NIRS—R—41

グループ研究「放射線に対する生体制御機構解明に関する研究」

第一研究グループ（生体制御研究グループ）

（平成７～12年度）

最終報告書

平成13年10月

放射線医学総合研究所

Final Report of the Group Research "Studies on Elucidation of Bioregulation Mechanisms against Radiation"

First Research Group (Bioregulation Research Group)

(April 1995 - March 2001)

October 2001

National Institute of Radiological Sciences
4-9-1 Anagawa, Inage-ku, Chiba 263-8555, Japan

目　　次
[CONTENTS]

序

本調査研究は、薬学研究部及び薬理化学研究部で行われていた活性酸素・フリーラジカルの生体影響研究をさらに発展・充実させるためにグループ研究として平成７年度から平成１２年度までの６年間に遂行されたものである。

本グループ研究の目的は放射線、紫外線、大気汚染あるいは化学物質などの環境ストレスによる生体障害の初期過程、遺伝子の発現調節や生体情報伝達、種々の疾患の発生、疾患の制御等における活性酸素・フリーラジカルの研究が世界的に行われはじめていることや本研究所において蓄積された研究成果を背景として、分子、遺伝子、細胞から個体レベルに至る放射線等の環境ストレスに対する生体制御機構を総合的に解明し、さらにそれらの予防、診断、治療等医学利用に寄与するために行われた。本グループ研究では6年間にその成果が期待できる４つのテーマを選び、それぞれサブグループを構成し、かつ研究材料および解析技術を共有できる共同研究型のグループ研究を実施した。

（１）第一サブグループ：生体ラジカルに関する研究

放射線等の酸化的ストレスにより生体内に生成される活性酸素・フリーラジカル種を電子スピン共鳴(ESR)法などの種々の分光学的手法を用いて同定し、反応性や生体内挙動をin vitroおよびin vivoで解析するとともに、抗酸化物質の評価法の確立を目指す。この結果を基に障害の初期過程が明らかにされ、引き続いて起こる障害や疾病の機構解明、さらには障害や疾病の予防、診断、治療などに寄与すことができる。

（２）第二サブグループ：生体制御物質の発現に関する研究

放射線・活性酸素に対する初期応答機構を解明するために、分子生物学的手法などを用いて初期応答に寄与する遺伝子のモチーフ構造の決定と活性化経路の分子解析、並びに、放射線防護剤および活性酸素制御物質の作用解析を行う。

障害の初期過程の解析により、引き続いて起こる障害や疾病の機構解明、さらには障害や疾病の予防、診断、治療などに寄与すことができる。

（３）第三サブグループ：細胞機能調節に関する研究

放射線による乳腺細胞の腫瘍化イニシエーションと卵巣ホルモン、下垂体ホルモンや一酸化窒素(NO)などのフリーラジカルとの関係、および放射線でイニシエートされた乳腺細胞が異常に増殖して腫瘍（がん）化する機序を解明するとともに、乳腺に作用する卵巣ホルモン、例えばエストラジオールの生合成時に起こる酸化的ストレスが生体に与える影響についても分子生物学的観点から明らかにする。

本課題の最終目標は、放射線に被ばくした乳腺の晩発障害の一つである腫瘍（がん）化を抑制する低毒性化合物を天然物や化学合成品から探索して発がんの予防に寄与することである。

（４）第四サブグループ：生体制御物質に関する探索研究

活性酸素・活性窒素と種々の疾患との関連が注目されている。これらの活性酸素・活性窒素による生体内障害は、DNAに対しては、塩基の酸化および鎖の開裂、タンパク質に対しては、酸化やニトロ化による不活性化、脂質に対しては過酸化である。本研究

では、生理活性物質や活性酸素・活性窒素の発生と消去に関連する生体制御物質を天然物や化学合成化合物から探索する。

グループ全体として得られた成果は、原著論文として８０報を越えている。少人数で研究費は研究グループの中では最も低かったが、逆に費用対効果はかなり高かったと考えられる。また、当初の研究目標の８割以上の達成度があったものと思われる。

グループ研究全体の成果としては、いくつかの生体制御物質の新規合成とその活性酸素・フリーラジカル消去活性を電子スピン共鳴(ESR)を用いるスピントラッピング法により明らかにしたことである。また、生理機能を有する一酸化窒素(NO)の新しいスピントラップ剤を開発したこともグループ研究としての成果である。これらの成果は特許出願中である。また、天然生薬（ウコン）の抽出物、クルクミンが放射線発がんの予防に有効であることを初めて明らかにした成果は放射線影響研究に大いに貢献した。

それぞれのサブグループで行われた研究成果は、小課題の研究成果にまとめられている。また、代表的な原著論文も末尾に載せてあるので詳細は省くが、本グループ研究において１）in vitro での活性酸素・フリーラジカルの生成法と検出法の確立及び反応性を明らかにすることができたこと、２）in vivo ESR を用いて個体レベルでの放射線による酸化ストレスを非侵襲的に評価する方法を確立した、３）遺伝子発現調節機構の解析方法を確立した、４）マウス細胞における内在レトロウイルスの発現制御とゲノム不安定性の関連を明らかにした、５）妊娠中や授乳中の乳腺は放射線感受性が高いことを内分泌学的に解明し、この高感受性動物を用いて放射線による腫瘍化を予防する物質を探索し、クルクミンが特に有効であることを明らかにした、６）乳腺細胞で NO が産生されることを証明し、NO 捕捉剤や NO 合成酵素阻害剤による発がん予防が可能であることを示唆した、７）本研究で合成した抗酸化剤の中で 2',4',3,4-hudroxychalcone が高いラジカル捕捉能を持つことを明らかにした、８）NO に対する新しいスピントラップ剤を開発した。また、放射線に対する防御機構や防御物質に関して放医研から様々な形で発信することができた。これらの研究成果は活性酸素・フリーラジカル研究が基盤をなす放射線障害の予防、防御研究あるいは２１世紀の大きな研究の柱となるであろう老化予防などの今後の放医研の研究に大きな寄与を果たすものと信ずる。

関係各位のご批判をいただければ幸いである。

グループリーダー　小澤　俊彦

Preface

Most environmental stress such as radiation, ultra-violet irradiation, air pollutants and chemical compounds cause damages to living organisms via reactive oxygen species (ROS) and free radicals produced in the organisms exposed to the stress. These ROS and free radicals react with various intracellular components such as DNA, proteins and lipids, and finally induce genomic damages and abnormality of cell functions.

This research group conducts research into biological effects from environmental stress from molecular and cellular levels to the whole-body level. This research started at April, 1995 and finished at March, 2001. Four subgroups have benn engaged in the following investigations: (1) studies on the bioradicals, (2) studies on the expression of the substances for bio-regulation, (3) regulation of cellular function, and (4) explorative study of bioregulation substances.

The significant results were published in appropriate international journals listed in the last part of this report. These findings will cntribute not only for the progress of the international free radical research, but also for better understanding of the antioxidants and radio-protection in biodefence mechanism against radiation and other environmental stress.

Toshihiko Ozawa
Director of Group Research

研究組織

本研究グループは、４つのサブグループから構成されており、第一サブグループでは生体ラジカルに関する研究、第二サブグループでは生体制御物質の発現に関する研究、第三サブグループでは細胞機能調節に関する研究、第四サブグループでは生体制御物質に関する探索研究を行った。以下に組織を略記する。

グループリーダー：小澤俊彦（平成７年４月～平成１３年３月）

第一サブグループ：小澤俊彦（併任）、島津良枝（平成７年４月～平成９年３月）、今井靖子（平成９年５月～平成１０年３月）、上田順市（平成７年４月～平成１３年３月）、安西和紀（平成７年４月～平成１０年３月）、竹下啓蔵（平成１０年６月～平成１３年３月）、三浦ゆり（科学技術特別研究員、平成７年４月～１０年３月）、有本豊子（重点研究支援研究員、平成１１年１月～平成１１年１２月）、西澤真裕（重点研究支援研究員、平成１２年１月～平成１２年１０月）

第二サブグループ：常岡和子（平成７年４月～平成１０年３月）、安西和紀（平成１０年４月～平成１３年３月）、古瀬雅子（平成７年４月～平成１３年３月）、石原弘（平成７年４月～平成１３年３月）、田中泉（平成７年４月～平成１３年３月）、万虹(STA Fellow、平成９年３月～平成１１年３月)

第三サブグループ：稲野宏志（平成７年４月～平成１３年３月）、鈴木桂子（平成７年４月～平成１３年３月）、小野田眞（平成７年４月～平成１３年３月）

第四サブグループ：伊古田暢夫（平成７年４月～平成１３年３月）、稲葉浩子（平成７年４月～平成１０年３月）、今井靖子（平成１０年４月～平成１３年３月）、中川秀彦（平成７年９月～平成１３年３月）、Ranjith Gamage (STA Fellow, 平成７年９月～平成９年９月)

Bioregulation Research Group

Group leader: Toshihiko Ozawa (1995. 4-2001. 3)

Sub-group:

1) Bioradical Research

Head: Toshihiko Ozawa (1995. 4-2001. 3)

Yoshie Shimazu (1995. 4-1997. 3)

Kiyoko Imai (1997. 5-1998. 3)

Jun-ichi Ueda (1995. 4-2001. 3)

Kazunori Anzai (1995. 4-1998. 3)

Keizo Takeshita (1998. 6-2001.3)

Yuri Miura* (1995. 4-1998. 3)

Toyoko Arimoto** (1999)

Masahiro Nishizawa** (2000)

2) Expression of Bioregulator Gene

Head: Kazuko Tsuneoka (1995. 4-1998. 3)

Head: Kazunori Anzai (1998. 4-2001. 3)

Hirosi Ishihara (1995. 4-2001. 3)

Masako Furuse (1995. 4-2001. 3)

Izumi Tanaka (1995. 4-2001. 3)

Wan Hong (1997. 3-1999. 3)

3) Radiation Effects on Endocrine Systems

Head: Hirosi Inano (1995. 4-2001. 3)

Keiko Suzuki (1995. 4-2001. 3)

Makoto Onoda (1995. 4-2001. 3)

4) Explorative Study of Bioregulation Substances

Head: Nobuo Ikota (1995. 4-2001. 3)

Hiroko Hama-Inaba (1995. 4-1998. 3)

Kiyoko Imai (1998. 4-2001. 3)

Hidehiko Nakagawa (1995. 9-2001. 3)

Ranjith Gamage***(1995. 9-1997. 9)

*National Institute Post Doctoral Fellow

**Priority Research Supporting Staff

***Science and Technology Agency Postdoctral Fellow

研究成果

Research Reports

生体ラジカルに関する研究

小澤俊彦、島津良枝、今井靖子、上田順市、安西和紀、竹下啓蔵、三浦ゆり、
有本豊子、西澤真裕（第１サブグループ）

Studies on the Bioradicals

Toshihiko Ozawa, Yoshie Shimazu, Kiyoko Imai, Junichi Ueda, Kazunori Anzai, Keizo Takeshita ,
Yuri Miura, Toyoko Arimoto, Masahiro Nishizawa

Most environmental stress-induced sources (radiations, UV, air pollutants, chemical substances, etc.) cause damages to living organisms via reactive oxygen species (ROS) such as superoxide ($O_2^{\cdot-}$), hydroxyl radical (OH), singlet oxygen ($^1O_2$) and hydrogen peroxide (H_2O_2) produced in the organisms exposed to the stress. These ROS react with various intracellular components such as DNA, proteins and lipids, and finally induce genetic damages and abnormality of cell functions. Therefore, it is important to know the chemical reactivites of these ROS, and to identify protective substances against them. It is known that OH is produced from the radiolysis of H_2O. Electron spin resonance (ESR)-spin trapping method using 5,5-dimethyl-1-pyrroline *N*-oxide (DMPO) as a spin trap and DNA strand scission assay showed that OH is also chemically generated from either the reaction of copper(II) complexes with H_2O_2 or UV photolysis of H_2O_2. By use of these hydroxyl radical generating system, it was elucidated that linoleic acid, a lipid model compound, was oxidized to generate linoleic hydroperoxide. On the other hand, by use of these hydroxyl radical detecting system, it was shown that almost all polyphenols including caffeic acid, catechin, or procatechuic acid scavenged OH.

Finally, it is also important to understand the generation of ROS and related phenomena in living organisms. Radiation increases the signal decay of a nitroxyl redox probe as measured with in vivo ESR technique. The increase may result from enhancement of radical reactions in the animal bodies, because antioxidants inhibit increase of signal decay. Thus, in vivo ESR system probing with nitroxyl radical may be available to evaluate not only the redox reaction in biological system but also the biological function.

Ⅰ．緒言

生体が放射線等の酸化的ストレスを受けることにより種々の障害や疾病が引き起こされることが知られているが、その起因の１つとして活性酸素・フリーラジカルの関与が推測されている。そこで放射線等の酸化的ストレスにより生体内で生成されると考えられる活性酸素・フリーラジカル種を種々の分光学的手法を用いて同定し、反応性や生体内挙動をin vitro及びin vivoで解析するとともに、抗酸化物質の評価法の確立を目指した。この結果を基に障害の初期過程が明らかになり、引き続いて発生する障害や疾病の機構解明、更にはそれらの予防、診断、治療などの医学利用に寄与することが出来ると考えられる。

Ⅱ．研究の内容・成果

(1) in vitroでの活性酸素・フリーラジカル種の同定と反応性の解析

①銅錯体と過酸化水素との反応、あるいは銅錯体と生体内還元剤との反応から生じる活性酸素種の同定

銅イオンと過酸化水素との反応により、あるいは銅イオンと生体内還元剤によりどのような活性酸素が発生するかをESRスピントラッピング法を用いて調べ、さらに同じ条件でＤＮＡ鎖切断が起こるかどうかをpBR322プラスミドを用いた電気泳動実験で調べた。銅イオンは生理的pH条件下ではフリーの状態ではなく、主に錯体を形成しているので、銅錯体を用いた。銅(II)錯体としては、Cu(HisGly) (HisGly: L-histidylglycine) 、Cu(HisGlyGly) (HisGlyGly;L-histidylglycylglycine)、$Cu(CyHH)_2$ (CyHH: cyclo(L-histidyl-L-histidyl))、$Cu(OP)_2$ (OP; o-phenanthroline) 、$Cu(en)_2$ (en; ethylenediamine) 溶液等を用いた。スーパーオキシドイオン ($O_2^{\cdot-}$) はhypoxanthine-xanthine oxidase系から発生させた。還元剤として、含ＳＨ化合物であるアセチルシスティン及びグルタチオン、アスコルビン酸、NADHを用いた。スピントラップ剤として5,5-dimethyl-1-pyrroline *N*-oxide (DMPO)を用いた。DMPO存在下、銅錯体とhypoxanthine-xanthine oxidase系、あるいは銅錯体と生体内還元剤を混合し、１分後にESRスペクトルを測定した。ESR装置はJEOL-RE-1Xを使用し、石英製扁平セルを用いて測定した。

スーパーオキシドラジカルを消去する物質として開発された有機化合物やペプチドを配位子とする銅錯体、例えば、Cu(HisGlyGly)、Cu(CyHH)$_2$、Cu(en)$_2$ 等、が図１に示すようにDMPOの$O_2^{\cdot-}$付加体のシグナル強度を減少させて、新たにDMPOの・OH付加体（DMPO-OH）を出現させた。これは、銅錯体が$O_2^{\cdot-}$を過酸化水素に換えるとともに、それを活性化して、より反応性の高いヒドロキシルラジカル(・OH)を発生させることを電子スピン共鳴（ＥＳＲ）ースピントラッピング法を用いて示した。さらに、生じた・OHはプラスミドpBR322のDNAの２本鎖を切断することを図２に示すように電気泳動法により明らかにした。

一方、銅錯体は過酸化水素がなくてもアスコルビン酸やグルタチオンなどの生体内還元剤が存在すると、酸素から過酸化水素を生成し、それを活性化して、・OHに変えることをＥＳＲースピントラッピング法を用いて示した。また、銅錯体と還元剤のみでプラスミドpBR322のDNA鎖切断が起こることを示した。これらの結果は、水の放射線分解から生ずる・OHが銅錯体ー過酸化水素系からも同様に生ずることをESR-スピントラッピング法と電気泳動法を用いたＤＮＡ鎖切断実験により明らかにした。さらに、銅イオンは細胞の核内に多く含まれており、過酸化水素やアスコルビン酸あるいはグルタチオンなどの生体内還元剤が核内に移行すると、ＤＮＡに結合した銅の周囲で・OHが生成し、ＤＮＡが傷害を受ける可能性を示唆した。

②抗酸化物質の評価法の確立

上記の方法が・OHを消去する物質の簡便な探索法として有用ではないかと考え、種々の化合物の・OH消去活性の評価を行った。化合物としてprocatechuic acid、catechin、 caffeic acid等のポリフェノール類、アスコルビン酸、Trolox C (vitamin E derivative)、尿酸、グルタチオン等の生体内物質、BHA等の市販の抗酸化物質を用いた。・OHはCu(II)(en)$_2$とH_2O_2 の反応から発生させた。スピントラップ剤としてDMPOを用いた。DMPO存在下、Cu(II)(en)$_2$、H_2O_2、化合物を混合し、１分後にESRスペクトルを測定した。化合物の抗酸化活性はDMPO-OHのESRシグナルの強度を半分にするときの化合物の濃度を求め、それの大小で比較した。その結果、ポリフェノール類と尿酸に強い消去活性を見い出した。

③ヒドロキシルラジカルによるリノール酸、リポソーム の過酸化過程の解明

活性酸素は、低密度リポ蛋白（ＬＤＬ）の酸化を通じて動脈硬化の原因となったり、生体膜に作用してイオン透過性を変化させることにより様々な病態・疾患の原因となっていると考えられている。その過程で、過酸化脂質の生成と分解が関与していると予想されるが、その詳細はまだ明らかにされていない。我々は、これまで銅錯体-過酸化水素(H_2O_2)系で発生する・OHとＤＮＡ等の生体構成成分との反応を調べてきた。銅錯体ーH_2O_2系で発生する・OHによるリノール酸の過酸化と分解機構の解明を分光学的に調べ、その機構の解明を行うとともに、・OHによるリン脂質の過酸化とイオン透過性との関係をリポソーム系においてK^+イオン選択性電極を用いて調べた。

・OHはCu(II)(en)$_2$ とH_2O_2 の反応から発生させた。共役ジエンの234nmの吸光度は日立U-3210分光光度計を用いて測定した。リノール酸(1.2 mM)、Cu(en)$_2$ (0.1 mM)及びH_2O_2 (1 mM又は10 mM)からなる反応液から一

Fig. 1. ESR spectra obtained from the hypoxanthine (HPX)-xanthine oxidase (XOD) system in the presence of DMPO. Reaction mixtures contained 0.5 mM HPX, 0.1 unit/ml XOD, 125 mM DMPO, and no addition (a); 0.025 mM Cu(II)(CyHH)$_2$ (b); 0.25 mM Cu(II)(CyHH)$_2$ (c).

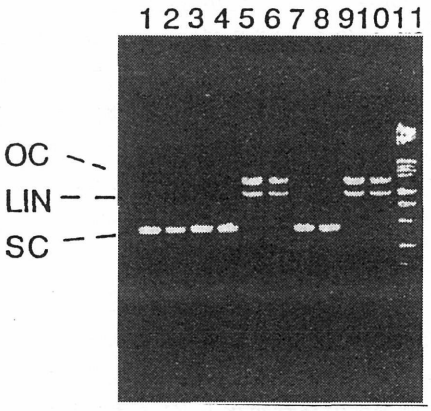

Fig. 2. Cleavage of supercoiled DNA by Cu(II) complexes and H_2O_2 system. Lane 1, DNA alone; lane 2, DNA + 25 mM H_2O_2; lanes 3 and 4, DNA + 0.25 mM Cu(II)(CyHH)$_2$; lanes 5 and 6, DNA + 0.25 mM Cu(II)(CyHH)$_2$ + 25 mM H_2O_2; lanes 7 and 8, DNA + 0.25 mM Cu(II)(Cim); lanes 9 and 10, DNA + 0.25 mM Cu(II)(Cim) + 25 mM H_2O_2; lane 11, DNA marker. Loading 0.5 μg DNA per lane.

定時間ごとに一定量とり、シクロヘキサン抽出してリノール酸の過酸化過程で生ずる共役ジエンの234nmの吸光度の経時変化を求めた。ＨＰＬＣは東ソー製多波長検出器とsilica 60カラムを、また溶離液としてhexane:isopropanol:acetic acid (80:1.25:0.1)を用いた。$Cu(en)_2$ (0.1 mM)とH_2O_2(1 mM)の場合、８時間の測定範囲内で234nmの吸収は時間とともに増加し２～４時間で最大となり、やがて減少した。しかし、・OHの発生量が多い$Cu(en)_2$ (0.1 mM)とH_2O_2(10 mM)の場合、234nmの吸収は同様に２～４時間で最大となったが、その吸光度はH_2O_2(1 mM)の場合の約半分であった。

次に、234nmの吸収がリノール酸の過酸化物由来であることをHPLCで確認した。シクロヘキサン抽出物中のリノール酸酸化物を順相HPLCにより解析したところ、・OHによるリノール酸過酸化物は４種類の異性体（13-E,Z 異性体, 13-E,E 異性体, 9-E,Z 異性体, 9-E,E 異性体）をほぼ同量含んでいることが明らかになった。さらに、リノール酸過酸化物のピークがH_2O_2濃度が10 mMの方が1 mMよりも少ないことが示されたが、これは生成したリノール酸の過酸化物が・OHによりさらに酸化されて分解されたためと考えられる。これを確かめるために、別途リポキシゲナーゼから合成したリノール酸過酸化物と$Cu(en)_2$ (0.1 mM)及びリノール酸過酸化物、$Cu(en)_2$ (0.1 mM)とH_2O_2(10 mM)との反応を調べた。$Cu(en)_2$ (0.1 mM)のみではリノール酸過酸化物の分解はほとんど見られなかったが、$Cu(en)_2$ (0.1 mM)とH_2O_2 (10 mM)の反応液はリノール酸過酸化物を分解した。この結果は、リノール酸過酸化物が・OHにより酸化されたことを示唆する。

次に、脂質の過酸化と分解が膜機能にどのように関与するのかを知る目的で、・OHによる卵黄レシチン（eggPC）リポソームの過酸化の過程で生ずる共役ジエンの234nmの吸光度の経時変化とK^+イオン選択性電極を用いてリポソームからのK^+透過性との関連性を調べた。リポソームはeggPCより逆相蒸発法により調製した。$Cu(en)_2$ (1 mM)とH_2O_2 (100 mM)によるeggPCのリポソームの234nmの吸光度の増加は少なかったが、eggPCのリポソームからのK^+の流出が見られた。これに対して、2,2'-azobis(2-amidinopropane) dihydrochloride (AAPH)による活性酸素発生系では、eggPCリポソームの過酸化過程で生ずる共役ジエンの233 nmの吸光度は大きく増加したが、eggPCリポソームからのK^+イオンの流出は見られなかった。これらの結果は、脂質過酸化物の生成よりも分解がリポソームのK^+イオン透過性に影響を与えることを示唆する。

このように、・OHによる生体構成成分の一つである脂質の酸化過程を分光学的手法とHPLCを用いて調べ、・OHによる不飽和脂肪酸の過酸化物の生成、更にそれらに引き続く酸化、膜の破壊を明らかにした。

④銅錯体によるリノール酸 の過酸化過程の解明

次に、銅錯体による脂質のモデル化合物、リノール酸の過酸化過程を分光学的手法と高速液体クロマトグラフィー（ＨＰＬＣ）を用いて検討した。銅(II)錯体としては、種々の酸化還元電位を持った５種の錯体、$Cu(BC)_2$ (BC; bathocuproinedisulfonic acid)、$Cu(CyHH)_2$、$Cu(OP)_2$、Cu(HisGlyGly)、$Cu(en)_2$ 溶液を用いて比較した。反応はpH 7.4のリン酸緩衝液中で行った。リノール酸と銅錯体を含んだ反応液から一定時間ごとに一定量取り、シクロヘキサン抽出してリノール酸の過酸化過程で生ずる共役ジエンの234 nmの吸光度の経時変化を求めた。その結果、Cu(II)錯体溶液(0.1 mM)によるリノール酸(1.2 mM)の過酸化において、２４時間の測定範囲内で共役ジエンの234nmの吸収は、反応時間とともに増加し、ある時間で最大となり、やがて減少した。反応産物のＨＰＬＣは４種類のリノール酸過酸化物(LOOH)の生成とともにその後の分解を示した。234nmの吸収が最大となった時間は$Cu(II)(BC)_2$ > $Cu(II)(CyHH)_2$ = $Cu(II)(OP)_2$ > $Cu(II)(en)_2$ > Cu(II)(HGG)の順番であった。この順番は銅(II)錯体の酸化還元電位の大小に似ており、これから、酸化還元電位の高い $Cu(II)(BC)_2$ が酸化還元電位の低い Cu(II)(HGG) よりも容易にリノール酸を酸化し、さらに分解することが示唆された。

⑤活性酸素種相互間の変換の可能性

活性酸素種相互の変換については$O_2\cdot^-$, H_2O_2, ・OH間ではよく調べられている。しかし、これらと一重項酸素（$^1O_2$）との間の変換についてはあまりわかっていない。$^1O_2$は可視、紫外の光線曝露により生体内で生成する可能性があり、これがより強力な障害性をもつ・OHへの変化について$^1O_2$生成系であるウロポルフィリン（UP）光増感反応を用いて検討した。スピントラップ剤, DMPO, の存在下、UPに可視光線を照射したところ、NADPH依存的にDMPOの・OH付加体（DMPO-OH）のESRシグナルが観測された。このシグナルの強度はエタノール、ぎ酸等の・OH消去剤の存在下で3～30％に減少し、それぞれ・$CH(OH)CH_3$、$CO_2\cdot^-$のDMPO付加体のESRシグナルが出現した（図3）。また、NaN_3やヒスチジン等の$^1O_2$ 消去剤によってもESRシグナルはほぼ完全に消失したが、SOD, カタラーゼ、desferrioxamineではほとんど影響がなかった。$^1O_2$ を2,2,6,6-tetramethyl-4-piperidone (TEMPD)の酸化により測定したところ、NADPH非存在下ではTEMPD酸化体のESRシグナルが検出されたが、NADPH存在下ではTEMPD酸化体シグナルの出現にラグタイムが生じ、そのラグタイムはNADPH濃度依存的に延長された。一方、同じ条件で検出試薬をDMPOに変えてNADPH濃度依存性を調べたところ、DMPO-OHのシグナルはNADPH濃度依存的に大きくなった。このことはNADPH存在下では$^1O_2$がTEMPDと反応する前にNADPHと反応し、・OHを生じたことを示唆する。また、照射によりH_2O_2 の生成が確認されたが、反応系にH_2O_2 を添加してもDMPO-OHのシグナルは増加しなかった。これらのことから、NADPH存在下で$^1O_2$依存的に・OHが生成するこ

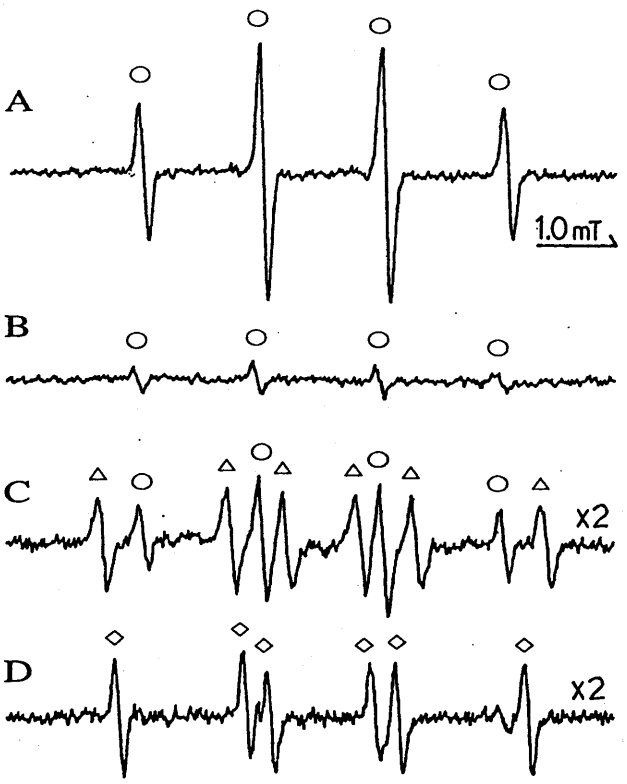

Fig. 3. ESR spectra of DMPO spin adducts formed during irradiation of UP. (A) 14 μM UP, 167 μM NADPH and 48 mM DMPO in 20 mM phosphate buffer, pH 7.4, was irradiated with visible light for 2 minutes; (B) same conditions except without NADPH. Samples containing (C) 600 mM ethanol and (D) 143 mM sodium formate were irradiated in the presence of NADPH. (△) ・CH(OH)CH3 adduct of DMPO, (◇) ・CO2- adduct of DMPO.

とが明らかとなり、それがO_2・⁻やH_2O_2を介さない可能性があることが示唆される。

続いて、ここで生成したDMPO-OHがフリーの・OHの生成に由来するか否か、そして、他の還元性物質の存在下で同様な反応が起こるか否かを調べた。$^1O_2$はUPの光増感反応あるいは3-(1,4-epidioxyl-4-methyl-1,4-dihydro-1-naphtyl)propionic acid (EPA)の熱分解により発生させた。還元剤としてNADPHの代わりにTrolox Cあるいはグルタチオンを用いたところ、いずれの場合にもDMPO-OH生成量が顕著に増加した。DMPO-OH生成量の増加はEPA系に比べUP光増感反応系で顕著であった。UP光増感反応系でスピントラップ剤としてDMPOの代わりに5-(diethoxyphosphoryl)-5-methyl-1-pyrroline-N-oxide (DEPMPO)を用いたところ、いずれの還元剤を用いた場合にもDEPMPO-OH生成量が増加した。しかし、Fenton反応により・OHを発生させたときに比べてDMPO-OH生成量に対するDEPMPO-OH生成量が極めて少なかった。以上のことより、UP光増感反応で還元剤の存在によるDMPO-OH形成のほとんどは・OH由来ではないこと、そしてその生成には光増感剤の反応が関わっていることが示唆された。さらに、$^1O_2$発生系として紫外線の1つであるUVAによるヘマトポルフィリン(HP)の光増感反応を用いてフェノール化合物の$^1O_2$消去活性を評価し、酸化電位の低いフェノール化合物が酸化電位の高いフェノール化合物よりも効率良く$^1O_2$を消去することを見い出した。

⑥ラクトペルオキシダーゼ(LPO)と過酸化水素(H_2O_2)の反応から生じるラジカル種の同定

ラクトペルオキシダーゼ(LPO)と過酸化水素(H_2O_2)の反応から生じるラクトペルオキシダーゼ compound I、IIは生体内還元剤であるNADHやGSHを酸化して各々のラジカル種を生成させ、これらのラジカル種が酸素をO_2・⁻に変換することが知られている。そこで、LPO/H_2O_2とNADH、あるいはGSHとの反応から生ずるラジカル種の生成に対するフェノール化合物の効果についてESR—スピントラッピング法を用いて検討した。フェノール化合物としては、estradiol, *p*-chlorophenol, phenol, quercetin, Troloxを含む19種類の化合物を用いた。さらに、フェノール化合物の化学的性質として、安定ラジカル, DPPHに対する消去活性を求め、DMPO付加体のシグナル強度の増減との間の相関性の有無について検討した。pH 7.4の0.1 Mリン酸緩衝液中、スピントラップ剤 DMPO、NADH, LPOとphenolを混合し、1分後に石英製扁平セルを用いてESRスペクトルを測定した。ESR装置はJEOL-RE-1X （日本電子製）を使用した。100 mM DMPO存在下、4 mM NADH, LPO (5 U/ml)と10 μM PhenolからDMPO付加体の12本線のESRスペクトルが得られた。超微細結合定数値（a^N =1.42, a_β^H=1.25, a_γ^H=0.12 mT）はO_2・⁻のDMPO付加体の文献値と一致した。スーパーオキシドジスムターゼ(SOD)の添加により、12本線のESRシグナルが消失したことからO_2・⁻のDMPO付加体であることが確認された。phenolを反応系から取り除くとこのシグナル強度は減少するので、phenolがO_2・⁻の発生を促進することが示唆される。LPO/H_2O_2/phenol系によるNADH酸化からのO_2・⁻の発生機序は次のように考えられる。

$$\text{LPO} + H_2O_2 \rightarrow \text{LPO-I} + H_2O \quad (1)$$
$$\text{LPO-I} + \text{PhOH} \rightarrow \text{LPO-II} + \text{PhO}\cdot \quad (2)$$
$$\text{LPO-II} + \text{PhOH} \rightarrow \text{LPO} + \text{PhO}\cdot \quad (3)$$
$$2\,\text{PhO}\cdot + 2\,\text{NADH} \rightleftarrows 2\,\text{PhOH} + 2\,\text{NAD}\cdot \quad (4)$$
$$2\,\text{NAD}\cdot + 2\,O_2 \rightarrow 2\,\text{NAD}^+ + 2\,O_2\cdot^- \quad (5)$$

LPO-I, LPO-IIはそれぞれラクトペルオキシダーゼ compound I、IIを表す。

他のフェノール化合物についても同様の実験を行い、得られた結果を表1に示す。phenol, estradiol, *p*-chlorophenol等の添加でO_2・⁻のDMPO付加体のシグナル強度は増加したが、Trolox, Quercetin等の添加では

逆にシグナル強度は減少した。Phenol による$O_2 \cdot^-$の生成増はLPO/H_2O_2/phenol系によるNADH酸化において式(4)が律速段階であり、NAD・/NADH (282 mV)よりも高い酸化電位を持つphenol (PhO・/PhOH = 970 mV)により式(4)の右の反応が加速されたためと考えられる。

次に、100 mM DMPO存在下、4 mM GSH, LPO (5 U/ml) と10 μM phenolの反応液から4本線のESRスペクトルが得られた。超微細結合定数値 (a^N =1.51, a_β^H =1.62 mT) はGS・のDMPO付加体の文献値と一致した。LPO/H_2O_2 /Phenol系によるGSH酸化からのGS・の発生機序はNADHの場合と同様に式(6)が律速段階のように考えられる。

$$PhO\cdot + GSH \rightleftarrows PhOH + GS\cdot \qquad (6)$$

他のフェノール化合物についても同様の実験を行い、得られた結果を表1に示す。

一方、DPPHとフェノール化合物を混合し、正確に1分後にESRスペクトルを測定し、DPPHのESRシグナル強度を50%低下させる時のフェノール化合物濃度を求め、これをフェノール化合物のDPPH消去活性とした。フェノール化合物のDPPH消去活性としてDPPHのESRシグナル強度を50%減少させる時のフェノール化合物の濃度を求め、その結果を表1に纏めて示した。estradiol, *p*-chlorophenol, phenol等はDPPH消去活性が弱く、quercetin, Trolox C等はかなり強いDPPH消去活性を示した。表1は、DPPH消去活性の弱いフェノール化合物ほど$O_2 \cdot^-$及びGS・のDMPO付加体のシグナル強度が高くなること、即ち$O_2 \cdot^-$及びGS・のラジカル発生量が大きいことを示す。DMPO付加体のシグナル強度に対するフェノール化合物のDPPH消去活性をプロットして解析を行ったところ、相関係数がそれぞれ0.666、0.914を示した。この結果は、未知の、或は合成フェノール化合物のDPPH消去活性を知ることによりそれらがLPO/H_2O_2によるNADHやGSHを酸化して各々のラジカル種を生成させるかどうかを予測できることを示唆した。

(2) in vivo ESR(生体計測用電子スピン共鳴装置)を用いた放射線障害の評価法の開発

X線照射による酸化的ストレスを生きた動物で調べるために、ニトロキシルラジカルをプローブとした*in vivo* ESR法を行った。ニトロキシルラジカルをマウスに投与し、マウス上腹部及び頭部で測定を行ったところ、それぞれ放射線照射によりニトロキシルラジカルの消失速度が増加し、in vivo ESRを放射線障害の非侵襲的評価法に応用できる可能性が示唆された。

一方、重粒子線は難治がん治療に有効な方法として期待されているが、in vivo における正常組織への障害メカニズムはほとんどわかっていない。重粒子線照射マウスにおいてin vivo ESRの結果と障害との関係について、照射線量依存性並びに照射後の時間変化を調べた。マウスに重粒子がん治療装置により重粒子線 (290MeV 炭素線, 6cm-SOBP, LET60keV/μm) を照射した。

Table1. Relationship between DPPH scavenging ability and signal intensities of DMPO/$O_2^{\cdot-}$ or DMPO/GS· adducts[a].

Compounds	IC50 (μM)[b]	DMPO/$O_2^{\cdot-}$ (a.u.)	DMPO/GS· (a.u.)
None		0.29 (1.0)[c]	1.28 (1.0)[c]
p-Chlorophenol	> 2500	2.88 (9.9)	9.46 (7.4)
17β-Estradiol	> 2500	2.61 (9.0)	4.83 (3.8)
3,4-Dimethylphenol	> 2500	2.20 (7.6)	6.40 (5.0)
Phenol	> 2500	1.26 (4.3)	8.19 (6.4)
Bisphenol A	> 2500	1.06 (3.7)	5.74 (4.5)
p-Hydroxyphenylacetic acid	> 2500	0.45 (1.6)	1.94 (1.5)
p-Hydroxybenzoic acid	> 2500	0.29 (1.0)	2.16 (1.7)
Acetaminophen	1940	0.65 (2.2)	5.01 (3.9)
Diethylstilbestrol	1460	0.47 (1.6)	4.28 (3.3)
Guaiacol	880	0.21 (0.7)	1.80 (1.4)
p-Methoxyphenol	265	0.11 (0.4)	1.95 (1.5)
p-Eugenol	263	0.50 (1.7)	1.98 (1.6)
Buthylated hydroxyanisole	204	0.30 (1.0)	0.93 (0.7)
Curcumin	45	0.41 (1.4)	1.89 (1.5)
Isoeugenol	32	0.28 (1.0)	1.85 (1.5)
Trolox	17	0.27 (0.9)	0.41 (0.3)
2-Hydroxyestradiol	17	0.22 (0.8)	0.99 (0.8)
Quercetin	16	0.00 (0.0)	1.45 (1.1)
Gallic acid	10	0.16 (0.6)	0.91 (0.7)

[a] Values are expressed as the mean (n = 3).
[b] [DPPH] = 105 μM.
[c] Relative signal intensity.

マウスをペントバルビタールナトリウムにより麻酔したのち、尾静脈より3-carbamoyl-2,2,5,5-tetramethylpyrrolidine-1-oxyl (carbamoyl-PROXYL) を投与し、直ちに上腹部をループ・ギャップ型共振器(幅5 mm) を装着したL-band ESR分光計により測定した。ESRシグナルの消失速度(/min)をスピンクリアランスとした。重粒子線照射4日目の生存率は7.5Gy 照射群では100%、15 Gy照射群では70%(5/7)であった。生き残ったマウスの障害の程度を調べたところ、体重は7.5 Gy照射群、15 Gy 照射群共に未照射群の約60%程度に減少し、肝重量は7.5Gy照射群で約40%、15 Gy照射群で約60%に減少した。また、血清GOT値は7.5Gy照射群で有意に増加した。過酸化の指標として肝のTBARSを測定したところ、7.5Gy、15Gy共に非照射群に比べて有意な増加が見られた。さらに、照射1-2時間後の上腹部におけるスピンクリアランスを測定したところ、7.5Gy照射群、15Gy照射群共に非照射群に比べて有意に増加し、その程度は両照射群で同程度であった。X線照射マウスで行った実験では照射1時間後の上腹部のスピンクリアランスが照射線量依存的に増加しており、重粒子線とX線の線量依存性の違いは生物学的効果の違いを反映しているものと思われる。7.5Gyの重粒子線照射後に経時的に障害指標を調べたところ、照射約1日後から体重並びに肝重量の減少が見られ、血清GOT値が上昇した。また、肝のTBARS値は照射2日後から4日後にかけて増加した。同線量において上腹部のスピンクリアランスを調べたところ、照射1-2時間後では非照射群より高く、16-17時間後及び35-36時間後では逆に非照射群より低くなる傾向が見られた（図4）。
照射16時間以降で見られたスピンクリアランスの照射群、非照射群の間での逆転現象は、障害の進行に関係しているものと思われる。類似の現象は15GyのX線照射でも見られている。

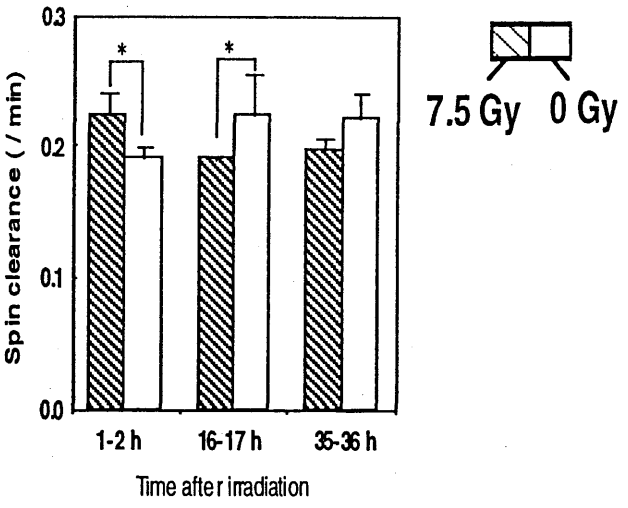

Fig. 4. Time course of spin clearance measured at upper abdomen of mice irradiated with high LET heavy ion beams. Mice (ddY, 4 weeks old) received carbon ion beam (60 keV/μm, 7.5 Gy) irradiation or sham irradiation. Carbamoyl-PROXYL (50 μL, 280 mM) was injected intravenously to the mice on the day indicated, and decay rates of ESR signal (spin clearance) were measured at upper abdomen of the mice with a L-band ESR spectrometer. Data were expressed as mean ± S.D (n=3-4). * indicates that the difference between the two groups is significant ($P<0.05$).

III. 結論

*in vitro*で銅錯体が$O_2^{\cdot -}$を不均化して過酸化水素に換え、さらにこれを活性化して、・OHを発生させること、及び発生した・OHがＤＮＡや脂質を酸化することを明らかにした。さらに、・OHの検出方法として電子スピン共鳴—スピントラッピング法とＤＮＡ鎖切断実験と組み合わせる方法を編み出した。炎症などの疾病の起因の一つとして活性酸素が考えられている。そのような活性酸素の中で・OHが最も反応性が高く、生体に障害を与えると推測されている。それ故に、・OHの発生抑制又は消去物質の探索は重要である。ヒドロキシルラジカルの検出方法として電子スピン共鳴—スピントラッピング法とＤＮＡ鎖切断実験の組み合わせる方法を用いることにより・OHの消去物質の探索を短時間で行うことが可能であることを示した。

一方、ニトロキシルラジカルを投与したマウスの上腹部及び頭部で、生体計測用ESRを測定したところ、投与直後からニトロキシルラジカルのシグナルが観測され、時間経過とともにシグナル強度が減少した。さらに、酸化的ストレスとしてマウスにX線照射したところ、このシグナル減少速度が低下することが明らかになった。これらの結果より、スピンプローブとしてニトロキシルラジカルを用いることで、生体内の酸化的ストレスによる影響を無侵襲的に測定できる可能性を示唆した。

IV. 研究発表

(1) Ueda, J., Shimazu, Y. and Ozawa, T.: Reactions of copper(II)-oligopeptide complexes with hydrogen peroxide: Effects of biological reductants, *Free Rad. Biol. Med.*, **18**, 929-933, 1995.

(2) Miura, Y., Ueda, J., and Ozawa, T.: Formation of the DMPO-OH adduct from Ti(IV) and DMPO in aqueous solution - the first ESR evidence. *Inorg. Chim. Acta*, **234**, 169-171, 1995.

(3) Sakamoto, S., Mihara, H., Matsuo, E., Niidome, T., Anzai, K., Kirino, Y. and Aoyagi, H.: Enhanced membrane-perturbing activities of bundled amphiphilic α-helix polypeptides on interaction with phospholipid bilayer, *Bull. Chem. Soc. Jpn.*, **68**, 2931-2939, 1995.

(4) Anzai, K., Yoshioka, Y., Hatanaka, K. and Kirino, Y.: Phosphatidylserine-specific transbilayer lipid translocation in synaptosomal plasma membranes

from *Narke japonica*, *J. Biochem.*, **117**, 1232-1237 , 1995.

(5) Ueda, J., Hanaki, A. and Nakajima, T.: Catalytic activities and coordination environments of the copper ions in the imidazole clusters of histidine-peptides, $His(His)_nGly$ and N-acetyl-$His(His)_nGly$ (n=3, 8, and 18), *Chem. Pharm. Bull.*, **43**, 359-361, 1995.

(6) Ueda, J., Hanaki, A., Yoshida, N. and Nakajima, T.: Proton nuclear magnetic resomance studies of the complexes of zinc(II) with glycyl-L-histidylglycine. *Chem. Pharm. Bull.*, **43**, 2042-2047, 1995.

(7) Ueda, J., Saito, N. and Ozawa, T.: Detection of free radicals produced from reactions of lipid hydroperoxide model compounds with Cu(II) complexes by ESR spectroscopy, *Arch. Biochem. Biophys.*, **325**, 65-76, 1996

(8) Ueda, J., Saito, N., Shimazu, Y. and Ozawa, T.: A comparison of scavenging abilities of antioxidants against hydroxyl radicals, *Arch. Biochem. Biophys.*, **333**, 377-384, 1996.

(9) Ozawa, T., Miura, Y. and Ueda, J.: Oxidation of spin-traps by cholorine dioxide (ClO_2) radical in aqueous solutions: First ESR evidence of formation of new nitroxide radicals, *Free Rad. Biol. Med.*, **20**, 837-841, 1996.

(10) Fujiwara-Hirashima, C., Anzai, K., Takahashi, M. and Kirino, Y.: A voltage-dependent chloride channel from *Tetrahymena* ciliary membrane incorporated into planar lipid bilayers, *Biochim. Biophys. Acta*, **1280**, 207-216, 1996.

(11) Ozawa, T. and Nakano, Y.: The radical scavenging abilities of a new antinephritic drug, OPC-15161, *Biochem. Mol. Biol. Int.*, **38**, 231-238, 1996.

(12) Ueda, J., Saito, N. and Ozawa, T.: ESR spin trapping studies on the reactions of hydroperoxides with Cu(II) complexes, *J. Inorg. Biochem.*, **64**, 197-206, 1996

(13) Ueda, J., Miyazaki, M., Matsushima, Y. and Hanaki, A.: Glycylsarcosyl-L-histidylglycine, A peptide with a "breakpoint" in the complex formation: hydrolysis of the complex $[CuH_{-1}L]$, *J. Inorg. Biochem.*, **63**, 29-39, 1996.

(14) Suzuki, K.T., Rui, M., Ueda, J. and Ozawa, T.: Production of ascorbate and hydroxyl radicals in the liver of LEC rats in relation to hepatitis, *Res. Commun. Mol. Pathol. Pharmacol.*, **96**, 137-146, 1997.

(15) Noda, Y., Anzai, K., Mori, A., Kohno, M., Shinmei, M. and Packer, L.: Hydroxyl and superoxide anion radical scavenging activities of natural source antioxidants using the computerized JES-FR30 ESR spectrometer system, *Biochem. Mol. Biol. Internatl.*, **42**, 35-44, 1997.

(16) Lee, S., Kiyota, T., Kunitake, T., Matsumoto, E., Yamashita, S., Anzai, K. and Sugihara, G.: *De Novo* Design, Synthesis, and Characterization of a Pore Forming Small Gloublar Protein and Its Insertion into Lipid Bilayers, *Biochemistry*, **36**, 3782-3791, 1997.

(17) Miura, Y., Anzai, K., Urano, S. and Ozawa, T.: *In vivo* electron paramagnetic resonance studies on oxidative stress caused by x-irradiation in whole mice, *Free Rad. Biol. Med.*, **23**, 533-540, 1997.

(18) Suzuki, K. T., Rui, M., Ueda, J. and Ozawa, T.: Production of ascorbate and hydroxyl radicals in the liver of LEC rats in relation to hepatitis, *Res. Commun. Mol. Pathol.*, **96**, 137-146, 1997.

(19) Miura, Y. Anzai, K., Takahashi, S. and Ozawa, T.: A novel lipophilic spin probe for the measurement of radiation damage in mouse brain using *in vivo* electron spin resonance (ESR), *FEBS Lett.*, **419**, 99-102, 1997.

(20) Ueda, J., Hanaki, A., Yoshida, N. and Nakajima, T.: Proton nuclear magnetic resonance studies of the complexation of Zn(II) with histidine-containing peptides, L-histidyl-L-histidylglycylglycine and L-histidylglycyl-L-histidylglycine, *Chem. Pharm. Bull.*, **45**, 1108-1113, 1997.

(21) Ueda, J., Takai, M., Shimazu, Y. and Ozawa, T.: Reactive oxygen species generated from the reaction of copper(II) complexes with biological reductants cause DNA strand scission, *Arch. Biochem. Biophys.*, **357**, 231-239, 1998.

(22) Hamada, T., Kodama, H., Takeshita, K., Utsumi, H. and Iba, K.: Characterization of transgenic tabacco with an incresed α-linoleic acid level, *Plant Physiol.*, **118**, 591-598, 1998.

(23) Anzai, K., Ogawa, K., Kuniyasu, A., Ozawa, T., Yamamoto, H. and Nakayama, H.: Effects of hydroxyl radical and sulfhydryl reagents on the open probability of the purified cardiac ryanodine receptor channel incorporated into planar lipid bilayers, *Biochem. Biophys. Res. Commun.*, **249**, 938-942 , 1998.

(24) Anzai, K., Miura, Y., Ueda, J., Ozawa, T., Noda, Y., Mori, A. and Packer, L.: *In vitro* studies of the antioxidant activity of EPC-K1, a conjugate of vitamin C and vitamin E, *Res. Commun. Biochem.Cell & Mol. Biol.*, **2 (1&2)**, 129-138, 1998.

(25) Ueda, J., Anzai, K., Miura, Y. and Ozawa, T.: Oxidation of linoleic acid by copper(II) complexes: effects of ligand, *J. Inorg.Biochem.*, **76**, 55-62 , 1999.

(26) Takeshita, K., Hamada, A. and Utsumi, H.: Mechanisms related to reduction of radical in mouse lung using an L-band ESR spectrometer, *Free Radic. Biol. & Med.*, **26**, 951-60, 1999.

(27) Miura, Y., Anzai, K., Ueda, J. and Ozawa, T.: Novel approach to in vivo screening for radioprotective activity in whole mice: in vivo electron spin resonance study probing the redox reaction of nitroxyl, *J. Radiat. Res.*, **41**, 103-111, 2000.

(28) Hirose, J., Minakami, M., Settu, K., Tsukahara, K., Ueda, J. and Ozawa, T.: Reaction mechanism of electron transfer from $Fe^{II}(CN)_6^{4-}$ or $W^{IV}(CN)_8^{4-}$ to the cupric ions in human copper, zinc superoxide dismutase, *Arch. Biochem. Biophys.*, **383**, 246-255, 2000.

(29) Takeshita, K., Olea-Azar, C. A., Mizuno, M. and Ozawa, T.: Singlet oxygen-dependent hydroxyl radical formation during uroporphyrin-mediated photosensitization in the presence of NADPH, *Antiox. Redox Signal.*, **2**, 355-362, 2000.

(30) Hanaki, A., Kinoshita, T. and Ozawa, T.: Kinetic studies on the autoxidation of cysteine catalyzed by copper complexes: catecholamines stimulate the autoxidation, *Bull. Chem. Soc. Jpn.*, **73**, 73-80, 2000.

(31) Ueda, J., Hanaki, A., Hatano, K. and Nakajima, T.: Autoxidation of ascorbic acid catalyzed by the copper(II) bound to L-histidine oligopeptides, (His)iGly and acetyl-(His)iGly (i = 9, 19, and 29). Relationship between catalytic activity and coordination mode, *Chem. Pharm. Bull.*, **48**, 908-913, 2000.

(32) Ueda, J., Tsuchiya, Y. and Ozawa, T.: Relationship between effects of phenolic compounds on the generation of free radicals from lactoperoxidase-catalyzed oxidsation of NAD(P)H or GSH and their DPPH scavenging ability, *Chem. Pharm. Bull.*, **49**, 299-304 , 2001.

(33) Miura, Y., Anzai, K., Ueda, J. and Ozawa, T.: Pathophysioological significance of *in vivo* ESR signal decay in brain damage caused by x-irradiation - radiation effect on nitroxyl decay of lipophilic spin probe in head region, *Biochem. Biophys. Acta*, **1525**, 167-172, 2001.

生体制御物質の発現に関する研究

安西和紀、石原　弘、古瀬雅子、田中　泉、常岡和子、万　虹
（第２サブグループ）

Studies on the Expression of the Substances for Bio-regulation

Kazunori Anzai, Hiroshi Ishihara, Masako Furuse, Izumi Tanaka, Kazuko Tsuneoka, Wan Hong

Bioorganisms possess defense mechanisms against damages induced by x-irradiation or chemical treatments. However, our understanding of the early responsive molecular mechanism against these stresses is still poor. In the present study, we investigated the early responsive mechanism against radiation and reactive oxygen species (ROS) using cellular and molecular biological methods. By a modified reporter assay, it appeared that IL-1β and *jun*B genes, which relate to the inflammatory process, are activated via specific binding of nuclear protein with nucleotide sequences positioned far-upstream region of the genes. Furthermore, an endogenous retrovirus that contributes to genomic instability of somatic cells is activated in regenerated hematopoietic cells damaged by x-ray irradiation. One kind of radioprotector, heat-killed *Lactobacillus casei* preparation, was found to modulate inflammation. This modulation may be responsible for the increase of the survival rate of mice after whole-body x-irradiation at lethal dose. Another kind of radioprotectors, methoxycarbonyl-PROXYL, POBN, and PBN, belonging to antioxidants, were also effective against lethal dose x-irradiation. These findings can be used to study the relationship between molecular mechanisms activated by irradiation or ROS and regulatory mechanisms by reduction/oxidation balance in bioorganisms.

Ⅰ．緒言

生体の放射線障害は、電離放射線により生体内で出現した活性酸素化合物が生体高分子に損傷を与えることにより発生する。電離放射線照射後の哺乳類細胞で活性化する遺伝子群の産物の内には生体の酸化的ストレスの軽減もしくは耐性亢進に寄与するものが含まれる。このことから、生体は放射線や酸化・還元状態の変動など、生体内外のストレスによる多様な障害を軽減する防御機構を有するものと考えられている。しかしながら、その初期反応機構、特にその分子機構に関しては未知の部分が多い。

本小課題は、放射線・活性酸素に対する初期防御応答機構を解明するために、細胞及び分子生物学的手法を用いて初期応答に寄与する遺伝子のモチーフ構造の決定と活性化経路の分子解析、並びに、活性酸素制御物質の作用解析を行うことを目的とした。さらに、放射線防護剤を検索し、それらの作用機作を上記初期防御応答反応と関連づけて検討することも行った。

放射線・活性酸素に対する初期防御応答過程の解析により、引き続いて発生する障害や疾病の発症機構を解明する有力な情報が得られる。そして、その結果はそれら障害や疾病の予防、診断、治療などの医学利用に寄与することができる。

Ⅱ．研究の内容・成果

１．遺伝子発現調節機構の解析方法の確立

電離放射線の初期刺激により転写調節因子やサイトカインの遺伝子が活性化する。これらの遺伝子産物は直接または信号伝達経路を介して、多種多様な生体反応を活性化する。すなわち、初期の刺激から時間を経るに従って放射線応答とは直接関係の無い応答機構が活性化することになる。本研究では放射線・活性酸素刺激に特異性の高い応答機構を解析するために、刺激直後に注目して解析を進めた。転写レベルでの発現調節を解析するためには、第一に Electrophoretic mobility-shift assay（EMSA）法など、遺伝子周囲の塩基配列に対する核蛋白質の特異的な結合を測定する生化学的手法がある。第二にレポーターアッセイなど、生きた細胞にレポーター遺伝子を導入してその遺伝子機能を調べる細胞生物学的手法がある。しかし、後者は通常一次刺激から数日後のレポーター蛋白機能を測定するので、刺激直後の応答の分析には適さない。我々は刺激直後の分析に使用できるようにレポーターアッセイの改良を試みた。誘導性および非誘導性プロモーターを用いて条件を検討した結果、chloram-phenicol acetyl transferase（*cat*）レポーターRNA を定量することにより刺激直後の反応が分析できるようになった（Figs 1, 2）。

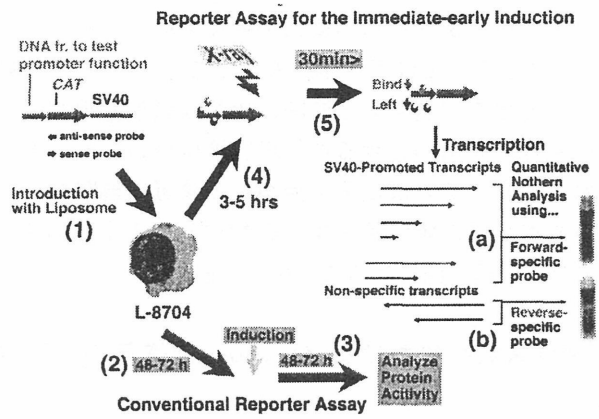

Fig. 1. Principle of the Reporter RNA Assay

Reporter gene that contains tested DNA and a coding region of reporter gene is transferred into cells (1). In conventional method, the cells are stimulated after incubation for 2-3 days to stabilize the exogenous DNA (2). Function of the reporter protein is measured 2-3 days after the stimulation (3).

In the reporter RNA assay, cells are harvested 30 minutes after stimulation (5) following 3-5 hours after introduction of reporter DNA (4). The amounts of reporter RNAs for both forward and backward RNAs are separately measured. To measure promoter function, the reporter RNAs at backward direction that correspond to nonspecific transcripts are subtracted from the reporter RNAs at forward direction that include both promoted and read-through RNA.

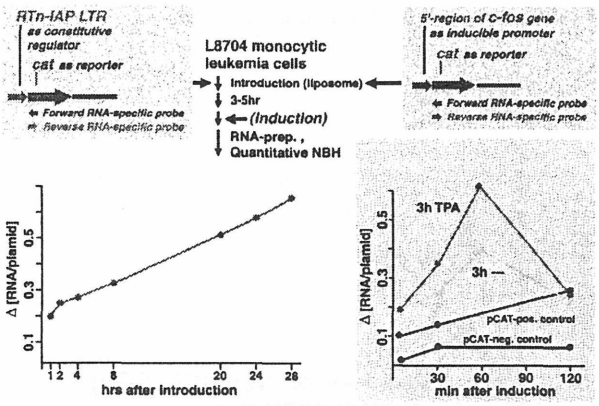

Fig. 2. Promoter Function Measured by the Reporter RNA Assay

Long terminal repeats (LTRs) of endogenous retrovirus that are constitutively activated in myeloid cells of C3H/He inbred mouse are placed at upstream region of chloramphenicol acetyl transferase (cat) gene (upper left). Three hours after transfer of the reporter DNA into a linearized macrophage-like leukemia (L8704) cells by liposome method, the cells are harvested at a time interval. Promoter function was calculated by separately measuring of forward and reverse cat RNAs by northen hybridization (lower left).

To test inducible promoter, upstream region of protooncogene c-fos that possesses phorbor ester responsible element was combined to cat gene (upper right). Three hours after introduction of the reporter into L8704 cells, cells were further incubated in the presence (3h TPA) or absence (3h ---) of phorbor ester. Promoter function was measured in the cells that were harvested at a time interval from 30 to 120 min after the induction (lower right).

レポーターDNA を細胞に導入後 3 時間という早い時期に外来遺伝子に由来する RNA が出現した。非誘導性内在レトロウイルス LTR をプロモーターとして使用したところ、*cat* RNA 量は次第に増加した。一方 TPA 応答モチーフを所持する *c-fos* 由来の誘導性プロモーターを使用した場合、TPA 添加直後に *cat* RNA 量が一過性に増加した (Fig. 2) 。このことは、細胞にレポーターを導入して 3 時間で刺激誘導をかけ、正および逆方向 *cat* RNA それぞれについて定量することで、初期応答が分析できることを示していた。この方法を利用して IL-1βならびに *fos/jun* 族遺伝子発現の調節を研究した。

2．マウス造血系細胞における Interleukin-1β (IL-1β) 遺伝子の発現制御

電離放射線照射直後のマウスの造血系細胞において、放射線防護蛋白質である IL-1β遺伝子は転写レベルで発現増強する(Ishihara *et al.*, *Radiat. Res.*, 133, 321-326, 1993)。IL-1β遺伝子は放射線刺激のみならず、様々なサイトカイン刺激や細胞分化刺激によっても持続的に発現するので、放射線の寄与の大きい照射直後の一過性発現調節機構を解析した。

20 Gy の放射線照射直後のマクロファージ系細胞から核蛋白質を分離し、独自に単離したマウス IL-1β遺伝子周囲のゲノム領域との特異結合を分析した。その結果、IL-1β遺伝子の遠上流に相当する三ケ所の部位に対して特異結合する核蛋白質が、放射線照射 30 分後に消失していた (Fig. 3)。

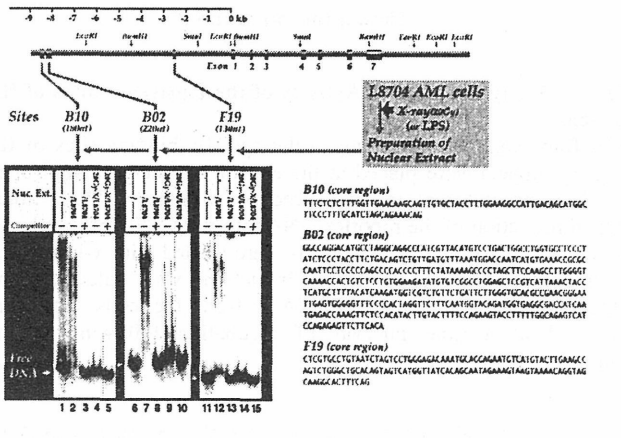

Fig. 3. Specific Binding of Nuclear Protein to Upstream Sites of IL-1β Gene

Three specific binding sites (B10, B02 and F19) in the upstream region of IL-1β gene (upper left) were found by electrophoretic mobility-shift assay. The labeled fragments (lanes 1, 6, 11) were bound to the nuclear proteins from non-irradiated macrophage-like cell line L8704 (lanes 2, 7, 12). The binding was prevented in the presence of non-labeled DNAs as competitors (lanes 3, 8, 13). The binding activity also disappeared when nuclear extract from the irradiated cells was used (lane 3, 9, 14).

この特異結合部位の位置は従来報告されてきた遺伝子発現調節部位と異なり、コード領域から著しく離れた部位に相当しており、既知の調節モチーフ配列は見出されなかったことから、独自の調節機構の存在が示唆された。そのうち一ケ所（Fig. 3、B02 部位）は、内在レトロウイルス GLN の LTR に相当し、その内部には p53 特異結合配列が存在していた。致死線量照射により、p53 媒介アポトーシスの発生することが知られているが、20 Gy の線量はマクロファージ様細胞では非致死線量に相当する。この状態で p53 が関与したとすると、アポトーシス経路とは異なる伝達経路の活性化している可能性がある。

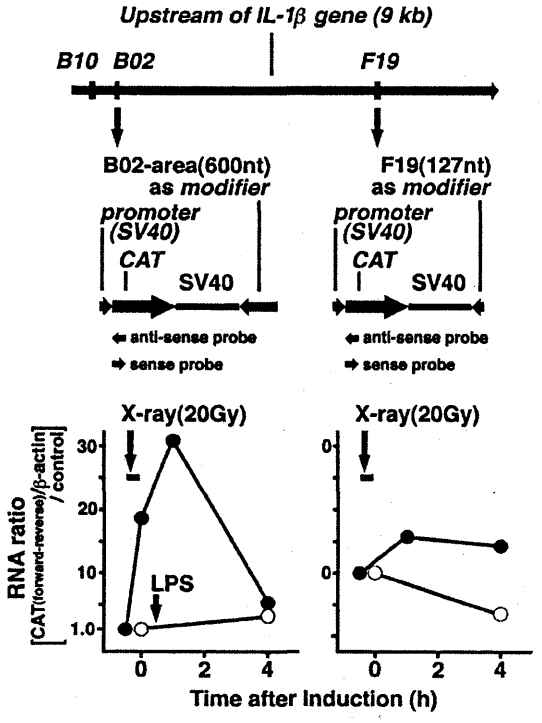

Fig. 4. X-ray Responsive Activity of the Upstream Sites of IL-1β Gene
DNA fragments corresponding to the specific binding sites of IL-1β gene (upper) were placed at the end of the cat gene controlled by SV40 promoter at reverse direction (middle). Three hours after introduction of the reporter DNA into the L8704 macrophage-like cells by liposome method, cells were treated with x-irradiation or lipopolysaccharide (LPS). Induction was calculated by measurement of the reporter RNA s from the cells that were harvested at a time interval of incubation following to the induction (lower).

これらの核蛋白質に特異結合する塩基配列の生体内における機能を調べるために、前記のレポーターRNA アッセイを行った（Fig. 4）。その結果 B10 部位には応答性が認められなかったが、B02 および F19 部位に X 線照射に対して一過性の応答性が認められた。B02 部位の応答性は F19 部位よりも強力であったが、両者ともに LPS による応答性は検出されず、X 線への特異性が示された。

以上の結果から、IL-1β遺伝子の遠上流に位置する B02 および F19 部位に対して特異結合する核蛋白質が電離放射線照射直後のマクロファージ様細胞において消失し、周囲のプロモーターからの遺伝子転写を促進することが示唆された。IL-1βは炎症蛋白質としてリンパ球や骨髄球などの分化を促進すると同時に致死線量放射線被曝マウスの生存率を増加させる放射線防護作用のあることが知られており、その遺伝子上流からの核蛋白解離ならびに転写レベルでの発現促進は、X 線に対する生体のストレス応答機構の一環であることが考えられる。

3．マウス細胞における *fos/jun* 族遺伝子の発現制御

前述の IL-1β遺伝子と同様に、*fos/jun* 族プロトオンコジーンの RNA が放射線照射直後に増加することが報告されている。これらの遺伝子産物はロイシンジッパー蛋白をコードしており、ヘテロダイマーを形成することで遺伝子の転写を調節する。このことから、*fos/jun* 族遺伝子発現に引き続いて活性化する遺伝子群の産物が放射線防護または損傷修復に寄与することが予想されている。しかし、*fos/jun* 族遺伝子はその産物の機能的な差異が明らかではなく、これらの発現のプロフィールは細胞の種類ならびに照射条件により著しく異なる。我々は放射線・活性酸素刺激後における各種 *fos/jun* 族遺伝子の発現を検討し、多くのマウス細胞では *jun*B 遺伝子の発現が増強することを明らかにした（Fig. 5）。

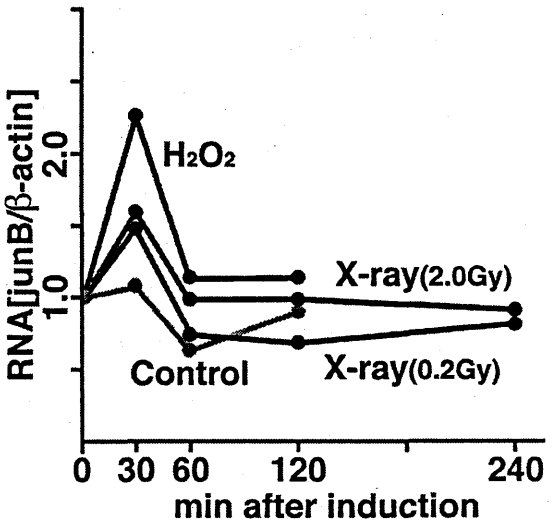

Fig. 5. Induction of junB Gene after Low Dose X-irradiation
Primary culture of murine spleen cells were treated with x-irradiation at low-dose or hydroperoxide. Cells were harvested after indicated times of incubation. RNA levels of *jun*B and β-actin were measured by quantitative northern hybridization.

0.2 Gy 程度の低線量 X 線および低濃度の過酸化水素を処理した細胞において *jun*B RNA の一過性発現が観察された。また、nuclear run-on アッセイならびに転写阻

害剤の作用分析から、これらの発現は IL-1βと同様に転写レベルで調節を受けていることが判明した。

*jun*B 遺伝子周辺の放射線・活性酸素応答に寄与する部位を検索するために、*jun*B 遺伝子上流を *cat* 遺伝子に連結してレポーターRNA アッセイを行った(Fig. 6)。その結果、*jun*B 遺伝子の 600-900 塩基上流に初期発現応答に寄与する機能のあることが判明した。これまで血清やキナーゼによる *fos/jun* 族遺伝子の発現増強に上流 500 塩基以下の配列が寄与することが報告されてきたが、IL-1β遺伝子の場合と同様に放射線・活性酸素独自の調節経路のあることが示唆された。一方、照射後 3 時間後には 250-600 塩基および 900-1500 塩基上流の配列による転写が増加した。照射 3 時間後には細胞に内在する遺伝子産物が増加する段階であることから、二次的発現にこれらの配列が寄与するものと考えられた。

*jun*B 遺伝子上流で見出された放射線・活性酸素に対する初期応答の標的配列にも既知物質に対する誘導性モチーフないし IL-1β遺伝子上流のモチーフとの類似性は認められなかった。放射線・活性酸素による刺激の標的塩基配列の特徴は、既知のキナーゼ活性化因子や様々な誘導物質に応答するモチーフ類に比べると、第一に配列類似性が乏しく、第二にその位置が遺伝子の遠上流に位置し、第三に標的配列の範囲が広く結合も弱いという特徴のあることが明らかになった。

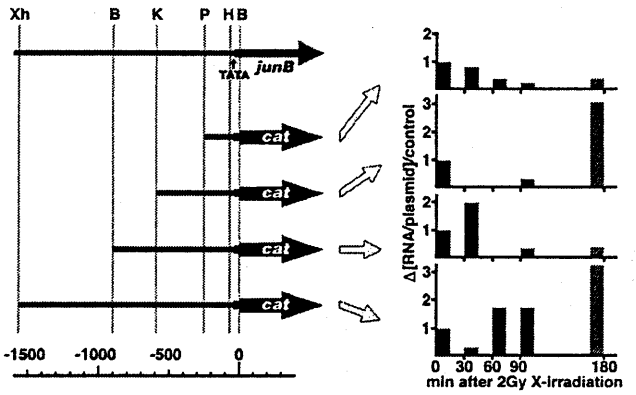

Fig. 6. Analysis of the Immediate-early Inducible Function in the Upstream Region of *jun*B Gene
Series of DNA fragments that correspond to an upstream region of *jun*B gene (upper left) were bind to cat gene were constructed as reporter genes (left). After 2Gy of x-irradiation to the cells following introduction of reporter genes, the cells were collected at different time of intervals. Promoter activity is designated as relative levels of forward cat RNA measured by quantitative northern hybridization (right).

4. マウス細胞における内在レトロウイルスの発現制御とゲノム不安定性の関連

Intracisternal A-particle (IAP) DNA エレメントは、正常マウスゲノムに数千コピー散在する塩基配列であり、レトロウイルス cDNA がゲノムに組込まれた構造である LTR-*gag-pol-env*-LTR からなる配列である。レトロウイルスと異なり、env 遺伝子が欠損しているためにウイルス粒子が細胞外には放出されないが、マウス細胞内には多数のレトロウイルス類似の構造体が存在している。ある種のマウス細胞では IAP RNA が発現し、レトロウイルスに酷似した分子機構によって IAP cDNA 合成とゲノムの新たな部位への組込みが発生する。その組込み部位の周囲に遺伝子があれば、機能異常を引き起こす。このレトロトランスポジションの発生頻度は著しく低いものの、マウス生殖細胞系列で発生した IAP cDNA 組込みが世代を重ねることで、現在の数千コピーまで増加したものと考えられている。

C3H 近交系マウスは電離放射線障害により骨髄性白血病が発生するという特徴があり、放射線発癌モデルとして使用されてきた。我々は骨髄性白血病細胞のゲノム解析の結果、放射線の初期障害から白血病発生に至る過程において、上記の IAP DNA エレメントの媒介するゲノム異常が頻発することを明らかにした。放射線による造血系組織障害から白血病発生までには多数の過程の蓄積することが予測されているが、その少なくとも一部に IAP の媒介するゲノム構造機能の不安定化という事象も寄与することが示された。

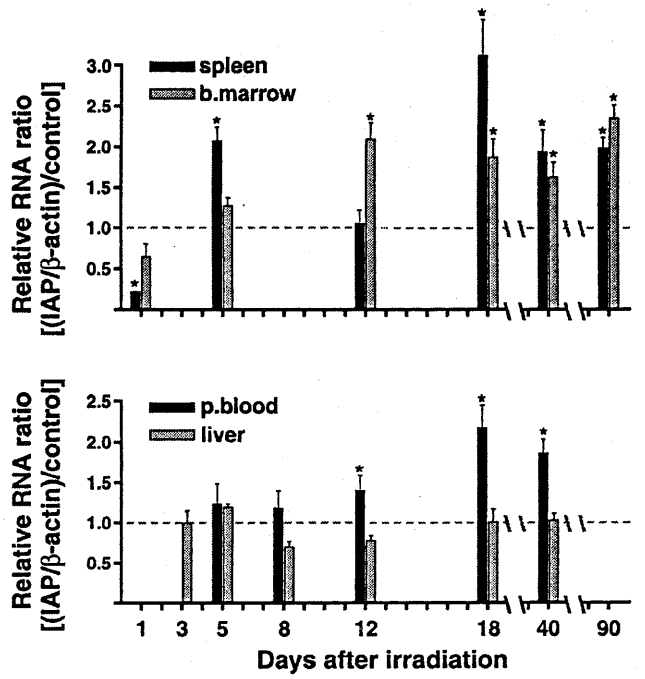

Fig. 7. IAP Expression during Hematopoietic Regeneration after X-irradiation
Spleen, bone marrow, liver and blood were isolated on the days indicated after irradiation. For each period, 3 mice were used and the samples were analyzed separately. The RNA ratio of IAP/β-actin calculated after quantitative Northern hybridization was divided by that of non-irradiated cells. The obtained relative RNA ratio in spleen, bone marrow, peripheral blood and liver are shown. Mean and standard deviation values for the relative RNA ratio of IAP/β-actin among the 3 mice at each point are shown. Asterisks indicate data at $p<0.05$ versus control by t-test.

この IAP 媒介レトロトランスポジションの第一段階は IAP RNA の生産である。電離放射線照射直後における IAP RNA 変動の有無を分析した。その結果、骨髄性白血病を頻発する C3H マウスの骨髄細胞に IAP RNA が高レベルに蓄積していること、更に電離放射線照射障害後に再生した骨髄細胞において、IAP RNA の発現が更に増加した状態が長期間維持されることを見出した(Fig. 7)。IAP RNA 増加は IAP 媒介レトロトランスポジションの発生頻度を亢進することが予想されることから、放射線照射後に再生した骨髄細胞集団並びに骨髄性白血病細胞で観察されてきた染色体構造の不安定化および遺伝的不安定性という従来の知見に対する分子生物学的証拠のひとつであると考えられる。

5．細胞膜への活性酸素の作用とその制御

放射線により発生する活性酸素・フリーラジカルの作用点として細胞膜が考えられる。活性酸素・フリーラジカルが細胞膜に作用すると、イオン透過性の変化を通じて細胞内情報伝達系が変動し、最終的に生体制御物質の発現に影響を与える可能性がある。そこで、細胞レベルでのイオン透過性の変化を細胞内カルシウム濃度の変動として、また、膜レベルでの変化を脂質のイオンバリアー能と膜イオンチャネル活性の変化として調べた。

白血病細胞株 HL60 とその過酸化水素耐性変異株 HP100 の細胞内カルシウム濃度を蛍光色素 Fura-2 を用いて測定した。ATP や過酸化水素で刺激した時、一過的な細胞内カルシウム濃度の変化が観測され、この変化は HL60 と HP100 とで異なることを見いだした。差異の原因として、ATP 刺激に対しては、細胞膜のアデノシン受容体の活性の違いが、また過酸化水素刺激に対しては細胞のカタラーゼ活性の違いが大きく寄与していることがわかった。

心筋小胞体膜のイオン透過性に対する活性酸素の影響を脂質平面膜法（微小膜電流測定法）を用いて調べた。ヒドロキシルラジカルは、脂質のみからなる膜のイオン透過性は上昇させなかったが、精製カルシウム遊離チャンネル（リアノジン受容体）を組込んだ膜のチャンネルの開口確率を上昇させた（Fig. 8）。この系では精製チャンネルを用いているので、活性酸素の作用点はチャンネル蛋白質自身にあると結論された。この結果は、心筋細胞障害メカニズムの一つとして活性酸素による細胞内カルシウム貯蔵部位の障害を示唆しており、治療分野への応用の基礎として重要である。

このような膜における活性酸素の障害を防御する化合物として、ビタミンEとビタミンCを結合した EPC-K1 を検討した。EPC-K1 は、細胞傷害性の高いヒドロキシルラジカルを防御する活性が高いことを見出した。この活性の機構として、溶液中の鉄イオンのキレーティングと生じたヒドロキシラジカルのスカベンジングの両面があることを明らかにした。

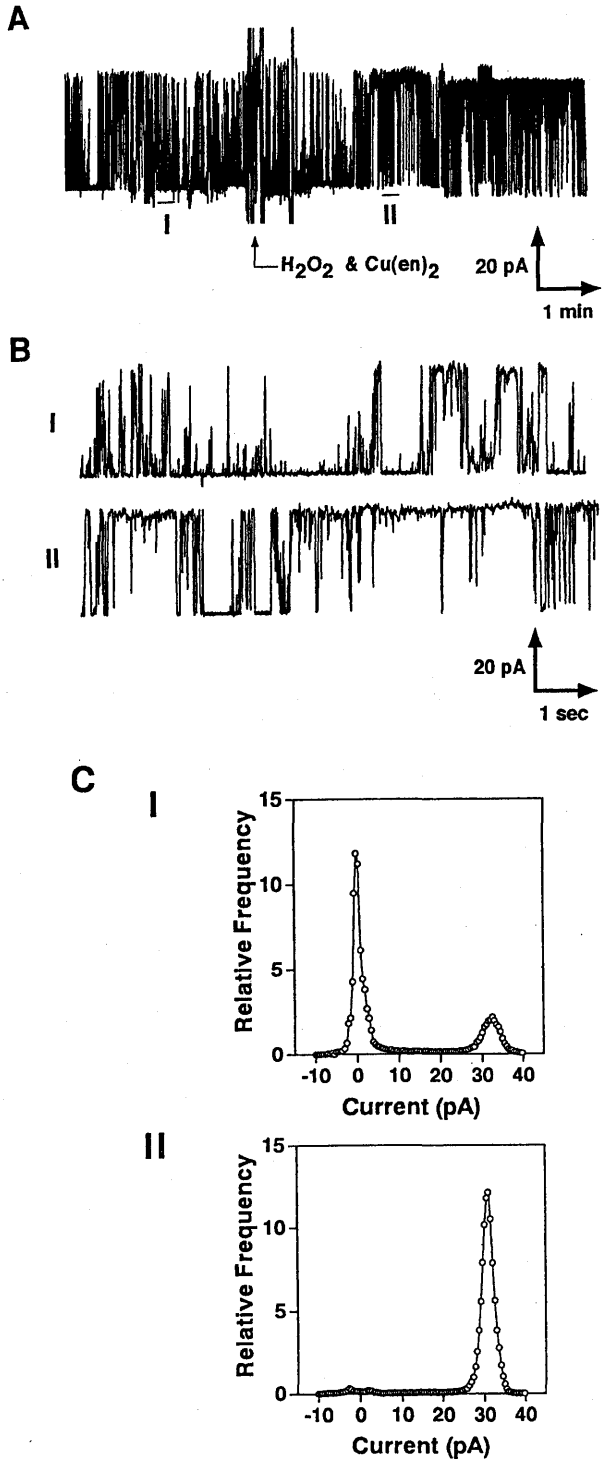

Fig. 8. Effect of hydroxyl radical on the open probability of the ryanodine receptor channel incorporated into planar bilayer
(A) 10 mM H_2O_2 and 0.1 mM $Cu(en)_2$ were added to the cis compartment of the chamber at the arrow. (B) The expanded trace of parts I (upper) and II (lower) of trace A. (C) The amplitude histograms corresponding to part I (before the application of the hydroxyl radical) and part II (after the application of the hydroxyl radical) of trace A.

6．放射線防護物質の作用機序の研究

我々はこれまでに、致死線量の放射線を照射したマウスに乳酸菌 *Lactobacillus casei* の菌体成分（LC9018）および M-CSF を投与することにより、放射線による致死率が軽減することを見出してきた。ここでは、これらの物質投与による放射線初期反応の関連を解析した。乳酸菌菌体成分投与および M-CSF をアルゼット浸透圧ポンプ埋植による連続投与のいずれにおいても、照射後 13 日目において白血球数が回復することをフローサイトメトリー分析により明らかにした（Fig. 9）。また、乳酸菌成分投与による致死率軽減効果は抗炎症剤により無効になり、これは特異的だった。このことから、炎症作用からリンパ球分化促進に至る骨髄細胞集団の変動が放射線障害の軽減に寄与することが示唆された。

この回復期造血系の修飾により、乳酸菌加熱製剤投与時に酷似した結果が得られたことから、両者の放射線防護作用における関連が示された。グラム陽性菌および M-CSF 投与によるマクロファージの活性化は IL-1β機能を介して初期炎症を誘発することから、放射線防護物質の作用と IL-1β発現調節系の変動の相関のあることが示唆された。

一方で、乳酸菌成分とは異なる機構による放射線防護作用を有する化合物の検索を行った。抗酸化活性を有する化合物から検索した結果、新たに、安定スピンプローブである methoxy-carbonyl-PROXYL(MC-PROXYL) やスピントラップ剤である PBN、POBN に放射線防護効果があることを見出した。乳酸菌菌体成分と MC-PROXYL との併用投与の実験から、両者の放射線防護作用の機構は異なることが確認された。

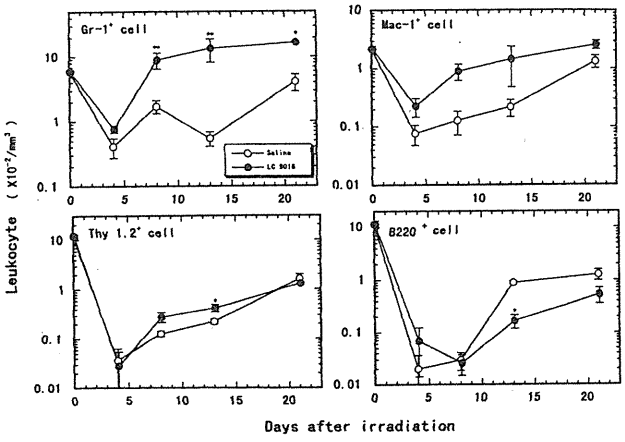

Fig. 9. Time Coarse of Cell Populations of Leukocytes in 6.0 Gy Irradiated Mouse Blood Measured by Flow Cytometry
Open circles (○) and closed circles (●) represent the data of saline treated- and LC-9018 treated-mouse blood, respectively. Asterisks indicate significant differences from saline treatment; $p < 0.01$ (**), $p < 0.05$ (*).

III．結論

本研究に着手する時点で、我々は、放射線防護作用を持つサイトカインである Interluekin-1β（IL-1β）蛋白質をコードする遺伝子発現が放射線照射により転写レベルで活性化することを見出していた。本研究ではその成果を土台として、放射線・活性酸素による遺伝子発現調節機構の解析を進めた。そして、放射線照射直後に発生する事象を解析するための分子生物学的ならびに細胞生物学的技術を開発し、当該技術を利用して放射線照射直後に発性する IL-1β遺伝子発現調節を解析した。さらに、低線量放射線・低濃度活性酸素刺激により活性化する *fos/jun* 族転写調節蛋白質遺伝子並びにその調節機構を明らかにした。この一連の研究の結果、両遺伝子コード配列の上流に位置して放射線・活性酸素による応答に関与する領域の塩基配列を明らかにすることができた。

放射線により発生する活性酸素・フリーラジカルは細胞膜に作用して障害を与える。本研究では、カルシウム貯蔵器官の膜に存在するカルシウムチャネルに対する活性酸素の影響を分子レベルで調べた。その結果、心筋細胞においては、活性酸素のうちのヒドロキシルラジカルが細胞内小器官である小胞体の膜に作用してカルシウムチャネルの活性を上昇させ、それにより細胞内カルシウム濃度の増加が惹起されることが明らかとなった。細胞内カルシウム濃度は、種々の細胞内生化学反応を制御していることが知られており、この増加により、それに引き続く一連の細胞内応答機構が働くものと予想される。

一方、マウスに対する非致死線量放射線の照射により、骨髄細胞のゲノムが不安定化して骨髄性白血病の発生することが知られている。この事象を解析するために、内在性レトロウイルスを指標として、ゲノム不安定性を誘発する遺伝子制御機構の解析を行った。その結果、骨髄性白血病を頻発する C3H マウスの骨髄細胞にレトロウィルスのひとつである IAP の RNA が高レベルに蓄積していること、また、放射線障害後に再生した骨髄細胞においても IAP の RNA が高レベルに維持されていることを明らかにした。

マウス個体を用いた放射線防護作用の研究により、炎症誘発物質である細菌菌体成分とマクロファージ-コロニー刺激因子（M-CSF）の造血系における効果が強い連関を持つことを明らかにした。また、新たなタイプの放射線防護化合物を見出すことができた。

本研究により、放射線・活性酸素刺激直後の生体の遺伝子転写調節という初期反応が明らかになり、その後に引き続いて発生する多種多様な信号伝達系ならびに骨髄細胞集団の変動およびその修飾を解析するための知見が得られた。

Ⅳ. 研究発表

1. Tanaka, I. and Ishihara, H.: Unusual long target duplication by insertion of intracisternal A-particle element in radiation-induced acute myeloid leukemia in mice. *FEBS Lett.*, **376**, 146-150, 1995.
2. Ishihara, H., Tanaka, I., Nemoto, K., Tsuneoka, K., Cheeramakara, C., Yoshida, K., and Ohtsu, H.: Immediate early transient induction of the interleukin-1β gene in mouse spleen macrophages by ionizing radiation. *J. Radiat. Res.*, **36**, 112-124, 1995.
3. Nemoto, K., Ishihara, H., Tanaka, I., Suzuki, G., Tsuneoka, K., Yoshida, K., and Ohtsu, H.: Expression of IL-1β mRNA in mice after whole body x-irradiation. *J. Radiat. Res.*, **36**, 125-133, 1995.
4. Furuse, M., Tsuneoka, K., Uchida, K., and Nomoto, K.: Acceleration of granulocytic cell recovery in irradiated mice by a single subcutaneous injection of a heat-killed Lactobacillus casei preparation. *J. Radiat. Res.*, **38**, 111-120, 1997.
5. Ishihara, H. and Tanaka, I.: Detection and cloning of unique integration sites of retrotransposon, intracisternal A-particle element in the genome of acute myeloid leukemia cells in mice. *FEBS Lett.*, **418**, 205-209, 1997.
6. Anzai, K., Ogawa, K., Kuniyasu, A., Ozawa, T., Yamamoto, H., and Nakayama, H.: Effects of hydroxyl radical and sulfhydryl reagents on the open probability of the purified cardiac ryanodine receptor channel incorporated into planar lipid bilayers. *Biochem. Biophys. Res. Commun.*, **249**, 938-942, 1998.
7. Anzai, K., Miura, Y., Ueda, J., Ozawa, T., Noda, Y., Mori, A., and Packer, L.: In vitro studies of the antioxidant activity of EPC-K1, a conjugate of vitamin C and vitamin E. *Res. Commun. Biochem. Cell & Mol. Biol.*, **2**, 129-138, 1998.
8. Lee, D., Anzai, K., Hirashima, N., and Kirino, Y.: Phospholipid translocation from the outer to the inner leaflet of synaptic vesicle membranes isolated from the electric organ of Japanese electric ray *Narke japonica*. *J. Biochem.*, **124**, 798-803, 1998.
9. Ando, S., Nojima, K., Majima, H., Ishihara, H., Suzuki, M., Furusawa, Y., Yamaguchi, H., Koike, S., Ando, K., Yamauchi M., and Kuriyama, T.: Evidence for mRNA expression of vascular endothelial growth factor by X-ray irradiation in a lung squamous carcinoma cell line. *Cancer Letters*, **132**, 75-80, 1998.
10. Ueda, J., Anzai, K., Miura, Y., and Ozawa, T.: Oxidation of linoleic acid by copper(II) complexes: Effects of ligand. *J. Inorg. Biochem.*, **76**, 55-62, 1999.
11. Anzai, K., Ogawa, K., Goto, Y., Senzaki, Y., Ozawa, T., and Yamamoto, H.: Oxidation-dependent changes in the stability and permeability of lipid bilayers. *Antioxidants & Redox Signaling*, **1**, 339-347, 1999.
12. Ishihara, H., Tanaka, I., Furuse, M., and Tsuneoka, K.. Increased expression of intracisternal A-particle RNA in regenerated myeloid cells after x-irradiation in C3H/HeMs inbred mice. *Radiat. Res.*, **153**, 392-397, 2000.
13. Anzai, K., Ogawa, K., Ozawa, T., and Yamamoto, H.: Oxidative modification of ion channel activity of ryanodine receptor. *Antioxidants & Redox Signaling*, **2**, 35-40, 2000.
14. Miura, Y., Anzai, K., Ueda, J., and Ozawa, T.: Novel approach to in vivo screening for radioprotective activity in whole mice: In vivo electron spin resonance study probing the redox reaction of nitroxyl. *J. Radiat. Res.*, **41**, 103-111, 2000.
15. Ando, S., Nojima, K., Ishihara, H., Suzuki, M., Ando, M., Majima, H., Ando, K., and Kuriyama, T.: Induction by carbon-ion irradiation of the expression of vascular endothelial growth factor in lung carcinoma cells. *Int. J. Radiat. Biol.*, **76**, 1121-1127, 2000.

細胞機能調節に関する研究

稲野宏志、鈴木桂子、小野田眞（第３サブグループ）

Regulation of Cellular Function

Hiroshi Inano, Keiko Suzuki and Makoto Onoda

Radiation is being used increasingly for medical and occupational reasons and is a cause of mammary tumors, leukemia and other tumors in both humans and experimental animal models. Epidemiological observations of atomic-bomb survivors have shown that women of reproductive age exposed to radiation developed mammary cancer in life. Radiation-induced tumorigenesis in mammary glands is considered to be influenced by the developmental stage of the glands at exposure. During pregnancy in rats, the concentrations of estradiol and progesterone in serum increase gradually, but the prolactin level remains low. During lactation, the serum prolactin level is increased, but the estradiol level remains low. On the other hand, reactive oxygen species and other free radicals, which generated excessively in cell body under diverse environmental conditions, are also considered as risk factors in the carcinogenic process and tumor progression. In this project, to clarify the effect of radiation on the induction of mammary tumors, we studied the effects of hormones and nitric oxide, a unique gaseous radical on the initiation of mammary tumorigenesis by radiation and on the promotion of tumorigenesis from primordial cells initiated with radiation. Also, since the prevention of radiation-induced tumors is a matter of interest in modern human life styles that depend upon atomic energy, we focused on recent concepts in the prevention of mammary tumorigenesis induced by radiation. In addition, we propose appropriate strategies for future clinical chemoprevention trials of radiation-induced tumors.

I. 緒　　言

性質の異なる多種類の細胞群で構成されている臓器（器官）は細胞間に複雑な調節機構が存在している。特に雌性動物の乳腺組織は思春期発来、性周期、妊娠、出産、授乳、閉経等の生理的変化に伴ってホルモンが変動して分化、増殖、退縮等が顕著におこる特徴を有しており、これらの組織学的変化は乳腺細胞の放射線に対する感受性にも影響を及ぼすことが考えられている。一方、長い期間炎症が続くことは発癌リスクの要因の一つであり、また炎症性メディエーターの一酸化窒素ラジカル（NO）を合成する酵素が乳腺腫瘍に存在していることなどから、過剰の NO 産生と発癌との関連性が指摘されている。本研究課題では放射線による乳腺細胞の腫瘍化イニシエーションと卵巣ホルモン、下垂体ホルモンやNOなどのフリーラジカルとの関係、および放射線でイニシエートされた乳腺細胞が異常に増殖して腫瘍（癌）化する機序を解明すると共に、乳腺に作用する卵巣ホルモン、例えばエストラジオールの生合成時に起こる酸化的ストレスが生体に与える影響についても分子生物学的観点から明らかにすることを試みた。本課題の最終目標は、放射線に被曝した乳腺の晩発障害の一つである腫瘍（癌）化を抑制する低毒性化合物を天然物や化学合成品から探索して発癌の予防に寄与することである。

II. 経　　過

平成７年度から５年間のグループ研究を開始するにあたって、以下のような研究計画を立てて内分泌関連細胞、特に乳腺細胞に対する放射線の影響の解明およびその低減化を目的に総合的な研究に着手した。すなわち、

(i) ラジカル消去化合物による放射線誘発乳腺腫瘍の抑制、およびラジカル消去作用をもつ低毒性天然物による腫瘍発生の予防

(ii) 内分泌器官に対する生体調節因子の作用および調節因子に応答した細胞で誘導される遺伝子の解析

(iii) 一酸化窒素合成酵素の細胞内局在性と挙動、および内分泌器官の発達や分化と一酸化窒素生成系の相関

の三本柱で研究遂行中、研究期間が１年間延長されて６年間に及んだグループ研究を平成１２年度に終了した。この間研究を効率的に行うため平成７年度に蛍光顕微鏡、

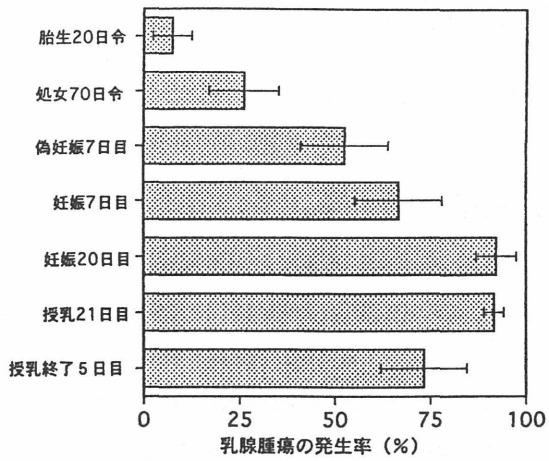

Figure 1, Induction of mammary tumors by irradiation with gamma-rays at various stages

平成８年度に mRNA 解析装置、平成１０年度に PCR サーマルサイクラー、平成１１年度にクリオスタット等の機器を購入して、以下に述べるような成果をあげる事ができた。

III. 成果・考察

1, 放射線発癌とホルモンの関係

放射線被曝によって発生する乳腺腫瘍を予防する研究の開始前に、乳腺の特性であるホルモン作用による組織発達や機能分化と放射線感受性の相関を解明して、研究の基礎データとした。

(a) 雌性生殖サイクルと乳腺の放射線感受性[(1,2)]：生殖サイクルによる内分泌学的環境の変化が乳腺の放射線感受性に与える影響を明らかにするため、胎生２０日令、処女７０日令、偽妊娠７日目、妊娠７日目、妊娠２０日目、授乳２１日目、授乳終了５日目のウィスター--MS 系ラットに ^{60}Co のガンマー線を全身照射し、その後一ヶ月を経てから、プロモーターとしてジエチルスチルベストロール（DES）を投与して乳線腫瘍の発生を１年間観察した。乳線腫瘍（腺腫と腺癌）の発生率は、2.6Gy(0.1-0.15Gy/min)を照射した時、胎生期被曝では 7.4% (2 匹／27 匹)、処女期被曝では 26.1% (6 匹／23 匹)、偽妊娠時被曝では 52.6%(10 匹／19 匹)、妊娠 7 日目の被曝では 66.7%(12 匹／18 匹)、妊娠末期被曝では 92.3%(24 匹／26 匹)、授乳期被曝では 91.7%(22 匹／24 匹)、授乳終了後被曝では 73.3%(11 匹／15 匹)であった (Fig. 1)。妊娠末期や授乳中の発達している乳腺は放射線に対する感受性が非常に高く、この時期に放射線に被曝すると高率に乳腺に腫瘍が発生したことから、乳腺の発達や分化に関与しているホルモンが放射線感受性を変化させている重要な因子である可能性が示唆された (Fig. 2)。しかし、妊娠期に乳腺を発達させる主なホルモンは卵巣から分泌されているエストラジオールとプロゲステロンで、脳下垂体から分泌されているプロラクチンは関与していない。一方、授乳期乳腺に作用して乳汁生成などの機能分化を促進しているホルモンは主にプロラク

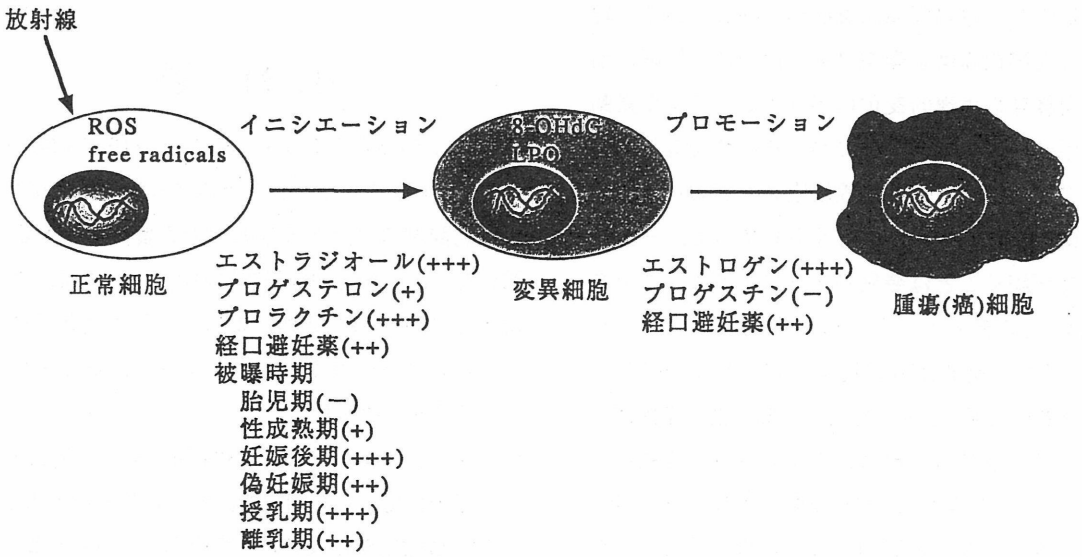

Figure 2, Modification of radiation-induced initiation and estrogen-induced promotion for mammary tumorigenesis

チンで卵巣ホルモンは関与せず、妊娠期と授乳期では乳腺に作用するホルモン環境が全く異なっているにもかかわらず、乳腺腫瘍の発生率はほぼ同値を示した。妊娠中や授乳中に 0.1-1.5Gy を照射したラットの乳腺の腺腫と腺癌の発生率を比較すると、明らかに授乳中に被曝したラットの方が悪性腫瘍(腺癌)の発生率が高く統計学的にも有意だった。ヒトでは、胎児に対する影響から放射線事故以外では妊娠中の母親の乳腺が被曝することは殆どないが、しかし授乳中の母親の医療被曝については十分な注意が払われていないのが現状である。我々のラットを用いた研究結果から、授乳中の乳腺は放射線に対する感受性が非常に高く放射線被曝により将来悪性腫瘍や良性腫瘍の乳腺腫瘍が発生する可能性が大きいことが示されたことから、ヒトの場合、授乳中に放射線を用いた診断や治療を行う時は慎重な対応が望まれる。

(b) 乳腺の放射線感受性に対するホルモンの影響[3-5]： 乳腺の発達や分化には卵巣ホルモン、脳下垂体ホルモン、副腎皮質ホルモン以外に甲状腺ホルモンやインスリン等の多くのホルモンが関与している。妊娠中は分娩後の乳仔への授乳に備えて、主にエストラジオールとプロゲステロンの作用で乳腺組織が増殖して発達し、出産後は乳腺に作用するホルモン環境が妊娠中と全く変わり主にプロラクチンの作用で乳汁の生合成を開始する。これらのホルモンの作用で発達、分化した乳腺組織の放射線に対する感受性を直接解明するため、性周期が発来する以前の 23 日令のラットおよび性成熟した 84 日令のラットの両側卵巣を摘除した。卵巣摘除した未成熟ラットが 74 日令に成熟した時、ガンマー線(2.6Gy)を照射、1 ヶ月後からプロモーターとして DES を投与して乳腺腫瘍の発生を観察した。その結果、乳腺腫瘍の発生率は 26.1% (6 匹／23 匹)だった (Table 1)。この値は成熟時に卵巣を摘除したラットに照射した場合の乳腺腫瘍の発生率(30%、9 匹／30 匹)と差がなかった。未成熟時または成熟時の卵巣摘除により照射時の乳腺組織は細い乳管の伸長が観察されたが、これは甲状腺ホルモンやインスリン等の作用によるもので性ホルモン非依存性の発達と考えられている。この未成熟時に卵巣を摘除したラットが 60 日令になった時、エストラジオール-3-ベンゾエートやプロゲステロンをそれぞれ 2 週間単独投与または併用投与後ガンマー線(2.6Gy)照射をして同様に観察をすると、エストラジオール-3-ベンゾエートを投与したラットの乳腺腫瘍の発生率は 57.1% (12 匹／21 匹)、プロゲステロンを投与したラットは 32.0%(8 匹／25 匹)、 併用投与したラットは 39.1%(9 匹／23 匹)であった。一方、成熟時に卵巣を摘除して 2 週間同様にホルモンを投与した後照射した場合は、エストラジオール-3-ベンゾエートを投与したラットの乳腺腫瘍の発生率は 90.5%(19 匹／21 匹)、プロゲステロンを投与したラットも 90.5%(19 匹／21 匹)、併用投与したラットでは 40.0%(8 匹／20 匹)であった。成熟時に卵巣を摘除したラットの方が放射線による乳腺腫瘍の発生率が高いのは、卵巣摘除前にすでに卵巣から分泌されたエストラジオールやプロゲステロンが乳腺に作用して乳腺幹細胞を分化させたためであると考えられる。また、成熟時に卵巣を摘除した実験で、エストラジオール-3-ベンゾエートの照射前投与とプロゲステロンの前投与により乳腺腫瘍の発生率が同値を示したが、発生した全腫瘍に対する腺癌の割合はエストラジオール-3-ベンゾエート投与群が 59.0%、 プロゲステロン投与群が 29.3%、 併用投与群が 11.8%で、エストロゲンの乳腺に対する直接作用または間接作用より発達、分化した組織は放射線被曝により悪性腫瘍の発生頻度が高くなる傾向を示した。エストロゲンの乳腺に対する間接作用とは、エストロゲンが脳下垂体に作用してプロラクチンの分泌を促進して、プロラクチンが乳腺組織を発達させる経路である。したがって、エストラジオール-3-ベンゾエート投与ラットの乳腺が放射線被曝により癌の発生が高かったのはエストロゲンとプロラクチンの相乗作用の結果であると考えられる。

次に、プロラクチン単独で分化した乳腺の放射線感受性を検討するため、性周期発来前のラットの卵巣を摘除し、成熟後、他のラットの脳下垂体を腎臓の皮膜下に移植することにより、ラットのホルモン環境を高プロラクチン／低性ホルモン状態にしてガンマー線(2.6Gy)を全身照射して同様に実験に供した。卵巣を摘除して脳下垂体を移植しない対照群の乳腺腫瘍の発生率は 21.6%(8 匹／37 匹)であったが、脳下垂体を移植して高プロラクチ

Table 1, Mammary tumorigenesis in irradiated rats treated with estradiol (E2B) and/or progesterone

Treatment	No. of rats used	No. of rats with tumors		No. of tumors[b]		No. of tumors per tumors-bearing rat
		No.	%	AC	FA	
Ovariectomy at immature						
Olive oil	23	6	(26.1)	1	5	1.0 ± 0.0
E2B	21	12	(57.1)	4	14	1.6 ± 0.1
Progesterone	25	8	(32.0)	2	9	1.3 ± 0.3
E2B + Progesterone	23	9	(39.1)	3	7	1.3 ± 0.2
Ovariectomy at mature						
Olive oil	30	9	(30.0)	7	10	1.9 ± 0.4
E2B	21	19	(90.5)	23	16	2.4 ± 0.3
Progesterone	21	19	(90.5)	12	29	2.3 ± 0.2
E2B + Progesterone	20	8	(40.0)	2	15	1.7 ± 0.3

a, All rats were treated with DES, as a tumor promoter, for 1 year after irradiation.
b, AC, adenocarcinoma; FA, fibroadenoma.

ン状態にして照射をすると、腫瘍の発生率が 77.8% (14匹／18 匹、$P < 0.0001$)に上昇した。また、悪性腫瘍である腺癌の発生率も対照群の 5.4% から下垂体移植により 50% ($P < 0.05$)に増加したことから、プロラクチンが乳腺の放射線感受性を上昇させていることが判明した。

(c) 乳腺に対する医薬品と放射線の複合影響[6,7] **：** 生体に対する 放射線単独の影響については多くの研究が行われてデータが蓄積されてきているが、放射線と医薬品や環境ホルモン等の他因子との複合影響については未知の事が多く、今後重要性が増すと考えられている。特に長い期間連続服用する医薬品による放射線影響の修飾については全く研究が行われていないのが現状である。わが国では平成１１年に経口避妊薬(ピル) が認可されたが、ピルは排卵を抑制する作用以外に乳腺や子宮の細胞にも作用して増殖させる作用がある。ピルの服用中に疾病の診断や治療等のため放射線を被曝することは容易に予測されることである。また、日本ではピルが正式に承認される前は治療用の高用量ホルモン剤を経口避妊薬として転用していた経緯があることから、本研究ではピルとして承認されている低用量ホルモン剤と高用量ホルモン剤を用いて、乳腺の放射線感受性におよぼす影響を検討した。

放射線に被曝する 1 ヶ月前から低用量の 17α -エチニルエストラジオール (EE_2)と 19-ノルエチステロン(NET)を性成熟した処女ラットに投与してガンマー線(2.6Gy)を全身照射し、その後もホルモン剤を１年間連続投与すると乳線腫瘍の発生率は33.3% (6匹／18匹)で、この値は非投与群(9 匹／27 匹)と同じであった (Table 2)。しかし、処女ラットに高用量の EE_2-NET 剤を照射する前後それぞれ１ヶ月間投与すると、１年間の乳腺腫瘍の発生率が 58.3% (14 匹／24 匹) になり、この値は非投与群の発生率(21.7%、5 匹／23 匹)の 2.8 倍である($P < 0.01$)。さらに、出産後授乳しているラットにガンマー線(2.6Gy)を照射して、１ヶ月後から低用量 EE_2-NET 剤を１年間投与すると、乳腺腫瘍の発生率が 90% (18 匹／20匹)にはね上がり、この値はピル非投与群の発生率(31.3%、10 匹／32 匹)の 3 倍である($P < 0.0001$)。このピル非投与群の放射線被曝ラットに発生した乳腺腫瘍(15 個)は全て良性の腺腫であったが、放射線被曝後に低用量ピルを１年間投与したラットには47個の乳腺腫瘍が発生して、そのなかの 27 個が悪性腫瘍の腺癌であった。

以上の結果から、高用量の EE_2-NET を含むピルは処女ラットの乳腺の放射線に対する感受性を増幅させて腫瘍の発生頻度を上昇させ、低用量 EE_2-NET ピルは授乳時に被曝した経産ラットの乳腺に発癌プロモーターとして作用して乳癌の発生を促進させることが明らかになった。

ピルによる血栓症等の副作用はその中の成分のエストロゲンに由来することから、エストロゲンを含まないピルの開発が行われ、クロロマジノンアセテート(CMA)が作られた。しかし、排卵抑制作用がエストロゲン含有ピルと比べると弱いためピルとしての製品化は断念し、前立腺肥大症の治療薬として用いられている。授乳終了時に内因性エストロゲンを排除するため両側卵巣を摘除したラットに、ガンマー線(2.6Gy)を全身照射し、1 ヶ月後から CMA の投与を開始して１年間続けても乳腺腫瘍の発生率(8.0%、2 匹／25 匹)は CMA 非投与の対照群の発生率(4.3%、1 匹／23 匹)と統計学的に差がなかった。

(d) 雄性乳腺の放射線感受性[8] **：** ヒトの場合、全乳癌患者の約 1%が男性で症例が少ないため男性の乳癌研究は殆ど行われていないのが現状である。特に精巣機能と放射線による雄性乳腺腫瘍(癌)の発生のイニシエーションについては未知のことが多いことから、ウィスター--MS、フィシャー--344、SD の３系統の雄ラットを用いて、精巣のアンドロゲン生合成酵素の活性と乳腺の放射線感受性の相関を検討した。 乳腺腫瘍の自然発生率は SD 系雄性ラットが 6.7% (1 匹／15 匹) を示し、他系統の雄性ラットは発生しなかった。性成熟した２ヶ月令の時、ガンマー線(2.6Gy)を全身照射して１年間観察すると、フィッシャー--344 系ラット(20 匹)は乳腺腫瘍を発生しないが、SD 系ラットの発生率は 9.5%(2 匹／21匹)、ウィスター--MS 系は 6.9%(2 匹／29 匹)を示した。さらに、2 ヶ月令の時、全身照射して 1 ヶ月後から、前記の雌性ラットの実験と同様に DES をプロモーターとして１年間投与して腫瘍の発生を観察すると、SD 系ラットが最も放射線感受性が高く発生率が 80.9%(17 匹／21 匹)を示し、以下ウィスター--MS 系が 35.0%(7 匹／20

Table 2, Radiation-induced mammary tumors in virgin and parous rats administered contraceptive steroids

Treatment[a]	No. of rats used	No. of rats with tumors No.	%	No. of tumors AC	FA	No. of tumors per tumor-bearing rat
Virgin rats						
Cholesterol	23	5	(21.7)	2	5	1.4 ± 0.2
EE2+ NET (high dose)	24	14	(58.3)	2	15	1.2 ± 0.1
Cholesterol	27	9	(33.3)	3	10	1.4 ± 0.2
EE2 + NET (low dose)	18	6	(33.3)	0	8	1.3 ± 0.2
Parous rats						
Cholesterol	32	10	(31.3)	0	15	1.5 ± 0.2
EE2 + NET (low dose)	20	18	(90.0)	27	20	2.6 ± 0.5

a, EE2,17α –ethinylestradiol; NET, norethisterone

匹)、フィッシャー-344 系が 9.4%(3 匹／32 匹)を示した。精巣の機能と放射線感受性を明らかにするため精巣内のアンドロゲン生合成に関与している酵素の活性を測定した結果、テストステロン生合成の律速反応を触媒しているΔ^5-3β-ヒドロキシステロイド脱水素酵素の活性が、SD 系ラットが最も高く、ウィスター-MS 系は SD 系の 1/3、フッシャー-344 系は約 1/5 で、乳腺腫瘍の発生率と正の相関を示した。血中のテストステロン濃度を測定すると、Δ^5-3β-ヒドロキシステロイド脱水素酵素の活性が高い SD 系ラットが最も高かった。テストステロンはエストロゲンの前駆体であるから SD 系ラットの血中エストロゲン値が高いため放射線に高感受性であることが予想された。しかし、雄性ラットの血中エストロゲン値をラジオイムノアッセー法で測定すると血中の脂質が測定に影響して正確な値を得る事ができなかったため、雄性ラットの乳腺の放射線感受性に対するエストロゲンの関与は不明であるが、精巣機能と関連していることは証明された。

2, 卵胞ホルモン生合成時の酸化的ストレス

卵巣でのエストロゲン等のホルモン生合成は脳下垂体から分泌される性腺刺激ホルモンによって調節されている。この調節機構および性腺刺激ホルモンによる卵巣内での酸化的ストレスを明らかにするため、モデル系としてラットを用いて以下の実験を行った。23 日令の未成熟ラットに PMSG（妊馬血清性腺刺激ホルモン）を投与して卵胞が発育後、hCG（ヒト胎盤性性腺刺激ホルモン）を注射すると一時的に（30 分以内に）エストロゲン生合成の前駆体のテストステロンが卵巣内に増加し、1 時間後にはテストステロンは hCG 投与前のレベルに戻った。一方、以前報告したようにテストステロン合成酵素の 1 つ lyase の活性は 3 時間後には hCG 投与前の 50%、さらに 6 時間後にはほぼ 0%になった。この機構を明らかにするため以下の実験を行った。この失活が lyase の活性中心にあるヘムを分解するヘムオキシゲネース(HO)-1 の発現が原因かどうかを検討するため、その発現量を PCR サーマルサイクラーと mRNA 解析装置を用いて検討したが、HO-1 mRNA の増加は hCG 投与後 3 時間まで観察されなかった。また、HO-1 阻害剤の Zinc protoporphyrin を hCG 投与の 1 時間後と 3 時間後に投与したが、lyase の活性低下を防ぐことはできなかった。以上の結果から、hCG による lyase の活性低下はヘムの分解が原因でないことが示された。

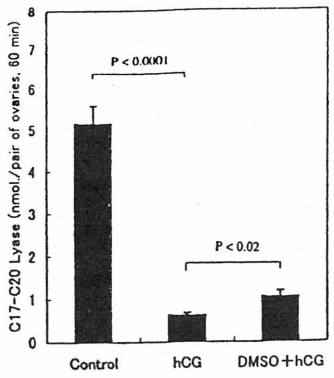

Figure 3, Effect of DMSO upon hCG-induced decrease of the lyase activity

次に、ステロイドホルモン産生臓器で hCG のような刺激ホルモンにより短時間に発現する steroidogenic acute regulatory protein (StAR) の lyase の活性低下への関与を調べた。hCG 投与の 20 分後には StAR の mRNA が増加するのが見られた。また hCG による lyase の活性低下における活性酸素種 (ROS) の関与を検討するため、hCG を投与する 3 時間前と 12 時間前に抗酸化剤の dimethyl sulfoxide (DMSO) をラットに投与した。hCG 投与の 6 時間後、lyase の活性は hCG 非投与群（対照群）の 11%にまで低下したが、ほぼ極量の DMSO を前投与しても対照群の 21%までの回復にとどまった(Fig. 3)。既に知られているように hCG を投与して 30 分後には RNA 合成を介さないコレステロールの急激な供給により、コレステロール側鎖切断酵素 (SCC) によるステロイド合成が一時的に亢進したことが確認された。また、この速いが一時的な反応より遅れて StAR 遺伝子の発現が継続的に誘導されたことから、StAR が継続的にコレステロールをミトコンドリア外膜から、内膜にある SCC に運搬すると考えられる。この 2 段階の SCC 反応の亢進により、SCC の代謝産物のプレグネノロンが lyase の局在するミクロソームへ大量に供給され、それに伴い NADPH 依存性の lyase 反応の回転が高まり ROS が発生してミクロソーム内の lyase の分解に少なくとも一部関与したことが示された。

3, 乳腺組織における一酸化窒素合成酵素の発現と NO 産生の制御

NO は免疫系、血管系、神経系などにおいて多岐にわたる重要な役割を担っている。中でも、免疫系の細胞が示す抗炎症、抗腫瘍活性などの一部は NO の細胞に対する毒性作用によると考えられている。一方、長期間の感

染や炎症が発癌リスクの要因の一つと言われているが、細胞内で NO を産生する一酸化窒素合成酵素（NOS）が乳腺腫瘍(癌)の細胞にも存在している事が報告され、過剰の NO 産生と発癌との関連性が指摘され始めた。

本研究では、パラクリンやオートクリン機構における制御因子の一つとしての NO の役割に着目し、正常乳腺組織や内分泌器官などにおける NOS の局在や NO の産生能に関する基礎的知見を得ると共に、それらの組織や器官などの発達、分化、機能などと NO 生成系との関連性を明らかにした。

(a) 培養乳腺細胞による NO の産生[9]：ラットの乳腺細胞を分離、培養し、その NO 産生能について検討するため、雌性ウィスター-MS 系ラット(8~9 週令)の乳腺組織を無菌的に摘出し、3 回の酵素処理後、乳腺細胞の小集塊を得た。この乳腺細胞画分を 10%ウシ胎児血清（FCS）を含む DMEM（ダルベッコ改良培地）に懸濁し、ペトリ皿上で 6 時間前培養した後、未接着の細胞集塊を回収して最終乳腺細胞画分とした。この乳腺細胞を 24 穴培養プレートに播種し、培養を続け、密集状態を確認した後実験に供した。培養乳腺細胞の細胞集団の組成はケラチン、ビメンチン、α-アクチンに対する特異的な抗体を用いて免疫細胞化学的に処理を施した後、蛍光顕微鏡で観察して確認した。培養した乳腺細胞に炎症誘発物質であるリポ多糖（LPS：5~2000ng/ml 培養液）と NO を捕捉するカルボキシ-PTIO（100 μM）を添加し、培地中に放出された NO 量を 48 時間まで経時的に測定した。NO 量はグリース反応を用いて定量した NO_2 濃度から推定した。

培養乳腺細胞はケラチン陽性の上皮性細胞がおよそ70%を占め、乳腺上皮細胞が多い培養系であった。培養乳腺細胞は LPS で刺激すると、6 時間程のラグタイムの後、急速に NO が産生され、少なくとも 48 時間まで NO の産生を持続した。この NO の産生は NOS を阻害するヒドロコルチゾン（グルココルチコイドの一種）やアミノグアニジンなどで完全に阻害された。これらの事から、培養乳腺細胞では炎症性刺激により NOS の誘導が起こり、多量の NO の産生が促進される事が明らかになった。

Table 3, Nitric oxide production by cultured rat mammary glands

Treatment	Produced NO_2 (nmol/ml)[b]
Control	6.4 ± 0.4
w/LPS (0.5 μg/ml)	29.9 ± 1.9[c]
w/LPS, hydrocortisone (3 μM)	7.5 ± 0.6

[a]Three pieces of the mammary glands were cultured, and at the end of culture the conditioned media were collected for the determination of nitrite (NO_2^-) concentration. NO produced and secreted by mammary glands into culture medium was estimated by measuring nitrite converted from NO with Griess reagent as described in Materials and Methods.
[b]Values represent mean ± SE obtained from three independent experiments. Each experiment contained 6–8 cultures per replicate.
[c]Significant difference from control, $p<0.001$.

(b) 乳腺組織における NOS の分布[9,10]：ラットの乳腺組織における NOS の局在性を、乳腺の組織培養系と NOS イソフォームに特異的な抗体を用いて免疫組織化学的に検討した。ウィスター-MS 系雌ラット(8 週令)にエストラジオールとプロゲステロンの各錠剤を皮下に移植して人為的に乳腺を発達させた後、乳腺組織を無菌的に摘出し、約 3mm 角の組織片を切り出した。3 個の組織片を 24 穴培養皿の各ウェルに移し 10%FCS/DMEM にて 24～48 時間培養した。その後、LPS(0.5 μg/ml)を含む 10%FCS/DMEM/カルボキシ-PTIO で 48 時間培養した。培養した乳腺組織片を中性ホルマリンで固定後にクリオスタットによって凍結切片(12 μm)を作成し、iNOS（誘導型）、eNOS（内皮型）、bNOS（脳／神経型）に特異的な抗体を用いて免疫組織化学的に染色を施し、蛍光顕微鏡下で観察した。一方、正確な局在性を判定する上で、乳腺組織中の上皮細胞を特異的に判別することが重要であることから、乳腺では上皮細胞のみが産生、分泌する乳汁タンパク質のカゼインに対する特異的な抗体を当研究室で作製した。この抗ラットカゼイン抗体と抗ラットトランスフェリン抗体を用いて同様に免疫組織化学的に染色して、乳腺上皮細胞の判定の基準とした。また、NOS が保持する NADPH-diaphorase の活性染色も行い、NOS の免疫組織化学的染色の結果と比較した。さらに、一部の培養乳腺組織のホモゲネートを調製し上記の各種抗体を用いてウェスタン・ブロット解析を試みた。培養上清中の NO_2 濃度はグリース反応から推定した。

培養した乳腺組織片による NO 産生量は概して低く(~10nmol/ml)、LPS 刺激によって対照群の 3～5 倍量の NO 産生が惹起された (Table 3)。この刺激効果はヒドロコルチゾンによって完全に抑えられた。これらの結果は前記の乳腺上皮細胞が多い培養系で得られた結果と良く一致した。乳腺ホモゲネートのウェスタン解析において、iNOS 抗体と反応する分子量約 122kDa のバンドが対照群でほんの僅かに認められ、LPS 処理群ではこのバンドが数倍に増加していた。これは NO の産生が LPS 添加後に 3～5 倍量増加した事と良く一致する結果であった (Fig. 4)。eNOS 抗体と反応する分子量約 152kDa

のバンドは両群に認められたが、LPS の処理により減少した (Fig. 5)。これは LPS で誘導された iNOS により過剰に産生された NO のネガティブフィードバック制御

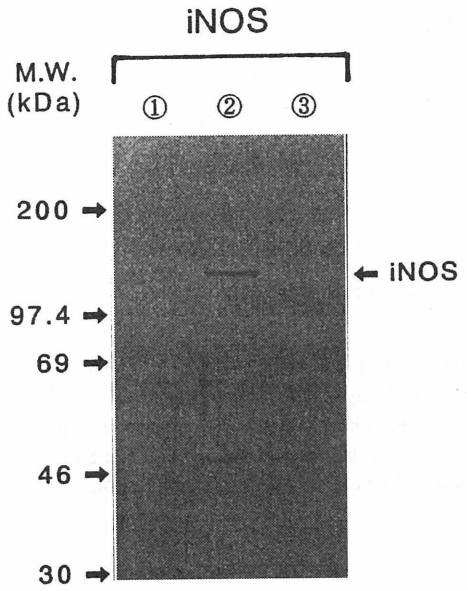

Figure 4, Immunoblot analysis of iNOS in extracts obtained from cultured rat mammary glands. The homogenates (10 μg/lane) were loaded onto the SDS-PAGE system and the immunoreactive substances were visualized by Western blot analysis with an alkaline phosphatase-conjugated secondary antibody. Lane 1, control; Lane 2, control + LPS (0.5 μg/ml); Lane 3, control + LPS + hydrocortisone (3 μM)

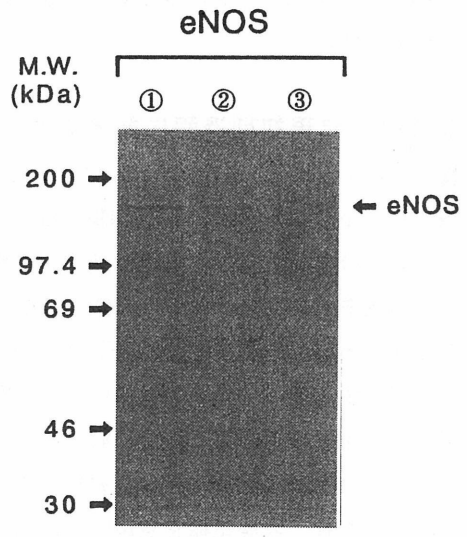

Figure 5, Immunoblot analysis of eNOS in extracts obtained from cultured rat mammary glands. The homogenates (18 μg/lane) were loaded onto the SDS-PAGE system and the immunoreactive substances were visualized by Western blot analysis with an alkaline phosphatase-conjugated secondary antibody. Lane 1, control; Lane2, control + LPS (0.5 μg/ml); Lane 3, control + LPS + hydrocortisone (3 μM)

によるものと考えられる。iNOS の組織内の局在性は、免疫組織化学的実験から、カゼインやトランスフェリンの局在とは異なり、乳管や乳腺房の基底層(myoepithelium)と血管内皮層に陽性染色が認められ、NADPH-diaphorase の局在性と一致した。eNOS 抗体による染色でも iNOS の局在パターンと類似した結果が得られた。bNOS 抗体では弱いながら乳腺房の上皮細胞層が陽性に染まった。これらの結果から、乳腺組織では介在血管だけでなく、乳腺の実質細胞にも 3 種類の NOS イソフォームが存在していることが明らかになり、cNOS（介在型の eNOS や bNOS など）は乳腺組織の生理作用を調節している可能性が示唆された。その一方で、iNOS は乳腺細胞の炎症時に、*de novo* 合成された後に NO 産生を促進し、これらの事象に対応している事が示された。

(c) 培養乳腺組織による NO 産生に対するクルクミンの影響[11]：NO は生体の多岐にわたる機能と密接な関わりを持つ事が知られているが、我々はラット乳腺組織にも 3 種類の NOS イソフォームが局在し、NO 産生を介して乳腺の生理的機能や病態生理学的状態を統御している事を明らかにした。一方、秋ウコン(*Curcuma longa* LINN)の根茎に含まれているクルクミンには、抗炎症作用や抗腫瘍作用（後述）が期待されている事から、ここでは、培養したラット乳腺組織の NO 産生に対するクルクミンの影響を検討した。ウィスター-MS 系雌ラット(8 週令)にエストラジオールとプロゲステロンの各錠剤を皮下移植して人為的に乳腺を発達させた後、乳腺組織を無菌的に摘出し、約 3mm 角の組織片を切り出した。1 個の組織片を 24 穴培養皿の各ウェルに移し 5%FCS/DMEM 培地にて 24～48 時間培養した。その後、LPS(0.5 μg/ml)あるいは、LPS とクルクミン(～100 μM)を含む新鮮な培地で 48 時間培養した。他の実験においては、LPS で 24 時間前処理した後、LPS を洗い流してからクルクミンだけを含有する培養液に交換して培養を続けた。培養上清中の NO_2 濃度をグリース反応によって定量し、NO 産生量を推定した。また、培養後に乳腺組織のホモゲネートを調製し、抗 NOS 抗体を用いてウエスタン・ブロット解析を試みた。さらに、NO 供与剤の NOC12（N-エチル-2-(1-エチ-2-ヒドロキシ-2-ニトロソヒドラジノ)エタンアミン）とクルクミンを直接試験管内で混合し、NOC12 から放出される NO ラジカルをクルクミンが直接捕捉出来るか否かについても検討を加えた。

乳腺組織片(1 個/2ml)の培養により僅かな NO の自発

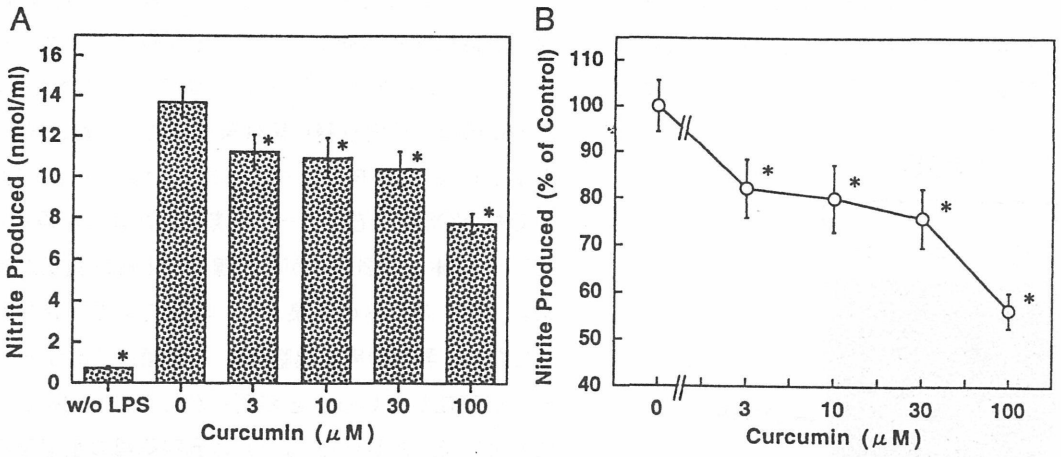

Figure 6, Inhibition of NO production in LPS-stimulated rat mammary glands by curcumin. A piece of the mammary gland was cultured in the presence or absence of LPS (0.5 g/ml) for 2 days, after which the conditioned medium was collected for the determination of the nitrite (NO_2^-) concentration. The curcumin concentration was maintained throughout the culture period. the actual concentration of the nitrite and relative concentration to the LPS-stimulated control culture are indicated in A and B, respectively. * Significant difference from LPS alone control, $P < 0.001$.

的産生(～0.5nmol/ml)が認められたが、LPS 添加によって約 20 倍量の NO 産生が惹起された。LPS で刺激された乳腺による NO の産生はクルクミンの用量に依存して低下したが、クルクミン 30μM と 100μM で NO 産生量は、それぞれ 76%、56%にまで低下した (Fig. 6)。クルクミンの培養液への難溶性は添加量に制限を来たし、高用量の効果判定をすることはできなかった。LPS 前処理をした後に培養系から LPS を除去すると、その後の乳腺組織による NO 産生量は著しく減少するが、それでも、LPS による前処理中にすでに誘導された iNOS による NO 産生は検出可能なレベルにあった。これに対して、LPS 前処理後の培養系に後からクルクミンを添加しても、すでに誘導された iNOS による NO 産生を阻害する事は出来なかった。乳腺のホモゲネートを用いてウェスタン解析を行うと、抗 iNOS、抗 eNOS 抗体と反応する分子量約 122kDa と分子量約 152kDa のタンパク質バンドが未処理の乳腺ホモゲネート中に検出された。LPS で刺激した乳腺組織中では抗 iNOS 抗体と反応するタンパク質バンドが著しく増加していたが、eNOS の発現は明らかに低下していた。また、クルクミン(100μM)の添加によって iNOS の発現量は明らかに減少したが、eNOS の発現量は未処理の乳腺組織における eNOS のレベルにまで回復していた。これらの結果は培養液中の NO 量の増減の結果とも良く一致していた。これらのことは乳腺における過剰の NO 産生には継続的な刺激物質 (LPS など) の存在が不可欠であること、また、クルクミンは iNOS の *de novo* 誘導前に共存しないと iNOS の発現を抑制する効果が無いことを示すものである。一方、無細胞の系で NOC12 から放出される NO の量は NOC12 の用量に依存して増加したが、クルクミン (30、100μM) の共存によって用量依存的に溶液中の NO 濃度は減少していた。これらの事から、乳腺がある種の侵襲などに際して産生する過剰の NO ラジカルに対して、クルクミンは捕捉能を有しているばかりではなく、iNOS 誘導の阻害効果も有している事が示され、ラジカルによる障害に対する防護作用が期待された。

(d) 乳腺の NOS 発現初期過程に対するクルクミンの影響[12]： クルクミンは乳腺において、LPS 刺激により誘導される NO レベルの増加を抑制するが、これはクルクミンの NO ラジカル捕捉効果と iNOS の発現抑制効果による事を先に示した。そこで、iNOS 遺伝子の発現を調節している誘導型転写活性化因子の NF-κB とその制御因子 IκB の挙動に対するクルクミンの影響について、培養ラット乳腺組織を用いて検討した。ウィスター-MS 系雌ラット(8 週令)をホルモン処理して人為的に乳腺を発達させた後、乳腺組織を無菌的に摘出し、約 3mm 角の組織片を切り出した。組織片 1 個を 24 穴培養皿の各ウェルに移し 5%FCS/DMEM 培地にて 24～48 時間培養した。その後、LPS あるいは、LPS とクルクミンを含む新鮮な培地で 30～60 分間培養した。培養後、乳腺組織のホモゲネートを調整し、核画分と細胞質画分を得た。各画分について抗 NF-κB(p65)抗体、抗 IκBα抗体を用いてウェスタン・ブロット解析を試みた。

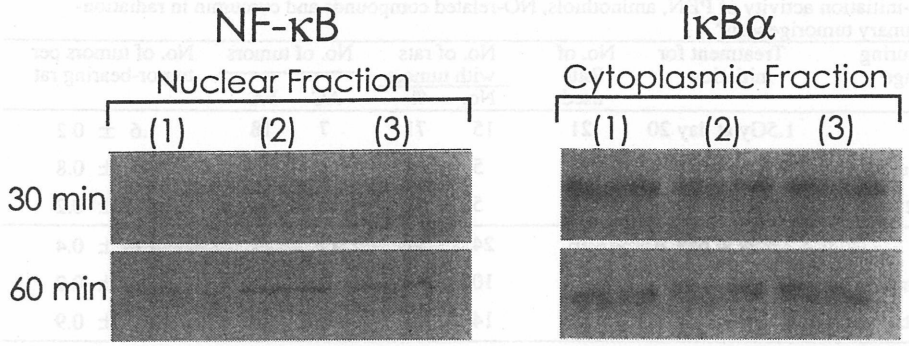

Figure 7, Immunoblot analysis of NF-κB and IκBα in nuclear and cytoplasmic fractions, respectively, obtained from cultured rat mammary glands. The nuclear fraction (20 μg/lane) and cytoplasmic fraction (10 μg/lane) were loaded onto the SDS-PAGE system and the immunoreactive substances were visualized by Western blot analysis with an alkaline phosphatase-conjugated secondary antibody. Lane 1, control; Lane 2, control + LPS (0.1 μg/ml); Lane 3, control + LPS + curcumin (100 μM)

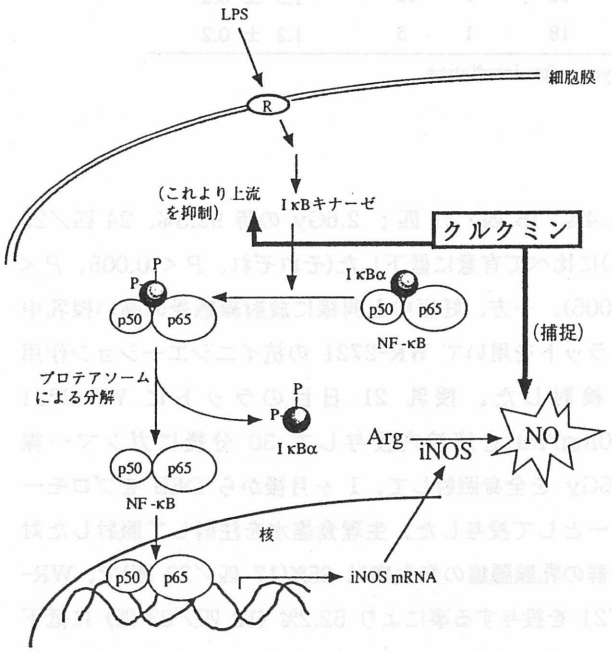

Figure 8, Inhibitory mechanism on iNOS induction by NF-κB activation and NO-scavenging activity of curcumin

培養乳腺組織片に LPS (0.1 または 0.5μg/ml) を添加して 30～60 分後では、いずれの LPS 刺激においても細胞質画分の NF-κB 量に著しい変化は認められなかったが、核画分へ移行した NF-κB 量は明らかに増加していた。この時、細胞質画分の IκBα量の若干の減少も認められた。これに対して、LPS とクルクミン(100μM)を同時に添加した場合、高用量の LPS (0.5μg/ml) 刺激下では NF-κB の核画分への移行を抑制することが出来なかったが、低用量の LPS (0.1μg/ml) で刺激した時には明らかに NF-κB の核画分への移行を抑制していた (Fig. 7)。そして、細胞質画分の IκBα減少も回復していた。以上の結果から、乳腺の病態生理的状況下における侵襲的な NO の産生に対して、クルクミンによる iNOS の誘導を阻害する作用の一部は，iNOS 遺伝子の発現の初期過程における NF-κB の活性化カスケード(多分、IκBα分解よりも上流過程) の抑制が関与している可能性が示唆された (Fig. 8)。

4, 抗イニシエーション化合物の探索

放射線が乳腺腫瘍(癌)発生のイニシエーターであることは我々の研究結果から明らかである。特に妊娠後期や授乳中の発達、分化している乳腺組織は放射線に対する感受性が高く、放射線被曝により高い頻度で腫瘍(癌)化するが、そのメカニズムとして次のような事が考えられている。

(i) 放射線により細胞内にフリーラジカルが生成されて DNA 等に修復不可能な損傷を与える。

(ii) フリーラジカルによる酸化的ストレスが癌遺伝子の活性化または癌抑制遺伝子の不活性化を誘導する。

これらの現象がエストロゲンやプロラクチンの作用を受けた乳腺の幹細胞で特に起こりやすいと考えられている。抗イニシエーション化合物の探索では、フリーラジカルを捕捉して無害化するアミノチオール化合物や植物成分のクルクミンを用いて検討を行った。

(a) システアミン[13]：放射線に対する感受性が高い妊娠後期のラットにシステアミン(25mg/rat)を腹腔内に投与して 30 分後にガンマー線(1.5 または 2.6Gy)を全身照射した。授乳終了後 1 ヶ月目からプロモーターとして

Table 4. Anti-initiation activity of PBN, aminothiols, NO-related compounds and curcumin in radiation-induced mammary tumorigenesis[a]

Treatment during initiation stage	Treatment for initiation	No. of Rats used	No. of rats with tumors		No. of tumors		No. of tumors per tumor-bearing rat
			No.	%	AC	FA	
Control	1.5Gy at day 20	21	15	71	7	18	1.6 ± 0.2
WR-2721 (50mg/rat,i.p.)	of pregnancy	21	5	24	2	7	1.8 ± 0.8
Cysteamine(25mg/rat,i.p.)		24	5	21	2	4	1.2 ± 0.2
Control	2.6Gy at day 20	26	24	92	17	21	1.6 ± 0.4
WR-2721(50mg/rat,i.p.)	of pregnancy	23	10	44	3	15	1.8 ± 0.2
Cysteamine(25mg/rat,i.p.)		21	14	67	6	15	1.6 ± 0.9
Control	1.5Gy at day 21	20	17	85	11	15	1.5 ± 0.3
WR-2721(50mg/rat,i.p.)	of lactation	23	12	52	7	8	1.2 ± 0.1
Cysteamine(25mg/rat,i.p.)		25	10	40	1	11	1.2 ± 0.1
Control	2.6Gy at day 21	28	27	96	16	16	1.2 ± 0.1
WR-2721(50mg/rat,i.p.)	of lactation	23	22	96	18	28	2.1 ± 0.3
Cysteamine(25mg/rat,i.p.)		22	20	91	22	32	2.8 ± 0.4
Control	1.5Gy at day 20	27	19	70	9	19	1.5 ± 0.2
Curcumin (1%, in diet)	of pregnancy	27	5	18	1	5	1.2 ± 0.2

a, All rats were treated with DES, as a tumor promoter, for 1 year after irradiation.

DES を1年間連続投与して乳腺腫瘍の発生を観察した。生理食塩水を注射して照射した対照群では、1.5Gy を照射したラットの乳腺腫瘍の発生率は71.4%(15匹／21匹)、2.6Gy の場合は 92.3%(24 匹／26 匹)であった。これに対して、システアミン投与後、1.5Gy を照射したラットの乳腺腫瘍の発生率は 20.8%(5 匹／24 匹、$P<0.001$) に、2.6Gy の時は 66.7%(14 匹／21 匹、$P < 0.005$)に腫瘍発生率が有意に低下した (Table 4)。

(b) WR-2721[13,14] : WR-2721 は米国 Walter Reed Army Institute of Research が核戦争に備えて合成したもので、1969 年 Yuhas 等が担癌マウスを用いて正常組織に対しては放射線被曝の影響を予防するが、腫瘍組織の放射線感受性は修飾しないことを発見して以来、癌の放射線療法に応用できる化合物として注目された。WR-2721 は細胞の中に入る時アルカリフォスファターゼで分解されて放射線防護作用をもつ活性型化合物，WR-1065、に変化すると考えられている。システアミンの投与実験と同様に、WR-2721(50mg/rat)を妊娠後期のラットの腹腔内に投与して 30 分後にガンマー線(1.5 および 2.6Gy)を全身照射し、授乳終了後プロモーターとして DES を1年間連続投与して乳腺腫瘍の発生を観察した。1.5Gy を照射したラットの発生率は 23.8%(5 匹／21 匹)、 2.6Gy の時は 43.5%(10 匹／23 匹)で (Table 4)、WR-2721 を投与しない対照群の発生率(1.5Gy の時 71.4%、15 匹／21 匹； 2.6Gy の時 92.3%、24 匹／26 匹)に比べて有意に低下した(それぞれ、$P < 0.005$、$P < 0.005$)。一方、妊娠中と同様に放射線感受の高い授乳中のラットを用いて WR-2721 の抗イニシエーション作用を検討した。授乳 21 日目のラットに WR-2721 (50mg/rat)を腹腔内投与して 30 分後にガンマー線 1.5Gy を全身照射して、1 ヶ月後から DES をプロモーターとして投与した。生理食塩水を注射して照射した対照群の乳腺腫瘍の発生率は 85%(17 匹／20 匹)で、WR-2721 を投与する事により 52.2% (12 匹／23 匹) に低下して、統計学的($P < 0.022$)に有意であった。しかし、線量を増やして 2.6Gy を WR-2721 投与後照射した時は有意な防護効果が得られなかった。これは授乳中の乳腺の方が妊娠乳腺よりも放射線に対する感受性が高いためで、同じ線量を照射しても WR-2721 で消去することが出来なかったラジカルが授乳中の乳腺細胞に損傷を与えたために防護効果がみられなかったと思われる。

(c) クルクミン[15]：前記のシステアミンや WR-2721 はラジカルを消去する作用以外に毒性もあるのでヒトへの利用がほとんど行われていない。毒性がなく放射線の障害を予防する化合物の検索は多くの研究者によって行われているが、我々は本プロジェクトを開始した 1996 年以来、植物から有効成分の探索を行い、秋ウコンの根茎に含まれている黄色色素のクルクミンに着目して、放

射線により誘発される乳腺腫瘍および脳下垂体腫瘍の発生過程のイニシエーション時投与における抗腫瘍(癌)効果を評価した。

妊娠 11 日目から出産日(妊娠 23 日目)まで 1%クルクミンを混合した餌でラットを飼育し、妊娠 20 日目に ^{60}Co のガンマー線(1.5Gy)で全身照射し、授乳が終了した後プロモーターとして DES を連続投与して乳腺腫瘍の発生を観察した。対照群としてクルクミンを含まない基礎飼料で飼育して照射したラットの場合は、乳腺腫瘍の発生率は 70.3%(19 匹／27 匹)であったが (Table 4)、放射線で腫瘍発生のイニシエーションを行う時クルクミンを摂取すると乳腺腫瘍の発生率は 18.5% (5 匹／27 匹) に低下した($P < 0.0001$)。また、脳下垂体腫瘍の発生率も、対照群の 29.6% (8 匹／27 匹) からクルクミン摂取により 18.5% (5 匹／27 匹) に低下した($P < 0.005$)。妊娠中のクルクミンの摂取は、胎児への影響や母親ラットへの影響がないことから、ヒトに応用が可能な化合物である。クルクミンが放射線による発癌を予防するメカニズムは,

(i) 放射線によって生体内で発生した $\cdot OH$、O_2^- や NO 等のフリーラジカルを直接消去する。

(ii) クルクミンはシクロオキシゲネース-2 やキサンチンオキシデースを阻害し、また一酸化窒素合成酵素の発現を抑制して生体内で発生するフリーラジカルを減少させる。

(iii) クルクミンは SOD、カタラーゼ、グルタチオンパーオキシデース等の抗酸化酵素を活性化して生体内のフリーラジカルを低下させる。

(iv) 放射線による NF-κB の活性化をクルクミンが抑制して腫瘍(癌)の発生を予防する。

等が考えられている。

5, 抗プロモーション化合物の探索

放射線被曝によって発癌イニシエーションが細胞内に誘導されて正常細胞が変異細胞に変化しても、変異細胞の増殖、発育を抑制する事ができれば結果的に発癌を防ぐことができる。放射線でイニシエートされた変異細胞がアポトーシスで組織から排除される場合は発癌に至らないが、変異細胞の寿命が長い場合は抗プロモーション化合物を長期間服用する必要がある。しかし、抗プロモーション作用があるからといって「薬物」を長期間服用することは現実的でない。そこで植物から毒性が低くて抗プロモーション作用を持つ有効成分の同定を行った。また放射線でイニシエートされた乳腺細胞が卵巣から分泌されているエストロゲンの直接作用、またはエストロゲンが脳下垂体に作用してプロラクチンの分泌を促進する間接作用がプロモーションになって、腫瘍(癌)化することを確認するため、抗エストロゲン剤の評価を行った。一方、食事の欧米化による高脂血症や高コレステロール血症が乳癌発生の要因の一つと考えられていることから、これらが放射線誘発乳腺腫瘍の発生過程の合成エストロゲン(DES)によるプロモーション作用に及ぼす影響を明らかにするための研究も行った。

(a) ベザフィブレート[16]： ベザフィブレートはクロフィブレート誘導体で高脂血症の治療薬として用いられている薬剤である。放射線に高感受性の妊娠 20 日目のウィスター-MS 系ラットをガンマー線(2.6Gy)で全身照射し、授乳終了直後から 0.15%ベザフィブレート含有飼料で飼育して、1 ヶ月後から腫瘍プロモーターとして DES を投与した。DES の投与期間は 1 年間で、その間ベザフィブレートを混合した飼料を与えて乳腺腫瘍の発

Table 5, Anti-promotion activity of DHEA, cholesterol lowering agents, tamoxifen and curcumin on DES-dependent promotion for tumorigenesis from primordial cells initiated by radiation[a]

Treatment during promotion with DES	Treatment for initiation	No. of rats used	No. of rats with tumors		No. of tumors		No. of tumors per tumor-bearing rat
			No.	%	AC	FA	
Control diet	2.6Gy at day 20	26	25	96	18	35	2.1 ± 0.4
DHEA (0.6%, in diet)	of pregnancy	20	7	35	9	6	2.1 ± 1.1
Control diet	2.6Gy at day 20	48	43	90	27	47	2.0 ± 0.2
Bezafibrate(0.15%, in diet)	of pregnancy	22	6	27	2	5	1.2 ± 0.2
Control diet	2.6Gy at day 20	57	50	88	29	56	1.9 ± 0.2
Simvastatin (0.03%, in diet)	of pregnancy	22	8	36	2	13	1.9 ± 0.4
Control pellet	1.5Gy at day 21	20	17	85	11	15	1.5 ± 0.3
Tamoxifen (30%, in pellet)	of lactation	23	1	4	0	1	1.0
Control diet	2.6Gy at day 20	39	33	85	19	44	1.9 ± 0.2
Curcumin (1%, diet)	in of pregnancy	25	7	28	1	6	1.0 ± 0.0

a, All rats were treated with DES, as a tumor promoter, for 1 year after irradiation.

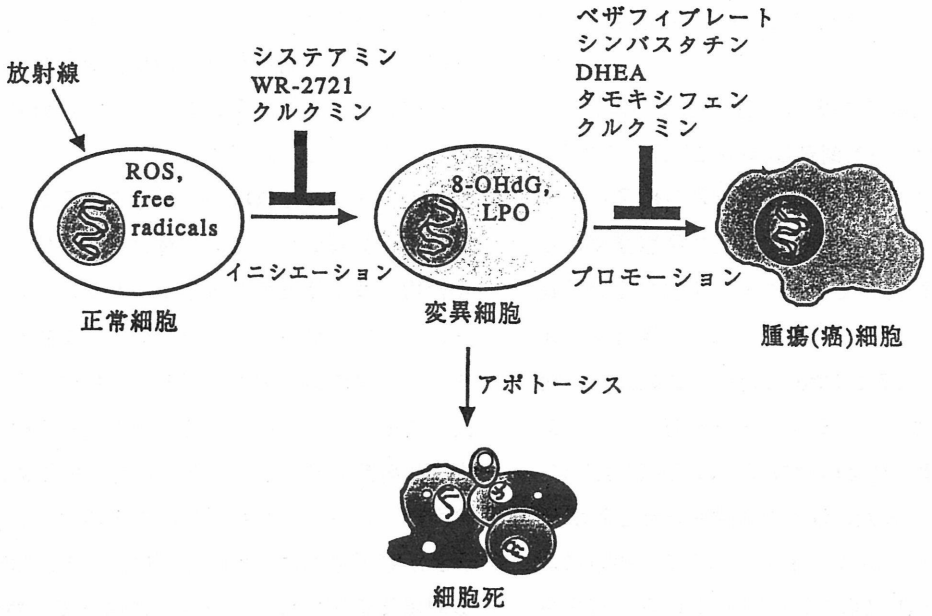

Figure 9, Prevention of radiation-induced mammary tumorigenesis

生を観察した。ベザフィブレートを含まない基礎飼料を与えた対照群の乳腺腫瘍の発生率は 89.6%(43 匹／48 匹)であったのに対し (Table 5)、ベザフィブレートを摂取した実験群の腫瘍の発生率は 27.3% (6 匹／22 匹)まで有意に低下した($P < 0.0001$)。ベザフィブレート摂取により血中の中性脂肪のトリグリセリドが対照群の約 60%まで低下し、また、乳腺腫瘍の発生と深い関係がある血中プロラクチン濃度も約 60%まで低下したことが、乳腺腫瘍の発生を予防した原因と考えられている。

(b) シンバスタチン[17]**：**シンバスタチンは酵母(*Aspergillus terreus*)の培養液から分離同定されたロバスタチン誘導体のラクトン環化合物で、生体内でジヒドロキシ酸に変換されて活性型になりコレステロール生合成の律速反応を触媒する酵素の 3-ヒドロキシ-3-メチルグルタール-CoA (HMG-Co)還元酵素の活性を阻害する薬剤で高コレステロール血症の治療に用いられている。放射線に高感受性の妊娠 20 日目のラットをガンマー線(2.6Gy)で全身照射し、授乳終了直後から 0.03%シンバスタチン含有飼料で飼育して、1 ヶ月後から腫瘍プロモーターの DES の投与を始めた。DES は 1 年間投与して、その間シンバスタチンを混合した飼料を与え続けて乳腺腫瘍の発生を観察した。シンバスタチンを摂取した実験群の乳腺腫瘍の発生率は 36% (8 匹／22 匹) で (Table 5)、この値はシンバスタチンを含まない基礎飼料で飼育した対照群の腫瘍発生率(88%、50 匹／57 匹)と比較して有意に低下した($P < 0.0001$)。シンバスタチンを摂取したラットの血中コレステロール値は低下せず、乳腺腫瘍の発生に関与している血中エストラジオール値が対照群の値の 20% にまで低下したことが腫瘍の発生を抑制した原因と考えられている。

(c) デヒドロエピアンドロステロン[18]**：**デヒドロエピアンドロステロン(DHEA)は副腎皮質で生合成されているアンドロゲンである。ヒトの場合、乳癌患者の血中 DHEA 濃度は正常人と比較すると有意に低いことから、DHEA と乳癌発生の関係が注目されてきた。放射線に高感受性の妊娠 20 日目のラットをガンマー線(2.6Gy)で全身照射し、授乳終了直後から 0.6%DHEA を含有する飼料で飼育を開始して、1 ヶ月後から腫瘍プロモーターの DES を投与した。DES は 1 年間投与し、その期間中 DHEA 含有飼料を与えて乳腺腫瘍の発生を観察した結果、腫瘍発生率は 35.0% (7 匹／20 匹) で (Table 5)、DHEA を含まない飼料で飼育した対照群の乳腺腫瘍の発生率(96.2%、25 匹／26 匹))と比較すると有意に低下した($P < 0.01$)。DES の投与により脳下垂体が肥大してプロラクチン分泌が促進されて放射線でイニシエートされた乳腺細胞が腫瘍化するが、DHEA は脳下垂体の肥大化を抑えると同時にプロラクチン分泌も抑制する事が乳腺腫瘍の発生を予防した原因の一つである。また、DHEA 投与により、肝臓肥大が認められたが、肝細胞内小器官のペルオキシソームの増加がみられた。ペルオキ

シソーム内の酵素系により脂肪酸のβ-酸化が促進して、過酸化水素が過剰産生されるが、この過酸化水素はHMG-Co 還元酵素の活性を阻害することによりファルネシル-ピロリン酸の生合成量が低下し、発癌遺伝子産物の $p21^{ras}$ のイソプレニル化を抑制し、結果的に腫瘍化を予防したカスケードも一つの可能な機構と考えられる。

(d) タモキシフェン[14]：放射線でイニシエートされた乳腺細胞から腫瘍(癌)になるには卵巣から分泌されているエストロゲンがプロモーターとして重要であるから、抗エストロゲン作用が強いタモキシフェンをプロモーション期間中投与して、その腫瘍(癌)化予防効果を検討した。放射線高感受性の授乳終了時のラットにガンマー線(1.5Gy)を全身照射し、1 ヶ月後から DES とタモキシフェンを含有するペレットを1年間投与して乳腺腫瘍の発生を観察した結果、腫瘍の発生率は 4.4% (1 匹／23 匹)で (Table 5)、DES のみを投与した群の発生率(85.0%、17 匹／20 匹)と比較すると有意に低下した($P < 0.0001$)。また、DES もタモキシフェンも投与しない場合、すなわち卵巣から分泌されているエストロゲンがプロモーターになっている群の発生率(26.0%、6 匹／23 匹)と比較しても有意に低下した($P < 0.01$)。一方、前述のラジカル捕捉剤の WR-2721 を投与した後、乳腺細胞を放射線照射によってイニシエーション後、プロモーション期間中 DES とタモキシフェンで処理すると、乳腺腫瘍は発生せず完全に予防 (0 匹／23 匹)することができた。タモキシフェンは乳腺のエストロゲン受容体と結合してエストロゲンの作用を阻害すると共に、脳下垂体のエストロゲン受容体とも結合してプロラクチンの生合成、分泌を抑制して抗プロモーション作用を示した。

(e) クルクミン[19]：酸化的ストレスの原因となる生体内で発生する種々のフリーラジカルや活性酸素を秋ウコンの根茎に含まれているクルクミンが消去または産生を抑制することは既に述べた。放射線に高感受性ラットを照射後、DES をプロモーターとして投与すると乳腺腫瘍が高頻度に発生するが、DES は生体内でキノン体に代謝されることから、その過程でラジカルが産生されることが知られている。放射線に高感受性の妊娠 20 日目のラットにγ-線を全身照射(2.6Gy)し、授乳終了時から1%クルクミン含有飼料で飼育を開始して、さらに 1 ヶ月後からプロモーターとして DES を投与した。DES は1年間投与してその期間中クルクミン含有飼料を与えて乳腺腫瘍の発生を観察した。対照群はクルクミンを含まない基礎飼料を与えた。クルクミンを与えた実験群の腫瘍の発生率は 28.0% (7 匹／25 匹)で (Table 5)、対照群の発生率(84.6%、33 匹／39 匹)の 1/3 であった。この値は統計学的に有意($P < 0.0001$)な減少であった。放射線でイニシエートされた乳腺細胞から DES のプロモーション作用で腫瘍(癌)化するのをクルクミンが予防したのは、クルクミンが DES による血中プロラクチン濃度の上昇を抑えたことが大きく寄与している。また 1%クルクミン含有飼料でラットを1年間飼育しても顕著な副作用が現れなかったことから、クルクミンは毒性が低くヒトへの臨床応用が可能な化合物であることが証明された。

IV. 結　論

乳腺は放射線に被曝すると腫瘍(癌)化しやすい臓器として知られている。ヒトの場合、放射線に被曝した時の年令と乳癌の発生との相関については原爆被曝者を対象とした疫学研究で調査されている。しかし、乳腺に対するホルモン環境が異なる生殖サイクルと放射線感受性の関係については不明であった。本研究の動物実験から、妊娠中や授乳中の発達している乳腺は特に放射線に対する感受性が高く、放射線により容易に腫瘍(癌)化イニシエーションを受け、卵胞ホルモン(エストロゲン)がプロモーターになって高頻度に腫瘍(癌)化することが証明された。ラット乳腺の化学発癌物質(例えば DMBA)に対する感受性は未分化乳腺組織の方が高いことから、乳腺の放射線発癌と化学発癌ではメカニズムが異なり、化学発癌実験は放射線発癌のモデルにならないことが示された。放射線によるイニシエーションには被曝で乳腺細胞内に誘導される iNOS の発現が亢進して、この酵素反応で過剰に産生される NO ラジカルの関与の可能性が高く、引き続き詳細に検討中である。ヒトでは、妊娠中は胎児に対する影響から妊婦が被曝することは放射線事故以外にありえないが、しかし、授乳中の母親の放射線被曝については十分に注意が払われていないのが現状ある。今後、この点については積極的な啓蒙活動が必要である。また、妊娠や授乳以外に、ピルのような排卵抑制作用の他に乳腺にも作用して組織を増殖させる医薬品を服用している場合も乳腺の放射線感受性が高くなることが分かった。

乳腺腫瘍(癌)の発生過程の放射線によるイニシエーションを抑制するにはラジカルを捕捉する化合物が有効で、特に、秋ウコンの根茎に含まれているクルクミンは放射線誘発乳腺腫瘍(癌)の抑制作用が強いことが証明された。その抑制作用の機序として、クルクミンの作用は多様性

を示すが、その中でも NO を捕捉するとともに、iNOS の発現を阻害して細胞内の NO レベルを低下させることがイニシエーションを抑える理由の一つと考えられる。またクルクミンは毒性が低いことからヒトへの応用を考えると有望な化合物である。また、放射線でイニシエートされた乳腺の変異細胞からエストロゲンのプロモーション作用で腫瘍(癌)化するのを抑制するには、抗高脂血症薬や抗エストロゲン剤が有効であったが、これらの医薬品以外に、前記のクルクミンが抗プロモーション作用も示して腫瘍(癌)の発生を強力に予防した (Fig. 9)。

V. 研究発表（原著論文）

1, Inano, H., Suzuki, K., Onoda, M. and Yamanouchi, H.: Susceptibility of fetal, virgin, pregnant and lactating rats for the induction of mammary tumors by gamma rays, *Radiat. Res.* **145,** 708-713, 1996.

2, Inano, H. and Suzuki K.: Radiation-induced mammary tumorigenesis in pseudopregnant rats mated with vasectomized partners, *Cancer Lett.* **116,** 241-245, 1997.

3, Yamanouchi, H., Ishii-Ohba, H., Suzuki, K., Onoda, M., Wakabayashi, K. and Inano, H.: Relationship between stages of mammary development and sensitivity to gamma-ray irradiation in mammary tumorigenesis in rats, *Int. J. Cancer,* **60,** 230-234, 1995.

4, Inano, H., Yamanouchi, H. Suzui, K., Onoda, M. and Wakabayashi,K.: Estradiol-17β as an initiation modifier for radiation-induced mammary tumorigenesis of rats ovaietomized before puberty, *Carcinogenesis,* **16,** 1871-1877, 1995.

5, Inano, H., Suzuki, K., Onoda, M., Kobayashi, H. and Wakabayashi, K.: Radiation-induced tumorigenesis of mammary glands in pituitary transplanted rats ovariectomized before onset of estrus cycle, *Cancer Lett.* **138,** 93-100, 1999.

6, Inano, H., Onoda, M., Suzuki, K., Kobayashi, H. and Wakabayashi, K.: Raiation-induced mammary tumors in virgin and parous rats administered contraceptive steroids, 17α–ethinylestradiol and norethisterone, *Carcinogenesis,* **21,** 1043-1050, 2000.

7, Inano, H., Suzuki, K. Onoda M., Kobayashi, H. and Wakabayashi, K.: Comparative effect of chlormadinone acetate and diethylstilbestrol as promoters in mammary tumorigenesis in rats irradiated with γ-rays during lactation, *Breast Cancer Res. Treat.* **53,** 153-160, 1999.

8, Inano, H., Suzuki, K., Onoda, M. and Wakabayashi, K.: Relationship between induction of mammary tumors and change of testicular function in male rats following gamma-ray irradiation and/or diethylstilbestrol, *Carcinogenesis,* **17,** 355-360, 1996.

9, Onoda, M. and Inano, H.: Localization of nitric oxide synthases and nitric oxide production in the rat mammary gland, *J. Histochem. Cytochem.* **46,** 1269-1278, 1998.

10, Onoda, M. and Inano, H.: Distribution of casein-like proteins in various organs in rat, *J. Histochem. Cytochem.* 45, 663-674, 1997.

11, Onoda, M. and Inano, H.: Effect of curcumin on the production of nitric oxide by cultured rat mammary gland, *Nitric Oxide, Biol. Chem.* **4,** 505-515, 2000.

12, Onoda, M. and Inano, H.: 論文作成中

13, Inano, H., Onoda, M., Suzuki, K., Kobayashi, H. and Wakabayashi, K.: Inhibitory effects of WR-2721 and cysteamine on tumor initiation in mammary glands of pregnant rats by radiation, *Radiat. Res.* **153,** 68-74, 2000.

14, Inano, H., Onoda, M., Suzuki, K., Kobayashi, H. and Wakabayashi, K.: Prevention of radiation-induced mammary tumors in rats by combined use of WR-2721 and tamoxifen, *Int. J. Radiat. Biol.* **76,** 1113-1120, 2000.

15, Inano, H., Onoda, M., Inafuku, N., Kubota, M., Kamada, Y., Osawa, T., Kobayashi,H. and Wakabayashi, K.: Potent preventive action of curcumin on radiation-induced initiation of mammary tumorigenesis in rats, *Carcinogenesis,* **21,** 1835-1841, 2000.

16, Inano, H., Suzuki, K. and Wakabayashi, K.: Chemoprevention of radiation-induced mammary tumors in rats by bezafibrate administered together with diethylstilbestrol as a promoter, *Carcinogenesis,* **17,** 2641-2646, 1996.

17, Inano, H., Suzuki, K., Onoda, M. and Wakabayashi, K.: Anti-carcinogenic activity of simvastatin during the promotion phase of radiation-induced mammary tumorigenesis of rats, *Carcinogenesis,* **18,** 1723-1727, 1997.

18, Inano, H., Ishii-Ohba, H., Suzuki, K., Yamanouchi, H., Onoda, M. and Wakabayashi, K.: Chemoprevention by dietary dehydroepiandrosterone against promotion/progression phase of radiation-induced mammary tumorigenesis in rats, *J. Steroid Biochem Mol. Biol.* **54,** 47-53, 1995.

19, Inano, H., Onoda, M., Inafuku, N., Kubota, M., Kamada, Y., Osawa, T., Kobayashi, H. and Wakabayashi, K.: Chemopre-

vention by curcumin during the promotion stage of tumorigenesis of mammary gland in rats irradiated with γ-rays, *Carcinogenesis*, **20,** 1011-1018, 1999.

生体制御物質に関する探索研究

伊古田暢夫、浜-稲葉浩子、今井靖子、中川秀彦、
Ranjith Gamage（第４サブグループ）

Explorative Study of Bioregulation Substances

Nobuo Ikota, Hiroko Hama-Inaba, Kiyoko Imai, Hidehiko Nakagawa, Ranjith Gamage

Reactive oxygen species (ROS) and reactive nitrogen species (RNS) have been implicated in a variety of diseases. Radiation-induced tissue damage is also a direct result of radical-mediated toxicity. Therefore the prevention from oxidative stress-induced damage is a subject of investigation. In this study, the bioregulation substances such as glycosidase inhibitors, polyhydroxylated pyrrolidine and pyyrolididines, are efficiently synthesized and the enzymatic activity was evaluated. Among the synthetic antioxydants, 2',4',3,4-tetrahydroxychalcone showed very strong scavenging activity against superoxide and hydroxyl radical examined by the ESR spin trapping method using DMPO (5,5-dimethyl-1-pyrroline N-oxide) as a spin trapping reagent. Scavenging activity against peroxynitrite has been examined using HPLC by monitoring the formation of 3-nitrotyrosine and dityrosine in the reaction of peroxynitrite with L-Tyr. Gluthathione, sulfur-containingcompound, N-ethylmercapto-3,4-dihydroxy-2-hydroxymethyl pyrrolidine, and selenium-containing compound, 2-amino-3,4-dihydroxy-5-phenylselenopentan-1-ol, exhibited a strong inhibitory effect on nitrotyrosine and dityrosine formation. On the other hand, endogeneous compounds, α-lipoic acid, melatonin, and 5-methoxytryptamine inhibit only the nitrotyrosine formation. This is the first finding of selective inhibition for nitrotyrosine formation in the reaction of L-Tyr with peroxinitrite. Iron complexes of dithiocarbamates of L-hydroxyproline and N-methylserine derivatives have been synthesized and used as a spin trapping reagent for nitric oxide. When the synthesized iron-complexes were injected into LPS (lipopolysaccaride)-treated mice intravenously, NO adducts were detected both in the liver and blood by X- and L-band ESR. Interestingly, NO adduct of iron-complex with the dithiocarbamate of trans-4-mehtoxymehtyloxy-L-proline was not detected in the liver but in blood, unlike typical spin traps for NO previously reported. This reagent may be used to estimate the amount of NO generation in blood. The production of superoxide and nitric oxide induced in U87 glioma cells treated with lipopolysaccharide (LPS) and interferon-γ (IFN-γ) was examined by ESR spectroscopy using a newly designed flow-type quartz cuvette without detaching cells from the culture plate. By the ESR measurement of cells on culture plates without detachment stress, it was found that the production of superoxide was induced by LPS/IFN-γ, but that of nitric oxide was not, in U87 glioma cells.

I. 緒言

活性酸素と種々の疾患との関連が注目されている。酸素は一電子還元を受けスーパーオキシドになり、スーパーオキシドジスムターゼにより、酸素と過酸化水素に不均化され、過酸化水素はさらにカタラーゼやグルタチオンペルオキシダーゼにより消去される。しかし、過酸化水素が消去しきれない場合には鉄や銅が存在するとヒドロキシルラジカルを生成する。またヒドロキシルラジカルは水への放射線照射や過酸化水素の紫外線照射によっても生成する。また最近、ArgからNOS（一酸化窒素合成酵素）によって生成するNO（一酸化窒素）とスーパーオキシドから生成するパーオキシナイトライトが新たな障害因子として注目されている。これらの活性酸素による生体内の障害は、DNAに対しては、塩基の酸化および鎖の開裂、蛋白質に対しては、酸化やニトロ化による不活性化、脂質に対しては過酸化である。本研究では、生理活性物質や、活性酸素・活性窒素の発生と消去に関連する生体制御物質を天然物や化学合成化合物から探索した。

II. 研究の成果・考察

1. 生体制御物質（グリコシダーゼ阻害剤、抗酸化剤）の探索

(1) ポリヒドロキシピロリジンおよびピロリジディン、ならびにカルコン類の開発

ポリヒドロキシピロリジンおよびピロリジディン類はポリヒドロキシアミン類のひとつで、グリコシダーゼ阻害作用、抗ウイルス作用、免疫調節作用、抗ガン作用などの有用な生理活性を有する物質であり、それらは光学活性体として存在する。またヒドロキシル基とアミノ基の立体配置に関しては多様な組み合わせがあり、光学異性体の数は不斉炭素の数に従って倍増する。本研究では、これらのポリヒドロキシアミン類をその光学異性体も含めて効率良く合成する方法を開発するものである。(S)-pyroglutamic acidより導かれるα-phenylseleno-γ-lactam(1)を共通の出発物質に用いてα,β-不飽和ラクタム(2)、α,β-不飽和ラクトン(3)、*trans*-α,β-不飽和エステル(4)を合成し、オスミウム酸にてジヒドロキシル化を行い、異なった立体配置を有するジヒドロキシル体を合成し、それらをchiral building blockとして利用した。α,β-不飽和ラクタムとα,β-不飽和ラクトンの*cis*-ジヒドロキシル化は高い選択性で進行し、それぞれ 5, 6を与えた。*trans*-α,β-不飽和エステルのcis-ジヒドロキシル化の選択性は高くなかった(7:8=2.5:1)。

hydroquinine誘導体をキラルリガンドとして用いる*trans*-α,β-不飽和エステルのオスミウム酸による重複不斉ジヒドロキシル化では7が98%deにて生成した。一方hydroquinidine誘導体を用いると62%deで8が優位に生成した。また*cis*-α,β-不飽和エステル(9) またはその誘導体(10)を(R)-セリンから合成し、*cis*-ジヒドロキシル化を行うと、そのアリリックストレインのためコンフォメーションが変わり、6および11が優位に生成した(up to 61% de)。以上のように共通の出発物質 1 を用い、種々の立体配置を有するchiral building blockが効率良く得ることができた(Fig. 1)。

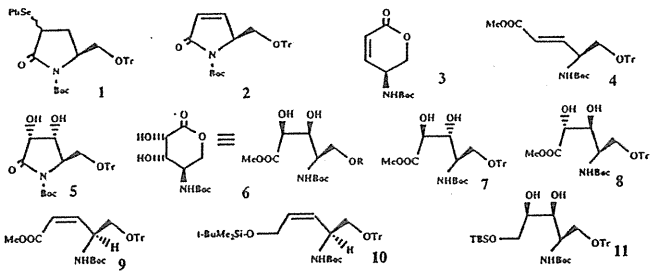

Fig. 1 Synthesis of chiral building blocks

最近、ポリヒドロキシピロリジディンのC-3位にヒドロキシメチル基を有し、さらに5個の連続した不斉炭素を有するアレキシン類が見い出された。そこで新規アレキシン光学異性体を(S)-ピログルタミン酸より合成し、その酵素活性を明らかにし、またこれらはアザシュガーと考えられるので、ヒドロキシルラジカルのような活性酸素に対する消去作用を調べた。

①研究方法および結果

Fig. 2に示すように(S)-ピログルタミン酸よりchiral building block 5 を経て合成した(3R,4R,5R)-N-tert-ブトキシカルボニル-3,4-イソプロピリデンジオキシ-5-トリチルオキシメチル-2-ピロリジノン(12)を水酸化リチウムにて加水分解後、ジアゾメタンにてメチルエステル化し、さらにこのメチルエステルを水素化ほう素ナトリウムにて還元し、1,1-ジメチルエチル N-[(1R,2R,3S)-4-ヒドロキシ-2,3-イソプロピリデンジオキシ-1-(トリチルオキシメチル)ブチル]カルバメート(13)を収率79%で得た。

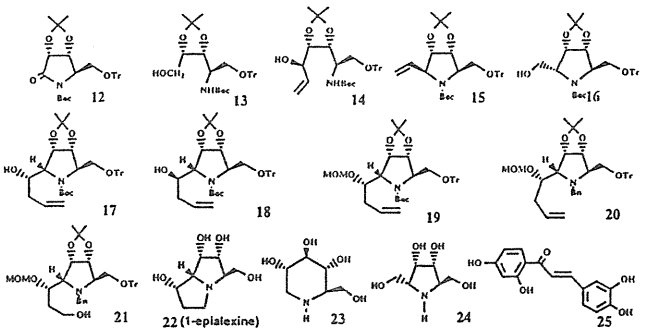

Fig. 2 Synthesis of alexine stereoisomers, 1-deoxynojirimicin, polyhydroxylated pyrrolidine, and hydroxychalcon.

このアルコール体をSwern酸化して対応するアルデヒドに導いた後、-78℃にてビニルマグネシウムブロミドにてビニル化し、1,1-ジメチルエチル N-[(1R,2R,3S,4R)-ヒドロキシ-2,3-イソプロピリデンジオキシ-1-トリチルオキシメチル-5-ヘキセニル]カルバメート(14)のみを収率71%で得た。このアリルアルコール体の水酸基をメシル化後、カリウム tert-ブトキシド処理してピロリジン環に閉環し、(2R,3R,4S,5S)-5-ビニルピロリジン誘導体(15)を収率88%で得た。この末端二重結合をオゾン処理した後、水素化ほう素ナトリウムで還元して(2R,3R,4S,5S)-5-ヒドロキシメチルピロリジン(16) が収率82%で得られた。このピロリジンの一級水酸基をSwern酸化して対応するアルデヒドに導いた後、-78℃にてアリルマグネシウムクロリドにてアリル化し、カラムクロマトグラフィーにて精製すれば、(2R,3R,4S,5S)-N-tert-ブトキシカルボニル-3,4-イソプロピリデンジオキシ-2-トリチルオキシメチル-5-[(1S)- および (1R)-1-ヒドロキシ-3-ブテニル]ピロリジン(17 および18) がそれぞれ収率52%および収率25%で得られた。

主生成物である17の二級水酸基をメトキシメチルエーテル化(19)した後、N-Boc基をN-ベンジル基(20)に変換した(収率48%)。なおMOM体(19)は結晶化し、アリル化反応により新たに生じた不斉炭素の絶対配置をX-線結晶解析にてSと決定した(Fig. 3)。

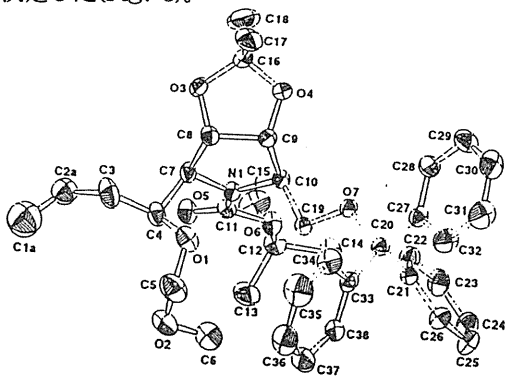

Fig. 3 ORTEP structure of 19

N-ベンジルピロリジン(20)をオゾン処理ならびに水素化ほう素ナトリウム還元を行い21を収率60%で得た。21 をメタンスルホニルクロリドにてメシル化するとメシル体は直ちにピロリジディン骨格に閉環する。このピロリジディンを10% パラジウム-炭素にて接触還元を行いベンジル基を除去し、次に酸にてメトキシメチル基とイソプロピリデン基、ならびにトリチル基を加水分解し、イオンカラムクロマトグラフィー (Dowex 50W-X8 (H^+ form、15 ml)，溶出液：0.6 Nアンモニア水) にて精製し凍結乾燥すれば、1-エピアレキシン(22) が 収率65%で得られた。 またchiral building block 7より1-デオキシノジリマイシン(23) を、16より2,5-ジヒド ロキシメチル-3,4-ジヒドロキシピロリジン(24) を合成した。また2,4-ジヒドロキシアセトフェノンと3,4-ジヒドロキシベンズアルデヒドより2',4',3,4-テトラヒドロキシカルコン(25)を合成した。

②グリコシダーゼ阻害活および抗酸化能評価。

グリコシダーゼ阻害活性は、50mMクエン酸ークエン酸ナトリウム液 (pH 4.8)中、基質に2mM パラニトロフェノール-β-D-グルコピラノシド、酵素に5 mg/ml β-グルコシダーゼ(SIGMA G-4511)を用い、基質200 μl、 各種濃度の阻害剤200 μl、酵素200 μl、を用い、25 ℃ にて15分間インキュベーションした。1N水酸化ナトリウム水溶液(400 μ)を加え

て反応を停止させ、分光計にて400nmの吸収を測定し、各阻害剤の50%阻害濃度を求めた。ポジティブコントロールとして1-デオキシノジリマイシンを用いた。Table 1 に結果を示すがいずれの化合物もIC_{50}は1-デオキシノジリマイシンより低濃度であった。

Table 1 22,23,24のグリコシダーゼ阻害能

化合物	IC_{50}
1-デオキシノジリマイシ(22)	3.0 $x10^{-4}$ M
1-エピアレキシン(23)	2.5 $x10^{-5}$ M
2,5-ジヒドロキシメチル-3,4-ジヒドロキシピロリジン(24)	6.2 $x10^{-5}$ M

抗酸化能の評価はESR-スピントラッピング法で行った。スーパーオキシドの場合はリン酸緩衝液(0.1 ml)、2 mM ヒポキサンチン(HPX, 0.1 ml)、0.5 M DMPO (0.1 ml)、最後に 0.4 unit/ml キサンチンオキシダーゼ (XOD, 0.1 ml) を加え室温でESRの測定を行った。ヒドロキシルラジカルの場合はリン酸緩衝液(0.1 ml)、1mMの銅錯体(0.1 ml)、100mM DMPO (0.1 ml)、最後に100mM 過酸化水素(0.1 ml)を加えESRの測定を行った。抗酸化剤存在下での DMPO-O_2^-体ならびにDMPO-OH体のESRシグナル強度の減少度により、抗酸化剤のO_2^-ならびにヒドロキシルラジカルに対する消去能力として評価した。スーパーオキシドに対する消去能は22, 23, および24では低かったが、25のIC_{50}は13 μMとグルタチオンやビタミンEより強かった。ヒドロキシルラジカルに対するIC_{50}は2, 23, および24では6-8 mMだったが、25では100 μMとグルタチオンより強かった。

(2) 細胞を用いた活性酸素、放射線防御系の解析

① 活性酸素に対する防御系の解析

CHO・K1細胞より活性酸素生成剤であるプランバギンに高感受性を示す変異株を多数分離した。これらは、活性酸素増産剤メチルビオロゲン、DNA架橋剤マイトマイシンCにも交差感受性を示し、前者に対しては、3遺伝子相補群、後者に対しては4群（3群は共通）の存在が確認された。

これらのうち、メチルビオロゲンに最も感受性の高いPb15株は、活性酸素消去能に異常があると考えられたが、SOD, カタラーゼ、グルタチオンペルオキシダーゼの発現（ウェスタンブロット法）は、親株と比べ有意な差はなかった。また、SOD活性、O_2^-の消去能(ESRスピントラッピング法)にも有意な差は認められず、DPPHトラッピング能は減少の傾向が見られた。

② 放射線誘発アポトーシスに対する新規合成抗酸化剤の効果

a, ラット胸腺細胞アポトーシスの阻害

5Gy照射では、4時間後にアポトーシスは約60%に達する。その進行に平行して、細胞体積の減少、クロマチン凝縮やパーオキサイドの産生が認められる。テストした合成抗酸化剤のうちカルコン（25）は、TEMPOLと同様にアポトーシスを抑制し、パーオキサイドの増加も抑制した。ビタミE様抗酸化剤(HTMP : 4-hexyl-2,3,6-trimethylphenol) にも部分的抑制効果が認められた。このテスト系では、グルタチオン, N-アセチルシステインなどの水溶性抗酸化剤は効果がなかった. 細胞膜に対する作用や、細胞内への取り込みが重要と考えられる。

b, L5178Y細胞の放射線照射による致死の抑制

各種の合成抗酸化剤存在下にX線照射した細胞の生存率を、コロニー生成法により調べた。ラジカル消去に必要と考えられる濃度では、薬剤のみで細胞の生存率を下げるものが多く、細胞系への総合的評価には、多くの系でのテストが必要と考えられる。テストした合成酸化剤の中では、HTMPはL5178Y細胞に対する毒性が低く、またX線に対する生存率を増加させた。

③ 細胞の増殖と死の制御（放射線誘発アポトーシスのシグナル伝達と放射線抵抗性の誘導）

a, X線高感受性マウスリンパ腫細胞3SBのX線誘発アポトーシスシグナル伝達を解析し、PKCの関与が示唆された。

b, X線繰り返し照射によるX線抵抗性株の分離とその抵抗性を解析し、X線感受性（抵抗性）は、セラミドやダウノルビシン感受性と平行しており、抵抗性に関与していると考えられる遺伝子の発現解析などから、細胞膜を経るシグナル伝達が3SB細胞のアポトシスの初期過程には重要と考えられた。

(3) パーオキシナイトライト(peroxynitrite) に対する防御物質の開発に関する研究

一酸化窒素とその酸化活性種である活性窒素種が酸化的ストレスによる障害に関与していることが報告されている。活性窒素種のなかでパーオキシナイトライトは生体内においてはスーパーオキシドと一酸化窒素から生成する化合物で非常に高い酸化活性を有する。ストレス付加時には生体内でスーパーオキシドと一酸化窒素がある程度多量に、また同時に産生されてると考えられ、パーオキシナイトライトが生成している可能性が高い。このことからパーオキシナイトライトはlow-density lipoprotein (LDL) oxidation, 脂質の過酸化、DNA strand breakageなどを通して様々な疾患に関わる可能性が指摘されている。さらにパーオキシナイトライトの特徴的な反応としてあげられるのがTyr残基のニトロ化である。ニトロ化によって生じるニトロチロシンはパーオキシナイトライトによりその部位で酸化的障害が引き起こされているマーカーとなるほか、機能タンパク質のTyr残基がニトロ化されること自体がリン酸化等の障害となって毒性を発揮しているとも考えられる。そこで、ニトロ化反応と酸化反応それぞれに対する防御化合物として合成抗酸化剤や天然の抗酸化物質を比較検討し、パーオキシナイトライトによる生体障害に有効な抗酸化剤を探索した。ニトロ化物として3-nitro-L-tyrosineを、酸化生成物としてdityrosineを指標に抗酸化剤の効果を検討した。Fig.4に使用した抗酸化剤を示す。

①研究方法

a, パーオキシナイトライトの調整

パーオキシナイトライトは過酸化水素と亜硝酸ナトリウムを酸性条件下反応させることにより調製した。反応液は

直ちにアルカリ性にして低温保存した。濃度は300nm付近の極大吸収の吸光度より決定し使用直前に0.01N水酸化ナ

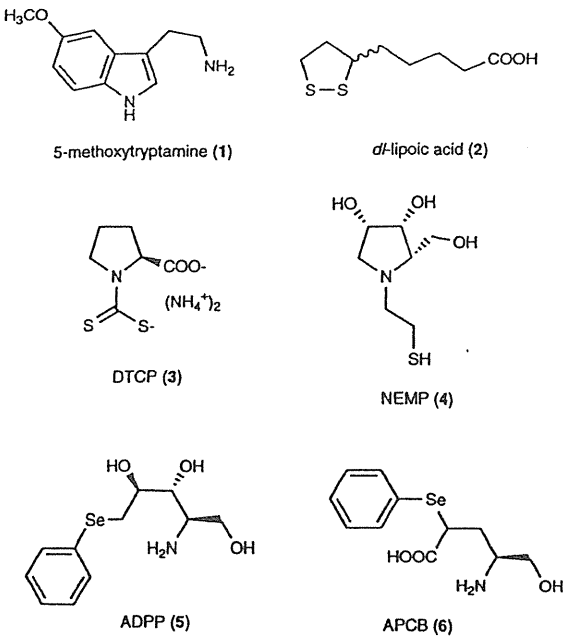

Fig. 4 Structures of Tested Compounds

The structures of endogenous and synthetic compounds used here are shown, except melatonin, serotonin, glutathione and L-cystine.

トリウム水溶液を用いて目的の濃度に希釈した。反応系中には未反応の過酸化水素と亜硝酸塩が残留しているが、対照実験を行いこれらの残留物はチロシンのニトロ化とdityrosineの生成に影響しないことを確認した。

b, パーオキシナイトライトとL-Tyrosineの反応

L-tyrosine(0.5 - 2mM)の緩衝液溶液とパーオキシナイトライトの10mM NaOH溶液をstopped flow反応装置で等量混合し200msec後までの355nmの吸光度をモニターした。得られた吸光度変化から反応初速度を求めた。次にL-tyrosine (final 0 - 2 mM)をpH7.4の緩衝液中パーオキシナイトライト(final 0 - 8 mM)と37℃で10分間反応させ、内部標準物質としてp-fluorotyrosineを加え(final 0.91 mM)、逆相HPLCを用いて分析した。3-nitro-L-tyrosineを274nmの吸光度で、dityrosineを励起波長295nm蛍光波長410nmの蛍光で測定した。なお標品のdityrosineは、pH9.5の緩衝液中、Horseradish peroxidase存在下L-tyrosineと過酸化水素を37℃で反応させ調製した。またニトロ化反応に及ぼすpH変化(7.4, 9.5, 11.5)の影響を調べた。

c, パーオキシナイトライトに対する阻害剤の防御能評価

種々の濃度の阻害剤 (0 mM - 2mM)存在下、L-tyrosine (final 1mM)をpH7.4の緩衝液中パーオキシナイトライト (final 0.2 mM)と37℃で10分間反応させ、内部標準物質としてp-fluorotyrosineを加え(final 0.91 mM)、HPLCにて3-nitro-L-tyrosineとdityrosineを分析した。阻害能はIC_{50}として算出した。

d, Tyrosyl RadicalのESRスピントラッピング

DMPO (90mM)をpH9.5緩衝液中でパーオキシナイトライトと室温で混合し、パーオキシナイトライトから由来するラジカルをESRにて測定した。また、L-tyrosine と2-methyl-2-nitrosopropane (MNP)の混合液中にパーオキシナイトライトを加え、直ちに室温でESRスペクトルを測定し、L-tyrosine とパーオキシナイトライトの反応から生成するラジカル種を観測した。

e, パーオキシナイトライトによるPlasmid DNA Strand切断と5-methoxytryptamine(5-MT)の防御効果

Plasmid pBR322(0.05 mM)をPBS中にて5-MT存在あるいは非存在下、60秒間パーオキシナイトライト(final 0.05 - 2.5 mM)処理し、2%アガロースゲルで電気泳動し、ethidium bromideにて染色しUV luminometerを用いて検出した。

②結果

a, 3-nitro-L-tyrosineの生成についてstopped flow法を用いて検討した結果、両者は速やかに反応し、生成速度はパーオキシナイトライト及びL-tyrosine量にほぼ比例していた。この条件で二次反応速度定数は約$3.6 \times 10^2 M^{-1}sec^{-1}$と求められた。また、パーオキシナイトライトを分解した対照実験から、この反応は残留する過酸化水素や亜硝酸塩によっては進行せず、パーオキシナイトライトによって起きることが確かめられた。

b, パーオキシナイトライトとL-Tyrosineの反応においてpH変化を調べた結果、高いpHでは3-nitro-L-tyrosineの生成は抑制されていた。このことはパーオキシナイトライトとL-Tyrosineの反応はパーオキシナイトライトのプロトン化した形で反応していることを意味している。

c, 各種抗酸化化合物について、3-nitro-L-tyrosine、dityrosineそれぞれに対する生成阻害能を検討した。その結果、Fig.5およびTable 2 に示したように3-nitro-L-tyrosineについては天然化合物でglutathione、lipoic acid、melatoninに強い生成阻害活性が、5-methoxytryptamine

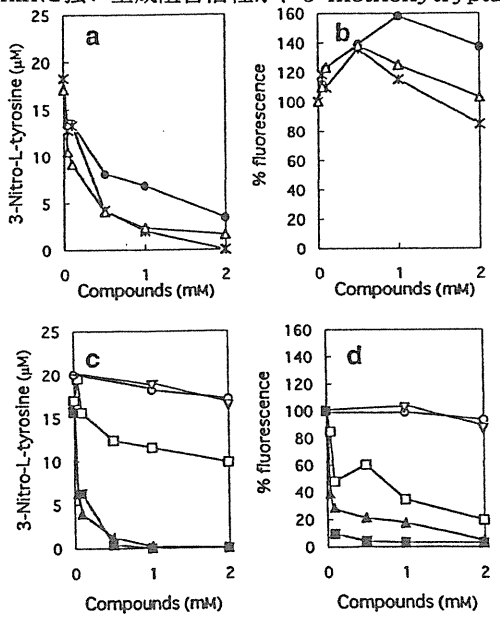

Fig. 5. Inhibitory Effects of Endogenous Compounds and DMPO on the Formation of 3-Nitro-L-tyrosine and 2,2'-Dityrosine by PN

PN and L-tyrosine were mixed in sodium phosphate buffer at pH 7.4 in the presence of various concentrations of test compounds. The formation of 3-nitro-L-tyrosine and 2,2'-dityrosine in the reaction mixture was detected. panel a and c: formation of 3-nitro-L-tyrosine, panel b and d: percent change of 2,2'-dityrosine fluorescence at 410 nm (ex. 295 nm). closed circles: 5-MT, asterisks: melatonin, open triangles: *dl*-LA, open squares: L-cystine, closed triangles: glutathione, closed squares: serotonin, open circles: DMPO, inverted triangles: PBN.

で中程度の生成阻害活性が見られた。また含硫黄化合物であるDTCPやポリアミノチオール誘導体であるNEMPで強い活性が見られた。dityrosineについては、glutathioneで強い活性が見られ、lipoic acid、melatonin, 5-methoxy-tryptamineではむしろ生成量が増加した。DTCP、NEMPでは強い生成阻害活性を示した。これに対しDMPOやPBNなどのスピントラップ剤では阻害効果はほとんど見られなかった。

Table 2 Inhibitory Effects of Endogenous and Synthetic Compounds on 3-Nitro-L-Tyrosine and 2,2′-Dityrosine Formation

Compound	IC_{50} value (mM)	
	3-Nitro-L-tyrosine	2,2′-Dityrosine
Glutathione	0.04	0.042
Serotonin	0.08	0.055
L-Cystine	—a)	—b)
5-MT (1)	0.44	—c)
Melatonin	0.29	—c)
dl-LA (2)	0.15	—c)
DTCP (3)	0.032	0.035
NEMP (4)	0.038	0.038
ADPP (5)	1.53	0.15
APCB (6)	0.50	0.37

a) The compound did not inhibit the formation more than 50%. *b*) The IC_{50} value was not calculated. *c*) The formation of 2,2′-dityrosine was enhanced.

d, この反応にラジカル種が関与しているかを検討するため、2種のスピントラップ剤を用いてスピントラッピングを行った。L-tyrosineを用いずパーオキシナイトライトのみでDMPOによるスピントラッピングを行うと、超微細結合定数がa_N=14.0G、a_H=14.0Gの4本線のシグナル(1:2:2:1)が得られ、このシグナルは速やかに減衰した。これはDMPO-OHアダクトに類似しており、これまで報告されているものと同様の結果であった。次にMNPによるスピントラッピングを行い、超微細結合定数がa_N=15.8Gの3本線のシグナルが得られ、これはtyrosyl radicalの1位にMNPが結合したスピンアダクトであった。

e, plasmid pBR322 のパーオキシナイトライトによる切断実験では、使用するパーオキシナイトライトの濃度依存的にOC(open-circular form, single strand scission) とLN(linear form, double strand scission)は増加した(Fig. 6)。しかしFenton反応の系ではほとんどSC(super coiled form) が検出されずOCとLNに切断されるの対し、パーオキシナイトライトの系では相対的な切断能は弱かった。5-MTの添加は大量に加えた場合にわずかに防御効果がみとめられたが、ほとんど切断を防がなかった。このことは、パーオキシナイトライトによるDNA鎖の切断がヒドロキシルラジカルのような活性酸素によるものであることを示している。しかしスピントラップ剤の実験結果よりパーオキシナイトライトはそれほど大量のヒドロキシルラジカル、あるいはその等価体を生成していない。

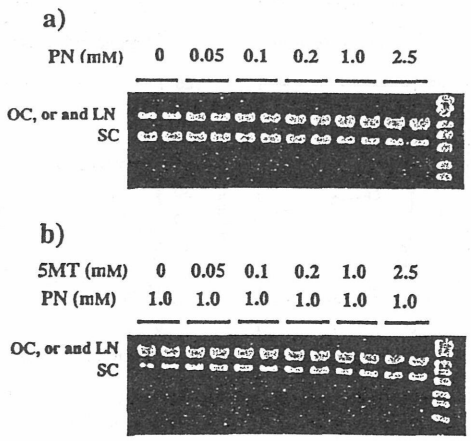

Fig. 6. Effect of 5-MT on the Plasmid DNA Scission by PN

Plasmid DNA pBR322 treated with PN was analyzed in the presence (a) and absence (b) of 5-MT by agarose gel electrophoresis and ethidium bromide staining. Three forms of pBR322 plasmid DNA, SC, OC and LN, were detected using a UV luminometer.

②考察

パーオキシナイトライトとL-tyrosineの反応でpHの低下に伴い3-nitro-L- tyrosineの生成量が増大すること、塩基性でパーオキシナイトライトが安定であることから、反応にはperoxynitrous acid(O=N-OOH)が関与していると考えられる。天然及び合成抗酸化剤を用いた3-nitro-L-tyrosine及びdityrosine生成の阻害実験で、チオール基及びdithiocarbamate基を有する化合物（glutathione、DTCP、NEMP）がパーオキシナイトライトの酸化活性・ニトロ化活性に対し有効に防御することが示された。また、lipoic acid、melatonin、5-methoxy- tryptamineにおいては3-nitro-L-tyrosineの生成のみを阻害してdityrosineの生成はむしろ増加させたことから、これらの化合物はL-tyrosineのニトロ化のみを選択的に阻害することが示された。ESRスピントラッピング法を用いた実験から、L-tyrosineとperoxynitriteの反応にはパーオキシナイトライト由来のhydroxyl radical様活性種、及びtyrosyl radicalが関与していることが示された。従って、tyrosineはhydroxyl radical様活性種でtyrosyl radicalとなった後、2分子が会合してdityrosineを、二酸化窒素ラジカルが付加して3-nitro-L-tyrosineを生成すると考えられる。しかしこの反応機構からはtyrosineのニトロ化のみを選択的に阻害する化合物の存在を説明しにくく、またラジカル捕捉剤であるDMPOやPBNが、他の抗酸化化合物に比べ生成阻害活性が非常に弱かったことから、L-tyrosineとパーオキシナイトライトの反応においては、ラジカル様活性種の反応の寄与は多くなく、親電子的な付加反応による生成が寄与している可能性が考えられた。

2. 生体内一酸化窒素検出用スピントラップ剤の開発

一酸化窒素（NO）は、血管平滑筋弛緩、神経伝達、ならびに興奮性細胞毒性など重要な生体反応に関与することが報告されている内因性の化合物である。化学的には低分子（分子量30）でラジカルであり、酸素分子と速やかに反応するなど比較的高い反応性を有し、不安定で短寿命な物質である。従って生体内NOの測定は難しく、現在のところ決定的な方法はなく、Griess法、化学発光法、電極法、生体内のnitrosyl Hbを測定する方法などが用いられている。これに対し、ESRスピントラッピング法は不安定ラジカル

種を測定する有効な手段の一つであり、不安定なラジカルをスピントラップ剤と反応させて安定なラジカル化合物へ導き、このESRシグナルを測定することで間接的に不安定ラジカルを測定する方法である。

NOは不安定な短寿命ラジカルであり、ESRスピントラッピング法による検出を検討した。NOのスピントラップ法に関しては、現在までにいくつかの報告がなされ、生体内で生成するNOの測定に応用した例もある。また生体内のHbに付加したNOを測定する方法もスピントラッピングの一種と考えることができる。しかし、そこで用いられているスピントラップ剤は非常に種類が少なく、特に生体系に応用可能であると考えられる水溶性のスピントラップ剤についてはFe(MGD)$_2$およびFe(DTCS)$_2$の２種が報告されているのみである。また体内動態に関しては特に肝臓に蓄積しやすいことが知られている。そこで生体内一酸化窒素の発生部位や挙動、および役割を探るうえで体内動態等の異なるスピントラップ剤を見出だすべく研究を行った。

(1)スピントラップ剤の合成(Fig. 7)

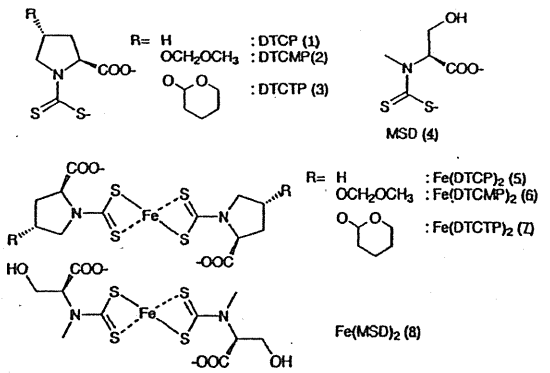

Fig. 7 Structures of synthesized dithiocarbamates and their iron complexes.

水酸基を有するアミノ酸は、その水酸基の修飾により種々の誘導体の合成が可能なため、L-プロリン、4位に水酸基を持つL-ヒドロキシプロリン、ならびに水酸基を有するセリンを用いて、dithiocarboxy基導入後、その鉄錯体を合成した。常法により得られるN-ベンジルオキシカルボニル-(2S,4R)-4-ヒドロキシ-2-ピロリジンカルボン酸ベンジルエステル、またはN-メチルベンジルオキシカルボニル-(S)-セリン メチルエステルをメトキシメチルエーテル化(MOM化)、あるいはテトラヒドロピラニル化(THP化) 後、生成したO-アルキルアミノ酸誘導体を水素-パラジウム炭素を用いる接触還元にて N-ベンジルオキシカルボニル基およびベンジルエステル基を除去してO-アルキルプロリン誘導体に導いた。一方、N-メチルベンジルオキシカルボニル-O-メトキシメチル-(S)-セリン メチルエステルをアルカリにてメチルエステルを加水分解した後、パラジウム炭素-水素により接触還元を行い、N-メチル-O-メトキシメチル-(S)-セリンを得た。これらをアンモニア水中で二硫化炭素と反応させて対応するジチオカルバメートアンモニウム塩((DTCP(1)、DTCMP(2)、DTCTP(3), MSD(4)) を合成した。これらのジチオカルバメート体はさらにトリス塩酸バッファー(40mM, pH 7.4) 中アルゴン気流下、硫酸鉄と反応させて鉄錯体 (Fe(DTCP)$_2$ (5)、Fe(DTCM)$_2$P (6)、Fe(DTCTP)$_2$ (7)、 Fe(MSD)$_2$ (8)) を得た。

(2) (S)-ヒドロキシプロリン誘導体ジチオカルバメート-鉄錯体、ならびにN-メチル-L-セリンジチオカルバメート- 鉄錯体の一酸化窒素捕捉能

水溶液中における各錯体の一酸化窒素捕捉能をESRスピントラッピング法を用いて検討した。一酸化窒素の水溶液を、嫌気下40mMのトリス塩酸バァファー(pH 7.4)中に一酸化窒素ガスを 吹き込んで作製した。その濃度はグリース法にて定量した。種々の濃度の一酸化窒素水溶液を0.5mMのヒドロキシアミノ酸誘導体ジチオカルバメート- 鉄錯体に加え、生成する一酸化窒素付加体をX-band ESRにて測定した。Fig. 8に6、7、および8を用いた結果を示す。いずれの錯体も一酸化窒素濃度に比例して付加体生成曲線を与え、各錯体間においてその差は少なく、効率良く一酸化窒素を捕捉することが判 明 した。

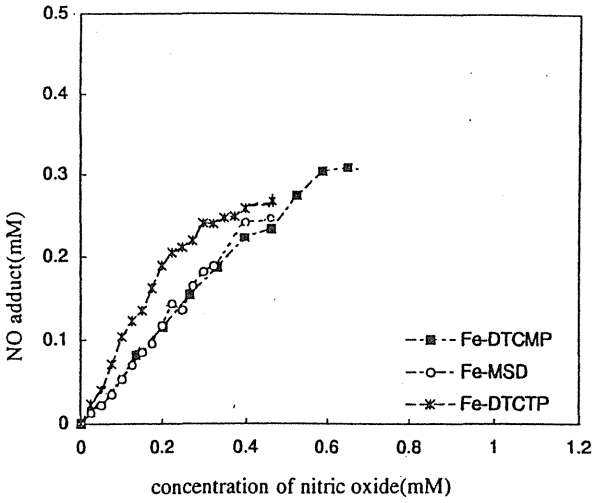

Fig. 8 Trapping ability of Fe(DTC)$_2$ for nitric oxide

(3)鉄錯体- 一酸化窒素付加体の in vivo ESR 測定

DTCMPの鉄錯体溶液 (6) に嫌気下一酸化窒素ガスを吹き込み一酸化窒素付加体を得る。この一酸化窒素付加体をマウスに静脈投与(50 mM溶液を200μl)し、腹部のESRスペクトルをL-band ESR装置を用いて測定すると、一酸化窒素付加体 のシグ ナルが30 分以上にわたって検出され、一酸化窒素付加体はマウス体内で比較的安定に存在することが示された。また、Fe(DTCMP)$_2$の一酸化窒素付加体はこれまで報告されているFe(DTCS)$_2$の一酸化窒素付加体と同等のシグナル強度を有していた。

(4) LPS (リポポリサッカライド) にて誘導されたマウスの一酸化窒素のスピントラッピング

リポポリサッカライド (LPS, E.coli 026:B6) を静脈内投与(20 mg/Kg)したマウス (ICR(雌, 5 週齢)、または ddY(雌、5 週齢)) に6時間後、Fe(MSD)$_2$(8) 溶液を静脈内投与 (0.42 mM/Kg)した。投与後２時間してL-band ESRにて、マウス生体内に発生した一酸化窒素を非侵襲的に測定した。このシグナルのS/N比は従来用いられているスピントラップ剤であるFe(MGD)$_2$ よりも優れていた。Fig. 9に示すように一酸化窒素付加体のシグナルを効率良く検出した。一方、鉄錯体の体内動態を調べるためLPS投与して

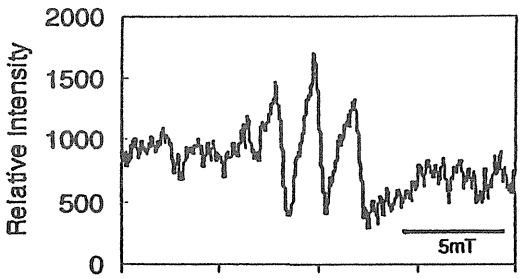

Fig. 9 In vivo ESR spectrum of nitric oxide trapped by Fe(MSD)2 in the body of LPS-treated mouse.

To the ICR mice (5w, female) which were treated with LPS (E. coli 026B6, 5 or 10mg/kg i.v.) 5 hr before, the synthesized Fe(MSD)2 and Fe(MGD)2 (110mg/kg as iron) were injected subcutaneously. The spectra of the mouse body (upper abdomen) were measured 2 hr after the treatment of the iron complex using a low frequency ESR spectrometer with a loop-gap resonator.

6時間後、種々の鉄錯体 ($Fe(DTCMP)_2$ (6), $Fe(DTCTP)_2$ (7)、および $Fe(MSD)_2$(8)) を投与 (0.42 mM/Kg)し、30分後に血液をヘパリン処 理済みのキャピラリーに採取しX-band ESRで一酸化窒素付加体を測定した。また肝ホモジネートを調製し同様に測定した。 Fig. 10に示すように

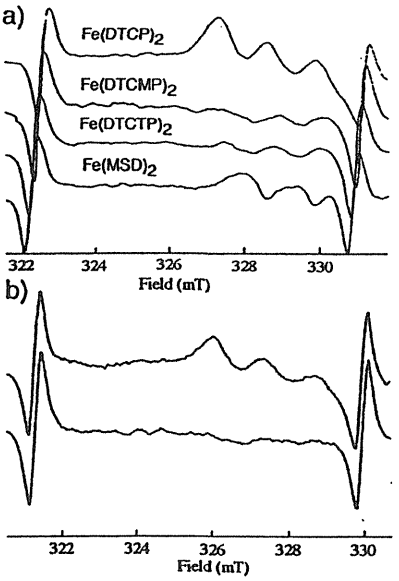

Fig. 10 ESR spectra of nitric oxide adducts of Fe(DTC)2 derivatives in LPS-pretreated mouse blood.

The spectra were modified by the computer using the smoothing method for excluding noises. Fe(DTC)2 derivatives as spin traps were injected intravenously to the mice (ddY, male, 5w) which had been pretreated with lipopolysaccharide (LPS, E.coli 026:B6, 250mg/kg) intravenously. The collected blood was measured with 9.5GHz ESR spectrometer within 6 min at the following settings; microwave frequency and power 9.43GHz/10mW, scan range 10mT, modulation frequency and range 100kHz/0.125mT. a); ESR spectra were measured at 5.5 hr after LPS treatment and at 0.5 hr after the injection of Fe(DTC)2 derivatives. b); Spectra from Fe(DTCP)2-injected mice (upper) and from L-NMMA- and Fe(DTCP)2-injected mice (lower) after LPS-treatment.

一酸化窒素付加体が観測された。なおこのシグナルは、一酸化窒素合成酵素(NOS)の阻害剤であるN^G-モノメチル-(S)-アルギニン((S)-NMMA)を投与しておくと観測されないので、このシグナルは一酸化窒素由来であることを確認した。またTable 3に血液中と肝臓中の相対的シグナル強度、ならびに肝ホモジネート中と血液中のシグナル強度比を示す。このシグナル強度比を図示したのがFig. 11であり、これまで知られている錯体である $Fe(MGD)_2$ と同様に、$Fe(DTCTP)_2$と$Fe(MSD)_2$の一酸化 窒素付加体は主として肝臓において検出された。特に$Fe(MSD)_2$の一酸化窒素付加体のシグ ナル強度は大きかった。これに対して $Fe(DTCMP)_2$ の一酸化窒素付加体のシグ ナルは肝臓中にはほとんど検出されず、血液中に見出された。この結果から $Fe(DTCMP)_2$ は血管中において発生した一酸化窒素を捕捉しているという特徴を有していることが判明した。

Table 3 Relative signal intensity of nitric oxide adducts in mouse liver and blood after LPS-treatment

$Fe(DTC)_2$	liver	blood	liver/blood ratio
$Fe(DTCP)_2$	0.70	0.37	1.89
$Fe(DTCMP)_2$	0.04	0.11	0.364
$Fe(DTCTP)_2$	0.77	0.11	6.81
$Fe(MSD)_2$	4.09	0.2	20.9

The liver/blood ratio was the average of two or three samples. Signal intensities were measured in mouse liver homogenate and blood at 0.5 hr after intravenous injection of $Fe(DTC)_2$ and at 5.5 hr after LPS treatment.

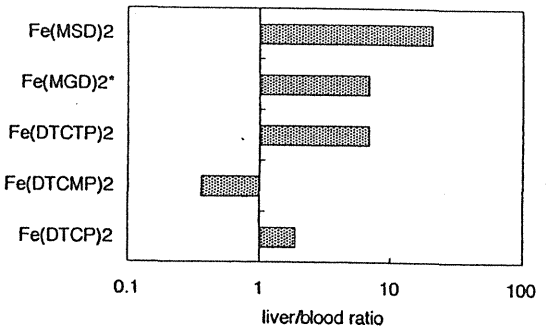

Fig. 11 Ratio of the amount of nitric oxide adducts between the liver and the blood of LPS-treated mouse.

The ratio between the liver and the blood was calculated by dividing the relative signal intensities in the liver by that in the blood. The ratio of Fe(MGD)2 (asterisked) was calculated from the result of a subcutaneous administration given in the literature (17). When Fe(MGD)2 was injected intravenously, the ratio was larger than that in the case of subcutaneous injection.

(5) 考察

LPS処理したマウスの生体ないで生成する一酸化窒素のスピントラップにおいて、用いた各錯体間でNO付加体が異なる血中濃度および異なる肝ホモジネート／血液比を示したことから、これらの錯体がマウス体内で異なる挙動を示すことが示された。特に$Fe(DTCMP)_2$ に関しては、1) 肝臓より血液中にて検出されること、2) LPSにて処理したマウスの肝臓ホモジネートと$Fe(DTCMP)_2$ をincubationした後、この錯体の一酸化窒素捕捉能を調べるとその捕捉能に変化なく一酸化窒素を捕捉すること、3) $Fe(DTCMP)_2$ の一酸化窒素付加体を静注しても肝臓では検出されないこと、4) 尿中には一酸化窒素付加体が検出されないこと、以上から血液中に生成した一酸化窒素を検出していると考えられる。

3. ESR用新規flow型石英cuvetteを用いるGlioma細胞のスーパーオキシド産生

スーパーオキシドと一酸化窒素は内在性のラジカル種で、炎症において防御因子として機能するほかシグナル伝達においても重要な役割を果たしている。最近それらが神経変性疾患に関連することが報告されている。抹消組織におけるマクロファージのような免疫細胞と同じように脳におけるグリア細胞は、感染や酸化的ストレスに対して防御的に働くと考えられている。一酸化窒素とスーパーオキシドの

産生はサイトカインやエンドトキシン処理により誘導される。しかし細胞においてスーパーオキシドや一酸化窒素の産生を測定しようという試みは少なく、発色法や電極法などによってわずかの例が報告されているのみである。前者は感度的に低く後者は電極を作るのに特別なテクニックを必要とする場合がある。一方ESRは生体内のラジカルを検出する有用な方法である。本研究では、U87 Glioma細胞におけるスーパーオキシドや一酸化窒素の産生を、ESRを用いスーパーオキシドに関してはニトロキシドスピンプローブのスーパーオキシドによるシグナル強度の減衰を、また一酸化窒素に関しては、スピントラッピング法により測定した。ESR測定には、特に接着細胞など培養プレートから細胞を分離するなどの操作によるストレスの影響を排除するため新たに考案したFlow型の石英cuvetteを用いて行った。

(1) 研究方法および結果

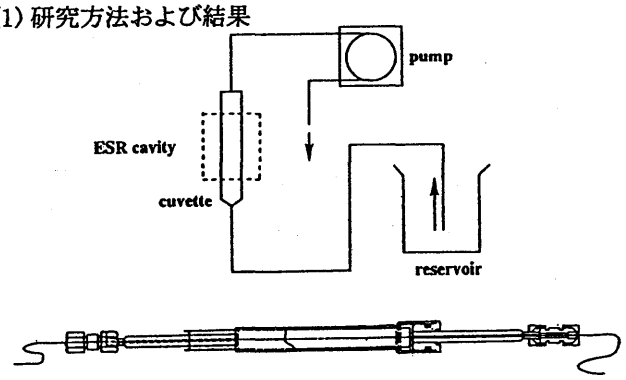

Fig. 12 The structure of the new flow-type quartz cell and a diagram of the ESR measurement system.

①スーパーオキシド産生能の定量的評価

U87 Glioma細胞をスライドグラス上で培養した後Flow型の石英cuvetteに直接挿入し、ESRスペクトルを測定した。。ESR測定系のflow systemはFig. 12 に示したように、石英cuvetteは37℃に暖められたreservoir tankに繋げられており、ペリスタポンプにてドレインされる。2 mlの7 mM TEMPOLをcuvetteに導入し、ESRスペクトルを1 5分毎に測定した。TEMPOLの低地磁場側のMnOシグナルに対する相対的な強度を時間軸に対してプロットする。またLPS(500 ng/ml)/INF-γ (150 units/ml)にて2 4時間処理したU87 Glioma細胞をSOD(100 units/ml)およびカタラーゼ(10 units/ml)存在または非存在下ESRスペクトルを測定した。U87 Glioma細胞とのTEMPOLシグナル強度は、擬一次反応速度で減少する(Fig. 13)。U87 Glioma細胞がなければシグナル強度は一定である。一方、LPS/INF-γにて2 4時間処理したU87 Glioma細胞のTEMPOLシグナル強度の減衰速度は加速された。(Fig. 13, Fig. 14) 見かけのTEMPOLシグナル強度の減衰速度定数は、LPS/INF-γにて処理しない場合　3.05×10^{-3}/min/10^6 cellであり、LPS/INF-γにて処理した場合6.14×10^{-3}/min/10^6 cellであった。この減衰速度の加速はSOD とcatalaseの添加により抑えられた。見かけの擬一次反応速度定数はSODおよびcatalase存在下LPS/INF-γにて処理したU87 Glioma細胞の場合3.39×10^{-3}/min/10^6 cellであった。SODおよびcatalase存在あるいは非存在下の見かけの反応速度定数の違いからTEMPOLとスーパーオキシドのシグナル減衰速度は2.75×10^{-3}/min/10^6 cellと算出される。TEMPOLとスーパーオキシドの反応速度定数は3.90×10^{-7} $M^{-1}min^{-1}$であるから、LPS/INF-γにて処理したU87 Glioma細胞に生成したスーパーオキシドの濃度は70.5 pM/10^6cellであった。

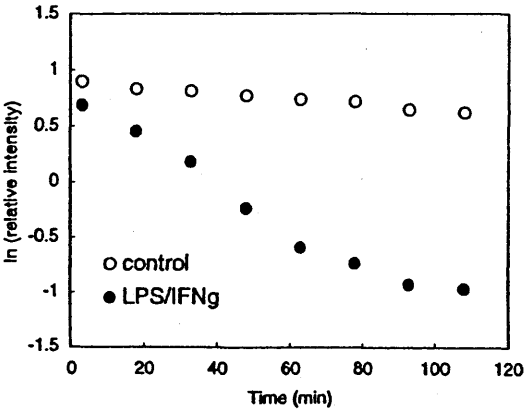

Fig. 13 ESR signal decay of TEMPOL with U87 glioma cells
The time course of the relative signal intensity measured at 15-min intervals

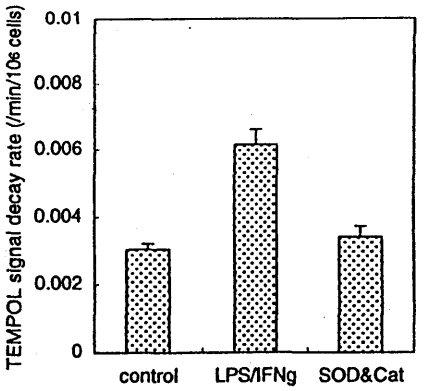

Fig. 14 Signal decay rate of TEMPOL by U87 glioma cells ESR spectra of the TEMPOL solution (the initial concentration is 7 μM) with U87 glioma cells on a quartz glass plate were obtained at 15 min intervals. The signal decay rate of TEMPOL with U87 glioma cells was calculated by measuring the decrease of ESR signal intensities of TEMPOL with U87 glioma cells treated with LPS/IFN-γ in the presence or absence of SOD and Cat. Values are presented as the mean ± S.E.M. of 3–5 experiments. One-way ANOVA indicated significant differences between groups ($P < 0.05$).

②一酸化窒素産生能のスピントラッピング法による評価

U87 Glioma細胞の培養スライドグラスをflow型の石英cuvetteに挿入し、Hank's balanced bufferで洗浄する。2mlの10mM Fe-DTCSまたはFe-MGD (0.25 Mグルコースを含むtris-HClバッファー中) をcuvetteに導入し、SODの存在または非存在下、ESRスペクトルを8分間隔で測定した。またLPS(500 ng/ml)/INF-γ (150 units/ml)で24時間前処理したU87 Glioma細胞の一酸化窒素の産生に対する効果を調べた。LPS/INF-γで前処理したU87 Glioma細胞ではFe-DTCSを用いた場合traceの一酸化窒素付加体のシグナルが最初のスキャンで観測された。しかしそれ以降は観測されなかった。SOD存在下においても同様の結果が得られた。Fe-MGDを用いた場合 一酸化窒素付加体のシグナルは検出されなかった。

③培養液中のNO_2^-/NO_3^-の濃度

LPS(500 ng/ml)/INF-γ (150 units/ml)で24時間前処理したU87 Glioma細胞の培養液中のNO_2^-//NO3-の濃度を

NO_2^-/NO_3^- detection kit Fにて測定した。培養液を取り15分室温で遠心(1000 xg)後、80 μlの上清を37℃でnitrate reductaseとco-enzymeで一時間処理し、さらに酸性条件下、2,3-diaminonaphtaleneと室温15分反応させた。水酸化ナトリウムで中和後、naphtalenetriazoleからの蛍光をプレートリーダーで測定した。NO_2^-/NO_3^-の濃度はLPS/INF-γ で24時間前処理しても変化せず、L-N-monomethylarginineによって減少した(Fig. 15)。したがって一酸化窒素は産生しているがLPS/INF-γによって誘導されたものではないことが明らかになった。

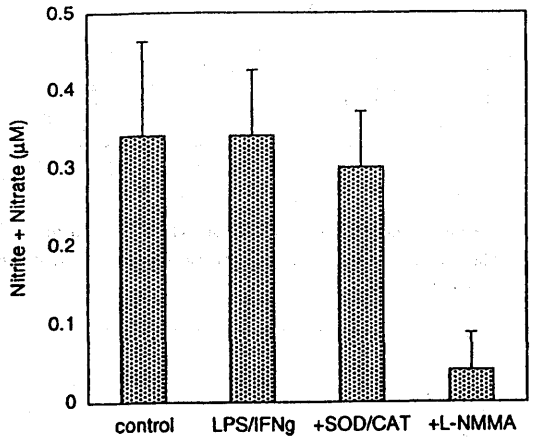

Fig. 15 Concentration of nitrite and nitrate in the culture media of U87 cells treated with LPS and IFN-γ. U87 cells at 7.3×10^4 cells per well were treated with LPS/IFN-γ for 24 h in culture media without serum and phenol red. After a reduction of nitrate to nitrite with nitrate reductase and a reaction with 2,3-diaminonaphtharene under acidic conditions, the concentration of nitrite in 80 μl of the media was evaluated by measuring the fluorescence intensity at 460 nm (excitation at 355 nm). Values are presented as the mean± S.E.M. of 10 samples.

(2) 考察

スーパーオキシドと一酸化窒素のU87グリオーマ細胞からの産生を接着細胞のために考案したFlow型の新規cuvetteを用い接着細胞を培養プレートから分離することなくESRにて測定した。この新しいシステムはトリプシン処理や物理的にプレートから細胞を剥がすなどのストレスを与えることなくESRを測定することを可能にした。スーパーオキシドの産生を評価するために、TEMPOLのシグナルの減衰速度をSODとCatalase存在あるいは非存在下でESRにて測定した。減衰速度はLPS/INF-γ にて処理した細胞では加速し、その加速はSODとCatalase存在下抑えられた。この結果から、スーパーオキシドの産生はLPS/INF-γ による前処理により誘導されたと考えられる。TEMPOLのようなニトロキシドスピンプローブはスーパーオキシドスカベンジャー、またはSOD-mimicとして働くということが報告されている。従って、TEMPOLがスーパーオキシドにより酸化されてオキソアンモニウムカチオンになり、それが順にスーパーオキシドを酸素分子に酸化する。この反応においてはTEMPOLは触媒的にスーパーオキシドと反応するためTEMPOLのシグナル強度はスーパーオキシドによって減少しないかもしれない。しかし、本研究ではTEMPOLがスーパーオキシドに比較して大過剰存在するためスーパーオキシドとオキソアンモニウムカチオンの反応が無視でき、触媒的反応が抑制されてシグナル強度はスーパーオキシド産生に従って減少する。シグナル強度の減衰はスーパーオキシドの産生量を反映すると考えられる。

LPS/INF-γで前処理した細胞とTEMPOLの減衰速度はSOD存在下コントロールの反応速度と同じレベルまで下がるが、TEMPOLのシグナル自体はそれでも減衰する。このゆっくりした減衰は、TEMPOLを含むニトロキシドスピンプローブを還元する生体のreductantsに基づくと考えられる。U87 glioma細胞では、LPS/INF-γで前処理によって一酸化窒素の産生誘導は検出されなかった。ESRスピントラップ法、NO_2^-/NO_3^-の蓄積を測定する方法、いずれによってもLPS/INF-γ前処理による一酸化窒素の誘導は観察されなかった。L-N-monomethylarginine(L-NMMA)を添加することによりNO_2^-/NO_3^-量は減少したことから、微量の一酸化窒素化が無刺激のU87 Glioma細胞で産生されていることが示された。これは、constitutive NO synthaseによる一酸化窒素生成を反映している可能性がある。最近一酸化窒素はいくつかの悪性Glioma細胞において一酸化窒素の誘導能（あるいは誘導型一酸化窒素合成酵素の誘導）が見られないという報告がされている。LPS/INF-γによる一酸化窒素産生誘導能の欠如はU87 Glioma細胞のtumorigenic natureとよい整合性がある。

III. 結論

生体制御物質として、グリコシダーゼ阻害作用を有するポリヒドロキシアミン類の効率的な合成法を確立した。またスーパーオキシドやヒドロキシルラジカルに対する抗酸化剤としてヒドロキシルカルコンを、パーオキシナイトライトに対する防御物質としてポリヒドロキシアミノチオールを開発した。また、パーオキシナイトライトの反応機構について、パーオキシナイトライトのニトロ化と酸化反応のなかでニトロ化のみを阻害する物質を初めて見出し、ラジカル様の活性種のほかに、親電子的なニトロニウムカチオン(NO_2^+) のような活性種の関与を示した。

水酸基を有するアミノ酸であるL-ヒドロキシプロリンやL-セリン誘導体のジチオカルバメート体を合成し、その鉄錯体を生体内で発生する一酸化窒素をESRにて検出するためのトラップ剤として開発した。特に$Fe(MSD)_2$ は、LPS処理したマウスのL-バンドESR (in vivo ESR) にて、腹部に強い一酸化窒素付加体のシグナルを与えた。また$Fe(DTCMP)_2$ は、血管で発生する一酸化窒素を測定できる可能性を示した。

新規Flow型のESR用石英cuvetteを利用して、接着細胞をESR測定するのに適した、新しい測定系を構築した.このESR測定システムは、培養プレートから細胞を分離するなどのストレスを排除して、細胞系のESRを測定することを可能とした。これは、酸化的ストレス等のストレスを負荷する細胞系でのESR測定に非常に有用であり、この系を用いて、LPS/INF-γで処理したU87 Glioma細胞がスーパーオキシドの産生を誘導するが一酸化窒素産生は誘導しないことを明らかにした。

IV. 研究発表（原著論文）

(1) Ikota, N. : Synthesis of (2*R*,3*R*,4*R*,5*R*)-3,4-Dihydroxy-2,5-dihydroxymethylpyrrolidine and Anisomycin derivative from (*S*)-Pyroglutamic Acid Derivative. *Heterocycles*, **41**, 983-994 (1995).

(2) Hanaki, A., Saito, M. and Ikota, N. : Copper(II) Transport from a Leucine-containing Tripeptide to Cysteine. Relationship between the Position of Isobutyl Side Chain in the Peptide Chain and the Rate of Ligand-exchange . *Nippon Kagaku Kaishi*, 388-393 (1995).

(3) Hanaki, A., Nagai, A. and Ikota, N. : Pre- equilibrium Determination the rate and selectivity in the Ligand-exchange of Cu(II) Complex, Cu(II)(H-2Gly-Gly-X), with Cystein to Yield a Ternary Complex, (Cys)-Cu(II)(H-2Gly-Gly-X). *ChemistryLett.*, 611-612 (1995).

(4) Kanai, M., Muraoka, A., Tanaka, T., Sawada, M., Ikota, N. and Tomioka, K. : Conformational Preference and Diastereoselectivity of (*S*)-*N*-(α,β–Unsaturated carbonyl)-γ-trityloxymethyl-γ-butyrolactam, *Tetrahedron Lett.*, 36, 9349-9352 (1995).

(5) Tomioka, K., Kanai, M. and Ikota, N. : Theoretical Calculation Based Reproductiors and Cytotoxicity of Azasteganes. *Heterocycles*, 42, 43-45 (1996) .

(6) Ikota, N. and Hama-Inaba, H. , Chiral Pyrrolidine Derivatives as Catalyst for the Enantioselective Addition of Diethylzinc to Aldehydes. *Chem. Pharm. Bull.*, 44, 587-589 (1996).

(7) Irie, T., Fukushi, K., Namba, H. , Iyo, M., Tamagami, H., Nagatsuka, S,, Ikota, N..: Radioactive Acetylcholine Analog Method for Measuring Brain Acetylcholinesterase Activity byPET: Direct Validation of Tracer Sensitivity with Rat Model of Alzheimer's Disease. *J. Nucl. Med.*, 37, 649-655 (1996).

(8) Nakagawa, H., Nihonmatsu, N., Ohta, S. and Hirobe, M. : Effects of new endogenous nonprotein amino acids, 1,2,3,4-tetrahydroiso-quinoline-3-carboxylic acid derivatives, on behavior of mice. *Biochem. Biophys. Res. Comm.*, **225**, 1027-1034 (1996).

(9) Kitamura, K., Imazawa, Y., Morimoto, T., Sato, K., Higuchi, H., Imai, K. and Watari, K. :Determination of thorium in the organs of deceased Thorotrast patients. *J. Rdioanal. Nucl. Chem.* **217**, 175-178 (1997).

(10) Ikota, N., Hirano, J. , Gamage, R. , Nakagawa, H. and Hama-Inaba, H. : Improved Synthesis of 1-Deoxynojirimycin and Facile Synthesis of Its Stereoisomers from (*S*)-Pyroglutamic acid Derivative. *Heterocycles*, **46**, 637-643 (1997).

(11) Kawai, H. , Kitamura, Y., Nikaido, O., Tatsuka, M., Hama-Inaba, H., Muto, M. Ohyama, H. and Suzuki, F.: Isolation and Characterization of Apoptosis-resistant Mutants from a Rediosensitive Mouse Lymphoma Cell Line. *Radiat. Res.*, **149**, 41-51 (1998) .

(12) Hama-Inaba,H., Wang, B., Mori, M. , Matsushima, T., Saitoh, T. , Takusagawa, M., Yamada,T., Muto, M. , and Ohyama, H. : Radiosensitive murine thymoma cell line 3SB. Characterization of its apoptosis-resistant variants induced by repeated X-irradiation. *Mutation Res.*, **403**, 85-94 (1998) .

(13) Nakagawa, H., Ikota, N., Ozawa, T.,Masumizu, T., Kohno, M., Spin Trapping for Nitric Oxide Produced in LPS-treated Mouse Using Various New Dithiocarbamate ion Complexes Having Substituted Proline and Serine Moiety. *Biochem.Molec .Biol. Int.*, **45**, 1129- 1138 (1998).

(14) Ikota,N., Nakagawa, H., Ohno, S., Okuyama, K. and Noguchi, K. : Stereoselective Synthesis of Alexine Stereoisomers from (S)-Pyroglutamic Acid. *Tetrahedron*, **54**, 8985-8998 (1998).

(15)Nakagawa, H., Sumiki, E., Ikota, N., Matsushima, Y., Ozawa, T. : Endogenous and new Synthetic Antioxidants for Peroxynitrite: Selctive Inhibitory Effect of 5-Methoxytryptamine and α-Lipoic Acid on Tyrosine Nitration by Peroxynitrite. *Antioxidants and Redox Signaling*, **1**, 239- 244 (1999) .

(16) Shimokawa, T., Masutani, M., Nagasawa, S., Nozaki, T., Ikota, N., Aoki, Y., Nakagama, H. and Sugimura, T. : Isolation and Cloning of Rat Poly(ADP-ribose) Glycohydrolase: Presence of a Potential Nuclear Export Signal Conserved in Mammalian Orthologs. *J. Biochemistry*, **126**, 748-755 (1999).

(17) Takahata, H., Kubota, M., and Ikota,N. : A New Synthesis of All Four Stereoisomers of 2-(2,3-Dihydroxypropyl)piperidines *via* Iterative Asymmetric Dihydroxylation to Cause Enantiomeric Enhancement. Application to Asymmetric Synthesis of Naturally Occurring Piperidine Related Alkaloids. *J. Org. Chem.* , **64**, 8594-8601 (1999).

(18) Nakagawa, H., Sumiki, E., Takusagawa, M., Ikota, N., Matsushima, Y. and Ozawa, T. : Scavengers for Peroxynitrite: Inhibition of Tyrosine Nitration and Oxidation with Tryptamine Derivatives, α-Lipoic Acid and Synthetic Compounds *Chem. Pharm. Bull.*, **48**, 261-265 (2000).

(19) Nakagawa, H., Moritake, T., Tsuboi, K., Ikota, N. and Ozawa, T. : Induction of Superoxide in Glioma Cell Line U87 Stimulated with Lipopolysaccharide and Interferon Gamma: ESR Using a New Flow-type Quartz Cell. *FEBS Lett.* **471**, 187-190 (2000).

(20) Ueda, T., Irie, T., Fukushi, K., I kota, N., Takatoku, K., Yomoda, I. and Nagatsuka, S. : Synthesis of N-Methyl-3-(1-Hydroxy-5-[^{123}I] Iodopent-4-enyl)-4-Acetoxypiperidine, A Novel Candidate of Acetylcholinesterase Activity Imaging Agent . *J. Labelled Cpd. Radiopharm.* **43**, 753-765 (2000).

発表原著論文（抜粋）

Selected Papers

ELSEVIER

Free Radical Biology & Medicine, Vol. 20, No. 6, pp. 837–841, 1996

0891-5849/96 $15.00 + .00

SSDI 0891-5849(95)02092-6

Brief Communication

OXIDATION OF SPIN-TRAPS BY CHLORINE DIOXIDE (ClO_2) RADICAL IN AQUEOUS SOLUTIONS: FIRST ESR EVIDENCE OF FORMATION OF NEW NITROXIDE RADICALS

TOSHIHIKO OZAWA, YURI MIURA, and JUN-ICHI UEDA

Department of Bioregulation Research, National Institute of Radiological Sciences, Chiba, Japan

(*Received* 27 *June* 1995; *Revised* 6 *September* 1995; *Accepted* 11 *September* 1995)

Abstract—The reactivities of the chlorine dioxide (ClO_2), which is a stable free radical towards some water-soluble spin-traps were investigated in aqueous solutions by an electron spin resonance (ESR) spectroscopy. The ClO_2 radical was generated from the redox reaction of Ti^{3+} with potassium chlorate ($KClO_3$) in aqueous solutions. When one of the spin-traps, 5,5-dimethyl-1-pyrroline *N*-oxide (DMPO), was included in the Ti^{3+}-$KClO_3$ reaction system, ESR spectrum due to the ClO_2 radical completely disappeared and a new ESR spectrum [$a^N(1) = 0.72$ mT, $a^H(2) = 0.41$ mT], which is different from that of DMPO-ClO_2 adduct, was observed. The ESR parameters of this new ESR signal was identical to those of 5,5-dimethylpyrrolidone-(2)-oxyl-(1) (DMPOX), suggesting the radical species giving the new ESR spectrum is assignable to DMPOX. The similar ESR spectrum consisting of a triplet [$a^N(1) = 0.69$ mT] was observed when the derivative of DMPO, 3,3,5,5-tetramethyl-1-pyrroline *N*-oxide (M_4PO) was included in the Ti^{3+}-$KClO_3$ reaction system. This radical species is attributed to the oxidation product of M_4PO, 3,3,5,5-tetramethylpyrrolidone-(2)-oxyl-(1) (M_4POX). When another nitrone spin-trap, α-(4-pyridyl-1-oxide)-*N*-t-butylnitrone (POBN) was used as a spin-trap, the ESR signal intensity due to the ClO_2 radical decreased and a new ESR signal consisting of a triplet [$a^N(1) = 0.76$ mT] was observed. The similar ESR spectrum was observed when *N*-t-butyl-α-nitrone (PBN) was used as a spin-trap. This ESR parameter [$a^N(1) = 0.85$ mT] was identical to the oxidation product of PBN, PBNX. Thus, the new ESR signal observed from POBN may be assigned to the oxidation product of POBN, POBNX. These results suggest that the ClO_2 radical does not form the stable spin adducts with nitrone spin-traps, but oxidizes these spin-traps to give the corresponding nitroxyl radicals. On the other hand, nitroso spin-traps, 5,5-dibromo-4-nitrosobenzenesulfonate (DBNBS), and 2-methyl-2-nitrosopropane (MNP) did not trap the ClO_2 radical. This result indicates that an unpaired electron of the ClO_2 radical is localized on oxygen atom, because nitroso spin-traps cannot form the stable spin adduct with oxygen-centered radical.

Keywords—Chlorine dioxide, ClO_2, Oxidation of spin-traps, ESR, Nitrrone spin-traps, Nitroso spin-traps, Ti^{3+}, $KClO_3$, Free radicals

INTRODUCTION

The stable radical molecule, chlorine dioxide (ClO_2), usually exists as a yellow gas. Because the ClO_2 radical is an excellent bleaching agent or disinfectant, it is widely used industrially.[1] Recently, in the disinfection of drinking water the toxicity of the ClO_2 radical remaining has become a serious problem. Abdel-Rahman et al. have examined the toxicity of the ClO_2 radical and its metabolite, chlorite and chlorate, in drinking water towards rats.[2,3] They have demonstrated that the ClO_2 radical in the drinking water decreased blood gluthathione (GSH) and red blood cell (RBC) osmotic fragility in vivo , and that in vitro, when the ClO_2 radical was added with GSH to the blood, no effect on hemolysis was observed, but decreased hemolysis was observed with the ClO_2 radical treatment alone.[2]

By use of a rapid-mixing flow technique coupled with electron spin resonance (ESR) spectroscopy, we have recently found that the ClO_2 radical can be generated by redox reaction system such as Ti^{3+}-$KClO_3$ system in aqueous solutions.[4–7] There are several reports

Address correspondence to: Toshihiko Ozawa, Department of Bioregulation Research, National Institute of Radiological Sciences, 9-1, Anagawa-4-chome, Inage-ku, Chiba 263, Japan.

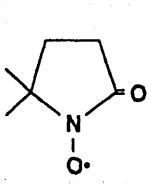

(1)

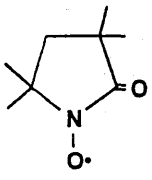

(2)

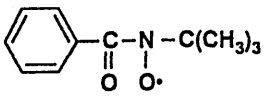

(3)

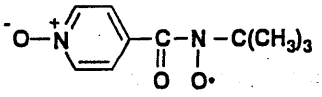

(4)

The Structure of Oxidized Nitrone Spin-Traps

Structure 1

concerning the reactive character of this radical.[8-11] However, as far as we know, there have been no reports that the ClO_2 radical is trapped by spin-traps. Therefore, we examined the reactivities of the ClO_2 radical towards some kinds of spin-traps by ESR spectroscopy.

MATERIALS AND METHODS

Reagent

Potassium chlorate ($KClO_3$), sulfuric acid, sodium hydroxide, and titanium trichloride solution ($TiCl_3$, dil. HCl soln., 20%) were purchased from Wako Pure Chemical Ind. Ltd. Nitrone spin-traps, 5,5-dimethyl-1-pyrrolinr *N*-oxide (DMPO), 3,3,5,5-tetramethylpyrroline-*N*-oxide (M_4PO), *N-tert*-butyl-α-phenyl-nitrone (PBN) and α-(4-pyridyl-1-oxide)-*N-tert*-butylnitrone (POBN), and nitroso spin-trap, 2-methyl-2-nitrosopropane (MNP) were obtained from LABOTEC. Another nitroso spin-trap, 3,5-dibromo-4-nitrosobenzenesulfonate (DBNBS) was synthesized as described previously.[12-15] Other reagents were of commercial grade.

Preparation of the ClO_2 radical

The ClO_2 radical was prepared from Ti^{3+}-$KClO_3$ reaction system in aqueous solutions at pH 2.0.[7]

ESR measurements

ESR measurements were carried out on a JEOL-RE-1X ESR spectrometer (X-band) with a 100 kHz field modulation. ESR parameters were calibrated by comparison with a standard Mn^{2+}/MgO marker and 2,2-diphenyl-1-picrylhydrazyl (DPPH, g = 2.0036). Further, the NMR field meter (JEOL ES-FC 5) and the microwave counter (Advantests) were used for more accurate calibration.

Procedure

All reaction solutions were prepared from deionized and triply distilled water, and their pH values were adjusted with sulfuric acid and sodium hydroxide. ESR spectrum was measured at 1 min after Ti^{3+} solution being added to $KClO_3$ solution with or without spin-trap. Reactions were done at pH 2.0.

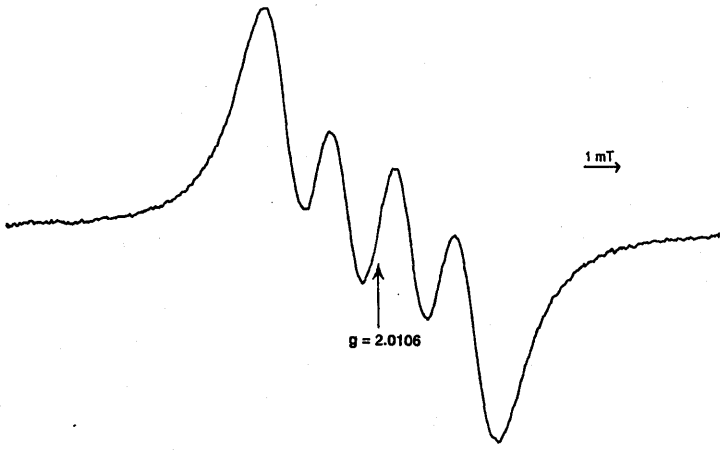

Fig. 1. ESR spectrum of the ClO_2 radical in aqueous solutions. Concentrations: $TiClO_3$, 3.25 mM; $KClO_3$, 50 mM. Instrumental settings: microwave power, 10 mW; modulation amplitude, 0.16 mT; time constant, 0.3 s; scan time, 8 min.

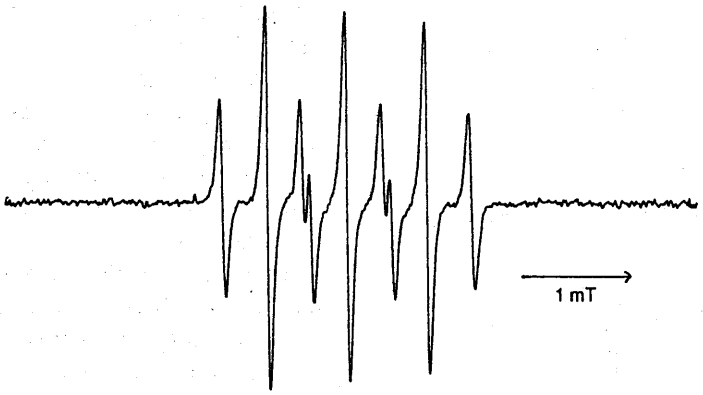

Fig. 2. ESR spectrum observed from the reaction of Ti^{3+} with $KClO_3$ in the presence of DMPO. Concentrations: $TiClO_3$, 2.2 mM; $KClO_3$, 33 mM; DMPO, 33 mM. Instrumental settings: microwave power, 10 mW; modulation amplitude, 0.05 mT; time constant, 0.1 s; scan time, 4 min.

RESULTS AND DISCUSSIONS

It is well known that in acidic aqueous solutions the ClO_2 radical is formed from the reaction of Ti^{3+} with $KClO_3$ as follows:[7]

$$ClO_3^- + H^+ \rightarrow HClO_3 \quad (1)$$

$$Ti^{3+} + O{=}Cl{-}OH \rightarrow Ti^{4+} + OH^- + ClO_2 \quad (2)$$

The reaction mixture of Ti^{3+} solution (3.25 mM) and $KClO_3$ solution (50 mM) gave the ESR spectrum due to the ClO_2 radical as shown in Fig. 1.

This spectrum consists of a quartet with a line intensity ratio of 1:1:1:1 and a hyperfine splitting of 1.85 mT centered at g = 2.0106.[4-7] Four lines with equal intensity could arise from hyperfine interaction with ^{35}Cl and ^{37}Cl nuclei, which have I = 3/2 and very similar magnetic moments (0.82091 and 0.6833 Mc, respectively).[4,7]

When DMPO (300 mM) was included in the Ti^{3+}-$KClO_3$ reaction system, the ESR spectrum due to the ClO_2 radical completely disappeared and a new ESR spectrum was observed as shown in Fig. 2. Figure 2 consists of a primary nitrogen triplet with each of the lines split into triplets in a 1:2:1 pattern, due to the interaction of the unpaired nitroxide electron with two γ-protons. The hyperfine coupling constants [$a^N(1)$ = 0.72 mT, $a^H(2)$ = 0.42 mT] are identical to those of 5,5-dimethylpyrrolidone-(2)-oxyl-(1) (DMPOX, **1**).[16,17] Therefore, the radical species giving the new ESR signal is assigned to DMPOX. Further, DMPOX was not detected when Ti^{3+} or $KClO_3$ was excluded from the reaction system. From this result, it is sug-

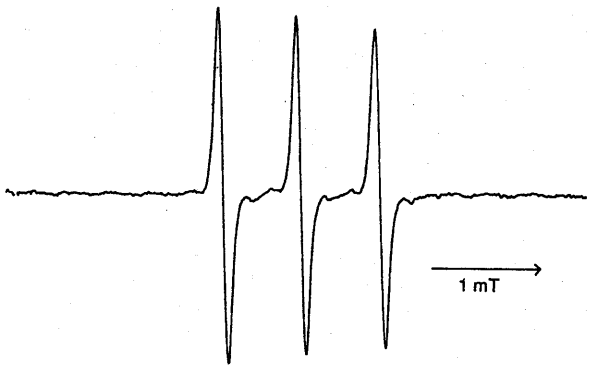

Fig. 3. ESR spectrum observed from the reaction of Ti^{3+} with $KClO_3$ in the presence of M_4PO. Concentrations: $TiClO_3$, 2.2 mM; $KClO_3$, 33 mM; M_4PO, 33 mM. Instrumental settings: microwave power, 10 mW; modulation amplitude, 0.05 mT; time constant, 0.1 s; acan time, 4 min.

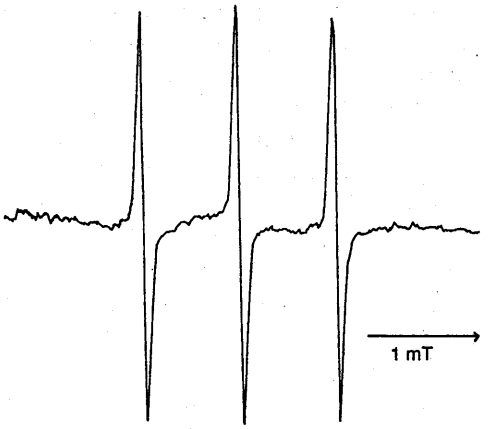

Fig. 4. ESR spectrum observed from the reaction of Ti^{3+} with $KClO_3$ in the presence of PBN. Concentrations: $TiClO_3$, 2.2 mM; $KClO_3$, 33 mM; PBN, 33 mM. Instrumental settings: microwave power, 10 mW; modulation amplitude, 0.05 mT; time constant, 0.1 s; scan time, 4 min.

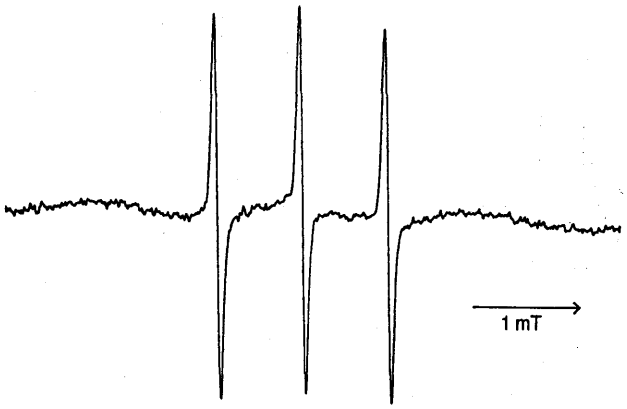

Fig. 5. ESR spectrum observed from the reaction of Ti^{3+} with $KClO_3$ in the presence of POBN. Concentrations: $TiCl_3$, 2.2 mM; $KClO_3$, 33 mM; POBN, 33 mM. Instrumental settings: microwave power, 10 mW; modulation amplitude, 0.05 mT; time constant, 0.1 s; scan time, 4 min.

gested that the ClO_2 radical is not directly trapped by DMPO, but oxidizes DMPO to give the oxidation product, DMPOX.

The same oxidation product was observed when M_4PO was used as a spin-trap. The ESR spectrum [$a^N(1) = 0.69$ mT] due to M_4POX (**2**)[18] was shown in Fig. 3. Figure 3 shows only a primary nitrogen triplet. Unlike DMPO, M_4PO does not have γ-protons to produce additional splitting of the ESR peaks in the primary nitroxide triplet.

When another nitrone spin-trap, PBN, was included in the Ti^{3+}-$KClO_3$ reaction system, the ESR spectrum due to the ClO_2 radical completely disappeared and a new ESR spectrum [$a^N(1) = 0.85$ mT] was observed as shown in Fig. 4. This ESR spectrum is different from that of PBN-ClO_2 adduct, because no hyperfine splitting due to β-protons was observed in Fig. 4. The hyperfine splitting constant was identical to that of the oxidation product of PBN, benzoyl-t-butylnitroxide (PBNX, **3**) which was produced in PBN in CCl_4 irradiated with X-rays.[19] Thus, the new ESR signal observed from the reaction of the ClO_2 radical with PBN is assignable to PBNX. The similar triplet ESR signal [$a^N(1) = 0.76$ mT] was observed when POBN was included in the Ti^{3+}-$KClO_3$ reaction system (Fig. 5). This ESR spectrum is different from that of ordinary POBN adduct with free radicals. Further, the hyperfine splitting constant is almost same as that of PBNX as mentioned above. Therefore, the new ESR signal observed from the reaction of the ClO_2 radical with POBN is assignable to the oxidation product of POBN, POBNX (**4**). As far as we know, this is the first report that ESR spectrum due to POBNX was observed.

On the other hand, when nitroso spin-traps, either DBNBS (100 mM) or MNP (100 mM), was included in the Ti^{3+}-$KClO_3$ reaction system, the ESR spectrum due to the ClO_2 radical was still observed without decreasing its signal intensity. These results indicate that an unpaired electron of the ClO_2 radical is localized on oxygen atom, because the nitroso spin-trap cannot form a stable spin adduct with oxygen-centered radicals.

From the results mentioned above, the reaction mechanisms between the ClO_2 radical with nitrone spin-traps may be assumed as follows (in this case, DMPO is used as a nitrone spin-trap):

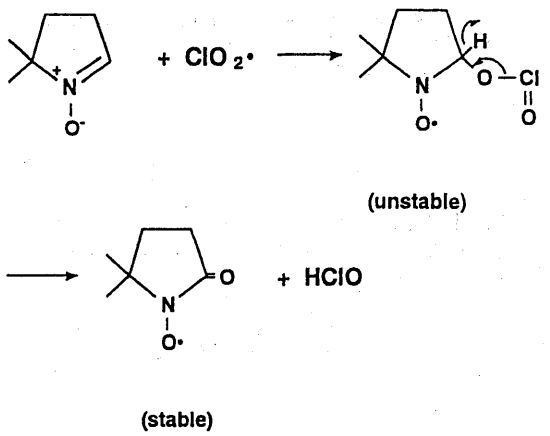

Scheme 1

In this reaction scheme, DMPO-ClO_2 adduct was not detected by ESR spectroscopy, because it may have a very short lifetime.

CONCLUSION

The ClO_2 radical, which is generated from the reaction of Ti^{3+} with $KClO_3$, was not trapped by DMPO, but oxidized it to yield the oxidation product, DMPOX. Other nitrone spin-traps, M_4PO, PBN and POBN, were also oxidized by the ClO_2 radical to give the corresponding oxidized radicals, respectively. On the other hand, nitroso spin-traps, both DBNBS and MNP did not form the stable spin adduct with the ClO_2 radical. From these results, it is indicated that an unpaired electron of the ClO_2 radical localizes on oxygen atom.

Acknowledgements—This work was partly supported by grants from the Hamaguchi Foundation for the Advancement of Biochemistry and the Nagase Science and Technology Foundation, and in part by a Grant-in-Aid for Scientific Research from the Ministry of Education, Science and Culture of Japan.

REFERENCES

1. Cotton, F. A.; Willkinson, G. *Advanced inorganic chemistry* 5th ed. New York: John Wiley & Sons; 1988.

2. Abdel-Rahman, M. S.; Couri, D.; Bull, R. J. Effect of exogenous glutathione, glutathione reductase, chlorine dioxide, and chlorite on osmotic fragility of rat blood in vitro. *J. Am. Coll. Toxicol.* **3**:269–275; 1984.
3. Abdel-Rahman, M. S.; Couri, D.; Bull, R. J. Toxicity of chlorine dioxide in drinking water. *J. Am. Coll. Toxicol.* **3**:277–284; 1984.
4. Ozawa, T.; Kwan, T. Electron spin resonance studies of chlorine dioxide (ClO_2) in aqueous solutions. *Chem. Pharm. Bull.* **31**:2864–2867; 1983.
5. Ozawa, T.; Kwan, T. Electron spin resonance studies on the reactive character of chlorine dioxide (ClO_2) radical in aqueous solution. *Chem. Pharm. Bull.* **32**:1587–1589; 1984.
6. Ozawa, T.; Kwan, T. Detoxification of chlorine dioxide (ClO_2) by ascorbic acid in aqueous solutions: ESR studies. *Water Res.* **21**:229–231; 1987.
7. Ozawa, T. Chemical reactivities of chlorine dioxide, ClO_2, in aqueous solutions. *Trends Org. Chem.* **2**:51–58; 1991.
8. Hull, L. A.; Giordano, W. P.; Rosenblatt, D. H.; Davis, G. T.; Mann, C. K.; Milliken, S. B. Oxidations of amines. VIII. Role of the cation radical in the oxidation of triethylenediamine by chlorine dioxide and hypochlorous acid. *J. Phys. Chem.* **73**:2147–2152; 1969.
9. Davis, G. T.; Demek, M. M.; Rosenblatt, D. H. Oxidation of amines. X. Detailed kinetics in the reaction of chlorine dioxide with triethylenediamine. *J. Am. Chem. Soc.* **94**:3321–3325; 1972.
10. Masui, M.; Kamada, Y.; Ozaki, S. Oxidative bond fission of β-alkanolamines by chlorine dioxide and the effect of an oxymethylene group at the β-carbon on the reaction. *Chem. Pharm. Bull.* **31**:122–127; 1983.
11. Ben Amor, H.; De Laat, J.; Dore, M. Mode of action of chlorine dioxide on organic compounds in an aqueous medium. Chlorine dioxide consumption and reactions on phenolic compounds. *Water Res.* **18**:1545–1560; 1984.
12. Ozawa, T.; Hanaki, A. Spin-trapping of superoxide ion by a water-soluble, nitroso-aromatic spin-trap. *Biochem. Biophys. Res. Commun.* **136**:657–664; 1986.
13. Ozawa, T.; Hanaki, A. Spin-trapping of sulfite radical anion, SO_3^-, by a water-soluble nitroso-aromatic spin-trap. *Biochem. Biophys. Res. Commun.* **142**:410–416; 1987.
14. Ozawa, T.; Hanaki, A. Spin-trapping of alkyl radicals by a water-soluble nitroso-aromatic spin-trap, 3,5-dibromo-4-nitrosobenzenesulfonate. *Bull. Chem. Soc. Jpn.* **60**:2304–2306; 1987.
15. Ozawa, T.; Hanaki, A. The first esr spin-trapping evidence for the formation of hydroxyl radical from the reaction of copper(II) complex with hydrogen peroxide in aqueous solution. *J. Chem. Soc. Chem. Commun.* 330–332; 1991.
16. Makino, K.; Hagiwara, T.; Hagi, A.; Nishi M.; Murakami, A. Cautionary note for DMPO spin trapping in the presence of iron ion. *Biochem. Biophys. Res. Commun.* **172**:1073–1080; 1990.
17. Hanna, P. M.; Chamulitrat, W.; Mason, R. P. When are metal ion-dependent hydroxyl and alkoxyl radical adducts of 5,5-dimethyl-1-pyrroline N-oxide artifacts? *Arch. Biochem. Biophys.* **296**:640–644; 1992.
18. Arroyo, C. M.; Wade, J. W.; Ichimori, K.; Nakazawa, H. The scavenging of hydroxyl radical ($^{\cdot}OH$) by a prostacyclin analogue, taprostene. *Chem.-Biol. Interact.* **91**:29–38; 1994.
19. Halpern, A. Spin-trapping study of the radiolysis of CCl_4. *J. Chem. Soc. Faraday Trans. I.* **83**:219–224; 1987.

ARCHIVES OF BIOCHEMISTRY AND BIOPHYSICS
Vol. 333, No. 2, September 15, pp. 377–384, 1996
Article No. 0404

A Comparison of Scavenging Abilities of Antioxidants against Hydroxyl Radicals

Jun-ichi Ueda,* Natuko Saito,† Yoshie Shimazu,* and Toshihiko Ozawa*,[1]

National Institute of Radiological Sciences, 9-1 Anagawa 4-chome, Inage-ku, Chiba-shi 263, Japan; and †Kyoritsu College of Pharmacy, 1-5-30 Shibakoen, Minato-ku, Tokyo 105, Japan

Received January 24, 1996, and in revised form May 8, 1996

The reactivities of various antioxidative compounds including catechol derivatives and endogenous radical scavengers toward hydroxyl radical (·OH) were investigated by an electron spin resonance–spin trapping method, thiobarbituric acid method, and DNA strand scission assay. Hydroxyl radical was generated by both the reaction of Cu(II) complex with hydrogen peroxide (H_2O_2) and ultraviolet (uv) photolysis of H_2O_2. At physiological pH, catechol derivatives such as protocatechuic acid and catechin greatly suppressed the DNA strand scission by ·OH produced from the reaction of $Cu(en)_2$ with H_2O_2, whereas ascorbic acid and acetylcysteine accelerated DNA strand scission. The former case is due to the chelation of catechol derivatives to Cu(II) ion, forming of Cu(II) complexes being unable to react with H_2O_2, and the latter case is due to the acceleration of the reduction rate of Cu(II) to Cu(I). On the other hand, all compounds used here suppressed the DNA strand scission by ·OH produced from uv photolysis of H_2O_2. The differences of the reactivities between the reaction system of $Cu(en)_2$–H_2O_2 and the uv photolysis of H_2O_2 have been discussed.

Active oxygen species such as superoxide (O_2^-) and hydrogen peroxide (H_2O_2) have been implicated both in the aging process and in degenerative disease such as cancer (1, 2). In particularly, it is now recognized that the extremely reactive hydroxyl radical (·OH) derived from O_2^- and H_2O_2 is considered to cause the DNA strand scission in the cellular damage (3). The importance of removing active oxygen species from living organisms is becoming increasingly recognized, together with a growing interest in the protective mechanisms whereby antioxidants that scavenge active oxygen species may have a potential for therapeutic use (4, 5). In this connection, many studies have been followed concerning the exploration of antioxidative compounds having the scavenging abilities especially toward ·OH (6–16).

We have examined the hydroxyl radical scavenging abilities of the antioxidative compounds including catechol derivatives such as protocatechuic acid, caffeic acid, catechin and gallic acid, and endogeneous radical scavengers such as uric acid, ascorbic acid, trolox (water-soluble derivative of vitamin E), glutathione, and acetylcysteine and cimetidine. Protocatechuic acid (17), caffeic acid (7), catechin (18), and gallic acid (19) are well known as plant phenols. Uric acid, ascorbic acid, and glutathione are known to be cellular antioxidants (1). The chemical structures of the compounds examined here were described in the legend to Fig. 1.

To estimate the scavenging abilities of these compounds against ·OH, we have used an electron spin resonance (ESR)[2]–spin trapping method, thiobarbituric acid (TBA) method, and DNA strand scission assay. Hydroxyl radical was generated from both the reaction of $Cu(en)_2$ (en, ethylenediamine) with H_2O_2 (20, 21) and uv photolysis of H_2O_2 (22). The reactivities of antioxidative compounds toward ·OH produced from Fe(II) ion-catalyzed decomposition of H_2O_2 have been greatly investigated (11, 16, 23, 24). However, there have been few studies concerning copper ion, irrespective of an essential metal ion as well as iron. In this paper, we report the reactivities of antioxidants toward

[1] To whom correspondence should be addressed. Fax: (+81)-43-255-6819.

[2] Abbreviations used: ESR, electron spin resonance; DMPO, 5,5-dimethyl-1-pyrroline *N*-oxide; TBA, thiobarbituric acid; H_2O_2, hydrogen peroxide; en, ethylenediamine; SC, supercoiled circular form; OC, open circular form; LIN, linear form; TBARS, TBA reactive substance.

(1) Protocatechuic acid

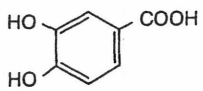

(2) Catechin

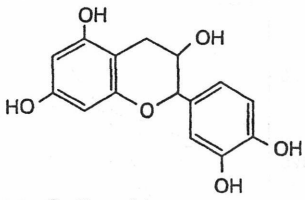

(3) Caffeic acid

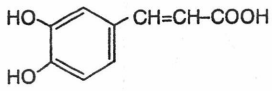

(4) Gallic acid

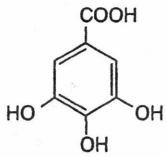

(5) Uric acid

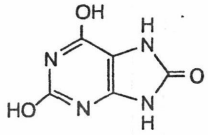

(6) Trolox

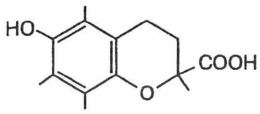

(7) Ascorbic acid

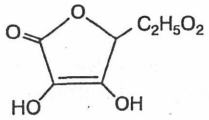

(8) Glutathione

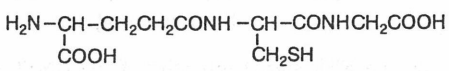

(9) Acetylcysteine

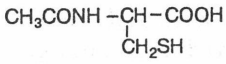

(10) Cimetidine

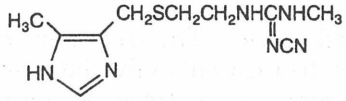

FIG. 1. Chemical structures of antioxidants used here.

•OH generated from both the reaction of $Cu(en)_2$ with H_2O_2 and uv photolysis of H_2O_2.

MATERIALS AND METHODS

Materials

Uric acid, cimetidine, glutathione, and acetylcysteine were purchased from Sigma Chemical Co. (USA). Catechin and protocatechuic acid were purchased from Nakalai Tesque Co. (Japan). Trolox was purchased from Aldrich Chemical Co. (USA). Ascorbic acid, gallic acid, caffeic acid, and H_2O_2 (30%) were purchased from Wako Pure Chemical Co. (Japan). 5,5-Dimethyl-1-pyrroline *N*-oxide (DMPO) was purchased from LABOTEC (Japan) and used without further purification. pBR322 plasmid DNA was purchased from Takara Co. (Japan). Chelex 100 was purchased from Bio-Rad Co. (USA).

$Cu(en)_2$ was synthesized as described previously (21). Phosphate buffer (0.1 M, pH 7.4) was treated with Chelex 100 resin.

Reactivities of Antioxidants Against •OH

(1) $Cu(en)_2$–H_2O_2 system. The apparent yield of •OH generated by the reaction of $Cu(en)_2$ (final concentration, 0.1 mM) with H_2O_2 (final concentration, 10 mM) in the presence and absence of different concentrations of antioxidants was checked by ESR using DMPO (final concentration, 25 mM) as a spin trap.

(2) uv photolysis of H_2O_2. The reaction mixture contained 150 μl of 10 mM DMPO and 150 μl of 10 mM H_2O_2 in phosphate buffer (0.1 M, pH 7.4) in a photometric quartz cuvette (1 × 1 cm). The reaction was also carried out in the presence of different concentrations of antioxidants in 150 μl. The final volume of the reaction mixture was made up to 0.6 ml by the addition of phosphate buffer. This solution was irradiated from a fixed distance (about 1 cm) by uv light for 1 min. The radiant energy (0.13 J/cm^2) was measured using a UVX radiometer (UVP Inc., USA). The yield of •OH generated by uv photolysis of H_2O_2 in the presence and absence of different concentrations of antioxidants was investigated by ESR using DMPO as a spin trap.

ESR Measurements

ESR measurements were carried out on a JEOL-RE-1X spectrometer (X-band) with 100 kHz field modulation. ESR spectra were recorded at room temperature in a JEOL flat quartz cell.

Detection of a TBA-Reactive Substance (TBARS) from Decomposition of Deoxyribose by Hydroxyl Radical

TBARS with oxidation products of deoxyribose by •OH was determined according to the described method (25).

DNA Strand Scission

(1) $Cu(en)_2$–H_2O_2 system. After the addition of H_2O_2 (final concentration, 25 mM) to the mixture of $Cu(en)_2$ (final concentration, 0.25

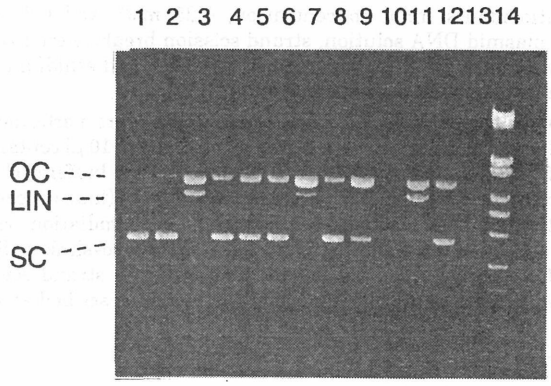

FIG. 2. Effects of various compounds on the protection of supercoiled DNA against •OH generated from the $Cu(en)_2$ and H_2O_2 system. Lane 1, DNA alone; lane 2, DNA + 25 mM H_2O_2; lane 3, DNA + 0.25 mM $Cu(en)_2$ + 25 mM H_2O_2; lane 4, DNA + 0.25 mM protocatechuic acid + 0.25 mM $Cu(en)_2$ + 25 mM H_2O_2; lane 5, DNA + 0.25 mM catechin + 0.25 mM $Cu(en)_2$ + 25 mM H_2O_2; lane 6, DNA + 0.25 mM caffeic acid + 0.25 mM $Cu(en)_2$ + 25 mM H_2O_2; lane 7, DNA + 0.25 mM gallic acid + 0.25 mM $Cu(en)_2$ + 25 mM H_2O_2; lane 8, DNA + 0.25 mM cimetidine + 0.25 mM $Cu(en)_2$ + 25 mM H_2O_2; lane 9, DNA + 0.25 mM trolox + 0.25 mM $Cu(en)_2$ + 25 mM H_2O_2; lane 10, DNA + 0.25 mM ascorbic acid + 0.25 mM $Cu(en)_2$ + 25 mM H_2O_2; lane 11, DNA + 0.25 mM glutathione + 0.25 mM $Cu(en)_2$ + 25 mM H_2O_2; lane 12, DNA + 0.25 mM uric acid + 0.25 mM $Cu(en)_2$ + 25 mM H_2O_2; lane 13, DNA + 0.25 mM acetylcysteine + 0.25 mM $Cu(en)_2$ + 25 mM H_2O_2; lane 14, DNA marker. Loading 0.5 μg DNA per lane. All reactions were performed in 100 mM phosphate buffer (pH 7.4) at room temperature for 1 min.

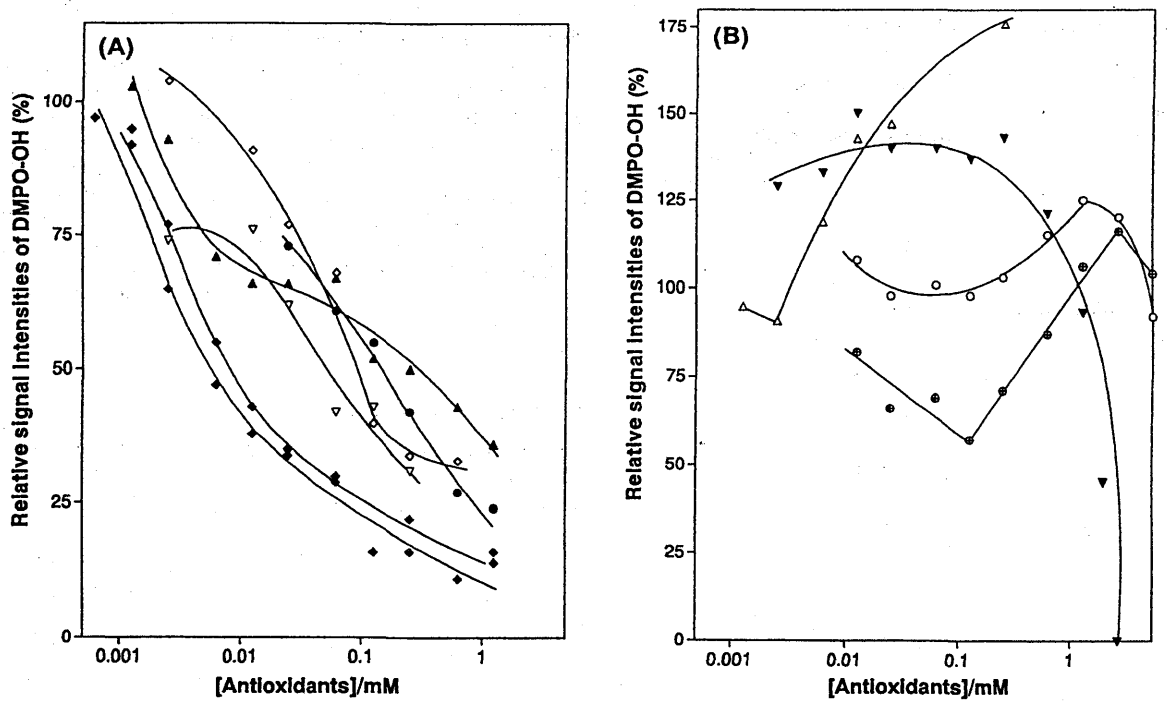

FIG. 3. Effect of varying the concentration of antioxidative compounds on the ESR signal intensity of the DMPO-OH adduct. Reaction conditions were described under Materials and Methods. (A) ⌖, protocatechuic acid; ●, catechin; ▲, caffeic acid; ▽, uric acid; ◇, glutathione; ◆, cimetidine; (B) ⊕, trolox; ○, ascorbic acid; △, gallic acid; ▼, acetylcysteine.

mM), antioxidants (final concentration, 0.25 mM), and 0.5 μg of pBR322 plasmid DNA solution, strand scission breaks were investigated by agarose gel electrophoresis of the DNA and ethidium fluorescence as described previously (26).

(2) uv photolysis of H_2O_2. The experiments were performed in 0.5-ml Eppendorf polypropylene tubes in a volume of 10 μl containing 0.5 μg of pBR322 plasmid DNA in 10 mM phosphate buffer (pH 7.4), H_2O_2 (final concentration, 2.5 mM), and antioxidants (final concentration, 0.25 mM). The reaction was started by uv irradiation with a radiant energy of 0.5 J/cm^2 using an XL-1000 uv crosslinker (Spectronics Co., USA). After the uv irradiation, DNA strand scission breaks were investigated by the same method as described above.

RESULTS

The Evaluation of Scavenging Abilities of Antioxidants against Hydroxyl Radical

(1) The reaction system of $Cu(en)_2$ with H_2O_2. The protecting activities of antioxidants against the DNA strand scission by ·OH generated from the reaction of $Cu(en)_2$ with H_2O_2 were investigated. Figure 2 shows the electrophoretic pattern of DNA after treatment of DNA with $Cu(en)_2$ (0.25 mM) and H_2O_2 (25 mM) in the presence and absence of antioxidative compounds (0.25 mM). DNA derived from pBR322 plasmid showed two bands on agarose gel electrophoresis (lane 1). The foremost moving band corresponded to the native form of supercoiled circular DNA (abbreviated as SC) and the slowly moving band was the open circular form (abbreviated as OC). The treatment of DNA with H_2O_2 only (lane 2) or $Cu(en)_2$ only (data not shown) did not change the migration pattern. When $Cu(en)_2$ plus H_2O_2 was used, however, DNA breakages to OC and the linear form (abbreviated as LIN) were observed (lane 3), indicating that ·OH generated from the reaction of $Cu(en)_2$ with H_2O_2 did cause DNA strand scission. The addition of protocatechuic acid (lane 4), catechin (lane 5), caffeic acid (lane 6), cimetidine (lane 8), trolox (lane 9), and uric acid (lane 12) to the reaction mixture of $Cu(en)_2$ and H_2O_2 showed a decrease of LIN and an increase of SC compared with the absence of antioxidant (lane 3), respectively. The addition of gallic acid (lane 7) and glutathione (lane 11) exhibited little protective effect against the DNA strand scission. In contrast, the addition of ascorbic acid (lane 10) and acetylcysteine (lane 13) caused fragmentation and enhanced DNA strand scission greater than that from the $Cu(en)_2$–H_2O_2 system itself (lane 3).

To understand the reactivities of antioxidative compounds toward ·OH, the reactions of these compounds with ·OH were investigated by the ESR–spin trapping and TBA methods. The ESR spectra of DMPO-OH adduct at the various concentrations of uric acid. Plots of the ESR signal intensities of DMPO-OH adduct against the various concentrations of antioxidative compounds were shown in Fig. 3. From Fig. 3A, it is shown that

protocatechuic acid, catechin, caffeic acid, uric acid, glutathione, and cimetidine are most effective in the suppression of $^{\bullet}OH$ generation among the compounds examined. In contrast, gallic acid, acetylcysteine, and ascorbic acid did not show the antioxidative activities (Fig. 3B). On the other hand, trolox showed a peculiar behavior (Fig. 3B). That is, the intensity of DMPO-OH decreased with an increase of concentration of trolox below 0.25 mM, but increased together with appearance of trolox radical above 0.25 mM. This result suggests that trolox reduces $Cu(II)(en)_2$ to give Cu(I) and trolox radical. Cu(I) formed thus reacts with H_2O_2 to give $^{\bullet}OH$ resulting the increase of signal intensity of DMPO-OH. Yoshida *et al.* reported the similar result that excessive amounts of α-tocopherol reacts with Cu(II) ion, giving the formation of α-tocopheroxyl radical and the reduction of Cu(II) ion to Cu(I) ion (27). It has been suggested that the tocopheroxyl radical can act as a prooxidant (28, 29).

The antioxidative activity can be represented as the concentration of 50% inhibition of the formation of DMPO-OH (IC_{50}). IC_{50} values of compounds examined by the ESR–spin trapping method are summarized in Table I. Plots of relative quantities of TBARS toward concentrations of antioxidative compounds were shown in Fig. 4. IC_{50} values obtained by the TBA method are summarized in Table I. The data of Table I show that catechol derivatives including protocatechuic acid, catechin, and caffeic acid are more effective in the suppression of $^{\bullet}OH$ generation than other compounds.

Further, we have examined whether antioxidative compounds can coordinate to $Cu(en)_2$. ESR spectra obtained from the reaction mixture of $Cu(en)_2$ with protocatechuic acid at room temperature were shown in Fig. 5. ESR spectrum of $Cu(en)_2$ exhibited four broad lines (g = 2.096), which is typical of Cu(II) complexes (21). The addition of an equivalent molar concentration of ascorbic acid to the $Cu(en)_2$ solution did not affect the pattern of the ESR spectrum of $Cu(en)_2$ but decreased its intensity. The same behavior was observed in the case of trolox, glutathione, acetylcysteine, and cimetidine. On the contrary, the addition of an equivalent molar concentration of protocatechuic acid to the $Cu(en)_2$ solution did change its ESR spectrum as shown in Fig. 5B, indicating that one molecule of protocatechuic acid coordinates to Cu(II) ion instead of at least one molecule of en, forming a ternary complex Cu(en)(protocatechuic acid), because the ESR spectrum (g = 2.114) obtained here was different from that (g = 2.127) obtained from the mixture of $CuSO_4$ with excess concentrations of protocatechuic acid (Fig. 5C). Similar results were obtained by catechin, caffeic acid, and gallic acid.

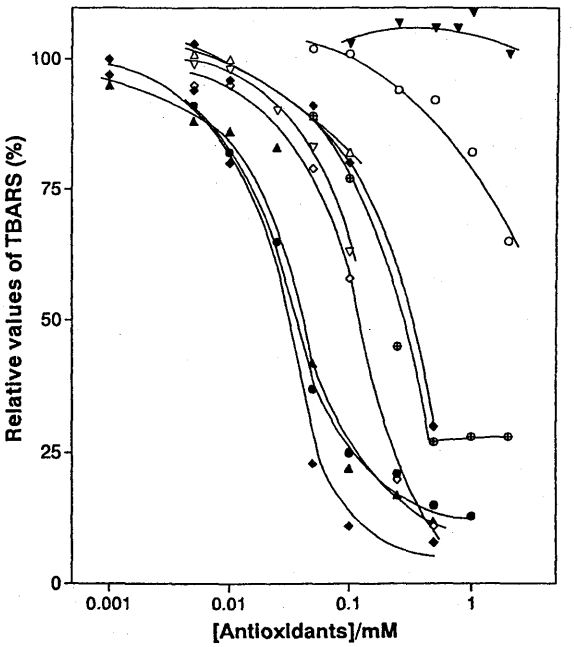

FIG. 4. Effect of varying the concentration of antioxidative compounds on the generation of TBARS. ●, catechin; ▲, caffeic acid; △, gallic acid; ▽, uric acid; ⊕, protocatechuic acid; ⊕, trolox; ○, ascorbic acid; ◇, glutathione; ▼, acetylcysteine; ◆, cimetidine.

TABLE I

Scavenging Abilities of Antioxidants against Hydroxyl Radical from the $Cu(en)_2$ and H_2O_2 by ESR-Spin Trapping and TBA Methods

Compounds	IC_{50}/mM	
	Spin trapping[a]	TBA[b]
Protocatechuic acid	0.01	0.02
Catechin	0.16	0.03
Caffeic acid	0.23	0.04
Gallic acid	>0.25	>0.1
Uric acid	0.04	>0.1
Trolox	>5.0	0.22
Ascorbic acid	>5.0	>2.0
Glutathione	0.09	0.12
Acetylcysteine	1.80	>2.0
Cimetidine	0.01	0.26

[a] $[Cu(en)_2]$ = 0.1 mM, $[H_2O_2]$ = 10 mM, [DMPO] = 25 mM, 100 mM phosphate buffer (pH 7.4).

[b] $[Cu(en)_2]$ = 0.1 mM, $[H_2O_2]$ = 10 mM, [deoxyribose] = 3.8 mM, 100 mM phosphate buffer (pH 7.4).

(2) uv photolysis of H_2O_2. Figure 6 shows the electrophoretic pattern of DNA after uv photolysis of H_2O_2 (2.5 mM) in the presence and absence of antioxidative compounds (0.25 mM). The uv irradiation to DNA in the presence of H_2O_2 (lane 2) caused breakage of SC DNA to OC and LIN, indicating that $^{\bullet}OH$ generated from uv photolysis of H_2O_2 did make DNA strand scission. All compounds used here suppressed the forma-

tion of LIN compared with the absence of antioxidative compounds (lane 2) as shown in Fig. 6.

To investigate the reactivities of antioxidants toward $^{\bullet}OH$, the reactions of these compounds with $^{\bullet}OH$ were investigated by the ESR–spin trapping method. Ascorbic acid, which did not have any antioxidative effect against $^{\bullet}OH$ generated by the $Cu(en)_2$–H_2O_2 reaction system, had been shown to be a very strong $^{\bullet}OH$ scavenger as seen in Fig. 7. Plots of relative ESR signal intensities of DMPO-OH adduct against the concentrations of antioxidative compounds were shown in Fig. 8. Ascorbic acid and acetylcysteine were the strongest $^{\bullet}OH$ scavengers among the antioxidants examined.

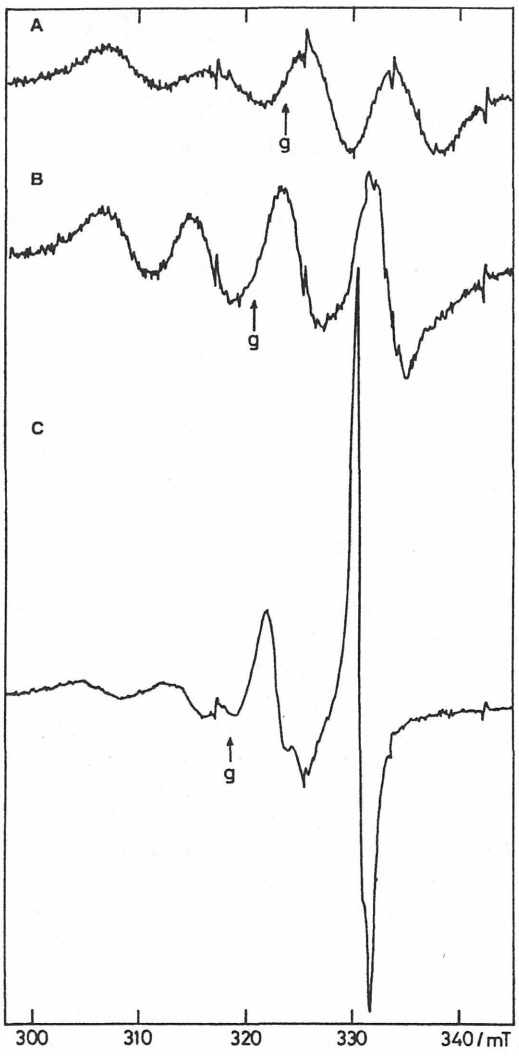

FIG. 5. ESR spectral change of $Cu(en)_2$ in the presence of antioxidants at room temperature. (A) $Cu(en)_2$ (1 mM); (B) $Cu(en)_2$ (1 mM) + protocatechuic acid (1 mM); (C) $CuSO_4$ (1 mM) + protocatechuic acid (5 mM). Instrumental conditions: microwave power, 10 mW; modulation amplitude, 0.079 mT; scan range, 100 mT; amplitude, 4.0×100; time constant, 0.3 s; scan time, 16 min.

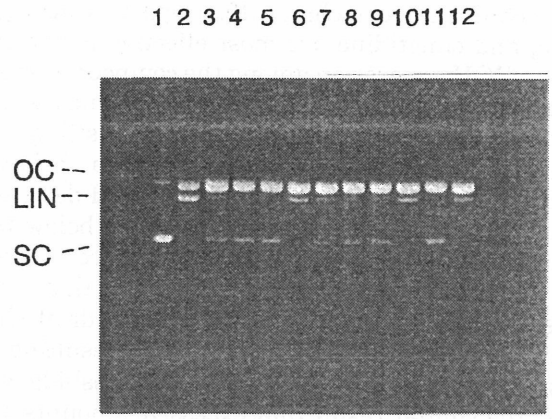

FIG. 6. Effects of various compounds on the protection of supercoiled DNA against $^{\bullet}OH$ generated from photolysis of H_2O_2. Lane 1, DNA alone; lane 2, DNA + 2.5 mM H_2O_2; lane 3, DNA + 0.25 mM protocatechuic acid + 2.5 mM H_2O_2; lane 4, DNA + 0.25 mM catechin + 2.5 mM H_2O_2; lane 5, DNA + 0.25 mM caffeic acid + 2.5 mM H_2O_2; lane 6, DNA + 0.25 mM gallic acid + 2.5 mM H_2O_2; lane 7, DNA + 0.25 mM cimetidine + 2.5 mM H_2O_2; lane 8, DNA + 0.25 mM trolox + 2.5 mM H_2O_2; lane 9, DNA + 0.25 mM ascorbic acid + 2.5 mM H_2O_2; lane 10, DNA + 0.25 mM glutathione + 2.5 mM H_2O_2; lane 11, DNA + 0.25 mM uric acid + 2.5 mM H_2O_2; lane 12, DNA + 0.25 mM acetylcysteine + 2.5 mM H_2O_2. Loading 0.5 μg DNA per lane. All reactions were performed in 100 mM phosphate buffer (pH 7.4).

Protocatechuic acid, caffeic acid, glutathione, and gallic acid showed moderate scavenging abilities. Catechin and trolox showed very weak scavenging activities against $^{\bullet}OH$. However, it is apparent from Figs. 6 and 8 that the protective activities of ascorbic acid and acetylcysteine against DNA strand scission by $^{\bullet}OH$ were not consistent with scavenging abilities obtained by the ESR–spin trapping method. This result suggests that ascorbic acid and acetylcysteine may react with the DMPO-OH formed. Then, the reactions of ascorbic acid and acetylcysteine with DMPO-OH were investigated. The addition of ascorbic acid to the solution of DMPO-OH adduct, which was produced from uv photolysis of H_2O_2 in the presence of DMPO, diminished the signal intensity of DMPO-OH. This result supports the suggestion that ascorbic acid reacts with DMPO-OH. Plots of the ESR signal intensities of DMPO-OH adduct against the various concentrations of antioxidative compounds are shown in Fig. 9. In analogy with ascorbic acid, acetylcysteine did react with DMPO-OH below 0.5 mM, but did not react above 0.5 mM. From Fig. 9, it was shown that antioxidative compounds except ascorbic acid and acetylcysteine did not react with DMPO-OH.

DISCUSSION

We have examined the scavenging abilities of antioxidative compounds toward $^{\bullet}OH$ generated from the re-

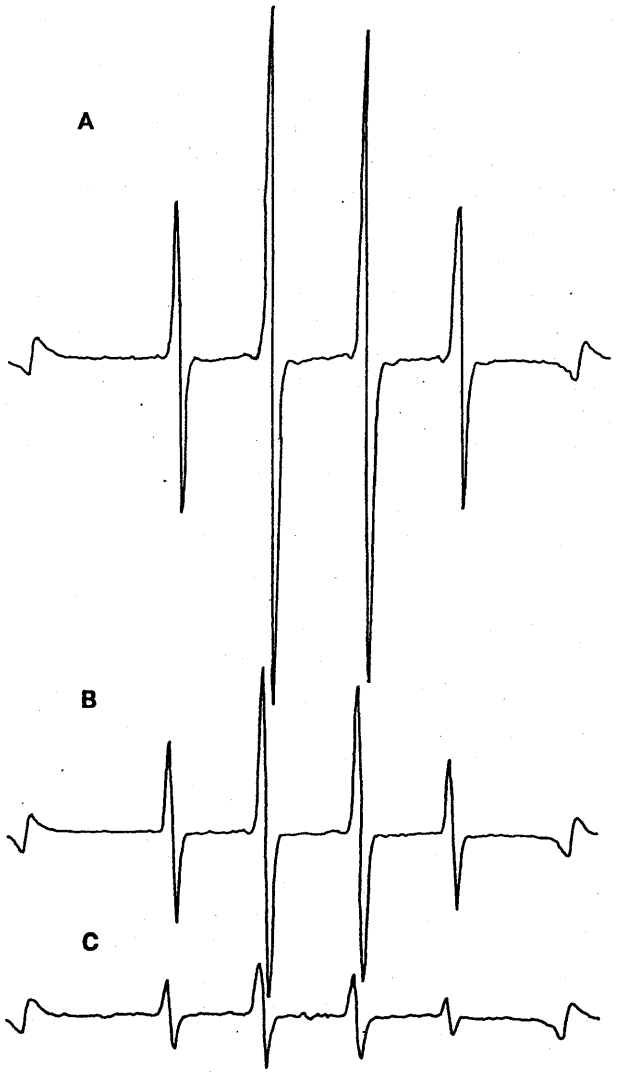

FIG. 7. Effect of varying the concentration of ascorbic acid on the signal intensity of the DMPO-OH adduct. [Ascorbic acid] = 0 mM (A); 0.025 mM (B); 0.063 mM (C). [H_2O_2] = 2.5 mM, [DMPO] = 2.5 mM, 100 mM phosphate buffer (pH 7.4). Instrumental conditions: microwave power, 10 mW; modulation amplitude, 0.079 mT; scan range, 10 mT; amplitude, 2 × 100; time constant, 0.03 s; scan time, 2 min. Spectra were recorded 60 s after mixing.

action of $Cu(en)_2$ with H_2O_2 using both ESR–spin trapping and TBA methods. From Table I, it was shown that protocatechuic acid, catechin, caffeic acid, glutathione and cimetidine were most effective in the suppression of $^{\bullet}OH$ generation among compounds examined. In particular, the remarkable antioxidative activities of catechol derivatives were found. In contrast, gallic acid, acetylcysteine and ascorbic acid did not show the antioxidative activities. DNA strand breaks caused by $Cu(en)_2$ plus H_2O_2 were suppressed by the addition of protocatechuic acid, catechin, caffeic acid, cimetidine, trolox, and uric acid as shown in Fig. 2. This result suggests that these compounds suppressed the generation of $^{\bullet}OH$ and protected the DNA. Addition of gallic acid and glutathione provided little protection against the DNA. In contrast, addition of ascorbic acid and acetylcysteine enhanced DNA strand scission greater than that from the $Cu(en)_2$–H_2O_2 system itself and caused fragments of DNA, indicating that these compounds accelerated the Cu(II)-dependent decomposition of H_2O_2.

There are two types of antioxidants against $^{\bullet}OH$: one suppresses the generation of $^{\bullet}OH$, and the other scavenges $^{\bullet}OH$ generated. In the former, the antioxidants may ligate to the metal ions which react with H_2O_2 to give the metal complexes. The metal complex thus formed could not further react with H_2O_2 to give $^{\bullet}OH$.

To understand the antioxidative mechanism of the compounds used here, we examined to which type these compounds belong. The reaction mixture of $Cu(en)_2$ with antioxidative compounds was measured by ESR spectroscopy at room temperature. As shown in Fig. 4, addition of ascorbic acid, trolox, glutathione, acetylcysteine, and cimetidine, respectively, to the $Cu(en)_2$ solution did not change the ESR spectrum of $Cu(en)_2$. On the other hand, addition of protocatechuic acid, catechin, caffeic acid, and gallic acid, respectively, to the $Cu(en)_2$ solution

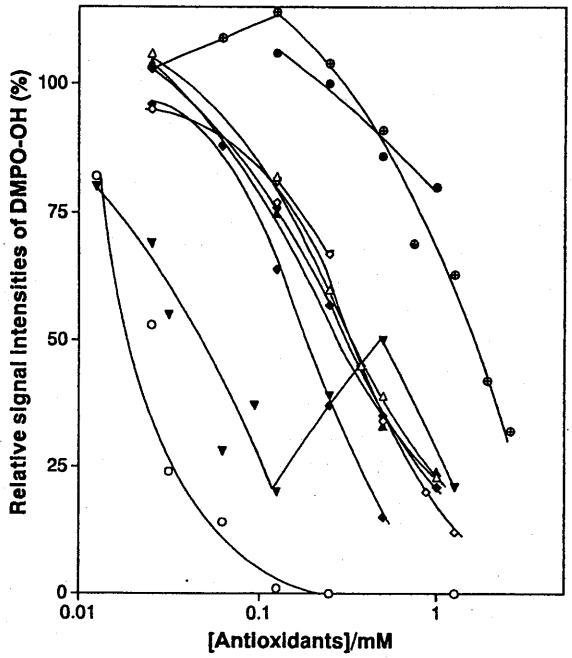

FIG. 8. Effect of varying the concentration of antioxidative compounds on the ESR signal intensity of the DMPO-OH adduct obtained during uv photolysis of H_2O_2. Reaction conditions were the same as described in the legend to Fig. 7. ●, catechin, ▲, caffeic acid, △, gallic acid, ▽, uric acid, ⌖, protocatechuic acid, ⊕, trolox, ○, ascorbic acid, ◇, glutathione, ▼, acetylcysteine; ◆, cimetidine.

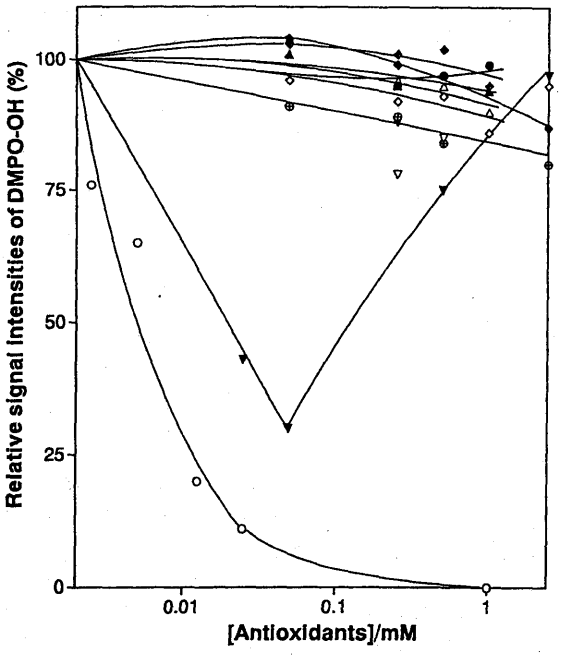

FIG. 9. Effect of varying the concentration of antioxidative compounds on the ESR signal intensity of the DMPO-OH adduct. DMPO-OH was obtained from the reaction of DMPO with ·OH generated from photolysis of H_2O_2. ●, catechin; ▲, caffeic acid; △, gallic acid; ▽, uric acid; ⌖, protocatechuic acid; ⊕, trolox; ○, ascorbic acid; ◇, glutathione; ▼, acetylcysteine; ♦, cimetidine.

did change the ESR spectrum of $Cu(en)_2$, indicating that one molecule of compound coordinates to the Cu(II) complex instead of at least one molecule of en, forming the ternary complex Cu(en)(L) (L, protocatechuic acid, catechin, caffeic acid, and gallic acid). This was supported from result that the ESR spectrum obtained here was different from $Cu(L)_2$ (Fig. 4). Thus, antioxidative activities of catechol derivatives except for gallic acid toward ·OH produced from the reaction of $Cu(en)_2$ with H_2O_2 are considered to be due to the chelation of catechol derivatives to the Cu(II) ion of which complexes cannot react further with H_2O_2. Iwahashi *et al.* reported that compounds with adjacent hydroxyl groups in aromatic rings might inhibit ·OH formation from the reaction of $FeCl_3$ with H_2O_2 in the presence of 3-hydroxyanthranilic acid and that this inhibitory effect may be due to the chelation of iron ion with the catechols (7). Although gallic acid may ligate to the Cu(II) ion, the Cu(II) complex of gallic acid thus formed is considered to be able to further react with H_2O_2 to give ·OH. On the other hand, ascorbic acid and acetylcysteine accelerated DNA strand scission. This is due to the acceleration of the reduction rate of Cu(II) to Cu(I) by these compounds, because these compounds could reduce Cu(II)–polyamine-*N*-polycarboxylate complexes such as Cu(II)-(edta) and Cu(II)(dtpa) to Cu(I) (30).

Further, to examine the direct scavenging abilities of these compounds toward ·OH, uv photolysis of H_2O_2 was used. Ascorbic acid and acetylcysteine, which did not have any antioxidative effect against ·OH generated by the reaction of $Cu(II)(en)_2$ with H_2O_2, were the strongest ·OH scavengers among the compounds examined as shown in Fig. 8. Protocatechuic acid, caffeic acid, glutathione, acetylcysteine, and gallic acid had moderate scavenging abilities. Catechin and trolox had very weak scavenging activities against ·OH. All compounds used here suppressed the formation of LIN compared with the absence of antioxidative compounds as shown in Fig. 6. These results indicate that antioxidative compounds used here suppressed the DNA strand scission by scavenging ·OH. In spite of high reactivity of ·OH, however, the extents of DNA strand scission in the presence of antioxidants were different. Notably, catechol compounds were more effective at suppressing DNA strand scission than glutathione. This may be due to the difference of the interaction between antioxidants and DNA. We are now investigating the interaction between antioxidants and DNA.

On the other hand, the results obtained from Figs. 6 and 8 indicate that the antioxidative activities of ascorbic acid and acetylcysteine against DNA strand scission caused by ·OH were not consistent with those observed by the ESR–spin trapping method. Certainly, ascorbic acid reacted with DMPO-OH as shown in Fig. 9. In the ESR–spin trapping method, ascorbate has been suggested to react with DMPO-OH (31, 32). The ascorbate reduction of nitroxyl in biological systems has been well known (33, 34). Therefore, no clear-cut antioxidative effect of ascorbic acid against ·OH could be obtained by the ESR–spin trapping method, because of the reduction of signal intensity of DMPO-OH by ascorbic acid. On the other hand, acetylcysteine showed the peculiar behavior in which the signal intensities of DMPO-OH first decreased and then increased, with a minimum value near 0.5 mM. We are further investigating this phenomenon.

In conclusion, catechol compounds such as protocatechuic acid, catechin, and caffeic acid greatly suppressed the generation of ·OH from the reaction of $Cu(en)_2$ with H_2O_2 by forming ternary Cu(en)(L) complexes. In contrast, ascorbic acid and acetylcysteine accelerated the reduction of Cu(II) to Cu(I) to yield ·OH. The antioxidative activities of these compounds against ·OH generated from uv photolysis of H_2O_2 were independent on their chemical structures. The results from the DNA strand scission caused by uv photolysis of H_2O_2 were not consistent with those of the ESR–spin trapping method in the presence of ascorbic acid or acetylcysteine. This is due to the reduction of DMPO-OH by ascorbic acid or acetylcysteine.

REFERENCES

1. Ames, B. N. (1983) *Science* **221,** 1256–1264.
2. Halliwell, B., and Gutteridge, J. M. C. (1989) *in* Free Radicals in Biology and Medicine, 2nd ed., Clarendon Press, Oxford.
3. Halliwell, B., and Gutteridge, J. M. C. (1990) *Methods Enzymol.* **186,** 1–85.
4. Oberley, L. W., and Buettner, G. R. (1979) *Cancer Res.* **39,** 1141–1149.
5. Rice-Evans, C. A., and Diplock, A. T. (1993) *Free Radical Biol. Med.* **15,** 77–96.
6. Aruoma, O. I., Laughton, M. J., and Halliwell, B. (1989) *Biochem. J.* **264,** 863–869.
7. Iwahashi, H., Ishii, T., Sugata, R., and Kido, R. (1990) *Arch. Biochim. Biophys.* **276,** 242–247.
8. Aruoma, O. I., and Halliwell, B. (1990) *FEBS Lett.* **244,** 76–80.
9. Zheng, S., Newton, G. L., Ward, J. F., and Fahey, R. C. (1992) *Radiat. Res.* **130,** 183–193.
10. Miura, T., Muraoka, S., and Ogiso, T. (1993) *Biochem. Mol. Biol. Int.* **31,** 125–133.
11. Ching, T.-L., Haenen, G. R. M. M., and Bast, A. (1993) *Chem.–Biol. Interact.* **86,** 119–127.
12. Hiramatsu, M., Liu, J., Edamatsu, R., Ohba, S., Kadowaki, D., and Mori, A. (1994) *Free Radical Biol. Med.* **16,** 201–206.
13. Fisher-Nielsen, A., Jeding, I. B., and Loft, S. (1994) *Carcinogenesis* **15,** 1609–1612.
14. Prasad, K., and Laxdal, V. A. (1994) *Mol. Cell. Biochem.* **135,** 153–158.
15. Prasad, K., and Laxdal, V. A. (1994) *Mol. Cell. Biochem.* **136,** 139–144.
16. Chan, W. K. M., Decker, E. A., Lee, J. B., and Butterfield, D. A. (1994) *J. Agric. Food Chem.* **42,** 1407–1410.
17. Tanaka, T., Kojima, T., Kawamori, T., Yoshimi, N., and Mori, H. (1993) *Cancer Res.* **53,** 2775–2779.
18. Morel, I., Lescoat, G., Cogrel, P., Sergent, O., Pasdeloup, N., Brissot, P., Cillard, P., and Cillard, J. (1993) *Biochem. Pharmacol.* **45,** 13–19.
19. Inoue, M., Suzuki, R., Koide, T., Sakaguchi, N., Ogihara, Y., and Yabu, Y. (1994) *Biochem. Biophys. Res. Commun.* **204,** 898–904.
20. Ozawa, T., and Hanaki, A. (1991) *Biochem. Int.* **25,** 783–788.
21. Ozawa, T., and Hanaki, A. (1991) *J. Chem. Soc. Chem. Commun.* 330–332.
22. Macgregor, R. B., Jr. (1992) *Anal. Biochem.* **204,** 324–327.
23. Aruoma, O. I., Evans, P. J., Kaur, H., Sutcliffe, L., and Halliwell, B. (1990) *Free Radical Res. Commun.* **10,** 143–157.
24. Hamada, H., Hiramatsu, M., Edamatsu, R., and Mori, A. (1993) *Arch. Biochim. Biophys.* **306,** 261–266.
25. Ozawa, T. , Goto, H., Takazawa, F., and Hanaki, A. (1988) *Nippon Kagaku Kaishi,* 459–465.
26. Ozawa, T. , Ueda, J., and Shimazu, Y. (1993) *Biochem. Mol. Biol. Int.* **31,** 455–461.
27. Yoshida, Y., Tsuchiya, J., and Niki, E. (1994) *Biochim. Biophys. Acta* **1200,** 85–92.
28. Maiorino, M., Zamburlini, A., Roveri, A., and Ursini, F. (1993) *FEBS Lett.* **330,** 174–176.
29. Bowry, V. W., and Stocker, R. (1993) *J. Am. Chem. Soc.* **115,** 6029–6045.
30. Ozawa, T., Hanaki, A., and Onodera, K. (1992) *Polyhedron* **11,** 735–738.
31. Halliwell, B. (1995) *Biochem. Pharmacol.* **49,** 1341–1348.
32. Floyd, R. A. (1983) *Biochim. Biochem. Acta* **756,** 204–216.
33. Iannone, A., and Tomasi, A. (1991) *Acta Pharm. Jugosl.* **41,** 277–297.
34. Vianello, F., Momo, F., Scarpa, M., and Rigo, A. (1995) *Magn. Reson. Imag.* **13,** 219–226.

A novel lipophilic spin probe for the measurement of radiation damage in mouse brain using in vivo electron spin resonance (ESR)

Yuri Miura[a], Kazunori Anzai[a], Sentaro Takahashi[b], Toshihiko Ozawa[a,*]

[a]*Department of Bioregulation Research, National Institute of Radiological Sciences, Anagawa 4-9-1, Inage-ku, Chiba-shi 263, Japan*
[b]*Environmental and Toxicological Sciences Research Group, National Institute of Radiological Sciences, Anagawa 4-9-1, Inage-ku, Chiba-shi 263, Japan*

Received 23 September 1997

Abstract **As a possible lipophilic spin probe of in vivo electron spin resonance (ESR), 3-methoxy carbonyl-2,2,5,5-tetramethyl-pyrrolidine-1-yloxy (MCPROXYL) was examined. The permeability of the blood-brain barrier to this compound was evaluated with a brain uptake index and autoradiography, with result that this probe is well distributed in the brain. The in vivo ESR spectra were measured in the head and the abdomen of MCPROXYL-injected living mice. The rate of signal decay of MCPROXYL in the head measured at one hour after X-irradiation was about 75% of that of the controls. The decrease in the head seems to be related to the early response of the brain to X-irradiation. This is the first report that the behavior of free radical such as MCPROXYL in the brain is influenced by X-irradiation. MCPROXYL is thus useful as a novel spin probe for in vivo ESR to monitor the radiation damage in the brain.**

Key words: In vivo electron spin resonance; Nitroxyl radical; Brain; Radiation; Blood-brain barrier; Free radical

1. Introduction

Oxidative stress such as radiation is known to generate active oxygens in living organisms, to vary the redox state significantly, and to cause various types of tissue damage. The brain may be especially susceptible to oxidative stress for the following reasons [1]: (1) The brain is exposed to a high amount of oxygen, because of its high and constant oxygen requirement, utilizing about one-fifth of the oxygen consumed by the whole body; (2) the brain membrane lipids enrich in oxidizable polyunsaturated fatty acids; (3) the brain has low levels of the antioxidant enzyme, catalase and only moderate amounts of superoxide dismutase and glutathione peroxidase; (4) the presence of non-protein-bound Fe^{3+} in the cerebrospinal fluid increases the formation of highly reactive hydroxyl radicals through the Haber-Weiss reaction. Therefore, oxidative damage in the brain is especially worthy of investigation.

A stable nitroxyl radical such as 3-carbamoyl-2,2,5,5-tetramethyl pyrrolidine-1-yloxy (carbamoyl-PROXYL) or 4-hydroxy-2,2,6,6-tetramethyl piperidine-1-yloxy (hydroxy-TEMPO) is often used for the in vivo ESR as a probe. The redox reaction of the nitroxyl radicals has been reported to correlate to the generation of free radicals and to changes of the physiological redox state caused by aging, ischemia-reperfusion, hyperoxia and hypoxia [2–6].

*Corresponding author. Fax: +81 (43) 255-6819.
E-mail: ozawa@nirs.go.jp

In our previous study [7], we reported that X-irradiation increases the signal decay rate, i.e. the reduction rate of carbamoyl-PROXYL in the mouse abdomen at 1 h postirradiation, indicating that early redox response of the mouse to the X-irradiation is detectable by an in vivo ESR system. However, carbamoyl-PROXYL is hydrophilic and does not pass through the blood-brain barrier (BBB) [8]. Similarly, most of the other nitroxyl compounds used conventionally are very soluble in water, and unlikely to pass through the BBB. Therefore, choosing a probe which can pass through the BBB is essential to monitor the redox reaction in the brain by in vivo ESR.

In the present study, we synthesized a lipophilic nitroxyl spin probe (3-methoxy carbonyl-2,2,5,5-tetramethyl-pyrrolidine-1-yloxy, MCPROXYL) as a novel spin probe which can monitor the physiological redox state in the brain. The permeability of the BBB to this probe and the effects of X-irradiation on the reduction rates of MCPROXYL in the head of living mice were examined.

2. Materials and methods

2.1. Chemicals

[^{14}C]Methanol (3 mCi/mmol) and [^{3}H]water (1 mCi/g) were purchased from Moravek Biochemicals, Inc. (Mercury Lane • Brea, CA, USA). [^{14}C]Sucrose was purchased from NEN Research Products (Boston, MA, USA). Soluene 350 (a tissue solubilizer) and Hionic-Fluor (scintillation mixture) were purchased from Packard Instrument Co. (Downers Grove, IL, USA). 3-Carboxy-2,2,5,5-tetramethyl-pyrrolidine-1-yloxy (carboxy-PROXYL) was purchased from Tokyo Kasei Kogyo, Co. (Tokyo, Japan). Pentobarbital (50 mg/ml) was obtained from Dainabot Co. (Osaka, Japan). Other reagents were of the highest purity commercially available.

2.2. Animals

Male Wistar rats (6 weeks, ca. 150 g body weight) for the brain transport studies, and female ddY mice (3–4 weeks, 15–20 g body weight) for the autoradiography and the ESR studies were purchased from Japan SLC (Hamamatsu, Japan).

2.3. Synthesis

MCPROXYL was synthesized from carboxy-PROXYL and diazomethane by the method of Rozantzev and Krinitzkaya [9]. The synthesized MCPROXYL was purified by column chromatography and distillation in vacuo: bp, 100°C (3 mm Hg). The purified MCPROXYL was characterized by [^{1}H]NMR and FT-IR. Since the NMR spectra of the nitroxyl radicals are quite broad, MCPROXYL was reduced to a diamagnetic *N*-hydroxyl derivative by the addition of a 1.5 equiv. of phenylhydrazine, in an NMR tube containing the nitroxyl dissolved in $CDCl_3$ [10]. [^{1}H]NMR δ 1.31, 1.22, 1.14, 1.02 (each 3H, each s, 4x-CH_3), 1.74 (1H, dd, J = 12.6, 8.4 Hz, H-4), 2.13 (1H, dd, J = 12.6, 11.0 Hz, H-4), 2.75 (1H, dd, J = 10.6, 8.3 Hz, H-3), 3.67 (3H, s, $-OCH_3$); ir ν_{max} (neat) 1740 cm^{-1}. [^{14}C]MCPROXYL was synthesized from carboxy-PROXYL and [^{14}C]methanol via the acid chloride of carboxy-PROXYL. To synthesize acid chloride, thionyl-

chrolide was added dropwise to a benzene solution of carboxy-PROXYL in the presence of pyridine. The synthesized [^{14}C]MCPROXYL was purified by column chromatography, and the purified nitroxyl showed a single spot in TLC. To verify the validity of this synthetic method, unlabeled MCPROXYL was synthesized by the same method via acid chloride. The MCPROXYL synthesized via acid chloride showed a [^{1}H]NMR spectrum identical to the one described above. The specific activity of [^{14}C]MCPROXYL was 2.92×10^{8} Bq/mol.

2.4. Brain transport studies

The brain transport of MCPROXYL was measured by the tissue-sampling single-injection technique (brain uptake index method) developed by Oldendorf [11]. A Wistar rat was anesthetized with intraperitoneal pentobarbital (80 mg/kg). The left common carotid artery of the rat was isolated and the mixture of [^{14}C]MCPROXYL and the internal reference compound, $^{3}H_2O$, was rapidly injected into the common carotid artery as an approximately 200 μl bolus of injection solution. The rat was decapitated 15 s after the injection. The cerebral hemisphere ipsilateral to the injection was removed from the cranium, solubilized in 1.5 ml of soluene 350 at 50°C for 3 h in an incubator, decolorized with 30% H_2O_2 and mixed with 10 ml Hionic-Fluor before double-isotope liquid scintillation counting. The brain uptake index (BUI) was calculated as follows [12]:

$$\text{BUI (\%)} = \frac{^{14}\text{C}/^{3}\text{H dpm (in brain)}}{^{14}\text{C}/^{3}\text{H dpm (in injection solution)}} \times 100.$$

2.5. Autoradiography

Mice were anesthetized with intraperitoneal pentobarbital. The mice were injected intravenously with [^{14}C]MCPROXYL or [^{14}C]sucrose at a dose of 0.3 μCi/mouse. Five min after the injection, the mice were frozen in dry ice/acetone after embedding in the 8% solution of carboxymethyl cellurose (CMC). The frozen mouse was cut into sections 20 μm thick by a microtome in a cryostat maintained at −10 to −15°C. The frozen sections of the mouse were adhered to cover slips at room temperature for a few seconds and then allowed to dry at −20°C for 2–3 days. The cover slips containing the freeze-dried sections were then covered by a thin plastic film (Lumilar Membrane, Nakagawa Co. Ltd., Tokyo, Japan) and placed in contact with an imaging plate (Type BAS III, Fuji Photo Film Co. Ltd., Tokyo, Japan) for 5 days. The radioactive images recorded on the imaging plate were read by a laser beam scanner and analyzed by an attached computer (BAS-2000, Fuji Photo Film Co. Ltd., Tokyo, Japan). Analysis settings were as follows: pixel, 100×100 μm; sensitivity, 10000; latitude, 4. In this image-analyzing system, the radioactivities in the tissue sections were provided as intensities of photostimulated luminescence. The ^{14}C concentrations in the tissue sections were reported to be proportional to the levels of photostimulated luminescence in the wide range [13].

2.6. X-irradiation

The irradiation of ddY mice was performed with X-rays (200 kV, 20 mA), using 0.5 mm copper and 0.5 mm aluminum filters, at a dose rate of 0.62–0.65 Gy/min. Several mice were simultaneously given a single whole body exposure in the irradiation chamber separated for individuals. Sham irradiation for control mice included comparable immobilization in the same irradiation chamber.

2.7. ESR measurement

MCPROXYL was dissolved in sodium phosphate-buffered saline (pH 7.4) at 140 mM, and the solution of MCPROXYL was sterilized before the injection to mice. The in vivo ESR measurements were performed as follows. Mice were anesthetized by an intramuscular injection of pentobarbital (120 mg/kg) and fixed on a Teflon holder. The mouse fixed on the holder was placed in a resonator of the in vivo ESR apparatus. Immediately after the injection of the sterilized solution of MCPROXYL to a tail vein (80 μl), ESR spectra were measured in the head or the abdomen. In vivo ESR spectrometer (JES-PE, JEOL, Tokyo) was equipped with an L-band microwave power unit (ES-LB1A, JEOL) and a loop-gap resonator. The kinetic constants of signal decay of MCPROXYL were calculated from the slope of the spin clearance curves, which were determined from semilogarithmic plots of the peak heights of the ESR signal at the lower magnetic field, as described previously [7].

Table 1
Partition coefficients of various nitroxyl compounds

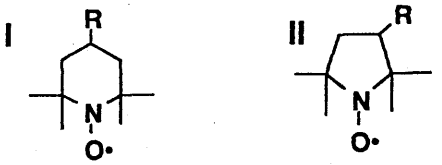

Nitroxyl compounds	Structure	Partition coefficients
CAT1	I R=$N^{+}(CH_3)_3I^{-}$	0.006
Carbamoyl-PROXYL	II R=$CONH_2$	0.6
Hydroxy-TEMPO	I R=OH	3.6
MCPROXYL	II R=$COOCH_3$	8.6

1-Octanol/water partition coefficients were determined.

3. Results and discussion

Since the permeability to the BBB is dependent on the lipophilicity and molecular weight of the compound, we examined the partition coefficients of various nitroxyl compounds. Table 1 partition coefficients between 1-octanol and water. The partition coefficients of carbamoyl-PROXYL and hydroxy-TEMPO were approximately consistent with those reported by Fuchs et al. [14]. MCPROXYL was more lipophilic than carbamoyl-PROXYL and the other spin probes, predicting the good permeability to the BBB of this compound.

Table 2 summarizes the BUI values for MCPROXYL. The BUI was calculated as described in Section 2. The BUI values for MCPROXYL were considerably higher than those for diazepam [15], suggesting that MCPROXYL can pass through the BBB and distribute well in the brain. This finding is consistent with the results reported by Sano et al. [16]. The result that the BUI decreased with the increase of the concentration of MCPROXYL coincided with the previous report for choline by Oldendorf and Braun [17].

We have confirmed the penetration of MCPROXYL to BBB and its distribution to the brain tissue by autoradiography using [^{14}C]sucrose as a control. Fig. 1 shows typical auto-

Table 2
Brain uptake index for MCPROXYL

Drug	BUI ± S.E. (%)	Reference
Acetylsalicylic acid (0.3 mM)	4.1 ± 1.1	[15]
Chloramphenicol (0.3 mM)	9.7 ± 0.7	[15]
Diazepam (0.3 mM)	94.4 ± 3.7	[15]
MCPROXYL (114.3 mM)	95.2 ± 4.6 (3)	This work
MCPROXYL (31.8 mM)	97.3 ± 1.5 (5)	This work
MCPROXYL (15.9 mM)	132.0 ± 2.8 (6)	This work
MCPROXYL (7.9 mM)	179.0 ± 6.8 (6)	This work

Values in parentheses are numbers of rats.

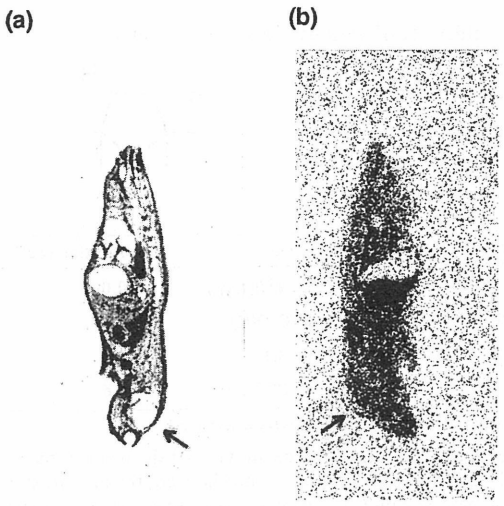

Fig. 1. Autoradiograms of the mice 5 min after injection. a: [^{14}C]Sucrose and b: [^{14}C]MCPROXYL. Details of the preparation are described in Section 2. The arrows show the mouse brain.

radiograms 5 min after injection of [^{14}C]sucrose (Fig. 1a) and [^{14}C]MCPROXYL (Fig. 1b), respectively. Fig. 2 shows a photograph of the corresponding section to Fig. 1. As shown in Figs. 1 and 2, [^{14}C]sucrose, which is known to be impermeable to BBB, was distributed to the blood vessel well but not to the brain cavity. On the other hand, [^{14}C]MCPROXYL was distributed to the liver and the brain cavity as well as to the blood vessel. The difference between the MCPROXYL and sucrose distribution to the brain was quantitatively estimated by analyzing the BAS image obtained through the simultaneous contact of MCPROXYL and sucrose sections (autoradiograms not shown). The areas of the regions of interest were 5.2 mm^2 for both the brain and the background. The intensities of photostimulated luminescence in three regions of interest in the brain were measured, subtracted the level of background, and then averaged. The intensity of the photostimulated luminescence, which is proportional to the ^{14}C concentration, was 1.07 ± 0.38 for the mouse to which sucrose was injected, while it was 5.52 ± 0.31 for the MCPROXYL-injected mouse. The ^{14}C concentration in the brain cavity of MCPROXYL-injected mouse was more than 5 times larger than that of sucrose-injected mouse. The results clearly show that MCPROXYL can penetrate to BBB and be well distributed to the brain tissue.

Fig. 3 shows the in vivo ESR spectra in the head (a) and the abdomen (b) of mice 1 min after the injection of MCPROXYL. In both regions, the spectrum consisting of three lines due to nitroxyl was observed. The hyperfine splitting was 1.65 mT, and the intensity of the three lines was not equivalent. The non-equivalent intensity due to a restriction of the rotational motion may be derived from the binding of MCPROXYL with biological materials such as protein. In both the head and the abdomen, a weak signal of the nitroxyl in the lipid phase was observed as a shoulder at the highest magnetic field peak. Since hyperfine structures and g-tensors of the ESR spectrum depend on the polarity of the environment in which the spin probe exists, the high field line may partially resolve into two lines. This result was consistent with the spectra of 2,2,6,6-tetramethyl piperidine-1-yloxy [18] and 2,2,6,6-tetramethyl-4-oxopiperidine-1-yloxy [19] in phospholipid membranes measured by X-band ESR. Komarov et al. have also

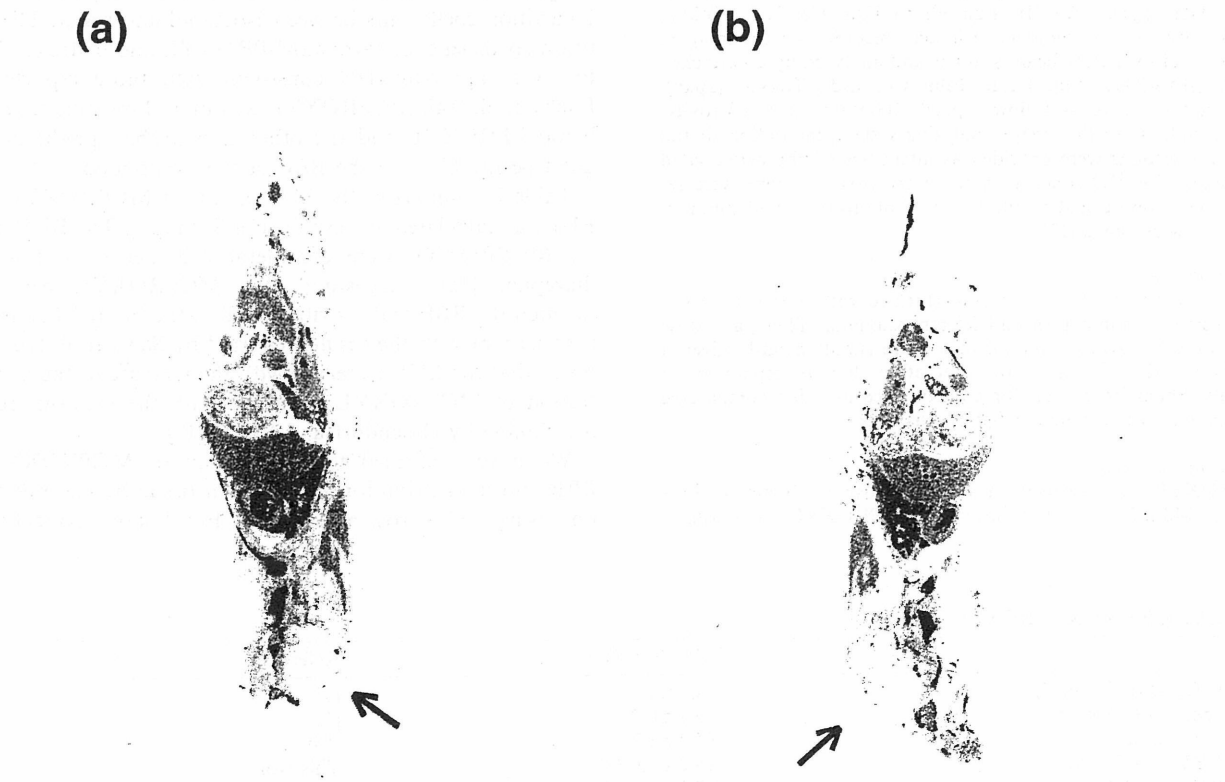

Fig. 2. A photograph of the same section as Fig. 1. a: [^{14}C]Sucrose and b: [^{14}C]MCPROXYL. Details of the preparation are described in Section 2. The arrows show the mouse brain.

Table 3
Effects of X-irradiation on kinetic constants of signal decay in the mouse head and abdomen

Dose of X-irradiation (Gy)	Head		Abdomen	
	1 h after irradiation	4 days after irradiation	1 h after irradiation	4 days after irradiation
0	0.142 ± 0.014 (6)	0.131 ± 0.019 (4)	0.137 ± 0.012 (6)	0.167 ± 0.026 (6)
1	0.135 ± 0.009 (6)	0.132 ± 0.017 (6)	–	–
3	0.105 ± 0.008 (4)*	0.142 ± 0.009 (5)	0.129 ± 0.010 (6)	0.170 ± 0.015 (6)
7.5	0.104 ± 0.010 (5)*	0.131 ± 0.015 (7)	0.128 ± 0.024 (4)	0.152 ± 0.015 (7)
15	O.110 ± 0.007 (5)*	–	0.125 ± 0.025 (3)	

*$P < 0.01$, different from that of 0 Gy.
The kinetic constants (min^{-1}) are the means ± S.D. Values in parentheses are numbers of mice.

demonstrated the two components, derived from an aqueous phase and a lipid phase, of 2,2,6,6-tetramethyl piperidine-1-yloxy injected to a mouse measured by S-band ESR [20]. Since this non-equivalent intensity and the appearance of the component in the lipid phase in the ESR spectrum were not detected using the water-soluble spin probes, these are very characteristic of MCPROXYL with high lipophilicity.

The signals of MCPROXYL in both regions decreased gradually with time after the injection. The kinetic constants of signal decay were calculated as described in Section 2. The effects of X-irradiation on the kinetic constants of signal decay of MCPROXYL were examined (Table 3). In the head, the decay rates of MCPROXYL were decreased (−25%) 1 h after X-irradiation at the doses of 3 and 7.5 Gy. A decrease in the decay rate was not observed 4 days after irradiation. In the abdomen, radiation effects were not observed at 1 h and 4 days after irradiation. These findings demonstrate that the X-irradiation decreased the rates of signal decay of MCPROXYL in the brain immediately after the irradiation. We have reported that the decay rates of carbamoyl-PROXYL were increased by X-irradiation in the mouse abdomen [7]. The opposite effects in the decay rate between MCPROXYL and carbamoyl-PROXYL may be presumably considered both the difference of the measuring region, i.e. the head and the abdomen, and the difference in the pharmacokinetics between MCPROXYL and carbamoyl-PROXYL. The different pharmacokinetics is probably derived from the following factors; (1) tissue and sub-cellular distribution, (2) reactivities with metabolic enzymes, bioreductants and bioradicals, and (3) the rate of excretion.

In conclusion, it was demonstrated that MCPROXYL is fairly lipophilic and can permeate through the BBB to brain. The rate of the signal decay of MCPROXYL was decreased by X-irradiation in the head region. These findings indicate that MCPROXYL is a novel spin probe for in vivo ESR, which can monitor the changes of the physiological redox state in the brain and/or the damage of the brain function caused by X-irradiation.

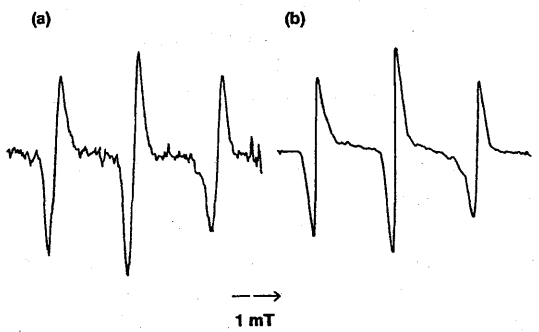

Fig. 3. In vivo ESR spectra of MCPROXYL in the head and abdomen of a living mouse. An anesthetized mouse was placed in a resonator. One min after the injection of MCPROXYL solution (140 mM, 80 μl) to a tail vein, the ESR spectrum was measured in the head (a) and the abdomen (b). The in vivo ESR spectrometer was equipped with an L-band microwave power unit and a loop-gap resonator. Details are described in Section 2.

Acknowledgements: We thank Dr. Nobuo Ikota and Dr. Hitoshi Ishizuka for providing us with the helpful discussion about the synthesis and the characterization of MCPROXYL, and the pharmacokinetics of MCPROXYL, respectively.

References

[1] Halliwell, B. (1989) Acta Neurol. Scand. 126, 23–33.
[2] Gomi, F., Utsumi, H., Hamada, A. and Matsuo, M. (1993) Life Sci. 52, 2027–2033.
[3] Masuda, S., Utsumi, H., and Hamada, A. (1992) in: Oxygen Radicals (Yagi, K., Kondo, M., Niki, E., and Yoshikawa, T. Eds.), pp. 175–178.
[4] Miura, Y., Utsumi, H. and Hamada, A. (1992) Biochem. Biophys. Res. Commun. 182, 1108–1114.
[5] Miura, Y., Utsumi, H. and Hamada, A. (1995) Free Radic. Res. 22, 209–214.
[6] Utsumi, H., Kawabe, H., Masuda, S., Takeshita, K., Miura, Y., Ozawa, T., Hashimoto, T., Ikehira, H., Ando, K., Yukawa, O. and Hamada, A. (1995) Free Radic. Res. Commun. 16, (1.5)
[7] Miura, Y., Anzai, K. and Ozawa, T. (1997) Free Radic. Biol. Med. 23, 533–540.
[8] Ishida, S., Matsumoto, S., Yokoyama, H., Mori, N., Kumashiro, H., Tsuchihashi, N., Ogata, T., Yamada, M., Ono, M., Kamada, H. and Yoshida, E. (1992) Magn. Reson. Imaging 10, 109–114.
[9] Rozantzev, E.G. and Krinitzkaya, L.A. (1965) Tetrahedron 21, 491–497.
[10] Keana, J.F.W. (1978) Chem. Rev. 78, 37–64.
[11] Oldendorf, W.H. (1970) Brain Res. 24, 372–376.
[12] Lin, T.-H., Sawada, Y., Sugiyama, Y., Iga, T. and Hanano, M. (1987) Biochem. Pharmacol. 36, 3425–3431.
[13] Takahashi, S., Kubota, Y., Koshimoto, C., Sato, H. and Hatashita, S. (1994) Radiat. Res. 140, 10–16.
[14] Fuchs, J., Nitschmann, W.H., Packer, L., Hankovszky, O.H. and Hideg, K. (1990) Free Radic. Res. Commun. 10, 315–323.
[15] Bezek, S., Trnovec, T., Scasnar, V., Durisova, M., Kukan, M., Kally, Z., Laginova, V. and Svoboda, V. (1990) Experientia 46, 1017–1020.
[16] Sano, H., Matsumoto, K. and Utsumi, H. (1997) Biochem. Mol. Biol. Int., in press.
[17] Oldendorf, W.H. and Braun, L.D. (1976) Brain Res. 113, 219–224.
[18] Wu, S.H.-W. and McConnell, H.M. (1975) Biochemistry 14, 847–854.
[19] Anzai, K., Yoshida, M. and Kirino, Y. (1990) Biochim. Biophys. Acta 1021, 21–26.
[20] Komarov, A.M. and Lai, C.S. (1994) Biochem. Biophys. Res. Commun. 201, 1035–1042.

Free Radical Biology & Medicine, Vol. 23, No. 4, pp. 533–540, 1997

0891-5849/97 $17.00 + .00

ELSEVIER

PII S0891-5849(97)00103-2

Original Contribution

IN VIVO ELECTRON PARAMAGNETIC RESONANCE STUDIES ON OXIDATIVE STRESS CAUSED BY X-IRRADIATION IN WHOLE MICE

YURI MIURA,* KAZUNORI ANZAI,* SHIRO URANO,† and TOSHIHIKO OZAWA*

*Department of Bioregulation Research, National Institute of Radiological Sciences, Anagawa, Inage-ku, Chiba-shi 263, Japan
†Tokyo Metropolitan Institute of Gerontology, Tokyo 173, Japan

(*Received* 2 *January* 1996; *Revised* 11 *July* 1996; *Re-revised* 4 *November* 1996; *Accepted* 4 *December* 1996)

Abstract—The effect of x-irradiation on the reduction rates of nitroxyl radicals was examined in whole mice using in vivo EPR. One hour after irradiation, the reduction rates of nitroxyl increased up to 15 Gy irradiation, but decreased over this dose. The enhancement of the reduction rate of nitroxyl was suppressed by preadministration of a radioprotector, cysteamine, suggesting that the enhancement of nitroxyl reduction is related to the radiation damage. Thiobarbituric acid-reactive substances (TBARS) in liver homogenate were increased by x-irradiation, indicating that x-irradiation induced oxidative stress in mice. Endogenous antioxidant, α-tocopherol, and the activities of antioxidative enzymes such as superoxide dismutase (SOD), catalase, and glutathione peroxidase were not induced by x-irradiation under these experimental conditions. Eventually the nitroxyl reduction in whole mice should be enhanced by the oxidative stress due to x-irradiation. An in vivo EPR system probing the nitroxyl reduction should be applicable to the noninvasive study on the oxidative stress caused by radiation. © 1997 Elsevier Science Inc.

Keywords—In vivo EPR, Radiation, X-irradiation, Nitroxyl radical, Oxidative stress, Active oxygens, α-Tocopherol, Antioxidative enzymes

INTRODUCTION

Radiation is known to produce various active oxygens in biological systems such as hydroxyl radical, superoxide, and hydrogen peroxide, and causes various types of tissue damage due to successive free radical reactions.[1] However, organisms have protective systems against free radical reactions, for example, endogenous antioxidants and antioxidative enzymes. Because these protective systems may well function in association with each other, in vivo studies are important to accurately estimate the oxidative stress in biological systems.

In vivo studies of radiation damage have been performed by invasive methods such as the measurement of lethal doses (e.g., LD_{50}) and tissue damage. These in vivo methods only show the final results of free radical reactions. Therefore, a noninvasive in vivo method to measure free radical reactions is necessary to investigate the mechanisms of radiation damage in the whole body.

The in vivo EPR spectrometer enables the detection of exogenous free radicals such as nitroxyl[2,3] and lithium phthalocyanine,[4] and endogenous free radicals such as nitric oxide[5–7] in the whole body. Oxidative stress and the redox state in biological systems have also been estimated by in vivo EPR spectroscopy.[8–12] The rates of nitroxyl reduction in the whole body were reported to be very susceptible to physiological redox state and oxidative stress, for example, ischemia-reperfusion,[8] γ-radiation damage,[9] aging,[10] hypoxia, and hyperoxia.[11,12]

In the present study, we examined the effects of x-irradiation on nitroxyl reduction by in vivo EPR, the lipid peroxidation in various organs, and the antioxidative systems in the whole body such as endogenous antioxidants and activities of antioxidative enzymes. We found that x-irradiation caused two phase dose-dependent effect on the nitroxyl reduction and that the effect should be attributable to oxidative stress due to x-irradiation.

Address correspondence to: Toshihiko Ozawa, Department of Bioregulation Research, National Institute of Radiological Sciences, 9-1, Anagawa-4-chome, Inage-ku, Chiba-shi 263, Japan.

MATERIALS AND METHODS

Chemicals

3-Carbamoyl-2,2,5,5-tetramethyl-pyrrolidine-N-yloxy (carbamoyl-PROXYL) was purchased from Aldrich Chemical Co. Inc. (Milwaukee, WI) and dissolved in sterilized distilled water (280 mM). Pentobarbital (50 mg/ml) was obtained from Dainabot Co., Ltd. (Osaka, Japan). Cysteamine was purchased from Wako Pure Chemical Industries, Ltd. (Osaka, Japan). α-Tocopherol and 2,2,5,7,8-pentamethyl-6-hydroxychroman (PMC) were gifts of the Eisai Co. Ltd. (Tokyo, Japan). Other reagents were of the highest grade commercially available.

Animals

Female ddY mice (3–4 weeks, 15–20 g body weight) were purchased from Japan SLC, Inc. (Hamamatsu, Japan).

X-irradiation

The irradiation of mice was performed with x-rays (200 kV, 20 mA), using 0.5 mm copper and 0.5 mm aluminum filters at a dose rate of 0.62–0.65 Gy/min. The x-ray dose delivered was measured with an AE-1321 exposure ratemeter. Several mice were simultaneously given a single whole-body exposure in individual chambers. Sham irradiation of the controls included comparable immobilization in the same irradiation chamber. Anesthetic was not administered to both irradiated and sham-irradiated mice.

In vivo EPR measurement

The mice were anesthetized by intramuscular injection of pentobarbital (100 mg/kg) and fixed on a Teflon holder, as described previously.[13] A mouse fixed in a holder was placed in a resonator of the in vivo EPR spectrometer and a sterilized solution of carbamoyl-PROXYL was injected into the tail vein of the mouse (50 μl). The EPR spectra were measured in the upper abdomen immediately after the injection with an EPR spectrometer (JES-PE, JEOL, Tokyo, Japan) equipped with an L-band microwave power unit (ES-LB1A, JEOL) and a loop-gap resonator. The sensitivity of the spectrometer was checked with DPPH powder attached to the Teflon holder. The rates of nitroxyl reduction were calculated from the spin clearance curves, which were determined from semilogarithmic plots of the peak heights of the EPR signal at the lower magnetic field.

Effects of x-irradiation on the rates of nitroxyl reduction

The mice were separated into six groups. Groups 1 and 2 were treated by sham irradiation as a control. Groups 3 and 4 were treated by x-irradiation at the dose of 7.5 Gy, and groups 5 and 6 were treated by 15 Gy irradiation as described above. One hour after irradiation, in vivo EPR measurement was performed in the upper abdomen of the mice of groups 1, 3, and 5; 4 or 5 d after irradiation, groups 2, 4, and 6 were measured by the same method.

The dependency of nitroxyl reduction on the radiation dose was examined as follows. One hour after x-irradiation at the dose of 1, 4, 7.5, 11, 15, 20, and 30 Gy, the rate of nitroxyl reduction was measured in the abdomen of mice as described above. The control mice were treated by sham irradiation.

Effects of preadministration of cysteamine

Cysteamine solution in saline adjusted to pH 7.0 was administered to the mice intraperitoneally 20 min before irradiation (0.5 or 2.0 mmol/kg). Saline was administered to the control mice (0.2 ml). The mice were separated into three groups, respectively; the rate of nitroxyl reduction was measured 1 h after sham irradiation, 1 h after 15 Gy irradiation, and 5 d after 7.5 Gy irradiation using in vivo EPR spectrometer.

Effects of x-irradiation on cyt. p-450 content and the activity of cyt. p-450 reductase

One hour after irradiation the mice were sacrificed and liver microsomes were prepared by the conventional method. The protein concentration in microsomes was determined by the method of Bradford.[14] The contents of cyt. P-450 was calculated by CO-difference spectra, and the activity of cyt. P-450 reductase was examined according to the method of Yasukochi and Masters.[15]

TBARS generation

Thiobarbituric acid-reactive substances (TBARS) were measured in the liver homogenates of the mice at 4 d postirradiation. Ten percent liver homogenates were prepared by the conventional method, and TBARS were measured by the method of Buege and Aust.[16] Protein assay was performed by the Bradford method.[14]

Contents of α-tocopherol

α-Tocopherol levels in the plasma, erythrocytes, and liver were determined as follows.[17] Blood collected

from murine hearts in heparinized tubes was centrifuged at 2000 rpm for 2 min at 4°C. From the plasma obtained, α-tocopherol was extracted with *n*-hexane. The suspension of erythrocytes was saponified by 60% KOH at 70°C for 30 min in the presence of 6% pyrogarrol. α-Tocopherol in erythrocytes was extracted with 10% ethyl acetate/*n*-hexane. α-Tocopherol in liver was extracted in a manner similar to that in erythrocytes after saponification. Pentamethyl-6-hydroxychroman (PMC) was used as an internal standard. α-Tocopherol was analyzed by reversed-phase HPLC equipped with an electrochemical detector (0.55 V, Nanospace SI-1, Shiseido, Tokyo, Japan).

Enzyme assays

At 1 h and at 5 d postirradiation, the 10% liver homogenates of mice were prepared and centrifuged at 3000 rpm for 20 min. Immediately after centrifugation, the activities of SOD, catalase and glutathione peroxidase in the supernatant were assayed by the methods of Oyanagui,[18] Aebi,[19] and Flohe and Gunzler[20] with slight modification, respectively.

RESULTS

Nitroxyl reduction in whole body

In EPR spectrum in abdomen of mice, three sharp lines were observed and these signals gradually decreased with time after injection of carbamoyl-PROXYL, as described previously.[11,12] We calculated the initial kinetic constants of signal decay in the abdomen from spin-clearance curves as described in Materials and Methods.

Table 1 summarizes the effects of x-irradiation on the kinetic constants of nitroxyl reduction in the abdomen. One hour after irradiation at the dose of 15 Gy, the reduction rate of nitroxyl was significantly enhanced (by 33 %) over that of sham irradiation. Four days after irradiation at the dose of 7.5 Gy, the reduction rate was significantly enhanced (+32%), while that following the dose of 15 Gy was significantly decreased (−40%), compared with that 4 or 5 d after sham irradiation. In sham controls, during 4 or 5 d the reduction rates of nitroxyl increased from 0.109 to 0.125, presumably due to the growth. The body weights of the mice that did not receive irradiation increased by about 20% for 5 d, while the weights of those exposed to 7.5 Gy and 15 Gy irradiation decreased 5 and 30%, respectively. Especially, the mice exposed to 15 Gy irradiation were damaged severely; about half of the mice died within 5 d after irradiation.

The dependency of nitroxyl reduction on the radiation dose was examined 1 h after irradiation (Fig. 1).

Table 1. Effects of X-Irradiation on the Reduction Rates of Nitroxyl in Mice Abdomen

Radiation Dose	Time after Radiation	Initial Kinetic Constants (/min) Mean ± SD
0 Gy	1 h	0.109 ± 0.015 (8)
	4–5 d	0.125 ± 0.031 (5)
7.5 Gy	1 h	0.130 ± 0.029 (7)
	4 d	0.165 ± 0.029* (6)
15 Gy	1 h	0.145 ± 0.021† (11)
	5 d	0.075 ± 0.008‡ (4)

*$p < .1$, different from that of 4–5 d after 0 Gy.
†$p < .001$, different from that of 1 h after 0 Gy.
‡$p < .05$, different from that of 4–5 d after 0 Gy.
Values in parentheses are numbers of mice.

The rates of nitroxyl reduction reached the maximum value at about 15 Gy irradiation, and then decreased.

The effects of cysteamine, which is known to be a radioprotector, on the enhancement of the nitroxyl reduction rate were examined (Fig. 2). Cysteamine was administered to mice intraperitoneally 20 min before irradiation. In the mice without irradiation, cysteamine did not affect the rate of nitroxyl reduction. However, 1 h after 15 Gy irradiation and 5 d after 7.5 Gy irradiation, the enhancement of nitroxyl reduction rates in the control mice (saline administration) were significantly suppressed by the preadministration of cysteamine.

TBARS generation

We examined the generation of TBARS as an indicator of lipid peroxidation in the whole body of mice. In liver homogenates, TBARS increased with x-irradiation (Fig. 3). In our experimental conditions, because x-irradiation gave significant oxidative stress to the mice, the lipid peroxidation was induced in tissue. These results agree with those of Ueda et al.[21] and Yamaoka et al.[22] Ueda reported the increase of TBARS after γ-irradiation at 10 Gy, and Yamaoka demonstrated the slight increase of TBARS in liver after a high dose of x-irradiation. However, Peltora et al. reported that TBARS decreased 1 or 7 d after x-irradiation at the dose of 0.5 and 3.0 Gy.[23] Yamaoka et al. have also reported that a low dose of x-irradiation decreased TBARS in various organs. The dose of x-irradiation is thus important for lipid peroxidation in organs.

α-tocopherol contents

Because α-tocopherol, an endogenous antioxidant, is known to have a radioprotective effect,[24] we examined the alteration of the contents of α-tocopherol due

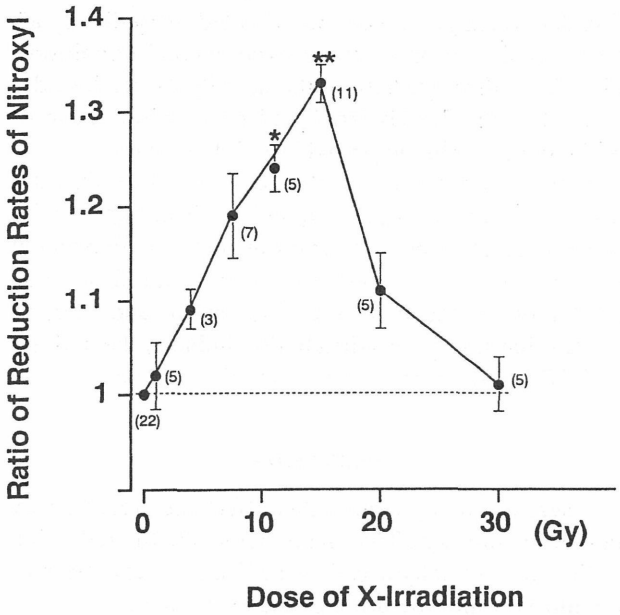

Fig. 1. The dependency of nitroxyl reduction rates on the radiation dose. X-irradiation was performed as described in Materials and Methods. The kinetic constants of nitroxyl reduction rates in the abdomen were calculated from the spin-clearance curves, which were measured 1 h after irradiation. Ordinate was the ratio of the kinetic constants of the irradiated mice to that of sham controls. The ratios are the means ± SE of several experiments. Values in parentheses are numbers of mice. *, **Significantly different from that of 0 Gy at $p < .05$ and .01, respectively.

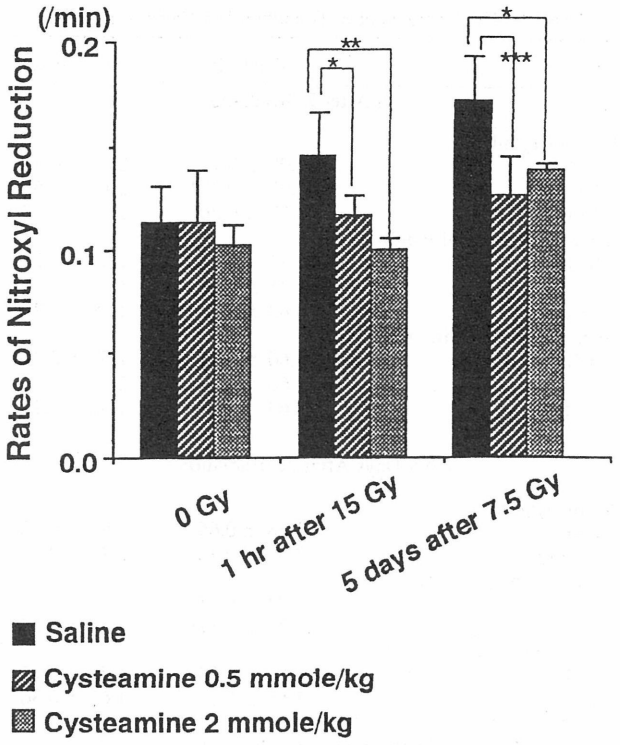

Fig. 2. Effects of preadministration of cysteamine on the increase of nitroxyl reduction rates. Cysteamine solution in saline adjusted to pH 7.0 by 0.1 M NaOH was administered to mice intraperitoneally 20 min before irradiation (0.5 or 2.0 mmol/kg). The mice were divided in three groups; 1 h after 15 Gy irradiation, 5 d after 7.5 Gy irradiation, and without irradiation. The kinetic constants of nitroxyl reduction rates in the abdomen were measured asdescribed in Materials and Methods. The kinetic constants are the means ± SD of five or six experiments. *, **, ***Significantly different from the kinetic constants of the mice administered saline at $p < .05$, .001, and .01, respectively.

to x-irradiation (Table 2). One hour after irradiation, the content of α-tocopherol in control mice decreased with x-irradiation in plasma, while there was no effect in erythrocytes or the liver. α-Tocopherol in plasma is mainly present in low density lipoprotein (LDL)[25] and functions to protect LDL against oxidative damage.[25,26] Therefore, these results suggest that LDL should be damaged oxidatively by x-irradiation, resulting in the consumption of α-tocopherol in plasma. Dierenfeld and McGuire[27] have also reported that the content of α-tocopherol in ruminant blood was lowered by γ-irradiation.

Five days after irradiation, the levels of α-tocopherol in the control mice were decreased by x-irradiation in the plasma and erythrocytes, while there was no effect in the liver. These results suggest that the consumption of α-tocopherol due to oxidative damage was progressing over the 5 d, and that the gastrointestinal injury due to x-irradiation lowered the uptake of α-tocopherol.

The preadministration of cysteamine suppressed the decrease of α-tocopherol due to x-irradiation in plasma 1 h after irradiation, suggesting that cysteamine protects the oxidative damage of LDL due to x-irradiation. In the nonirradiated group, the contents of α-tocopherol in the mice administered cysteamine were increased compared with those without cysteamine, indicating that cysteamine may be involved in the regeneration of α-tocopherol. α-Tocopheryl radical, which is formed from α-tocopherol in the process of the scavenging of

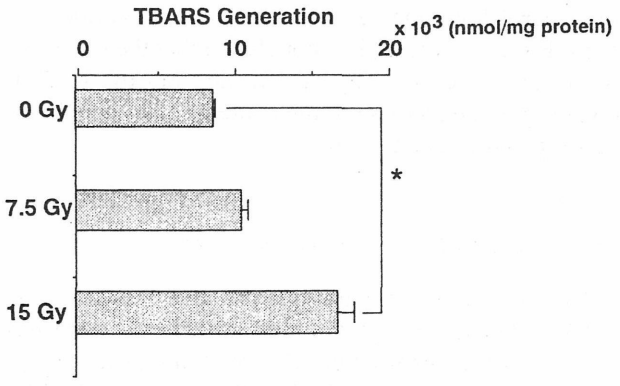

Fig. 3. TBARS generation due to x-irradiation. TBARS in the liver homogenates were measured as described in Materials and Methods after 4 d after irradiation. The data are the means ± SE of five or six experiments. *Significantly different from that of 0 Gy at $p < .01$.

Table 2. The Contents of α-Tocopherol in Various Tissues

	Control[a]	Cysteamine[b]
(a) 1 h After X-Irradiation		
Plasma (μg/ml)		
0 Gy	2.00 ± 0.16	2.41 ± 0.43
7.5 Gy	1.62 ± 0.30*	2.10 ± 0.52
15 Gy	1.60 ± 0.20†	2.33 ± 0.40
Erythrocytes (μg/ml RBC)		
0 Gy	1.72 ± 0.63	1.80 ± 0.26
7.5 Gy	1.48 ± 0.49	1.55 ± 0.15
15 Gy	1.82 ± 0.52	1.58 ± 0.27
Liver (μg/mg protein) $\times 10^2$		
0 Gy	1.60 ± 0.27	1.67 ± 0.47
7.5 Gy	1.60 ± 0.16	2.10 ± 0.38
15 Gy	1.63 ± 0.27	1.57 ± 0.17
(b) 5 Days After X-Irradiation		
Plasma (μg/ml)		
0 Gy	2.68 ± 0.65	2.84 ± 0.28
7.5 Gy	2.04 ± 0.42	2.44 ± 0.37
Erythrocytes (μg/ml RBC)		
0 Gy	2.04 ± 0.37	2.40 ± 0.76
7.5 Gy	1.26 ± 0.17†	1.47 ± 0.50*
Liver (μg/mg protein) $\times 10^2$		
0 Gy	1.61 ± 0.34	1.78 ± 0.17
7.5 Gy	1.68 ± 0.33	1.62 ± 0.36

* $p < .05$, † $p < .01$ Different from that of 0 Gy.
[a] Control group was administered saline (0.2 ml, IP).
[b] Cysteamine group was administered cysteamine solution (2.0 mmol/kg, IP).

the oxygen radicals, might be reduced to α-tocopherol by cysteamine, with the present result that the content of α-tocopherol increased compared with that in the mice without cysteamine. It has been reported that glutathione (GSH) can reduce α-tocopheryl radical to α-tocopherol and produce GS· radical.[28] Because cysteamine has a thiol group as the same as that of GSH, a similar reaction between cysteamine and α-tocopheryl radical might occur.

In the comparison of the content of α-tocopherol 1 h and 5 d after irradiation, in nonirradiated mice the α-tocopherol level increased significantly in various organs. From this result, it is concluded that the mice (3–4 weeks) were growing significantly during the 5 d, resulting in the increase of the contents of α-tocopherol accompanying the growth.

The activities of antioxidative enzymes

The activities of antioxidative enzymes such as SOD, catalase, and glutathione peroxidase were examined in the supernatant of liver homogenate (Fig. 4). One hour after x-irradiation, the activities of SOD, catalase, and glutathione peroxidase did not change significantly compared with those of the nonirradiated mice. These results suggest that the activities of antioxidative enzymes were not affected immediately after x-irradiation under these experimental conditions. Five days after irradiation, the activity of catalase decreased in the 7.5 Gy-irradiated mice, while those of SOD and glutathione peroxidase did not vary.

Effects of radiation on the activities of SOD, catalase, and glutathione peroxidase have been reported by several investigators.[21–23] Their results were dependent on the experimental conditions such as the dose of x-irradiation or the time after irradiation, and demonstrated that low-dose x-irradiation induced the activity of SOD, while high-dose x-irradiation did not.

DISCUSSION

There are many factors that affect the signal decay rate of the nitroxyl. Two main factors are the reduction of the nitroxyl to hydroxylamine[29] and the excretion of the nitroxyl into the urine or the excrement.[30]

Nitroxyl radical injected to the organisms is known to be reduced to hydroxylamine in the various tissues.[29] The signal decay of nitroxyl in the whole body has been reported to be due to the reduction immediately after injection of nitroxyl.[10,13] We also have found that the EPR signal intensity of carbamoyl-PROXYL in collected blood remains almost unchanged from the original intensity during 10 min after injection but decreased after 10 min, by the addition of potassium ferricyanide, an oxidizing agent of hydroxylamine to nitroxyl radical (data not shown). If the excretion of nitroxyl contributes to the signal decay of nitroxyl, the concentration of nitroxyl and hydroxylamine should decrease and then the EPR signal of oxidized sample 10 min after injection should be smaller than that immediately after injection. Therefore, we consider that the reduction to hydroxylamine is the main factor that is responsible to the signal decay of nitroxyl during the 10 min after injection.

Ionizing radiation generates active oxygen species through an excitation of water,[1] resulting in the exposure of the irradiated organisms to the oxidative stress. In the present study, we examined the effects of radiation on the reduction rates of nitroxyl in the whole body of mice. The reduction rates of nitroxyl increased up to the dose of 15 Gy but decreased over 15 Gy 1 h after irradiation, and decreased 5 d after 15 Gy irradiation (Table 1, Fig. 1). There are at least two factors that affect the reduction rate of the nitroxyl; one causing enhancement and another causing inhibition.

The activity of drug metabolism including cytochrome P-450 and cytochrome P-450 reductase was reported to be reduced 3 or 7 d after irradiation.[31]. Therefore, the decrease of the rates of nitroxyl reduction 5 d after 15 Gy irradiation may have been caused by injury

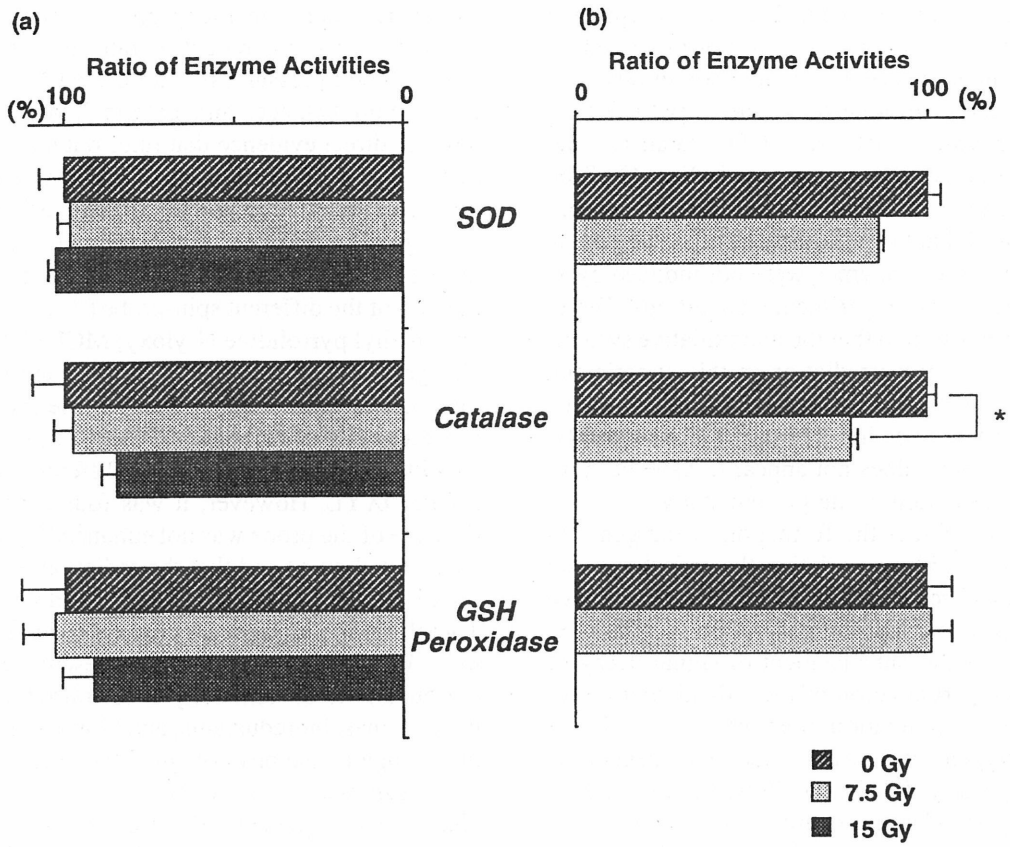

Fig. 4. The activities of antioxidative enzymes in the supernatant of 10% liver homogenate. Supernatant was prepared from liver homogenates and assayed as described in Materials and Methods. (a) One hour after x-irradiation; (b) 5 d after x-irradiation. The data are the means ± SE of five or six experiments. *Significantly different from that of 0 Gy at $p < .05$.

of the drug metabolic system. A similar decrease of nitroxyl reduction was reported in γ-irradiated mice.[9] Also, the result that the enhancement of nitroxyl reduction 1 h after irradiation was suppressed at the dose of more than 15 Gy, might have been explained by the injury of the reduction capability.

We will further discuss the increase of the reduction rate. Because the preadministration of cysteamine, a radioprotector, suppressed the increase of the reduction rates of nitroxyl by x-irradiation (Fig. 2), the enhancement of nitroxyl reduction should be related to the radiation damage. The body weights of mice and drug metabolism did not change significantly 1 h after irradiation (Table 3), suggesting that the enhancement of nitroxyl reduction 1 h after irradiation was not caused by the change of body weight or the functioning of the drug metabolism system.

The rates of nitroxyl reduction in the whole body have been reported to be sensitive to the physiological reducing capacity, and the generation of active oxygens and the subsequent free radical reactions in whole body.[8-12] Therefore, there are two possibilities in explanation of the increase of nitroxyl reduction by x-irradiation. One is the increase of reducing capacity caused by the induction of the defense system against oxidative stress in organism, and the other is the participation of active oxygens and various free radicals generated by the x-irradiation.

To test these two possibilities, we examined the induction of antioxidative systems by x-irradiation. The levels of α-tocopherol, an established endogenous antioxidant, were examined in plasma, erythrocytes, and

Table 3. Effects of X-Irradiation on Cytochrome P-450 Content and the Activity of Cytochrome P-450 Reductase

Irradiation Dose (Gy)	Cyt. P-450 Content (nmol/mg protein)	Activity of Cyt. P-450 Reductase (nmol/min/mg protein)
0	0.42 ± 0.02	105 ± 4
3	0.52 ± 0.03	103 ± 4
7.5	0.46 ± 0.02	95 ± 7
15	0.46 ± 0.01	113 ± 7

The mice were sacrificed 1 h after irradiation. The mice liver microsomes were prepared by the conventional method. Cyt. P-450 content and activity of cyt. P-450 reductase were examined as described in Materials and Methods.

liver (Table 2). From the data in Table 2, it is apparent that the levels of α-tocopherol were not increased by x-irradiation under these experimental conditions. Further, the effects of x-irradiation on the activities of antioxidative enzymes such as SOD, catalase, and glutathione peroxidase were examined (Fig. 4). Both 1 h and 5 d after irradiation the activities of antioxidative enzymes did not significantly change, suggesting that the antioxidative enzymes were not induced by x-irradiation under these experimental conditions. Therefore, it was demonstrated that the antioxidative systems were not induced by x-irradiation in this experiment, although these results are different from those observed in studies with low-dose irradiation.[22,32] Consequently, the reducing capacity does not appear to have been increased by x-irradiation in the present study.

X-irradiation induces the formation of oxygen radicals and causes lipid peroxidation through the subsequent free radical reactions in biological systems (see Fig. 3). It is possible that the generation of active oxygens may cause the enhancement of signal decay of nitroxyl; 1) the participation of the radical chain reaction caused by the generation of active oxygens, 2) the decrease of oxygen concentration due to the generation of active oxygens, and 3) the inhibition of reoxidation systems of hydroxylamine to nitroxyl by active oxygens. It has been reported that nitroxyl reacts with various oxygen radicals such as $\cdot OH$, O_2^-, $LO\cdot$, and $LOO\cdot$ in vitro.[33–35] Because the lifetimes of these free radicals primarily formed by x-irradiation are very short, it is impossible for these radicals to interact with nitroxyl radical directly 1 h after irradiation. However, the generation of active oxygens should give rise to the radical chain reaction in vivo, which is supported by the report that TBARS in various tissues have been increased for several days after irradiation.[21,22] Therefore, the direct interaction of nitroxyl with these secondary bioradicals in the whole body is possible and the enhancement of nitroxyl reduction may be attributable in part to the radical chain reaction due to the generation of active oxygens. Nitroxyl was also reported to be reduced more rapidly under hypoxia.[36,37] O'Hara et al.[38] have reported that the pO_2 in a murine tumor rapidly decreased several hours after irradiation. Consequently, there is a second possibility that the decrease of oxygen concentration might increase the reduction rates of nitroxyl radical. Hydroxylamine, reduced nitroxyl radical, is known to be oxidized to nitroxyl radical in biological systems.[39] As a third possibility, the reoxidation system of hydroxylamine might be damaged by active oxygens due to x-irradiation, with the result that the equilibrium of nitroxyl and hydroxylamine is perturbed and the apparent reduction rates of nitroxyl are increased.

Because these data were obtained from in vivo measurements, there are many physiological factors that indirectly affect the reduction rates of nitroxyl, for example, blood pressure, blood flow rates, body temperature, fluid balance, and caloric intake. Though we have no direct evidence that rules out the physiological factors for the enhancement of nitroxyl reduction, we think that the effect of the physiological factors is small or negligible because of the following findings. We have examined the radiation effects on the nitroxyl reduction of the different spin-probe (3-methoxy-2,2,5,5-tetramethyl pyrrolidine N-yloxy; MCPROXYL). If the change in the physiological factors caused by x-irradiation were the major reason for the increase of the reduction rate of carbamoyl-PROXYL, similar change should be observed with a different spin probe, MCPROXYL. However, it was found that the reduction rate of the probe was not enhanced by x-irradiation (data not shown) and that the radiation effect was distinct between the measurement in abdomen and head. Therefore, the increase of nitroxyl reduction of carbamoyl-PROXYL observed in the present study might be attributable to the reactivity of the nitroxyl with reducing enzymes, bioreductants, and bioradicals, rather than the change of the physiological factors.

In summary, x-irradiation on mice caused two phases dose-dependent effect on the reduction rate of carbamoyl-PROXYL observed at 1 h postirradiation in abdomen of the mice using in vivo EPR. The reduction rate increased up to 15 Gy irradiation, whereas it decreased over this dose. The increase was suppressed by the preadministration of a radioprotector, cysteamine, indicating that the increase of the reduction rate is related to the radiation damage. Antioxidative systems such as endogenous antioxidants and antioxidative enzymes were not induced by x-irradiation in the present conditions. Although the details of the mechanism that increased the reduction rate are still unclear, oxidative stress caused by x-irradiation should be the major factor for this effect. In vivo EPR system probing the nitroxyl reduction will continue to contribute to the noninvasive in vivo studies of radiation damage.

Acknowledgements — This work was supported in part by the Foundation for Life Science Research.

REFERENCES

1. Riley, P. A. Free radicals in biology: Oxidative stress and the effects of ionizing radiation. *Int. J. Radiat. Biol.* **65**:27–33; 1994.
2. Berliner, L. J.; Wan, X. In vivo pharmacokinetics by electron magnetic resonance spectroscopy. *Magn. Reson. Med.* **9**:430–434; 1989.
3. Ferrari, M.; Colacicchi, S.; Gualtieri, G.; Santini, M. T.; Sotgiu, A. Whole mouse nitroxide free radical pharmacokinetics by low frequency electron paramagnetic resonance. *Biochem. Biophys. Res. Commun.* **166**:168– 173; 1990.

4. Liu, K. J.; Gast, P.; Moussavi, M.; Norby, S. W.; Vahidi, N.; Walczak, T.; Wu, M.; Swartz, H. M. Lithium phthalocyanine: A probe for electron paramagnetic resonance oximetry in viable biological systems. *Proc. Natl. Acad. Sci. USA* **90**:5438–5442; 1993.
5. Komarov, A. M.; Mattson, D.; Jones, M. M.; Singh, P. K.; Lai, C. S. In vivo spin trapping of nitric oxide in mice. *Biochem. Biophys. Res. Commun.* **195**:1191–1198; 1993.
6. Lai, C. S.; Komarov, A. M. Spin trapping of nitric oxide produced in vivo in septic-shock mice. *FEBS Lett.* **345**:120–124; 1994.
7. Yoshimura, T.; Fujii, S.; Yokoyama, H.; Kamada, H. In vivo electron paramagnetic resonance imaging of NO-bound iron complex in a rat head. *Chem. Lett.* 309–310; 1995.
8. Masuda, S.; Utsumi, H.; Hamada, A. In vivo EPR studies on radical reduction in femoral ischemia-reperfusion of whole mice. In: Yagi, K.; Kondo, M.; Niki, E.; Yoshikawa, T., eds. *Oxygen radicals. Amsterdam: Elsevier Publishers B.V.; 1992:*175–178.
9. Utsumi, H.; Kawabe, H.; Masuda, S.; Takeshita, K.; Miura, Y.; Ozawa, T.; Hashimoto, T.; Ikehira, H.; Ando, K.; Yukawa, O.; Hamada, A. In vivo EPR studies on radical reaction in whole mice -Effects of radiation exposure. *Free Radic. Res. Commun.* **16**:1.5; 1992.
10. Gomi, F.; Utsumi, H.; Hamada, A.; Matsuo, M. Aging retards spin clearance from mouse brain and food restriction prevents its age-dependent retardation. *Life Sci.* **52**:2027–2033; 1993.
11. Miura, Y.; Utsumi, H.; Hamada, A. Effects of inspired oxygen concentration on in vivo redox reaction on nitroxide radicals in whole mice. *Biochem. Biophys. Res. Commun.* **182**:1108–1114; 1992.
12. Miura, Y.; Utsumi, H.; Hamada, A. In vivo EPR studies of antioxidant activity on free radical reaction in living mice under oxidative stress. *Free Radic. Res.* **22**:209–214; 1995.
13. Utsumi, H.; Muto, E.; Masuda, S.; Hamada, A. In vivo EPR measurement of free radicals in whole mice. *Biochem. Biophys. Res. Commun.* **172**: 1342–1348; 1990.
14. Bradford, M. M. A rapid and sensitive method for the quantitation of microgram quantities of protein utilizing the principle of protein-dye binding. *Anal. Biochem.* **72**:248–254; 1976.
15. Yashukochi, Y.; Masters, B. S. S. Some properties of a detergent-solubilized NADPH-cytochrome *c* (Cytochrome P-450) reductase purified by biospecific affinity chromatography. *J. Biol. Chem.* **251**:5337–5344; 1976.
16. Buege, J. A.; Aust, S. D. Microsomal lipid peroxidation. In: Fleischer, S.; Packer, L., eds. *Methods in enzymology—52.* New York: Academic Press; 1978:302–310.
17. Ueda, T. *Kagaku to Seibutsu.* **31**:44–48; 1993.
18. Oyanagui, Y. Reevaluation of assay methods and establishment of kit for superoxide dismutase activity. *Anal. Biochem.* **142**:290–296; 1984.
19. Aebi, H. Catalase in vitro. In: Packer, L., eds. *Methods in enzymology—105.* San Diego: Academic Press; 1984:121–126.
20. Flohe, L.; Gunzler, W. A. Assays of glutathione peroxidase. In: Packer, L., eds. *Methods in enzymology—105.* San Diego: Academic Press; 1984:114–121.
21. Ueda, T.; Toyoshima, Y.; Kushihashi, T.; Hishida, T.; Yasuhara, H. Effect of dimethyl sulfoxide pretreatment on activities of lipid peroxide formation, superoxide dismutase and glutathione peroxidase in the mouse liver after whole-body irradiation. *J. Toxicol. Sci.* **18**:239–244; 1993.
22. Yamaoka, K.; Edamatsu, R.; Mori, A. Increased SOD activities and decreased lipid peroxide levels induced by low dose x irradiation in rat organs. *Free Radic. Biol. Med.* **11**:-299–306; 1991.
23. Peltola, V.; Parvinen, M.; Huhtaniemi, I.; Kulmala, J.; Ahotupa, M. Comparison of effects of 0.5 and 3.0 Gy X-irradiation on lipid peroxidation and antioxidant enzyme function in rat testis and liver. *J. Androl.* **14**:267– 274; 1993.
24. Brown, M. A. Resistance of human erythrocytes containing elevated levels of vitamin E to radiation-induced hemolysis. *Radiat. Res.* **95**:303–316; 1983.
25. Frei, B.; Gaziano, J. M. Content of antioxidants, preformed lipid hydroperoxides, and cholesterol as predictors of the susceptibility of human LDL to metal ion-dependent and -independent oxidation. *J. Lipid Res.* **34**:2135–2145; 1993.
26. Sato, K.; Niki, E.; Shimasaki, H. Free radical-mediated chain oxidation of low density lipoprotein and its synergistic inhibition by vitamin E and vitamin C. *Arch. Biochem. Biophys.* **279**:402–405; 1990.
27. Dierenfeld, E. S.; McGuire, J. T. Effect of gamma irradiation on α- tocopherol levels in ruminant blood samples. *Int. J. Vit. Nutr. Res.* **61**:33–37; 1991.
28. Niki, E.; Tsuchiya, J.; Tanimura, R.; Kamiya, Y. Regeneration of vitamin E from α-chromanoxyl radical by glutathione and vitamin C. *Chem. Lett.* 789– 792; 1982.
29. Iannone, A.; Tomasi, A. Nitroxide radicals, their use as metabolic probes in biological model systems: An overview. *Acta Pharm. Jugosl.* **41**:277–297; 1991.
30. Bacic, G.; Nilges, M. J.; Magin, R. L.; Walczak, T.; Swartz, H. M. In vivo localized ESR spectroscopy reflecting metabolism. *Magn. Res. Med.* **10**:266–272; 1989.
31. Wolfle, G.; Bleyer, H.; Muller, D.; Klinger, W. The influence of the radiation syndrome on cytochrome P450-dependent monooxygenation in rat liver. *Exp. Pathol.* **43**:89–95; 1991.
32. Yamaoka, K.; Edamatsu, R.; Itoh, T.; Mori, A. Effects of low-dose X-ray irradiation on biomembrane in brain cortex of aged rats. *Free Radic. Biol. Med.* **16**:529–534; 1994.
33. Krishna, M. C.; Grahame, D. A.; Samuni, A.; Mitchell, J. B.; Russo, A. Oxoammonium cation intermediate in the nitroxide-catalyzed dismutation of superoxide. *Proc. Natl. Acad. Sci. USA* **89**:5537–5541; 1992.
34. Takahashi, M.; Tsuchiya, J.; Niki, E. Scavenging of radicals by vitamin E in the membranes as studied by spin labeling. *J. Am. Chem. Soc.* **111**:6350–6353; 1989.
35. Miura, Y.; Utsumi, H.; Hamada, A. Antioxidant activity of nitroxide radicals in lipid peroxidation of rat liver microsomes. *Arch. Biochem. Biophys.* **300**:148–156; 1993.
36. Chen, K.; Glockner, J. F.; Morse, P. D., II; Swartz, H. M. Effects of oxygen on the metabolism of nitroxide spin labels in cells. *Biochemistry* **28**:2496– 2501; 1989.
37. Miura, Y.; Utsumi, H.; Hamada, A. Effects of oxygen on the membrane structure and the metabolism of lipophilic nitroxide in rat liver microsomes. *J. Biochem.* **108**:516–518; 1990.
38. O'Hara, J. A.; Goda, F.; Liu, K. J.; Bacic, G.; Hoopes, P. J.; Swartz, H. M. The pO_2 in murine tumor after irradiation: An in vivo electron paramagnetic resonance oximetry study. *Radiat. Res.* **144**:222–229; 1995.
39. Chen, K.; Swartz, H. M. Oxidation of hydroxylamines to nitroxide spin labels in living cells. *Biochim. Biophys. Acta* **970**:270–277; 1988.

ABBREVIATIONS

cyt. P-450—cytochrome P-450
LD_{50}—lethal dose for 50% of irradiated animals
SOD—superoxide dismutase
TBARS—thiobarbituric acid-reactive substances

ARCHIVES OF BIOCHEMISTRY AND BIOPHYSICS
Vol. 357, No. 2, September 15, pp. 231–239, 1998
Article No. BB980811

Reactive Oxygen Species Generated from the Reaction of Copper(II) Complexes with Biological Reductants Cause DNA Strand Scission

Jun-ichi Ueda,[1] Mamiko Takai, Yoshie Shimazu, and Toshihiko Ozawa
National Institute of Radiological Sciences, 9-1 Anagawa 4-chome, Inage-ku, Chiba-shi 263, Japan

Received January 30, 1998, and in revised form June 4, 1998

The generation of hydroxyl radicals (•OH) from the reaction of Cu(II) complexes with biological reductants such as ascorbic acid, glutathione, acetylcysteine, and hydroquinone was confirmed by spin-trapping experiments using electron spin resonance (ESR). The following Cu(II) complexes were used: Cu(II)-(CyHH)$_2$ (CyHH, cyclo(L-histidyl-L-histidyl)), Cu(II)(OP)$_2$ (OP, *o*-phenanthroline), Cu(II)(HGG) (HGG, L-histidylglycylglycine), and Cu(II)(en)$_2$ (en, ethylenediamine). The methyl radical adduct of α-(pyridyl-4-*N*-oxide)-*N*-*tert*-butylnitrone (POBN-CH$_3$) was obtained from the reaction of ascorbic acid with all Cu(II) complexes used here in the presence of a spin trap, POBN, and dimethyl sulfoxide, indicating the generation of •OH. Glutathione, *N*-acetylcysteine, and hydroquinone reacted with both Cu(II)(CyHH)$_2$ and Cu(II)(OP)$_2$ to generate POBN-CH$_3$, while these reductants did not react with either Cu(II)(HGG) or Cu(II)(en)$_2$. Interestingly, the formation of POBN-CH$_3$ in the reaction of Cu(II)-(CyHH)$_2$ with glutathione or *N*-acetylcysteine was found only at a Cu(II)(CyHH)$_2$/glutathione or Cu(II)-(CyHH)$_2$/*N*-acetylcysteine ratio of 1. The DNA strand scission caused by reaction mixtures of Cu(II) complexes with reductants was investigated under the same conditions as the ESR spin-trapping experiments. Addition of ascorbic acid to mixtures of these four Cu(II) complexes and DNA resulted in DNA strand breakage. Hydroquinone plus Cu(II)(CyHH)$_2$ also caused DNA strand scission. In addition, DNA strand breakage was observed with the reaction of Cu(II)(OP)$_2$ with glutathione, *N*-acetylcysteine, and hydroquinone. In contrast, reaction mixtures of glutathione, *N*-acetylcysteine, or hydroquinone with Cu(II)-(HGG) or Cu(II)(en)$_2$ did not cause DNA strand scission within the concentration range used. The results obtained here suggest that there is a good correlation between POBN-CH$_3$ formation and DNA strand scission. Thus, DNA strand scission may be caused by •OH generated from the reaction of some Cu(II) complexes with biological reductants under aerobic conditions. Since ascorbic acid, glutathione, and *N*-acetylcysteine are present in living cells, some Cu(II) complexes may be capable of initiating DNA damage in the presence of these reductants.

Oxidative DNA damage from active oxygen species such as hydroxyl radicals (•OH) has been hypothesized to play a critical role in diverse physiological processes including mutagenesis, carcinogenesis, radiation damage, and cancer chemotherapy (1). Hydroxyl radicals may be produced by the metal-catalyzed Haber–Weiss reaction, i.e., metal-catalyzed reaction of superoxide ($O_2^{\bullet-}$) with hydrogen peroxide (H_2O_2) (2). Hydroxyl radicals are also considered to be generated during the reaction of iron with biological reductants in the presence of molecular oxygen (2).

Copper(II) (Cu(II)) is an important metal ion present in chromosomes (3) and which is closely associated with DNA bases (4). Consequently, interest in copper–DNA adducts stems from the possibility that endogenous, DNA-associated copper may be able to promote oxidative damage of DNA (5).

On the other hand, our previous studies suggested that DNA strand scission was caused by •OH generated from the reaction of various Cu(II) complexes with H_2O_2 (6–8). Since H_2O_2 may be generated *in situ* through the reduction of molecular oxygen by reduced copper ions (9, 10), we investigate what kind of Cu(II) complexes can react with biological reductants such as ascorbic acid, glutathione, *N*-acetylcysteine, or hydroquinone in the presence of molecular oxygen to gener-

[1] To whom correspondence should be addressed. Fax: (+81)-43-255-6819.

ate •OH using electron spin resonance (ESR)[2] spin-trapping methods and to cause DNA strand scissions. Ascorbic acid, glutathione, and *N*-acetylcysteine are known to be cellular antioxidants, and hydroquinone is a benzene metabolite.

MATERIALS AND METHODS

Materials. *N*-Acetylcysteine, glutathione (GSH), superoxide dismutase (SOD) (3200 U/mg), and catalase (11,000 U/mg) were purchased from Sigma Chemical Co. (U.S.A.). Ascorbic acid, hydroquinone, and dimethyl sulfoxide (DMSO) were purchased from Wako Chemical Co. (Japan). α-(Pyridyl-4-*N*-oxide)-*N*-*tert*-butylnitrone (POBN) was purchased from Aldrich Chemical Co. (U.S.A.). Cyclo(L-histidyl-L-histidyl) (CyHH) and L-histidylglycylglycine (HGG) were respectively synthesized by the method described in the literatures (11, 12). *o*-Phenanthroline (OP) was from Dojindo Laboratory (Japan). Cupric sulfate was purchased from E. Merck (Germany). Chelex 100 resin (sodium form) was purchased from Bio-Rad Co. (U.S.A.). Phosphate buffer (0.1 M, pH 7.4) was treated with Chelex 100 resin by the column method (13).

Preparation of reaction solutions of Cu(II) complexes. Cu(II)-$(CyHH)_2$ and Cu(II)$(OP)_2$ complexes were prepared by the addition of a 2.3-fold excess concentration of ligands to cupric sulfate. Cu(II)-(HGG) complex was prepared by the addition of a 1.1-fold concentration of HGG to cupric sulfate. Cu(II)$(en)_2$ was synthesized by the method described previously (14).

Cyclic voltammetry measurements. Using a Polarographic Analyzer P-1100 (Yanaco Co., Japan) system, cyclic voltammetric measurements were performed with a three-electrode system consisting of a glassy carbon electrode, a platinum counter electrode, and a saturated calomel electrode (SCE) as a reference. Cyclic voltammograms were recorded at a scan rate of 100 mV s^{-1}. Halfwave potential, $E_{1/2}$, was determined as the midpoint between the peak potentials Epc and Epa by following equation, $E_{1/2}$ = (Epc + Epa)/2. Redox potentials were calculated as the equation E^0 (NHE) = $E_{1/2}$ + 0.2515 (V). The concentration of Cu(II) was 1 mM.

Detection of hydroxyl radical formation by ESR spin trapping. A secondary spin-trapping technique was employed because the spin adduct of •OH is unstable (15). Methyl radical (•CH_3), which is easily formed by the reaction of •OH with DMSO, is then reacted with a spin trap, POBN, to form the relatively stable methyl radical adduct, POBN–CH_3, with a characteristic ESR spectrum. Reaction mixtures contained 25 mM POBN, 2.5% DMSO (v/v), 0.25–2.5 mM reductants and 0.25 mM Cu(II) complexes in 0.1 M phosphate buffer at pH 7.4. ESR spectra were recorded at 5 min after mixing unless otherwise stated. Experiment was performed in air-saturated solutions.

ESR measurements. ESR measurements were carried out on a JEOL-RE-1X spectrometer (X-band) with 100 kHz field modulation. ESR spectra were recorded at room temperature in a JEOL flat quartz cell. ESR parameters were calibrated by comparison with a standard Mn^{2+}/MgO marker.

Assay of DNA strand scission. DNA strand breaks were assayed by measuring the conversion of supercoiled DNA to open circular and linear DNA. At 5 min after addition of various concentrations of reductants to the mixing solutions of Cu(II) complexes (0.25 mM) and 0.5 μg of pBR322 plasmid DNA in 10 mM phosphate buffer (pH 7.4), DNA strand scission breakages were observed by agarose gel electrophoresis of the DNA and ethidium fluorescence as described previously (6). The experiment was performed in air-saturated solutions.

RESULTS

Figure 1 shows cyclic voltammograms of four Cu(II) complexes used in this study. The values of $E_{1/2}$ (vs NHE) obtained were in the following order: Cu(II)-$(CyHH)_2$ (0.282 V) > Cu(II)$(OP)_2$ (0.147 V) > Cu(II)-(HGG) (0.082 V) > Cu(II)$(en)_2$ (−0.014 V). This suggests that Cu(II)$(CyHH)_2$ is most easily reduced in the four Cu(II) complexes, and Cu(II)$(en)_2$ forms the most stable Cu(II) complex.

When ascorbic acid (0.2 mM) was added to Cu(II)-$(CyHH)_2$ (0.2 mM) solution containing DMSO (2%) and POBN (20 mM), a prominent six-line ESR signal with hyperfine splitting constants [$a^N(1)$ = 1.59 mT, $a^H(1)$ = 0.28 mT] (Fig. 2A), assignable to the POBN–CH_3 radical adduct by reference to the reported values (16), was observed. This result indicated the generation of •OH from the ascorbic acid/Cu(II)$(CyHH)_2$ system. In addition to the POBN–CH_3 adduct, a weak doublet signal from ascorbyl radical [a^H = 0.18 mT] (17) was observed. The addition of SOD (224 U/ml) into this reaction system did not affect the ESR spectrum (Fig. 2B). However, the addition of catalase (844 U/ml) markedly decreased the signal intensity of the POBN–CH_3 adduct (Fig. 2C), although boiled catalase did not (Fig. 2D). On the other hand, the addition of ascorbic acid (0.2 mM) to Cu(II)$(OP)_2$ (0.2 mM) solution gave a stronger signal intensity of POBN–CH_3 adduct than that to Cu(II)$(CyHH)_2$ solution (Fig. 3A). No ascorbyl radicals were observed. The addition of SOD (224 U/ml) further increased the signal intensity of POBN–CH_3 adduct (Fig. 3B), suggesting the increasing formation of H_2O_2 derived from the dismutation of $O_2^{\bullet-}$ by SOD. The signal intensity of POBN–CH_3 adduct was markedly decreased by the addition of catalase (844 U/ml) (Fig. 3C).

Variations in the ESR signal intensities of the POBN–CH_3 adduct against various concentrations of ascorbic acid at fixed concentrations of four Cu(II) complexes are shown in Fig. 4. The relative intensity of the POBN–CH_3 adduct reached a maximum when the ratios of ascorbic acid to Cu(II) complexes such as Cu(II)-$(CyHH)_2$, Cu(II)$(OP)_2$, and Cu(II)(HGG) were close to 2:1 and then decreased with increases in concentration of ascorbic acid. On the other hand, in the case of Cu(II)$(en)_2$, the maximal intensity of the POBN–CH_3 adduct was obtained when the molar ratio of ascorbic acid to Cu(II) was 5:1.

The addition of GSH (0.2 mM) to Cu(II)$(OP)_2$ (0.2 mM) solution containing DMSO (2%) and POBN (20 mM) gave a six-line ESR signal of the POBN–CH_3 adduct (Fig. 5A). The further addition of SOD (224 U/ml) into this reaction system did not affect the ESR

[2] Abbreviations used: ESR, electron spin resonance; GSH, glutathione; SOD, superoxide dismutase; POBN, α-(pyridyl-4-*N*-oxide)-*N*-*tert*-butylnitrone; CyHH, cyclo(L-histidyl-L-histidyl); HGG, L-histidylglycylglycine; OP, *o*-phenanthroline; en, ethylenediamine; DMSO, dimethyl sulfoxide; SC, supercoiled circular form; OC, open circular form; LIN; linear form.

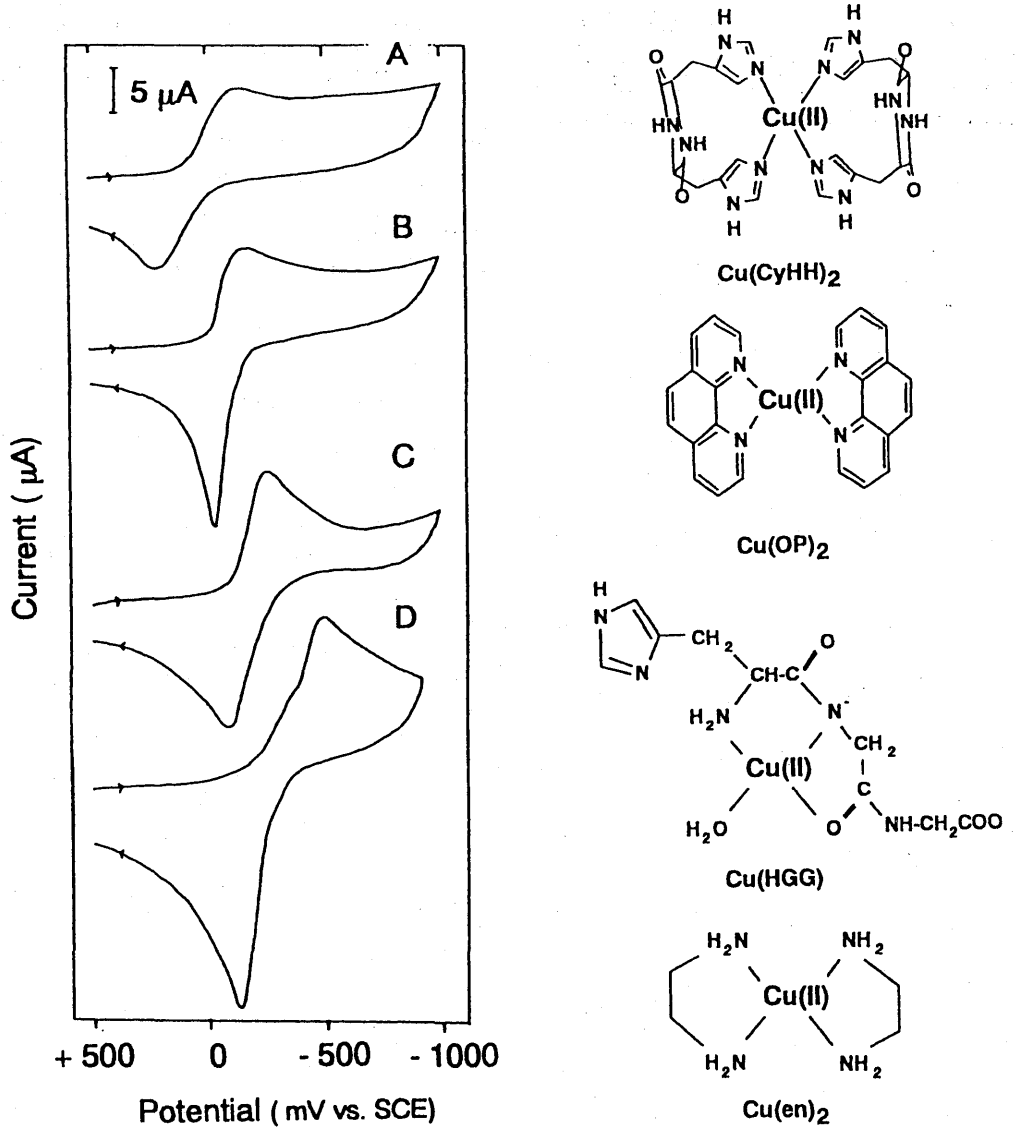

FIG. 1. Assumed chemical structures of Cu(II) complexes used here and their cyclic voltammograms. (A) $Cu(CyHH)_2$, (B) $Cu(OP)_2$, (C) Cu(HGG), (D) $Cu(en)_2$.

signal (Fig. 5B), but the signal intensity of the POBN–CH_3 adduct was markedly decreased by the addition of catalase (844 U/ml) (Fig. 5C). Variations in the ESR signal intensities of the POBN–CH_3 adduct against the various concentrations of GSH are shown in Fig. 6. The intensity of the POBN–CH_3 adduct reached a maximum when the GSH/$Cu(OP)_2$ ratio was close to 5:1, and then decreased with increases in concentration of GSH. On the other hand, a small amount of POBN–CH_3 adduct was observed only when the molar ratio of GSH to Cu(II)$(CyHH)_2$ was 1:1, as shown in Fig. 6. In contrast, the addition of GSH to Cu(II)(HGG) or Cu(II)-$(en)_2$ solution containing DMSO and POBN did not give any ESR signal within the range of GSH concentration used here. Similar results were obtained in the reaction of *N*-acetylcysteine with these four Cu(II) complexes (data not shown).

When hydroquinone (0.4 mM) was added to Cu(II)-$(CyHH)_2$ (0.2 mM) solution containing DMSO (2%) and POBN (20 mM), a prominent six-line ESR signal from the POBN–CH_3 adduct was observed, confirming the generation of $^{\bullet}OH$ (Fig. 7A). In addition to POBN–CH_3, the spectrum contained two weak signals (marked by asterisks in Fig. 7A), one probably from the methoxy adduct of POBN (POBN-OCH_3), which may be formed via a mechanism involving methylperoxyl radicals produced from the reaction of $^{\bullet}CH_3$ with molecular oxygen (17), and another from quintet semiquinone radical [a^H = 0.23 mT] (18). The addition of SOD (224 U/ml) into this solution system

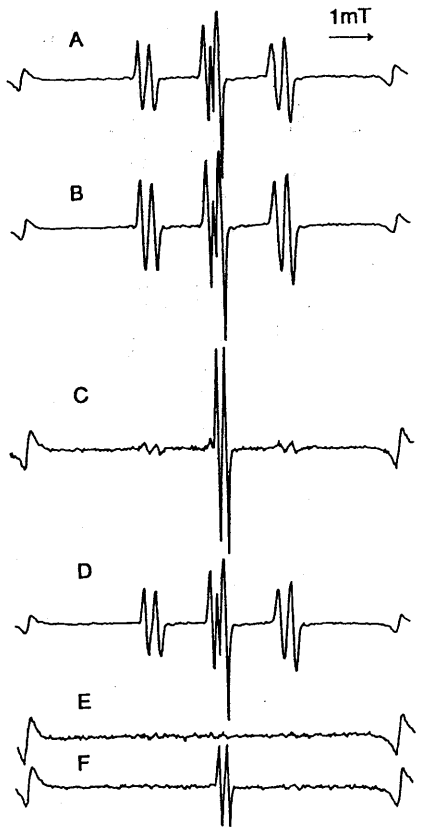

FIG. 2. Effects of SOD, catalase, or boiled catalase on the formation of the POBN–CH_3 adduct from the reaction of ascorbic acid (0.2 mM) with $Cu(CyHH)_2$ (0.2 mM) in the presence of DMSO (2%) and POBN (20 mM). (A) Complete system. (B) Same as A but with SOD (224 U/ml). (C) Same as A but with catalase (844 U/ml). (D) Same as A but with boiled catalase. (E) Same as A but without ascorbic acid. (F) Same as A but without $Cu(CyHH)_2$. Conditions: microwave power, 10 mW; modulation amplitude, 0.079 mT; scan range, 10 mT; time constants, 0.1 s; scan time, 2 min. Receiver gains in A, B, and D are 160, and those in C, E, and F are 320. Spectrum was recorded at 60 s after mixing.

did not affect the ESR spectrum (Fig. 7B). However, the signal intensity of the POBN–CH_3 adduct was markedly decreased by the addition of catalase (844 U/ml) (Fig. 7C). Variations in the ESR signal intensities of the POBN–CH_3 adduct against the various concentrations of hydroquinone are shown in Fig. 8. The intensity of the POBN–CH_3 adduct obtained from the reaction of $Cu(II)(CyHH)_2$ with hydroquinone increased progressively with the increasing hydroquinone concentration. On the other hand, the addition of hydroquinone to $Cu(II)(OP)_2$ solution gave a weaker intensity of POBN–CH_3 adduct than that of $Cu(II)(CyHH)_2$ (Fig. 8). In contrast, the addition of hydroquinone to both Cu(II)(HGG) and $Cu(II)(en)_2$ (0.2 mM) solutions containing DMSO (2%) and POBN (20 mM) did not give any ESR signal within the range of hydroquinone concentration used here (Fig. 8).

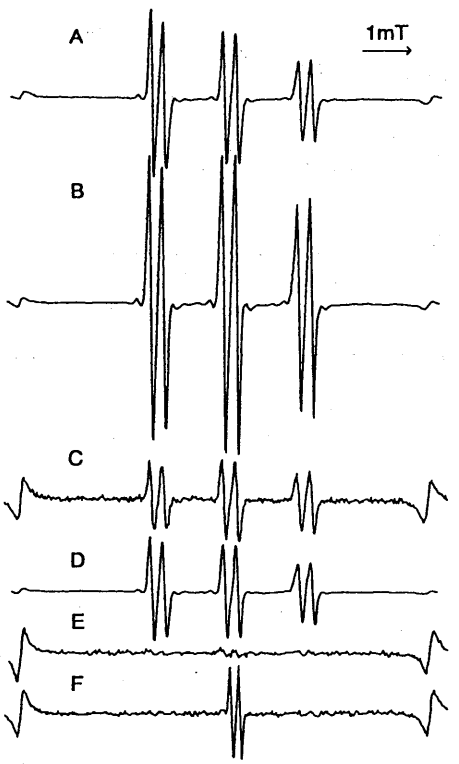

FIG. 3. Effects of SOD, catalase, or boiled catalase on the formation of the POBN–CH_3 adduct from the reaction of ascorbic acid (0.2 mM) with $Cu(OP)_2$ (0.2 mM) solution in the presence of DMSO (2%) and POBN (20 mM). (A) Complete system. (B) Same as A but with SOD (224 U/ml). (C) Same as A but with catalase (844 U/ml). (D) Same as A but with boiled catalase. (E) Same as A but without ascorbic acid. (F) Same as A but without $Cu(OP)_2$. Conditions except receiver gain were the same as those shown in Fig. 2. Receiver gains in A and B are 63, and those in C, E, and F are 320, and that in D is 32.

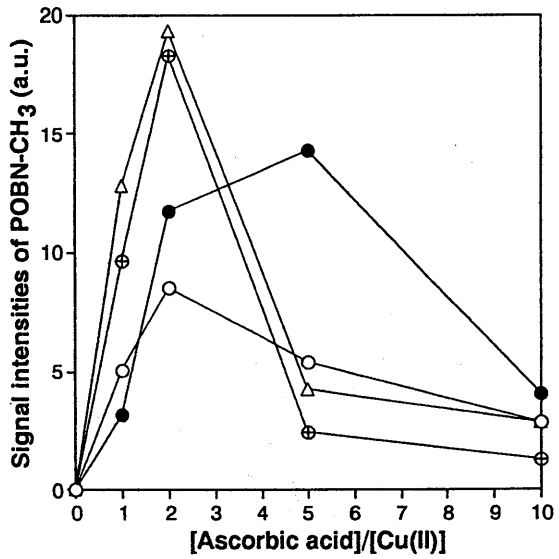

FIG. 4. Effects of varying the concentration of ascorbic acid on the ESR signal intensity of the POBN–CH_3 adduct. Reaction conditions were described under Materials and Methods. ○, $Cu(CyHH)_2$; ⊕, $Cu(OP)_2$; △, Cu(HGG); ●, $Cu(en)_2$.

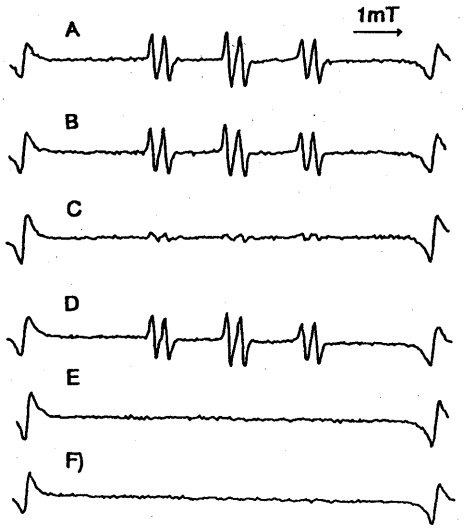

FIG. 5. Effects of SOD, catalase, or boiled catalase on the formation of the POBN–CH_3 adduct from the reaction of glutathione (0.2 mM) with $Cu(OP)_2$ (0.2 mM) solution in the presence of DMSO (2%) and POBN (20 mM). (A) Complete system. (B) Same as A but with SOD (224 U/ml). (C) Same as A but with catalase (844 U/ml). (D) Same as A but with boiled catalase. (E) Same as A but without glutathione. (F) Same as A but without $Cu(OP)_2$. Conditions except receiver gain were the same as those described in the legend to Fig. 2. Receiver gain is 320.

DNA strand scission by $^{\bullet}OH$ generated from the reaction of Cu(II) complexes with ascorbic acid was investigated. The effects of varying the concentration of ascorbic acid at fixed concentrations of Cu(II) complexes are shown in Fig. 9. Figure 9A shows the

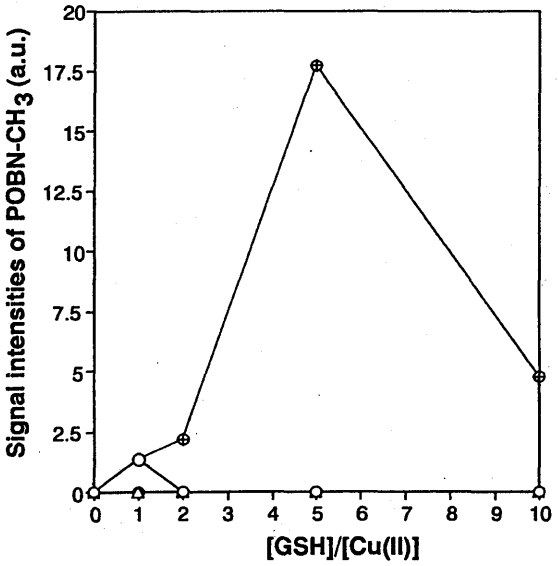

FIG. 6. Effects of varying the concentration of glutathione on the ESR signal intensity of the POBN–CH_3 adduct. Reaction conditions were described under Materials and Methods. ○, $Cu(CyHH)_2$; ⊕, $Cu(OP)_2$; △, Cu(HGG); ●, $Cu(en)_2$.

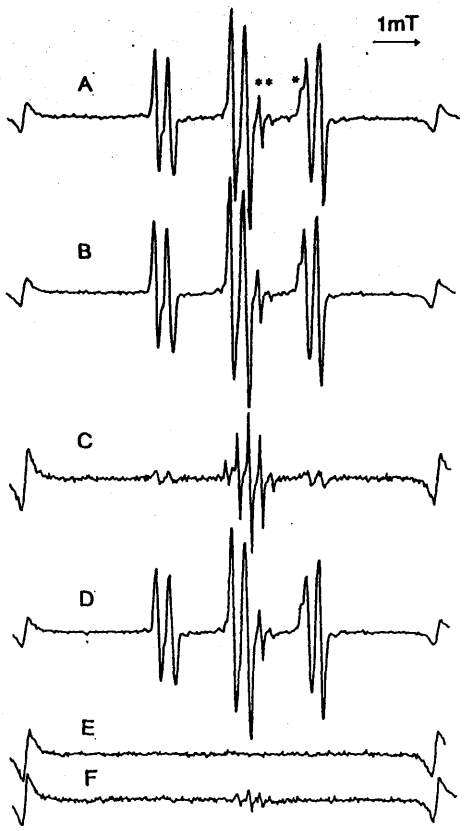

FIG. 7. Effects of SOD, catalase, or boiled catalase on the formation of the POBN–CH_3 adduct from the reaction of hydroquinone (0.4 mM) with $Cu(CyHH)_2$ (0.2 mM) solution in the presence of DMSO (2%) and POBN (20 mM). (A) Complete system. (B) Same as A but with SOD (224 U/ml). (C) Same as A but with catalase (844 U/ml). (D) Same as A but with boiled catalase. (E) Same as A but without hydroquinone. (F) Same as A but without $Cu(CyHH)_2$. (*) shows POBN–OCH_3 and (**) shows quintet semiquinone radical. Conditions except receiver gain were the same as those described in the legend to Fig. 2. Receiver gains in A, B, and D are 160, and those in C, E, and F are 320.

electrophoretic pattern after treatment of DNA with Cu(II)-$(CyHH)_2$ or $Cu(II)(OP)_2$ and ascorbic acid. DNA derived from pBR322 showed two bands on agarose gel electrophoresis (lane 1). The foremost moving band corresponded to the native form of supercoiled circular DNA (abbreviated as SC) and the slower moving band was the open circular form (abbreviated as OC). Treatment of the DNA with ascorbic acid alone (lane 2) or Cu(II) complexes alone (lanes 3 and 4) did not change the migration pattern. When both Cu(II) complexes plus ascorbic acid were used, however, DNA breakage of OC and the linear form (abbreviated LIN) was observed (lanes 5–12), indicating that $^{\bullet}OH$ generated from the reaction of Cu(II) complexes with ascorbic acid caused DNA strand scission. On the other hand, both Cu(II)(HGG) and Cu(II)-$(en)_2$ also caused DNA strand scission in the presence of ascorbic acid as shown in Fig. 9B. Especially

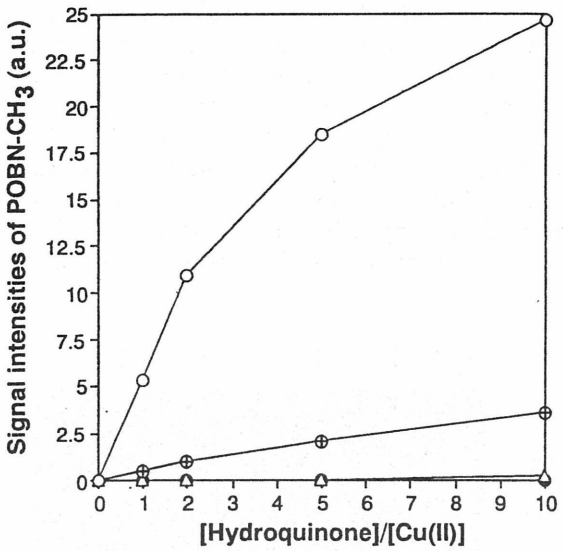

FIG. 8. Effects of varying the concentration of hydroquinone on the ESR signal intensity of the POBN–CH_3 adduct. Reaction conditions were described under Materials and Methods. ○, $Cu(CyHH)_2$; ⊕, $Cu(OP)_2$; △, Cu(HGG); ●, $Cu(en)_2$.

in $Cu(II)(OP)_2$, increases in the concentration of ascorbic acid caused fragmentation and enhanced DNA strand scissions greater than those from other Cu(II) complexes.

Figure 10A shows the electrophoretic pattern of DNA after treatment of DNA with $Cu(II)(CyHH)_2$ or $Cu(II)(OP)_2$ complex and various concentrations of GSH. Treatment of DNA with GSH alone (lane 2) or either Cu(II) complex alone (lanes 3 and 4) did not change the migration pattern. When the $Cu(II)(CyHH)_2$ complex plus an equimolar concentration of glutathione were used, however, a slight DNA breakage from SC to OC was observed (lane 5), indicating that $^{\bullet}OH$ generated from the reaction of $Cu(II)(CyHH)_2$ complex with equimolar GSH caused DNA strand scission. This result was consistent with one obtained from the ESR spin-trapping experiment. On the other hand, the addition of GSH to $Cu(II)(OP)_2$ caused fragmentation and enhanced DNA strand scission (lanes 9–12), which depended on the concentration of GSH. In contrast, Cu(II)(HGG) or $Cu(II)(en)_2$ plus GSH did not cause any DNA strand scission (Fig. 10B).

When *N*-acetylcysteine was used in place of GSH, the same results were obtained.

Figure 11A shows the electrophoretic pattern after treatment of DNA with $Cu(II)(CyHH)_2$ or $Cu(II)(OP)_2$ complex and various concentrations of hydroquinone. Treatment of DNA with hydroquinone alone (lane 2) or Cu(II) complexes alone (lanes 3 and 4) did not change the migration pattern. When both Cu(II) complex and hydroquinone were used, DNA breakage to OC was observed, indicating that $^{\bullet}OH$ generated from the reaction of both Cu(II) complexes with hydroquinone caused DNA strand scission. In particular, $Cu(II)(OP)_2$ enhanced DNA strand scission to a greater extent than the $Cu(II)(CyHH)_2$ complex. This was the only case in which the concentration of the POBN–CH_3 adduct generated was not correlated with the extent of DNA strand scission. In contrast, Cu(II)(HGG) or $Cu(II)(en)_2$ plus hydroquinone did not cause any DNA strand scission, irrespective of the concentration of hydroquinone used (Fig. 11B).

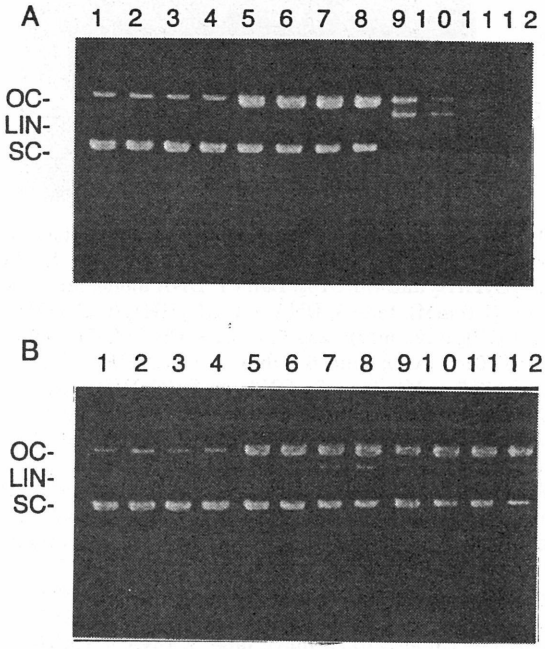

FIG. 9. Effects of various concentrations of ascorbic acid on DNA stand scission in the presence of Cu(II) complexes. (A) In the presence of $Cu(CyHH)_2$ and $Cu(OP)_2$: Lane 1, DNA alone; lane 2, DNA + ascorbic acid (2.5 mM); lane 3, DNA + $Cu(CyHH)_2$ (0.25 mM); lane 4, DNA + $Cu(OP)_2$ (0.25 mM); lane 5, DNA + $Cu(CyHH)_2$ (0.25 mM) + ascorbic acid (0.25 mM); lane 6, DNA + $Cu(CyHH)_2$ (0.25 mM) + ascorbic acid (0.5 mM); lane 7, DNA + $Cu(CyHH)_2$ (0.25 mM) + ascorbic acid (1.25 mM); lane 8, DNA + $Cu(CyHH)_2$ (0.25 mM) + ascorbic acid (2.5 mM); lane 9, DNA + $Cu(OP)_2$ (0.25 mM) + ascorbic acid (0.25 mM); lane 10, DNA + $Cu(OP)_2$ (0.25 mM) + ascorbic acid (0.5 mM); lane 11, DNA + $Cu(OP)_2$ (0.25 mM) + ascorbic acid (1.25 mM); lane 12, DNA + $Cu(OP)_2$ (0.25 mM) + ascorbic acid (2.5 mM). Loading 0.5 μg DNA per lane. All reactions were performed in 100 mM phosphate buffer (pH 7.4) at room temperature for 5 min. (B) In the presence of Cu(HGG) and $Cu(en)_2$: Lane 1, DNA alone; lane 2, DNA + ascorbic acid (2.5 mM); lane 3, DNA + Cu(HGG) (0.25 mM); lane 4, DNA + $Cu(en)_2$ (0.25 mM); lane 5, DNA + Cu(HGG) (0.25 mM) + ascorbic acid (0.25 mM); lane 6, DNA + Cu(HGG) (0.25 mM) + ascorbic acid (0.5 mM); lane 7, DNA + Cu(HGG) (0.25 mM) + ascorbic acid (1.25 mM); lane 8, DNA + Cu(HGG) (0.25 mM) + ascorbic acid (2.5 mM); lane 9, DNA + $Cu(en)_2$ (0.25 mM) + ascorbic acid (0.25 mM); lane 10, DNA + $Cu(en)_2$ (0.25 mM) + ascorbic acid (0.5 mM); lane 11, DNA + $Cu(en)_2$ (0.25 mM) + ascorbic acid (1.25 mM); lane 12, DNA + $Cu(en)_2$ (0.25 mM) + ascorbic acid (2.5 mM). Loading 0.5 μg DNA per lane. All reactions were performed in 100 mM phosphate buffer (pH 7.4) at room temperature for 5 min.

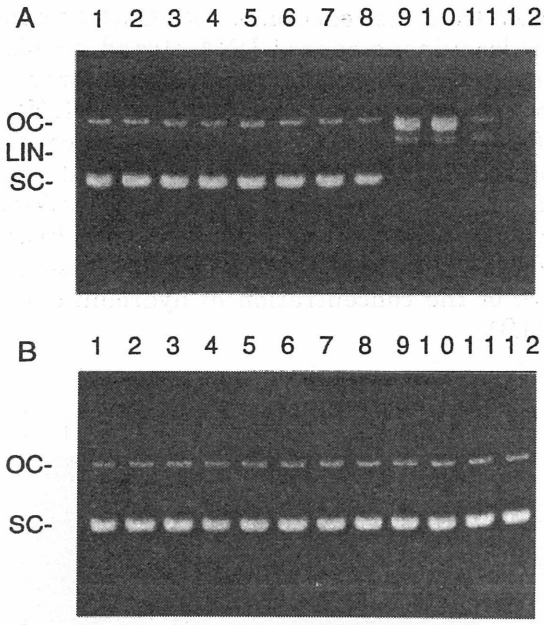

FIG. 10. Effects of various concentrations of glutathione on DNA stand scission in the presence of Cu(II) complexes. (A) In the presence of $Cu(CyHH)_2$ and $Cu(OP)_2$: Lane 1, DNA alone; lane 2, DNA + glutathione (2.5 mM); lane 3, DNA + $Cu(CyHH)_2$ (0.25 mM); lane 4, DNA + $Cu(OP)_2$ (0.25 mM); lane 5, DNA + $Cu(CyHH)_2$ (0.25 mM) + glutathione (0.25 mM); lane 6, DNA + $Cu(CyHH)_2$ (0.25 mM) + glutathione (0.5 mM); lane 7, DNA + $Cu(CyHH)_2$ (0.25 mM) + glutathione (1.25 mM); lane 8, DNA + $Cu(CyHH)_2$ (0.25 mM) + glutathione (2.5 mM); lane 9, DNA + $Cu(OP)_2$ (0.25 mM) + glutathione (0.25 mM); lane 10, DNA + $Cu(OP)_2$ (0.25 mM) + glutathione (0.5 mM); lane 11, DNA + $Cu(OP)_2$ (0.25 mM) + glutathione (1.25 mM); lane 12, DNA + $Cu(OP)_2$ (0.25 mM) + glutathione (2.5 mM). Loading 0.5 μg DNA per lane. All reactions were performed in 100 mM phosphate buffer (pH 7.4) at room temperature for 5 min. (B) In the presence of Cu(HGG) and $Cu(en)_2$: Lane 1, DNA alone; lane 2, DNA + glutathione (2.5 mM); lane 3, DNA + Cu(HGG) (0.25 mM); lane 4, DNA + $Cu(en)_2$ (0.25 mM); lane 5, DNA + Cu(HGG) (0.25 mM) + glutathione (0.25 mM); lane 6, DNA + Cu(HGG) (0.25 mM) + glutathione (0.5 mM); lane 7, DNA + Cu(HGG) (0.25 mM) + glutathione (1.25 mM); lane 8, DNA + Cu(HGG) (0.25 mM) + glutathione (2.5 mM); lane 9, DNA + $Cu(en)_2$ (0.25 mM) + glutathione (0.25 mM); lane 10, DNA + $Cu(en)_2$ (0.25 mM) + glutathione (0.5 mM); lane 11, DNA + $Cu(en)_2$ (0.25 mM) + glutathione (1.25 mM); lane 12, DNA + $Cu(en)_2$ (0.25 mM) + glutathione (2.5 mM). Loading 0.5 μg DNA per lane. All reactions were performed in 100 mM phosphate buffer (pH 7.4) at room temperature for 5 min.

DISCUSSION

Although $^{\bullet}OH$ can be directly trapped by the spin trap, 5,5-dimethyl-1-pyrroline *N*-oxide (DMPO), the DMPO–OH adduct formed was suggested to be readily destroyed via reaction with metal ions and/or reducing agents, and therefore DMPO may not always give a reliable indication of $^{\bullet}OH$ concentration (19). We therefore employed a secondary radical trapping technique for the detection of $^{\bullet}OH$ using POBN (15, 20).

The generation of $^{\bullet}OH$ from the reaction of Cu(II) complexes with ascorbic acid was ascertained by ESR spin-trapping experiments as shown in Figs. 2–4. The reduction of Cu(II) to Cu(I) by ascorbic acid was supported by the disappearance of room temperature ESR signal due to Cu(II) (data not shown). Cu(I) thus formed can take part in electron transfer reactions with molecular oxygen (O_2) to generate $O_2^{\bullet-}$. Cu(I) reacts further with H_2O_2 generated by dismutation of $O_2^{\bullet-}$ to give $^{\bullet}OH$. The generation of $^{\bullet}OH$ was not inhibited by SOD, but by catalase. These observations indicate that the production of $^{\bullet}OH$ from the ascorbic acid/

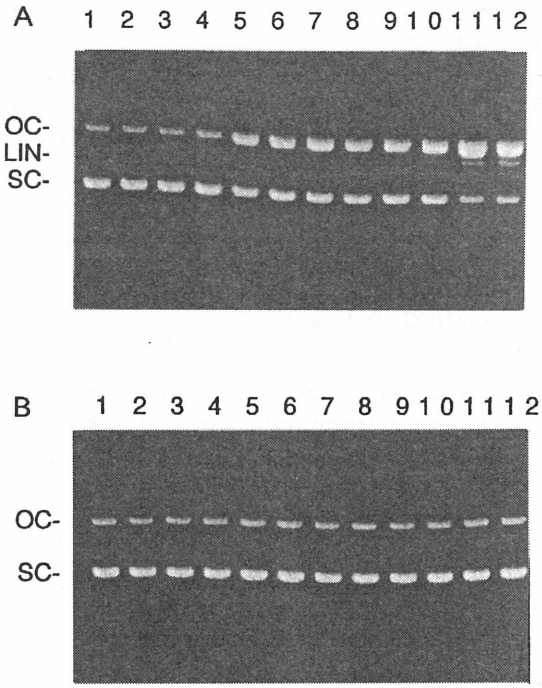

FIG. 11. Effects of various concentrations of hydroquinone on DNA stand scission in the presence of Cu(II) complexes. (A) In the presence of $Cu(CyHH)_2$ and $Cu(OP)_2$: Lane 1, DNA alone; lane 2, DNA + hydroquinone (2.5 mM); lane 3, DNA + $Cu(CyHH)_2$ (0.25 mM); lane 4, DNA + $Cu(OP)_2$ (0.25 mM); lane 5, DNA + $Cu(CyHH)_2$ (0.25 mM) + hydroquinone (0.25 mM); lane 6, DNA + $Cu(CyHH)_2$ (0.25 mM) + hydroquinone (0.5 mM); lane 7, DNA + $Cu(CyHH)_2$ (0.25 mM) + hydroquinone (1.25 mM); lane 8, DNA + $Cu(CyHH)_2$ (0.25 mM) + hydroquinone (2.5 mM); lane 9, DNA + $Cu(OP)_2$ (0.25 mM) + hydroquinone (0.25 mM); lane 10, DNA + $Cu(OP)_2$ (0.25 mM) + hydroquinone (0.5 mM); lane 11, DNA + $Cu(OP)_2$ (0.25 mM) + hydroquinone (1.25 mM); lane 12, DNA + $Cu(OP)_2$ (0.25 mM) + hydroquinone (2.5 mM). Loading 0.5 μg DNA per lane. All reactions were performed in 100 mM phosphate buffer (pH 7.4) at room temperature for 5 min. (B) In the presence of Cu(HGG) and $Cu(en)_2$: Lane 1, DNA alone; lane 2, DNA + hydroquinone (2.5 mM); lane 3, DNA + Cu(HGG) (0.25 mM); lane 4, DNA + $Cu(en)_2$ (0.25 mM); lane 5, DNA + Cu(HGG) (0.25 mM) + hydroquinone (0.25 mM); lane 6, DNA + Cu(HGG) (0.25 mM) + hydroquinone (0.5 mM); lane 7, DNA + Cu(HGG) (0.25 mM) + hydroquinone (1.25 mM); lane 8, DNA + Cu(HGG) (0.25 mM) + hydroquinone (2.5 mM); lane 9, DNA + $Cu(en)_2$ (0.25 mM) + hydroquinone (0.25 mM); lane 10, DNA + $Cu(en)_2$ (0.25 mM) + hydroquinone (0.5 mM); lane 11, DNA + $Cu(en)_2$ (0.25 mM) + hydroquinone (1.25 mM); lane 12, DNA + $Cu(en)_2$ (0.25 mM) + hydroquinone (2.5 mM). Loading 0.5 μg DNA per lane. All reactions were performed in 100 mM phosphate buffer (pH 7.4) at room temperature for 5 min.

TABLE I

The Relationship between the Generation of •OH and DNA Scission Caused by Reaction Mixtures of Cu(II) Complexes with Reductants

Cu(II) complexes	Reductants					
	Ascorbic acid (2 mM)		Glutathione (5 mM)		Hydroquinone (10 mM)	
	•OH generation	DNA scission	•OH generation	DNA scission	•OH generation	DNA scission
$Cu(CyHH)_2$ (0.282 V)	+	+	−	−	++	+
$Cu(OP)_2$ (0.147 V)	++	+++	++	+++	+	++
Cu(HGG) (0.082 V)	++	++	−	−	−	−
$Cu(en)_2$ (−0.014 V)	+	++	−	−	−	−

Note. −, not detectable; +, low level; ++, medium level; +++, high level.

Cu(II) complex system is directly dependent on H_2O_2 but not $O_2^{\bullet-}$. In Fig. 3A, the signal from the POBN–CH_3 adduct is seen to decay during recording. This decay probably reflects reduction of the spin adduct by $Cu(I)(OP)_2$ (21), which is generated efficiently by $Cu(II)(OP)_2$/ascorbic acid mixtures. Therefore, although the signal intensity of POBN–CH_3 in the $Cu(II)(OP)_2$ reaction system is the same as that of the Cu(II)(HGG) reaction system in Fig. 4, $Cu(II)(OP)_2$ may actually generate more hydroxyl radicals than Cu(II)(HGG) in the presence of ascorbic acid. Furthermore, Fig. 4 shows that $Cu(II)(en)_2$ is the most difficult complex to reduce by ascorbate, reflecting its low potential. On the other hand, $Cu(II)(CyHH)_2$ demonstrated the lowest POBN–CH_3 signal intensity. This may be explained by the assumption that $Cu(II)(CyHH)_2$ has the highest redox potential; therefore, it should be the easiest to reduce. However, the higher redox potential of the Cu(II)/Cu(I) couple results in a stable Cu(I) complex, thereby making the oxygen reduction more difficult.

On the other hand, the reaction mixtures of ascorbic acid with all Cu(II) complexes caused DNA strand scission as shown in Fig. 9. Interestingly, with the exception of $Cu(II)(OP)_2$ addition of a large excess of ascorbic acid to Cu(II) complexes showed the same extent of DNA strand scission as addition of a small amount of ascorbic acid. This suggested that a large amount of ascorbic acid scavenged •OH before the interaction of •OH with DNA. In contrast, $Cu(II)(OP)_2$ progressively caused DNA strand scission with increases in the concentration of ascorbic acid. This may be explained by the assumption that $Cu(I)(OP)_2$ generated from the reduction of $Cu(II)(OP)_2$ by ascorbic acid can intercalate into DNA and react with H_2O_2 to generate •OH, and the resultant •OH caused DNA strand scission site-specifically, because it has been suggested that $Cu(I)(OP)_2$ binds to the minor groove of DNA (22–25).

GSH reacted with $Cu(II)(CyHH)_2$ to generate •OH and caused DNA strand scission only at a $Cu(II)(CyHH)_2$ to GSH ratio of 1. On the other hand, the amount of •OH generated from the reaction of $Cu(II)(OP)_2$ with GSH increased with increases in the concentration of GSH, and reached a maximum when the molar ratio of GSH to $Cu(II)(OP)_2$ was 5, subsequently decreasing (Fig. 6). The decrease in the signal intensity of POBN–CH_3 suggested that a 10-fold excess of GSH reacted with $Cu(II)(OP)_2$ to generate the Cu(I)–GSH complex, which could not react with O_2, or POBN–CH_3 was reduced to a hydroxylamine by $Cu(I)(OP)_2$ or GSH. The third assumption can be excluded because it was reported that GSH does not reduce nitroxide radicals (26). $Cu(II)(OP)_2$ progressively caused DNA strand scission with increases in the concentration of GSH. We observed that excess GSH inhibits hydroxyl radical (i.e., POBN–CH_3) formation by $Cu(II)(OP)_2$, but excess GSH does not suppress DNA fragmentation. This may be explained by two theories. One is that excess GSH can compete effectively with OP for the binding of Cu(I) under ESR spin-trapping experimental conditions, but cannot compete effectively with OP for the binding of Cu(I) in the presence of DNA (20), and hence the reactive $Cu(I)(OP)_2$ complex that remains in the reaction mixture causes DNA damage. The other theory is that $Cu(OP)_2$ generates the largest amount of hydroxyl radicals in the presence of GSH, although it appears to generate less because the POBN–CH_3 adduct is removed by $Cu(I)(OP)_2$, which was generated from the reaction of $Cu(II)(OP)_2$ and GSH.

On the other hand, GSH did not react with either Cu(II)(HGG) or $Cu(II)(en)_2$ to generate •OH. To elucidate whether GSH can reduce both Cu(II)(HGG) and $Cu(II)(en)_2$, the ESR spectra of these Cu(II) complexes were measured in the presence of GSH. The addition of GSH to both Cu(II)(HGG) and $Cu(II)(en)_2$ caused the

disappearance of the ESR spectra due to these Cu(II) complexes (data not shown), suggesting the formation of Cu(I) complexes. This result suggests that although GSH can reduce both Cu(II)(HGG) and Cu(II)$(en)_2$, Cu(I)(HGG) and Cu(I)$(en)_2$ thus formed are very unstable and easily exchangeable to the Cu(I)–GSH complex which cannot react with O_2 as a result of stabilization of Cu(I) through chelation (27, 28).

At physiological pH, the autoxidation of hydroquinone has been suggested to occur through a semiquinone anion radical as an intermediate (29, 30). Hydroquinone reacted with Cu(II)$(CyHH)_2$ to generate a large amount of $^{\bullet}OH$ compared with the three other Cu(II) complexes as shown in Fig. 8, suggesting that hydroquinone easily reduced Cu(II)$(CyHH)_2$ to Cu(I)-$(CyHH)_2$ concomitant with the generation of semiquinone radical. Since hydroquinone cannot coordinate to Cu(I) instead of CyHH to form a stable Cu(I)–hydroquinone complex, Cu(I)$(CyHH)_2$ reacts with O_2 to generate H_2O_2, and further $^{\bullet}OH$. The results obtained from ESR measurement of Cu(II) complexes in the presence of hydroquinone indicated that hydroquinone could slowly reduce Cu(II)$(OP)_2$, but could not reduce either Cu(II)(HGG) or Cu(II)$(en)_2$ (data not shown). These results suggest that the reactivities of Cu(II) complexes toward hydroquinone depend on their redox potential. Despite the generation of a large amount of $^{\bullet}OH$ from Cu(II)$(CyHH)_2$ compared to Cu(II)$(OP)_2$, however, more DNA strand scission was observed in Cu(II)$(OP)_2$ than in Cu(II)$(CyHH)_2$ as shown in Fig. 11. This suggests that the intercalation of Cu(I)$(OP)_2$ into DNA is also important in DNA strand scission by Cu(II)-$(OP)_2$ plus hydroquinone. Since CyHH does not have a benzene ring, Cu(II)$(CyHH)_2$ cannot intercalate into DNA.

In conclusion, the results obtained here suggest that there is a good correlation between POBN–CH_3 formation and the extent of DNA strand scission as shown by the results in Table I. Thus, DNA strand scission may be caused by $^{\bullet}OH$ which is generated by the reactions of Cu(II) complexes with biological reductants. Since ascorbic acid, *N*-acetylcysteine, and GSH are present in living cells, some Cu(II) complexes may be capable of initiating DNA damage *in vivo*.

REFERENCES

1. Burkitt, M. J. (1994) *Methods Enzymol.* **234,** 66–79.
2. Halliwell, B., and Gutteridge, J. M. C. (1990) *Methods Enzymol.* **186,** 1–75.
3. Bryan, S. E., Vizard, D. L., Beary, D. A., LaBiche, R. A., and Hardy, K. J. (1981) *Nucleic Acids Res.* **9,** 5811–5823.
4. Geierstanger, B. H., Kagawa, T. F., Chen, S.-L., Quigley, G. J., and Ho, P. S. (1991) *J. Biol. Chem.* **266,** 20185–20191.
5. Chevion, M. (1988) *Free Radical Biol. Med.* **5,** 27–37.
6. Ozawa, T., Ueda, J., and Shimazu, Y. (1993) *Biochem. Mol. Biol. Int.* **31,** 455–461.
7. Ueda, J., Shimazu, Y., and Ozawa, T. (1994) *Biochem. Mol. Biol. Int.* **34,** 801–808.
8. Ueda, J., Shimazu, Y., and Ozawa, T. (1995) *Free Radical Biol. Med.* **18,** 929–933.
9. Graham, D. R., Marshall, L. E., Reich, K. A., and Sigman, D. S. (1980) *J. Am. Chem. Soc.* **102,** 5419–5421.
10. Chiou, S.-H. (1983) *J. Biochem.* **94,** 1259–1267.
11. Arena, G., Bonomo, R. P., Impellizzeri, Izatt, R. M., Lamb, J. D., and Rizzarelli, E. (1987) *Inorg. Chem.* **26,** 795–800.
12. Ueda, J., Ikota, N., Hanaki, A., and Koga, K. (1987) *Inorg. Chim. Acta* **135,** 43–46.
13. Kotake, Y., and Janzen, E. G. (1991) *J. Am. Chem. Soc.* **113,** 9503–9506.
14. Ozawa, T., and Hanaki, A. (1991) *J. Chem. Soc. Chem. Commun.* 330–332.
15. Kadiiska, M. B., Hanna, P. M., Hernandez, L., and Mason, R. P. (1992) *Mol. Pharmacol.* **42,** 723–729.
16. Buettner, G. R. (1987) *Free Radical Biol. Med.* **3,** 259–303.
17. Sharma, M. K., and Buettner, G. R. (1993) *Free Radical Biol. Med.* **14,** 649–653.
18. Li, Y., Kuppusamy, P., Zweier, J. L., and Trush, M. A. (1995) *Chem.-Biol. Interact.* **94,** 101–120.
19. Burkitt, M. J., and Mason, R. P. (1991) *Proc. Natl. Acad. Sci. USA* **88,** 8440–8444.
20. Milne, L., Nicotera, P., Orrenius, S., and Burkitt, M. J. (1993) *Arch. Biochem. Biophys.* **304,** 102–109.
21. Burkitt, M. J., Tsang, S. Y., Tam, S. C., and Bremner, I. (1995) *Arch. Biochem. Biophys.* **323,** 63–70.
22. Aronovitch, J., Godinger, D., Samuni, A., and Czapski, G. (1987) *Free Radical Res. Commun.* **2,** 241–258.
23. Stoewe, R., and Prütz, W. A. (1987) *J. Free Radical Biol. Med.* **3,** 97–105.
24. Sigman, D. S., Landgraf, R., Perrin, D. M., and Pearson, L. (1996) *in* Metal Ions in Biological Systems (Sigel, A., and Sigel, H., Eds.), pp. 485–513. Dekker, New York.
25. Veal, J. M., and Rill, R. L. (1991) *Biochemistry* **30,** 1132–1140.
26. Ueda, J., Saito, N., Shimazu, Y., and Ozawa, T. (1996) *Arch. Biochem. Biophys.* **333,** 377–384.
27. Österberg, R., Ligaarden, R., and Persson, D. (1979) *J. Inorg. Biochem.* **10,** 341–355.
28. Hanna, P. M., and Mason, R. P. (1992) *Arch. Biochem. Biophys.* **295,** 205–213.
29. Li, Y., and Trush, M. A. (1993) *Carcinogenesis* **14,** 1303–1311.
30. Li, Y., and Trush, M. A. (1993) *Arch. Biochem. Biophys.* **300,** 346–355.

ELSEVIER

www.elsevier.nl/locate/jinorgbio

Journal of Inorganic Biochemistry 76 (1999) 55–62

JOURNAL OF Inorganic Biochemistry

Oxidation of linoleic acid by copper(II) complexes: effects of ligand

Jun-ichi Ueda *, Kazunori Anzai, Yuri Miura [1], Toshihiko Ozawa

Bioregulation Research Group, National Institute of Radiological Sciences, 9-1 Anagawa 4-chome, Inage-ku, Chiba-shi 263-8555, Japan

Received 12 January 1999; received in revised form 30 June 1999; accepted 9 July 1999

Abstract

The oxidation of linoleic acid (LH) by cupric (Cu(II)) complexes was investigated by absorption spectroscopy and high performance liquid chromatography (HPLC). The following Cu(II) complexes were used: $Cu(II)(BC)_2$ (BC: bathocuproinedisulfonic acid), $Cu(II)(CyHH)_2$ (CyHH: cyclo(L-histidyl-L-histidyl)), $Cu(II)(OP)_2$ (OP: *o*-phenanthroline), Cu(II)(HGG) (HGG: L-histidylglycylglycine), and $Cu(II)(en)_2$ (en: ethylenediamine). The absorbance at 234 nm observed during Cu(II)-catalyzed oxidation of LH increased with incubation time, reached a maximum level, and subsequently decreased. HPLC chromatograms of oxidation products indicated the appearance of peaks corresponding to four isomers of linoleic acid hydroperoxide (LOOH) and subsequent complete decomposition of LOOH. The time to reach the maximal value of absorbance at 234 nm within 24 h was in the following order: $Cu(II)(BC)_2 > Cu(II)(CyHH)_2 = Cu(II)(OP)_2 > Cu(II)(en)_2 > Cu(II)(HGG)$. These observations suggested that $Cu(II)(BC)_2$ can produce LOOH from linoleic acid more rapidly than Cu(II)(HGG) and decompose the LOOH generated more easily. The absorbance at 234 nm observed in the reaction of Cu(II)(HGG) or $Cu(II)(en)_2$ with LH in the presence of H_2O_2 increased with incubation time more rapidly than in the absence of H_2O_2. Hydroxyl radical generation from the reaction of Cu(II)(HGG) or $Cu(II)(en)_2$ with H_2O_2 may initiate the oxidation of LH. In contrast, the addition of H_2O_2 inhibited the oxidation of LH by $Cu(II)(BC)_2$.

Keywords: Linoleic acid; Lipid peroxidation; Copper; Bathocuproinedisulfonic acid; Redox potential

1. Introduction

Lipid peroxidation has been suggested to be the most important and probably the primary event in inflammation, reoxygenation injury and parasitic infections, as well as degenerative diseases such as cancer, atherosclerosis, rheumatoid arthritis and aging [1–3]. Such oxidation usually continues by a free radical chain mechanism and its initial event is the generation of reactive oxygen species such as hydroxyl radicals that induce the chain initiation [3].

Copper ions have been shown to initiate lipid peroxidation in erythrocytes [4], methyl linoleate [5,6], liposomes [4,6], and low density lipoprotein (LDL) [7–11]. In the oxidation of LDL by copper ions, it is considered necessary for apo B protein of LDL to form a complex with copper ion in vitro [12–14]. Although it is reasonable to assume that the bound copper is in a redox-active state and capable of producing free radicals initiating the chain reaction, the mechanism of initiation of copper-induced peroxidation of LDL is still unclear. Linoleic acid is the most abundant polyunsaturated fatty acid in LDL [7]. Thus, we examined the mechanism of peroxidation of linoleic acid by some cupric (Cu(II)) complexes as model compounds of copper bound to apo B protein of LDL. The following Cu(II) complexes were used; $Cu(II)(BC)_2$ (BC: bathocuproinedisulfonic acid), $Cu(II)(CyHH)_2$ (CyHH: cyclo(L-histidyl-L-histidyl)), $Cu(II)(OP)_2$ (OP: *o*-phenanthroline), Cu(II)(HGG) (HGG: L-histidylglycylglycine), and $Cu(II)(en)_2$ (en: ethylenediamine). Differences in ligands in the Cu(II) complexes may induce variation in the redox potentials of Cu(II) complexes [6]. Therefore, experimental results obtained from the oxidation of linoleic acid by Cu(II) complexes with a variety of redox potentials may be expected to reveal the mechanism of peroxidation of LDL by Cu(II) ions. BC, a cuprous ion (Cu(I)) chelator, is often used to confirm that the Cu(II)/Cu(I) redox cycle plays an important role in copper-catalyzed reactions, due to the formation of a stable $Cu(I)(BC)_2$ complex. For example, Lynch and Frei [9] showed that LDL reduced Cu(II) ions to Cu(I) ions using BC. Multhaup et al. [15] also demonstrated the reduction of Cu(II) ions to Cu(I) ions by amyloid precursor protein using BC. Although BC was used to confirm the reduction of

* Corresponding author. Fax: +81-43-255-6819; e-mail: ueda@nirs.go.jp

[1] Present address: Laboratory of Biochemistry and Isotopes, Tokyo Metropolitan Institute of Gerontology, 35-2 Sakaecho, Itabashiku, Tokyo 173-0015, Japan.

Cu(II) ions, there have been few studies of the reactivity of Cu(II)$(BC)_2$ complex [16,17]. Therefore, we investigated the reactivity of Cu(II)$(BC)_2$ against polyunsaturated fatty acid.

We reported previously that the generation of hydroxyl radicals ($^{\cdot}OH$) by the reaction of various Cu(II) complexes with hydrogen peroxide (H_2O_2) [18,19] resulted in pBR 322 DNA strand scission [20–22]. In this study, we investigated whether linoleic acid is oxidized by $^{\cdot}OH$ generated from the reaction of various Cu(II) complexes with H_2O_2, because Cu(II) complexes may interact with H_2O_2 generated by the enzymatic or nonenzymatic dismutation of superoxide ions in biological systems.

In this study, we first showed that five Cu(II) complexes reacted with linoleic acid to yield linoleic acid hydroperoxide and furthermore degraded it to the corresponding hydroxy derivatives and oxodienoic acids by absorption spectroscopy and high performance liquid chromatography (HPLC). Furthermore, the addition of H_2O_2 accelerated oxidation of linoleic acid by Cu(II)(HGG) or Cu(II)$(en)_2$, but suppressed the oxidation by Cu(II)$(BC)_2$.

2. Materials and methods

2.1. Materials

Linoleic acid (purity higher than 99.0%), which was used without further purification, ascorbic acid, cyclohexane and H_2O_2 (30%) were purchased from Wako Pure Chemical Ind. (Japan). The amount of preformed linoleic acid hydroperoxide contained in the linoleic acid used was determined by comparing the peak area with a calibration curve of the peak area of a standard amount of 13-hydroperoxy-*cis*-9, *trans*-11-octadecaneoic acid (13ZE-HPODE) (0.2–2 μg) using HPLC and its amount was 0.06% that of linoleic acid. The lower detection limit of this HPLC method was 0.2 μg for the amount of 13ZE-HPODE. BC and OP were purchased from Dojindo Laboratory (Japan). HGG and CyHH were synthesized by the method described previously [23,24]. Cu$(en)_2$ was synthesized as described previously [18]. Cupric sulfate was purchased from Merck (Germany). Soybean lipoxygenase (1.4×10^5 units mg^{-1}), 13ZE-HPODE and 13-hydroxy-*cis*-9, *trans*-11-octadecaneoic acid (13ZE-HODE) were purchased from Sigma Chemical Co. (USA).

2.2. Preparation of reaction solutions of Cu(II) complexes

Cu$(CyHH)_2$ and Cu$(OP)_2$ complex solutions were prepared by addition of a 2.5-fold higher concentration of ligands to Cu(II) ion. Cu(HGG) was prepared by addition of a 1.2-fold higher concentration of HGG to Cu(II) ion. Cu(II)$(BC)_2$ was prepared by addition of a 20-fold higher concentration of BC to Cu(II) ion.

2.3. Reaction conditions

Standard reaction mixtures containing 1.2 mM linoleic acid (or 0.3 mM linoleic acid hydroperoxide) dissolved in 2.5% ethanol and 0.1 mM Cu(II) complexes in 4 ml of phosphate buffer (0.1 M, pH 7.4) were incubated at 37°C. Aliquots (0.5 ml) were withdrawn from reaction mixtures at appropriate time points for chemical analysis of peroxidation products. They were immediately transferred into sample bottles containing 3 ml of cyclohexane and 0.5 ml of diethylenetriamonepentaacetic acid (DTPA) (2 mM) cooled on ice to suppress peroxidation during handling, and the sample bottles were stirred vigorously on a vortex mixer for 1 min. Lipid peroxidation was immediately measured by following the increase in absorption at 234 nm of the cyclohexane layer with a Hitachi U-3210 spectrophotometer (Japan) at room temperature. The absorbance at 234 nm described in the case of OP has been already subtracted from the OP absorbance in the experimental data. We think that a slight excess of the ligand against copper(II) ion is needed for the complexation of Cu(II), and unbound ligand does not influence the absorbance kinetics. In fact, addition of various concentrations of BC to copper(II) ion did not affect the time course of absorbance at 234 nm. In the case of Cu(I), the reaction mixture contained 0.3 mM linoleic acid hydroperoxide dissolved in 2.5% ethanol, 0.1 mM Cu(II) complexes, and 0.2 mM ascorbic acid in 4 ml of phosphate buffer (0.1 M, pH 7.4) was incubated at 37°C for 8 h. Aliquots (0.5 ml) were withdrawn from the reaction mixture at 0.05, 1, 2, 4, 6 and 8 h for chemical analysis of peroxidation products. All experiments were performed in air-saturated solutions.

The standard reaction mixture contained 1.2 mM linoleic acid dissolved in 2.5% ethanol, 0.1 mM Cu(II) complex, and 1 mM H_2O_2 in 4 ml of phosphate buffer (0.1 M, pH 7.4) was incubated at 37°C for 8 h. Aliquots (0.5 ml) were withdrawn from reaction mixtures at 0, 2, 4, 6 and 8 h.

2.4. Synthesis of linoleic acid hydroperoxide

Linoleic acid hydroperoxide was synthesized enzymatically by the reaction of linoleic acid with soybean lipoxygenase according to the method described in the literature [25]. Lipoxygenase (280 units ml^{-1}) was added to a solution of linoleic acid (1.68 mM) in 0.1 M borate buffer, pH 9.0, with vigorous stirring. The reaction was monitored spectrophotometrically at 234 nm, and stopped by acidification to pH 3 with 1 M HCl after the absorbance reached a plateau. The reaction mixture was extracted with ethyl ether three times, and the organic layers were washed with saturated aqueous NaCl, dried over anhydrous magnesium sulfate, and evaporated to dryness. The lipid hydroperoxide obtained as a colorless oil was dissolved in ethanol and stored at −20°C. Hydroperoxide concentration was determined using a molar extinction coefficient of $2.7\times10^4\,M^{-1}\,cm^{-1}$ at 234 nm [26].

2.5. High performance liquid chromatography (HPLC) measurement

Aliquots (2 ml) of the same cyclohexane layer used for measurement of the absorbance at 234 nm were evaporated under vacuum, and the residue was redissolved in 100 μl of HPLC eluent. This solution (20 μl) was injected into a normal phase silica 60 column (TOSOH, 0.46×25 cm). Hexane–isopropanol–acetic acid (80:1.25:0.1, v/v/v) at 1 ml min^{-1} was used as the mobile phase, and the increase or decrease of conjugated diene and the increase of oxodine were determined by monitoring UV absorbance at 234 and 270 nm, respectively. HPLC analyses were performed with a TOSOH instrument with CCPS pumps and a PD 8020 UV detector.

3. Results

3.1. The formation of linoleic acid hydroperoxide from the reaction of Cu(II) complexes with linoleic acid

The oxidation of linoleic acid by Cu(II) complexes was investigated by absorption spectroscopy and HPLC. The absorbance at 234 nm observed during the oxidation of linoleic acid by $Cu(II)(BC)_2$ increased with incubation time for 2 h, reached a maximum level, and decreased gradually thereafter (Fig. 1). As shown in Fig. 1, the plot of absorbance at 234 nm against incubation time exhibited a 'bell-shaped' curve. The time to reach the maximal value of absorbance at 234 nm was in the following order: $Cu(II)(BC)_2$ > $Cu(II)(CyHH)_2$ = $Cu(II)(OP)_2$ > $Cu(II)(en)_2$ > Cu(II)-(HGG).

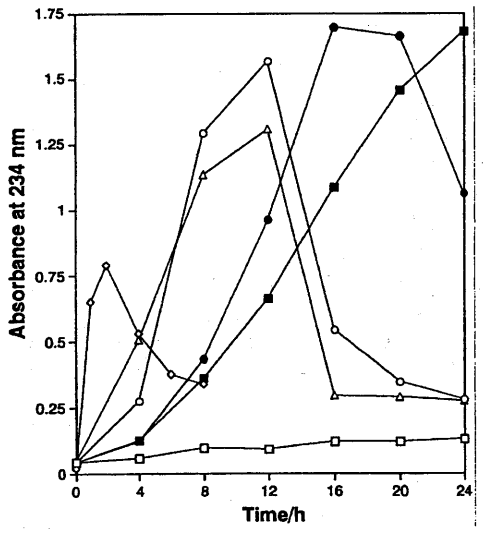

Fig. 1. Time course of change in absorbance at 234 nm of the conjugated diene in the oxidation products after incubation of linoleic acid (1.2 mM) with 0.1 mM Cu(II) complexes for 0–24 h in 0.1 M phosphate buffer (pH 7.4): □, none; ◇, $Cu(BC)_2$; ○, $Cu(CyHH)_2$; △, $Cu(OP)_2$; ■, Cu(HGG); ●, $Cu(en)_2$. Data of one representative experiment from three are shown.

The increase in absorbance at 234 nm due to the formation of conjugated dienes suggested that linoleic acid was oxidized by Cu(II) complexes to yield linoleic acid hydroperoxide. HPLC chromatograms of linoleic acid oxidized by $Cu(II)(BC)_2$ after incubation for 2 h indicated the formation of four isomers (peaks 2–5) of linoleic acid hydroperoxide (Fig. 2(b)). Peak 2 was identified according to its retention time as 13ZE-HPODE. The other peaks 3, 4, and 5 were tentatively attributed to 13EE-HPODE, 9-hydroperoxy-*trans*-10, *cis*-12-octadecaneoic acid (9EZ-HPODE) and 9EE-HPODE, respectively, as reported by Spiteller and Spiteller [27]. This was further supported by the disappearance of peaks 2 to 5 followed by increases in the intensities of peaks 1, 4b, 6 and 7 on addition of sodium borohydride (data not shown), which leads to the stoichiometric conversion of LOOH to LOH [28]. HPLC chromatograms of linoleic acid oxidized by $Cu(II)(CyHH)_2$ or $Cu(II)(OP)_2$ and $Cu(II)(en)_2$ or Cu(II)(HGG) showed the appearance of a

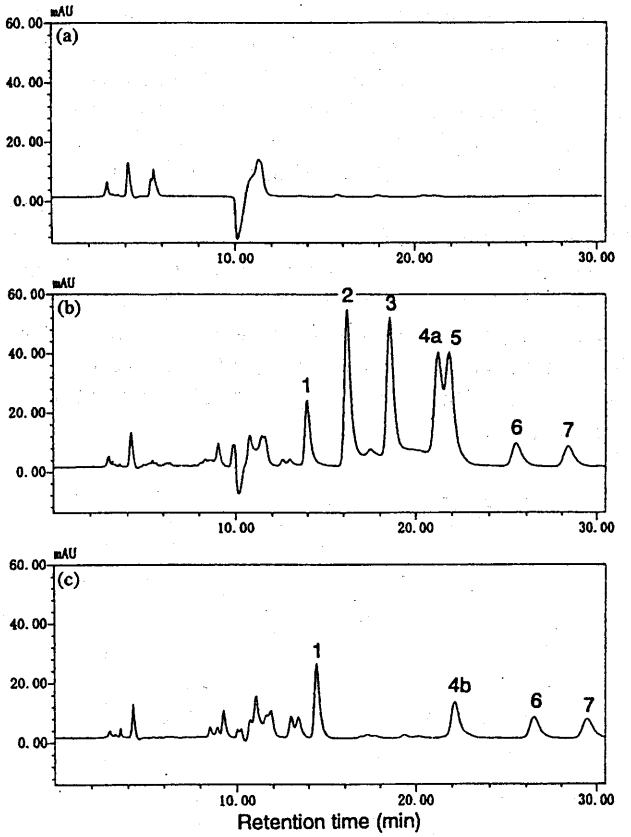

Fig. 2. Results of HPLC of linoleic acid and its oxidation products after incubation of linoleic acid (1.2 mM) with $Cu(II)(BC)_2$ (0.1 mM) for 0–8 h in 0.1 M phosphate buffer (pH 7.4): (a) 0 h; (b) 2 h; (c) 8 h. The numbered peaks represent: (1) 13-hydroxy-*cis*-9, *trans*-11-octadecadienoic acid; (2) 13-hydroperoxy-*cis*-9, *trans*-11-octadecadienoic acid; (3) 13-hydroperoxy-*trans*-9, *trans*-11-octadecadienoic acid; (4a) mixture of 9-hydroperoxy-*trans*-10, *cis*-12-octadecadienoic acid and 13-hydroxy-*trans*-9, *trans*-11-octadecadienoic acid; (4b) 13-hydroxy-*trans*-9, *trans*-11-octadecadienoic acid; (5) 9-hydroperoxy-*trans*-10, *trans*-12-octadecadienoic acid; (6) 9-hydroxy-*trans*-10, *cis*-12-octadecadienoic acid; (7) 9-hydroxy-*trans*-10, *trans*-12-octadecadienoic acid.

large amount of linoleic acid hydroperoxide after 12 and 20 h of incubation, respectively (data not shown).

3.2. The decomposition of linoleic acid hydroperoxide by Cu(II) complexes or Cu(I) complexes

The decrease in absorbance at 234 nm as shown in Fig. 1 suggested that linoleic acid hydroperoxide (LOOH) formed was further decomposed by Cu(II) complexes or Cu(I) complexes. To elucidate whether LOOH formed during the oxidation of linoleic acid is decomposed by Cu(II) or Cu(I) complexes produced from the reduction of Cu(II) complexes by hydroperoxides, the reactions of LOOH with both types of copper complexes were investigated by absorption spectroscopy and HPLC. 13-Hydroperoxyoctadecaneoic acid (abbreviated as 13-LOOH) was separately prepared from soybean lipoxygenase. The absorbance at 234 nm of 13-LOOH decreased more rapidly with incubation time in the presence of both Cu(II)$(BC)_2$ and Cu(II)$(OP)_2$, decreasing gradually in the case of Cu(II)$(CyHH)_2$ or Cu(II)$(en)_2$, and declined slightly in the case of Cu(II)(HGG) (Fig. 3). The rate of disappearance of 13-LOOH was in the following order: Cu(II)$(BC)_2$ = Cu(II)$(OP)_2$ > Cu(II)$(CyHH)_2$ > Cu(II)$(en)_2$ > Cu(II)(HGG). HPLC chromatograms of oxidation products obtained from the reaction of 13-LOOH with Cu(II) complexes indicated that disappearance of the peak corresponding to 13-LOOH depended on Cu(II) complexes, similarly to the decrease in the UV absorbance of 234 nm. Interestingly, in the reaction of 13-LOOH with Cu(II)$(BC)_2$, 9-hydroxyoctadecaneoic acids (9-LOH) derived from 9-LOOH, an isomer of 13-LOOH, accompanied by the disappearance of 13-LOOH was observed together with 13-hydroxyoctadecaneoic acids (13-LOH) (Fig. 4(c)). However, these phenomena could not be observed with other Cu(II) complexes.

All Cu(I) complexes generated by the reduction of Cu(II) complexes with excess ascorbic acid rapidly decreased the absorbance at 234 nm due to LOOH within 1 h of incubation (Fig. 5). The results shown in Fig. 5 suggested that Cu(I) complexes can decompose LOOH faster than the correspond-

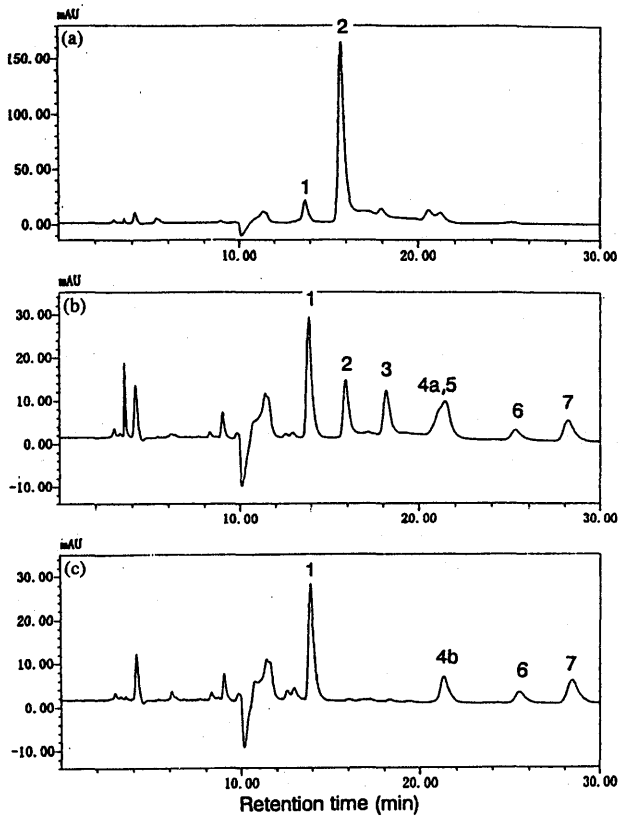

Fig. 4. Results of HPLC after incubation of LOOH (0.3 mM) with 0.1 mM Cu(II)$(BC)_2$ in 0.1 M phosphate buffer (pH 7.4) for 0 h (a), 2 h (b) and 8 h (c). The numbered peaks are the same as those described in Fig. 2.

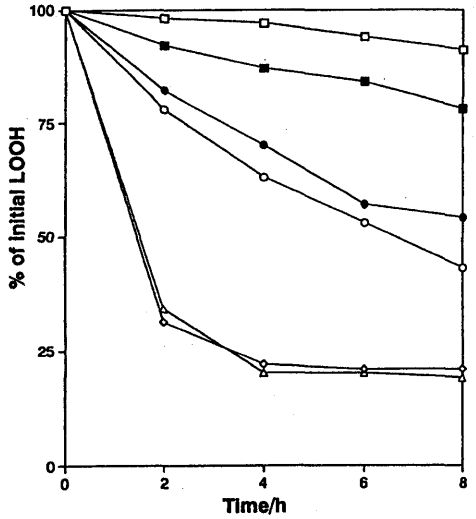

Fig. 3. Time course of reaction of linoleic acid hydroperoxide (LOOH) (0.3 mM) with 0.1 mM Cu(II) complexes for 0–8 h in 0.1 M phosphate buffer (pH 7.4): □, none; ◇, Cu$(BC)_2$; ○, Cu$(CyHH)_2$; △, Cu$(OP)_2$; ■, Cu(HGG); ●, Cu$(en)_2$. Data of one representative experiment from three are shown.

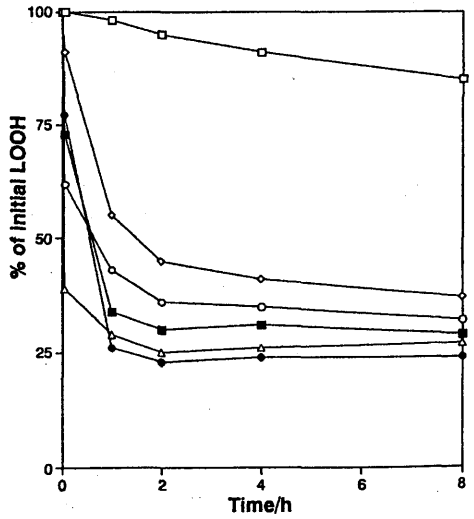

Fig. 5. Time course of changes in absorbance at 234 nm after incubation of LOOH (0.3 mM) with 0.1 mM Cu(II) complex and 0.2 mM ascorbic acid for 0–8 h in 0.1 M phosphate buffer (pH 7.4): □, none; ◇, Cu$(BC)_2$; ○, Cu$(CyHH)_2$; △, Cu$(OP)_2$; ■, Cu(HGG); ●, Cu$(en)_2$. Data of one representative experiment from three are shown.

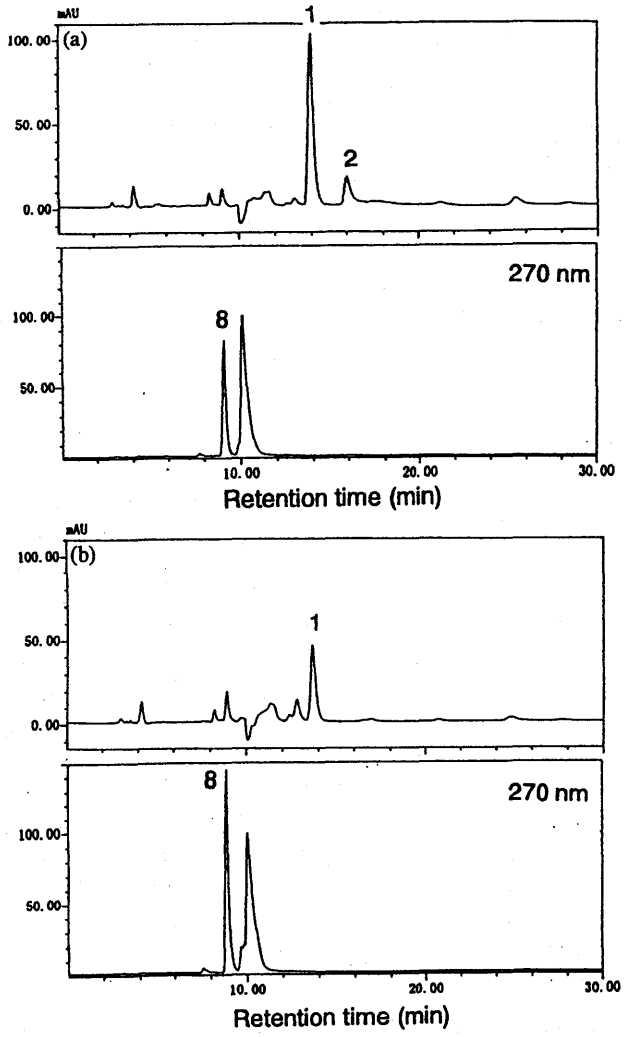

Fig. 6. Results of HPLC after 2 h incubation of LOOH (0.3 mM) with 0.1 mM Cu(II)$(BC)_2$ (a) and Cu(II)$(en)_2$ (b) in the presence of 0.2 mM ascorbic acid in 0.1 M phosphate buffer (pH 7.4). The numbered peaks are the same as those described in Fig. 2. Peak 8 corresponds to 13-oxo-9,11-octadecadienoic acid.

ing Cu(II) complexes. HPLC of oxidation products obtained from the reaction of LOOH with Cu(II)$(BC)_2$ or Cu(II)$(en)_2$ in the presence of ascorbic acid after 2 h of incubation indicated almost complete disappearance of LOOH and increase in the corresponding LOH and a peak with absorbance at 270 nm (peak 8) (Fig. 6). Interestingly, the relative signal intensity of LOH among oxidation products obtained from the reaction of Cu(I) complexes with LOOH was larger than those of Cu(II) complexes.

3.3. Reaction of Cu(II) complexes with linoleic acid in the presence of H_2O_2

Lipid peroxidation may be initiated by hydroxyl radicals ($^{\cdot}OH$) [3]. On the other hand, Cu(II) complexes were shown to react with H_2O_2 to generate $^{\cdot}OH$ [18,19]. Therefore, the addition of H_2O_2 to reaction mixtures of linoleic

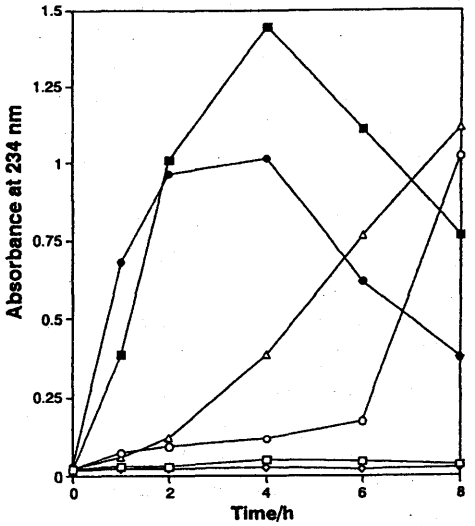

Fig. 7. Time course of changes in absorbance at 234 nm after incubation of linoleic acid (1.2 mM), and linoleic acid (1.2 mM) with 0.1 mM Cu(II) complexes for 0–8 h in the presence of 1 mM H_2O_2: □, none; ◇, Cu$(BC)_2$; ○, Cu$(CyHH)_2$; △, Cu$(OP)_2$; ■, Cu(HGG); ●, Cu$(en)_2$. Data of one representative experiment from three are shown.

acid and Cu(II) complexes was expected to accelerate the oxidation due to generation of reactive $^{\cdot}OH$. The addition of H_2O_2 to Cu(II)(HGG) or Cu(II)$(en)_2$ rapidly increased the absorbance at 234 nm, whereas the addition of H_2O_2 to Cu(II)$(CyHH)_2$ suppressed the increase in absorbance at 234 nm over a 6 h incubation period (Fig. 7). Furthermore, no oxidation of linoleic acid was evoked by Cu(II)$(BC)_2$ in the presence of H_2O_2 within the experimental period (8 h), suggesting that H_2O_2 reduces Cu(II)$(BC)_2$ and then prevents initiation of lipid peroxidation.

4. Discussion

The absorbance at 234 nm in the reaction of Cu(II)$(BC)_2$ with linoleic acid increased with incubation time for 2 h and decreased gradually thereafter (Fig. 1). Lipid peroxidation proceeds through a chain reaction initiated by the abstraction of a hydrogen atom from polyunsaturated fatty acids containing unconjugated 1,4-dienes to yield conjugated dienes with a characteristic UV absorption around 234 nm [3]. Therefore, the increase in absorbance at 234 nm suggested that linoleic acid was oxidized by Cu(II)$(BC)_2$ and converted to LOOH with a conjugated diene. On normal phase HPLC after 2 h of incubation (Fig. 2), four isomers (from peak 2 to peak 5) of LOOH were observed and attributed to 13ZE-HPODE, 13EE-HPODE, 9ZE-HPODE, and 9EE-HPODE, respectively, according to previous reports [27,29–31]. On the other hand, plots of absorbance at 234 nm against incubation time in the reaction of linoleic acid with five Cu(II) complexes exhibited a 'bell-shaped' curve (Fig. 1). The time to reach the maximal value of absorbance at 234 nm was in the following order: Cu(II)$(BC)_2$ > Cu(II)$(CyHH)_2$ = Cu(II)-

$(OP)_2$ > Cu(II)$(en)_2$ > Cu(II)(HGG). This result suggested that lipid peroxidation, i.e. the formation of lipid hydroperoxide, may depend on the redox potential of Cu(II) complexes, since the redox potential of Cu(II)$(BC)_2$, 620 mV (versus NHE) [32,33], was the highest among the five Cu(II) complexes examined here. The redox potentials of the other four Cu(II) complexes were in the following order: Cu(II)$(CyHH)_2$ (282 mV) > Cu(II)$(OP)_2$ (147 mV) > Cu(II)(HGG) (82 mV) > Cu(II)$(en)_2$ (−14 mV) [34]. It has been reported that the change in redox potential of copper markedly influenced the rate of oxidation of lipids induced by copper [6].

The decrease in absorbance at 234 nm during the reaction of Cu(II) complexes with linoleic acid shown in Fig. 1 suggested the decomposition of LOOH formed during oxidation by Cu(II) complexes. Then, the reaction of LOOH, which was separately prepared from the reaction of linoleic acid with soybean lipoxygenase, with five Cu(II) complexes were investigated by absorption spectroscopy and HPLC. As shown in Fig. 3, Cu(II)$(BC)_2$ or Cu(II)$(OP)_2$ decomposed LOOH rapidly, Cu(II)$(CyHH)_2$ or Cu(II)$(en)_2$ moderately, and Cu(II)(HGG) slowly. This result suggested a good correlation between the decomposition of LOOH and redox potential of the Cu(II) complexes used here. The results obtained by HPLC were similar to those obtained by UV spectroscopy. Interestingly, the HPLC chromatogram observed in the reaction of Cu(II)$(BC)_2$ with 13-LOOH indicated the presence of 9-HODE (peaks 6 and 7) in addition to 13-HODE. Also, the corresponding derivatives of *E*/*Z* isomers of 9- and 13-HODE were formed. The presence of these isomers of 9- and 13-HODE is in accordance with the observation of Porter [35] who reported that peroxyl radicals decompose by loss of oxygen, allowing a second-step reoxygenation in either position 9 or 13 with double-bond isomerization. However, at present we cannot explain why this was not observed in HPLC analysis of other Cu(II) complexes.

Furthermore, to ascertain whether the decomposition of LOOH was caused by Cu(I) complexes generated during oxidation of LOOH by Cu(II) complexes, the reactions of LOOH with Cu(I) complexes were investigated by electronic absorption spectroscopy and HPLC. All Cu(I) complexes, which were generated by the reduction of Cu(II) complexes with excess ascorbic acid, rapidly decreased the amount of LOOH (Fig. 5). In particular, Cu(I)$(en)_2$ was more reactive toward hydroperoxide than Cu(I)$(BC)_2$. HPLC analysis of the products obtained from the reaction of LOOH with Cu(I) complexes suggested that amounts of LOH and oxooctadienoic acids with an absorbance peak at 270 nm were larger than those produced in the case of Cu(II) complexes. Furthermore, epoxyhydroxyoctadecenoic acids could also be produced from the alkoxyl radical as observed in the reaction of 13-LOOH with Fe(II) ion [27,36]. A large amount of LOH may be generated from the reduction of alkoxyl radicals by either ascorbic acid [37] or Cu(I) complexes, or from hydrogen abstraction of alkoxyl radicals accompanied by the formation of oxodienoic acids [36,38].

Thus, a mechanism of Cu(II)-dependent oxidation of linoleic acid occurs involving the cleavage of preformed LOOH in linoleic acid and can be proposed as follows [5,39]:

$$Cu(II) + LOOH \rightarrow Cu(I) + LOO^{\cdot} + H^{+} \quad (1)$$

$LOO^{\cdot}$ abstracts the hydrogen atom (H) from other linoleic acid molecules (LH) to yield the alkyl radical ($L^{\cdot}$) (Eq. (2)). $L^{\cdot}$ combines with O_2 under aerobic conditions to give the peroxyl radical, $LOO^{\cdot}$ (Eq. (3)), and then the chain reaction of lipid peroxidation can continue:

$$LOO^{\cdot} + LH \rightarrow LOOH + L^{\cdot} \quad (2)$$

$$L^{\cdot} + O_2 \rightarrow LOO^{\cdot} \quad (3)$$

Lichtenberg and co-workers [40] reported that peroxidation of LDL is initiated by copper-catalyzed decomposition of LOOH into peroxyl radicals. In addition, Trolox, which is a potent peroxyl radical scavenger [41], suppressed the peroxidation of linoleic acid by Cu$(CyHH)_2$ or Cu$(OP)_2$ (data not shown). These results suggested that peroxyl radicals generated by reaction of Cu(II) complex with LOOH in linoleic acid may participate in the initiation stage of peroxidation of linoleic acid and the generation of peroxyl radicals may be dependent on the redox potential of Cu(II) complexes.

LOOH, which was produced and accumulated during the oxidation of linoleic acid, could then be decomposed by Cu(II) complex (Eq. (1)). The resultant Cu(I) could also cleave LOOH in a reaction analogous to the Fenton reaction (Eq. (4)):

$$Cu(I) + LOOH \rightarrow Cu(II) + LO^{\cdot} + HO^{-} \quad (4)$$

$LOO^{\cdot}$ or $LO^{\cdot}$ decompose to give a variety of products:

$$LOO^{\cdot} \rightarrow \text{degradation products} \quad (5)$$

$$LO^{\cdot} \rightarrow \text{degradation products} \quad (6)$$

The decomposition of LOOH may be dependent on the redox potential of Cu(II) complexes as shown in Fig. 1.

The contribution of the $^{\cdot}OH$ formed by the Fenton or Haber–Weiss reaction in the peroxidation of lipids has been the subject of extensive discussion [42]. The oxidation of linoleic acid by Cu(II)(HGG) or Cu(II)$(en)_2$ occurred faster in the presence than in the absence of H_2O_2, as shown in Figs. 1 and 7. H_2O_2 reduces Cu(II)(HGG) or Cu(II)$(en)_2$ to yield these corresponding Cu(I) complexes. Although Cu(I) complexes cannot oxidize linoleic acid, the unstable Cu(I) complexes formed thus react with H_2O_2, being equal to the concentration of linoleic acid to yield a large amount of $^{\cdot}OH$ (data not shown) [18,20], which may primarily oxidize linoleic acid to yield LOOH. In contrast, the addition of H_2O_2 suppressed the oxidation of linoleic acid by Cu(II)$(BC)_2$ or Cu(II)$(CyHH)_2$. This suggested that the Cu(II) complex having the higher redox potential such as Cu(II)$(BC)_2$ is reduced by H_2O_2 to result in the correspond-

ing stable Cu(I) complex, thereby making the reaction with H_2O_2 more difficult. Although $Cu(I)(BC)_2$ can react with LOOH to give lipid alkoxyl radicals (Fig. 6), small amounts of alkoxyl radical thus formed probably cannot oxidize linoleic acid. On the other hand, addition of H_2O_2 to the reaction mixture of linoleic acid and $Cu(OP)_2$ hardly changed the product pattern; almost all $^{\cdot}OH$ generated may be reduced by $C(I)(OP)_2$ to HO^- before it can react with linoleic acid.

5. Conclusions

Cu(II) complexes with a high redox potential could oxidize preformed LOOH to generate peroxyl radicals, which may readily oxidize linoleic acid to yield lipid alkyl radicals. The lipid alkyl radical thus formed further reacts with oxygen to yield peroxyl radicals [5,39], although we cannot exclude the possibility of direct oxidation of polyunsaturated lipids by Cu(II) complexes. These results obtained suggest that copper(II) ions bound into lipoprotein with high redox potential may induce rapid oxidation of low density lipoprotein.

6. Abbreviations

HPLC	high performance liquid chromatography
LDL	low density lipoprotein
BC	bathocuproinedisulfonic acid
CyHH	cyclo(L-histidyl-L-histidyl)
OP	*o*-phenanthroline
HGG	L-histidylglycylglycine
en	ethylenediamine
LOOH	linoleic acid hydroperoxide
13ZE-HPODE	13-hydroperoxy-*cis*-9, *trans*-11-octadecaneoic acid
13ZE-HODE	13-hydroxy-*cis*-9, *trans*-11-octadecaneoic acid
9EZ-HPODE	9-hydroperoxy-*trans*-10, *cis*-12-octadecaneoic acid
9EZ-HODE	9-hydroxy-*trans*-10, *cis*-12-octadecaneoic acid
13EE-HPODE	13-hydroperoxy-*trans*-9, *trans*-11-octadecaneoic acid
9EE-HPODE	9-hydroperoxy-*trans*-10, *trans*-12-octadecaneoic acid

Acknowledgements

This work was supported in part by a Grant-in-Aid from the Ministry of Education, Science, and Culture, Japan.

References

[1] D. Steinberg, Circulation 76 (1987) 508.
[2] C.E. Cross, B. Halliwell, E.T. Borish, W.A. Pryor, B.N. Ames, R.L. Saul, J.M. McCord, D. Harman, Ann. Int. Med. 107 (1987) 526.
[3] B. Halliwell, J.M.C. Gutteridge, Free Radicals in Biology and Medicine, 2nd ed., Clarendon Press, Oxford, 1989.
[4] P.C. Chan, O.G. Peller, L. Kesner, Lipids 17 (1982) 331.
[5] Y. Yoshida, E. Niki, Arch. Biochem. Biophys. 295 (1992) 107.
[6] Y. Yoshida, S. Furuta, E. Niki, Biochim. Biophys. Acta 1210 (1993) 81.
[7] H. Esterbauer, J. Gebicki, H. Puhl, G. Jurgensm, Free Rad. Biol. Med. 13 (1992) 341.
[8] W. Sattler, G.M. Kostner, G. Waeg, H. Esterbauer, Biochim. Biophys. Acta 1081 (1991) 65.
[9] S.M. Lynch, B. Frei, J. Biol. Chem. 270 (1995) 5158.
[10] A. Kontush, S. Meyer, B. Finckh, A. Kohlschütter, U. Beisiegel, J. Biol. Chem. 271 (1996) 11106.
[11] J. Neuzil, S.R. Thomas, R. Stocker, Free Rad. Biol. Med. 22 (1997) 57.
[12] B. Kalyanaraman, W.E. Antholine, S. Parthasarathy, Biochim. Biophys. Acta 1035 (1990) 286.
[13] M. Kuzuya, K. Yamada, T. Hayashi, C. Funaki, M. Naito, K. Asai, F. Kuzuya, Biochim. Biophys. Acta 1123 (1992) 334.
[14] S.P. Gieseg, H. Esterbauer, FEBS Lett. 343 (1994) 188.
[15] G. Multhaup, A. Schlicksupp, L. Hesse, D. Beher, T. Ruppert, C.L. Masters, K. Beyreuther, Science 271 (1996) 1406.
[16] C. Perugini, M. Seccia, E. Albano, G. Bellomo, Biochim. Biophys. Acta 1347 (1997) 191.
[17] F.P. Patel, D. Svistunenko, M.T. Wilson, V.M. Darley-Usmar, Biochem. J. 322 (1997) 425.
[18] T. Ozawa, A. Hanaki, J. Chem. Soc., Chem. Commun. (1991) 330.
[19] J. Ueda, T. Ozawa, M. Miyazaki, Y. Fujiwara, J. Inorg. Biochem. 55 (1994) 123.
[20] J. Ueda, Y. Shimazu, T. Ozawa, Biochem. Mol. Biol. Int. 34 (1994) 801.
[21] J. Ueda, A. Sudo, A. Mori, T. Ozawa, Arch. Biochem. Biophys. 315 (1994) 185.
[22] J. Ueda, Y. Shimazu, T. Ozawa, Free Rad. Biol. Med. 18 (1995) 929.
[23] G. Arena, R.P. Bonomo, G. Impellizzeri, R.M. Izatt, J.D. Lamb, E. Rizzarelli, Inorg. Chem. 26 (1987) 795.
[24] J. Ueda, N. Ikota, A. Hanaki, K. Koga, Inorg. Chim. Acta 135 (1987) 43.
[25] M.R. Egmond, M. Brunori, P.M. Fasella, Eur. J. Biochem. 61 (1976) 93.
[26] W.A. Pryor, L. Castle, Methods Enzymol. 105 (1984) 293.
[27] P. Spiteller, G. Spiteller, Biochim. Biophys. Acta 1392 (1998) 23.
[28] B. Frei, Y. Yamamoto, D. Niclas, B.N. Ames, Anal. Biochem. 175 (1988) 120.
[29] J.I. Teng, L.L. Smith, J. Chromatogr. 350 (1985) 445.
[30] M.L. Lenz, H. Hughes, J.R. Mitchell, D.P. Via, J.R. Guyton, A.A. Taylor, A.M. Gotto Jr., C.V. Smith, J. Lipid Res. 31 (1990) 1043.
[31] Z. Wu, D.S. Robinson, C. Domoney, R. Casey, J. Agric. Food Chem. 43 (1995) 337.
[32] A.G. Lappin, M.P. Youngblood, D.W. Margerum, Inorg. Chem. 19 (1980) 407.
[33] N. Al-Shatti, A.G. Lappin, A.G. Sykes, Inorg. Chem. 20 (1981) 1466.
[34] J. Ueda, M. Takai, Y. Shimazu, T. Ozawa, Arch. Biochem. Biophys. 357 (1998) 231.
[35] N.A. Porter, Methods Enzymol. 105 (1984) 273.
[36] H.W. Gardner, Free Rad. Biol. Med. 7 (1989) 65.

[37] K.L. Retsky, B. Frei, Biochim. Biophys. Acta 1257 (1995) 279.
[38] A. Loidl-Stahlhofen, K. Hannemann, G. Spiteller, Biochim. Biophys. Acta 1213 (1994) 140.
[39] C.E. Thomas, R.L. Jackson, J. Pharmacol. Exp. Ther. 256 (1991) 1182.
[40] I. Pinchuk, E. Schnitzer, D. Lichtenberg, Biochim. Biophys. Acta 1389 (1998) 155.
[41] G.W. Winston, F. Regoli, A.J. Dugas Jr., J.H. Fong, K.A. Blanchard Free Rad. Biol. Med. 24 (1998) 480.
[42] K.M. Schaich, Lipids 27 (1992) 209.

ANTIOXIDANTS & REDOX SIGNALING
Volume 2, Number 2, 2000
Mary Ann Liebert, Inc.

Original Research Communication

Singlet Oxygen-Dependent Hydroxyl Radical Formation during Uroporphyrin-Mediated Photosensitization in the Presence of NADPH

KEIZO TAKESHITA,[1] CLAUDIO A. OLEA-AZAR,[1,3] MICHIKO MIZUNO,[1,2] and TOSHIHIKO OZAWA[1]

ABSTRACT

The conversion of singlet oxygen ($^1O_2$) to hydroxyl radical ($^{\cdot}OH$) during photosensitization of uroporphyrin (UP) in the presence of NADPH was examined by a spin-trapping technique with 5,5-dimethyl-1-pyrroline-*N*-oxide (DMPO). Significant electron spin resonance (ESR) signals of DMPO-OH adduct were observed during irradiation of the UP-NADPH system with visible light. Scavengers of $^{\cdot}OH$ reduced the signal intensity to 3–30% of control, indicating that more than 70% of DMPO-OH results from freely diffusing $^{\cdot}OH$. The ESR signal was almost completely lost when quenchers of $^1O_2$ were added, and was enhanced when the amount of deutrated solvent was increased. The appearance of $^1O_2$, as determined by the oxidation of 2,2,6,6-tetramethyl-4-piperidone (TEMPD), was delayed with an increase in the concentration of NADPH, whereas the production of $^{\cdot}OH$ was upregulated. These observations indicate that conversion of $^1O_2$ to $^{\cdot}OH$ occurs quickly in the presence of NADPH. Hydrogen peroxide (H_2O_2) was produced $^1O_2$-dependently during irradiation of UP in the presence of NADPH. However, neither catalase nor desferrioxamine decreased the DMPO-OH signal, and addition of H_2O_2 did not increase the signal. SOD increased the signal only slightly. These results suggest that the production of $^{\cdot}OH$ from $^1O_2$ involves neither superoxide anion radical nor H_2O_2. Antiox. Redox Signal. 2, 355–362.

INTRODUCTION

PHOTOSENSITIZERS SUCH AS PORPHYRIN DERIVATIVES are used as agents for photodynamic therapy (Calzavara-Pinton *et al.*, 1996) but are causative of porphyrias (Brun and Sanberg, 1991). The therapeutic effect and the tissue damage are explained by the generation of reactive oxygen species (ROS) such as superoxide anion radical ($O_2^{\cdot -}$), hydroxyl radical ($^{\cdot}OH$), hydrogen peroxide (H_2O_2), and singlet oxygen ($^1O_2$), during photodynamic reactions and their successive reactions with biologically important molecules. The pathways for generating reactive oxygen species usually fall into two major categories: (1) type I reactions involving electron or hydrogen transfer between the substrate and the triplet excited sensitizer, with generation of free radicals and other reactive intermediates, *e.g.*, $O_2^{\cdot -}$, $^{\cdot}OH$, and H_2O_2, and (2) type II reactions involving energy transfer from the triplet sensitizer to oxygen, ac-

[1]Bioregulation Research Group, National Institute of Radiological Sciences, Chiba 263-8555, Japan.
[2]Kyoritsu College of Pharmacy, Tokyo 105-8512, Japan.
[3]Present address: Faculty of Science and Pharmacy, University of Chile, Olivos 1007, Independencia, Casila 233 Santiago 1, Chile.

companying the formation of $^1O_2$. Formation of $O_2^{\cdot -}$ was demonstrated during the reaction of $^1O_2$ with NAD(P)H by monitoring the reductions of benzoquinone (Peters and Rodgers,1981) and *p*-nitrotetrazolium blue (Inoue *et al.*, 1984). $^1O_2$-mediated formation of H_2O_2 was reported in the presence of SOD (Menon *et al.*, 1989) and NADPH (Bodaness and Chan, 1977). Furthermore, Buettner (1985) demonstrated $^1O_2$-mediated formation of ·OH in the presence of cysteine. These reports suggest that conversion of $^1O_2$ to other ROS is possible in the presence of certain biological substances. Reaction manners and biological effects vary depending on the kind of ROS (Ryter and Tyrrell, 1998; Halliwell and Gutteridge, 1999). Nevertheless, how $^1O_2$ is converted to other ROS is not fully understood. In the present study, we studied the conversion of $^1O_2$ to highly toxic ·OH in the presence of NADPH in a uroporphyrin (UP) photosensitizing system and demonstrated that ·OH is generated without the intermediates $O_2^{\cdot -}$ or H_2O_2.

MATERIALS AND METHODS

Materials

Uroporphyrin I dihydrochloride was obtained from Porphyrin Products (Logan, UT). 5,5-Dimethyl-1-pyrroline-*N*-oxide (DMPO) was purchased from Labotec (Tokyo). NADPH was obtained from Kohjin Co., Ltd. (Tokyo). Catalase (Bovine Liver), superoxide dismutase (SOD, Bovine Erythrocyte), horseradish peroxidase (type VI), 2,2,6,6-tetramethyl-4-piperidone hydrochloride (TEMPD) and desferrioxamine mesylate (DFO) were obtained from Sigma (St. Louis, MO). Deuterium oxide (D_2O) was purchased from Aldrich (Milwaukee, WI). Pure water was freshly prepared with a Millipore Milli-Q Labo (Bedford, MA). All other reagents were of the highest purity commercially available.

Electron spin resonance measurements

Oxygen radicals were determined by spin-trapping method with DMPO as the trapping agent, and TEMPD was used for the determination of $^1O_2$. The detection of $^1O_2$ is based on the oxidation of TEMPD to corresponding nitroxide radical, 2,2,6,6-tetramethyl-4-piperidone-*N*-oxyl (TEMPON) (Lion *et al.*, 1976; Moan and Wold, 1979). A sample solution was transferred to a quartz flat cell (Labotec, Tokyo) and irradiated with visible light at room temperature (24–25°C). X-band ESR spectra were recorded with a JEOL JES RE-1X spectrometer at 0.079 mT of 100 kHz field modulation. Manganese oxide was used as an internal standard.

Measurement of H_2O_2

Photodynamic generation of H_2O_2 was assayed according to the method of Frew *et al.* (1983) with a slight modification. In this method, H_2O_2 oxidatively couples with 4-aminoantipyrine and phenol to yield a quinoneimine chromogen with a maximum absorption at 505 nm. A 2.4-ml volume of sample solution in a quartz cubet was irradiated with visible light for 10 min at room temperature (24–25°C). To the solution was added 0.4 ml of a reagent which contains 0.5 wt/vol % 4-aminoantipyrine, 1.2 wt/vol % phenol, 0.1 μM horseradish peroxidase, and 12.5 μM H_2O_2. The sample solution incubated in the dark was used as a negative control. The absorbance of the resulting solution was measured at 505 nm. The concentration of H_2O_2 was determined with spectrophotometrically standardized H_2O_2 (ϵ = 43.5 $M^{-1}cm^{-1}$ at 240 nm).

Light source

A 750 W tungsten bulb (Philips AP-12) equipped with a reflector and a condensing lens was used as a visible light source. Using a model IL1400A radiometer/photometer with a SL021/FQI detector (International Light, Inc., Newburyport, MA), the light intensity was determined to be 0.7 W/m^2 for spin-trapping experiments and 10 W/m^2 for H_2O_2 determination experiments.

RESULTS

Irradiation of UP with visible light in the presence of NADPH and DMPO produced a four-line (1:2:2:1) ESR spectrum with hyperfine

splittings ($a^N = a^H = 1.49$ mT) characteristic of the ·OH adduct of DMPO (DMPO-OH) (Fig. 1A) (Buettner, 1987; Ozawa and Hanaki, 1991). The signal intensity of DMPO-OH was obviously reduced when NADPH was excluded from the reaction mixture (Fig. 1B), and no signal was observed on incubation in the dark (data not shown). The addition of ethanol and sodium formate during irradiation resulted in a reduction in the intensity of signal of DMPO-OH and the appearance of a six-line ESR signal which was assigned to the $\cdot CH(OH)CH_3$ adduct of DMPO ($a^N = 1.59$ mT, $a^H = 2.29$ mT) and the $\cdot CO_2^-$ adduct of DMPO ($a^N = 1.57$ mT, $a^H = 1.87$ mT), respectively (Fig. 1C, D) (Buettner, 1987). Addition of ethanol, sodium formate, or dimethyl sulfoxide (DMSO) reduced the signal intensity to 3–30% of control (Table 1). These observations suggest that more than 70% of DMPO-OH results from freely diffusing ·OH produced during irradiation of UP and NADPH, but not from decay of the $O_2^{\cdot -}$ adduct of DMPO. Similar results were obtained when NADH was used instead of NADPH.

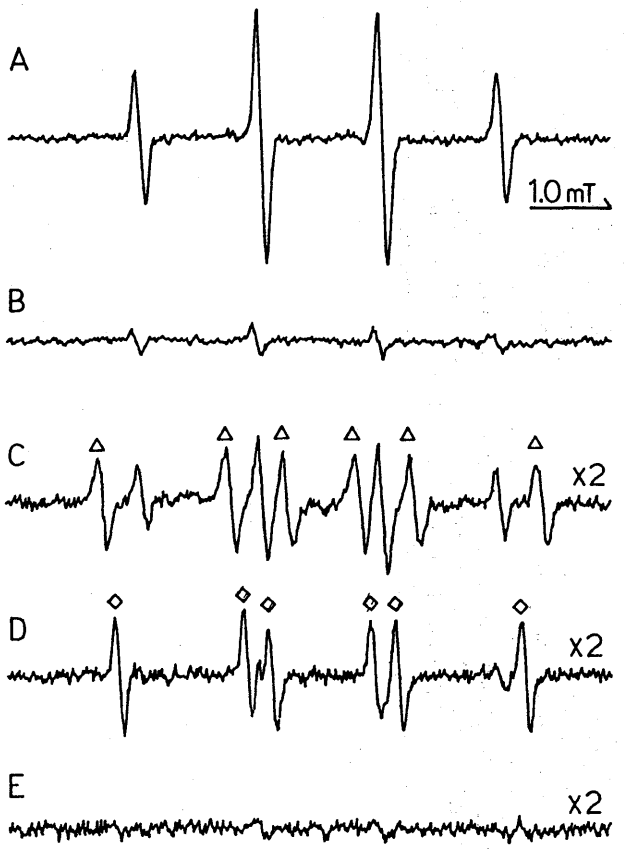

Fig. 1. ESR spectra of DMPO spin adducts formed during irradiation of UP. (**A**) 14 μM UP, 167 μM NADPH, and 48 mM DMPO in 20 mM phosphate buffer, pH 7.4, was irradiated with visible light for 2 min. (**B**) Same conditions except without NADPH. Samples containing 600 mM ethanol (**C**), 143 mM sodium formate (**D**), and 5 mM NaN_3 (**E**) were irradiated in the presence of NADPH. (△) $\cdot CH(OH)CH_3$ adduct of DMPO; (◇) $\cdot CO_2^-$ adduct of DMPO.

The signal of DMPO-OH was almost completely lost on addition of quenchers of $^1O_2$ such as sodium azide, L-histidine, and 1,4-diazabicyclo[2.2.2]octane (DABCO) (Table 1). No $N_3^{\cdot}$ adduct of DMPO was observed (Fig. 1E). To obtain evidence of the involvement of $^1O_2$ in the production of ·OH, the formation of DMPO-OH was examined in the deuterated solvent where the half-life of $^1O_2$ is known to be elongated. Replacement of 97% of H_2O with D_2O clearly increased both the rate and extent of DMPO-OH formation (Fig. 2). These observations strongly indicate that $^1O_2$ is an intermediate of ·OH.

Role of $^1O_2$ in the ·OH formation was further clarified by examining the oxidation of TEMPD by $^1O_2$. Signal heights for TEMPON formation in the presence of different concentrations of NADPH were measured along with time and were superimposed on those for DMPO-OH formation obtained under the same concentrations of UP and NADPH (Fig. 3). In the absence of NADPH, the signal of TEMPON increased with increase of irradiation time. This signal significantly decreased when irradiation was performed in the presence of quenchers of $^1O_2$ such as NaN_3 and L-histidine, although ·OH scavengers, catalase, and SOD had less or no effect (Table 1), indicating that oxidation of TEMPD to TEMPON is specific to $^1O_2$ under this condition. The presence of NADPH delayed the appearance of TEMPON signal (Fig. 3). The lag time increased with the concentration of NADPH, whereas the rate of formation of DMPO-OH increased with the concentration of NADPH. These observations imply that $^1O_2$ is converted to ·OH NADPH dependently, and that the apparent reaction rate constant of $^1O_2$ for NADPH is much larger than the rate constant of $^1O_2$ for TEMPD ($4–8 \times 10^7\ M^{-1}\cdot s^{-1}$) (Lion *et al.*, 1976; Moan and Wold, 1979).

One-electron reduction of $^1O_2$ by NAD(P)H (Peters and Rodgers, 1981; Inoue *et al.*, 1984) has been proposed in chemical reactions. This reaction gives $O_2^{\cdot -}$ as a product. On the other

TABLE 1. EFFECTS OF INHIBITORS ON DMPO-OH FORMATION AND H_2O_2 PRODUCTION IN A UP-NADPH PHOTOSENSITIZING SYSTEM AND ON TEMPON PRODUCTION IN A UP-PHOTOSENSITIZING SYSTEM

Inhibitors	*Concentrations*	*DMPO-OH (relative signal intensity) in UP-NADPH-light system*[a]	*TEMPON (relative signal intensity) in UP-light system*[b]	*H_2O_2 (μM) in UP-NADPH-light system*[c]
None		1.89 ± 0.26 (100)	0.396 ± 0.084 (100)	51.4 ± 7.6 (100)
Ethanol	600 m*M*	0.53 ± 0.03 (27)	0.393 ± 0.020 (99)	ND
DMSO	143 m*M*	0.33 ± 0.14 (18)	0.276 ± 0.031 (70)	ND
Sodium formate	143 m*M*	0.06 ± 0.03 (3)	0.275 ± 0.022 (67)	ND
NaN_3	5 m*M*	0.06 ± 0.02 (3)	0.135 ± 0.025 (34)	3.2 ± 0.5[d] (6)
L-Histidine	5 m*M*	0.06 ± 0.02 (3)	0.000 ± 0.000 (0)	ND
DABCO	5 m*M*	0.26 ± 0.01 (14)	0.295 ± 0.025 (74)	ND
DFO	20 μ*M*	2.03 ± 0.21 (107)	0.282 ± 0.087 (71)	59.0 ± 1.6[e] (115)
SOD	100 U/ml	2.93 ± 0.59 (155)	0.425 ± 0.060 (107)	ND
Catalase	280 U/ml	2.43 ± 0.40 (129)	0.391 ± 0.027 (99)	0.0 ± 0.1[f] (0)
SOD + catalase	100 U/ml + 280 U/ml	2.70 ± 0.20 (143)	ND	ND

Each value is the mean ± SD for triplicate experiments. Numbers in parentheses are the percentage to the value for no inhibitor. ND, Not determined.
[a]Sample solutions containing 14 μ*M* UP, 167 μ*M* NADPH, 48 m*M* DMPO, and indicated concentrations of inhibitor were irradiated.
[b]Sample solutions containing 14 μ*M* UP, 50 m*M* TEMPD, and indicated concentrations of inhibitor were irradiated.
[c]Sample solutions containing 2.5 μ*M* UP, 0.17 m*M* NADPH, and indicated concentrations of inhibitor were irradiated.
[d]6 m*M* NaN_3 was used.
[e]17 μ*M* desferrioxamine was used.
[f]120 U/mL catalase was used.

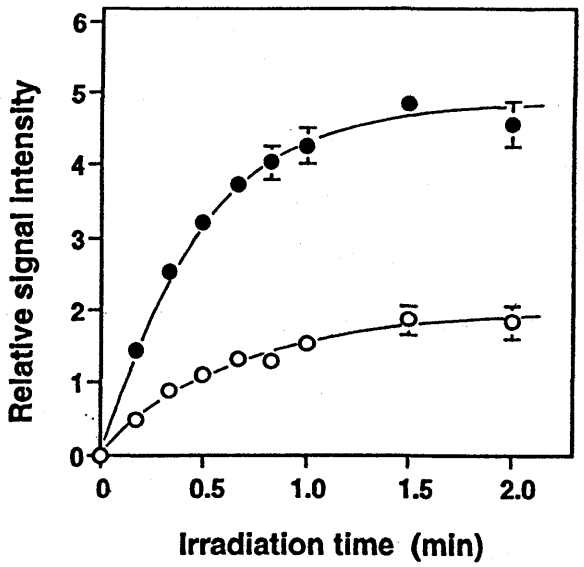

Fig. 2. Enhancement of DMPO-OH formation in deuterated solvent. Irradiated with visible light was 14 μM UP, 167 μM NADPH, and 48 mM DMPO in 5 mM phosphate buffer, pH 7.4, prepared with H_2O (○) or 97% D_2O (●). The ratio of the signal intensity of the second low-field peak to that of the manganese peak (internal standard) was plotted. Data are presented as mean values of duplicate experiments. Error bars indicate deviations.

hand, two-electron reduction of $^1O_2$ to H_2O_2 by NADPH was also suggested in a hematoporphyrin photodynamic system (Bodaness and Chan, 1977). $O_2^{\cdot -}$ and/or H_2O_2 may produce ·OH through metal-catalyzed reactions. To confirm whether or not the generation of ·OH observed in the present study occurs through $O_2^{\cdot -}/H_2O_2$, effects of DFO, a Fe-chelator, SOD, and catalase on DMPO-OH formation were examined in a UP-NADPH photodynamic system. DFO and catalase did not reduce the DMPO-OH formation at the concentration indicated in Table 1. SOD somewhat enhanced the DMPO-OH formation, but the increase was not inhibited by addition of catalase, indicating that the effect does not result from H_2O_2 formation enhanced by SOD. Catalase was not effective even at a higher concentration (21,000 U/ml). At a higher concentration (0.7 mM), DFO decreased the rate of DMPO-OH formation (data not shown).

To clarify the reaction pathway further, the amount of H_2O_2 produced during the UP-NADPH photodynamic reaction was determined. As shown in Table 1, about 50 μM of H_2O_2 was produced in the presence of 2.5 μM

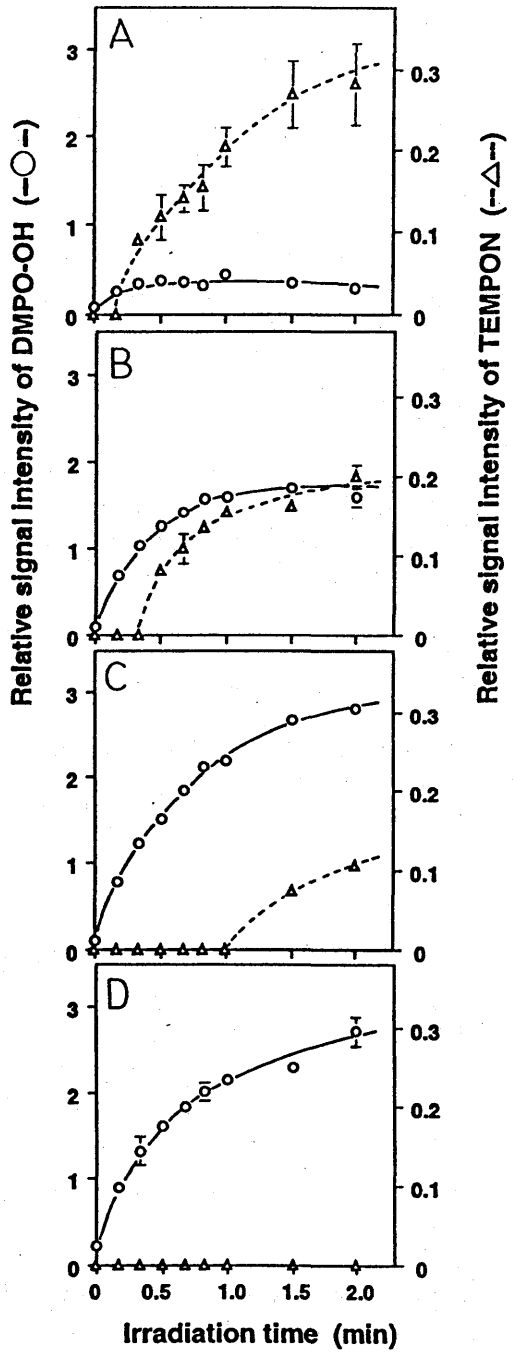

Fig. 3. Effects of NADPH on the formations of DMPO-OH and TEMPON during photosensitization of UP. Irradiated with visible light in the presence of either 48 mM DMPO or 50 mM TEMPD were 14 μM UP and various concentrations of NADPH in 20 mM phosphate buffer, pH 7.4. Concentrations of NADPH were (A) 0 μM, (B) 7 μM, (C) 33 μM, and (D) 167 μM. The second low-field peak for DMPO-OH and the first low-field peak for TEMPON were used to obtain relative signal intensities. Data are presented as mean values of duplicate experiments. Error bars indicate deviations.

UP and 2 m*M* NADPH. SOD exhibited no effect on the production of H_2O_2, while catalase or NaN_3 completely inhibited it. DFO increased the rate of formation of H_2O_2 little. To confirm the involvement of H_2O_2 in the production of ·OH, UP, and UP-NADPH systems were irradiated in the presence of 0.63 m*M* H_2O_2. As shown in Fig. 4, the formation of DMPO-OH was not upregulated, even in the presence of H_2O_2. This result strongly indicates that conversion of H_2O_2 to ·OH hardly occurs, even if H_2O_2 is produced during irradiation, and suggests that the enhancing effect of SOD and reducing effect of DFO on DMPO-OH formation is a side-effect of these reagents; at high concentration, SOD is known to induce Cu-catalyzed ·OH production (Yim *et al.* 1990), and DFO is known to scavenge ·OH (Halliwell, 1989).

DISCUSSION

The present study clearly demonstrated that $^1O_2$ is an intermediate in the production of ·OH during the photodynamic reaction of UP in the presence of NADPH. $^1O_2$-dependent production of ·OH has been reported in various photodynamic reaction systems. The following three pathways were proposed:

$$^1O_2 \xrightarrow{e^-} O_2^{\cdot -} \xrightarrow{e} H_2O_2 \xrightarrow{Metals} {\cdot OH} \xrightarrow{DMPO} \text{DMPO-OH} \quad (1)$$

$$^1O_2 \rightarrow [\text{DMPO-}^1O_2] \xrightarrow{H^+} \text{DMPO-OH} + {\cdot OH} \xrightarrow{DMPO} \text{DMPO-OH} \quad (2)$$

$$^1O_2 \xrightarrow{-SH} -SOOH \rightarrow -SO\cdot + {\cdot OH} \xrightarrow{DMPO} \text{DMPO-OH} \quad (3)$$

$^1O_2$-mediated $O_2^{\cdot -}$ and H_2O_2 production have been reported in the presence of NADPH (Bodaness and Chan, 1977; Peters and Rodgers, 1981). If transition metal ion is present, ·OH can be formed from H_2O_2 (pathway 1). In the present study, addition of H_2O_2 to the reaction mixture did not increase the intensity of DMPO-OH signal either in the presence or absence of NADPH, although $^1O_2$-mediated production of H_2O_2 was observed during the UP-NADPH photodynamic reaction. Neither catalase nor DFO affected NADPH-enhanced DMPO-OH production. These observations show that ·OH is derived from a pathway other than pathway 1. Pathway 2 has been proposed in photosensitizing reaction of bacteriochlorin a (Hoebeke *et al.*, 1997), merocyanine 540 (Feix and Kalyanaraman, 1991), and C-phycocyanin (Zhang *et al.*, 1999). Formation of DMPO-OH through this pathway is involved in the decomposition of a product of the reaction of DMPO with $^1O_2$. However, this possibility can be ruled out in the present case for the following reasons: (1) more than 70% of the DMPO-OH signal was lost in the presence of ·OH scavengers, although one-half of DMPO-OH results from decay of the reaction product [DMPO-$^1O_2$], and the rest from free ·OH in pathway 2; and (2) if the reaction of $^1O_2$ with DMPO gives DMPO-OH signal, an equivalent signal of DMPO-OH should be observed regardless of the presence of NADPH, assuming that NADPH does not affect the generation of $^1O_2$. Buettner (1985) observed $^1O_2$-dependent formation of DMPO-OH in a photodynamic reaction of hematoporphyrin derivative in the presence of cysteine and proposed that ·OH is

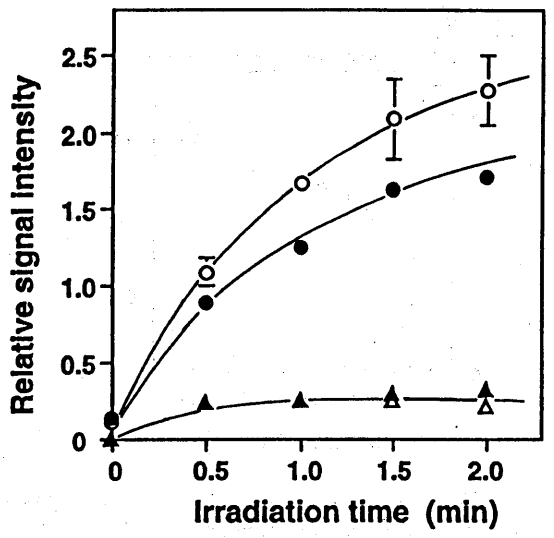

Fig. 4. Effect of H_2O_2 addition on the formation of DMPO-OH during photosensitization of UP. Samples of 14 μM UP, 167 μM NADPH, and 48 m*M* DMPO in 20 m*M* phosphate buffer, pH 7.4, were irradiated with visible light in the presence (●) or absence of 0.63 m*M* H_2O_2 (○). Samples of 14 μM UP and 48 m*M* DMPO in 20 m*M* phosphate buffer, pH 7.4, were irradiated with visible light in the presence (▲) or absence (△) of 0.63 m*M* H_2O_2. The ratio of signal intensity of the second low-field peak to that of the manganese peak (internal standard) was plotted. Data are presented as mean values of duplicate experiments. Error bars indicate deviations.

produced by homolytical cleavage of -SOOH, a product of the reaction of thiol with $^1O_2$. We could not determine whether or not a similar reaction occurs in the present system, but results obtained here indicate the existence of unknown pathways.

In conclusion, we obviously demonstrated $^1O_2$-derived ·OH formation in a UP-NADPH photodynamic reaction system and suggested the occurrence of other pathways for conversion of $^1O_2$ to ·OH than metal-catalyzed reactions of $O_2^{\cdot -}$ and H_2O_2 derived from $^1O_2$, although details of the pathway are still unknown. NADPH and NADH are continuously produced in the cells. This suggests that ·OH generated from $^1O_2$ contributes at least in part to the mechanism of porphyria phototoxicity and photodynamic therapeutic effect.

ACKNOWLEDGMENTS

This study was supported by a Grant-in-Aid for Scientific Research (No. 10357021) from the Ministry of Education, Science, Sports and Culture of Japan, and by the Cosmetology Research Foundation. We thank JISTEC for scholarship of C. A. O.-A.; Professor Y. Matsushima, Kyoritsu College of Pharmacy, and Dr. J. Ueda, NIRS, for helpful discussions; and the Division of Environmental Chemistry, National Institute of Health Sciences for use of a radiometer.

ABBREVIATIONS

DABCO, Diazabicyclo[2.2.2]octane; DMPO, 5,5-dimethyl-1-pyrroline-*N*-oxide; DFO, desferrioxamine mesylate; D_2O, deuterium oxide; DMSO, dimethyl sulfoxide; ESR, electron spin resonance; H_2O_2, hydrogen peroxide; $^1O_2$, singlet oxygen; ·OH, hydroxyl radical; $O_2^{\cdot -}$, superoxide anion radical; ROS, reactive oxygen species; SOD, superoxide dismutase; TEMPD, 2,2,6,6-tetramethyl-4-piperidone hydrochloride; TEMPON, 2,2,6,6-tetramethyl-4-piperidone-*N*-oxyl; UP, uroporphyrin.

REFERENCES

BODANESS, R.S., and CHAN, P.C. (1977). Singlet oxygen as a mediator in the hematoporphyrin-catalyzed photooxidation of NADPH to $NADP^+$ in deuterium oxide. J. Biol. Chem. **10,** 8554–8560.

BRUN, A., and SANDBERG, S. (1991). Mechanisms of photosensitivity in porphyric patients with special emphasis on erythropoietic protoporphyria. J. Photochem. Photobiol. B:Biol. **10,** 285–302.

BUETTNER, G.R. (1985). Thiyl free radical production with hematoporphyrin derivative, cysteine and light: a spin-trapping study. FEBS Lett. **177,** 295–299.

BUETTNER, G.R. (1987). Spin trapping: ESR parameters of spin adducts. Free Radic. Biol. Med. **3,** 259–303.

CALZAVARA-PINTON, P.G., SZEIMIES, R.-M., ORTEL, B., and ZANE, C. (1996). Photodynamic therapy with systemic administration of photosensitizers in dermatology. J. Photochem. Photobiol. B:Biol. **36,** 225–231.

FEIX, J.B., and KALYANARAMAN, B. (1991). Production of singlet oxygen-derived hydroxyl radical adducts during merocyanine-540–mediated photosensitization: Analysis by ESR-spin trapping and HPLC with electrochemical detection. Arch. Biochem. Biophys. **291,** 43–51.

FREW, J.E., JONES, P., and SCHOLES, G. (1983). Spectrophotometric determination of hydrogen peroxide and organic hydroperoxides at low concentration in aqueous solution. Anal. Chim. Acta **155,** 139–150.

HALLIWELL, B. (1989). Protection against tissue damage in vivo by desferrioxamine; what is its mechanism of action? Free Rad. Bio. Med. **7,** 645–651.

HALLIWELL, B., and GUTTERIDGE, J.M.C. (1999). *Free Radicals in Biology and Medicine, Third Edition.* (Oxford University Press, New York).

HOEBEKE, M., SCHUITMAKER, H.J., JANNINK, L.E., DUBBELMAN, T.M.A. R., JAKOBS, A., and VAN DE VORST, A. (1997). Electron spin resonance evidence of the generation of superoxide anione, hydroxyl radical and singlet oxygen during the photohemolysis of human erythrocytes with bacteriochlorin a. Photochem. Photobiol. **66,** 502–508.

INOUE, K., MATSUURA, T., and SAITO, I. (1984). A convenient method for detecting the superoxide ion from singlet oxygen reactions of biological systems: Superoxide formation from hydrogenated nicotinamide adenine dinucleotide and 5-hydroxytryptophan. J. Photochem. **25,** 511–518.

LION, Y., DELMELLE, M., and VAN DE VORST, A. (1976). A new method of detecting singlet oxygen production. Nature **263,** 442–443.

MENON, I.A., BECKER, M.A., PERSAD, S.D., and HABERMAN, H.F. (1989). Quantitation of hydrogen peroxide formed during UV-visible irradiation of protoporphyrin, coproporphyrin and uroporphyrin. Clin. Chim. Acta **186,** 375–381.

MOAN, L.E., and WOLD, E. (1979). Detection of singlet oxygen production by ESR. Nature **279,** 450–451.

OZAWA, T., and HANAKI, A. (1991). The first ESR spin-trapping evidence for the formation of hydroxyl radical from the reaction of copper(II) complex with hydrogen peroxide in aqueous solution. J. Chem. Soc. Chem. Commun. 330–332.

PETERS, G., and RODGERS, M.A.J. (1981). Single-electron

transfer from NADH analogues to singlet oxygen. Biochim. Biophys. Acta **637,** 43–52.

RYTER, S.W., and TYRRELL, R.M. (1998). Singlet molecular oxygen ($^1O_2$): A possible effector of eukaryotic gene expression. Free Radic. Biol. Med. **24,** 1520–1534.

YIM, M.B., CHOCK, P.B., and STADTMAN, E.R. (1990). Copper, zinc superoxide dismutase catalyzes hydroxyl radical production from hydrogen peroxide. Proc. Natl. Acad. Sci. USA **87,** 5006–5010.

ZHANG, S., XIE, J., ZHANG, J., ZHAO, J., and JIANG, L. (1999). Electron spin resonance studies on photosensitized formation of hydroxyl radical by C-phycocyanin from *Spirulina platensis*. Biochim. Biophys. Acta **1426,** 205–211.

Address reprint requests to:
Dr. Toshihiko Ozawa
Bioregulation Research Group
National Institute of Radiological Sciences
Chiba 263–8555, Japan

E-mail: ozawa@nirs.go.jp

Received for publication September 13, 1999; accepted December 10, 1999.

Free Radical Biology & Medicine, Vol. 28, No. 4, pp. 854–859, 2000

0891-5849/00/$–see front matter

ELSEVIER

PII S0891-5849(00)00162-3

Forum: Oxidative Stress Status

NONINVASIVE STUDY OF RADIATION-INDUCED OXIDATIVE DAMAGE USING IN VIVO ELECTRON SPIN RESONANCE

YURI MIURA* and TOSHIHIKO OZAWA†

*Department of Biochemistry and Isotopes, Tokyo Metropolitan Institute of Gerontology, Tokyo, Japan and †Department of Bioregulation Research, National Institute of Radiological Sciences, Chiba, Japan

(*Received* 30 *September* 1999; *Revised* 29 *December* 1999; *Accepted* 10 *January* 2000)

Abstract—Nitroxyl radicals injected into a whole body indicate the disappearance of signal intensity of in vivo electron spin resonance (ESR). The signal decay rates of nitroxyl have reported to be influenced by various types of oxidative stress. We examined the effect of X-irradiation on the signal decay rate of nitroxyl in the upper abdomen of mice using in vivo ESR. The signal decay rates increased 1 h after 15 Gy irradiation, and the enhancement was suppressed by preadministration of cysteamine, a radioprotector. These results suggest that the signal decay of nitroxyl in whole mice is enhanced by radiation-induced oxidative damage. The in vivo ESR system probing the signal decay of nitroxyl could provide a noninvasive technique for the study of oxidative stress caused by radiation in a living body. © 2000 Elsevier Science Inc.

Keywords—In vivo ESR, Oxidative stress, Nitroxyl radical, ROS, Spin probe, Signal decay, Redox, Free radicals

INTRODUCTION

As it has become apparent that oxygen free radicals are involved in numerous pathophysiological conditions, there is a growing interest in the in vivo detection of free radicals by electron spin resonance (ESR). ESR was developed as an in vivo detector of bioradicals in the late 1980s. Because bioradicals such as nitric oxide, superoxide radical, and hydroxyl radical are present in extremely low concentrations in tissue and organs and because their lifetimes are extremely short, indirect detection employing spin trapping agents or spin probes is more useful.

The most widely used spin probe is a nitroxyl radical, which is relatively stable at room temperature and has low toxicity to organisms (Fig. 1). Nitroxyl radical is not stable in biological systems, however. In hepatic microsomes and various cultured cells, the reduction and reoxidation of nitroxyl compounds have been reported since the 1970s, suggesting that various biomolecules and enzymes such as cytochrome P-450, cytochrome P-450 reductase, mitochondrial electron transport systems, and ascorbic acid, are involved in the redox reaction of nitroxyl. Furthermore, it has become apparent that oxygen concentration, antioxidant content, and oxygen free radicals influence the rate of the redox reaction of nitroxyl in biological systems. Therefore, in in vitro or cell-level experiments, a nitroxyl compound may be used as a sensitive redox indicator by monitoring its redox reaction. In whole-body experiments, there have been several recent reports noting the redox change in organisms in pathophysiological conditions such as oxidative stress and examining the effects on the redox reaction of nitroxyl in vivo. Here, we review the recent in vivo ESR studies on the redox reaction of nitroxyl and discuss the

Yuri Miura graduated with a degree in pharmaceutical sciences from the University of Tokyo. She was a Research Assistant at the School of Pharmaceutical Sciences, Showa University, and received her Ph.D. degree from the University of Tokyo in 1994. She completed a postdoctoral fellowship with Dr. Toshihiko Ozawa at the National Institute of Radiological Sciences. She is currently a Research Scientist at Tokyo Metropolitan Institute of Gerontology. Her research interests include radiation biology of neuronal and glial cells. Toshihiko Ozawa graduated with a degree in pharmaceutical sciences from the University of Tokyo. In 1974, he received his Ph.D. degree from the same university and performed his postdoctoral work with Dr. James P. Collman at Stanford University before becoming a Senior Researcher at the National Institute of Radiological Sciences. He was then a Section Head, and in 1993, he assumed the position of Director of the Department of Bioregulation Research. He is also a Visiting Professor at the Graduate School of Natural Sciences at Chiba University. His research interests include in vivo detection and electron spin resonance imaging of active oxygens and free radicals.

Address correspondence to: Toshihiko Ozawa, Department of Bioregulation Research, National Institute of Radiological Sciences, Chiba 263-8555, Japan; Tel: +81 (43) 206 3120; Fax: +81 (43) 255 6819; E-Mail: ozawa@nirs.go.jp

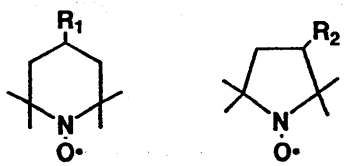

piperidine nitroxyl pyrrolidine nitroxyl

	Functional Group	Acronym
R_1	$-OH$	hydroxy-TEMPO
	$-N^+(CH_3)_4\Gamma$	Catl
	$-NH_2$	amino-TEMPO
R_2	$-CONH_2$	carbamoyl-PROXYL
	$-COOH$	carboxy-PROXYL
	$-COOCH_3$	MCPROXYL

Fig. 1. Chemical structures of nitroxyl compounds.

possibility of applying in vivo ESR to the in vivo non-invasive study of oxidative damage.

PHARMACOKINETICS OF NITROXYL RADICALS INJECTED TO WHOLE BODY

In in vivo ESR measurement, the signal intensity of a nitroxyl radical decreases with time after injection. The pharmacokinetics of a nitroxyl compound (carbamoyl-PROXYL) using L-band (approximately 1 GHz microwave) ESR was first reported by Berliner and Wan [1]. They detected the nitroxyl signal of carbamoyl-PROXYL and measured the signal disappearance in rat tails. Since then, a several groups have reported spectra and the signal decay of nitroxyl radical in the abdomen or head of living animals by L-band ESR [2–7].

The signal decay of nitroxyl in the whole body is ascribed to two factors: one is the metabolism of nitroxyl to a diamagnetic molecule and the other is the diffusion and excretion from the measured region to other organs.

In vitro, there are many reports of the reduction of nitroxyl radicals to the corresponding hydroxylamine in microsomes, mitochondria, and whole cells. In vivo, nitroxyl compounds also seem to be reduced to hydroxylamine, based on the fact that the signal intensity of the collected blood was recovered by the addition of potassium ferricyanide, which oxidized hydroxylamine to nitroxyl radical [8]. Takeshita et al. [9] extracted the metabolite of hydroxy-TEMPO from mouse lung and identified it as its hydroxylamine by means of thin-layer chromatography. The reduction rates of nitroxyl depend on the chemical structure of nitroxyl compounds. Komarov and Lai [10] have measured the in vivo reduction kinetics of about 20 different nitroxyl compounds by S-band (3.5 GHz microwave) ESR. They examined the effect of the chemical structures of nitroxyl compounds on the half-life of in vivo reduction, showing that pyrrolidine nitroxyl was more resistant to cellular metabolism in vivo than piperidine nitroxyl. In vivo, the reducing enzymes and ascorbate should be involved in the reduction of a nitroxyl radical similar to what occurs in vitro. Vianello et al. [11] calculated the ascorbate contribution to various nitroxyl removals on the basis of the ascorbate concentration in organs and the second-order kinetic constants of nitroxyl reduction measured in phosphate-buffered saline. They speculated that the disappearance of piperidine nitroxyl in the brain was controlled mainly by ascorbate, although that of pyrrolidine nitroxyl was not.

On the other hand, Bacic et al. [3] have reported the detection of an increase in nitroxyl signal in the bladder of a mouse injected with Catl using L-band ESR. Takechi et al. [12] examined the urine of rats that were administered 3-carboxy-PROXYL, and their results suggested that parent nitroxyl and its hydroxylamine were excreted into the urine 2 to 10 h after administration. These data suggest that water-soluble nitroxyl compounds were excreted into the urine.

EFFECTS OF VARIOUS TYPES OF OXIDATIVE STRESS ON SIGNAL DECAY RATES OF NITROXYL RADICALS

Because various types of oxidative stress are known to change the redox state and metabolic capacity of organisms, it is expected that they would affect the pharmacokinetics of nitroxyl radical in vivo. Thus, the effects of oxidative stress or the administration of various drugs were studied by examining the signal decay rates of various nitroxyls [8,13–21] (Table 1). The results are divided into two categories depending on whether the treatment caused an increase or decrease in the signal decay rate of nitroxyl radicals. In cases in which signal decay was inhibited, the results were attributed to a decrease in the reducing capacity of the organism [8,20, 21]. In contrast, treatment with idebenone or chronic administration of vitamin C was concluded to enhance the radical reducing ability in the living body, resulting in an increase in the decay rates of nitroxyl [18,19]. In cases of oxidative stress such as ischemia-reperfusion, hyperoxia, diabetes, iron overload, and CCl_4 administration [13–17], it was speculated that a free radical reaction occurring during the oxidative damage may have been involved in the enhancement. This was because the enhancement was suppressed by in vivo antioxidants and because in vitro nitroxyl radical reacts with various ROS such as superoxide, hydroxyl radicals, and peroxyl rad-

Table 1. Effects of Various Treatments in Animals on the Rates of Signal Decay of Nitroxyl Radicals

Effect	Treatment	Measured region	Spin probe	Experimental condition	Reference
Increase	Ischemia-reperfusion	Femoral	Amino-TEMPO	Occlusion	[13]
Increase	Hyperoxia	Abdomen	Carbamoyl-PROXYL	Exposed to 80% O_2 and 20% N_2	[14]
Increase	Diabetes	Abdomen	Carbamoyl-PROXYL	Streptozotocin-induced	[15]
Increase	Iron overload	Abdomen	Carbamoyl-PROXYL	Subcutaneously loaded with ferric-citrate	[16]
Increase	CCl_4	Abdomen	Carbamoyl-PROXYL	Oral administration	[17]
Increase	Idebenone	Head	Carbamoyl-PROXYL	Intracerebroventricular injection	[18]
Increase	Vitamin C	Head	Hydroxy-TEMPO	Vitamin C–containing food	[19]
Decrease	Aging	Head	Carbamoyl-PROXYL	6, 30, and 39 month old mice	[8]
Decrease	Seizure	Head	Carbamoyl-PROXYL	Kainic acid–induced	[20]
Decrease	CCl_4	Hepatic and pelvic domain	Hydroxy-TEMPO	Intraperitoneal administration	[21]

icals, leading to the signal disappearance. The results of CCl_4 administration were different between the report of Inaba et al. [21] and that of Utsumi et al. [17]. Inaba et al. [21] injected CCl_4 intraperitoneally and measured in vivo ESR 48 h after injection, and Utsumi et al. [17] used oral administration and measured in vivo ESR 30 min after injection. CCl_4 injected into an organism is metabolized by cytochrome P-450 in liver microsomes, which accompanies the generation of ROS, causing hepatic damage and a decrease in metabolic capacity. It seems that there is a change in the degree of the damage between 30 min and 48 h after administration. Therefore, these results suggest that different stages of oxidative stress should yield different effects on the signal decay rate of nitroxyl radical.

EFFECTS OF RADIATION ON SIGNAL DECAY RATES OF CARBAMOYL-PROXYL IN THE ABDOMENS OF MICE

Radiation produces various ROS such as hydroxyl radicals, superoxide, and hydrogen peroxide in the whole body not only directly but also indirectly through a subsequent free radical reaction and inflammation, resulting in a change in the redox status of the organism. We have examined the effects of radiation on the decay rate of a nitroxyl radical (carbamoyl-PROXYL) using L-band ESR [22].

In experiments in noncysteamine-treated mice, the mice were separated into six groups. Groups 1 and 2 were treated by sham irradiation as a control. Groups 3 and 4 were treated by X-irradiation at a dose of 7.5 Gy, which is approximately the $LD_{50/30}$ of mice, and groups 5 and 6 were treated by 15 Gy irradiation. In vivo ESR measurement was performed 1 h after irradiation in groups 1, 3, and 5, and 4 or 5 d after irradiation in groups 2, 4, and 6. In cysteamine-treated mice, cysteamine was injected into the mice intraperitoneally 20 min before irradiation (2.0 mM/kg). Whole-body irradiation was performed at a dose rate of approximately 0.6 Gy/min. Sham irradiation of the controls included comparable immobilization in the same irradiation chamber. Anesthetic was not administered to either irradiated or sham-irradiated mice. The in vivo ESR spectra of the nitroxyl radical were measured as follows. A mouse was anesthetized using pentobarbital and placed in a loop-gap resonator. The solution of carbamoyl-PROXYL was injected into the tail vein, and ESR spectra were measured in the upper abdomen of the mouse repeatedly beginning immediately after injection. The rate constants of the signal decay of nitroxyl were calculated from the signal decay curves, which were determined from semilogarithmic plots of the peak heights of the ESR signal at the lower magnetic field.

Table 2 summarizes the kinetic constants of signal decay in the abdomens of the mice. One hour after

Table 2. Radiation Effects on the Signal Decay Rates (Gy/min) of Carbamoyl-PROXYL in the Abdomens of Mice

	1 h After irradiation		4 or 5 d After *irradiation	
	Without cysteamine	With cysteamine	Without cysteamine	With cysteamine
0 Gy	0.109 ± 0.015	0.102 ± 0.010	0.125 ± 0.031	—
7.5 Gy	0.130 ± 0.029	—	0.165 ± 0.029	0.138 ± 0.004
15.0 Gy	0.145 ± 0.021*	0.100 ± 0.005	0.075 ± 0.008†	—

* $p < .001$, different from that 1 h after 0 Gy (without cysteamine).
† $p < .05$, different from that 4 or 5 d after 0 Gy (without cysteamine).

irradiation, the signal decay rates increased by 15 Gy irradiation; 5 d after irradiation, these rates significantly decreased by 15 Gy irradiation. These data suggest that there are at least two factors that affect the signal decay rate of nitroxyl: one causing enhancement and another causing inhibition. Five days after irradiation, the mice exposed to 15 Gy irradiation were severely damaged; about half of the mice died within 5 d. The factor causing inhibition was believed to be the degeneration of the systemic condition, including metabolic and excretive capacities, as the result of high-dose irradiation.

To study the factor causing enhancement, we examined the effect of cysteamine, which is a radical scavenger and radioprotector, on the enhancement of the signal decay rate in nitroxyl (Table 1). It seemed that preadministration of cysteamine significantly suppressed the enhancement of the signal decay rate of nitroxyl as a result of X-irradiation. Other radioprotectors such as 5-HT, WR2721, hydroxy-TEMPO, IL-1β, and SCF also suppressed the enhancement of the signal decay rate of nitroxyl at the appropriate doses.

BIOLOGICAL MECHANISM OF THE ENHANCEMENT OF NITROXYL DECAY IN THE WHOLE BODY

What is the factor causing enhancement in this case? There are two possibilities: the induction of reducing capacity by oxidative stress and the participation of free radical reaction as a result of X-irradiation. We examined the activity of reducing enzymes (cytochrome P-450 and cytochrome P-450 reductase) and antioxidative enzymes (superoxide dismutase, catalase, and glutathione peroxidase) as well as the contents of endogenous antioxidants (vitamins E and C) under the present conditions. The results indicated that neither the activities of the reducing and antioxidative enzymes nor the contents of endogenous antioxidants increased 1 h after irradiation, suggesting that the reducing capacities in the mice were not induced 1 h after irradiation. Accordingly, free radical reactions in tissue caused by X-irradiation might be involved in the enhancement of the signal decay rate of nitroxyl. Although the lifetimes of primarily formed ROS are quite short as a result of X-irradiation, they should subsequently cause biological and chemical chain reactions, which, in turn, would produce fresh ROS. The fact that the radical scavenger cysteamine suppressed the enhancement seems to support the hypothesis that free radical reaction induced by X-irradiation participates in the enhancement of nitroxyl decay similar to what occurs in other types of oxidative stress [13–17]. Because in vivo ESR study is a whole-body experiment, however, physiological factors that affect the rate of tissue distribution or excretion of nitroxyl (e.g., blood pressure, blood flow rate, body temperature) cannot be ruled out.

EFFECT OF RADIATION ON SIGNAL DECAY RATES OF MCPROXYL IN THE HEADS OF MICE

The spin probe injected into peripheral blood cannot be distributed to brain tissue because of the blood brain-barrier (BBB). Thus, we synthesized BBB-permeable spin probe, and radiation damage to the brain was examined using in vivo ESR [23].

MCPROXYL was more lipophilic than carbamoyl-PROXYL and well distributed in brain tissue after intravenous injection. The signal decay rate of nitroxyl radical in the head region decreased 1 h after irradiation unlike that of carbamoyl-PROXYL in the upper abdomen. We examined the effect of radiation on the reducing activity of nitroxyl in the brain homogenate and the content of ascorbic acid in the brain, and the results showed that the reducing capacity was not decreased 1 h after irradiation. Although the biological mechanism of the radiation effect on MCPROXYL disappearance remains unclear, it is possible that the BBB-permeable spin probe might provide some information on radiation damage in the brain.

TOPICS

The analysis of in vivo ESR data is quite difficult because of the many factors affecting the signal decay rate of nitroxyl radicals in the whole body. Nevertheless, we can say for certain that the signal decay rate of nitroxyl radicals in vivo reflects the pathophysiological and/or physiological state of a living body. Therefore, we believe that in vivo ESR can be used for clinical applications so as to probe the change of the signal decay rate in nitroxyl.

Recently, there have been many in vivo ESR studies aiming to improve in vivo imaging. Nicholson et al. [24] have reported the in vivo imaging of nitroxyl clearance using a LODESR imaging apparatus to demonstrate that carboxy-PROXYL injected into rats shifted from the liver to the kidneys with time after injection. Yokoyama et al. [25] have reported ESR imaging for the signal decay of nitroxyl in the brains of rats. They used MCPROXYL, a BBB-permeable spin probe, and analyzed the effect of kainic acid–induced seizures on the signal decay rates in the hippocampus and cerebral cortex, showing that the half-life of nitroxyl radicals was significantly prolonged in the hippocampus but not in the cerebral cortex by kainic acid–induced seizure. In vivo imaging of the signal decay rate of nitroxyl should provide more information on the pathophysiology of the living body.

Conversely, it is also necessary to develop the spin probe, whose spectrum yields pathophysiological or physiological information on organisms. Here, we sum-

marize the recent reports on such spin probes. Gallez et al. [26] have developed a pH-sensitive nitroxyl compound, which is manifested in the ESR spectrum as a decrease in hyperfine coupling constant with pH-induced change, and Sotgiu et al. [27] have performed pH-sensitive imaging using this nitroxyl. Dragutan et al. [28] also synthesized pH-sensitive spin probes. Using these spin probes, in vivo ESR can provide a noninvasive technique for monitoring pH in tissue or organs. Furthermore, Yamaguchi et al. [29] synthesized spin-labeled triglyceride (SL-TG) and analyzed in vivo ESR spectra of lipid emulsion containing SL-TG in the chests of mice. Immediately after administration, ESR signal derived from lipid particles was observed; after that, ESR signal derived from free and immobilized fatty acids to which lipoprotein lipase in the blood hydrolyzed lipid particles was superimposed on the spectra. These investigators demonstrated that in vivo ESR can determine the pharmacokinetics of lipid emulsion in a noninvasive fashion, suggesting that oxidative damage of lipoproteins or blood cells in the living body may be analyzed by this method.

CONCLUSIONS

Nitroxyl radicals injected into an organism indicate the disappearance of signal intensity of in vivo ESR. It is shown that the signal decay rates of nitroxyl depend on various types of oxidative stress, including X-irradiation. Thus, in vivo ESR could provide a noninvasive technique for the study of oxidative stress in a living body.

Acknowledgements — This study was supported in part by a Grant-in-Aid for Scientific Research (No. 10357021) from the Ministry of Education, Science, Sports, and Culture of Japan, and by a Grant from the Cosmetology Research Foundation.

REFERENCES

[1] Berliner, L. J.; Wan, X. In vivo pharmacokinetics by electron magnetic resonance spectroscopy. *Magn. Reson. Med.* **9**:430–434; 1989.

[2] Ishida, S.; Kumashiro, H.; Tsuchihashi, N.; Ogata, T.; Ono, M.; Kamada, H.; Yoshida, E. In vivo analysis of nitroxide radicals injected into small animals by L-band ESR technique. *Phys. Med. Biol.* **34**:1317–1323; 1989.

[3] Bacic, G.; Nilges, M. J.; Magin, R. L.; Walczak, T.; Swartz, H. M. In vivo localized ESR spectroscopy reflecting metabolism. *Magn. Reson. Med.* **10**:266–272; 1989.

[4] Ferrari, M.; Colacicchi, S.; Gualtieri, G.; Santini, M. T.; Sotgiu, A. Whole mouse nitroxide free radical pharmacokinetics by low frequency electron paramagnetic resonance. *Biochem. Biophys. Res. Commun.* **166**:168–173; 1990.

[5] Utsumi, H.; Muto, E.; Masuda, S.; Hamada, A. In vivo ESR measurement of free radicals in whole mice. *Biochem. Biophys. Res. Commun.* **172**:1342–1348; 1990.

[6] Takeshita, K.; Utsumi, H.; Hamada, A. ESR measurement of radical clearance in lung of whole mouse. *Biochem. Biophys. Res. Commun.* **177**:874–880; 1991.

[7] Miura, Y.; Utsumi, H.; Hamada, A. Effects of inspired oxygen concentration on in vivo redox reaction of nitroxide radicals in whole mice. *Biochem. Biophys. Res. Commun.* **182**:1108–1114; 1992.

[8] Gomi, F.; Utsumi, H.; Hamada, A.; Matsuo, M. Aging retards spin clearance from mouse brain and food restriction prevents its age-dependent retardation. *Life Sci.* **52**:2027–2033; 1993.

[9] Takeshita, K.; Utsumi, H.; Hamada, A. Whole mouse measurement of paramagnetism—loss of nitroxide free radical in lung with a L-band ESR spectrometer. *Biochem. Mol. Biol. Int.* **29**: 17–24; 1993.

[10] Komarov, A. M.; Lai, C. S. In vivo pharmacokinetics of nitroxides in mice. *Biochem. Biophys. Res. Commun.* **201**:1035–1042; 1994.

[11] Vianello, F.; Momo, F.; Scarpa, M.; Rigo, A. Kinetics of nitroxide spin label removal in biological systems: an in vitro and in vivo ESR study. *Magn. Reson. Imaging* **13**:219–226; 1995.

[12] Takechi, K.; Tamura, H.; Yamaoka, K.; Sakurai, H. Pharmacokinetic analysis of free radicals by in vivo BCM (blood circulation monitoring)-ESR method. *Free Radic. Res.* **26**:483–496; 1997.

[13] Masuda, S.; Utsumi, H.; Hamada, A. In vivo ESR studies on radical reduction in femoral ischemia-reperfusion of whole mice. In: Yagi, K.; Kondo, M.; Niki, E.; Yoshikawa, T., eds. *Oxygen radicals.* Amsterdam: Elsevier, 1992:175–178.

[14] Miura, Y.; Hamada, A.; Utsumi, H. In vivo ESR studies of antioxidant activity on free radical reaction in living mice under oxidative stress. *Free Radic. Res.* **22**:209–214; 1995.

[15] Sano, T.; Umeda, F.; Hashimoto, T.; Nawata, H.; Utsumi, H. Oxidative stress measurement by in vivo electron spin resonance spectroscopy in rats with streptozotocin-induced diabetes. *Diabetologia* **41**:1355–1360; 1998.

[16] Phumala, N.; Ide, T.; Utsumi, H. Noninvasive evaluation of in vivo free radical reactions catalyzed by iron using in vivo ESR spectroscopy. *Free Radic. Biol. Med.* **26**:1209–1217; 1999.

[17] Utsumi, H.; Ichikawa, K.; Takeshita, K. In vivo ESR measurements of free radical reactions in living mice. *Toxicol. Lett.* **82/83**:561–565; 1995.

[18] Yokoyama, H.; Tsuchihashi, N.; Ogata, T.; Hiramatsu, M.; Mori, N. An analysis of the intracerebral ability to eliminate a nitroxide radical in the rat after administration of idebenone by an in vivo rapid scan electron spin resonance spectrometer. *MAGMA* **4**:247–250; 1996.

[19] Matsumoto, S.; Mori, N.; Tsuchihashi, N.; Ogata, T.; Lin, Y.; Yokoyama, H.; Ishida, S. Enhancement of nitroxide-reducing activity in rats after chronic administration of vitamin E, vitamin C, and idebenone examined by an in vivo electron spin resonance technique. *Magn. Reson. Med.* **40**:330–333; 1998.

[20] Ueda, Y.; Yokoyama, H.; Ohya-Nishiguchi, H.; Kamada, H. ESR spectroscopy for analysis of hippocampal elimination of a nitroxide radical during kainic acid-induced seizure in rats. *Magn. Reson. Med.* **40**:491–493; 1998.

[21] Inaba, K.; Nakashima, T.; Shima, T.; Mitsuyoshi, H.; Sakamoto, Y.; Okanoue, T.; Kashima, K.; Hashiba, M.; Nishikawa, H.; Watari, H. Hepatic damage influences the decay of nitroxide radicals in mice—an in vivo ESR study. *Free Radic. Res.* **27**:37–43; 1997.

[22] Miura, Y.; Anzai, K.; Urano, S.; Ozawa, T. In vivo electron paramagnetic resonance studies on oxidative stress caused by X-irradiation in whole mice. *Free Radic. Biol. Med.* **23**:533–540; 1997.

[23] Miura, Y.; Anzai, K.; Takahashi, S.; Ozawa, T. A novel lipophilic spin probe for the measurement of radiation damage in mouse brain using in vivo electron spin resonance (ESR). *FEBS Lett.* **419**:99–102; 1997.

[24] Nicholson, I.; Foster, M. A.; Robb, F. J. L.; Hutchison, J. M. S.; Lurie, D. J. In vivo imaging of nitroxide-free-radical clearance in the rat, using radiofrequency longitudinally detected ESR imaging. *J. Magn. Reson. (Series B.)* **113**:256–261; 1996.

[25] Yokoyama, H.; Lin, Y.; Itoh, O.; Ueda, Y.; Nakajima, A.; Ogata, T.; Sato, T.; Ohya-Nishiguchi, H.; Kamada, H. EPR imaging for in vivo analysis of the half-life of a nitroxide radical in the hippocampus and cerebral cortex of rats after epileptic seizures. *Free Radic. Biol. Med.* **27**:442–448; 1999.

[26] Gallez, B.; Mader, K.; Swartz, H. M. Noninvasive measurement

of the pH inside the gut by using pH-sensitive nitroxides. An in vivo EPR study. *Magn. Reson. Med.* **36**:694–697; 1996.
[27] Sotgiu, A.; Mader, K.; Placidi, G.; Colacicchi, S.; Ursini, C. L.; Alecci, M. pH-sensitive imaging by low-frequency EPR: a model study for biological applications. *Phys. Med. Biol.* **43**:1921–1930; 1998.
[28] Dragutan, H.; Caragheorgheopol, A.; Chiralen, F.; Mehlhorn, R. J. New amino-nitroxide spin labels. *Bioorg. Med. Chem.* **4**:1577–1583; 1996.
[29] Yamaguchi, T.; Itai, S.; Hayashi, H.; Soda, S.; Hamada, A.; Utsumi, H. In vivo ESR studies on pharmacokinetics and metabolism of parenteral lipid emulsion in living mice. *Pharm. Res.* **13**:729–733; 1996.

ABBREVIATIONS

ESR—electron spin resonance
ROS—reactive oxygen species
carbamoyl-PROXYL—3-carbamoyl-2,2,5,5-tetramethyl pyrrolidine-1-oxyl
hydroxy-TEMPO—4-hydroxy-2,2,6,6-tetramethyl piperidine-1-oxyl
Cat1—4-trimethylamino-2,2,6,6-tetramethyl piperidine-1-oxyl
carboxy-PROXYL—3-carboxy-2,2,5,5-tetramethyl pyrrolidine-1-oxyl
MCPROXYL—3-methoxymethyl-2,2,5,5-tetramethyl pyrrolidine-1-oxyl
CCl_4—carbon tetrachloride
$LD_{50/30}$—50% lethal dose for 30 d
5-HT—5-hydroxytryptamine
WR2721—S-2-(3-aminopropylamino)ethylphosphorothioic acid
IL-1β—interleukin 1β
SCF—stem cell factors
LODESR—longitudinally detected ESR

FEBS Letters 376 (1995) 146–150 FEBS 16333

Unusual long target duplication by insertion of intracisternal A-particle element in radiation-induced acute myeloid leukemia cells in mouse

Izumi Tanaka, Hiroshi Ishihara*

Bioregulation Research Group, National Institute of Radiological Sciences, Anagawa 4-9-1, Inage-ku, Chiba 263, Japan

Received 5 October 1995; revised version received 23 October 1995

Abstract **Retrotransmission into the IL-3/GM-CSF gene locus by the retrotransposon intracisternal A-particle (IAP) had been observed in distinct tumor cell lines. We analyzed the locus in genomes from 7 different myeloid leukemia cell strains which were originally generated by whole-body X-irradiation of the inbred C3H/He mice at a dose of 3 Gy and maintained by in vivo passage. In one leukemia cell strain out of 7 such cases, RFLP of an allele of the interleukin-3 gene was found. Sequence analysis after cloning from the genomic library showed that a type IΔ2 IAP element was inserted in the region upstream of the IL-3 gene in the head-to-head orientation. This suggests that the locus in myeloid cells is sensitive for integration of IAP elements. Additionally, an unusual long target duplication of 82 bp, 14-fold larger than normal one, was found at the junction of the element. This suggests the possibility of a radiation-induced integration mechanism which is distinct from normal retrotransmission.**

Key words: Retrotransposon; Intracisternal A-particle; Myeloid leukemia; Target duplication; Interleukin-3 gene; Genomic DNA cloning

1. Introduction

The intracisternal A-particle (IAP), believed to be a defective provirus, is the most studied retrotransposon in the mouse (see reviews in [1,2]). Like a retrovirus, the integrated form of IAP in the mouse genome has *gag-pol-env* genes between two direct repeats of a retroviral long terminal repeat (LTR) sequence. The copy number of the IAP element is approximately 1000 per haploid genome, which is probably the result of accumulation by retrovirus-like integration and maintenance by vertical transmission in germline cells. In the case of somatic cells, the most commonly observed novel insertion of the element is limited in several tumor cells which possess unique functions due to corresponding gene rearrangement. It is possible that activation or inactivation of several genes by novel integration of the IAP element contributes to tumorigenicity of the cells [1,2]. However, the large copy number prevents determination and isolation of the IAP-inserted loci which are tumor specific.

Interestingly, integration of the IAP element into the interleukin (IL)-3/granulocyte macrophage colony-stimulating factor (GM-CSF) gene locus with gene activation has been found frequently in distinct tumor cell lines [3–8]. If the IL-3/GM-CSF locus has a tendency to accept IAP elements, several tumor cell with gene rearrangements of IL-3 by retrotransmission should be detected. To confirm this supposition as well as to study the chronic effects of radiation, we used radiation-induced acute myeloid leukemia cells from the C3H/He mouse for analysis. Approximately 20–30% of whole-body X-irradiated C3H/He mice develop acute myeloid leukemia within 2 years with chromosomal aberrations [9,10]. Each leukemia cell strain from different individuals should be an 'independent' leukemia since they became tumorigenic by separate processes. In leukemia cells, not only tumor-specific but also radiation-specific events may be recorded in the genome.

We analyzed this locus and found integration of the IAP element in the IL-3 gene in one leukemia cell strain from a total of 7 independent leukemias. Additionally, an unusual long direct repeat of mouse DNA of 82 bp in length was generated at the insertion site of the IAP element, although the target duplication is no more than 6 bp in length in all the reported sequences suggesting a retroviral-like integration mechanism [3,5,6,8,11–19]. The long target duplication may reflect a specific event which occurs during radiation-induced leukemogenesis.

2. Materials and methods

2.1. Leukemia cells and DNA preparation

Radiation-induced myeloid leukemia cells were originally prepared by Yoshida et al. [9]. In brief, 6-week-old C3H/He mice inbred in our institute received whole-body X-irradiation at a dose of 3 Gy. Leukemia cells were isolated from leukemic individuals and were characterized histochemically [9]. After 5 cycles of in vivo passage for stabilization of histochemical phenotype [9] and chromosome number [10], leukemic cells were stored in liquid nitrogen. The frozen cells were thawed, washed with saline and injected intravenously ($1–10 \times 10^4$ cells per mice) into 6-week-old male C3H/He mice, and after 2–4 weeks, proliferated leukemia cells were isolated from the spleen of the leukemia mice. Total DNAs from the cells were prepared by the standard method [20].

2.2. Probes and the labeling

Probes for IL-3 cDNA corresponded to nucleotides (nt) 104–296 of the previously reported sequence (Genbank K01850). GM-CSF cDNA was a gift from Kirin Beer Inc., and cDNAs for IL-1α and IL-1β were from Yakult Central Institute. CDNAs for IL-3, IL-4, IL-5, IL-6 and IL-7 were supplied by the Japanese Association of Immunology. These cDNAs were labeled with [α-^{32}P]dCTP (NEN; 3000 Ci/mmol) using a random primer labeling kit (BRL).

2.3. Polymerase chain reaction (PCR)

Four primers used in the study are as follows: the J1F primer (5′-GAAGGCTCCTGTGGCTTCTT-3′) corresponding to nt −22 to −3 of the putative start site for transcription of the IL-3 gene at sense direction, the J1R primer (5′-AAGAAGCCACAGGAGCCTTC-3′) having complemental sequence to the J1F primer, the IAPF2 primer (5′-ATATGGGTGGCCTATTTGCT-3′) corresponding to the IAP element at sense orientation and the IAPR1 primer (5′-GGTTTCGGCACCAATTGTTA-3′) corresponding to the IAP element at antisense orientation. Twenty ng of total genomic DNA with these primers and

*Corresponding author. Fax: (81) (43) 256-9616.

The sequences reported in this paper will appear in the DDBJ, EMBL and GenBank nucleotide sequence databases with the following accession numbers D63766 and D63767.

Taq DNA polymerase (Perkin-Elmer) was amplified for 30 cycles (94°C; 1 m; 55°C; 1 m; 72°C; 5 m) using a thermal cycler (Perkin-Elmer model 480).

2.4. Southern blot hybridization

According to the standard method [20], 10 μg of total DNA was digested by an appropriate restriction enzyme, electrophoresed and transferred onto nylon membranes. The blots were prehybridized at 65°C for 1 h in 5 × SSC buffer containing 2 × Denhardt's solution, 10% SDS, 50 mM sodium phosphate, 50 mM Tris-HCl (pH 7.5) and 100 μg/ml sonicated salmon sperm DNA. Hybridization was performed by incubation at 65°C overnight after addition of radioactive probe. The membranes were washed twice with 2 × SSC buffer containing 5 mM sodium phosphate and 1 mM EDTA at 65°C for 30 min, and radioactive bands were visualized by the BAS 2000 system (Fuji Film Co., Japan) after exposure of the Imaging Plate.

2.5. Construction of genomic library, cloning and sequencing

Total DNAs from leukemia cells and from the liver of C3H/He mice were partially digested with *Mbo*I, size-fractionated by sucrose gradient centrifugation, ligated into lambda EMBL3 vector DNA, incorporated into phage particles using Giga pack gold (Stratagene), and introduced into *E. coli* P2–392 cells [20]. After amplification of the library containing 10^7 independent clones, 2×10^6 clones were screened by the plaque hybridization method [20] using IL-3 cDNA as a probe. Ten IL-3-positive clones were selected and purified by 4 cycles of single-plaque isolation. The inserted DNA fragments were subcloned using the plasmid vector pBluescript KS+ (Stratagene), and the nucleotide sequences were then determined using a SequenaseII sequencing kit (Stratagene).

3. Results

3.1. IL-3 gene rearrangement in radiation-induced myeloid leukemia in C3H/He mice

We used 7 independent populations of myeloid leukemia cells which were originally isolated from different leukemic individuals after whole-body irradiation of C3H/He mice. Fig. 1 shows data from Southern blot hybridization of total DNA from the leukemia cells using IL-3 cDNA as a probe. Of 7 leukemia cell populations, one (L-8028) harbored an RFLP of one allele of the IL-3 gene. No such rearrangement was found in genes for GM-CSF in any of the 7 leukemia cell populations. Remarkable expression of IL-3 or GM-CSF mRNA was not observed by Northern blot analysis (data not shown) in all the leukemia cell populations. Additionally, no rearrangements in genes for IL-1α, IL-1β, IL-2, IL-4, IL-5 and IL-6 were found in the genome of the L-8028 cells (data not shown).

3.2. Cloning and sequencing of rearranged region of the IL-3 gene

We constructed a genomic DNA library from L-8028 cells and isolated 2 independent clones possessing a rearranged IL-3 allele and 8 clones corresponding to the normal IL-3 allele from 2×10^6 clones. There was no difference between the normal allele of the leukemic cell and the germline configuration. Sequence and restriction analyses showed that the IAP element was inserted into the 5′-region of the IL-3 gene in head-to-head orientation as shown in Fig. 2. Unlike other reported target sites in the IL-3 gene, the insertion site was close to the promoter region of IL-3. The IAP element is 5.4 kb in length, categorized as type LΔ2, which is a subtype probably derived from the full-length IAP element by deletion. Nucleotide sequence analysis showed the 5′ side of the inverted repeat sequence was not present in the 5′-LTR sequences in this case, although inverted repeats of 3–4 bp have been reported at both ends of the LTR in most IAP elements (Fig. 3). Since this

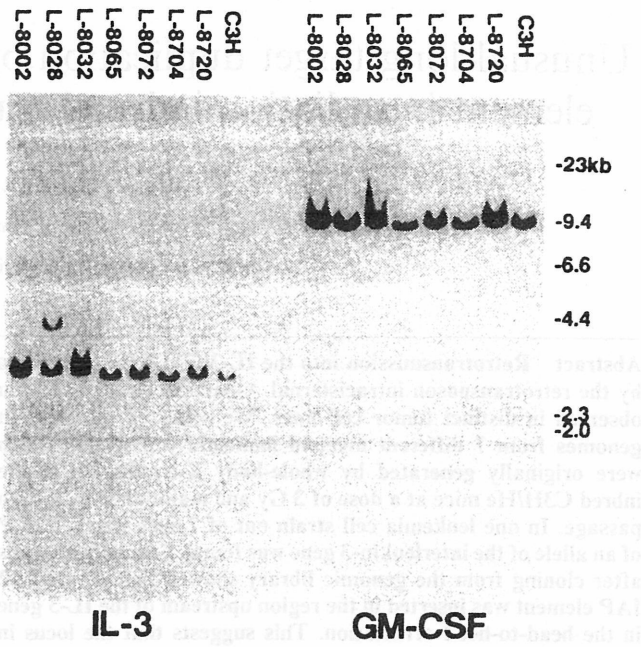

Fig. 1. Southern blot analysis of genomes from radiation-induced myeloid leukemia cells. Ten μg of *Bam*HI-digested DNA from liver of C3H/He and leukemia cells of different-origin (printed at the top of each lanes) were electrophoresed, blotted and hybridized with IL-3 cDNA (left panel) and GM-CSF cDNA (right panel).

incomplete inverted repeat was found only in the 5′-LTR, the defect should have occurred during or after integration. Additionally, complete identity of both LTRs suggest that the insertion event occurred during tumorigenesis in somatic cells. Except the polymorphic structure within the R-region [14], the LTR sequence was similar to other reported data such as the germline-derived LTR from MIA14 [14] at 82% identity, IL3/IAP from WEHI-3B [3] at 90% identity and that from FL5.12 [7] at 99.7% as shown in Fig. 3.

3.3. Unusual long target duplication surrounding IAP element

In the normal IL-3 allele, a single *Apa*I restriction site was present in the promoter region of the IL-3 gene (Fig. 2), as in the nucleotide sequence data from Genbank X02732 and K03233. However, the restriction map of the IL-3 gene locus in the rearranged allele showed the presence of two ApaI restriction sites close to junctions of the IAP element (Fig. 2). Sequence analysis of the junctions revealed that the IAP element lay between two unusual long direct repeats of the IL-3 gene 82 bp in length (Fig. 4a–c). The presence of an 82 bp target duplication in the IL-3 gene locus was further confirmed by allele-specific PCR amplification using L-8028 genomic DNA. Using a forward primer corresponding to the target duplication of the IL-3 gene at sense orientation (Fig. 4a, J1F) and a backward primer corresponding to the IAP element at sense orientation (Fig. 4a, IAPF2), DNA amplification of junction with 3′-LTR was observed only in the leukemia L-8028 (Fig. 4d, lane 3) but not in the germline (Fig. 4d, lanes 1 and 2). Similarly, the leukemia-specific amplification of junction with 5′-LTR was detected using a forward primer (Fig. 4a, IAPR1) corresponding to the IAP element at antisense orientation and a backward primer (Fig. 4a, J1R) having sequence complement

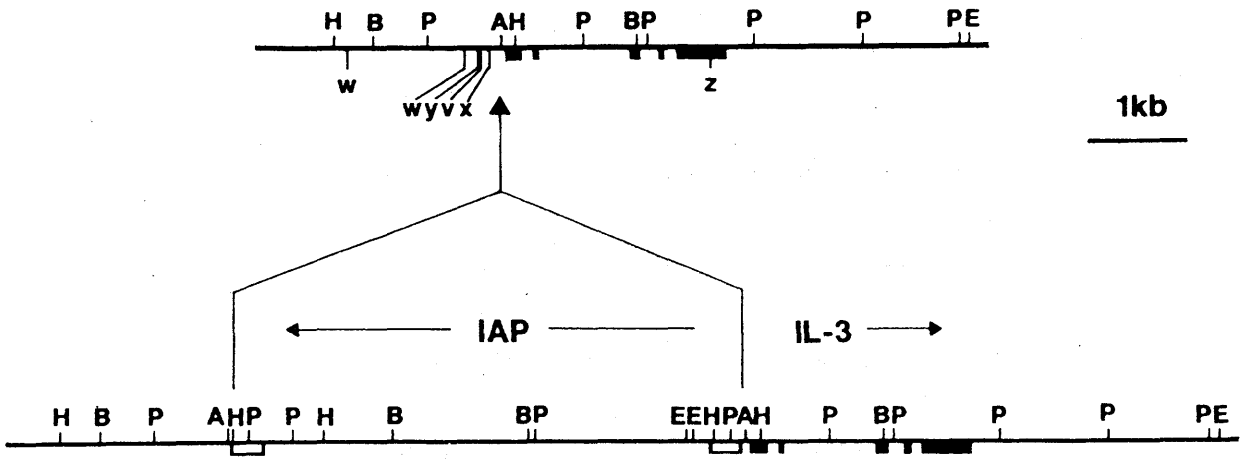

Fig. 2. Restriction map of IL-3 allele in L-8028 leukemia cells. Restriction maps of normal (upper line) and abnormal (lower line) IL-3 alleles were constructed of genomic clones from L-8028 leukemia cells and C3H/He liver cells. Closed boxes correspond to putative exons of the IL-3 gene, and open boxes represent LTR sequences of the IAP element. Restriction sites above both lines indicated are: E = *Eco*RI, B = *Bam*HI, H = *Hin*dIII, P = *Pst*I, A = *Apa*I. Insertion sites found in other previously published cell lines are indicated under the upper line as follows: v, [3]; w, [5]; x, [6]; y, [7]; z, [8].

to the J1F (Fig. 4d, lane 6). Thus, the long target duplication is present in an allele of the IL-3 gene in L-8028 leukemia cells.

4. Discussion

Integration by retrotransposon IAP element has the capacity to contribute to malignancy by activation or inactivation of genes, since at least some levels of IAP message are always present in normal cells [1,2]. Indeed, several established tumor cell lines have tumorigenic features generated at least in part by IAP element-derived activation of limited number of genes for c-mos [12], IL-3 [3,5–8], GM-CSF [4,5,6], IL-6 [16], IL-5 [21], IL-6 receptor [22], IL-2 receptor [23] and hox 2.4 [24]. Heidemann determined the efficiency of retrotransmission by IAP element as 1.5×10^{-6} per cell per generation in a teratocarcinoma cell line [25]. However, the large copy number (1000 copies per haploid genome) of the IAP element in the mouse genome strongly prevents further analyses such as determination and isolation of novel tumor-specific integration sites.

Activation of the IL-3 gene by integration of an IAP element in WEHI-3B cells causes factor-independence which contributes to malignancy [3]. Similar integration events by IAP elements at different sites in the IL-3/GM-CSF locus were found in factor-independent sublines from several cell lines including D35 myeloid [4], FDC-P1 myeloid [5], WEHI-274 myeloid [6], PB-3c mast cell [7] and FL-5.12 lymphoid [8]. Because most of these sublines produce a large amount of IL-3 or GM-CSF mRNA, they are probably selected from IL-3/GM-CSF-dependent population with dominant phenotype of factor-independence. Frequency of in IL-3/GM-CSF-independent clones which included IAP-transposed one at $4–70 \times 10^{-8}$ had been estimated in D35 cell line by Stocking et al.[4].

We found the IAP transposition into IL-3 gene in one strain (L-8028) out of 7 in vivo-passaged leukemia strains (Figs. 1, 2 and 3) which are not selected as factor-independent cells. Stimulation of IL-3 mRNA expression was not observed in the L-8028 cells unlike WEHI-3B cells, although IAP-LTR possessed trascriptional activity. It may be due to the excessively short distance between integration site and the promoter of the IL-3 gene (GC-rich region, Fig. 4a) in the cell, as compared with above-mentioned cell lines. The IAP-transposed IL-3 gene was found in one leukemia strain, even though we tested only 7 strains. This may suggest that the transposition into the IL-3 gene locus is a frequent event in some kind of cell types. The

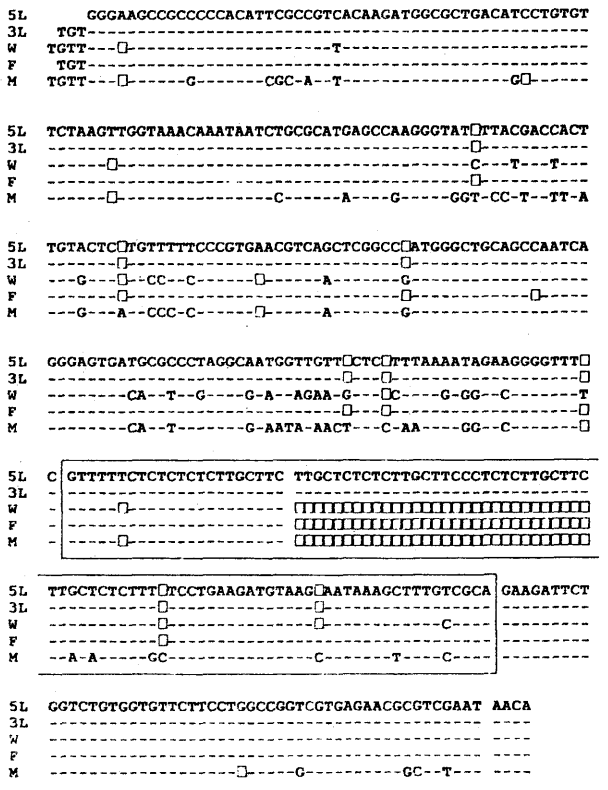

Fig. 3. Sequence comparison of IAP LTRs. Nucleotide sequence of 5′-LTR at the IL-3 allele from L-8028 cells (5L) was compared with the 3′-LTR from the allele (3L) and other LTRs containing IL-3-IAP from WEHI-3B (W)[2], IL3-IAP from FL5.12 (F)[8] and germline IAP of MIA14 (M)[14]. Comparisons to 5L are denoted as follows: – = same sequence; N = different sequence; □ = absent sequence. The R-region in the LTRs is boxed.

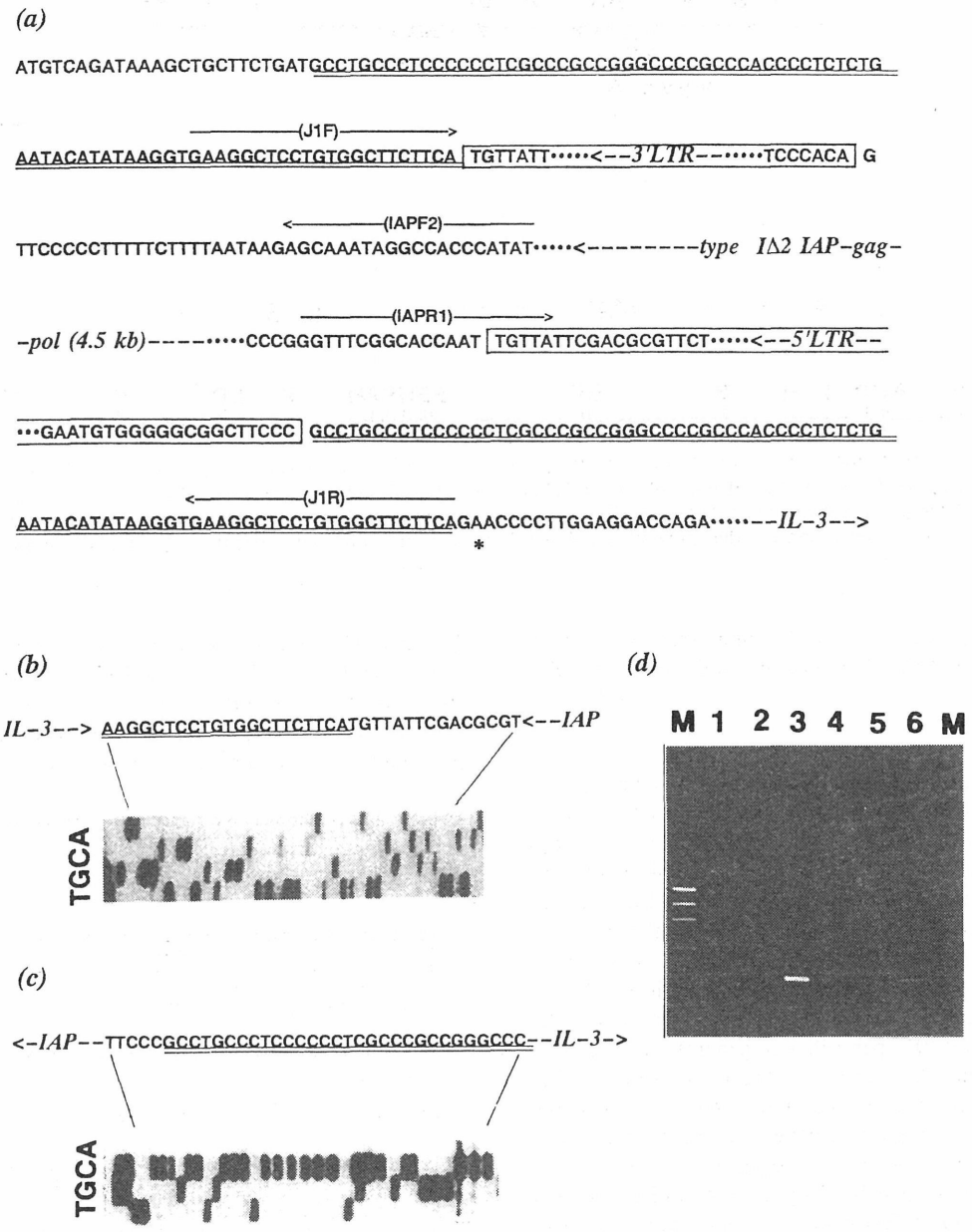

Fig. 4. Analyses of nucleotide sequence at junction of IAP element and IL-3 gene. (a) IAP element sequence is boxed and unique long target duplication sequences are double underlined. Four arrows above the line of sequence shows PCR primers (J1F, IAPF2, IAPR1 and J1R) for Fig. 4d. The asterisk in the bottom line of sequence indicates putative transcription start site. (b) Part of the nucleotide sequence gel showing the junction of the 3′-LTR/IL-3 gene. (c) Part of the sequence gel showing the junction of the 5′-LTR/IL-3 gene. (d) Electrophoresis of DNA after an amplification by PCR. Different lots of genomic DNA from C3H/He liver (lanes 1, 2, 4 and 5) and from L-8028 (lanes 3 and 6) were used for PCR with a set of the J1F and the IAPF2 primers (lanes 1–3), and a set of the J1R and the IAPR1 primers (lanes 4–6). The M is ϕX174DNA/*Hae*III as a molecular length standard.

presence of such a sensitive locus can be proposed based on recent evidence of insertions of IAP elements into the *agouti* locus in germline cells in three different hair color mutant mice [18,19]. At present, we cannot exclude possibility that we could accidentally found the integrated leukemia without selection. To estimate the sensitivity to the transposition in the IL-3/GM-CSF locus, further studies using numerous leukemia strains by wide-range analysis such as pulsed-field gel electrophoresis should be required.

We also found a unique long target duplication at the insertion site (Fig. 4). With the exception of one case with no target duplication [11], all junction sequences published have a 6 bp target duplication suggesting that the insertion was due to a retroviral integration mechanism [3,5,6,8,11–19]. In addition, an incomplete inverted repeat was found only in the 5′-LTR (Fig. 3). No supporting mechanisms nor speculations have yet to suggest that such features may be the recombination after integration.

An alternative mechanism to explain these observations is that both ends of the IAP cDNA with a small deletion bind to the 82 nucleotide cohesive ends. These DNA ends may be generated by artificial reactions induced by ionizing radiation

via superoxide. Gene rearrangement is still not well understood at the molecular level in radiation-induced tumor cells. However, speculative data were presented that X-irradiation increased in the level of message for VL30-retro element which is also a member of the mouse retrotransposon family [26]. If IAP message is increased with VL30 mRNA, then frequency of incorporation can be increased. Additionally, if a limited number of loci are chemically sensitive and subsequent DNA ends behave as acceptors for such elements, the insertion into these loci may be found. Further analyses of radiation- and nonradiation-induced tumors with regard to IAP integration should be performed to reveal the detailed mechanisms of retrotransmission and tumorigenesis.

References

[1] Kuff, E.L. and Lueders, K.K. (1988) Adv. Cancer Res. 51, 183–276.
[2] Keshet, E., Schiff, R. and Itin, A. (1991) Adv. Cancer Res. 56, 215–251.
[3] Ymer, S., Tucker, W.Q.J., Sanderson, C.J., Hapel, A.J., Campbell, H.D. and Young, I.G. (1985) Nature 317, 255–258.
[4] Stocking, C., Loliger, C., Suciu, S., Gough, N. and Ostertag, W. (1988) Cell 53, 869–879.
[5] Dührsen, U., Stahl, J. and Gough, N.M. (1990) EMBO J. 8, 1087–1096.
[6] Leslie, K.B., Lee, F. and Schrader, J.W. (1991) Mol. Cell. Biol. 11, 5562–5570.
[7] Hirsh, H.H., Nair, A.P.K. and Moroni, C. (1993) J. Exp. Med. 178, 403–411.
[8] Algate, P.A. and McCubrey, J.A. (1993) Oncogene 8, 1221–1232.
[9] Seki, M., Yoshida, K., Nishimura, M. and Nemoto, K. (1991) Radiat. Res. 127, 146–149.
[10] Hayata, I., Seki, M., Yoshida, K., Hirashima, K., Sado, T., Yamagiwa, J. and Ishihara, T. (1983) Cancer Res. 43, 367–373.
[11] Kuff, E.L., Feensta, A., Lueders, K., Smith, L., Hawley, R., Hozumi, N., and Shulman, M. (1983) Proc. Natl. Acad. Sci. USA 80, 1992–1996.
[12] Canaani, E., Dreazen, O., Klar, A., Rechavi, G., Rem, D., Cohen, J.B. and Givol, D. (1983) Proc. Natl. Acad. Sci. USA 80, 7118–7122.
[13] Burt, D.W., Reith, A.D. and Brammer, W.J. (1984) Nucleic Acid Res. 12, 8579–8593.
[14] Christy, R.J., Brown, A.R., Gourlie, B.B. and Huang, R.C.C. (1985) Nucleic Acid Res. 13, 289–302.
[15] Man, Y.M., Delius, H. and Leader, D.P. (1987) Nucleic Acids Res. 15, 3291–3304.
[16] Blankenstein, T., Qin, Z., Li, W. and Diamanstein, T. (1990) J. Exp. Med. 171, 965–970.
[17] David, L.B., Aberdam, D.A., Sachs, L. and Blatt, C. (1991) Virology 182, 382–387.
[18] Duhl, D.M.J., Vrieling, H., Miller, K.A., Wolff, G.L. and Barsh, G.S. (1994) Nat. Genet. 8, 59–64.
[19] Michaud, E.J., vanVugt, M.J., Bultman, S.J., Sweet, H.O., Davisson, M.T. and Woychik, R.P. (1994) Genes Dev. 8, 1463–1472.
[20] Sambrook, J., Fritsch, E.F. and Maniatis, T. (1989) Molecular Cloning: a Laboratory Manual, 2nd edn., Cold Spring Harbor Laboratory Press, Cold Spring Harbor, New York.
[21] Tohyama, K., Lee, K.H., Tashiro, K., Kinashi, T. and Honjo, T. (1990) EMBO J. 9, 1823–1830.
[22] Sugita, T., Tothsuka, T., Saito, M., Ymasaki, K., Taga, T., Hirano, T. and Kishimoto, T. (1990) J. Exp. Med. 171, 2001–2009.
[23] Kono, T., Doi, T., Yamada, G., Hatakeyama, M., Minamoto, S., Tsudo, M., Miyasaka, M., Miyata, T. and Taniguchi, T. (1990) Proc. Natl. Acad. Sci. USA 87, 1806–1810.
[24] Blatt, C., Aberdam, D., Schwarts, R. and Sachs, L. (1988) EMBO J. 7, 4283–4290.
[25] Heidmann, O. and Heidmann, T. (1991) Cell 64, 159–170.
[26] Panozzo, J., Bertonicini, D., Miller, D., Libertin, C.R. and Woloschack, E. (1991) Carcinogenesis 12, 801–804.

J. RADIAT. RES., 36, 112–124 (1995)

Immediate-early, Transient Induction of the Interleukin-1β Gene in Mouse Spleen Macrophages by Ionizing Radiation

HIROSHI ISHIHARA[1]*, IZUMI TANAKA[1], KUMIE NEMOTO[2], KAZUKO TSUNEOKA[1], CHEERARATANA CHEERAMAKARA[1]**, KAZUKO YOSHIDA[2] AND HIROSHI OHTSU[2]

[1]Division of Chemical Pharmacology,
[2]Division of Pathology and Physiology, National Institute of Radiological Sciences, 9-1 Anagawa 4-Chome, Inage-ku, Chiba-shi 263, Japan

(*Received, January 18, 1995*)
(*Revision received, April 28, 1995*)
(*Accepted, May 8, 1995*)

interleukin-1β/radiation-response/gene expression/mRNA/fos

In murine spleen cells, x ray irradiation induces the expression of the IL-1β gene at multiple phases of the peak time. We analyzed the immediate-early phase of IL-1β mRNA accumulation. To determine the lineage of cells that showed the immediate response to irradiation, normal spleen cells were analyzed by Northern blotting and *in situ* hybridization after separation by magnetic antibodies against specific cell-surface antigens. Although most of the spleen macrophages continuously expressed a low level of IL-1β mRNA, a portion of the macrophage population transiently accumulated large amounts of IL-1β message immediately after irradiation. A macrophage-like leukemia cell line that resembles these inducible macrophages was identified. A similar immediate-early and transient increase in the IL-1β mRNA level occurred when cultured spleen cells were irradiated with a low dose (3 Gy) of x rays. In contrast, the x ray-inducible expression of the IL-1β gene was immediate and continuous, not transient, in spleen cells from whole-body irradiated mice. Results of the run-on transcription assay and the determination of the decrease in the message using cultured spleen and macrophage-like leukemia cells indicated that x ray irradiation appears to activate the transcription of the IL-1β gene and partially stabilize the message. The results show that the x ray-induced immediate-early accumulation of IL-1β mRNA is regulated at both the transcriptional and post-transcriptional levels in an as yet unidentified population of spleen macrophages.

INTRODUCTION

Interleukin(IL)-1α and IL-1β are multifunctional cytokines that have important roles in a variety of biological reactions, including those in the immune system and inflammation. Results of extensive studies by Neta show that both IL-1α and IL-1β appear to function as radio-

* To whom correspondence should be addressed.
石原　弘：放射線医学総合研究所，生体制御研究グループ，千葉市稲毛区穴川4丁目9番1号　〒263
** Visiting Scientist from the Institute of Tropical Medicine, Mahidol University, Bangkok, Thailand.

protectors in lethally irradiated mice[1,2,3]. Radiation damage can be ameliorated by such functions of IL-1β as the stimulation of lymphocytes[4] and biochemical activation of Mn-superoxide dismutase[5]. The actual mechanism of IL-1 protection has yet to be clarified as a wide variety of biological reactions are stimulated by IL-1s, occasionally in conjunction with other cytokines[6,7]. IL-1α and IL-1β have the same biological functions, and their genes are closely linked on chromosome 2 in both humans and mice[8,9]. Although the intron-exon structures of their genes are similar, they have different nucleotide sequences, particularly in the upstream region. For example, only the IL-1β gene possesses a TATA box, which suggests that the genes are regulated by different mechanisms. The IL-1β, but not the IL-1α gene, is induced by ionizing radiation[10,11], which places it in the family of radiation-induced genes[12,13]. The fact that the IL-1β gene, which encodes a radioprotector, is radiation-inducible suggests the existence of mechanisms of resistance against ionizing radiation in mammals, including the regulation of IL-1β gene expression. To show what these mechanisms are, it is important to analyze the induction of the IL-1β gene by x rays.

IL-1β gene expression mainly is found in monocyte/macrophage cells and is induced by various stimuli such as ionizing radiation[10,11], ultraviolet light[14], lipopolysaccharide (LPS)[15], phorbol ester[16], tumor necrosis factor-α[17], and the IL-1β protein itself[18]. The variety of profiles of IL-1β mRNA accumulation seen after induction are dependent on inducers as well as cell type. Probably this is the result of complex regulatory mechanisms of the IL-1β gene. At the transcriptional level, activation of the gene is reported to be controlled by a number of recently defined nucleotide sequence motifs for the functional enhancer-like proteins present in the upstream region[19–23]. Additionally, the cellular level of the IL-1β message is regulated post-transcriptionally by an AUAAA motif in the mRNA molecule[24]. The relationship between these functions and the various ways in which the message is accumulated in a tissue-type and inducer-specific manner is not yet clear.

After IL-1β mRNA reaches its maximal level, regardless of the trigger of accumulation, that level usually is maintained for several hours to days[10,14–18]. We, however, found a unique profile of IL-1β mRNA accumulation immediately after exposure to x rays in cultured normal spleen cells and myeloid leukemia cells freshly isolated from mouse spleen[11]. A large amount of the message accumulated immediately after irradiation, subsequently decreasing within 1 hour. A similar transient expression reported following the administration of phorbol ester or calcium ionophore occurred simultaneously with expression of the *fos* protooncogene, a typical immediate-early gene, in myeloid leukemia cells[11]. To understand this early event, it is important to analyze the molecular mechanism of IL-1β gene activation by ionizing radiation. Immediate-early expression probably is driven by a minimal number of early biochemical reactions induced by radiation as compared with later expression which potentially is driven by numerous nuclear factors from the early response genes stimulated by irradiation. We therefore focused on the immediate-early events in IL-1β gene expression after exposure to ionizing radiation. Moreover, we made an analysis of the immediate accumulation of IL-1β mRNA in normal spleen. We found it to be regulated at both transcriptional and post-transcriptional levels by derivation of a macrophage cell line which is useful for molecular analysis. We also found that the responsive cells in the spleen are a population of macrophages which continuously produce small amounts

of the message. Similar induction by lower doses of x-rays was detected.

MATERIALS AND METHODS

Animals and irradiation

Specific pathogen-free male C3H/HeN mice 8–12 weeks of age were used. X rays were generated at 200 kVp/20 mA and filtered through 0.5 mm each of Cu and Al. The exposure rate was monitored with a Victoreen R meter. Dose rates of 0.682 Gy/min for whole-body irradiation and 0.899 Gy/min for the exposure of cultured cells were used.

Cell lines and the preparation of spleen cells

Spleen cells isolated from 5 mice above were pooled with RPMI medium (Sigma Chemical Co.) containing 10% fetal calf serum (FCS, Flow Laboratories). After being washed 3 times with the same medium, 1 ml samples of the cells were plated in 35 mm plastic Petri dishes at a density of 2×10^5/ml.

Myeloid leukemia cell lines, established from mice with radiation-induced leukemia[24], were maintained in culture in RPMI-10%FCS. Cell lines L8032 and L8075 were derived from non-adhesive myelomonocytic leukemia. Cell line L8704 was derived from adhesive macrophage-like leukemia.

Before irradiation, all the cultured cells were first incubated at 37°C in 5% CO_2 for 3 h. The cells in the dishes then were irradiated at room temperature and again brought to 37°C for further incubation for various periods. Immediately after incubation, the cells were chilled at 4°C, then transferred to polypropylene tubes and lysed for RNA preparation. Adhesive cells were lysed directly on the plate.

Probes and chemicals

The cDNA for mouse IL-1β (Yakult Central Institute), *v-fos* DNA (from Japanese Cancer Research Resources Bank), and the third exon DNA of human β-actin gene (Wako Pure Chemical Co.) were used as probes in the hybridization experiments. For Northern hybridization, they were labeled using the random primer DNA-labeling kit (Bethesda Research Laboratory) with [α^{32}P]dCTP (111TBq/mmol, ICN), and were diluted to a specific activity of 10^8 cpm/μg DNA. As the RNA probe for *in situ* hybridization, BssHII restriction fragments of pBluescriptIIKS+(Strategene) linked with the probes were incubated with T7- or T3-RNA polymerase (Bethesda Research Laboratory) in the presence of [α^{35}S]UTP (42TBq/mmol, NEN).

Antibodies, F4/80 (BMA) and MOMA2(BMA)[24] were used as the specific antibodies against murine macrophages. Anti-mouse CD3 (Gibco BRL), anti-mouse B220 (PharMingen) and anti-mouse granulocyte (PharMingen) antibodies also were used.

For the induction experiments, 83 n*M* 12-O-tetradecanoyl phorbol acetate (TPA, Sigma), 1 m*M* dibutyryl cyclic AMP (dbcAMP, BDH Ltd.), 2 μM calcium ionophore A23187(Calbio) 1 μg/ml LPS (Sigma), 10 μg/ml actinomycin D (Wako Pure Chemical Co.), 10 μg/ml α-amanitin

(Boehringer Ingelheim), 50 μg/ml H7(protein kinase C inhibitor, Seikagaku Kogyo Co.) and 25 μg/ml H8(protein kinase A inhibitor, Seikagaku Kogyo Co.) were used.

RNA preparation and Northern blot hybridization

Total RNA extracted by the guanidium/hot-phenol method was glyoxylated and electrophoresed according to the general method[27]. After electroblotting of the RNA onto positively-charged nylon membranes (IBI, Optiblot) by our quantitative method[28], the blots were prehybridized then hybridized by the method described previously[11]. The Imaging Plate (Fuji Photo Film Co.) was used to expose the blots. Quantitative autoradiograms were obtained by 2-dimensional measurement of the Imaging Plate with BAS 2000 System (Fuji Photo Film Co.).

Fractionation of spleen cells and in situ *hybridization*

Washed spleen cells were resuspended in RPMI-0.5%FCS medium at 5×10^5/ml at 0°C. Primary rat antibodies against the murine cell surface were added at the final concentration of $1\mu g/10^6$ cells and incubated at 0° for 30 min. After the cells had been washed 3 times with RPMI-0.5%FCS, Dynabeads M-450 coated with sheep anti-rat IgG (Dynal A. S., Norway) were transferred at a final ratio of 0.1 ml/10^6 cells and incubated at 0°C for 30 min. Antigen-positive and -negative cells were separated by the use of a magnetic platform and preincubated at 37°C for 3 h with RPMI-0.5% FCS. After irradiation, they were cytocentrifuged and fixed with 4% paraformaldehyde at room temperature. *In situ* hybridization was performed as described previously[29] using ^{35}S-labeled RNA probes.

Nuclear run-on transcription assay

Isolated nuclei were prepared by the lysis of 10^8 cells in 10 m*M* Tris-HCl(pH 8.0) buffer containing 5 m*M* KCl, 3 m*M* $MgCl_2$ and 0.5% Nonidet P-40. After being washed with ice-cold phosphate-buffered saline (PBS), the nuclei were incubated at 26°C for 45 min in 10 m*M* Tris-HCl(pH 8.3) buffer containing 15% glycerol, 70 m*M* KCl, 2.5 m*M* $MgCl_2$, 10 m*M* ethylenediamine tetraacetic acid (EDTA), 4 m*M* ATP, 4 m*M* CTP, 4 m*M* GTP, 2 m*M* UTP, 0.5 m*M* dithiothreitol, 630 units/ml RNA guard (Pharmacia) and 7.4 MBq α^{32}P-UTP (111TBq/ml, NEN). After sequential treatment of the mixture with DNaseI, proteinase K, and phenol/chloroform, the radioactive RNA was pelleted by isopropanol precipitation.

Plasmid DNAs were digested by restriction enzymes, then denatured by boiling and placed 10 μg per spot on nitrocellulose filters (Schleicher & Schuell). The blots were baked at 80°C in a vacuum for 2 h, then prehybridized at 42°C overnight in 2×SSC buffer containing 50% formamide, 0.2% sodium dodecyl sulfate, 0.2% Ficoll 400 (Pharmacia), 0.2% bovine serum albumin (Sigma, fraction V), 0.2% polyvinylpyrrolidone, 50 m*M* Tris-HCl (pH 8.0), 50 m*M* sodium phosphate (pH 6.5), 100 μg/ml tRNA, and 100 μg/ml sonicated salmon sperm DNA. Hybridization took place during incubation at 42°C for 3 days after the addition of radioactive RNA. The filters were washed 3 times at 60°C for 30 min with 2×SSC buffer containing 0.2% sodium dodecyl sulfate, 5 m*M* sodium phosphate (pH 7.0), and 1 m*M* EDTA, and autoradiograms obtained as above.

RESULTS

Immediate-early expression of the IL-1β gene induced by the x-irradiation of spleen cells

Lymphoid and myeloid cells at various stages of differentiation are present in the spleen. In a previous paper, we showed that some spleen cells transiently accumulate IL-1β message immediately after x-irradiation[11]. In contrast, differentiated macrophages are known to express IL-1β mRNA[11] constitutively. In specific pathogen-free (SPF) mice, the population of macrophage-lineage cells in the spleen is limited; consequently, the amount of IL-1β mRNA in the spleen is low. On irradiation with x rays, however, the immediate appearance and subsequent decrease of large amounts of IL-1β mRNA was observed. After incubation of the isolated spleen cells for 2 h with serum-free RPMI medium in plastic dishes, a small number of macrophage-like

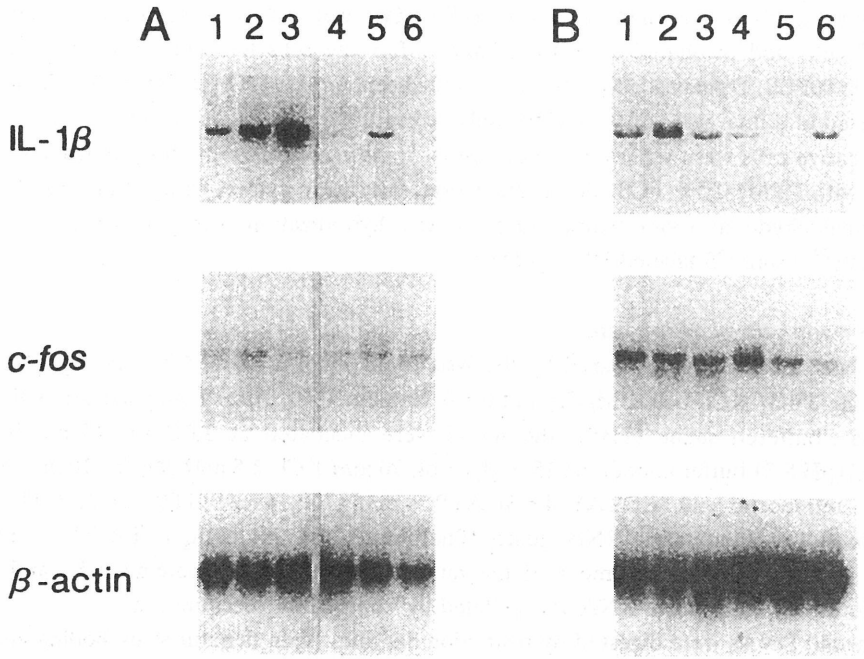

Fig. 1. Immediate accumulation of IL-1β mRNA after x irradiation. Each lane of the Northern blots contained 10 μg total RNA from cultured spleen cells (A) or L8704 leukemia cells (B) after the following treatments. The RNA was hybridized to IL-1β, *c-fos*, and β-actin DNA probes. (A). Tightly adhesive (lanes 1–3) and non-adhesive (lanes 4–6) cells were irradiated with 20 Gy x rays. Lanes 1 and 4: before irradiation; lanes 2 and 5: immediately after treatment (25 min after the start of irradiation); lanes 3 and 6: after 30 min of incubation subsequent to irradiation. (B). RNA prepared from L8704 leukemia cells was used after the following treatments. Lane 1: before treatment; lane 2: immediately after x-irradiation; lane 3: after 30 min of incubation subsequent to irradiation; lane 4: after 30 min of incubation after the addition of TPA; lanes 5 and 6: after 30 min (lane 5) or 60 min (lane 6) of incubation subsequent to the addition of LPS.

cells tightly adhered to the dishes. Immediately after irradiation, IL-1β mRNA was accumulated transiently in the mixture of weakly adhesive and non-adhesive cells (Fig. 1). In contrast, tightly adhesive cells were continuously produced IL-1β mRNA regardless of whether they were irradiated.

To distinguish the cell type showing the transient and inducible IL-1β expression after irradiation, spleen cells were separated using magnetic beads to which were linked cell surface-specific antibodies, and were analyzed by *in situ* hybridization. There was constitutive production of a small amount of IL-1β mRNA in most cells that expressed the antigens for macrophage-specific antibodies F4/80 and MOMA2 (Fig. 2). A large amount of IL-1β mRNA was accumulated in a subpopulation of cells that bound to F4/80 and MOMA2 after irradiation. Within 30 min, the message decrease to the control level in these cells during incubation after irradiation. In contrast, neither transient nor constitutive expression were observed in CD3 (T cell antigen)-positive or B220 (B cell antigen)-positive cells. This means that the x ray-inducible expression of the IL-1β gene originated in a subpopulation of macrophages.

Previously, we showed a similar transient expression of the IL-1β gene in non-linearized myeloid leukemia cells isolated from mouse spleen[11]. Although accumulation of mRNA for the *c-fos* protooncogene following x or γ irradiation is frequently observed in various linearized cells[30], including myeloid leukemia cells[11], the mRNA level in normal spleen cells is not clearly increased after irradiation. Linearized cells which reflect the radiation response in spleen cells are required for molecular studies. We analyzed three myeloid leukemia cell lines; two myelomonocytic cell lines, L8032 and L8075, and a macrophage-like cell line, L8704[25,29]. The two myelomonocytic leukemia cell lines showed no detectable IL-1β mRNA without irradiation, a small amount of the message being observed immediately after irradiation. These cells produced *c-fos* mRNA on irradiation as did other tumor cell lines (data not shown). In contrast, as shown in Fig. 1, L-8704 cells, a macrophage-like cell line, showed continuous low levels of IL-1β and *c-fos* transcripts without induction. Irradiation with 20 Gy x rays induced an increase in the IL-1β mRNA level 2.5-fold that prior to exposure, but no concomitant increase in the level of the *c-fos* message. These features are similar to those of normal spleen cells; therefore we used the L-8704 cell line in further experiments.

Transcriptional and post-transcriptional regulation of the transient expression of the IL-1β gene

Previously, we reported the contribution of the protein kinase(PK)C and PKA networks to the immediate accumulation of IL-1β[11]. This was supported by the observation that x ray-induced immediate-early accumulation of IL-1β mRNA was prevented by pretreatment of the spleen or L8704 cells with H7 (PKC inhibitor) or H8 (PKA inhibitor) (Fig. 3). If the activation of these kinase networks contributes to the accumulation of the IL-1β message after irradiation, then transcriptional regulation should function in the induction. The contribution of transcriptional regulation after irradiation was supported by the results of the run-on transcription assay of L8704 cell nuclear extract (Fig. 4).

The cellular level of the IL-1β message, however, is not only controlled by transcriptional regulation but is regulated post-transcriptionally; cytoplasmic regulation to stabilize or destabilize message using specific sequences besides the 3'-position of the molecule[24]. To clarify this

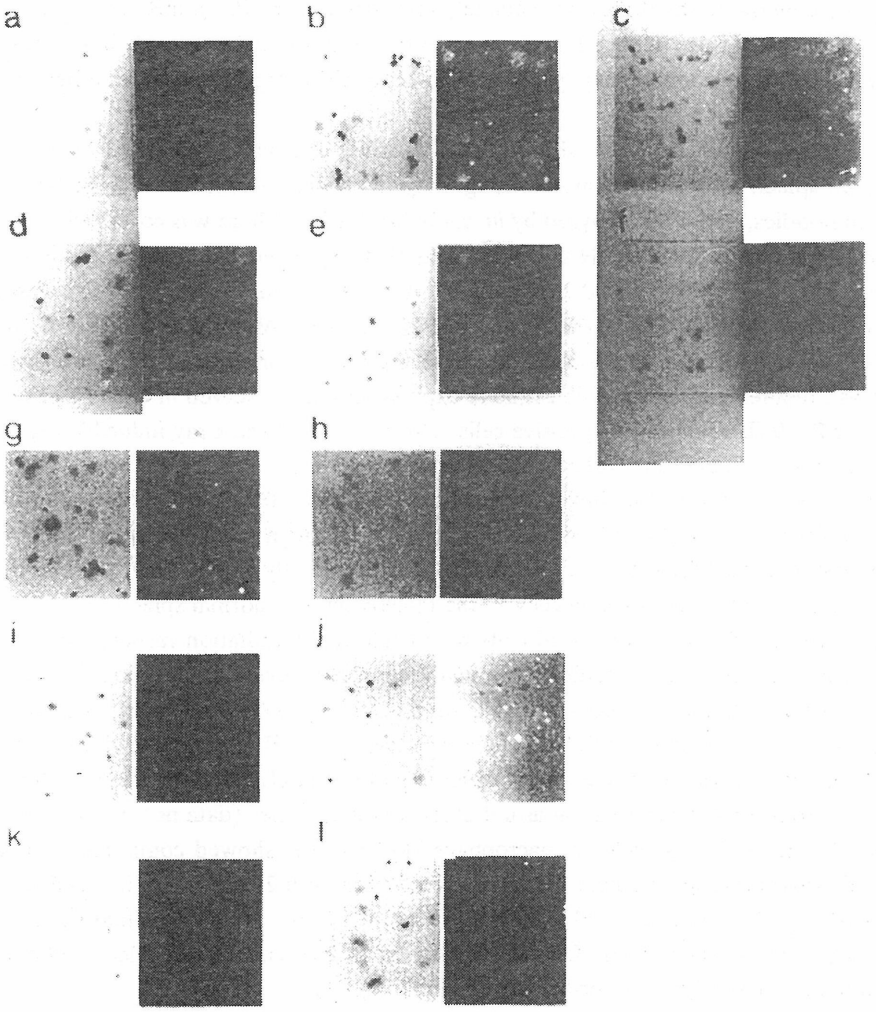

Fig. 2. Detection of IL-1β mRNA in normal spleen cells by *in situ* hybridization. Cells were separated using Dynabeads with bound F4/80 antibody (a, b, c), MOMA2 antibody (d, e, f), anti-gral antibody (g, h), anti-CD3 antibody (i, j), or anti-B220 antibody (k, l). The separated cells were cytocentrifuged before (a, d, g, i, k), or immediately after irradiation with 20 Gy x rays (b, e, h, j, l), or after 30 min of incubation subsequent to irradiation (c, f). Each pair of microphotographs shows the light-field (left) and dark-field (right) views of micro-autoradiographs of the same area. In the dark-field, many small grains are present around the IL-1β mRNA-producing cells. The large single grains are due to the presence of Dynabeads.

contribution to the x ray-induced expression of the mRNA, the decrease rate of the IL-1β message in leukemia cells was analyzed quantitatively in medium containing the transcriptional inhibitors α-amanitin and actinomycin D during x-irradiation. As shown in Fig. 5, the maximal

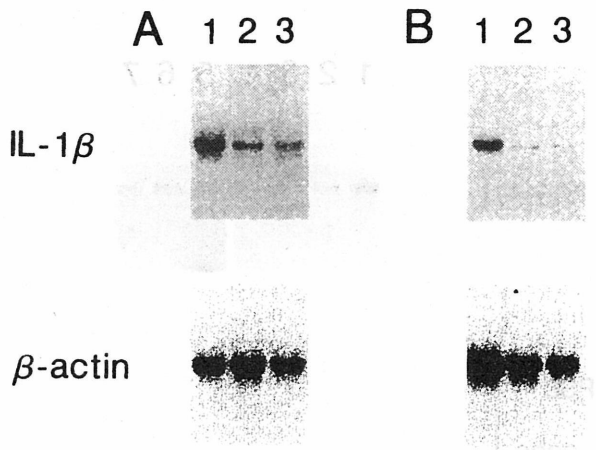

Fig. 3. Repression of IL-1β mRNA accumulation by protein kinase inhibitors. Each lane contains 10 μg of RNA from cultured spleen (A) or L8704 leukemia (B) cells. Cells were collected immediately after irradiation with 20 Gy x rays subsequent to pretreatment without (lanes 1 and 4) or with the PK inhibitors H7 (lanes 2 and 5) or H8 (lanes 3 and 6).

Fig. 4. Nuclear run-on transcription analysis. Nuclei were isolated before (A) or immediately after (B) irradiation with 20 Gy x rays. Spots on the nitrocellulose filter contain 10 μg of pBluescriptIIKS+(1) as the negative control, IL-1β cDNA (2) or β-actin DNA (3) as the positive control.

level of the message induced by dbcAMP decreased rapidly in the presence of these inhibitors in L8704 cells. When cells were irradiated with x rays immediately after the addition of the inhibitors, degradation of the message was prevented. These results show that the x ray-induced accumulation of the message is regulated at the transcriptional as well as the post-transcriptional levels.

A low dose of x rays induces transient expression of IL-1β mRNA in isolated spleen cells in vitro, *and constitutive expression in the spleen by whole-body irradiation* in vivo

In a previous paper[11], we showed that 20 Gy x-irradiation induced the immediate and transient accumulation of IL-1β mRNA in mouse spleen cells. To determine whether a dose of 20 Gy is necessary for this induction, we examined the effect of the lower dose of 3 Gy x-irradiation on the immediate and transient expression of the IL-1β gene in isolated mouse spleen cells. As shown in Fig. 6A, some IL-1β message was detectable in the isolated spleen cells containing adhesive and non-adhesive cells during preincubation in culture. The accumulation of the IL-1β message was detected 30 min after irradiation with 3 Gy x rays, and immediately after

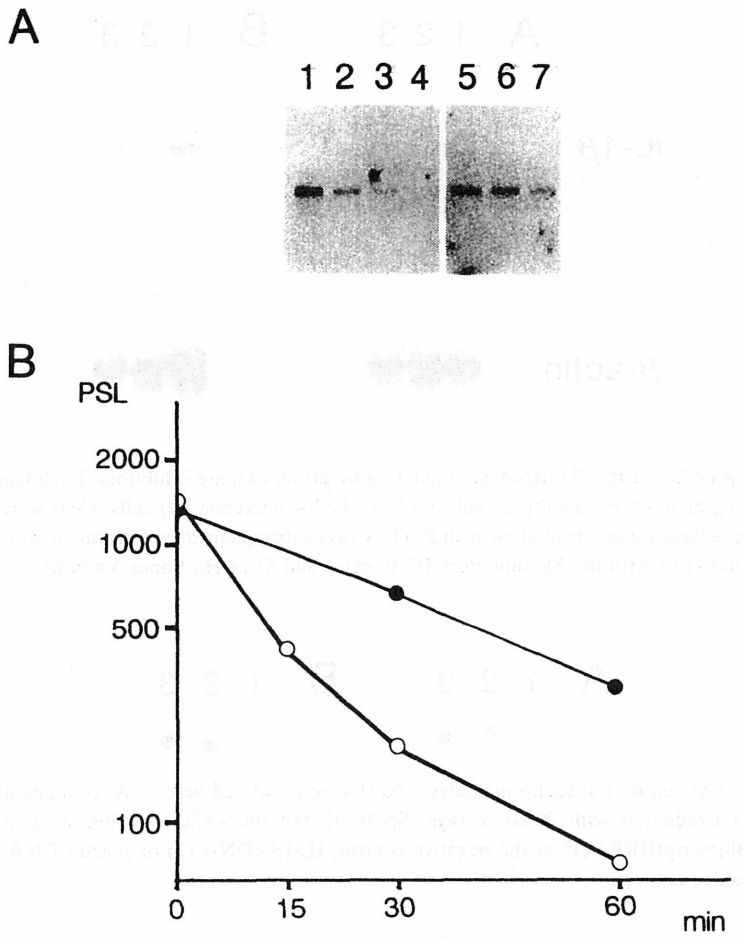

Fig. 5. Effect of x-irradiation on the rate of decrease in the IL-1β mRNA level. (**A**). L8704 cells pretreated with dbcAMP to emphasize IL-1β mRNA were treated with (lanes 3 to 5) or without (lane 1) the transcriptional inhibitors α-amanitin and actinomycin D. Immediately after the addition of the inhibitors, the cells were irradiated (lanes 4 and 5) for 30 min; lanes 2 and 3 are the non-irradiated controls. Total RNA was prepared from the cells before the addition of the inhibitors (lane 1) immediately after irradiation (lanes 2 and 4), or after being kept for 30 min after irradiation (lanes 3 and 5). Each lane of the Northern blots contained 10 μg of total RNA. (**B**). The radioactivity (PSL value) on the autoradiogram shown in panel A was quantified and plotted. Open circles: lanes 1–4; closed circles: lanes 5–7.

irradiation with 20 Gy x rays. In these experiments, irradiation times for 3 Gy and 20 Gy were 3.7 min and 25 min, respectively. The peak of immediate accumulation therefore was detectable 30 min after the initiation of irradiation. This shows that a dose of 3 Gy is sufficient to produce the early induction of IL-1β expression, and that the message accumulates during irradiation with 20 Gy.

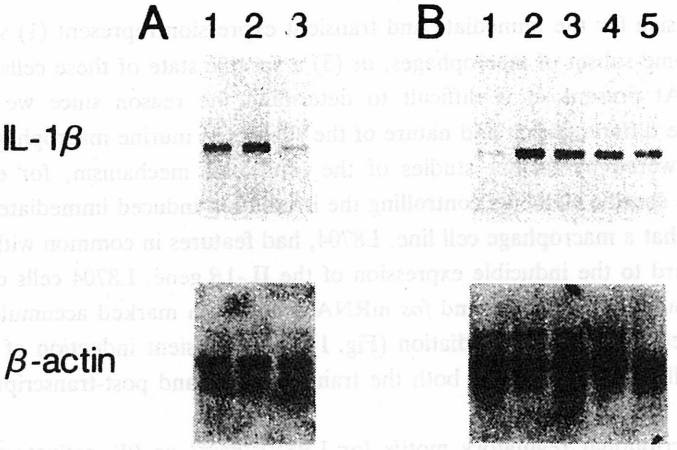

Fig. 6. Immediate-early expression of IL-1 mRNA in spleen cells after *in vivo* and *in vitro* irradiation. (**A**). RNA was prepared from cultured spleen cells before (lane 1) and after incubation for 30 min (lane 2) and 1 h (lane 3) subsequent to irradiation with the low dose of 3 Gy x rays. A 10 μg sample of the RNA was loaded to each lane for Northern blot hybridization. (**B**). Spleen cell RNA was prepared from mice before (lane 1) and after 30 min (lane 2), 1 h (lane 3), 2 h (lane 4) and 4 h (lane, 5), subsequent to whole-body irradiation with 18.5 Gy x rays.

To examine whether the immediate-early event occurs in spleen cells *in vivo*, we used immediately prepared spleen cells from whole-body-irradiated mice after various intervals. As shown in Fig. 6B, immediate accumulation was found 30 min after the initiation of irradiation with 18.5 Gy x rays, which was similar to the *in vitro* experiment; but, the increased level of the message was not decreased after 4 h. This suggests that the decrease phase in the message level cannot detected in spleen cells *in vivo*.

DISCUSSION

We previously showed that immediate accumulation and subsequent reduction of IL-1β mRNA occurs after x-irradiation of isolated spleen cells that contain normal undifferentiated blood cells and in myeloid leukemia cells[11] as well. Because the immediate mechanism reflected the early response of organisms against x rays, we focused on the mechanism of the immediate expression phase of the IL-1β gene after x-irradiation.

We found a cell type which contributed to the immediate-early expression of the IL-1β gene after x ray exposure in cultured spleen cells containing a heterogeneous mixture of undifferentiated lymphoid and myeloid cells: the inducible cells were macrophage antigen-positive cells (Fig. 2), and showed little adhesiveness to plastic dishes (Fig. 1). In contrast, a continuously low level of the message was detected in all the macrophage antigen-positive cells and rapidly adhesive cells. This continuous expression seems to be distinct from the immediate and transient accumulation of the message found in this study. There are several possibilities that the

macrophages responsive for the immediate and transient expression represent (1) subtly differentiated cells, (2) some subset of macrophages, or (3) a specific state of these cells determined by the cell cycle. At present, it is difficult to determine the reason since we know little concerning the subtle differentiation and nature of the subsets of murine macrophages. However, this will be answered by further studies of the molecular mechanism, for example, by determination of the specific elements controlling the irradiation-induced immediate reaction.

We also found that a macrophage cell line, L8704, had features in common with the spleen macrophages in regard to the inducible expression of the IL-1β gene. L8704 cells continuously expressed small amounts of the IL-1β and *fos* mRNAs and had a marked accumulation of the IL-1β message immediately after x-irradiation (Fig. 1). The transient induction of IL-1β gene expression in the cells was regulated at both the transcriptional and post-transcriptional levels (Figs. 3, 4, 5).

Recently, transcriptional regulatory motifs for LPS[19,20,22,23] or PK activator[21]-inducible expression were identified in the region upstream of the IL-1β coding sequences in the human and mouse. The presence of multiple regulation sequences is consistent with the observation that the gene shows various profiles of RNA accumulation depending on the range of inducers and cell types[15–18]. Intervals of several hours after the administration of the agents passed before the preparation of the nuclear and cellular extracts for the mobility-shift and CAT assays in these experiments, showing that the IL-1β gene can be activated by transcriptional regulators such as the *fos/jun* family genes which are activated by x irradiation[30–32]. In contrast, x ray induction of IL-1β expression was markedly transient with no activation of the *fos* gene in the L8704 (Fig. 1B) and normal spleen cells[11]. Molecular analysis using L8704 cells is a usefull tool with which to investigate the relationship between the immediate-early and moderate activations of IL-1β after x ray irradiation.

We also found immediate and transient expression of the IL-1β gene in cultured spleen cells after irradiation at doses of 20 Gy as well as 3 Gy (Fig. 6A). A similar immediate accumulation was detected in the same spleen cells isolated from mice after whole-body irradiation with 20 Gy x rays (Fig. 6B). These results show that the immediate accumulation of the message occurs not only in isolated cells but also in those within the living spleen. In the *in vivo* experiment, however, the IL-1β message level was maintained continuously at a high level following irradiation. The absence of a decrease in the message level may be the result of as yet unknown regulatory mechanisms mediated by cell-cell contact in the normal spleen.

We have showed that the immediate-early accumulation of IL-1β mRNA is one of the x ray-responsive events occurring in spleen macrophages. At present, it is still unclear why the expression of a gene for a cytokine as well as radioprotector should have an immediate responsive phase after x-irradiation, although most of the genes induced immediately by x rays encode nuclear factors. Further molecular analysis of the primary reaction to x rays and the immediate accumulation of IL-1β mRNA using the macrophage cell line L8704 is necessary.

REFERENCES

1. Neta, R. Douches, S. and Oppenheim, J. J. (1986) Interleukin 1 is a radioprotector. J. Immunol. **136**: 2483–2485.
2. Neta, R. (1988) Why should internists be interested in interleukin-1? Ann. Intern. Med. **190**: 1–2.
3. Neta, R., Oppenheim, J., Ledney, G. D. and MacVittie, T. J. (1992) Role of cytokines in innate and LPS-enhanced radioresistance. In Radiation Research: A Twentieth-Century Perspective, eds. W. C. Dewey, et al. Vol II, pp. 830–833. Academic Press, San Diego.
4. Bagby, Jr, G. C. (1989) Interleukin-1 and hematopoiesis. Blood Rev. **3**: 152–161.
5. Masuda, A., Longo, D. L., Kobayashi, Y., Appela, E., Oppenheim, J. J. and Matsushima, K. (1988) Induction of mitochondrial manganese superoxide dismutase by interleukin 1. FASEB J. **2**: 3087–3091.
6. Dinarello, C. (1984) Interleukin-1. Rev. Infect. Dis. **6**: 51–96.
7. Dinarello, C. (1991) Interleukin 1 and interleukin 1 antagonism. Blood **77**: 1627–1652.
8. Modi, W. S., Masuda, A., Yamada, M., Oppenheim, J. J., Matsushima, K. and O'Brien, S. J. (1988) Chromosomal localization of the human interleukin 1 α gene. Genomics **2**: 310–314.
9. Silver, A. R. J., Masson, W. K., George, A. M., Adam, J. and Cox, R. (1990) The IL-1 α and β genes are closely linked (<70 kb) on mouse chromosome 2. Somat. Cell. Mol. Genet. **16**: 549–556.
10. Woloschak, G. E., Chang-Liu, C. M., Jones, P. S. and Jones, C. A. (1990) Modulation of gene expression in Syrian hamster embryo cells following ionizing radiation. Cancer Res. **50**: 339–344.
11. Ishihara, H., Tsuneoka, K., Dimchev, A. B. and Shikata, M. (1993) Induction of the expression of the interleukin-1β gene in mouse spleen by ionizing radiation. Radiat. Res. **133**: 321–326.
12. Fornace Jr, A. J. (1992) Mammalian genes induced by radiation: Activation of genes associated with growth control. Annu. Rev. Genet. **26**: 507–526.
13. Herrlich, P., Ponta, H. and Rahmsdorf, H. J. (1994) DNA damage-induced gene expression: Signal transduction and relation to growth factor signalling. Rev. Physiol. Biochem. Pharmacol. **119**: 187–223.
14. Kupper, T. S., Chua, A. O., Flood, P., McGuire, J. and Gubler, U. (1987) Interleukin 1 gene expression in cultured human keratinocyte is augumented by ultraviolet irradiation. J. Clin. Invest. **80**: 430–436.
15. Schindler, R., Clark, B. D. and Dinarello, C. A. (1990) Dissociation between interleukin-1β mRNA and protein synthesis in human peripheral blood mononuclear cells. J. Biol. Chem. **265**: 10232–10237.
16. Fenton, M. J., Vermeulen, M. W., Clark, B. D., Webb, A. C. and Auron, P. E. (1988) Human pro-IL-1β gene expression in monocytic cells is regulated by two distinct pathways. J. Immunol. **140**: 2267–2273.
17. Turner, M., Chantry, D., Buchan, G., Barrett, K. and Feldmann, M. (1989) Regulation of human IL-1α and IL-1β genes. J. Immunol. **143**: 3556–3561.
18. Elias, J., Reynold, M., Kotloff, R. and Kern, J. (1989) Fibroblast interleukin-1β: Synergistic stimulation by recombinant interleukin-1 and tumor necrosis factor and post-transcriptional regulation. Proc. Natl. Acad. Sci. USA **86**: 6171–6175.
19. Buras, J. A., Monks, B. G. and Fenton, M. J. (1994) The NF-βA-binding element, not an overlapping NF-IL-6 binding element, is required for maximal IL-1β gene expression. J. Immunol. **152**: 4444–4454.
20. Zhang, Y. and Rom, W. N. (1993) Regulation of the interleukin-1β (IL-1β) gene by mycobacterial components and lipopolysaccharide is mediated by two nuclear factor-IL6 motifs. Mol. Cell. Biol. **13**: 3831–3837.
21. Serkkola, E. and Hurme, M. (1993) Synergism between protein-kinase C and cAMP-dependent pathways in the expression of the interleukin-1β gene is mediated via the activator-protein-1 (AP-1) enhancer activity. Eur. J. Biochem. **213**: 243–249.
22. Cogswell, J. P., Godlevski, M. M., Wisely, G. B., Clay, W. C., Leesnitzer, L. M., Ways, J. P. and Gray, J. G. (1994) NFκB regulates IL1β transcription through a consensus NFκB binding site and a

nonconsensus CRE-like site. J. Immunol. **153**: 712–723.
23. Godambe, S. A., Chaplin, D. D., Takava, T. and Bellone, C. J. (1994) Upstream NFIL6-like site located within a DNase I hypersensitivity region mediates LPS-induced transcription of the murine interleukin-1β gene. J. Immunol. **153**: 143–152.
24. Capt. D., Beutler, B., Hartog, K., Thayer, R., Shimer, S. B. and Cerami, A. (1986) Identification of a common nucleotide sequence in the 3'-untranslated region of mRNA molecules specifying inflammatory mediators. Proc. Natl. Acad. Sci. USA **83**: 1670–1674.
25. Seki, M., Yoshida, K., Nishimura, M. and Nemoto, K. (1991) Radiation-induced myeloid leukemia in C3H/He mice and the effect of predonisolone acetate on leukemogenesis. Radiat. Res. **127**: 146–149.
26. Breel, M., Mebius, R. E. and Kraal, G. (1987) Dendritic cells of the mouse recognized by two monoclonal antibodies. Eur. J. Immunol. **17**: 1555–1559.
27. Maniatis, T. Sambrook, J. and Fritsch, E. F. (1982) Molecular Cloning: A Laboratory Mannual. Cold Spring Harbor Laboratory, Cold Spring Harbor, NY.
28. Ishihara, H. and Shikita, M. (1990) Electroblotting of double-stranded DNA for hybridization experiments: DNA transfer is complete within 10 minutes after pulsed-field gel electrophoresis. Anal. Biochem. **184**: 207–212.
29. Ishihara, H., Yoshida, K., Nemoto, K., Tsuneoka, K. and Shikita, M. (1993) Constitutive overexpression of the c-fos gene in radiation-induced granulocytic leukemia in mice. Radiat. Res. **135**, 394–399.
30. Sherman, M. L., Datta, R., Hallahan, D. E., Weichselbaum, R. R. and Kufe, D. W. (1990) Ionizing radiation regulates expression of the c-jun protooncogene. Proc. Natl. Acad. Sci. **87**: 5663–5666.
31. Hallahan, D. E., Sukhatme, V. P., Sherman, M. L., Virudachalam, S., Kufe, D. and Weichselbaum, R. R. (1991) Protein kinase C mediates x-ray inducibility of nuclear signal transducers EGR1 and JUN. Proc. Natl. Acad. Sci. **88**: 2156–2160.
32. Manome, Y., Datta, R., Taneja, N., Shafman, T., Bump, E., Hass, R., Weichselbaum, R. and Kufe, D. (1993) Coinduction of c-jun gene expression and internucleosomal DNA fragmentation by ionizing radiation. Biochem. **32**: 10607–10613.

Detection and cloning of unique integration sites of retrotransposon, intracisternal A-particle element in the genome of acute myeloid leukemia cells in mice

H. Ishihara*, I. Tanaka

The First Research Group, National Institute of Radiological Sciences, Anagawa 4-9-1, Inage-ku, Chiba 263, Japan

Received 9 October 1997

Abstract **We previously found retrotransposition of the intracisternal A-particle (IAP) element in the genome of acute myeloid leukemia (AML) cells induced by X-irradiation of C3H/He mice (FEBS 16333). To analyze the occurrence of the IAP-mediated retrotransposition in AML cells, we compared integration sites of the IAP element by polymerase chain reaction (PCR) in the genomes of five AML strains derived from different C3H mice. Unique PCR products were found in all of the above independent leukemia cells, whereas no such products were detected in normal cells. Results of cloning, sequencing and Southern analyses showed that the PCR products were derived from novel integration sites of the IAP element in the genome. The data suggest that IAP-mediated retrotransposition occurs frequently in radiation-induced AML cells from C3H/He mice.**

Key words: Retrotransposon; Retrotransposition; Intracisternal A-particle; Gene rearrangement; Polymerase chain reaction; Nucleotide sequence

1. Introduction

Radiation-induced leukemia can be experimentally produced in several inbred mice. Acute myeloid leukemia (AML) occurs in 20–30% of C3H/He inbred mice 1–2 years after whole-body exposure to ionizing radiation [1,2]. The murine AML cells from different individuals with a wide variety of histochemical phenotypes can be treated as 'independent' strains. These cells can be used to analyze genetic events which are inscribed in the genome through initial radiation damage and leukemogenesis. We previously found that one of seven independent AML cells tested has a rearrangement in the interleukin-3 gene by integration of the intracisternal A-particle (IAP) element [3].

The IAP is one of the murine retrotransposons and is believed to be a kind of incomplete endogenous retrovirus [4]. Like retroviruses, the reverse transcription product can be introduced into genomic DNA by retrotransposition [5], resulting in an IAP element with two long terminal repeat (LTR) sequences containing enhancer/promoter function [6]. Whereas retroviral infection and subsequent events are rare in normal mice, normal genomes naturally contain large numbers (ca. 1000 copies/haploid) of the IAP element due to accumulation of retrotransposition in the germline cells [4,5]. This means that any normal cell has the possibility of being modified in the genome by IAP retrotransposition, so that the IAP is regarded as an endogenous mutagen in mouse cells [4,5]. Examples of IAP-mediated gene rearrangement that contributes to the specific features of the tumor have been observed in various tumor cell lines in mice [4,5,7–10]. If retrotransposition by the IAP commonly occurs in tumor cells or during tumorigenesis, the integrated IAP element should be observed in the genome from any tumor cell. However, the large copy number of the IAP provirus strongly prevents detection of the tumor-specific integration site.

Our previous finding of gene rearrangement by integration of the IAP element in AML cells from C3H/He mice led us to investigate the possibility that retrotransposition may be a frequent event in AML cells. In this study, we compared the integration sites of the IAP element in genomes of five independent AML cells and normal cells. Genomes of all the AML cells possessed unique integration sites of IAP, whereas no such retrotransposition was observed in normal cells. This suggests that IAP-mediated retrotransposition is a frequent event in radiation-induced AML in C3H/He mice.

2. Materials and methods

2.1. Mice and leukemia cells

Radiation-induced AML was generated 1–2 years after whole-body X-irradiation to C3H/He mice at a dose of 3 Gy [1]. Leukemia cells obtained from the AML mice were maintained by in vivo passage by injection of the cells into 6–8-week-old normal C3H/He mice inbred in our institute [1,3]. The amplified leukemia cells were collected from the spleen 2–4 weeks after injection. High molecular weight DNA samples of five independent leukemia strains derived from different AML mice were prepared by the standard method [11].

2.2. Primers, PCR and inverted PCR

The six PCR primers for detection of AML-specific integration sites are shown in Fig. 1. Four primers (RS-IAP-F, U-IAP-F, RS-IAP-R and U-IAP-R) correspond to IAP-LTR and two primers (SINE-B2-F and SINE-B2-R) correspond to the consensus sequence of the short interspersed element (SINE)-B2. 50 ng of total genomic DNA with a pair of the primers was amplified by PCR with 0.25 units of ExTaq DNA polymerase (Takara Shuzo Co.) (94°C, 1 min; then 32 cycles of 98°C, 20 s; 55°C, 1 min; 72°C, 8 min) using a thermal cycler (Perkin-Elmer model 480).

The inverted PCR [12] was used to clone the normal allele of the AML-specific rearranged DNA. After sequencing of the first PCR product specific for AML cells, a primer set suitable for the inverted PCR was prepared. Germline DNA was digested by appropriate restriction enzymes, end-filled by Klenow fragment of DNA polymerase I, and recircularized by T4 DNA ligase at low DNA concentration (2 ng/ml). The recircularized DNA was used for the inverted PCR with a

*Corresponding author. Fax: (81) (43) 255-6819.
E-mail: ishihara@nirs.go.jp

The sequences in this paper will appear in DDBJ, EMBL and GenBank nucleotide sequence databases under accession numbers D85906 and D85907.

set of primers and ExTaq DNA polymerase (35 cycles of 94°C, 1 min; 52°C, 1 min; 72°C, 4 min). By comparing the sequences between an AML-specific PCR product and the corresponding product of the inverted PCR from germline DNA, AML-specific insertion sites of the IAP element were determined. Since the first PCR product is one side of the AML-specific junction of the IAP element, the sequence corresponding to the other side of the junction in the AML genome can be predicted by a comparison. A primer matched to the other side was prepared, together with an IAP-LTR primer and AML genomic DNA, and was used for PCR (35 cycles of 94°C, 1 min; 55°C, 1 min; 72°C, 2 min) by Taq DNA polymerase (Perkin Elmer). The 6 primers (Q11-F, Q11-R, Q11-B, Q14-F, Q14-R and Q14-B) used in the subsequent PCR are shown in Fig. 3.

2.3. Nucleotide sequence analysis and Southern blot hybridization

The PCR products were electroeluted, cloned using the T-vector pMOSblue (Amersham), and sequenced using Sequenase-2 (USB). Probes for genomic Southern analysis were prepared from PCR products corresponding to the AML-specific insertion site in the normal allele which does not contain IAP- or SINE-derived sequences by appropriate primers (Q11-R plus Q11-B or Q14-R plus Q14-B) and germline DNA. Using the standard method [11], the probes were labeled with ^{32}P using a random primer labeling kit (BRL), hybridized with blots and analyzed with the BAS2000 system (Fuji Photo Film Co.).

3. Results

We have mainly studied whether IAP-mediated retrotransposition is a frequent event in the AML cells from C3H/He mice. If so, AML-specific integration sites of the IAP element should be detectable in the genomes of the AML cells from any type of independent AML. However, it is difficult to detect the specific integration sites due to the 1000 copies of the IAP provirus in the normal genome. Even though 2-dimensional genomic Southern blot analysis was used to visualize the whole provirus, non-IAP-derived genes and RFLP produced large numbers of background spots and interfered with the analysis.

3.1. Detection of AML-specific PCR product using IAP-specific primers

We attempted to amplify the integration sites by PCR using a primer corresponding IAP-LTR as one of a pair. To construct another primer, a sequence for the SINE-B2, a repetitive sequence with a high copy number (80 000–120 000) dispersed throughout the mouse genome, was used. Since both SINE-B2 and IAP have directions, four combinations can be analyzed as follows: (a) the region from the 5′-end of the IAP-LTR to the 3′-end of the SINE; (b) from IAP-LTR-5′ to SINE-5′; (c) from IAP-LTR-3′ to SINE-3′; (d) from IAP-LTR-3′ to SINE-5′.

To construct IAP-LTR-specific primers, we focused on the central area of the U3 region of the IAP-LTR. Examination of this area among IAP-LTR sequences registered in the GenBank database showed that they can be classified into two subtypes. One subtype is named the RS group which is similar to the IAP element isolated from C3H/He-derived AML cells [3], and the other is named the U group (Fig. 1a). Therefore, we constructed four primers for IAP-LTR (RS-IAP-F, U-IAP-F, RS-IAP-R and U-IAP-R). On the other hand, two primers in both directions corresponding to consensus sequences for SINE-B2 were prepared (SINE-B2-F and SINE-B2-R, Fig. 1b).

PCR amplification from SINE-B2 to IAP gave a limited number of DNA species which could be analyzed by agarose gel electrophoresis (Fig. 2). When the DNA area from the 5′-end of RS-IAP-LTR to the 3′-end of SINE-B2 was amplified using the reverse primer for RS-IAP-LTR and the forward primer for SINE-B2, the genomes of all leukemia cell strains, except L-8028, produced evident novel bands of different sizes (Fig. 2a, lanes 4–8) as compared with the normal genome (Fig. 2a, lanes 2 and 3). On the other hand, the U-IAP-LTR-specific primer gave different sizes and numbers of amplified bands (Fig. 2a, lane 1), though an AML genome-specific band was not detected (data not shown). Similarly, AML-specific bands were observed in the genomes of strains L-8028 and L-8065 at the area from RS-IAP-LTR-5′ to SINE-B2-5′ (Fig. 2b, lanes 5 and 7), in the L-8032 genome at the area from RS-IAP-LTR-3′ to SINE-B2-3′ (Fig. 2c, lane 6) and in the L-8002 and L-8032 genomes at the area from RS-IAP-LTR-3′ to SINE-B2-5′ (Fig. 2d, lanes 4 and 6). No RFLPs were observed among genomic DNA of spleen and liver from 15 different individuals of C3H/He mice containing different production lots (details not shown, see Fig. 2a–d, lanes 2 and 3). These results show that all five independent AML genomes have a novel structure lying between the IAP element and SINE-B2.

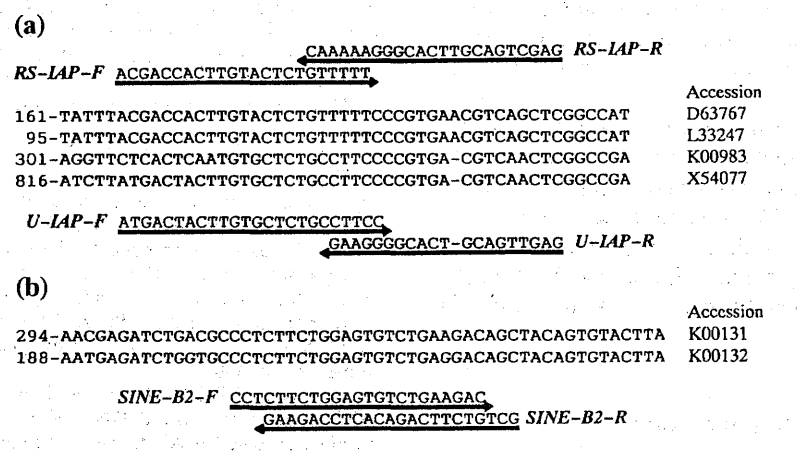

Fig. 1. Nucleotide sequences of parts of IAP-LTR and SINE-B2. a: Sequences at the center of the U3 region of IAP-LTR were compared with those from the GenBank database. Accession number D63767 is the sequence of IAP elements previously isolated from AML cells. PCR primers used in this study are mentioned at the top and bottom of the figure, with arrows indicating the direction (5′ to 3′) of the primers. b: The consensus sequence of SINE-B2 and corresponding primers are shown.

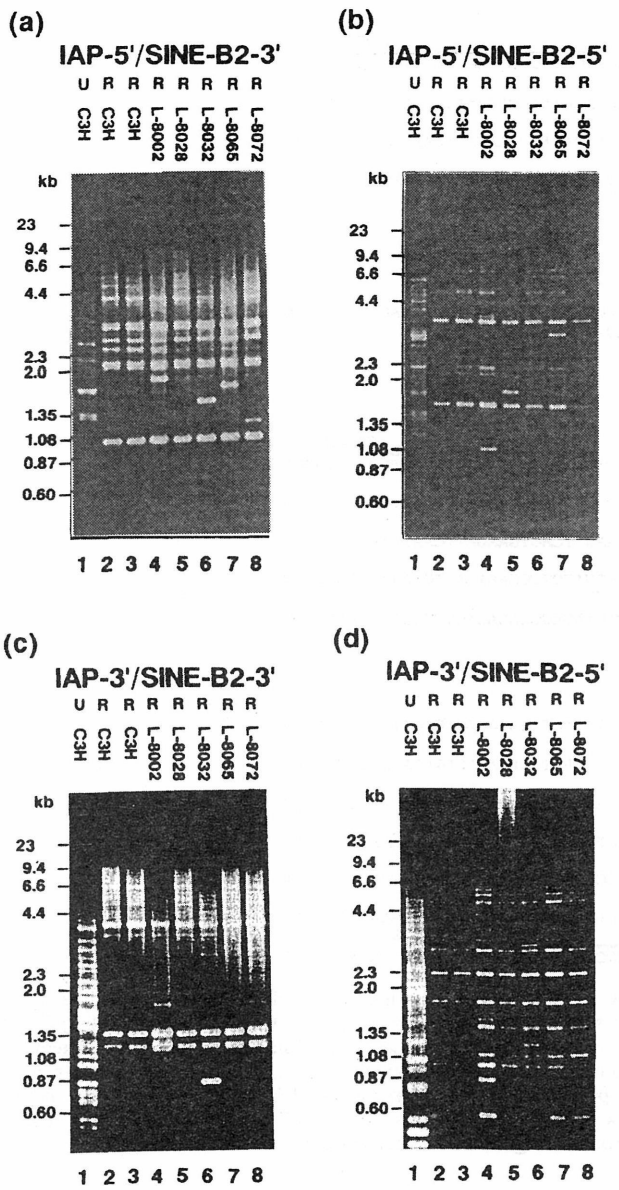

Fig. 2. PCR amplification of DNAs from germline and AML cells. DNAs from normal livers of C3H/He mice (lanes 2 and 3) and from AML cells of different origins (lanes 4–8) were PCR-amplified using RS-IAP-LTR primer (R) and SINE-B2 primer. Results of PCR following replacement of the RS-IAP-LTR primer with primer U (U) using germline DNA are shown in lane 1. a: Backward IAP-LTR plus forward SINE-B2. b: Backward IAP-LTR plus backward SINE-B2. c: Forward IAP-LTR plus forward SINE-B2. d: Forward IAP-LTR plus backward SINE-B2.

3.2. *Cloning and analysis of the AML-specific integration site of IAP*

The AML-specific PCR product was cloned and sequenced. Fig. 3a shows the nucleotide sequence at the junction of the IAP element isolated from the first PCR product of 1.7 kbp DNA derived from the L-8002 AML cell strain (Fig. 2a, lane 4). A sequence which was not found in the database was linked to the 5′-end of the IAP element.

To isolate the normal allele corresponding to the junction, inverted PCR was used. The nucleotide sequence of the first PCR product which was not related to any multicopy sequence recorded in the database was used to construct a pair of oligonucleotide primers (Q11-F and Q11-R, Fig. 3a) for the inverted PCR. The normal allele was amplified by inverted PCR when germline DNA was used. By comparing the sequences of the inverted PCR product and the first PCR product in Fig. 3a, the original structure before integration of the IAP element in L-8002 AML was estimated as shown in Fig. 3c. If the sequence is compatible with a normal allele, a part of the sequence which is not found in Fig. 3a must be linked to the 3′-end of the IAP element in the L-8002 genome. To confirm this, a PCR primer (Q11-B) was prepared based on the germline sequence shown in Fig. 3c. By priming Q11-B plus RS-IAP-F for PCR, amplification of a single band was detected using DNA from L-8002 AML cells but not using other genomic DNAs. The product was sequenced as shown in Fig. 3b and contained the junction of the 3′-end of the IAP element and the genomic sequence. When these three sequences were compared, a target duplication of 6 bp long which was generated by retrotransposition was found. Therefore, it is suggested that the construction of the AML-specific structure (Fig. 3a,b) occurred by retrotransposition of IAP at the normal site (Fig. 3c) during or after leukemogenesis of L-8002 AML cells.

Similarly, subsequent PCR and sequencing analyses were performed using the first PCR product of 1.5 kbp DNA derived from L-8065 AML (Fig. 2a, lane 7). The sequences obtained were compared as described above. Fig. 3d shows the target duplication site and surrounding germline sequence where the arrangement occurred in the L-8065 genome.

3.3. *Genomic Southern blot analysis*

Evidence for IAP-derived rearrangement in AML cells was further supported by Southern analysis of genomic DNA from normal and AML cells. It is expected that both PCR products of the normal allele using Q11-R plus Q11-B (Fig. 3c) or Q14-R plus Q14-B (Fig. 3d) primers can be used as probes for the analysis, since there are no repetitive or repeated sequences. Actually, a single size of DNA was definitely detected by PCR using either of these primer pairs (data not shown). These PCR products were thus used as probes. They hybridized to the corresponding allele in the genomic DNA without any artificial bands (Fig. 4). Rearrangement in half of the allele of the genome was observed only in L-8002 DNA with the Q11 probe (Fig. 4a, lane 2). When the Q14 probe was used, it appeared that both alleles in the L-8065 genome contained rearrangement (Fig. 4b, lane 5). No RFLP was detected among germline DNAs from 15 C3H/He mice in this study (data not shown).

4. Discussion

It is well known that the genomes of most tumor cells contain a variety of abnormal structures, and at least part of them contribute to properties of the tumor. Since rearranged genes activated by IAP-mediated retrotransposition were found in several murine tumor cell lines, the possibility that IAP-mediated retrotransposition is one of the mechanisms responsible for tumorigenic changes has been put forward [4,5]. Activation of the retrotransposition can increase the frequency of gene rearrangement and some of these events may affect the function of genes close to the integration site due to the insertion of a functional LTR sequence [6] or disruption of the target gene structure. Indeed, most of such

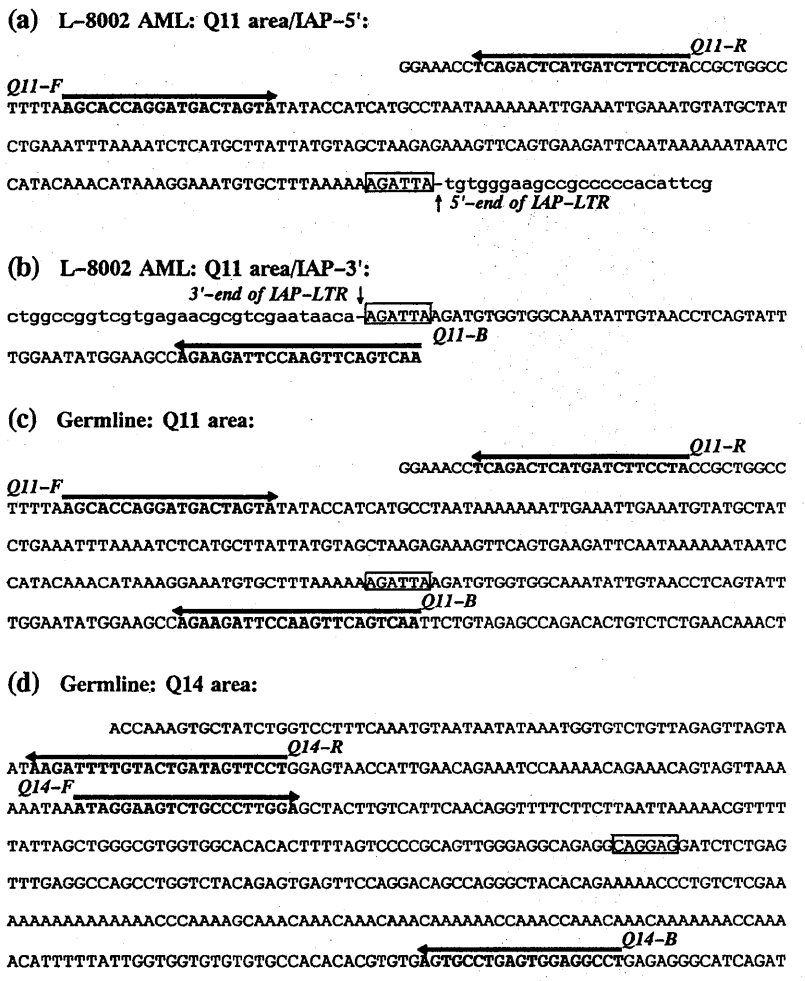

Fig. 3. Nucleotide sequences of target sites for IAP elements specific to AML strains. Small letters indicate the IAP-element-derived sequence. Bold letters with arrows showing the directions correspond to primers used in subsequent PCR analyses (Q11-F, Q11-R, Q11-B, Q14-F, Q14-R and Q14-B). The target duplication site for IAP-mediated retrotransposition site is boxed. a: Sequence of the junction of the IAP element (5'-side) from L-8002 AML cells of a 1.5 kb fragment (Fig. 2, lane 4). b: Sequence of another junction of the IAP element (3'-side) from an abnormal allele in L-8002 AML cells. c: Sequence of a normal allele corresponding to (a) and (b) estimated by comparison of (a) and the inverted PCR product from germline DNA. d: Sequence of a normal allele where the retrotransposition of IAP occurs in the L-8065 genome estimated by sequence comparison in subsequent analyses of a 1.5 kb PCR product (Fig. 2, lane 7) derived from L-8065 AML cells.

integrated genes are attributed to changes in gene function as discussed elsewhere [3]. If the retrotransposition occurs frequently in a tumor cell line, integrated IAP elements must be detectable with or without functional changes in the cell line. However, the tumor-specific insertion of an IAP element as a result of retrotransposition is hard to detect since the normal murine genome naturally possesses 1000 copies of the IAP element.

The IAP elements have been divided into subtypes based on their physical structure [5] and on the sequence heterogeneity of LTR [13,14]. Using 34 LTR sequences of different IAPs in the GenBank database, we compared the central area of the U3 region which has a low level of heterogeneity. Seven of these 34 sequences were similar to the IAP that was isolated from one of the AML cells reported previously [3] and were named as the RS subtype. The total amount of the RS subtype can be estimated at ca. 200 copies per mouse genome. We designated a PCR primer corresponding to the RS-LTR to analyze members of this group selectively (Fig. 1).

In this study, we amplified part of the integration site of the IAP element by PCR using a primer set of the RS-IAP and the SINE-B2, a retroposon which is a widely dispersed element in the mouse genome (Fig. 1). Therefore, sequences between the IAP element and SINE-B2 less than 4 kbp in size were analyzed. Whereas the PCR products of all genomic DNA from normal C3H/He mice were identical, unique bands were observed only when the genomes of AML cells were used (Fig. 2). The unique IAP integration sites were confirmed by subsequent analyses using two examples of the PCR product (Figs. 3 and 4). One allele in the L-8002 genome was rearranged at the Q11-related locus (Fig. 4a) showing the typical structure of retrotransposition-mediated rearrangement. However, both alleles in the L-8065 genome were rearranged at the Q14-related locus (Fig. 4b), and this was probably due to loss of the normal allele after retrotransposition by chromosomal heterogeneity. The most important point in this study was that unique integration sites were commonly observed among different AML cells generated independently (Fig. 2). This fact strongly suggests the universality of this event at least in radiation-induced AML from C3H/He mice.

In the PCR analyses, a total number of 30 sites (Fig. 2) were detected out of ca. 400 junctions of RS-type IAP in the

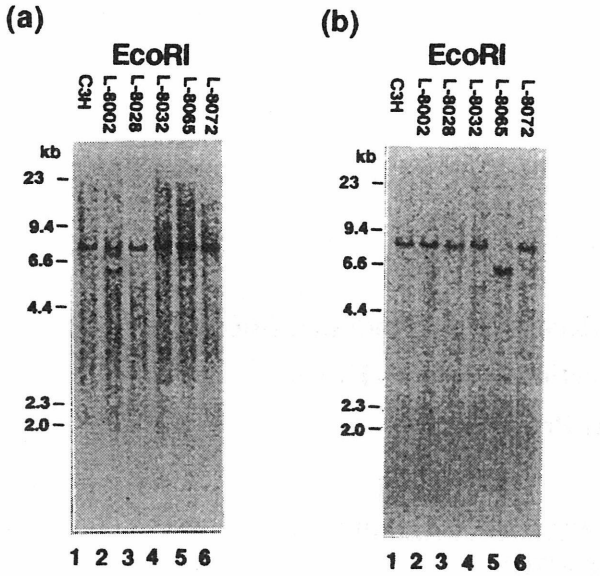

Fig. 4. Genomic Southern analysis. Each lane contained 10 mg of total DNAs from germline and AML cells digested with *Eco*RI. Probes from PCR products primed with Q11-R plus Q11-B (a) and with Q14-R plus Q14-B (b) were used. Lane 1, germline DNA; lane 2, L-8002 AML; lane 3, L-8028 AML; lane 4, L-8032 AML; lane 5, L-8065 AML; lane 6, L-8072 AML.

genome. From the fact that all independent AML cells tested gave 2–3 unique junctions, it is expected that there are 400/30 times the observed number present in the genome in AML cells. If the integration occurred randomly throughout the genome, this number seems too small to cause drastic changes in leukemia cells. However, IAP-mediated gene rearrangements have been observed around a locus of tens of kilobases containing the interleukin-3 gene in distinct cell lines [3,7–9,15,16]. Additionally, IAP-mediated retrotransposition adjacent to the *agouti* locus in germline cells was also reported by different authors [17,18]. Both of them suggest the presence of loci which are susceptible to incorporation of IAP elements in the mouse genome. If so, the 20–30 novel integration events may be sufficient to induce marked changes in the properties of AML cells. In addition, Lepage et al. reported that amplification of a multidrug resistance gene in a doxorubicin-resistant derivative of the P388 cell line is the consequence of insertion of an IAP element [19]. If insertion of the IAP element stimulates gene amplification at the target site, a limited number of IAP-mediated retrotransposition event gives greater cytological effects.

At present, there is no answer to the question whether the retrotransposition event is limited in C3H/He mouse-derived tumors, AML-related tumors or radiation-induced tumors. Investigation of a wide variety of types of cells including those from tumors and transformed cells by our method should answer the above question.

References

[1] Seki, M., Yoshida, K., Nishimura, M. and Nemoto, K. (1991) Radiat. Res. 127, 146–149.
[2] Hayata, I., Seki, M., Yoshida, K., Hirashima, K., Sado, T., Yamagiwa, J. and Ishihara, T. (1983) Cancer Res. 43, 367–373.
[3] Tanaka, I. and Ishihara, H. (1995) FEBS Lett. 376, 146–150.
[4] Keshet, E., Schiff, R. and Itin, A. (1991) Adv. Cancer Res. 56, 215–251.
[5] Kuff, E.L. and Lueders, K.K. (1988) Adv. Cancer Res. 51, 183–276.
[6] Lamb, B.T., Satyamoorthy, K., Solter, D., Basu, A., Xu, M.Q., Weinmann, R. and Howe, C.C. (1992) Mol. Cell. Biol. 12, 4824–4833.
[7] Ymer, S., Tucker, W.Q.J., Sanderson, C.J., Hapel, A.J., Campbell, H.D. and Young, I.G. (1985) Nature 317, 255–258.
[8] Hirsh, H.H., Nair, A.P.K. and Moroni, C. (1993) J. Exp. Med. 178, 403–411.
[9] Algate, P.A. and McCubrey, J.A. (1993) Oncogene 8, 1221–1232.
[10] Lepage, P., Devault, A. and Gros, P. (1993) Mol. Cell. Biol. 13, 7380–7391.
[11] Sambrook, J., Fritsch, E.F. and Maniatis, T. (1989) Molecular Cloning: A Laboratory Manual, 2nd edn., Cold Spring Harbor Laboratory, Cold Spring Harbor, NY.
[12] Triglia, T., Peterson, M.G. and Kemp, D.J. (1989) Nucleic Acids Res. 16, 8186.
[13] Christy, R.J., Brown, A.R., Gourlie, B.B. and Huang, R.C.C. (1985) Nucleic Acids Res. 13, 289–302.
[14] Mietz, J.A. and Kuff, E.L. (1992) Mamm. Genome 3, 447–451.
[15] Duhrsen, U., Stahl, J. and Gough, N.M. (1990) EMBO J. 9, 1087–1096.
[16] Leslie, K.B., Lee, F. and Schrader, J. (1991) Mol. Cell. Biol. 11, 5562–5570.
[17] Michaud, E.J., vanVugt, M.J., Bultman, S.J., Sweet, H.O., Davisson, M.T. and Woychik, R.P. (1994) Genes Dev. 8, 1463–1472.
[18] Duhl, D.M.J., Vrieling, H., Miller, K.A., Wolff, G.L. and Barsh, G.S. (1994) Nature Genet. 8, 59–64.
[19] Stocking, C., Loliger, C., Kawai, M., Suciu, S., Gough, N. and Ostertag, W. (1988) Cell 53, 869–879.

J. RADIAT. RES., 38, 111–120 (1997)

Acceleration of Granulocytic Cell Recovery in Irradiated Mice by a Single Subcutaneous Injection of a Heat-Killed *Lactobacillus casei* Preparation

MASAKO FURUSE[1], KAZUKO TSUNEOKA[1]*, KAZUMI UCHIDA[2] and KOJI NOMOTO[2]

[1]Bioregulation Research Group, National Institute of Radiological Sciences, 4–9–1 Anagawa, Inage-ku, Chiba 263, Japan.
[2]Yakult Central Institute for Microbiological Research, Yaho 1796, Kunitachi 186, Japan.

(*Received, March 27, 1997*)
(*Revision received, May 26, 1997*)
(*Accepted, June 2, 1997*)

***Lactobacillus casei*/flow cytometry/radioprotection/granulocyte/lymphocyte**

Flow cytometric analysis showed that the treatment of irradiated mice with a heat-killed *Lactobacillus casei* preparation (LC 9018) accelerated the recovery of granulocytic cell populations in peripheral blood, spleen and femur bone marrow. The recovery of the lymphocytic cell population was not accelerated while the recovery of the B-lymphocytic cell population was inhibited. Histological analysis also showed that the LC-9018 treatment markedly enhanced granulopoiesis in the spleen and bone marrow of irradiated mice. The same LC-9018 treatment significantly increased 30-day survival rates of athymic nude mice after lethal whole-body irradiation. The recovery of the granulocytic cell population in peripheral blood of irradiated athymic nude mice was also accelerated by LC-9018 treatment. Our results suggest that LC 9018 protected lethally irradiated mice from bone marrow death by enhancing granulopoiesis rather than lymphopoiesis and that the contribution of activated T lymphocytes to the enhancement of the granulopoiesis was small.

INTRODUCTION

Several kinds of cytokines and cytokine inducers exhibit a protective effect in irradiated animals by enhancing the recovery of the hematopoietic system[1–7]. Recombinant cytokines and cytokine inducers are used for medical treatment of myelosuppression in humans after radiation accidents[8,9] or chemotherapy and radiotherapy for cancer[10–13]. Cytokines and cytokine inducers seem to stimulate the cytokine network and activate the biodefense system in the body[14,15].

One cytokine inducer, a heat-killed *Lactobacillus casei* preparation (LC 9018), has been reported to accelerate the phagocytic function of the reticuloendothelial system in mice[16]. Administration of LC 9018

* Corresponding author

Abbreviations: LC 9018, a heat-killed preparation of *Lactobacillus casei* YIT 9018; G-CSF, granulocyte colony-stimulating factor; GM-CSF, granulocyte macrophage colony-stimulating factor; M-CSF, macrophage/monocyte colony-stimulating factor; IL-3, interleukin 3; CSA, colony-stimulating activity

enhanced the production of colony-stimulating activity (CSA) by the peritoneal macrophages. The CSA enhanced the maturation of the bone marrow cells to macrophages and polymorphonuclear cells that showed strong antitumor activity in vivo and in vitro[17]. We previously reported that administration of LC 9018 had a protective effect in mice given a lethal dose of irradiation when it was subcutaneously injected within 10 hrs after irradiation[18,19]. LC 9018 promoted the recovery of hematopoietic stem cells such as spleen colony forming units and colony forming cells in culture in irradiated mice. In the present study, we show that the enhancement of granulopoiesis contributes most to the radioprotective effect of LC 9018 on lethally irradiated mice and not the enhancement of lymphopoiesis. Further, we show that the T cell population does not contribute to the enhancement of the granulopoiesis by LC-9018 treatment.

MATERIALS AND METHODS

Mice and irradiation.

Male C3H/He and BALB/c (nu/nu) (athymic nude) mice (10–15 weeks old) were used. They were bred and maintained under specific pathogen free conditions in the facilities of our institute. Irradiation was to the whole body with a source of ^{137}Cs γ ray (Toshiba γ Ray Irradiator model RSG-50) at a dose rate of about 60 cGy/min. All other procedures were as described[19]. LC 9018 was suspended in saline and subcutaneously injected at a dose of 1 mg/mouse/0.1 ml into the inguinal region immediately after irradiation. A phosphate buffered saline was injected into the control mice immediately after irradiation.

Flow cytometric analysis of hematopoietic cells in the irradiated mice.

Peripheral blood was collected from the femoral artery under ether anesthesia. The spleen and bone marrow were taken from the sacrificed mice, and single cell suspensions were made. Flow cytometry was performed with a fluorescence activated cell sorter, FACScan (Becton Dickinson), following the method described in the manual. Briefly, to 100 μl of blood or 50 μl (10^6 cells) of spleen or bone marrow cell suspension, the lineage specific antibodies were added. After 20 min. incubation at 4°C, a lysing solution (Becton Dickinson) was added for lysis of the erythrocytes. After centrifugation at 350 × g, the cell pellet was washed with 2 ml of 0.1% NaN_3/1% FCS/PBS twice. For each sample, 10,000 events were collected using an open gate. Lysis II software (Becton Dickinson) was used for analysis. Fluorescein isothiocyanate (FITC) conjugated anti-mouse CD11b (Mac-1), R-Phycoerythrin (R-PE) conjugated anti-mouse CD45R/B220, FITC conjugated anti-mouse CD90 (Thy 1.2), and R-PE conjugated anti-mouse Gr-1/myeloid differentiation antigen monoclonal antibodies were used as the lineage specific antibodies. FITC conjugated rat IgG_{2a} and FITC conjugated rat IgG_{2b} were used as nonspecific controls. To block the Fc receptor, anti-mouse CD32/CD16 monoclonal antibody was used. All antibodies and labeled immunoglobulins were purchased from PharMingen (San Diego CA). The granulocyte area, the lymphocyte area and the monocyte area were gated in the forward scatter (cell size) versus the right angle light scatter (granularity) profile. The Gr-1 and Mac-1 positive cells gated in the granulocyte area were assigned to the granulocytic cells, while Thy 1.2 positive cells or B220 positive cells gated in the lymphocyte area were assigned to the T-lymphocytic or B-lymphocytic cells, respectively. The Gr-1 low and Mac-1 positive cells gated in the monocyte area were assigned to the monocytic cells.

Histological examination of hematopoietic tissue.

The spleen, the femoral bone marrow and the small intestines were removed from the mice subcutaneously treated with LC 9018 immediately after irradiation (8.5 Gy). The tissues were fixed in 10% buffered formalin and processed for paraffin sectioning, followed by hematoxylin-eosin (H-E) staining for photomicroscopy. Two mice were used at each point.

Other methods

Leukocytes were counted using a hematocytometer (Sysmex K 1000). The statistical processing was carried out by Student's t-test for cell number (Fig. 1–3) or generalized Willcoxson test for 30-day survival (Fig.4).

RESULTS

Cellularity in Irradiated Mouse Hematopoietic Tissues

The recovery of the nucleated cell number in irradiated mouse hematopoietic tissues treated with LC 9018 was promoted compared with those treated with saline (Fig. 1). On the 8th day after irradiation, the leukocyte numbers in blood and the nucleated cell numbers in spleen and femoral bone marrow were increased significantly in LC-9018 treated mice compared with saline treated mice. By day 13, a critical time for hematopoietic death, the leukocyte numbers in blood had increased 8-fold, and the nucleated cell number had increased 9-fold in the spleen, and 1.6-fold in the bone marrow in LC-9018 treated mice compared with saline treated mice. On day 21 after irradiation, in the LC-9018 treated mice, spleen cell numbers were slightly elevated over the normal level, but the leukocyte number in the blood and the nucleated cell number in the marrow had recovered almost to the levels in normal mice. In the saline treated mice, the leukocyte number in the blood and the nucleated cell number in the spleen surpassed those in the LC-9018 treated and normal mice. In the bone marrow, the recovery was slow despite an early beginning.

Flow Cytometric Analysis of Hematopoietic Cells on the 13th Day after Irradiation.

The 13th day after irradiation is a critical time for bone marrow death of lethally irradiated mice. To establish which lineage specific cell population contributed most to the protection of mice from bone marrow death, we analyzed in detail the hematopoietic cells using flow cytometry (Fig. 2). The results showed that the percentage of granulocytic cells (Gr-1 and Mac-1 positive cells) was high in the LC-9018 treated mice. In the peripheral blood, about 50% of the leukocytes were taken up by granulocytic cells. In the spleen, the granulocytic cell population was greater than normal, however it was the same as in the bone marrow. On the other hand, in saline treated mice, the percentage of granulocytic cells in the peripheral blood, the spleen and especially the bone marrow was low.

The B-lymphocytic cell population was reduced in the LC-9018 treated mice, while in the saline treated mice, it was increased relative to the normal mice. The percentage of B-lymphocytic cells to total nucleated cells was highest in the bone marrow (60%). The T-lymphocytic cell population in both irradiated groups was reduced relative to non-irradiated mice.

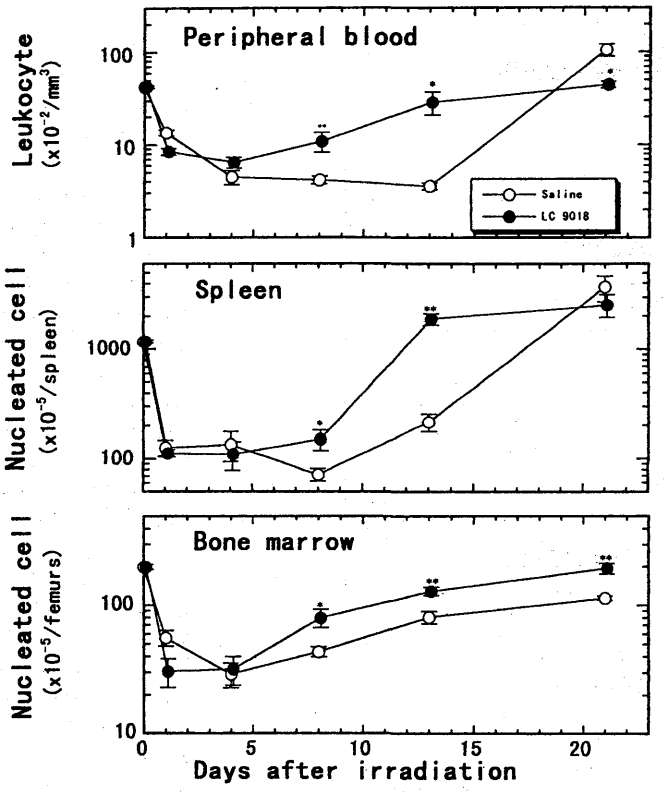

Fig. 1. Changes in blood leukocyte number and nucleated cell number in the spleen and bone marrow in 6.0-Gy whole-body irradiated mice. LC 9018 (closed circles) or saline (open circles) were injected into C3H/He male mice immediately after irradiation. Each point (upper panel) represents the mean value ± SE for 7–10 mice. Spleen or bone marrow cells were pooled for each group of 3 mice. Each point (middle and lower panels) represents the mean value ± SE for 3 independent experiments. Asterisks indicate statistical significance of the difference between the saline-treated and LC-9018 treated mice; $p < 0.01$(**), $p < 0.05$(*).

Change in the Cell Distribution in the Peripheral Blood of Irradiated Mice.

In the LC-9018 treated mice, the recovery of the granulocytic cell population was remarkably accelerated (Fig. 3). It increased to 3 times the normal level on the 13th day after irradiation. In contrast, in the saline treated mice, in spite of the increase in granulocytic cell number observed on day 8, a decrease was observed on day 13. A similar decrease in granulocytic cell population on day 13 after irradiation was observed in both the spleen and bone marrow of saline treated mice (data not shown). The T-lymphocytic cell population in the LC-9018 treated mice recovered slowly in a manner similar to that observed in the saline treated mice (Fig. 3) and had reached 3% of the normal level by day 13. The B-lymphocytic cell population also recovered slowly, as did the T-lymphocytic cell population. However, the B-lymphocytic cell population in the saline treated mice was 5-fold that in LC-9018 treated mice on day 13 after irradiation.

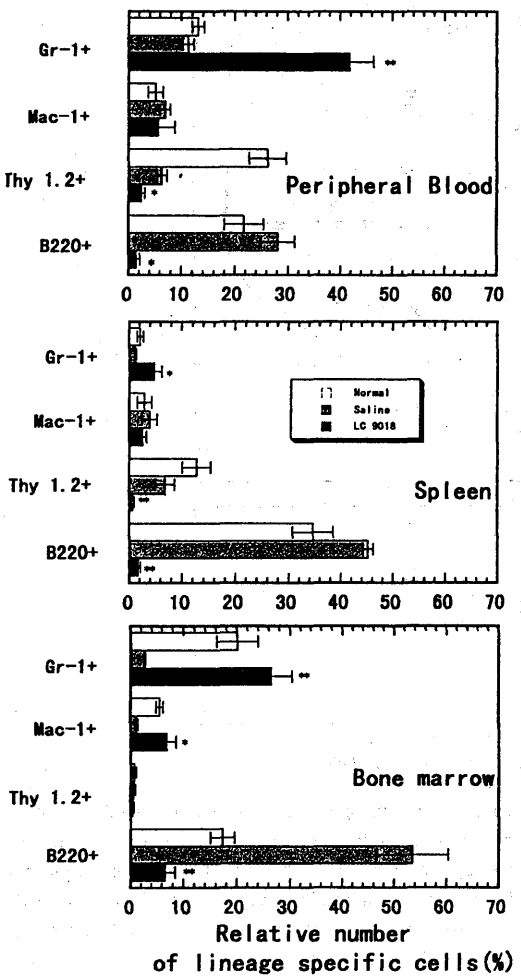

Fig. 2. Effect of LC-9018 treatment on the relative number of lineage specific hematopoietic cells on day 13 after 6.0-Gy irradiation. C3H male mice were treated as in Fig. 1. The same number of cells from individual mice were pooled for each group of 3 mice. Gr-1$^+$, Mac-1$^+$, Thy 1.2$^+$ and B220$^+$ in the Figure represent Gr-1 and Mac-1 positive cells (granulocytic cells), Gr-1 low Mac-1 positive cells (monocytic cells), Thy 1.2 positive cells and B220 positive cells, respectively. Each bar represents the mean value ± SE for 3 independent experiments (□, non-irradiated normal; ■, saline treatment; ■, LC-9018 treatment). Asterisks indicate statistical significance of the difference between the saline-treated and LC-9018 treated mice; $p < 0.01$(**), $p < 0.05$(*). Total white blood cell number was 42.3 ± 1.3 (non-irradiated normal), 3.6 ± 0.29 (saline treatment), and 29.1 ± 8.3 (LC-9018 treatment) × 10^2 per mm^3. Total nucleated cell number of spleen was 1183 ± 35 (non-irradiated normal), 217.6 ± 40 (saline treatment), and 1886 ± 228 (LC-9018 treatment) × 10^5 per spleen. Total nucleated cell number of bone marrow was 199.4 ± 8.4 (non-irradiated normal), 80.8 ± 9,0 (saline treatment), and 129.4 ± 10.2 (LC-9018 treatment) × 10^5 per two femurs.

Radioprotection of Lethally Irradiated Athymic Nude Mice by LC-9018 Administration.

Because the damage to lymphocytes in irradiated mice was more severe than to granulocytes or monocyte/macrophages, the recovery of T-lymphocytic cell numbers appeared later and had scarcely reached 3% of the normal lymphocytic cell numbers by day 13 after irradiation (Fig. 3), a critical time for bone marrow death. To establish whether the T-lymphocyte population contributed to the radioprotection of irradiated mice from bone marrow death, we injected LC 9018 into irradiated athymic nude mice. The administration of LC 9018 significantly increased the 30-day survival rates of lethally irradiated athymic nude mice (Fig. 4). On the 13th day after 4.5 Gy irradiation, the number of Gr-1 positive cells in the blood of the nude mice was 8.53 ± 1.27 (non-irradiated normal), 1.37 ± 0.08 (saline treatment), and 13.85 ± 7.95 (LC-9018 treatment) x 10^2/mm^3 (The mean value ± SE for 3 mice). Acceleration of granulocytic cell recovery by LC-9018 treatment was also observed in athymic nude mice.

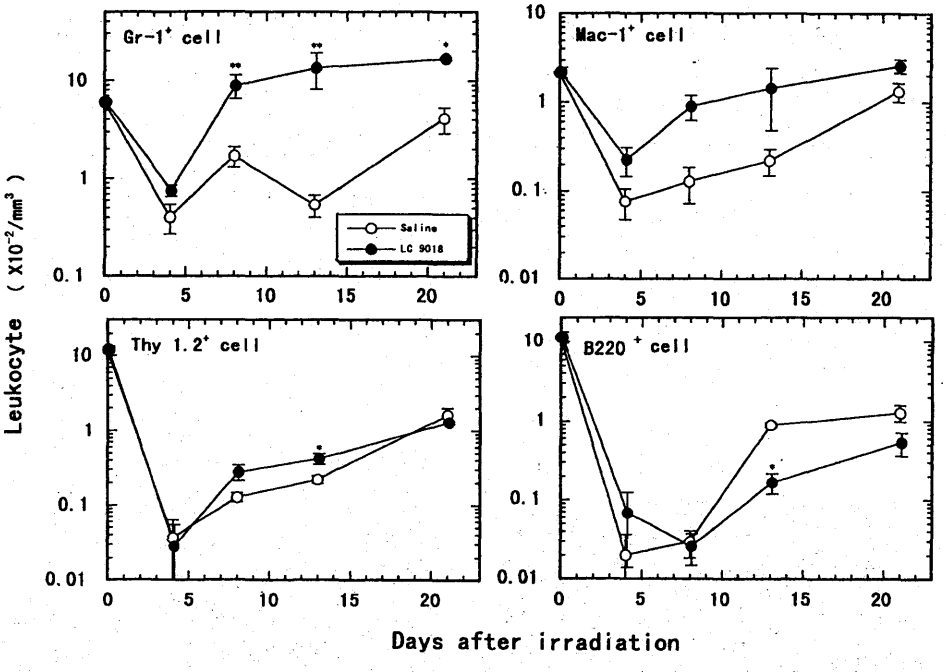

Fig. 3. Time cause of lineage specific cell populations of leukocytes in 6.0-Gy irradiated mouse blood. Mice were treated as in Fig. 1. The same number of leukocytes from individual mice were pooled for each group of 3 mice for flow cytometric analysis. The cell number in the figure indicates the relative cell number multiplied by the number of leukocytes in blood. Each point represents the mean value ± SE for 3 independent experiments (open circles, saline treatment; closed circles, LC-9018 treatment). Asterisks indicate significant differences from saline treatment; $p < 0.01$ (**), $p < 0.05$ (*)

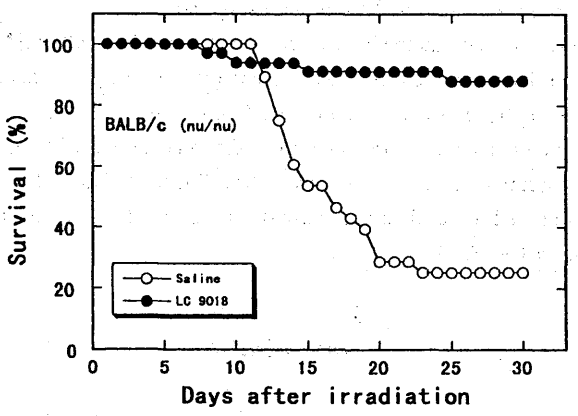

Fig. 4. The radioprotective effect of LC 9018 on 6.0-Gy irradiated athymic nude mice treated with LC 9018. Athymic nude mice, 15 weeks old, were treated with LC 9018 (n = 33, closed circles) or saline (n = 28, open circles) immediately after whole-body irradiation. The difference between LC-9018 treatment and saline treatment is statistically significant at $p < 0.001$ by the generalized Willcoxson test.

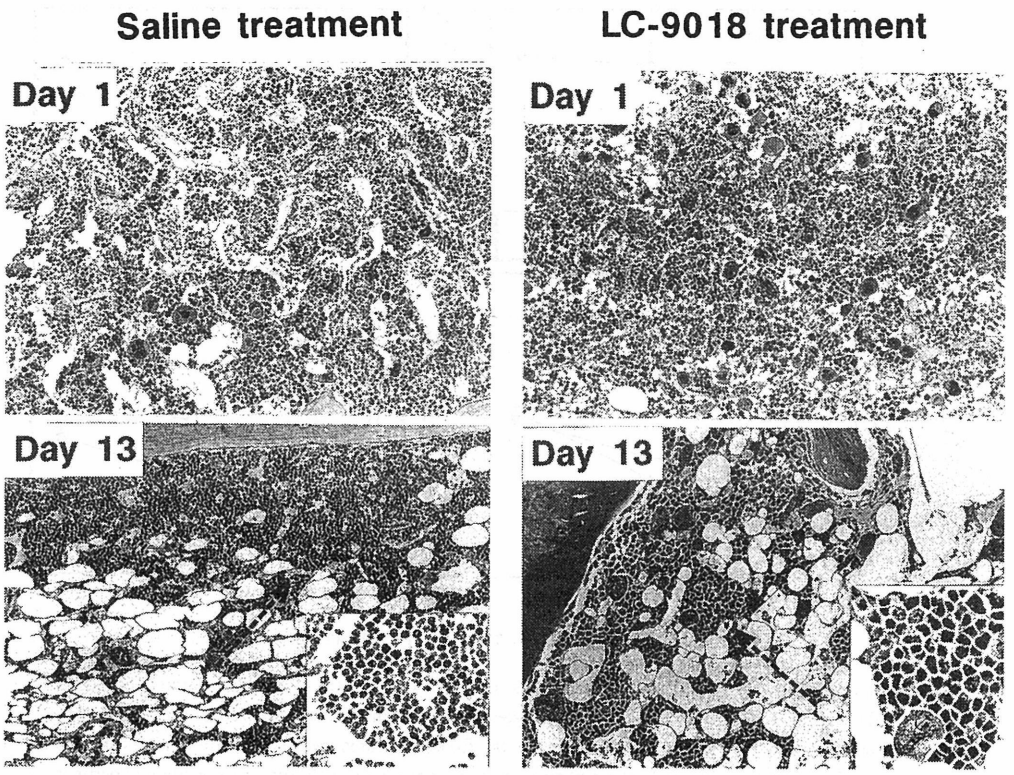

Fig. 5. Histology of the femoral bone marrow of 8.5-Gy irradiated mice (× 175). Further magnification of the area indicated by an arrow is shown in the lower right-hand corner (× 480).

Histological Examination of the Irradiated Mouse Hematopoietic Tissues.

Histological analysis showed that the bone marrow cells were markedly injured by 8.5-Gy total-body irradiation (Fig. 5 Day 1). There was no difference in the degree of injury to hematopoietic tissue by 8.5-Gy irradiation between the LC-9018 treatment and the saline treatment. On the 13th day after irradiation, granulopoiesis in the bone marrow was observed only in the mice treated with LC 9018 (Fig. 5 Day 13). In contrast, lymphopoiesis occurred in the bone marrow in the saline treated mice. Similar results were observed in the spleen of the irradiated mice (data not shown). These results were consistent with the results of analysis using flow cytometry (Fig.2).

DISCUSSION

To elucidate know which lineage specific cell population contributed to the protection of lethally irradiated mice from bone marrow death, we analyzed hematopoietic cells on the 13th day after irradiation. The results showed that the granulocytic cell population in LC-9018 treated mice was significantly increased relative to saline treated mice (Fig. 2). Cytokines have been reported to remove neutrophils from tissues and

put then into circulation about 10 hs after administration[20]. But the high percentage of granulocytic cells in irradiated mice treated with LC 9018 was not the cause of this removal because similar percentages were obtained in all tissues examined. An analysis of the time course of cellularity in peripheral blood also revealed an augmentation of granulocytic cell hemopoiesis in irradiated mice treated with LC 9018. We observed that LC 9018 increased myeloid progenitor cell numbers in sublethally irradiated mouse bone marrow on day 7 after administration[19]. This increase may prevent the depletion of the granulocytic cell population observed on day 13 in irradiated mice treated with saline (Fig. 3).

Kishimoto et al. have reported that both the expression and activity of Mac-1 are greatly increased after neutrophil activation[21]. Cells gated in the granulocyte area in the forward scatter versus the right angle light scatter profile were almost all Gr-1 and Mac-1 positive. But, no significant increase in the intensity of Mac-1 due to LC-9018 treatment was observed. Studies using flow cytometry are now in progress to determine the expressions of the other receptors related to neutrophil activation.

LC-9018 treatment accelerated the recovery of the granulocytic cell population, but inhibited the recovery of the B lymphocytic cell population on the 13th day (Fig. 2 and Fig. 3). Colony-stimulating factors such as G-CSF, GM-CSF or IL-3, and other cytokines have been reported to suppress primary B lymphopoiesis[22-25]. Various cytokines produced by LC-9018 treatment may participate in the acute inhibition of B lymphopoiesis in irradiated mice. It is unknown whether acute suppression of B lymphopoiesis by LC 9018 treatment is related to the enhancement of the granulocytic cell population.

Some substances have been reported to impart hematopoietic rescue via the activation of T cells, yet are ineffective in athymic nude mice[26,27]. In irradiated mice treated with LC 9018, the recovery of the T-lymphocytic cell population was slow, and was only 3% of the normal level on the 13th day after irradiation, a crucial time for bone marrow death. Lymphocytes seemed not to contribute to the radioprotective effects of LC 9018 in lethally irradiated mice. However, it is possible that a small portion of activated lymphocytes secrete the cytokines that protect the irradiated mice by stimulating myelopoiesis. To clarify whether the T lymphocytic cell population contributes to the radioprotective effect of LC 9018, we injected LC 9018 into the athymic nude mice. The LC-9018 treatment significantly increased the 30-day survival ratios of lethally irradiated nude mice (Fig. 4). This result indicates that there was little contribution by the T lymphocytes to the radioprotection of lethally irradiated mice. Kato et al. reported that LC-9019 treatment augmented the natural killer cell activity of spleen cells[28] and Su et al. reported T-cell-deficient mice (nude and scid mice) exhibited high NK cell activity for longer periods of time post-infection[29]. The radioprotective effect of LC 9018 on irradiated nude mice may be dependent on the activation of NK cells in addition to augmentation of granulocytic cell numbers.

We previously reported that LC 9018 increased the level of M-CSF mRNA and GM-CSF mRNA in irradiated mouse livers and increased the activity of macrophage colony-stimulating factor (M-CSF) in serum[18,19]. Okitsu-Negishi et al. have reported that the water-soluble cell wall extract from *Lactobacillus casei* stimulated the production of inflammatory cytokines such as IL-1, TNFα and IL-6 by mouse peritoneal macrophages in vitro[31]. On the other hand, Ishihara et al. showed that the expression of IL-1β mRNA in mouse spleen macrophages was enhanced by whole body X-irradiation[32,33]. LC-9018 treatment seems to further stimulate the body's biodefense system against irradiation and to result in enhancement of granulopoiesis in irradiated mice. Our results suggest that LC-9018 treatment protected mice exposed to a lethal dose of irradiation through the stimulation of granulopoiesis by cytokines induced by activated macrophages not by activated T lymphocytes.

ACKNOWLEDGEMENTS

We thank Dr. M. Shikita for helpful comments on the manuscript, and Dr. T. Yokokura for encouragement.

REFERENCES

1. Tanikawa, S., Nakao, I., Tsuneoka, K., and Nara, N. (1989) Effects of recombinant granulocyte colony-stimulating factor (rG-CSF) and recombinant granulocyte-macrophage colony- stimulating factor (rGM-CSF) on acute radiation hematopoietic injury in mice. Exp. Hematol. **17**: 883–888.
2. Zsebo, K. M., Smith, K. A., Hartley, C. A., Greenblatt, M., Cooke, K., Rich, W. and McNiece, I. K. (1992) Radioprotection of mice by recombinant rat stem cell factor. Proc. Natl. Acad. Sci. USA **89**: 9464–9468.
3. Macvittie, T. J., Monroy, R. L., Patchen, M. L. and Souza, L. M. (1990) Therapeutic use of recombinant human G-CSF (rh G-CSF) in a canine model of sublethal and lethal whole-body irradiation. Int. J. Radiat. Biol. **57**: 723–736.
4. Aoki, Y. (1986) Protective action of OK-432 (Picibanil^{R}) on the radiation-induced myelosuppression: Examination of its action in the whole body irradiated mice. Nippon Acta Radiologica **46**: 1324–1330.
5. Kalechman, Y., Gafter, U., Barkai, I. S., Albeck, M. and Sredni, B. (1993) Mechanism of radioprotection conferred by the immunomodulator AS101. Exp. Hematol. **21**: 150–155.
6. Guenechea, G., Albella, B., Bueren J. A., Maganto, G., Tuduri, P., Guerrero, A., Pivel, J. P. and Real. A. (1997) AM218, a new polyanionic polysaccharide, induces radioprotection in mice when administered shortly before irradiation. Int. J. Radiat. Biol. **71**: 101–108.
7. Fedorocko, P., Brezani. P. and Mackova, N. O. (1992) Radioprotection of mice by the bacterial extract Broncho-Vaxom^{R}: haemopoietic stem cells and survival enhancement. Int. J. Radiat. Biol. **61**: 511–518.
8. Gale, P. R. and Butturini, A, (1990) The role of hematopoietic growth factors in nuclear and radiation accidents. Exp. Hematol. **18**: 958–964.
9. Butturini, A., Souza, P. C. D., Gale, R. P., Cordiero, J. M., Lopes, D. M., Neto, C., Cunha, C. B., Souza, C. E. P. D., Ho, W. G., Tabak, D. G., Sanpai, J. M., Burla, A. and The Navy Hospital Radiation Team (1988) Use of recombinant granulocyte- macrophage colony stimulating factor in the Brazil radiation accident. The Lancet, August **27**: 471–475.
10. Adamietz, I. A., Rosskopf, B., Dapper, F. D., Lieven, H. and Boettcher, H. D. (1996) Comparison of two strategies for the treatment of radiogenic leukopenia using granulocyte colony stimulating factor. Int. J. Radiat. Oncol. Biol. Phys. **35**: 61– 67.
11. Sakata, K., Aoki, Y., Muta, N., Therahara, A., Karasawa, K., Onogi, Y., Nakagawa, K., Hasezawa, K., Sasaki, Y. and Akanuma, A.(1993) Effect of human granulocyte colony- stimulating factor on neutropenia induced by radiotherapy and chemotherapy. Oncology **50**: 238–240.
12. Yoshida, T., Hirashima, K., Asano, S. and Takaku, F. (1991) A phase II trial of recombinant human granulocyte colony- stimulating factor in the myelodysplastic syndromes. Brit. J. Haematol. **78**: 378–384.
13. Makidono, R., Makidono, A. and Matsuura, K.(1977) Leukopenia and lymphopenia during the radiation therapy and their recovery by anti-leukopenia drugs. Nippon Acta Radiologica **37**: 1153–1167.
14. Gilmore, G. L., DePasquale, D. K., Fisher, B. C. and Shadduck, R. K. (1995) Enhancement of monocytopoiesis by granulocyte colony-stimulating factor: evidence for secondary cytokine effects in vivo. Exp. Hematol. **23**: 1319–1323.
15. Jacobson, S. E. W., Ruscetti, F. W., Dubois, C. M. and Keller, J. R. (1992) Tumor necrosis factor α directly and indirectly regulates hematopoietic progenitor cell proliferation: role of colony-stimulating factor receptor modulation. J. Exp. Med. **175**: 1759–1772.
16. Kato, I., Yokokura, T. and Mutai, M. (1983) Macrophage activation by *Lactobacillus casei* in mice. Microbiol.

Immunol. **27**: 611–618.
17. Shimizu, T., Nomoto, K., Yokokura, T. and Mutai, M. (1987) Role of colony-stimulating activity in antitumor activity of *Lactobacillus casei* in mice. J. Leukocyte Biol. **42**: 204–212.
18. Tsuneoka, K., Ishihara, H., Dimchev, A. B., Nomoto, K., Yokokura, T. and Shikita, M. (1994) Timing in administration of a heat-killed *Lactobacillus casei* preparation for radioprotection in mice. J. Radiat. Res. **35**: 147–156.
19. Nomoto, K., Yokokura, T., Tsuneoka, K. and Shikita, M.(1991) Radioprotection of mice by a single subcutaneous injection of heat-killed *Lactobacillus casei* after irradiation. Radiat. Res. *125*: 293–297.
20. Ulich, T. R., Castillo, J. D., McNiece, I. K., Yin, S., Irwin, B., Busser, K. and Guo, K. (1990) Acute and subacute hematologic effects of multi-colony stimulating factor in combination with granulocyte colony-stimulating factor in vivo. Blood **75**: 48–53.
21. Kishimoto, T. K., Jutila, M. A., Berg, E. L. and Butcher, E. C. (1989) Neutrophil Mac-1 and MEL-14 adhesion proteins inversely regulated by chemotactic factors. Science **245**: 1238–1241.
22. Ball, T. C., Hirayama, F. and Ogawa, M. (1996) Modulation of early B lymphopoiesis by interleukin 3. Exp. Hematol. **24**: 1225–1231.
23. Neben, S., Donaldson, D., Fitz, L., Calvetti, J., Neben, T., Turner, K., Hirayama, F. and Ogawa, M. (1996) Interleukin-4 (IL-4) in combination with IL-11 or IL-6 reverses the inhibitory effect of IL-3 on early B lymphocyte development. Exp. Hematol. **24**: 783–789.
24. Lee, M. Y., Fevold, K. L., Dorshkind, K., Fukunaga, R., Nagata, S. and Rosse, C. (1993) In vivo and in vitro suppression of primary B lymphocytopoiesis by tumor-derived and recombinant granulocyte colony-stimulating factor. Blood **82**: 2062–2068.
25. Dorshkind, K. (1991) In vivo administration of recombinant granulocyte-macrophage colony-stimulating factor results in a reversible inhibition of primary B lymphopoiesis. J. Immunol. **146**: 4204–4208.
26. Maestroni, G. J. M., Covacci, V. and Conti, A. (1994) Hematopoietic rescue via T-cell-dependent, endogenous granulocyte-macrophage colony-stimulating factor induced by the pineal neurohormone melatonin in tumor-bearing mice. Cancer Res. **54**: 2429–2432.
27. Horiuchi, K. and Miyamoto, T. (1992) Radioreductive effect of bestatin (Ubenimex) in BALB/c mice. Int. J. Radiat. Biol. **62**: 73–80.
28. Kato, I., Yokokura, T. and Mutai, M. (1984) Augmentation of mouse natural killer cell activity by *Lactobacillus casei* and its surface antigens. Microbiol. Immunol. **28**: 209–217.
29. Su, H. C., Ishikawa, R. and Biron, C. A. (1993) Transforming growth factor-β expression and natural killer cell responses during virus infection of normal, nude, and scid mice. J. Immunol. **151**: 4874–4890.
30. Okitsu-Negishi, S., Nakano, I., Suzuki, K., Hashira, S., Abe, T. and Yoshino, K. (1996) The induction of cardioangitis by *Lactobacillus casei* cell wall in mice. 1. The cytokine production from murine macrophage by *Lactobacillus casei* cell wall extract. Clin. Immunol. Immunopathol. **78**: 30–40.
31. Ishihara, H., Tanaka, I., Nemoto, K., Tsuneoka, K., Cheeramakara, C., Yoshida, K. and Ohtsu, H. (1995) Immediate-early, transient induction of the interleukin-1β gene in mouse spleen macrophages by ionizing radiation. J. Radiat. Res. **36**: 112–124.
32. Nemoto, K., Ishihara, H., Tanaka, I., Suzuki, G., Tsuneoka, K., Yoshida, K. and Ohtsu, H. (1995) Expression of IL-1β mRNA in mice after whole body X-irradiation, J. Radiat. Res. **36**: 125–133.

BIOCHEMICAL AND BIOPHYSICAL RESEARCH COMMUNICATIONS 249, 938–942 (1998)
ARTICLE NO. RC989244

Effects of Hydroxyl Radical and Sulfhydryl Reagents on the Open Probability of the Purified Cardiac Ryanodine Receptor Channel Incorporated into Planar Lipid Bilayers

Kazunori Anzai,* Kunitaka Ogawa,† Akihiko Kuniyasu,‡ Toshihiko Ozawa,* Haruhiko Yamamoto,‡ and Hitoshi Nakayama‡

Bioregulation Research Group, National Institute of Radiological Sciences, Japan; †Department of Applied Bioscience, Faculty of Science, Kanagawa University, Japan; and ‡Faculty of Pharmaceutical Sciences, Kumamoto University, Japan

Received July 27, 1998

We examined the effects of hydroxyl radical on the ion permeability of the ryanodine receptor, a calcium releasing channel of sarcoplasmic reticulum. The cardiac ryanodine receptor, purified from pig heart, was reconstituted to proteoliposomes and then incorporated into a planar bilayer membrane. A single channel activity with a conductance of 724 pS in 900/200 mM (*cis/trans*) KCl and an ion selectivity of $P_K:P_{Cl}$ = 1:0.08 was observed. These characteristics are similar to those observed by the incorporation of the channel through sarcoplasmic reticulum vesicles. Hydroxyl radicals chemically generated by the reaction of H_2O_2 and Cu(ethylenediamine)$_2$ at the *cis* compartment increased the open probability of the channel. Treatment with SH oxidizing reagents from the *cis* compartment also increased the open probability, and dithiothreitol, a SH reducing agent, reversed the effect. These findings suggest that hydroxyl radicals react with some SH groups of the ryanodine receptor and increase the Ca^{2+} release from sarcoplasmic reticulum through the ryanodine receptor.

The ryanodine receptor (RyR) is involved in the physiological Ca^{2+} release from sarcoplasmic reticulum (SR) in both skeletal and cardiac muscles [1]. Various oxidative stresses have been shown to alter the Ca^{2+} permeability of the SR membranes [2]. Reconstitution of the SR vesicles to planar bilayers has suggested that ionic current through the RyR channel is modified by oxidative stress [3-5]. In these studies, however, it was not determined whether hydroxyl radical is involved as the crucial oxidant, or whether the oxidative stress directly alters the RyR molecule itself. In the present study, to clarify these points, we used a system involving purified RyR protein and a chemically generated hydroxyl radical. The purified RyR was incorporated into a planar lipid bilayer membrane, and the effects of the hydroxyl radical on the channel activity were examined. The effects of SH reagents on the channel activity were also examined as a reference.

Abbreviations: DTDP, 4,4′-dithiodipyridine; DTT, dithiothreitol; en, ethylenediamine; P_o, open probability; RyR, ryanodine receptor; SR, sarcoplasmic reticulum.

MATERIALS AND METHODS

The heavy fraction of cardiac SR membrane vesicles was prepared from a porcine heart [6] obtained at a local slaughterhouse. Cardiac RyR was purified and reconstituted into proteoliposomes with asolectin according to a method described previously [7].

Planar lipid bilayers were formed by the folding method [8] using phosphatidylethanolamine (Avanti Polar Lipid, Alabaster, AL, USA) as the membrane forming lipid. The RyR was incorporated into the planar bilayer by the fusion of either heavy SR vesicles or reconstituted proteoliposomes to the bilayer. The membrane potential was defined as the potential at the *cis* compartment (in which samples were added) with respect to the *trans* compartment (opposite to the *cis* compartment). We detected K^+ current instead of Ca^{2+} current as the activity of the RyR channel, since the RyR permeates the K^+ ion if the Ca^{2+} concentration is very low and since the K^+ current is larger than the Ca^{2+} current [7]. The channel data were stored with a DAT data recorder (RD-120TE, TEAC, Tokyo) and analyzed later with a personal computer.

Hydroxyl radical was generated by the reaction of 1-10 mM H_2O_2 and 0.1 mM Cu(en)$_2$. The continuous generation of hydroxyl radical for more than 30 min was confirmed by the ESR spin trapping technique [9].

RESULTS AND DISCUSSION

The purified cardiac RyR incorporated into the planar bilayer membrane showed a single channel ac-

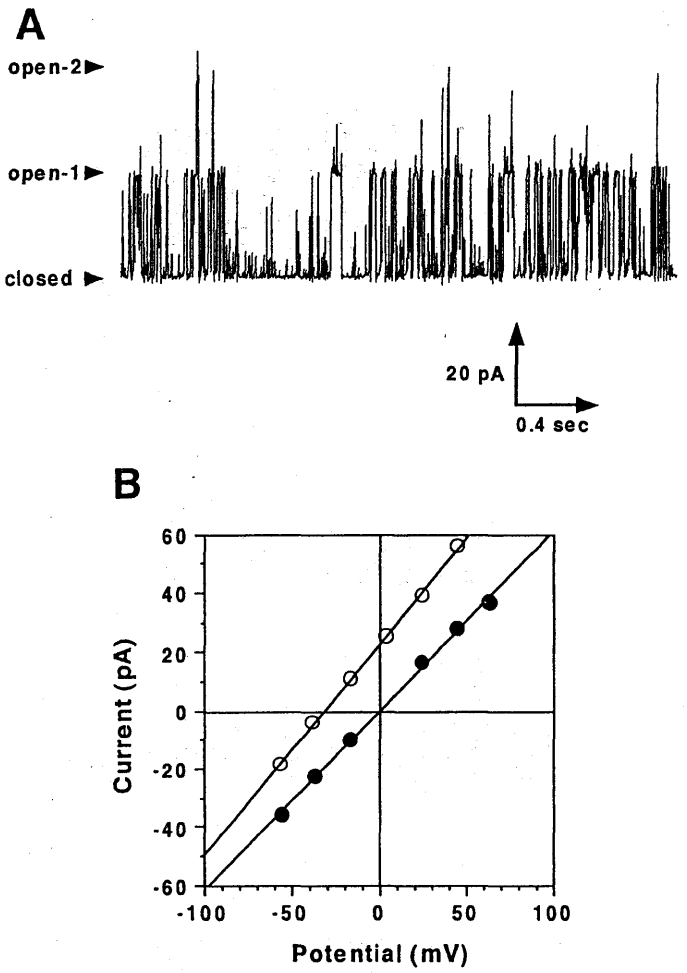

FIG. 1. (A) Single channel activity of the cardiac purified ryanodine receptor incorporated into a planar bilayer membrane formed with egg phosphatidylethanolamine in 900/200 mM (*cis/trans*) KCl and 10 mM Tris-Hepes (pH 7.4). Two open levels with the same current (open-1 and open-2) are observed, suggesting that at least two channels were incorporated. The membrane potential at the *cis* compartment with respect to the *trans* compartment was 3.6 mV. (B) Membrane current-potential relationship of the single channel activity of the ryanodine receptor in the planar bilayer in symmetrical 200 mM KCl (l) and asymmetrical 900/200 mM (*cis/trans*) KCl (m) both containing 10 mM Tris-Hepes (pH 7.4).

tivity (Fig. 1A). The conductance was 614 pS and 724 pS in symmetrical 200 mM KCl and asymmetrical 900/200 mM (*cis /trans*) KCl both containing 10 mM Tris-Hepes (Fig. 1B). The ion selectivity was calculated to be P_K:P_{Cl}=1:0.08 from the reversal potential (−31.8 mV) using the Goldman-Hodgkin-Katz equation (Fig. 1B). ATP (1 mM) added at the *cis* compartment significantly increased the open probability (P_o) of the channel (Fig. 2A). Ryanodine (1 μM) added at the *cis* compartment reduced the conductance to half of the original conductance, whereas it resulted in the steady open state of the channel (Fig. 2B). These characteristics are similar to those of the RyR incorporated into the planar bilayer membranes through the fusion of SR membrane vesicles [10], suggesting that factors other than RyR protein do not affect the conductance or the ion selectivity of the channel. In addition, this finding confirmed that the RyR maintained its channel activity during the purification process.

Hydroxyl radicals chemically generated by the reaction of H_2O_2 and $Cu(en)_2$ at the *cis* compartment increased the P_o of the channel from 0.27 to 0.94 after a lag time of about 2 min, without affecting the conductance (Fig. 3). Further addition of dithiothreitol (DTT, 3 mM), an SH reducing reagent, decreased the P_o (data not shown). The addition of H_2O_2 without $Cu(en)_2$ did not significantly increase the P_o (Fig. 4). The addition of $Cu(en)_2$ alone did not affect the P_o. Since the hydroxyl radical generated by the reaction of H_2O_2 and $Cu(en)_2$

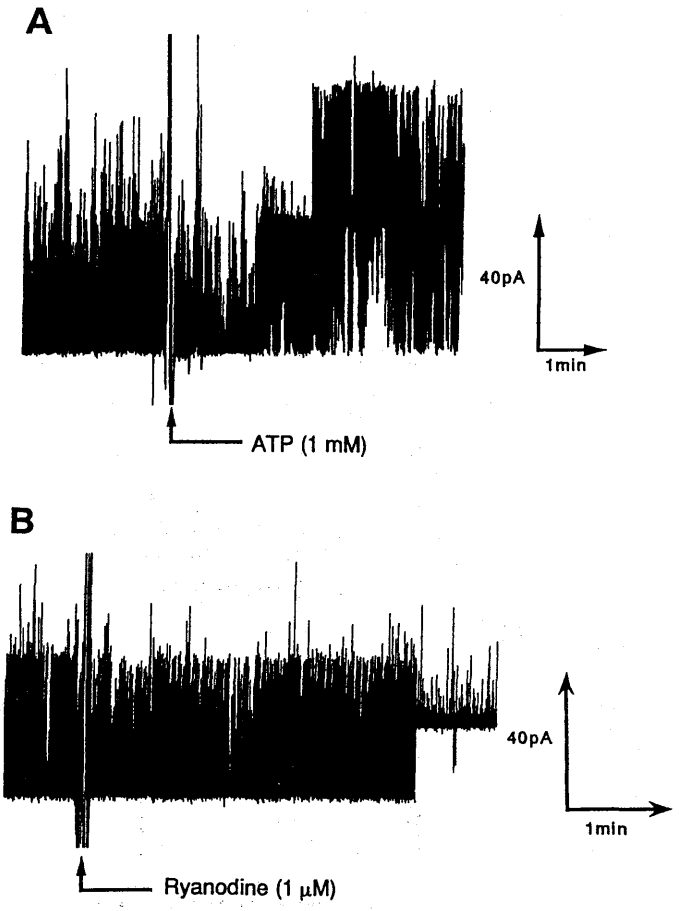

FIG. 2. Effect of ATP (A) and ryanodine (B) on the channel activity of the ryanodine receptor. The cardiac ryanodine receptor channel was incorporated into the planar bilayer membrane and the membrane current was measured similarly as in the Fig. 1. ATP (final 1 mM) and ryanodine (final 1 μM) were added to the *cis* compartment of the chamber at the point marked by the allow in traces A and B, respectively.

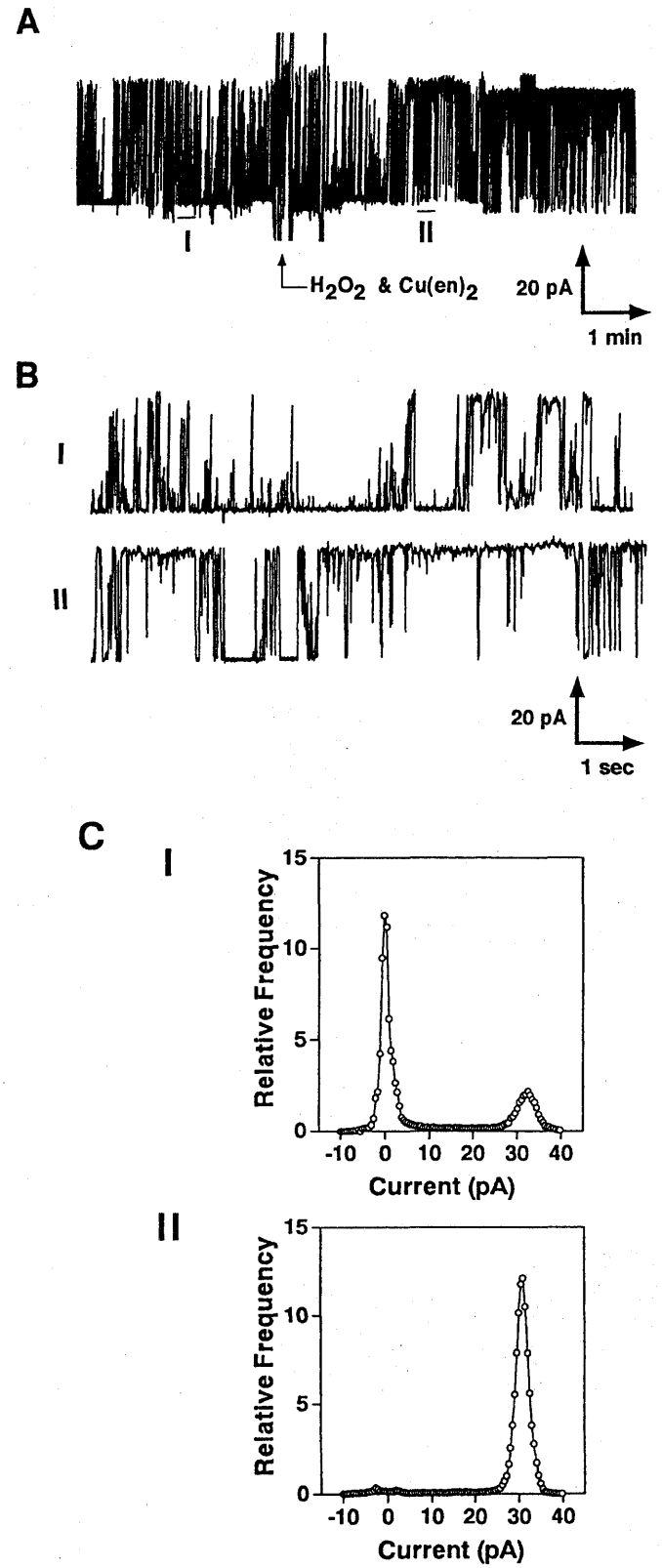

FIG. 3. Effect of hydroxyl radical generated by the reaction of H_2O_2 and Cu(en)$_2$ on the open probability of the ryanodine receptor channel incorporated into the planar bilayer. (A) 10 mM H_2O_2 and 0.1 mM Cu(en)$_2$ were added to the *cis* compartment of the chamber at the arrow. (B) The expanded traces of parts I (upper) and II (lower) of trace A. (C) The amplitude histograms corresponding to part I (before the application of the hydroxyl radical) and part II (after the application of the hydroxyl radical) of trace A. The open probability, P_o, for parts I and II were estimated to be 0.27 and 0.94, respectively.

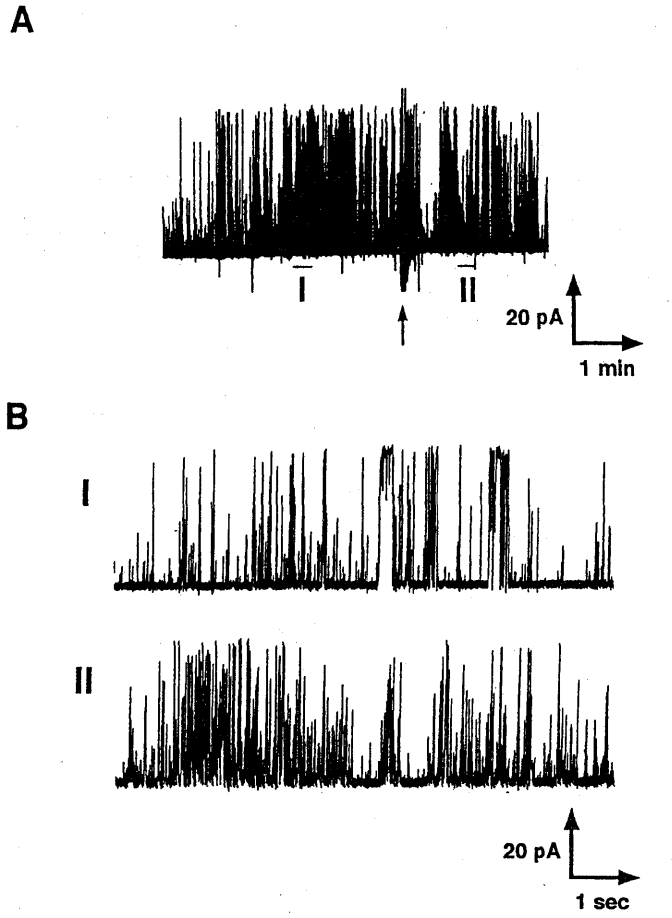

FIG. 4. Effect of H_2O_2 on the ion channel activity of the ryanodine receptor incorporated into the planar bilayer. (A) 10 mM H_2O_2 was added to the *cis* compartment of the chamber at the arrow. (B) Time-expanded traces of parts I and II of trace A.

did not increase the permeability of pure lipid bilayers nor peroxidize the membrane lipids in this time range [11], these results indicate that the chemically generated hydroxyl radical modified the RyR channel protein itself and increased the P_o of the channel without changing the conductance.

When 4,4′-dithiodipyridine (DTDP, 9.3 μM), an SH oxidizing reagent, was added to the *cis* compartment, the single channel P_o increased significantly from 0.31 to 0.85, and DTT (3 mM) reversed the effect of DTDP (Fig. 5). N-succinimidyl 3-(2-pyridyldithio)propionate (60 μM), another SH oxidizing reagent, also increased the P_o from 0.59 to 0.77 (data not shown). These find-

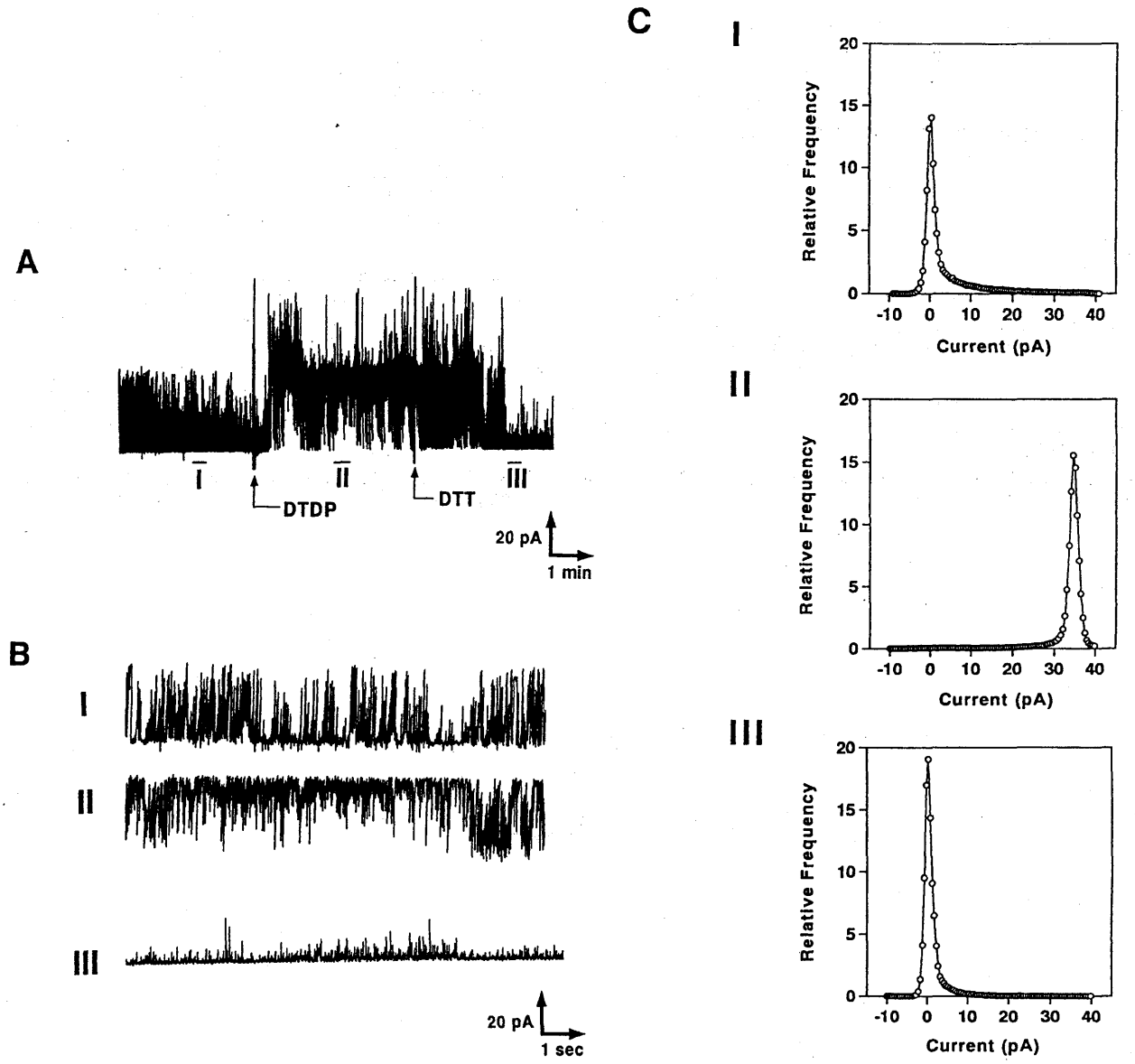

FIG. 5. Effects of 4,4′-dithiodipyridine (DTDP) and dithiothreitol (DTT) on the channel activity of the ryanodine receptor incorporated into the planar bilayer. (A) DTDP (final 9.3 μM) and DTT (final 3 mM) were added to the *cis* compartment of the chamber at the first and second arrows, respectively. (B) The time scales of parts I, II, and III in trace A were extended 60 times. (C) The amplitude histograms corresponding to parts I, II and III. The P_o values of parts I, II, and III were 0.31, 0.85, and 0.20, respectively.

ings indicate that the oxidation/reduction of some SH groups of the RyR channel protein regulates its open probability.

The application of both hydroxyl radical and SH oxidizing reagents from the cytoplasmic side increased the P_o of the RyR channel. Since hydroxyl radical is a potent oxidant, this correlation suggests that the channel opening effect of the hydroxyl radical is derived from the oxidation of the same SH group which is oxidized by the SH reagents. The RyR from rabbit cardiac muscle has about 5,000 amino acid residues, and about 3,100 residues from the N-terminus exist at the cytoplasmic side [12]. Since the number of cysteine residues within 3,100 residues from the N-terminus is 55, the SH groups affected by the hydroxyl radical and the SH oxidizing reagents should be within these cysteine residues. In addition to the cytoplasmic SH groups, the activation of the RyR channel from frog muscle by the oxidation of sulfhydryls on the luminal side by H_2O_2 treatment was recently reported [13]. Further, the nitrosylation of several SH groups of RyR also increased the P_o of the channel, and the P_o depended on the number of the nitrosylated SH groups [14]. Therefore, the modification of SH groups of the RyR channel may well

have general importance for its physiological regulation. In cardiac muscle cells, hydroxyl radicals generated for various reasons may increase the Ca^{2+} release from SR by the modification of RyR on the SR membrane, and the increase of the Ca^{2+} release may cause physiologically harmful effects on the cardiac muscle cells.

REFERENCES

1. Meissner, G. (1994) *Annu. Rev. Physiol.* **56,** 485–508.
2. Okabe, E., Odajima, C., Taga, R., Kukreja, R., Hess, M. and Ito, H. (1988) *Molecular Pharmacology* **34,** 388–394.
3. Stoyanovsky, D. A., Salama, G. and Kagan, V. E. (1994) *Arch. Biochem. Biophys.* **308,** 214–221.
4. Boraso, A. and Williams, A. J. (1994) *Am. J. Physiol.* **267,** H1010–H1016.
5. Favero, T. G., Zable, A. C. and Abramson, J. J. (1995) *J. Biol. Chem.* **270,** 25557–25563.
6. Sitsapesan, R. and Williams, A. J. (1990) *J. Physiol.* **423,** 425–439.
7. Lindsay, A. R. G. and Williams, A. J. (1991) *Biochim. Biophys. Acta* **1064,** 89–102.
8. Anzai, K., Kadono, H., Hamasuna, M., Lee, S., Aoyagi, H. and Kirino, Y. (1991) *Biochim. Biophys. Acta* **1064,** 256–266.
9. Ozawa, T. and Hanaki, A. (1991) *J. Chem. Soc., Chem. Commun.* **1991,** 330–332.
10. Coronado, R., Morrissette, J., Sukhareva, M. and Vaughan, D. (1994) *Am. J. Physiol.* **266,** C1845–C1504.
11. Anzai, K., Ogawa, K., Goto, Y., Ueda, J., Miura, Y. and Ozawa, T. (1998) in Biological Oxidants & Antioxidants: Molecular Mechanisms & Health Effects (Packer, L. and Ong, A. H. S., eds.), pp. 79–89, AOCS Press, Champaign.
12. Otsu, K., Willard, H., Khanna, V., Zorzato, F., Green, N. and MacLennan, D. (1990) *J. Biol. Chem.* **265,** 13472–13483.
13. Oba, T., Ishikawa, T. and Yamaguchi, M. (1998) *Am. J. Physiol.* **274,** C914–C921.
14. Xu, L., Eu, J., Meissner, G. and Stamler, J. (1998) *Science* **279,** 234–237.

ANTIOXIDANTS & REDOX SIGNALING
Volume 1, Number 3, 1999
Mary Ann Liebert, Inc.

Original Research Communication

Oxidation-Dependent Changes in the Stability and Permeability of Lipid Bilayers

KAZUNORI ANZAI,[1] KUNITAKA OGAWA,[2] YASUKO GOTO,[1] YUMIKO SENZAKI,[1] TOSHIHIKO OZAWA,[1] and HARUHIKO YAMAMOTO[2]

ABSTRACT

Peroxidation-dependent change in the permeability of lipid bilayers was mesaured by using artificial membrane systems, that is, planar lipid bilayers and liposomes. The unsaturated fatty acyl chains of phospholipids in small unilamellar vesicles were peroxidized time-dependently by the hydroxyl radical chemically generated by the reaction of H_2O_2 and $Cu(en)_2$. In contrast, at the same hydroxyl radical concentration and time ranges, no ionic current through the planar lipid bilayers and no release of K^+ from the liposomes were observed. These findings indicate that accumulation of lipid peroxide within lipid bilayers is not responsible for the permeability increase that is often observed in biomembranes exposed to oxidative stresses. Higher concentration of the hydroxyl radical caused break-down of the planar lipid bilayers composed of the mixture (7:3) of phosphatidylethanolamine (PE) and phosphatidylcholine (PC). The bilayer containing 100% PE at least at one leaflet of the bilayer (facing the hydroxyl radical-generating solution) was not broken-down by the application of the hydroxyl radical, suggesting that PE stabilizes the planar lipid bilayer against the attack of the hydroxyl radical. Antiox. Redox Signal. 1, 339–347.

INTRODUCTION

RECENTLY, IT HAS BEEN WIDELY ACCEPTED that oxidants regulate cellular responses by affecting signal transduction and gene expression. Reactive oxygen species (ROS) may affect the cellular responses directly by acting as signal transduction messengers (Sen, 1998). ROS may also affect the cellular responses indirectly through changes in intracellular ionic environment, especially in intracellular Ca^{2+} homeostasis (Trump and Berezesky, 1992; Kaneko *et al.*, 1994; Dreher and Junod, 1995). For example, involvement of intracellular Ca^{2+} in oxidant-induced NF-κB activation was reported (Sen *et al.*, 1996). Therefore, it is important to know the effect of ROS on the intracellular ionic concentrations. The ionic concentration is determined by the ion flux through the plasma membrane and/or through the membranes of internal ionic stores. The ion flux occurs either at ion-transporting membrane proteins, such as ion pumps and ion channels, or at lipid bilayer.

There have been few studies that strictly measured oxidation-dependent change in the ion permeability of lipid bilayers (Nakazawa and Nagatsuka, 1980; Kunimoto *et al.*, 1981). Artificial lipid bilayers, *i.e.*, liposomes and pla-

[1]Bioregulation Research Group, National Institute of Radiological Sciences, Japan, and [2]Department of Applied Bioscience, Faculty of Science, Kanagawa University, Japan.

nar lipid bilayers, are good systems to measure the permeability of the lipid bilayer part of membranes independent of the ion-transporting proteins involved in biomembranes. In the present study, by using these artificial membrane systems, we have measured the effects of chemically generated hydroxyl radical (•OH) and peroxyl radical (ROO•) on the peroxidation, stability, and permeability of the lipid bilayers.

MATERIALS AND METHODS

Materials

Egg phosphatidylcholine (PC) and egg phosphatidylethanolamine (PE) were purchased from Avanti Polar Lipid (Alabaster, AL). The acyl chain composition of the PE was identical to that of the PC, because the PE was the product transesterified from the PC. Cu(II)(ethylenediamine)$_2$ complex (Cu(en)$_2$) was prepared as described previously (Ozawa *et al.*, 1988). 5,5'-Dimethyl-1-pyrroline-*N*-oxide (DMPO) was obtained from LABOTEC (Tokyo, Japan). Other chemicals were of analytical grade and used without further purification.

Generation and detection of hydroxyl radical and peroxyl radical

The hydroxyl radical (•OH) was generated chemically by the reaction of the Cu(en)$_2$ complex with hydrogen peroxide (H_2O_2) as described previously (Ozawa and Hanaki, 1991). The generation of •OH was monitored by the ESR (electron spin resonance) spin-trapping technique. The time course of the •OH generation rate was measured as follows. Various concentrations of H_2O_2 and Cu(en)$_2$ were mixed to be 100 and 1 m*M*, 50 and 0.5 m*M*, or 10 and 0.1 m*M*, respectively, with a buffer solution containing 150 m*M* KCl and 10 m*M* Tris-HEPES, pH 7.4. From time to time, a 100-μl aliquot was withdrawn from the reaction solution and mixed with 100 μl of 100 m*M* DMPO solution. The mixture was transferred to an ESR flat cell and ESR spectra were measured with X-band ESR spectrometer (JEOL RE-1X, Tokyo, Japan) within 1 min after the mixing of the sample and DMPO. Typical conditions for the ESR measurement were as follows: magnetic field, 333 ± 5 mT, frequency 9.44 GHz, scan 2 min, response 0.3 sec, and amplitude 2,000. Peroxyl radical (ROO•) was generated from 2,2'-azobis(2-amidinopropane)dihydrochloride (AAPH) (Niki, 1990).

Liposomes

Small unilamellar vesicles (SUVs) were prepared by sonication with a bath-type sonicator (Iuchi VS-70U, Osaka, Japan) of multilamellar vesicles composed of PE/PC = 7:3 or 100% PC in 150 m*M* KCl and 10 m*M* Tris-HEPES, pH 7.4. Large unilamellar vesicles (LUVs) were prepared by the reverse-phase evaporation method (Kaneda *et al.*, 1987) as follows. Fifty milligrams of PE/PC = 7:3 or 100% PC was dissolved in a 3-ml solution of isopropyl ether and chloroform (64:36). A water-phase solution of 150 m*M* KCl and 10 m*M* Tris-HEPES, pH 7.4, was added to the lipid solution, and the mixture was sonicated briefly with the bath-type sonicator. The organic solvent of the resultant suspension was evaporated with a rotary evaporator and a 10-ml solution of 150 m*M* KCl and 10 m*M* Tris-HEPES, pH 7.4, was added to the residue to form LUVs. It was impossible to form LUVs with 100% PE. For the measurement of K^+ release with an K^+ selective electrode, LUVs were washed twice with 150 m*M* NaCl and 10 m*M* Tris-HEPES, pH 7.4, by centrifugation with an ultracentrifuge (Hitachi SCP70H, Tokyo) at 41,000 rpm for 30 min. The recovery of the LUVs by this treatment was 100% based on the comparison of phosphorus measured with a kit (Wako, Osaka) before and after the centrifugation.

Measurement of phospholipid peroxidation

Formation of peroxidized phospholipids was analyzed using liposomes (SUVs) with the same lipid composition (PE/PC = 7:3) as the planar bilayer membrane. Lipid peroxidation by hydroxyl radical was initiated by the addition of various concentrations of Cu(en)$_2$ and H_2O_2 to the liposomal suspension (2 mg phospholipid/ml). The reaction was stopped at an appropriate time by chelating the Cu with 2 m*M* diethylenetriamine-*N*,*N*,*N'*,*N''*,*N''*-pentaacetic acid (DTPA) and cooling down the so-

lution to 0°C. A 5-ml solution of chloroform/methanol (2:1) was added to the reaction mixture (1 ml), mixed well, and the mixture was centrifuged at 1,000 × *g* for a few min with a centrifuge (05P-21, Hitachi, Tokyo). The upper layer was discarded and 3 ml of distilled water was added to the lower layer. Mixing and centrifugation were repeated as above. From the lower layer, 2.5 ml was withdrawn and the solvent was evaporated. For the diene conjugation assay (Buege and Aust, 1978), the resulting residue was dissolved in cyclohexane and the absorbance at 233 nm was measured with a spectrophotometer (Hitachi U-3210, Tokyo). Lipid peroxidation by ROO• generated by the decomposition of AAPH was performed in a manner similar to the peroxidation by •OH generated by the reaction of $Cu(en)_2$ and H_2O_2 described above. The reaction was stopped just by cooling down the reaction mixture. Iodometric assay of lipid peroxide was occasionally performed according to the literature method (Buege and Aust, 1978; Jessup *et al.*, 1994).

Potassium ion-selective electrode

K^+ release from liposomes was measured with a K^+-selective electrode, which was made according to the literature method (Katsu *et al.*, 1986). At first, a calibration curve was made for the electrode to use with known concentration of KCl. Next, the electrode was immersed in the suspension of LUVs, and the output voltage was continuously measured. The sample was stirred with a magnetic stirrer and kept at 37°C using a cuvette (volume ~2 ml) with a water jacket. At an appropriate time, $Cu(en)_2$ and H_2O_2 or AAPH was added to generate •OH or ROO•. At the end of the measurement, 2 m*M* Triton X-100 was added to the sample to release completely the K^+ in the LUVs. The output voltage was converted to the K^+ concentration with the calibration curve made at the beginning of the measurement.

Planar bilayer lipid membrane

Planar bilayer membranes were made at a small hole (200 μm in diameter) on a very thin Teflon septum (25 μm thick) in 150 m*M* KCl and 10 m*M* Tris-HEPES, pH 7.4, by the folding method as described previously (Anzai *et al.*, 1991). The lipid composition of the planar bilayer was PE/PC = 7:3 or 100% PE. An asymmetrical bilayer consisting of PE/PC = 7:3 for one leaflet (*cis* side) and 100% PE for the other leaflet (*trans* side) of the bilayer or *vice versa* was also made by the folding method. The Teflon chamber, Teflon septum, and electric setting were the same as described previously (Anzai *et al.*, 1991). $Cu(en)_2$ and H_2O_2 or AAPH was added to one side (*cis* side) of the chamber, and the electric current through the bilayer was measured under a voltage clamp condition at room temperature.

RESULTS

Time course of •OH generation

Hydroxyl radical was generated chemically by the reaction of H_2O_2 and $Cu(en)_2$. The •OH generation rate was detected by the spin trapping technique. Figure 1 shows the time course of the •OH generation rate in several $Cu(en)_2/H_2O_2$ concentrations. The ratio of $Cu(en)_2$ and H_2O_2 was kept constant (1:100). When high concentration of H_2O_2 and $Cu(en)_2$

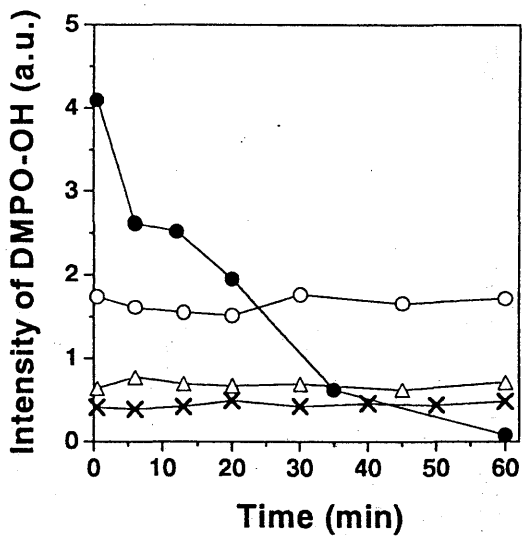

FIG. 1. Time course of hydroxyl radical generation by the reaction of various concentrations of $Cu(en)_2$ and H_2O_2. (●) 100 m*M*/1 m*M*; (○) 50 m*M*/0.5 m*M*; (△) 20 m*M*/0.2 m*M*; and (X) 10 m*M*/0.1 m*M* for the concentrations of $Cu(en)_2/H_2O_2$, respectively. The hydroxyl radical was trapped by 25 m*M* DMPO. The relative intensity of the ESR signal of DMPO-OH adduct to that of MnO, an external standard, is shown.

was used (100 m*M* and 1 m*M*, respectively), the peak height of the DMPO-OH adduct decreased in time and even reached a negligible value in 1 hr. On the other hand, at lower concentrations of the generators, the generation rate was constant and no decrease of the signal was observed at least for 1 hr. At 50 m*M* H_2O_2 and 0.5 m*M* $Cu(en)_2$, the •OH generation gradually decreased after 1 hr, but the rate was still a half of the initial rate even at 4 hr; at 10 m*M* H_2O_2 and 0.1 m*M* $Cu(en)_2$, the •OH generation rate was constant at least for 8 hr (data not shown). The initial generation rates at the initial stage corresponded well to the concentration of the generators.

Lipid peroxidation by •OH and ROO•

Figure 2A shows the increase of conjugated diene in SUVs (PE/PC = 7/3) by the treatment of •OH generated chemically by the reaction of several concentrations of H_2O_2 and $Cu(en)_2$. The peroxidation proceeded rapidly and reached a plateau at 30–60 min. The diene-conjugated assay and the iodometric assay showed similar values for the amount of peroxidized phospholipid (data not shown). The initial peroxidation rate was high for the condition of high •OH generation rate. In contrast, the plateau value was low for such a condition.

Lipid peroxidation proceeded by the addition of 20 m*M* AAPH at 37°C, but the rate was smaller than that observed in the •OH generating system (Fig. 2B). The peroxidation reaction did not reach a plateau even at 3 hr.

Effect of •OH and ROO• on K^+ permeability through liposomes

Figure 3 shows the effect of •OH generated with 100 m*M* H_2O_2 and 1 m*M* $Cu(en)_2$ (Fig. 3A) and ROO• generated with 20 m*M* AAPH (Fig. 3B) on the K^+ release from the LUVs (PE/PC = 7/3). Although gradual release of K^+ from the LUVs occurred naturally, no significant additional release of K^+ was observed on exposure of the LUVs to either •OH or ROO• at the initial stage (0–60 min) of the time course. However, a significant difference was observed at a later stage (after 60 min) for the sample exposed to •OH.

Effect of •OH on the permeability of planar bilayer membrane

Planar bilayer membranes were used to assess the relationship between lipid peroxida-

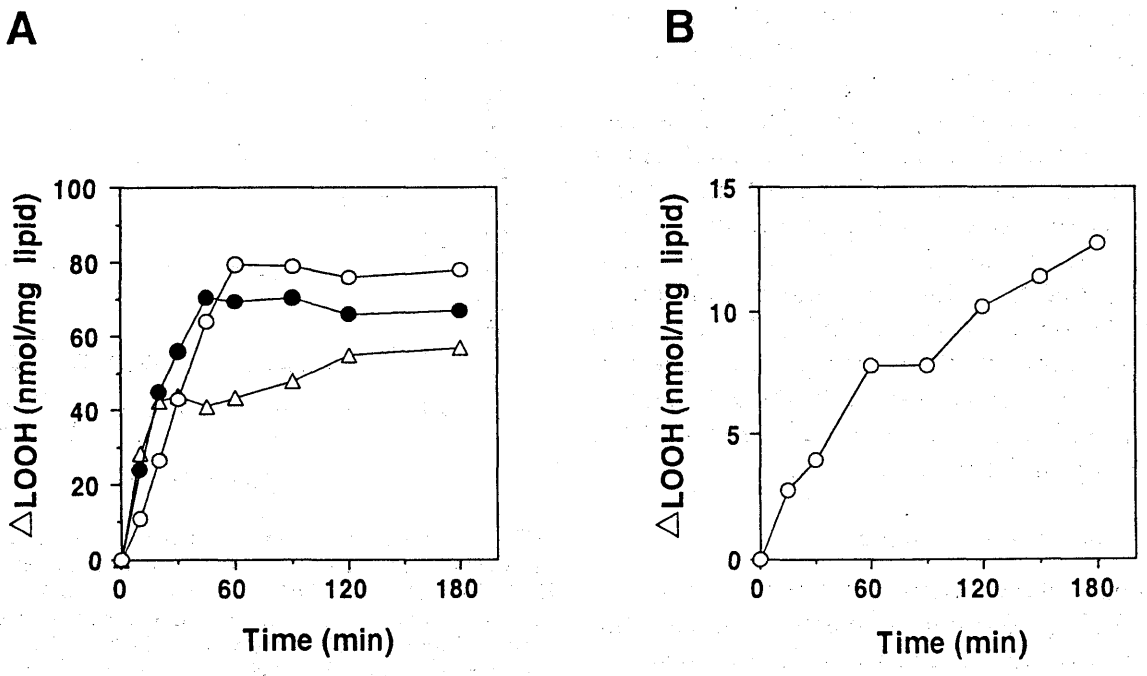

FIG. 2. Formation of phospholipid hydroperoxide in PE/PC (7/3) liposomes. A. Application of hydroxyl radical generated by various concentrations of $Cu(en)_2/H_2O_2$ at 37°C: (△) 100 m*M*/1 m*M*; (●) 50 m*M*/0.5 m*M*; (○) 10 m*M*/0.1 m*M*. **B.** Application of peroxyl radical generated by 20 m*M* AAPH at 37°C.

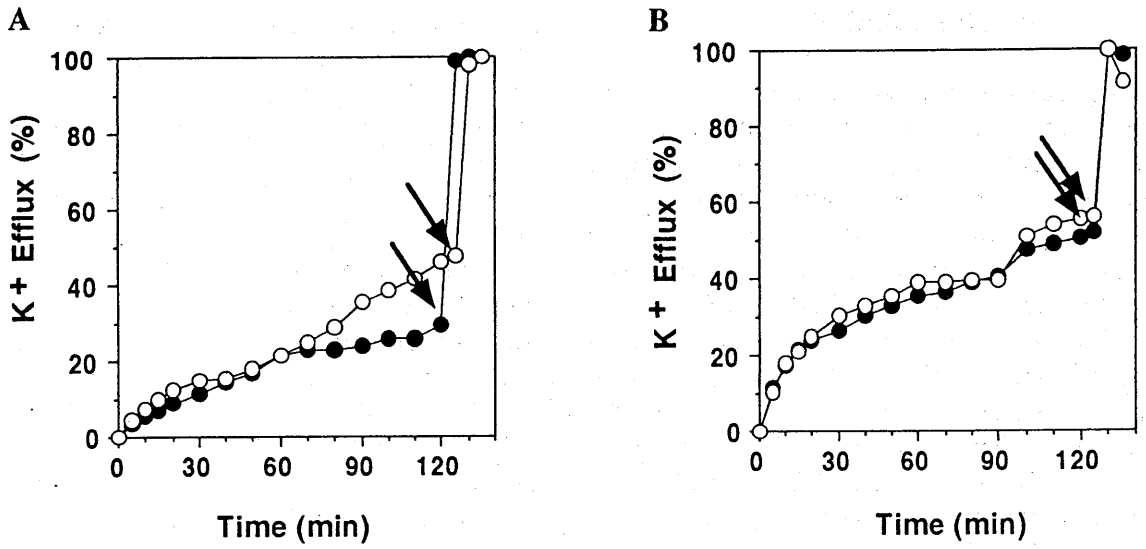

FIG. 3. **Effects of hydroxyl radical and peroxyl radical on the K^+ permeability of PC liposomes. A.** The time-course of K^+ release from the liposomes was measured with a K^+-selective electrode in the presence of hydroxyl radical generated by 100 m*M* H_2O_2/1 m*M* $Cu(en)_2$ (○) and in its absence (●). **B.** The time-course of K^+ release from the liposomes was measured with a K^+-selective electrode in the presence of peroxyl radical generated by 20 m*M* AAPH (○) and in its absence (●).

tion and the integrity and permeability of the lipid part of bilayer membranes. Figure 4 shows no change in the membrane current for more than 40 min after application of 50 m*M* H_2O_2 and 0.5 m*M* $Cu(en)_2$ (trace A) or 10 m*M* H_2O_2 and 0.1 m*M* $Cu(en)_2$ (trace B). No current change was observed up to 90 min in these conditions (data not shown).

When higher concentration of •OH was generated by 100 m*M* H_2O_2 and 1 m*M* $Cu(en)_2$, the membrane current gradually increased at about 10 min (Fig. 5). The current increased exponentially with increased noise, and the membrane collapsed suddenly at around 16 min.

The stability of the planar lipid bilayer was dependent on the composition of the polar head group of the bilayer lipid. When a symmetrical bilayer was formed by PE/PC = 7:3, application of a high concentration of •OH by 100 m*M* H_2O_2 and 1 m*M* $Cu(en)_2$ increased the membrane current and produced bilayer breakdown (Fig. 5). The bilayer made of 100% PE was, however, relatively stable and membrane breakdown did not occur until 70 min after the application of •OH (Fig. 5B). When an asymmetrical bilayer with PE/PC = 7:3 for the leaflet of *cis* side (the side of H_2O_2 and $Cu(en)_2$ addition) and 100% PE for the leaflet of *trans* side was used, high concentration of •OH collapsed the bilayer within 30 min (Fig. 5C). On the other hand, when an asymmetrical bilayer with 100% PE for the *cis* side and PE/PC = 7:3 for the *trans* side was used, the asymmetrical bilayer was more stable and no breakdown of the bilayer occurred within 60 min.

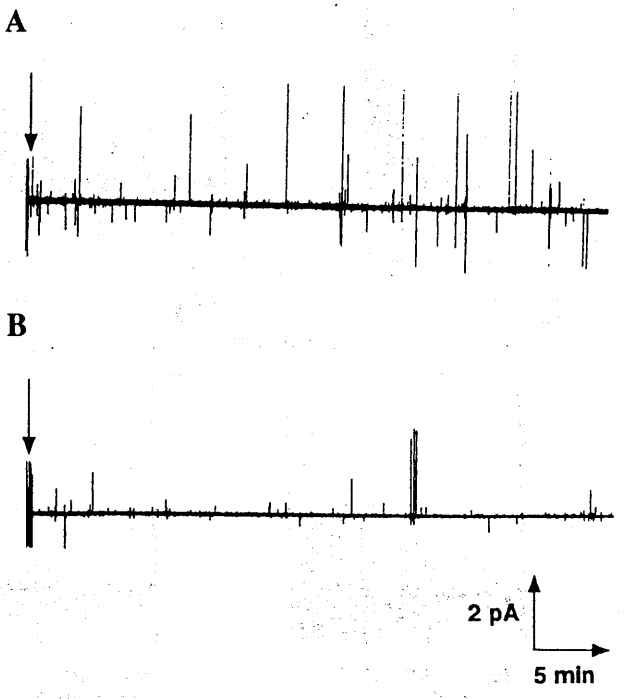

FIG. 4. **Effect of hydroxyl radical generated by (A) 0.5 mM $Cu(en)_2$ and 50 mM H_2O_2 and (B) 0.1 mM $Cu(en)_2$ and 10 mM H_2O_2 on the current through the symmetrical planar lipid bilayer of PE/PC (7/3).** The arrows indicate the time of the addition of $Cu(en)_2$ and H_2O_2 to the *cis* compartment of the chamber.

DISCUSSION

A conjugated diene was formed time-dependently by the exposure of liposomes to •OH or ROO•. A similar time course of the formation of peroxidized lipid was observed by the iodometric assay (data not shown). Therefore, the acyl chains of PC and PE in SUVs were peroxidized by the exposure to •OH or ROO•. The peroxidation reached a plateau at about 60 min by the application of •OH (Fig. 2), whereas it still proceeded even at 180 min when ROO• was applied from 20 m*M* AAPH at 37°C. During the first 60 min, •OH was constantly generated, except at high concentrations of H_2O_2 and $Cu(en)_2$ (100 m*M* and 1 m*M*, respectively), by which the generation rate decreased gradually with time and reached almost zero at 60 min. The formation of ROO• by the decomposition of AAPH and additional reaction of O_2 was reported by Niki (1990). Radical formation from AAPH was detected by spin-trapping method (Sato *et al.*, 1995; Krainev and Bigelow, 1996).

The apparent saturation of the peroxidation seen in Fig. 2 at 100 m*M* H_2O_2 and 1 m*M* $Cu(en)_2$ is not the real saturation, because a slow increase of peroxidized lipid is seen after 1 hr. The peroxidation level at 1 hr was higher when lower concentrations of the •OH generators were used. Because the •OH generation proceeded for more than 4 hr when 50–10 m*M* H_2O_2 and 0.5–0.1 m*M* $Cu(en)_2$ was used, the saturation of lipid peroxidation observed for these conditions must be due to the consumption of the substrate (unsaturated double bonds), whereas the apparent saturation at 30 min observed for 100 m*M* H_2O_2 and 1 m*M* $Cu(en)_2$ should be ascribed to the stop of the •OH generation.

The acyl chain composition of PC was reported as 32% $C_{16:0}$, 1.0% $C_{16:1}$, 16.0% $C_{18:0}$,

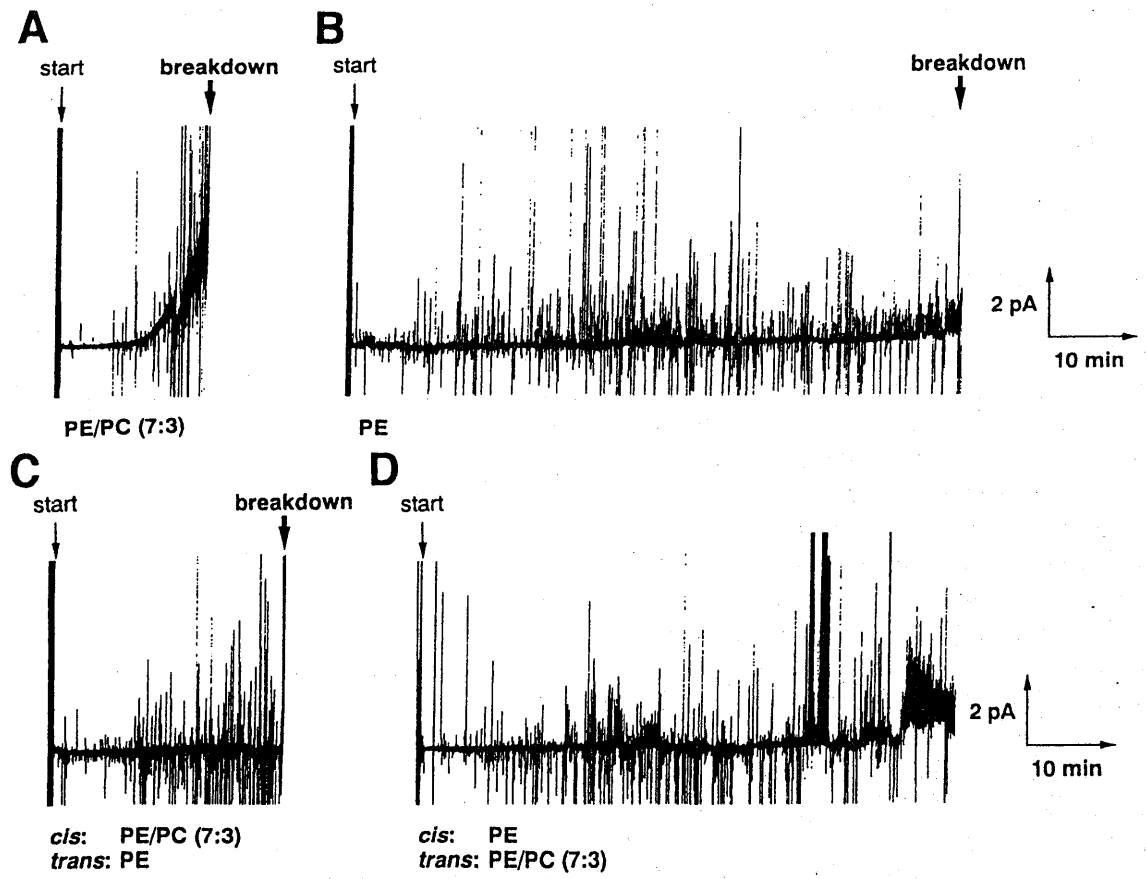

FIG. 5. Effect of hydroxyl radical generated by 1 m*M* $Cu(en)_2$ and 100 m*M* H_2O_2 on the current through: the (A) symmetrical planar lipid bilayer of PE/PC (7/3); (B) symmetrical planar lipid bilayer of PE only; (C) asymmetrical planar lipid bilayer (*cis*, PE/PC (7/3); *trans*, PE only); and (D) asymmetrical planar lipid bilayer (*cis*, PE only; *trans*, PE/PC (7/3)).

30.0% $C_{18:1}$, 17.0% $C_{18:2}$, and 3.0% $C_{20:4}$ (White, 1973). Because the PE we used was the product transesterified from PC, the acyl chain composition should be identical to that of PC. We assume that $C_{18:2}$ and $C_{20:4}$ contribute mainly to the conjugated diene formation; that is, about 20% of the lipid undergoes peroxidation. Assuming that the average molecular weight of the phospholipids is 800 and all the $C_{18:2}$ and $C_{20:4}$ are peroxidized, the saturation level of the conjugated diene is calculated to be 250 nmol/mg lipid. The saturation level observed (about 75 nmol/mg lipid) was about 30% of the calculated value. Because the •OH-generating agents are water soluble, •OH should be generated outside the liposomes, causing peroxidation of only the outer leaflet of the liposomes. In addition, the liposomes we used were not completely unilamellar. These factors may explain the observed peroxidation level of 30% of the total peroxidizable part of the acyl chains. The lower saturation level at 100 m*M* H_2O_2 and 1 m*M* $Cu(en)_2$ may represent a progress of the reaction to decompose the formed lipid peroxide. This kind of decomposition also explains the lower level of peroxidation than expected. The increase of the absorbance at 270 nm supports the occurrence of further decomposition (data not shown).

The K^+-selective electrode detected a slow release of K^+ ion entrapped inside the liposomes. Application of •OH or ROO• did not enhance the leak out of K^+ ion significantly in the first 60 min. This result indicates that the formation of peroxidized lipid in the lipid bilayer does not necessarily increase the ion permeability of the bilayer. When high concentrations of the •OH generating system were used (100 m*M* H_2O_2 and 1 m*M* $Cu(en)_2$), significant increase of K^+ efflux was observed (Fig. 3A). Because the •OH generation stopped after 60 min in this condition, this increase should be due to some after effect such as deformation or disintegration of liposomes. Also, 100 m*M* H_2O_2 alone or 1 m*M* $Cu(en)_2$ alone did not enhance the K^+ efflux (data not shown), indicating that the enhancement was caused not by H_2O_2 or $Cu(en)_2$ but by •OH.

When •OH generated from $H_2O_2/Cu(en)_2$ (50/0.5 m*M* or 10/0.1 m*M*) was applied to one side of the planar bilayer composed of PE/PC = 7/3, no increase of the membrane current was observed (Fig. 4). Because •OH generated from these concentrations of $H_2O_2/Cu(en)_2$ peroxidized the acyl chain of the phospholipid (Fig. 2), this observation supports the idea based on the result of K^+ efflux from liposomes: that is, the formation of lipid peroxide itself does not cause the increase of the ion permeability of the lipid bilayer membrane.

When high concentrations of $H_2O_2/Cu(en)_2$ (100/1 m*M*) were used, the membrane current began to increase at about 10 min after the application of •OH to the PE/PC (7/3) bilayer, and the bilayer was suddenly broken down at about 16 min (Fig. 5A). When the planar bilayer made of 100% PE was used, no increase of the membrane current was observed and the bilayer was broken down only at about 70 min (Fig. 5B). Therefore, the stability of the planar lipid bilayer against •OH was dependent on the composition of the head group of the phospholipids. Because •OH was produced at the *cis* side of the planar bilayer, •OH should first attack the phospholipid molecules of the leaflet facing the •OH generating system (*cis* side). The asymmetrical bilayer made of 100% PE and PE/PC (7/3) for the *cis* and *trans* leaflet of the bilayer, respectively, was more stable than the asymmetrical bilayer of opposite composition. The head group of PE may protect the unsaturated fatty acyl chains from the attack by •OH. Formation of a Schiff base between PE head groups and aldehyde formed by the decomposition of lipid peroxide and/or the cross-linking between the ethanolamine head groups may also contribute to the more stable bilayer containing more PE (van Duijn *et al.*, 1984). The composition of the head group at the *cis* leaflet is an important factor determining the stability of the planar bilayer.

Many reports showed that the ion permeability of biological membranes was increased under the condition of oxidative stress. According to the results of this study, the increase of the ion permeability is not due to the increase at the lipid bilayer by the formation of lipid peroxide. Rather, the degradation products of peroxidized lipid, such as various aldehydes, are important to the change of membrane permeability through modification of membrane ion-transporting proteins (Halliwell and Gut-

teridge, 1989). In addition, direct modification of membrane proteins would be also important for the increase of the ion permeability of the membrane induced by the oxidative stress. Indeed, several reports suggested that modification of sulfhydryl groups of ion channel proteins increased the ion permeation through the channels (Anzai *et al.*, 1998; Xu *et al.*, 1998; Bouzat *et al.*, 1991; Abramson *et al.*, 1995; Serre *et al.*, 1995).

ACKNOWLEDGMENTS

The authors thank Drs. Jun-ichi Ueda and Yuri Miura for helpful discussion.

ABBREVIATIONS

AAPH, 2,2′-azobis(2-amidinopropane) dihydrochloride; $Cu(en)_2$, Cu(II)(ethylenediamine)$_2$ complex; DMPO, 5,5′-dimethyl-1-pyrroline-*N*-oxide; DTPA, diethylenetriamine- *N,N,N′, N″,N″*-pentaacetic acid; ESR, electron spin resonance; H_2O_2, hydrogen peroxide; LUVs, large unilamellar vesicles; •OH, hydroxyl radical; PC, egg phosphatidylcholine; PE, egg phosphatidylethanolamine; ROO•, peroxyl radical; ROS, reactive oxygen species; SUVs, small unilamellar vesicles.

REFERENCES

ABRAMSON, J.J., ZABLE, A.C., FAVERO, T.G., and SALAMA, G. (1995). Thimerosal interacts with the Ca^{2+} release channel ryanodine receptor from skeletal muscle sarcoplasmic reticulum. J. Biol. Chem. **270,** 29644–29647.

ANZAI, K., OGAWA, K., GOTO, Y., UEDA, J., MIURA, Y., and OZAWA, T. (1998). Effects of hydroxyl radicals and peroxyl radicals on ion permeability of membranes. In *Biological Oxidants & Antioxidants: Molecular Mechanisms & Health Effects.* L. Packer and A.H.S. Ong (eds.). (Champaign, AOCS Press) pp. 79–89.

ANZAI, K., KADONO, H., HAMASUNA, M., LEE, S., AOYAGI, H., and KIRINO, Y. (1991). Formation of ion channels in planar lipid bilayer membranes by synthetic basic peptides. Biochim. Biophys. Acta **1064,** 256–266.

BOUZAT, C., BARRANTES, F.J., and SIGWORTH, F.J. (1991). Changes in channel properties of acetylcholine receptors during the time course of thiol chemical modifications. Pflugers Arch. **418,** 51–61.

BUEGE, J.A., and AUST, S.D. (1978). Microsomal lipid peroxidation. Methods Enzymol. **52,** 302–310.

DREHER, D., and JUNOD, A.F. (1995). Differential effects of superoxide, hydrogen peroxide, and hydroxyl radical on intracellular calcium in human endothelial cells. J. Cell. Physiol. **162,** 147–153.

HALLIWELL, B., and GUTTERIDGE, J.M.C. (1989). *Free Radicals in Biology and Medicine.* (Oxford University Press, New York, NY).

JESSUP, W., DEAN, R.T., and GEBICKI, J.M. (1994). Iodometric determination of hydroperoxides in lipids and proteins. Methods Enzymol. **233,** 289–303.

KANEDA, Y., UCHIDA, T., KIM, J., ISHIURA, M., and OKADA, Y. (1987). The improved efficient method for introducing macromolecules into cells using HVJ (Sendai virus) lipodomes with gangliosides. Exp. Cell Res. **173,** 56–69.

KANEKO, M., MATSUMOTO, Y., HAYASHI, H., KOBAYASHI, A., and YAMAZAKI, N. (1994). Oxygen free radicals and calcium homeostasis in the heart. Mol. Cell. Biochem. **139,** 91–100.

KATSU, T., KOBAYASHI, H., and FUJITA, Y. (1986). Mode of action of gramicidin S on *Escherichia coli* membrane. Biochim. Biophys. Acta **860,** 608–619.

KRAINEV, A.G., and BIGELOW, D.J. (1996). Comparison of 2,2′-azobis(2-amidinopropane) hydrochloride (AAPH) and 2,2′-azobis(2,4-dimethylvaleronitrile (AMVN) as free radical initiators: a spin-trapping study. J. Chem. Soc., Perkin Trans. 2 **1996,** 747–754.

KUNIMOTO, M., INOUE, K., and NOJIMA, S. (1981). Effect of ferrous ion and ascorbate-induced lipid peroxidation on liposomal membranes. Biochim. Biophys. Acta **646,** 169–178.

NAKAZAWA, T., and NAGATSUKA, M. (1980). Radiation-induced lipid peroxidation and membrane permeability in liposomes. Int. J. Radiat. Biol. **38,** 537–544.

NIKI, E. (1990). Free radical initiators as source of water- or lipid-soluble peroxyl radicals. Methods Enzymol. **186,** 100–109.

OZAWA, T., and HANAKI, A. (1991). The first ESR spin-trapping evidence for the formation of hydroxyl radical from the reaction of copper(II) complex with hydrogen peroxide in aqueous solution. J. Chem. Soc., Chem. Commun. **1991,** 330–332.

OZAWA, T., TAKAZAWA, F., GOTO, H., and HANAKI, A. (1988). *Formation of Hydroxyl Radical from the Reaction of Copper (11) Complexes with Hydrogen Peroxide.* (Nippon Kagaku Kaishi) pp. 459–465.

SATO, Y., KAMO, S., TAKAHASHI, T., and SUZUKI, Y. (1995). Mechanism of free radical-induced hemolysis of human erythrocytes: hemolysis by water-soluble radical initiator. Biochemistry **34,** 8940–8949.

SEN, C.K. (1998). Redox signaling and the emerging therapeutic potential of thiol antioxidants. Biochem. Pharmacol. **55,** 1747–1758.

SEN, C.K., ROY, S., and PACKER, L. (1996). Involvement of intracellular Ca^{2+} in oxidant-induced NF-kB activation. FEBS Lett. **385,** 58–62.

SERRE, V., ILDEFONSE, M., and BENNETT, N. (1995). Effects of cysteine modification on the activity of the cGMP-gated channel from retinal rods. J. Membr. Biol. **146,** 145–162.

TRUMP, B.F., and BEREZESKY, I.K. (1992). The role of cytosolic Ca^{2+} in cell injury, necrosis and apoptosis. Curr. Opin. Cell Biol. **4,** 227–232.

VAN DUIJN, G., VERKLEIJ, A.J., and DE KRUIJFF, B. (1984). Influence of phospholipid peroxidation on the phase behavior of phosphatidylcholine and phosphatidylethanolamine in aqueous dispersions. Biochemistry **23,** 4969–4977.

WHITE, D.A. (1973). The phospholipid composition of mammalian tissues. In *Form and Function of Phospholipids.* C.B. Ansell, J.N. Hawthorne, and P.M.C. Dawson (eds.). (Elsevier Scientific Publishing Company, Amsterdam) vol. 3, pp. 441–482.

XU, L., EU, J.P., MEISSNER, G., and STAMLER, J.S. (1998). Activation of the cardiac calcium release channel (ryanodine receptor) by poly-S-nitrosylation. Science **279,** 234–237.

Address reprint requests to:
Dr. Kazunori Anzai
Bioregulation Research Group
National Institute of Radiological Sciences
4-9-1 Anagawa, Inage-ku,
Chiba 263-8555, Japan

E-mail: anzai@NIRS.go.jp

RADIATION RESEARCH 153, 392–397 (2000)
0033-7587/00 $5.00

Increased Expression of Intracisternal A-Particle RNA in Regenerated Myeloid Cells after X Irradiation in C3H/He Inbred Mice

Hiroshi Ishihara,[1] Izumi Tanaka, Masako Furuse and Kazuko Tsuneoka

First Research Group, National Institute of Radiological Sciences, Anagawa 4-9-1, Inage-ku, Chiba-shi, Chiba 263-8555, Japan

Ishihara, H., Tanaka, I., Furuse, M. and Tsuneoka, K. Increased Expression of Intracisternal A-Particle RNA in Regenerated Myeloid Cells after X Irradiation in C3H/He Inbred Mice. *Radiat. Res.* 153, 392–397 (2000).

Myeloid leukemia cells were derived from regenerated hematopoietic cells damaged by sublethal doses of X radiation in C3H/He inbred mice. We previously found that within the genome of the myeloid leukemia cells, a retrotransposon, the intracisternal A-particle (IAP) element, is integrated. Levels of IAP RNA, the source of cDNA for the integration, were analyzed quantitatively in C3H mice. Higher levels of IAP transcripts were observed in normal cells, particularly in hematopoietic cells, from C3H/He mice, than in those from C57BL/6J and STS/A mice. In the C3H/He mice, an approximately twofold increase in IAP RNA was found in the regenerated spleen and bone marrow cells at 5 days and from 12 to 90 days after whole-body X irradiation. In addition, an increased level of IAP RNA was observed in all the myeloid leukemia cells derived from C3H/He mice. This suggests that the elevated levels of IAP RNA in the regenerated hematopoietic cells after irradiation contribute to the increase in retrotransposition of IAP found in myeloid leukemia cells from C3H/He mice. © 2000 by Radiation Research Society

INTRODUCTION

Intercisternal A-particle (IAP) is a murine retrotransposon that is a noninfectious retrovirus-like particle (*1–3*). Like the provirus of retroviruses, the IAP DNA element is composed of a *gag-pol-(env)*-like sequence with a long terminal repeat (LTR) at each end. The transcript from 5′-LTR is reverse-transcribed to form intact cDNA, and then the cDNA is integrated into a novel locus of the mouse genome (*1*). The presence of 1000 copies of the IAP element in the normal mouse genome is due to the occurrence of the retrotransposition in the germ line. The inserted IAP element can interfere with the function of the adjacent gene. Examples of IAP-mediated mutagenesis have been found in various tumor cells (*2*) and mutant mice (*4*).

C3H/He inbred mice can be used as a model system to obtain radiation-induced myeloid leukemia. When the mice are exposed to 3 Gy whole-body radiation, hematopoietic progenitor cells are damaged (*5*). Although the damaged hematopoietic cells are regenerated at a normal level 2–4 weeks after irradiation (*6*), 20–30% of the mice develop leukemia within 2 years (*5*). The isolated leukemia cells from different individual mice show various histochemical and morphological phenotypes. Thus "leukemia lines" in various lineages and differentiation stages are obtained (*7, 8*). Genomes of all the various leukemia cell lines contained novel integration sites for the IAP element (*9*). Since the functions of the interleukin-3 gene are modified by the IAP-mediated retrotransposition in one of the leukemia cell lines (*10*), it is suggested that the IAP-mediated event contributes to the unique features of the leukemia cells as in the WEHI-3B leukemia cell line (*11*).

The frequent occurrence of IAP-mediated retrotransposition among all the leukemia cell lines from different mice suggests that any sequential mechanism of retrotransposition can be activated during or after the generation of the leukemia cells, regardless of the etiology of the leukemogenesis. Since transcription of the IAP element is the initial step of the transposition, we analyzed the changes in the message level in myeloid cells from normal C3H mice after X irradiation.

MATERIALS AND METHODS

Mice, Irradiation and Preparation of RNA

C3H/HeMs, C57BL/6J and STS/A inbred mice produced in our Institute were used in this study. Specific pathogen-free male mice were irradiated with X rays at 10 weeks of age at a dose rate of 0.682 Gy/min at 2000 kVp/20 mA filtered through 0.5 mm each of copper and aluminum. Three mice were killed humanely on each scheduled day after irradiation, and the tissue samples from different mice were isolated separately and used for the preparation of RNA. Spleen, thymus, liver and blood were isolated immediately after the killing of mice anesthetized with ether. Total RNA was prepared by the guanidium hot phenol method (*12*) and the concentration of RNA was measured by Bioprofil™ (Vilber Loumat) as the intensity of bands after staining with ethidium bromide of the electrophoresis gel with standard RNAs. The myeloid leukemia cell lines used in the study have been described previously (*9*). All animals received humane care in compliance with the guidelines of the Committee of Safety and Ethics of Experimental Animals of the National Institute of Radiological Sciences.

[1] Author to whom correspondence should be addressed.

FIG. 1. IAP expression in tissues of inbred mice. RNAs from the bone marrow (B), spleen (S), thymus (T) and liver (L) of inbred strains (as indicated) were analyzed by Northern blot hybridization. Arrows show the main band of IAP and β-actin as standard.

Probes

The IAP 5′-LTR DNA fragment was prepared from C3H mouse genomic DNA by PCR using the primers 5′-TTGGGAAGCCGCCCCCACAT-3′ and 5′-TCTGGAATGAGGTATCCCTCCT-3′ (corresponding to the sequence from 114 to 556 in the DDBJ-EMBL-GenBank database, accession number D63766). Similarly, mouse β-actin DNA (nucleotide position 286 to 686 of the DDBJ-EMBL-GenBank database sequence, accession number X03765) was prepared by genomic PCR. The DNAs were labeled with [α-^{32}P-dCTP] (NEN, 111 TBq/mmol) using the random hexamer primer extension kit (Gibco-BRL). The specific activity of both probes was adjusted to 5×10^8 cpm/μg DNA by addition of unlabeled DNA.

For the subtype-specific quantification of IAP-LTR, we used two probes with a variation at nucleotide position 227 to 249 (accession number D63766) (*9*). These two DNA oligomers, RS-IAP-R (5′-GAGCTGACGTTCACGGGAAAAAC-3′) and U-IAP-R (5′-GAGCGTGACGTCACGGGGAAG-3′), were end-labeled with [γ-^{32}P]ATP (NEN, 222 TBq/mmol) by T4 polynucleotide kinase.

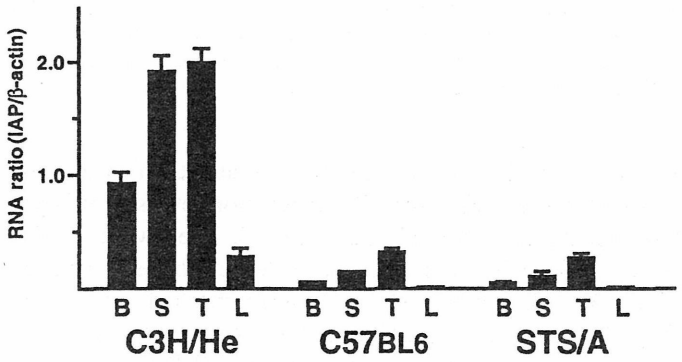

FIG. 2. Relative IAP expression levels among different tissues from inbred mice. From three mice per strain, bone marrow (B), spleen (S), thymus (T) and liver (L) were isolated and used for quantitative Northern hybridization as described in the Materials and Methods. Mean and standard deviation values of the relative RNA ratio of IAP/β-actin among the three mice are indicated. The mean level ± SD for three membrane is as follows: 0.94 ± 0.07 (B), 1.93 ± 0.15 (S), 2.01 ± 0.15 (T) and 0.29 ± 0. 06 (L) in C3H/HeMs mice; 0.07 ± 0.03 (B), 0.16 ± 0.02 (S), 0.34 ± 0.02 (T) and 0.01 ± 0.01 (L) in C57BL/6J mice; and 0.06 ± 0.01 (B), 0.12 ± 0.03 (S), 0.23 ± 0.06 (T) and 0.02 ± 0.01 (L) in STS/A mice.

Quantitative Northern Blot Hybridization

To compare the amount of IAP RNA among different samples, the ratio of IAP to β-actin RNA levels was calculated using blot membranes prepared as follows. The RNA samples from each mouse were electrophoresed and analyzed separately. To prepare multiple Northern blot membranes with the same samples in the same amounts, total RNA was glyoxylated, divided, electrophoresed at least in duplicate at 10 μg per lane, and transferred to a nylon membrane (Amersham, Hybond N+) by the standard methods (*12*). Using the series of membrane copies, hybridization with appropriate probes was done. After washing, the membrane was exposed to an ImagingPlate™ (Fuji Photofilm Co.). From the record on the ImagingPlate™, the radioactivities of the IAP and β-actin bands of each sample were measured using the BAS 2000 system (Fuji). The β-actin RNA level during regeneration did not fluctuate markedly (maximal difference was 8 ± 8%; data not shown); we chose this level as an internal standard. To calculate relative RNA ratios of IAP to β-actin, the value of the IAP RNA band minus the mean background level was divided by the value of β-actin RNA minus the background. Finally, the RNA ratios for the individual mice were obtained.

RESULTS

Enhanced IAP Expression in C3H/HeMs Inbred Mice

First, we compared basal levels of IAP RNAs in cells from the spleen, thymus and liver among inbred mouse strains by Northern blot hybridization (Fig. 1). Expression of IAP RNA of 5–7 kb was detected in the bone marrow and spleen of C3H/HeMs mice and in the thymus from all the mice tested. Small IAP RNA bands were detected in the liver cells from C3H/HeMs mice, probably due to the deleted derivatives of IAP elements (*1*). Since transposition of the full-length type at 7 kb or I-delta 1 type at 5 kb of IAP occurs in most of the tumor cells, we focused on the hybridized area of 5–7 kb with the elimination of the small IAP RNA for subsequent quantitative analyses. To compare relative IAP levels, IAP/β-actin ratios were calculated using three sets of separate membranes in triplicate. All the membranes were hybridized simultaneously to IAP and β-actin probes (Fig. 2). A high level of long IAP transcript was detected in hematopoietic cells in C3H/HeMs inbred mice.

Spleen, thymus and marrow cells expressed approximately six-, six- and threefold more IAP RNA than liver cells, respectively. In contrast, cells from STS/A and C57BL/6J mice expressed less IAP RNA. Even though thymus cells expressed the highest level of IAP RNA among all the cells from STS/A and C57BL/6J mice, the RNA ratio for IAP/β-actin was lower than that of the liver cells from C3H/HeMs mice. Thus it was confirmed that hematopoietic cells in C3H/HeMs mice possess three- to sixfold more IAP RNA than any cells in other inbred mice.

Modulation in the Level of IAP RNA during Regeneration of Hematopoietic Cells

After whole-body irradiation with a sublethal dose (3 Gy) of X rays, hematopoietic cells were damaged and regenerated. We analyzed the fluctuations in the numbers of the cells and IAP RNA levels (Fig. 3). At various times after irradiation, tissues from three mice were separately isolated and analyzed. The numbers of cells in the spleen and marrow were diminished at 1 day but then increased gradually (Fig. 3a). In spleen and bone marrow cells, the RNA ratios of IAP/β-actin were decreased at day 1 and increased above the normal level at day 5 and day 12. The levels remained elevated for at least 90 days after irradiation (Fig. 3b). In peripheral blood, the RNA ratio was normal on day 5 and elevated after day 12 (Fig. 3c). No such fluctuation was observed in the liver. Since IAP RNA levels may be different in mice of the same strain from different colonies, we conducted similar experiments using three groups of mice from different colonies and birth dates. The ratio increased in IAP RNA at day 5 in spleen, at day 12 in bone marrow, and after day 18 in both spleen and bone marrow. In peripheral blood cells, an increase in IAP RNA was detected after day 18 (data not shown). Mean ratios of IAP/β-actin/control of 2.04 (SD = 0.31, SEM = 0.103) at day 5 and 2.31 (SD = 0.85, SEM = 0.11) at day 18 were obtained in spleen cells from these mice. The results show that an increase in IAP RNA is characteristic of regenerated cells present in spleen, marrow and blood.

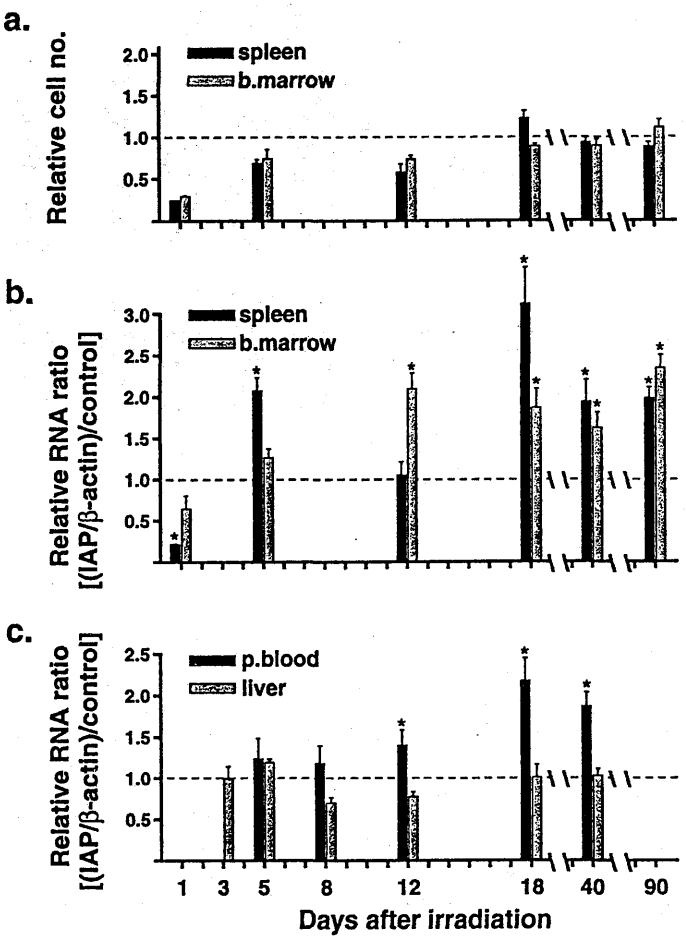

FIG. 3. Number of cells and IAP expression during hematopoietic regeneration. Spleen, femur, liver and blood were isolated on the days indicated after irradiation. For each period, three mice were used and the samples were analyzed separately. Panel a: Total numbers of the cells from spleen and femur bone marrow were counted and the relative ratio compared to nonirradiated mice is shown. Panels b, c: The RNA ratio of IAP/β-actin calculated after quantitative Northern hybridization was divided by that of nonirradiated cells. The relative RNA ratio for spleen (b), bone marrow (b), peripheral blood (c) and liver (c) are shown. The mean and ± SD for the relative RNA ratio of IAP/β-actin among the three mice at each point are shown. Asterisks (*) indicate data at $P < 0.05$ compared to controls by a t test.

Enhanced Increase in RNA of IAP in Myeloid Leukemia Cells

Cells from myeloid leukemia lines derived from C3H/HeMs mice have a genome retrotransposed with the IAP element. In the nucleotide database, there are two major sequence variations at position 116 to 140 of IAP LTR, a U-type sequence that occupies the majority of the IAP LTR sequence and an RS type (Fig. 4a). We previously found that only RS-type IAP elements are transposed in the leukemia cells derived from C3H mice (*9*). The LTR-type specific expression was quantified using the subtype-specific oligonucleotide probes. No difference in the expression levels could be detected in regenerating spleen cells after irradiation (data not shown). In the RNA samples from the leukemia cells, the levels of the RS-type IAP element in all the myeloid cells were twofold greater than in the normal spleen cells (Fig. 4b). The expression levels of RS-type IAP among the myeloid leukemia cell lines were similar, although the RNA levels of one of the retrotransposons, the virus-like 30s particle element, were markedly increased (Fig. 4d). In contrast, all the leukemia and normal spleen cells possess similar levels of U-type IAP RNA (Fig. 4c). This implies that the increase in the RNA level of a limited subset of the IAP element, which contributes to retrotransposition, is a common feature of leukemia cell lines.

DISCUSSION

We previously found transposed IAP elements in the genomes of myeloid leukemia cells induced by X irradiation

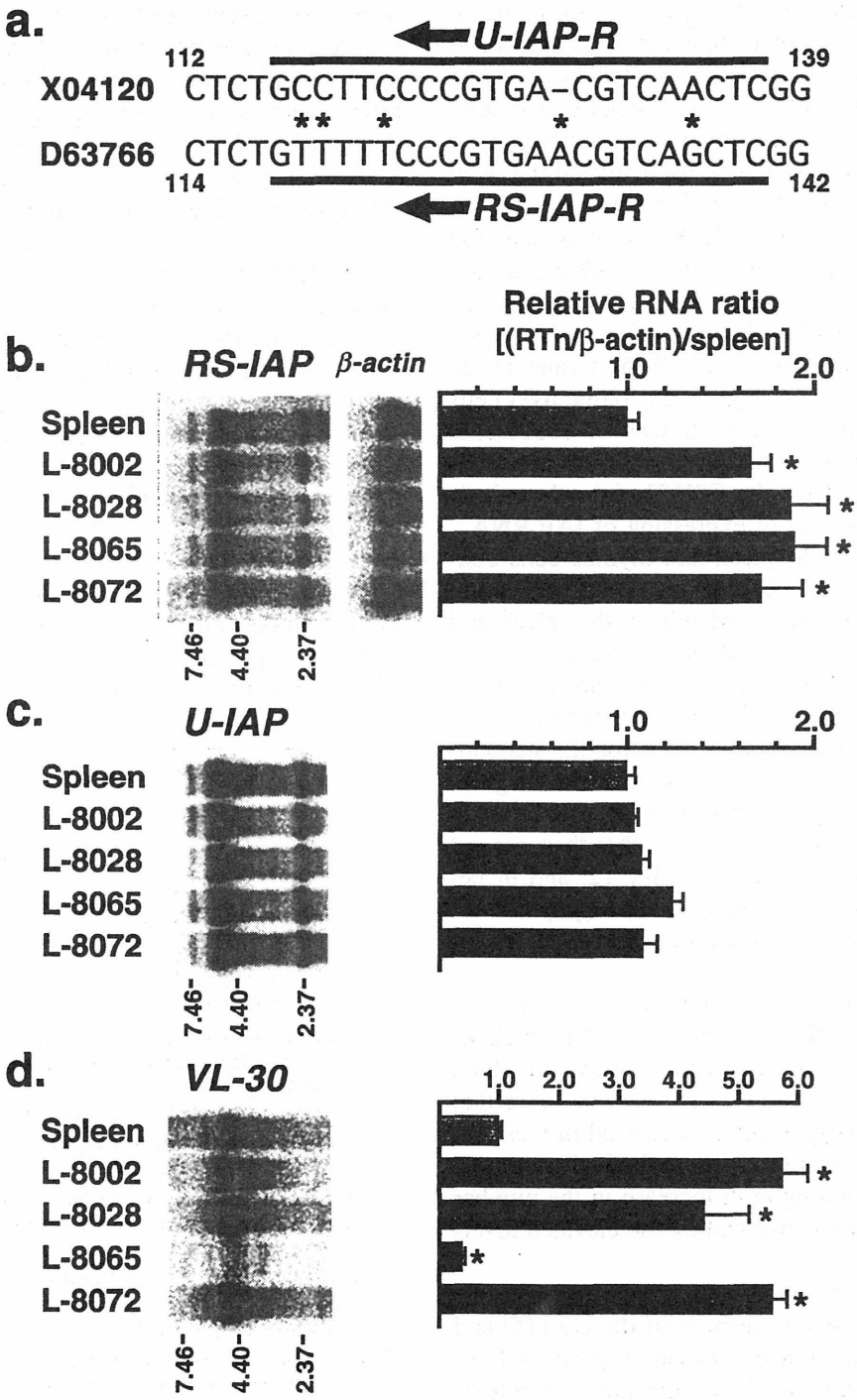

FIG. 4. IAP RNA expression in myeloid leukemia cells. Panel a: Sequence variation in LTR was used to analyze IAP subtype-specific expression. Sequences of accession no. X04120 from WEHI-3B cells (upper) and D63766 from leukemia cells derived from C3H/HeMS mice (lower) are shown. Differences in nucleotides are indicated by asterisks. Numbers indicate the site of the nucleotide from the 5′ end of LTR in both sequences. Areas for oligonucleotide probes are underlined. Panels b–d: RNAs from normal spleen and four myeloid leukemia lines, L-8002, L-8028, L-8065 and L-8072, were used. Twelve electrophoresis gels with 10 μg of total RNA per sample were prepared and blotted. They were divided into four groups for triplicate hybridization probed with RS-type IAP (b), U-type IAP (c), virus-like 30S (d) and β-actin (b) as standard. After exposure of the ImagingPlate™ (left panels), the intensity of the main RNA band was measured and the ratio of IAP (or VL30)/β-actin was calculated. The data are represented as the relative RNA ratio compared to the expression in normal spleen (right panels). The mean ± SD of the relative RNA ratio of IAP/β-actin for three mice for each point are indicated. Asterisks (*) indicate data at $P < 0.05$ compared to control by a t test.

of C3H/He mice (*9, 10*). The IAP-mediated retrotransposition includes the transcription to generate RNA that is 200 nucleotides shorter than the original IAP element, reverse-transcription to generate full-length IAP cDNA, and integration into genomic DNA. Since the intermediates and the cDNA are difficult to detect *in vivo*, we analyzed the level of the transcription product of the IAP element.

Since the generation of myeloid leukemia by X radiation is a unique to C3H/He mice, we compared IAP expression levels among three inbred mouse strains. Similar to the findings in BALB/c mice (*13*), the expression of IAP RNA in cells was highest in the thymus of all the tissues tested in STS/A and C57BL/6J mice (Figs. 1, 2). While liver cells expressed a lower level than other tissues in C3H/HeMs mice, the level was similar to that in the thymus from STS/A and C57BL/6J mice. Thus the C3H/He inbred strain is characterized by a high level of expression of IAP RNA.

In C3H/HeMs mice, both spleen and thymus cells contain a large amount of IAP RNA (Figs. 1, 2). When the mice were irradiated, the number of cells in the spleen and marrow and the RNA ratio of IAP/actin recovered to the normal level simultaneously at day 5 after irradiation (Fig. 3). Although the number of cells ultimately returns to the normal level, it takes more than 15 days for the hematopoietic system to recover as indicated by the levels of granulocyte-macrophage colony-forming units (*6*). As shown in Fig. 3b and c, the IAP RNA level was higher than normal in spleen at day 5, in bone marrow at day 12, and in peripheral blood at day 18. This implies that cell populations with a high level of IAP RNA in the hematopoietic system expand during the repair period.

The level of IAP RNA was elevated for a long period in the hematopoietic tissues (Fig. 3). Since elevated levels of IAP RNA are found in tumor cells with a genome in which the IAP element is integrated (*14, 15*), it is possible that the frequency of retrotransposition is increased in these regenerated cells. The retrotransposition in the leukemia cells may be improved by the long-term increase in the number of undifferentiated myeloid cells and by the elevated levels of IAP RNA.

IAP elements can be classified by structure (*1*), or by the differences in the nucleotide sequences of the U3 (*15*) and R region (*16, 17*). We previously focused on position 118–140 of the IAP LTR and found that the novel retrotransposition in leukemia is mediated by the RS type of IAP element (Fig. 4a, ref. *9*). Even though leukemia cells from different mice express various amounts of a retrotransposon, VL30 (*3*), all of them exhibited similar levels of IAP RNA. The levels of RS-type IAP RNA in the cells from all the leukemia lines were twofold higher than those in normal spleen cells, although similar levels of expression of non-RS (U) type were found among leukemia and spleen cells. Since this subtype of the IAP element contributes to both the increase in the RNA level and retrotransposition in all the leukemia cells, this limited subtype may be activated in the cells. Alternatively, one of the spleen cells from which the leukemia cells originate may acquire a phenotype of accumulation of RS-IAP RNA at some stage after X irradiation. However, the relationship is obscure because little is known about the sequence variation of the IAP element when there are 1,000 copies in the genome. Thus further analyses of IAP RNA accumulation and the retrotransposition using the IAP subtype are required.

The elevated expression of IAP warrants study in hematopoietic cells, since IAP has the potential to change genomic structures and functions. The mechanism by which the IAP transcripts are activated has been studied, and three enhancer sites have been identified at different positions of LTR in cells of embryonic (*18*), plasmacytoma (*19*) and myeloid (*20*) cell lines. In addition to the cell-type specificity, the enhancer activities exhibit diverse nucleotide sequences (*19, 20*). Moreover, DNA methylation also alters the enhancer activities (*18–21*). Since those studies used cells of tumor cell lines, the mechanisms may not be the same as those in normal cells from C3H/HeMs inbred mice. Further studies on the mechanism of strain- and tissue-specific IAP expression in normal cells will help to clarify the effect of radiation on endogenous function in hematopoietic cells.

Received: May 4, 1999; accepted: December 8, 1999

REFERENCES

1. E. L. Kuff and K. K. Lueders, The intracisternal A-particle gene family: Structure and functional aspects. *Adv. Cancer Res.* **51**, 183–276 (1988).
2. E. L. Kuff, Intracisternal A-particles in mouse neoplasia. *Cancer Cells* **2**, 398–400 (1990).
3. E. Keshet, R. Schiff and A. Itin, Mouse retrotransposons: A cellular reservoir of long terminal repeat (LTR) elements with diverse transcriptional specificities. *Adv. Cancer Res.* **56**, 215–251 (1991).
4. T. J. Wasicek, L. Zang, X. J. Guan, T. Zhang, F. Costantini and S. M. Tilghman, Two dominant mutations in the mouse fused gene are the result of transposon insertions. *Genetics* **147**, 777–786 (1997).
5. M. Seki, K. Yoshida, M. Nishimura and K. Nemoto, Radiation-induced myeloid leukemia in C3H/He mice and the effect of prednisolone acetate on leukemogenesis. *Radiat. Res.* **127**, 146–149 (1991).
6. K. Nemoto, H. Ishihara, I. Tanaka, G. Suzuki, K. Tsuneoka, K. Yoshida and H. Ohtsu, Expression of interleukin-1β mRNA in mice after whole body X-irradiation. *J. Radiat. Res.* **36**, 125–133 (1995).
7. K. Yoshida, K. Nemoto, M. Nishimura, I. Hayata, T. Inoue and M. Seki, Nature of leukemic stem cells in murine myelogenous leukemia. *Int. J. Cell Cloning* **4**, 91–102 (1986).
8. H. Ishihara, K. Yoshida, K. Nemoto, K. Tsuneoka and M. Shikita, Constitutive overexpression of the c-*fos* gene in radiation-induced granulocytic leukemia in mice. *Radiat. Res.* **135**, 394–399 (1993).
9. H. Ishihara and I. Tanaka, Detection and cloning of unique integration sites of retrotransposon, intracisternal A-particle element in the genome of acute myeloid leukemia cells in mice. *FEBS Lett.* **418**, 205–209 (1997).
10. I. Tanaka and H. Ishihara, Unusual long target duplication by insertion of intracisternal A-particle element in radiation-induced acute myeloid leukemia cells in mouse. *FEBS Lett.* **376**, 146–150 (1995).
11. S. Ymer, W. Q. J. Tucker, C. J. Sanderson, A. J. Hapel, H. D. Campbell and I. G. Young, Constitutive synthesis of interleukin-3 by leukemia cells line WEHI-3B is due to retroviral insertion near the gene. *Nature* **317**, 255–258 (1985).

12. T. Maniatis, J. Sambrook and E. F. Fritsch, *Molecular Cloning: A Laboratory Manual*, pp. 187–206. Cold Spring Harbor Laboratory, Cold Spring Harbor, NY, 1982.

13. E. L. Kuff and J. W. Fewell, Intracisternal A-particle gene expression in normal mouse thymus tissue: Gene products and strain-related variability. *Mol. Cell. Biol.* **5**, 474–483 (1985).

14. G. L. C. Shen-ong and M. D. Cole, Amplification of a specific set of intracisternal A-particle genes in a mouse plasmacytoma. *J. Virol.* **49**, 171–177 (1984).

15. K. K. Luders, J. W. Fewell, V. E. Morozov and E. L. Kuff, Selective expression of intracisternal A-particle genes in established mouse plasmacytomas. *Mol. Cell. Biol.* **13**, 7439–7446 (1993).

16. R. J. Christy, A. R. Brown, B. B. Gourlie and R. C. C. Huang, Nucleotide sequence of murine intracisternal A-particle LTRs extensive variability within the R region. *Nucleic Acid Res.* **13**, 289–302 (1985).

17. J. A. Mietz and E. L. Kuff, Intracisternal A-particle-specific oligonucleotides provide multilocus probes for genetic linkage studies in the mouse. *Mamm. Genome* **3**, 447–451 (1992).

18. K. Satyamoorthy, K. Park, M. Atchison and C. C. Howe, The intracisternal A-particle upstream element interacts with transcription factor YY1 to activate transcription: Pleiotropic effects of YY1 on distinct promoter elements. *Mol. Cell. Biol.* **13**, 6621–6628 (1993).

19. M. Falzon and E. J. Kuff, A variant binding sequence for transcription factor EBP-80 confers increased promoter activity on a retroviral long terminal repeat. *J. Biol. Chem.* **265**, 13084–13090 (1990).

20. X. Y. Wang and J. A. McCubrey, Differential effects of retroviral long-terminal repeats on interleukin-3 gene expression and autocrine transformation. *Leukemia* **11**, 1711–1725 (1997).

21. A. Feensta, J. Fewell, K. Lueders and E. Kuff, *In vitro* methylation inhibits the promoter activity of a cloned intracisternal A-particle LTR. *Nucleic Acid Res.* **14**, 4343–4352 (1986).

Carcinogenesis vol.16 no.8 pp.1871–1877, 1995

Estradiol-17β as an initiation modifier for radiation-induced mammary tumorigenesis of rats ovariectomized before puberty

Hiroshi Inano, Hiroshi Yamanouchi[1], Keiko Suzuki, Makoto Onoda and Katsumi Wakabayashi[2]

The First Research Group, National Institute of Radiological Sciences, 9-1 Anagawa-4-chome, Inage-ku, Chiba-shi 263 and [2]Institute for Molecular and Cellular Regulation, Gunma University, Maebashi-shi 371, Japan

[1]Present address: First Department of Anatomy, Wakayama Medical College, Wakayama-shi 640, Japan

This investigation evaluated the roles of estradiol-17β, progesterone and prolactin in the initiation of mammary tumorigenesis by irradiation. Sixty day old Wistar-MS rats ovariectomized bilaterally at 23 days of age were injected daily with olive oil, estradiol-3-benzoate (E_2B), progesterone or haloperidol for 14 days, and were then irradiated with γ-rays (260 cGy) on the morning following the last injection. Diethylstilbestrol pellets were administered by implantation 30 days after the irradiation. Following treatment with E_2B, the incidence of mammary tumors was increased 2.2-fold, in comparison with that in the corresponding control rats. Bilateral ovariectomy before puberty caused the mammary glands of adult rats to atrophy, and a low degree of differentiation with long narrow ducts was observed in whole mounts. The DNA synthesis in the mammary glands and serum prolactin level of E_2B-treated rats were markedly increased and the terminal ducts showed distinctly increased differentiation into terminal end buds and alveolar buds with prolactin receptors. When progesterone, another ovarian hormone, or haloperidol, a dopamine antagonist in adenohypophysis, was injected into the rats under estrogen-free conditions, neither expression of prolactin receptors nor stimulation of DNA synthesis was observed in the mammary glands, and the incidence of mammary tumors induced by irradiation was lower than that observed in rats treated with E_2B. Combined treatment with E_2B and progesterone resulted in a reduction in the incidence of mammary tumors and in serum prolactin levels compared with those in E_2B alone, in spite of the synergistic effects on prolactin receptor concentration and DNA synthesis by the two hormones. On the other hand, concurrent administration of haloperidol did not reduce the E_2B-induced tumor incidence or prolactin concentration in serum. Many of the mammary tumors which developed in the ovariectomized rats were of the ER(−)PgR(−) type. The incidence of development of ER(+)PgR(+) tumors was increased by treatment with E_2B before the irradiation, and no ER(−)PgR(−) tumors were observed in this group. Our results suggest that estrogen is a direct or indirect sensitizer for tumor initiation by radiation, and is also one of the regulatory factors for hormone dependence of radiation-induced mammary tumors.

Introduction

During pregnancy in rats, the concentrations of estradiol and progesterone in serum increase gradually, but the prolactin level remains unchanged at a low level (1). When rats receive γ-ray irradiation during pregnancy, a significantly higher incidence of mammary tumors is observed in the presence of the tumor promotion diethylstilbestrol (DES*) (2,3). On the other hand, during lactation, the serum prolactin level is markedly high, but the estradiol level remains relatively constant at a low level (1). The high concentrations of prolactin receptor and estrogen receptor are observed in the mammary glands at days 5–10 of lactation (4,5), but no progesterone receptor is detected (5). Irradiation in the lactating rats followed by DES treatment results in a high incidence of mammary tumors (6). If tumor initiation by radiation is cell-stage dependent, mammary cell proliferation stimulated by hormones would increase the number of cells at risk. In previous studies (7) to establish whether the mechanisms differ in pregnancy- and lactation-dependent initiation for mammary tumors by radiation, rats were treated with estrogen and/or progesterone immediately after bilateral ovariectomy in adulthood and were then exposed to radiation. The incidence of mammary tumors in the treated rats was significantly higher than that in the controls in the presence of DES. In that condition, the mammary glands had previously been affected by ovarian hormones—estrogens and progestins—before the ovariectomy. In the present study, we used rats ovariectomized bilaterally before the onset of the estrous cycle to evaluate the role of estradiol under progesterone-free conditions and the role of progesterone in the absence of estrogen-priming in the sensitivity for the initiation of mammary tumors by irradiation. Based on the results, the relationships between mammary tumorigenesis and the endocrinological, histological and cytological stages at the time of irradiation are discussed.

Materials and methods

Materials

Progesterone, DES, haloperidol and calf thymus DNA were purchased from Sigma (St Louis, MO). 17β-Estradiol-3-benzoate (E_2B), cholesterol and olive oil were purchased from Wako Chemical Co. (Tokyo, Japan). [2,4,6,7-^{3}H]Estradiol-17β (sp. act. 4.0 TBq/mmol), [17α-methyl-^{3}H]R5020 (sp. act. 3.0 TBq/mmol) and non-labeled R5020 were obtained from Du Pont/NEN Research Products (Boston, MA). [Methyl-^{3}H]thymidine (sp. act. 2.6 TBq/mmol) and ^{125}I in NaOH solution (3.7 GBq/ml) were purchased from Amersham (Aylesbury, UK). Pellets were prepared in a medical grade Silastic tube (Dow Corning Co. Midland, MI, 1.98 mm i.d., 3.18 mm o.d.), and were filled with 3 mg of DES mixed with 27 mg of cholesterol.

Animals and treatment

Female Wistar-MS rats, bred at our institute, were kept at 23 ± 1°C in a controlled light environment (14 h light/10 h dark). Tap water and diet were taken *ad libitum*. In the protocol (Figure 1), 227 rats were ovariectomized bilaterally at 23 days of age, and were then divided into six groups at 60 days of age. Group I consisted of 40 rats receiving olive oil (0.2 ml/day, s.c.) for 14 days; group II (35 rats) were treated with E_2B (50 μg/0.2 ml olive oil/day, s.c.); group III (38 rats) with progesterone (5 mg/0.2 ml olive oil/day, s.c.); group IV (37 rats) with haloperidol (50 μg/0.2 ml 0.3% tartaric acid/day, s.c.); group V (38 rats) with a combination of E_2B (50 μg) and progesterone

*Abbreviations: DES, diethylstilbestrol; E_2B, 17β-estradiol-3-benzoate; R5020, 17α,21-dimethyl-19-nor-4,9-pregnadiene-3,20-dione; haloperidol (or halo), 4-[4-(*p*-chlorophenyl)-4-hydroxypiperidino]-4-fluorobutyrophenone; ER, estrogen receptor; PgR, progesterone receptor; LH, luteinizing hormone; FSH, follicle stimulating hormone; TSH, thyroid stimulating hormone.

(5 mg) in 0.2 ml olive oil; and group VI (39 rats) with E_2B (50 μg/0.2 ml olive oil/day) together with haloperidol (50 μg/0.2 ml 0.3% tartaric acid/day). Each group was further divided into two subgroups following the last injection; one (20–25 rats/group) for the observation of mammary tumorigenesis and the other (13–17 rats/group) for morphological and biochemical studies. For the observation of mammary tumorigenesis, rats received whole-body irradiation of 260 cGy γ-rays (15 cGy/min) from a ^{60}Co source on the morning following the last injection, and were then implanted with the DES pellets 30 days after the irradiation. The pellets were implanted s.c. in the interscapular region under Nembutal (sodium pentobarbital, Abbott Laboratories, North Chicago, IL) anesthesia. The pellets were replaced every 8 weeks until the end of the experiment. The estimated DES release was 0.38 ± 0.01 μg DES/day (3). The rats were observed for detection of palpable mammary tumors for 1 year after the initiation of DES treatment. When a tumor >2 cm in diameter was detected, the rat was killed by carbon dioxide asphyxiation and the tumor excised. The tumor incidence was calculated from the total number of mammary tumors that developed within 1 year.

Whole mounts of mammary glands

After the hormone treatment for 14 days, the entire inguinal mammary glands were dissected from the inner surface of the skin, retaining as much of the connective tissue as possible, and spread and dried slightly on filter paper. After fixing in 10% formalin buffered with 0.1 M phosphate buffer (pH 7.2) and defatting in acetone, the preparations were stained with alum carmin, destained in ethanol and stored in Cedar oil (8).

Histological examination

The mammary tumors were fixed immediately in 10% neutral buffered formalin. Each paraffin section (4 μm in thickness) was prepared and stained with H&E. The tumors were classified as fibroadenoma or adenocarcinoma according to the criteria for the classification of rat mammary tumors (9).

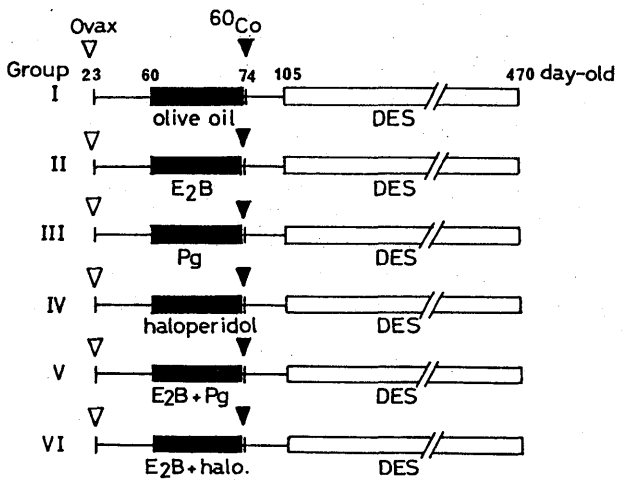

Fig. 1. Experimental schedule of ovariectomy, hormone treatments and irradiation. (▽) Bilateral ovariectomy (Ovax) at 23 days of age; (▼) γ-ray irradiation with ^{60}Co (260 cGy) and assays of DNA synthesis and prolactin receptors in mammary glands and serum hormone concentration at 74 days of age; closed bar, period of hormone treatment; open bar, period of DES treatment.

Assay of receptors

The tumor tissues (1.0 g) were homogenized with 10 mM Tris−HCl buffer (pH 7.4) containing 1.5 mM EDTA-Na and 1 mM dithiothreitol. Homogenates were centrifuged at 105 000 *g* for 1 h at 4°C, and the cytosol fraction (0.4 mg protein/0.2 ml) was incubated with variable amounts of [2,4,6,7-^{3}H]estradiol-17β at 4°C for 16–18 h for assay of estrogen receptor (ER). The incubation mixture was mixed with 0.0025% dextran-coated 0.25% charcoal at 4°C for 30 min to remove the unbound ligand. Also, the cytosol fraction was incubated with [^{3}H]estradiol-17β in the presence of a 1000-fold excess non-radiolabeled estrogen for the determination of non-specific binding (10). For progesterone receptor (PgR), the cytosol fraction (0.4 mg protein/0.1 ml) was incubated with variable amounts of [17α-methyl-^{3}H]R5020 at 4°C for 2 h, and an equal volume of 60% glycerol was added to the incubation mixture. After further incubation at 4°C for 2 h, the dextran-coated charcoal suspension was added. The mixture was shaken vigorously at 4°C for 30 min. Excess non-labeled R5020 was used (11) to determine non-specific binding. For analysis of prolactin receptor in the mammary glands, ovine prolactin (NIDDK-oPRL I-2) for binding assay was generously supplied by the National Hormone and Pituitary Program (Baltimore, MD). ^{125}I-Iodinated prolactin (sp. act. 0.9 MBq/μg) was prepared by the chloramine-T method (12). After hormone treatment for 14 days, the membrane fraction of the mammary glands was prepared according to the method of Posner *et al.* (13). The membranes were treated with 4 M $MgCl_2$ for 5 min at room temperature to remove endogenously bound prolactin from its receptor (14). The membrane preparations (300 μg protein) were incubated with [^{125}I]prolactin (10 000 c.p.m.) at 25°C for 15 h in the presence of various concentrations of unlabeled prolactin. Maximum binding sites and dissociation constant (K_d) values for the receptors were determined by a Scatchard plot analysis (15).

Incorporation of [methyl-^{3}H]thymidine into DNA

On the day following the last hormone treatment, rats were injected i.p. with [methyl-^{3}H]thymidine (22.2 MBq/kg body wt) to the right abdomen. The left inguinal mammary glands and heart were isolated after 1 h, washed with ice-cold saline to remove blood, frozen in liquid nitrogen, and stored at −80°C until assay. The tissues were then homogenized, and DNA was extracted by the method of Chung and Coffey (16) with some modification. A portion of the DNA solution was transferred into scintillation fluid (Clearsol-I, Nacalai Tesque, Tokyo) and its radioactivity was measured with a liquid scintillation spectrometer for a time sufficient to reduce the counting error to <5%. DNA concentrations in the extracts were determined by diphenylamine method at 595 nm after diluting the sample to suitable concentrations, using calf thymus DNA as a standard (17). The incorporation rate was expressed as d.p.m./μg DNA/h. *De novo* DNA synthesis in the mammary glands was expressed as a percentage of the incorporation rate obtained in the heart (18).

Radioimmunoassay

A blood sample was collected from each rat by cardiocentesis under anesthesia. The blood was allowed to clot and centrifuged to obtain serum. The sera were frozen immediately at −80°C until assay was started. Concentrations of luteinizing hormone (LH), follicle-stimulating hormone (FSH), thyroid-stimulating hormone (TSH) and prolactin were determined with NIDDK radioimmunoassay kits kindly supplied by Dr A.F.Parlow, National Hormone and Pituitary Program. The concentration of progesterone was assayed with a commercially available RIA kit (BioMerieux, Marcy-l'Etiole, France), and estradiol-17β was measured by modified methods of Watanabe *et al.* (19).

Iball's index and statistical analysis

Iball's index was defined so that the ratio of incidence (%) to the average latency period in days was multiplied by 100 (20). Statistical analyses were

Table I. Body weight gain and organ weights in bilaterally ovariectomized rats after treatment with hormones

Group	Treatment (*n*)	Body weight (g)			Mammary glands (g)	Pituitary glands (mg)	Uterus (mg)	Adrenal glands (mg)
		Before	After	Gain				
I	olive oil (n = 7)	243.0±6.8	277.0±8.2	+34.0±2.3	6.44±0.25	10.3±0.4	52.3±6.0	91.9±4.4
II	E_2B (n = 6)	234.7±4.3^{c}	213.3±4.7^{a}	−21.6±1.7^{a}	3.51±0.17^{a}	19.3±0.8^{a}	413.2±68.9^{a}	86.5±3.3^{c}
III	progesterone (n = 5)	231.8±4.3^{c,f}	267.5±3.2^{c,d}	+35.7±2.9^{c,d}	5.41±0.45^{c,d}	11.0±0.4^{c,d}	75.6±7.2 ^{c,d}	109.4±3.8^{b,d}
IV	haloperidol (n = 6)	241.8±4.9^{c,f}	262.6±4.9^{c,d}	+21.8±3.4^{a,d}	7.11±0.38^{c,d}	10.2±0.2^{c,d}	42.0±5.0^{c,d}	87.0±4.5^{c,f}
V	E_2B + progesterone (n = 6)	220.5±7.1^{b,f}	217.3±6.5^{a,f}	−3.2±2.6^{a,d}	3.87±0.44^{a,f}	16.2±0.3^{a,d}	210.5±18.7^{a,d}	74.0±3.9^{a,e}
VI	E_2B + haloperidol (n = 6)	247.8±7.3^{c,f}	225.2±7.8^{a,f}	−22.6±2.9^{a,f}	4.93±0.46^{b,e}	20.7±0.9^{a,f}	365.2±16.9^{a,f}	99.8±3.5^{c,e}

$^{a}P < 0.01$, $^{b}P < 0.05$, ^{c}not significant compared with olive oil treatment.
$^{d}P < 0.01$, $^{e}P < 0.05$, ^{f}not significant compared with E_2B treatment.

conducted using Fisher's exact probability test for incidence, and Dunnett's test for the level of significance of differences by multiple comparisons.

Results

Biological effects by treatment with hormones

A significant reduction ($P < 0.01$) of body weight gain was observed in all rats receiving E_2B with or without haloperidol for 2 weeks (Table I). However, the gain in body weight of the rats injected with progesterone was comparable to that of the controls administered olive oil. Compared with the controls, rats injected with E_2B showed hypertrophied pituitary glands (1.9-fold, $P < 0.01$) and uterus (7.9-fold, $P < 0.01$) as well as decreased weight of mammary glands (50% of the control, value $P < 0.01$). The same findings were observed in the rats treated with the combination of E_2B and progesterone and with E_2B and haloperidol. Several of the enlarged pituitary glands were seen macroscopically to have friable hemorrhagic tumors. The significant weight loss of the mammary glands ($P < 0.01$) induced by E_2B was due to disappearance of adipose tissues from the glands. Marked stagnation of the biological fluids in the uterus was observed in the group injected with E_2B. No significant difference among the groups in adrenal weight was observed.

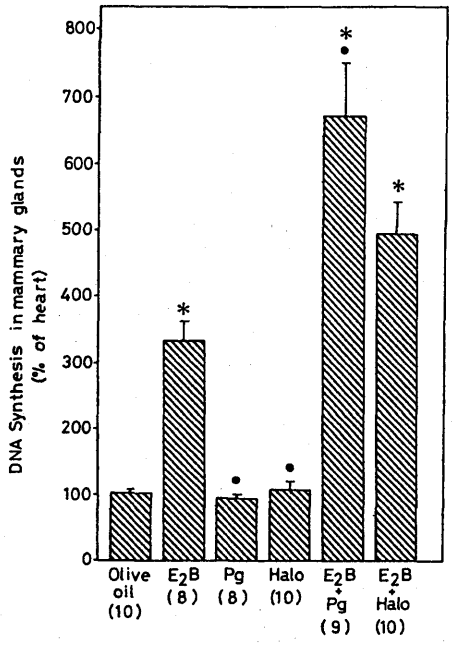

Fig. 2. DNA synthesis in mammary glands of bilaterally ovariectomized rats treated with hormones. Arabic numerals in parentheses indicate the number of experiments. Mean ± SE, (*) significant difference from the control (olive oil treatment), $P < 0.01$, and (●), significant difference from E_2B-treated group, $P < 0.01$. For details, see the text.

DNA synthesis in mammary glands at time of irradiation

On the day following the final hormone treatment, the incorporation of [^{3}H]thymidine into DNA was assayed as an index of cellular proliferation in the mammary glands. In comparison with that in the control rats, the E_2B injection group (group II) showed increased DNA synthesis (3.2-fold, $P < 0.01$), but no effect was found in the progesterone group (group III) and in the haloperidol group (group IV) (Figure 2). Combined injection of E_2B and progesterone (group V) and of E_2B and haloperidol (group VI) resulted in marked synergistic elevation ($P < 0.01$) in DNA synthesis in the glands.

Serum concentration of hormones

The concentration of hormones was assayed using serum collected 24 h after the last treatment. The serum prolactin concentration in the rats injected with E_2B was 32-fold higher ($P < 0.01$) than that in the rats injected with olive oil (Table II). In the rats treated with E_2B combined with progesterone, the serum prolactin level was reduced ($P < 0.05$) to 55% of that observed in the E_2B alone group, but the value was still 18-fold higher ($P < 0.01$) than that in the control rats. No change in prolactin concentration was observed in the haloperidol-treated rats. E_2B markedly reduced the serum concentrations of LH and FSH, and increased the TSH concentration, while these effects of E_2B were not influenced by the presence of progesterone. The estradiol concentration in the

Table II. Serum hormone concentrations of bilaterally ovariectomized rats after treatment with hormones

Group	Treatment (n)	Prolactin (ng/ml)	LH (ng/ml)	FSH (ng/ml)	TSH (ng/ml)	Estradiol-17β (ng/ml)	Progesterone (ng/ml)
I	olive oil (n = 5)	5.3±1.0	3.2±0.3	22.1±2.9	0.58±0.14	0.010±0.001	23.4±0.9
II	E_2B (n = 5)	172.9±18.9[a]	1.0±0.3[a]	8.3±0.4[a]	2.90±0.36[a]	1.36±0.21[a]	44.4±7.6[a]
III	progesterone (n = 5)	15.7±3.7[a,d]	3.4±0.4[c,d]	18.4±0.4[c,d]	1.32±0.22[b,e]	0.014±0.001[c,d]	75.7±3.8[a,e]
IV	haloperidol (n = 5)	8.0±1.2[c,d]	4.3±0.4[c,d]	20.9±0.5[c,d]	0.90±0.11[a,d]	0.006±0.001[c,d]	68.3±6.3[a,f]
V	E_2B + progesterone (n = 5)	96.2±12.1[a,e]	0.5±0.1[a,d]	8.9±1.9[a,f]	3.64±1.13[a,f]	2.68±0.66[a,e]	176.6±12.4[a,d]
VI	E_2B + haloperidol (n = 5)	214.7±14.9[a,f]	1.2±0.1[a,f]	9.2±0.6[a,f]	2.64±0.74[a,f]	1.96±0.25[a,f]	37.4±6.2[b,f]

[a]$P < 0.01$, [b]$P < 0.05$, [c]not significant compared with olive oil treatment.
[d]$P < 0.01$, [e]$P < 0.05$, [f]not significant compared with E_2B treatment.

Table III. Expression of prolactin receptors in mammary glands of bilaterally ovariectomized rats according to hormone

Group	Treatment (n)	K_d value ($\times 10^{-9}$ M)	Maximum binding capacity (fmol/mg protein)
I	olive oil (n = 2)	–	0
II	E_2B (n = 2)	0.50±0.05	32.1 ± 0.1
III	progesterone (n = 2)	–	0
IV	haloperidol (n = 2)	–	0
V	E_2B + progesterone (n = 1)	1.09	54.6
VI	E_2B + haloperidol (n = 2)	0.55±0.18	22.3±6.3

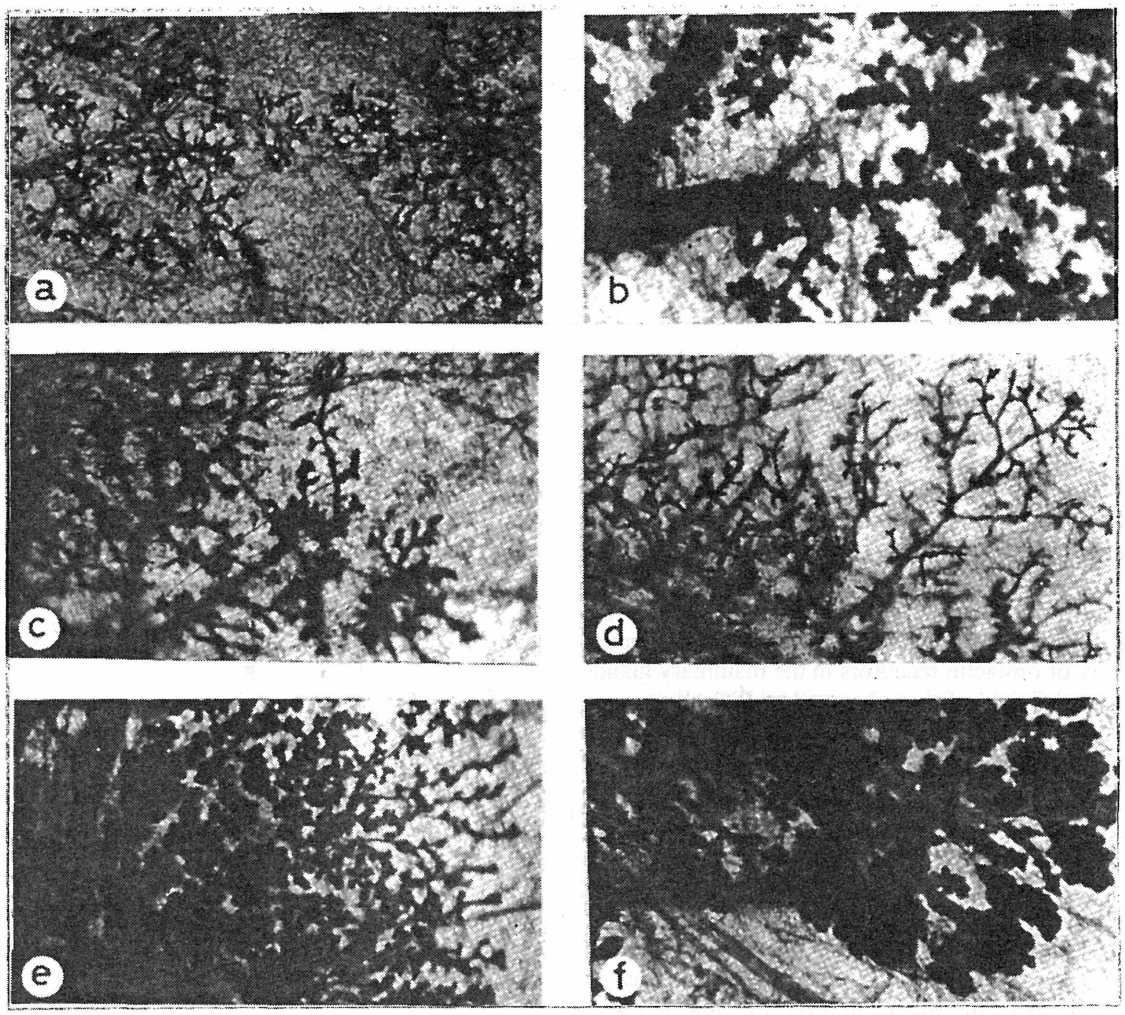

Fig. 3. Whole mount preparation of mammary glands. (**a**) group I (olive oil); (**b**) group II (E_2B); (**c**) group III (progesterone); (**d**) group IV (haloperidol); (**e**) group V (E_2B and progesterone); (**f**) group VI (E_2B and haloperidol). ×13.

Table IV. Development of mammary tumors in bilaterally ovariectomized irradiated rats

Group	Treatment	Rats used	No. of rats with tumors (%)	No. of tumors			Latency period (months)	Iball's index	Tumor weight (g)
				FA[c]	AC[d]	Total (/rat)			
I	olive oil	23	6 (26.1)	5	1	6 (1.0±0.0)	8.8±0.9	9.9	14.9±4.4
II	E_2B	21	12 (57.1)[a]	14	4	18 (1.6±0.1)	9.9±0.4	19.2	4.1±1.4
III	progesterone	25	8 (32.0)[b]	9	2	11 (1.3±0.3)	10.3±0.3	10.4	9.6±3.6
IV	haloperidol	20	6 (30.0)[b]	8	3	11 (1.2±0.1)	10.5±0.4	13.6	13.3±6.2
V	E_2B + progesterone	23	9 (39.1)[b]	7	3	10 (1.3±0.2)	9.6±0.6	13.6	9.7±4.3
VI	E_2B + haloperidol	23	13 (56.5)[a]	14	0	14 (1.1±0.1)	10.3±0.5	18.3	4.3±1.1

[a] $P < 0.05$, [b] not significant compared with olive oil treatment, [c] fibroadenoma, [d] adenocarcinoma.

control rats, ovariectomized bilaterally at 23 days of age, was near the detection limit measurable by radioimmunoassay. That in the E_2B-treated rats was 130- to 260-fold higher ($P < 0.01$) than that in the controls. On the other hand, the concentration of progesterone was not reduced completely by ovariectomy before puberty.

Expression of prolactin receptors in mammary glands according to hormone treatment

Prolactin receptors were not detected in the mammary glands of adult female rats ovariectomized bilaterally before puberty, but expression of prolactin receptors was observed in the

Table V. Expression of ER and PgR in mammary tumors

Group	Treatment	No. of tumors analyzed	Receptors			
			ER(+)PgR(+)	ER(+)PgR(−)	ER(−)PgR(+)	ER(−)PgR(−)
I	olive oil	6	1	1	0	4
II	E_2B	10	7	0	3	0
III	progesterone	10	3	1	0	6
IV	haloperidol	7	3	1	2	1
V	E_2B + progesterone	6	5	0	1	0
VI	E_2B + haloperidol	9	9	0	0	0

ovariectomized rats injected with E_2B (50 μg/day) for 14 days (Table III). The maximum binding capacity of prolactin receptors in the mammary glands in this treatment group (32.1 ± 0.1 fmol/mg protein) was only 2.6% of that (1215 ± 458 fmol/mg protein) observed on day 10 of lactation, which was the highest level observed during lactation (6). Neither progesterone treatment nor haloperidol treatment induced the expression of prolactin receptors in the mammary glands of estrogen-free conditioned rats. However, when the E_2B treatment was combined with progesterone, the maximum binding capacity of prolactin receptors in the mammary glands was increased to 1.7-fold of that observed in E_2B alone.

Whole mounts

The mammary glands of bilaterally ovariectomized rats obtained prior to the irradiation demonstrated a low degree of differentiation with long narrow ducts that branched profusely into terminal ducts (Figure 3a). In the rats treated with E_2B for 14 days, the ducts were apparently thicker than those in the ovariectomy only rats, and the terminal ducts were differentiated into terminal end buds and alveolar buds (Figure 3b). However, no alveolar bud was observed in any area of the mammary glands of the ovariectomized rats injected with progesterone alone for 14 days (Figure 3c), or was identified in rats given haloperidol alone for 14 days (Figure 3d). The mammary glands of rats injected with both E_2B and progesterone contained a small lobule of alveoli and were lacking in terminal end buds (Figure 3e). Thin ducts and differentiated lobuloalveolar structures were observed in the mammary glands of rats treated with E_2B combined with haloperidol (Figure 3f).

Mammary tumorigenesis

Of the 23 rats ovariectomized bilaterally before puberty and administered whole-body irradiation with 260 cGy γ-rays in adulthood (group I), only six (26.0%) developed mammary tumors during the 1 year period of DES implantation (Table IV). Treatment with E_2B of ovariectomized rats before the irradiation (group II) increased the incidence of mammary tumors within the 1 year period to 2.2-fold ($P < 0.05$) and the number of tumors per rat (from 1.0 ± 0.0 to 1.6 ± 0.2). In the rats injected with progesterone (group III) or haloperidol (group IV) before irradiation, the tumor incidence was lower than that observed in the rats treated with E_2B ($P = 0.078$ and 0.075 respectively). In those treated with both E_2B and haloperidol before irradiation (group VI), the development of mammary tumors was comparable to that in the rats injected with E_2B alone (group II), but was significantly higher than that in the ovariectomy only rats ($P < 0.05$). A low incidence of tumors was observed in the rats treated with both E_2B and progesterone (group V), compared with that in group II. The tumor incidence of group V was not significantly different from that in the control rats, and was comparable to those in the rats injected with progesterone alone (group III). The latency period until the first appearance of tumor showed no change associated with the type of hormonal treatment before the irradiation, and also no statistically significant difference in fibroadenoma and adenocarcinoma.

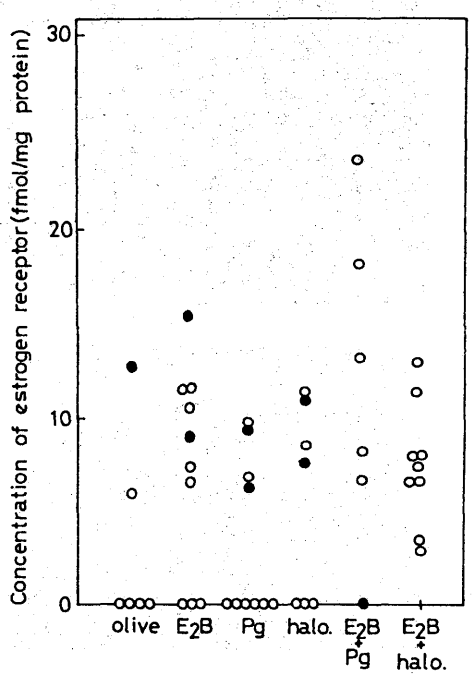

Fig. 4. Maximum binding capacities of ER in mammary tumors. Open and closed circles represent data for fibroadenomas and adenocarcinomas respectively.

ER and PgR in mammary tumors

The results of analysis using a Scatchard plot of ER and PgR in the cytosol fraction of homogenized portions of the mammary tumors >2 cm in diameter are shown in Table V. Many of the mammary tumors which developed in bilaterally ovariectomized rats (group I) were of the ER(−)PgR(−) type. On the other hand, group II rats showed increased incidence of ER(+)PgR(+) tumors, and no ER(−)PgR(−) tumors were detected. Similar results were observed in groups V and VI. Group III showed three ER(+)PgR(+) and six ER(−)PgR(−) tumors. The tumors that expressed ER—7/10 tumors in group II, 5/6 tumors in group V and all tumors in group VI—also have detectable PgR levels.

There were no significant differences among the groups in the concentration of ER in the mammary tumors induced by the irradiation after the hormone treatment (Figure 4). The K_d values of ER in all mammary tumors that developed in rats

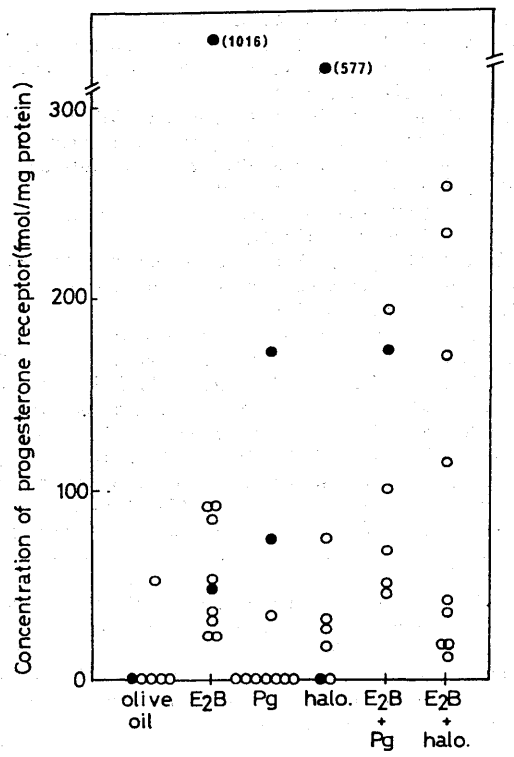

Fig. 5. Maximum binding capacities of PgR in mammary tumors. Open and closed circles represent data for fibroadenomas and adenocarcinomas respectively.

pretreated with both E_2B and progesterone (group V) were $<10^{-10}$ M. As shown in Figure 5, it was clearly suggested that PgR was expressed in all mammary tumors arising from the estrogen-dependent differentiated mammary glands (Figure 3b,e,f) following irradiation.

Discussion

Our experiments clearly established that E_2B induces stimulation of DNA synthesis and expression of prolactin receptors in the mammary glands, and prolactin secretion from the pituitary glands, with development of end buds from terminal ducts. Nicholson *et al.* (21) have reported that the stimulatory actions of estradiol on the growth of mammary glands of ovariectomized rats were not the result of the capacity of this steriod to increase circulating prolactin levels. The results of experiments in which estradiol was administered daily to ovariectomized rats have inspired the hypothesis that estrogen acts not only directly on the mammary glands but also indirectly, through pituitary factors such as prolactin (7). Therefore, our experiments were designed to induce hyperprolactinemia under estrogen-free conditions. Haloperidol, which blocks dopamine receptors in the adenohypophysis, was injected daily to previously ovariectomized rats for 14 days, and the rats were irradiated 24 h after the last injection. The cumulative incidence of mammary tumors was not increased by the haloperidol administration, because there was no change in the differentiation and DNA synthesis in the mammary glands by the treatment. In spite of haloperidol treatment, a low serum prolactin concentration assayed 24 h after the last injection was observed in the present study. Demarest *et al.* (22) have reported that the serum prolactin concentration was increased to its maximum level 4 h after the s.c. injection of haloperidol, and was then restored to the basal level 24 h after the treatment. The contrasting effects on prolactin concentration of E_2B and haloperidol can be explained as follows: daily injection of haloperidol for 2 weeks is considered to pulse stimulation in prolactin secretion from the pituitary glands; E_2B dissolved in olive oil stimulates prolactin secretion continuously, as previously reported by Labrie *et al.* (23,24).

In recent studies, progesterone has been reported to inhibit some estrogen-induced biological responses. For example, estradiol has been shown to increase rapidly the number of prolactin-producing cells in the pituitary glands (25) and the prolactin mRNA level (26). The increases in the number of these cells (25) and in the mRNA level (27) were suppressed by progestin. In another study, estrogen- (28,29) and chemical carcinogen- (30) induced tumorigeneses of mammary glands were found to be decreased by chronic treatment with progesterone. Estradiol also rapidly induced expression of the nuclear protooncogene c-*fos* in rat uterus (31), and progesterone delayed transcriptional response of the gene by estrogen (32). While, in the present study, progesterone was antagonistic to estrogen-dependent increases in the radiation-induced tumor, serum prolactin concentration and pituitary weight, it showed synergistic acceleration of the increase of DNA synthesis in the mammary gland elicited by E_2B.

The cells of the terminal end buds have been considered to be a stem cell population (33) and the main site of action of chemical carcinogens (34). The DMBA-induced mammary carcinogenesis was inhibited in rats which had completed pregnancy and lactation prior to exposure to the carcinogen (35). On the other hand, the rat mammary tumor induced by radiation is dependent on the developmental stage of the mammary glands at the time of irradiation (2,7). In contrast, Clifton (36) has reported that stem-cell-like clonogens, the number of which peaked around the beginning of puberty (37), were the ultimate targets of radiation in initiation of mammary cancer. The reasons for the difference of physiological influences on the inductive action of chemicals and radiation in the mammary glands are not clear, but it is considered that the target sites of mammary tumorigenesis due to radiation might be a specific stem cell population maintained throughout the reproductive life cycle.

Hormone-dependent mammary tumors develop in rats in response to chemical carcinogens. The growth of such tumors is regulated by a number of hormones, such as estradiol and prolactin. The roles of these two hormones vary with the model. Of the two widely studied models in rats, 7,12-dimethylbenz[*a*]anthracene-induced tumors show predominantly prolactin-dependent growth (38–40), while those induced by *N*-nitroso-*N*-methylurea are thought to be more estrogen dependent (41,42). Under both the estrogen- and progesterone-free conditions (group I) in this experiment, the growth of the many mammary tumors induced by radiation was mainly hormone independent. On the other hand, when the bilaterally ovariectomized rats were irradiated after treatment with estrogen alone or in combination with progesterone (or haloperidol), many of the mammary tumors which developed were ER(+)PgR(+). During promotion of radiation-initiated mammary tumorigenesis as well, estrogen was found to induce the development of ER(+)PgR(+) tumors (3). Our data suggest that the susceptibility of the mammary glands to radiation depends upon estrogen-stimulated differentiation at the time of exposure, and also that estrogen is one of the regulatory factors for expression of ER and PgR in these radiation-induced mammary tumors.

Acknowledgements

The authors are indebted to Dr H.Ishii for histological examination. This work was partly supported by a project research grant for 'Experimental Studies on the Radiation Health, Detriment and its Modifying Factors', of the National Institute of Radiological Sciences, and also by grants to H.Y. from the Research Development Corporation of Japan (JRDC) and Foundation for Life Science Research.

References

1. Marchetti,B., Fortier,M.-A., Poyet,P. and Follea,N. (1990) β-Adrenergic receptors in the rat mammary gland during pregnancy and lactation: characterization, distribution, and coupling to adenylate cyclase. *Endocrinology*, **126**, 565–574.
2. Inano,H., Suzuki,K., Ishii-Ohba,H., Ikeda,K. and Wakabayashi,K. (1991) Pregnancy-dependent initiation in tumorigenesis of Wistar rat mammary glands by ^{60}Co-irradiation. *Carcinogenesis*, **12**, 1085–1090.
3. Inano,H., Suzuki,K., Ishii-Ohba,H., Yamanouchi,H., Takahashi,M. and Wakabayashi,K. (1993) Promotive effects of diethylstilbestrol, its metabolite (*Z,Z*-dienestrol) and a stereoisomer of the metabolite (*E,E*-dienestrol) in tumorigenesis of rat mammary glands pregnancy-dependently initiated with radiation. *Carcinogenesis*, **14**, 2157–2163.
4. Jahn,G.A., Edery,M., Belair,L., Kelly,P.A. and Djiane,J. (1991) Prolactin receptor gene expression in rat mammary gland and liver during pregnancy and lactation. *Endocrinology*, **128**, 2976–2984.
5. Sharoni,Y., Feldman,B., Teuerstein,I. and Levy,J. (1984) Protein kinase activity in the rat mammary gland during pregnancy, lactation, and weaning: a correlation with growth but not with progesterone receptor levels. *Endocrinology*, **115**, 1918–1924.
6. Suzuki,K., Ishii-Ohba,H., Yamanouchi,H., Wakabayashi,K., Takahashi,M. and Inano,H. (1995) Susceptibility of lactating rat mammary glands to gamma-ray-irradiation-induced tumorigenesis. *Int. J. Cancer*, **56**, 413–417.
7. Yamanouchi,H., Ishii-Ohba,H., Suzuki,K., Onoda,M., Wakabayashi,K. and Inano,H. (1995) Relationship between stages of mammary development and sensitivity to γ-ray irradiation in mammary tumorigenesis in rats. *Int. J. Cancer*, **60**, 230–234.
8. Rothschild,T.C., Boylan,E.S., Calhoon,R.E. and Vonderhaar,B.K. (1987) Transplacental effects of diethylstilbestrol on mammary development and tumorigenesis in female ACI rats. *Cancer Res.*, **47**, 4508–4516.
9. World Health Organization (1981) *Histological Typing of Breast Tumors*, 2nd edn. WHO, Geneva, pp. 15–25.
10. Johnson,R.B.Jr., Nakamura,R.M. and Libby,R.M. (1975) Simplified Scatchard plot assay for estrogen receptor in human breast tumors. *Clin. Chem.*, **21**, 1725–1730.
11. Johnson,R.B. and Nakamura,R.M. (1978) Simplified Scatchard plot assay for progesterone receptor in breast cancer: comparison with single point and multipoint assay. *Clin. Chem.*, **24**, 1170–1176.
12. Hunter,W.M. and Greenwood,F.C. (1962) Preparation of iodine-131 labeled human growth hormone of high specific activity. *Nature*, **194**, 495–496.
13. Posner,B.I., Kelly,P.A., Shiu,R.P.C. and Friesen,H.G. (1974) Studies of insulin, growth hormone and prolactin binding, tissue distribution, species variation and characterization. *Endocrinology*, **95**, 521–531.
14. Kelly,P.A., Leblanc,G. and Djiane,J. (1979) Estimation of total prolactin-binding sites after *in vitro* desaturation. *Endocrinology*, **104**, 1631–1638.
15. Scatchard,G. (1949) The attractions of proteins for small molecules and ions. *Ann. NY Acad. Sci. USA*, **51**, 660–672.
16. Chung,L.W.K. and Coffey,D.S. (1971) Biochemical characterization of prostatic nuclei. II, Relationship between DNA synthesis and protein synthesis. *Biochim. Biophys. Acta*, **247**, 584–596.
17. Burton,K. (1968) Determination of DNA concentration with diphenylamine. *Methods Enzymol.*, **12B**, 163–166.
18. Evans,R.D. and Williamson,D.H. (1989) Lipid metabolism during the initiation of lactation in the rat. The effects of starvation and tumor growth. *Biochem. J.*, **262**, 887–895.
19. Watanabe,G., Taya,K. and Sasamoto,S. (1990) Dynamics of ovarian inhibin secretion during the oestrous cycle of the rat. *J. Endocrinol.*, **126**, 151–157.
20. Iball,J. (1939) The relative potency of carcinogenic compounds. *Am. J. Cancer*, **35**, 188–190.
21. Nicholson,R.I., Gotting,K.E., Gee,J. and Walker,K.J. (1988) Action of oestrogens and antioestrogens on rat mammary gland development: relevance to breast cancer prevention. *J. Steroid Biochem.*, **30**, 95–103.
22. Demarest,K.T., Moore,K.E. and Riegle,G.D. (1985) Adenohypophysial dopamine content and prolactin secretion in the aged male and female rat. *Endocrinology*, **116**, 1316–1323.
23. Labrie,F., Ferland,L., Denizeau,F. and Beaulieu,M. (1980) Sex steroids interact with dopamine at the hypothalamic and pituitary level to modulate prolactin secretion. *J. Steroid Biochem.*, **12**, 323–330.
24. Raymond,V., Beaulieu,M., Labrie,F. and Biossier,J. (1978) Potent antidopaminergic activity of estradiol at the pituitary level on prolactin release. *Science*, **200**, 1173–1175.
25. Oliveira,M.C., Spritzer,P., Poy,M., Coronel,A.X., Dahlem,N., Moraes,J.T. and Barbosa-Coutinho,L.M. (1993) Progestin effects on prolactin secretion and on immunoreactive prolactin cells in estradiol-treated ovariectomized rats. *Hormone Metab. Res.*, **25**, 600–602.
26. Maurer,R.A. (1982) Estradiol regulates the transcription of the prolactin gene. *J. Biol. Chem.*, **257**, 2133–2136.
27. Cho,B.N., Suh,Y.H., Yoon,Y.D., Lee,C.C. and Kim,K. (1993) Progesterone inhibits the estrogen-induced prolactin gene expression in the rat pituitary. *Mol. Cell. Endocrinol.*, **93**, 47–52.
28. Segaloff,A. (1973) Inhibition by progesterone of radiation–estrogen-induced mammary cancer in the rat. *Cancer Res.*, **33**, 1136–1137.
29. Inoh,A., Kamiya,K., Fujii,Y. and Yokoro,K. (1985) Protective effects of progesterone and tamoxifen in estrogen-induced mammary carcinogenesis in ovariectomized W/Fu rats. *Jpn J. Cancer Res.*, **76**, 699–704.
30. Gottardis,M., Erturk,E. and Rose,D.P. (1983) Effects of progesterone administration on *N*-nitrosomethylurea-induced rat mammary carcinogenesis. *Eur. J. Cancer Clin. Oncol.*, **19**, 1479–1484.
31. Loose-Mitchell,D.S., Chiappetta,C. and Stancel,G.M. (1988) Estrogen regulation of c-*fos* messenger ribonucleic acid. *Mol. Endocrinol.*, **2**, 946–951.
32. Kirkland,J.L., Murthy,L. and Stancel,G.M. (1993) Progesterone inhibits estrogen-induced increases in c-*fos* mRNA level in the uterus. *Rec. Prog. Hormone Res.*, **48**, 477–480.
33. Williams,J.M. and Daniel,C.W. (1983) Mammary ductal elongation: differentiation of myoepithelium and basal lamina during branching morphogenesis. *Dev. Biol.*, **97**, 274–290.
34. Russo,I.H. and Russo,J. (1988) Hormone prevention of mammary carcinogenesis: a new approach in anticancer research. *Anticancer Res.*, **8**, 1247–1264.
35. Russo,J. and Russo,I.H. (1987) Biological and molecular bases of mammary carcinogenesis. *Lab. Invest.*, **57**, 112–137.
36. Clifton,K.H. (1990) The clonogenic cells of the rat mammary and thyroid glands: their biology, frequency of initiation, and promotion/progression to cancer. In Moolgavkar,S.H. (ed.), *Scientific Issues in Quantitative Cancer Risk Assessment*. Birkhauser, Boston, MA, pp. 1–21.
37. Shimada,Y., Yasukawa-Barnes,J., Kim,R.Y., Gould,M.N. and Clifton,K.H. (1994) Age and radiation sensitivity of rat mammary clonogenic cells. *Radiat. Res.*, **137**, 118–123.
38. Arafah,B.M., Manni,A. and Pearson,O.H. (1980) Effects of hypophysectomy and hormone replacement on hormone receptor levels and the growth of 7,12-dimethylbenz(*a*)anthracene-induced mammary tumors in the rat. *Endocrinology*, **107**, 1364–1369.
39. Manni,A., Trujillo,J.E. and Pearson,O.H. (1977) Predominant role of prolactin in stimulating the growth of 7,12-dimethylbenz(*a*)anthracene-induced rat mammary tumor. *Cancer Res.*, **37**, 1216–1219.
40. Shoyab,M. (1983) Enhancement by fluphenazine of dimethyl benz(*a*)-anthracene-induced mammary tumorigenesis in rats. *Cancer Lett.*, **18**, 297–303.
41. Ratko,T.A. and Beattie,C.W. (1985) Estrous cycle modification of rat mammary tumor induction by a single dose of *N*-methyl-*N*-nitrosourea. *Cancer Res.*, **45**, 3042–3047.
42. Braun,R.J., Pezzuto,J.M., Anderson,C.H. and Beattie,C.W. (1989) Estrous cycle status alters *N*-methyl-*N*-nitrosourea (NMU)-induced rat mammary tumor growth and regression. *Cancer Lett.*, **48**, 205–211.

Received on February 3, 1995; revised on April 24, 1995; accepted on April 24, 1995

Int. J. Cancer: **60**, 230–234 (1995)

Publication of the International Union Against Cancer
Publication de l'Union Internationale Contre le Cancer

RELATIONSHIP BETWEEN STAGES OF MAMMARY DEVELOPMENT AND SENSITIVITY TO GAMMA-RAY IRRADIATION IN MAMMARY TUMORIGENESIS IN RATS

Hiroshi YAMANOUCHI[1], Hiroko ISHII-OHBA[1], Keiko SUZUKI[1], Makoto ONODA[1], Katsumi WAKABAYASHI[2] and Hiroshi INANO[1,3]

[1]*Division of Chemical Pharmacology, National Institute of Radiological Sciences, 9-1 Anagawa-4-chome, Inage-ku Chiba-shi 263; and* [2]*Hormone Assay Center, Gunma University, Showa-machi, Maebashi-shi 371, Japan.*

Mature Wistar-MS rats were ovariectomized and treated with estradiol benzoate and/or progesterone. Control animals were treated with olive oil. The rats were then exposed to γ-rays and implanted with a pellet of diethylstilbestrol. The incidence of mammary tumors in rats treated with estradiol benzoate or with progesterone was significantly higher than in rats in the non-treated control group, whereas, in rats treated with both estradiol benzoate and progesterone, the incidence was not significantly different from that in the controls. Histological examination of the mammary tumors showed 2 types of neoplasm: adenocarcinoma and fibroadenoma. Interestingly, over half of all the tumors in the rats treated with estradiol benzoate were adenocarcinomas, while fibroadenomas were mainly induced in the rats treated with progesterone or with both estradiol benzoate and progesterone. The expression of estrogen and progesterone receptors in the tumor tissues showed some differences according to whether the groups were treated with estradiol benzoate or with progesterone. Morphologically, mammary glands at irradiation showed well-developed lobuloalveoli in both the estradiol-benzoate-treated rats and in those rats treated with both estradiol benzoate and progesterone. This was consistent with the higher incorporation of [^{3}H]thymidine into the DNA in the mammary glands of rats in both of these groups. Our findings suggest that a more advanced developmental stage of the mammary glands, dependent upon ovarian hormones, is related to a higher incidence of mammary tumors induced by irradiation.

In the course of sexual maturation, the mammary glands develop to ensure lactation after childbirth. This development occurs in several phases, each phase being characterized by different anatomical and histological features, and being influenced by different hormones. Pituitary hormones such as prolactin, and ovarian hormones such as estrogens and progesterone, are the major hormones involved in development of the mammary glands. Many studies have shown that estrogens promote terminal end-bud development and duct elongation in mammary glands, while progesterone promotes duct enlargement and ductule formation and growth (Dulbecco *et al.*, 1982). The synergistic effect of ovarian hormones and prolactin in the development of mammary glands has also been implicated in tumorigenesis in the mammary glands (Welsch and Nagasawa, 1977).

Whole-body irradiation of female rats results in a higher incidence of mammary tumors than that observed in non-irradiated normal female rats; the highest incidence of such tumors occurs in rats irradiated in late pregnancy and then treated with DES (Inano *et al.*, 1991). We have shown that altering the concentrations of estradiol and progesterone in the serum of pregnant rats leads to different stages of mammary gland development, and the induction of mammary tumors in these rats depends on the stage of the mammary glands at irradiation (Suzuki *et al.*, 1994). In this study, we carried out further investigations to clarify the relationship between the induction of mammary tumors by irradiation and the developmental stage of the mammary glands regulated by the action of ovarian and pituitary hormones.

MATERIAL AND METHODS

Material

[2,4,6,7-^{3}H]estradiol-17β (specific activity 4.0 TBq/mmol) and [17α-methyl-^{3}H]17α,21-dimethyl-19-nor-4,9-pregnandiene -3,20-dione (R5020) (specific activity 3.0 TBq/mmol) were purchased from Du Pont/NEN (Boston, MA), and estradiol-6-[(o-carboxymethyl) oximino-(2-[^{125}I] iodohistamine)] (specific activity 74 TBq/mmol) and [methyl-^{3}H]thymidine (3.15 TBq/mmol) were purchased from Amersham (Aylesbury, UK). NIDDK radioimmunoassay kits for rat luteinizing hormone (LH), rat follicle-stimulating hormone (FSH), rat prolactin and ovine prolactin (NIDDK-oPRL I-2) for receptor assay were supplied by the National Hormone and Pituitary Program of the University of Maryland School of Medicine, Baltimore, MD. Antiserum against estradiol (GDN 244) was a gift of Dr. K. Taya, Tokyo University of Agriculture and Technology, who had received it from Dr. G.D. Niswender. All other reagents and chemicals were purchased from Sigma (St Louis, MO) unless otherwise noted in the text.

Animals and treatment with irradiation and hormones

All experiments were carried out using virgin female Wistar-MS rats bred in this Institute. The animals were maintained at 23°C with controlled lighting (14-hr light, 10-hr dark). They received water and food *ad libitum*. All rats were ovariectomized at 70 days of age; they were then divided into 4 groups and treated with the agents indicated below, daily for 2 weeks. Group I (control) rats were treated s.c. with 0.2 ml olive oil, Group II with 50 μg estradiol benzoate in 0.2 ml olive oil, Group III with 5 mg progesterone in 0.2 ml olive oil, and Group IV with 50 μg estradiol benzoate plus 5 mg progesterone in combination. After 14 days, each group was further divided into 2 subgroups; one for the observation of mammary tumorigenesis and the other for biochemical studies and morphological examination. For the observation of mammary tumorigenesis, rats were exposed to whole-body irradiation of 260 cGy γ-rays (17 cGy/min) from a ^{60}Co source. One month after the irradiation, a pellet containing 3 mg DES and 27 mg cholesterol was implanted s.c. in the interscapular region. The pellets were replaced by a fresh pellet of the same composition every 8 weeks. Rats were observed for 1 year to detect palpable mammary tumors. When palpable tumors had grown to more than 2 cm in diameter, the rats bearing them were killed by CO_2 asphyxiation and the tumors were removed for further experiments. Part of the tumor tissue was fixed in 10% formalin/0.1 M sodium phosphate buffer (pH 7.2) for histological examination. The remainder was frozen at −80°C until use for receptor assays of prolactin and steroids. The remaining rats were killed 1 year after the initiation of DES implantation, and were autopsied to ascertain whether they had any non-palpable tumors (Inano *et al.*, 1993). Tumor incidence was

[3]To whom correspondence and reprint requests should be addressed, at the Division of Chemical Pharmacology, National Institute of Radiological Sciences, 9-1 Anagawa-4-chome, Inage-ku, Chiba-shi 263, Japan. Fax: 011 81 43 255 6819.

Received: June 7, 1994 and in revised form September 4, 1994.

TABLE I – TUMORIGENESIS IN MAMMARY GLANDS INDUCED BY WHOLE-BODY IRRADIATION AND DES IMPLANTATION

Group	Treatment	Number of rats used	Rats with tumors		Number of tumors			Latency period (months)[3]	Iball's index
			Number	%	Fibroadenoma	Adenocarcinoma	Total (/rat[3])		
I	Olive oil	30	9	30.0	10 (58.8%)	7 (41.2%)	17 (1.9 ± 0.4)	9.5 ± 0.4	10.5
II	Estradiol benzoate	21	19	90.5[1]	16 (41.0%)	23 (59.0%)	39 (2.4 ± 0.3)	9.3 ± 0.4	32.4
III	Progesterone	21	19	90.5[1]	29 (70.7%)[2]	12 (29.3%)[2]	41 (2.3 ± 0.2)	9.3 ± 0.4	32.4
IV	Estradiol benzoate + progesterone	20	8	40.0	15 (88.2%)[2]	2 (11.8%)[2]	17 (1.7 ± 0.3)	10.7 ± 0.4	12.5

[1]Difference from control (group I): $p \leq 0.01$.–[2]Difference from estradiol benzoate-treated group (group II): $p \leq 0.05$.–[3]Values represent means ± SE.

calculated from the total number of palpable and non-palpable tumors.

Radioimmunoassays

A blood sample was collected from each rat by cardiocentesis under pentobarbital anesthesia. The blood was allowed to clot and centrifuged to obtain serum. Sera were frozen immediately at −80°C until the assay was started. Prolactin, LH and FSH were measured with NIDDK radioimmunoassay kits. The concentration of estradiol in serum was determined with a double-antibody RIA system, using [^{125}I]-iodohistamine estradiol as a radioligand (Taya *et al.*, 1985). Progesterone was measured with a radioimmunoassay kit from bioMérieux (Marcy-l'Etoile, France).

Determination of estrogen and progesterone receptors

The cytosol fraction of the tumor tissues was prepared by a previously described method. Estradiol receptors and progesterone receptors were analyzed by the dextran-coated-charcoal method, with [2,4,6,7-^{3}H]estradiol-17β and [17α-methyl-^{3}H]R5020, respectively, as radioligands (Inano *et al.*, 1993).

Prolactin receptor

Prolactin (NIDDK-oPRL I-2) was iodinated to a specific activity of 0.9 MBq/μg by a chloramine-T method (Hunter and Greenwood, 1962). Membrane fractions of mammary glands were prepared according to the method of Posner *et al.* (1974). Crude membranes were treated with 4 M $MgCl_2$ to remove endogenously bound prolactin from its receptor. Membrane preparations (300 μg protein/tube) were incubated with [^{125}I]-prolactin (10,000 cpm) and various concentrations of unlabeled prolactin at 25°C for 15 hr in 25 mM Tris-HCl (pH 7.6) containing 25 mM $MgCl_2$ and 0.1% BSA. Equilibrium parameters, *i.e.*, the dissociation constant (K_D) and number of binding sites (capacity), were obtained by analysis of Scatchard plots.

Measurement of DNA synthesis

[methyl-^{3}H]Thymidine (22.2 MBq/kg body wt) made up to 0.5 ml with saline was administered to rats by i.p. injection. One hour later, the rats were killed by CO_2 asphyxiation, and the inguinal mammary glands and heart were isolated and frozen in liquid nitrogen. The samples were then minced and homogenized, and DNA was extracted by the method of Chung and Coffey (1971) with some modification. The radioactivity of a portion of the DNA solution was measured in a liquid scintillation counter. DNA concentration was assayed by the method of Burton (1968), somewhat modified, using calf thymus DNA as a standard. The rate of DNA synthesis was expressed as dpm/hr/mg of DNA but, for the purposes of comparing rates between disparate groups, the results are presented as a percentage of the rate obtained in the heart.

Histological examination and whole-mount preparation

A paraffin section (4 μm thick) was prepared from the fixed mammary tumor and stained with hematoxylin and eosin. Tumors were classified by applying the criteria developed in the consensus on classification of rat mammary tumors (WHO, 1981). The right inguinal mammary glands, in their entirety, were prepared as a whole mount by the method of Rothschild *et al.* (1987), with modifications.

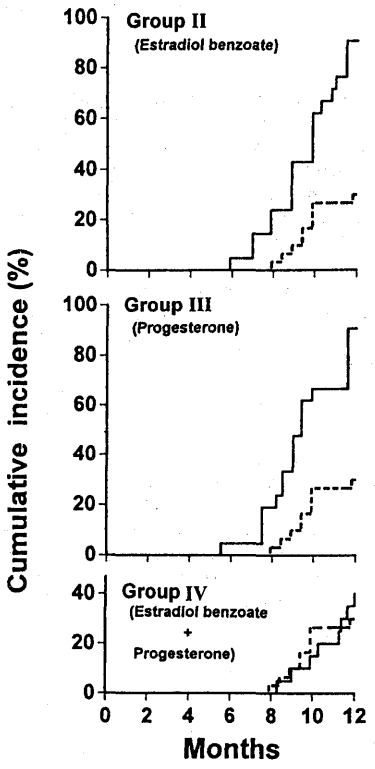

FIGURE 1 – Cumulative incidence of mammary tumors in rats treated with estradiol benzoate (group II), progesterone (group III) or estradiol benzoate plus progesterone (group IV) before whole-body irradiation. Solid lines indicate the rate of incidence in each experimental group, and dotted lines indicate the rate of incidence in the controls (group I).

Iball's index and statistical analysis

Iball's index is defined as 100 times the ratio of incidence (%) to the average latency period in days (Suzuki *et al.*, 1994). Differences in the incidence of tumors between any 2 groups were compared using Fischer's exact probability test. The level of significance of differences of mean values of hormone concentrations, values in the binding assays and DNA synthesis rates were evaluated by multiple comparisons of Dunnett's test. Differences were considered significant when $p \leq 0.05$.

RESULTS

Development of mammary tumors by irradiation

The incidence of mammary tumors in rats treated with estradiol benzoate (group II: 90.5%) and with progesterone (group III: 90.5%) was significantly higher ($p \leq 0.01$) than

TABLE II – HORMONE CONCENTRATIONS IN SERUM AT IRRADIATION

Group (treatment)	Estradiol (pg/ml)	Progesterone (ng/ml)	Prolactin (ng/ml)	LH (ng/ml)	FSH (ng/ml)
I (Olive oil)	16.3 ± 5.5	43.6 ± 2.0	21.5 ± 1.9	1.93 ± 0.27	21.3 ± 0.8
II (Estradiol benzoate)	660.6 ± 118.4[1]	42.2 ± 8.4	165.1 ± 20.9[1]	0.31 ± 0.03[1]	12.9 ± 0.5[1]
III (Progesterone)	19.0 ± 5.2	117.0 ± 25.4	27.6 ± 4.5	2.16 ± 0.29	24.6 ± 0.5[2]
IV (Estradiol benzoate + progesterone)	1056.0 ± 112.4[1]	124.4 ± 10.5[2]	78.5 ± 8.4[2]	0.33 ± 0.10[1]	12.9 ± 1.5[1]

Values represent means ± SE from 6 rats.–[1]Difference from control (group I): $p \leq 0.01$.–[2]Difference from control (group I): $0.01 < p \leq 0.05$.

TABLE III – BINDING AFFINITY AND MAXIMUM NUMBER OF BINDING SITES FOR PROLACTIN IN MAMMARY GLAND

Group	Treatment	Equilibrium dissociation constant K_D (nM)	Maximum number of binding sites (fmol/mg protein)
I	Olive oil	0.80 ± 0.06	58.4 ± 6.8
II	Estradiol benzoate	1.04 ± 0.03	64.2 ± 8.0
III	Progesterone	1.67 ± 0.15	124.7 ± 2.2[1]
IV	Estradiol benzoate + progesterone	1.21 ± 0.31	101.6 ± 21.5

Values represent means ± SE of triplicate determinations.–[1]Difference from control (group I): $0.01 < p \leq 0.05$.

that in control rats (group I: 30.0%) at the end of the 1-year experimental period (Table I). The incidence of mammary tumors in rats treated with estradiol benzoate plus progesterone in combination (group IV) was 40.0%; this was not significantly different from that in the control group.

Histological examination of the tumors induced by irradiation after the hormone treatment showed that there were 2 types of tumor; fibroadenoma and adenocarcinoma. Adenocarcinoma accounted for 59% of tumors in the estradiol benzoate-treated rats, but for less than 41.2% of the tumors in the 3 other groups. There were no significant differences between groups in the latency period or in the number of tumors per rat. Iball's index was higher in groups II and III than in the control group.

The cumulative number of tumors and the time-course of mammary tumorigenesis in rats irradiated after treatment with hormones are shown in Figure 1. The first appearance of palpable tumors in both groups II and III was 5.9 and 5.5 months, respectively, after DES implantation was initiated and these tumors appeared approximately 2 months earlier than in the controls (group I) (7.9 months). In group IV, the time of the first appearance of tumors (8.3 months) was almost the same as in the control group.

Hormone concentrations in serum

As shown in Table II, the concentration of estradiol was significantly higher in rats treated with estradiol benzoate (groups II and IV) than in the control animals (group I). The concentration of progesterone was also higher in rats treated with progesterone (groups III and IV) than in the group-I rats. The concentration of prolactin was significantly higher than the control level in rats treated with estradiol benzoate (groups II and IV), while there was no significant difference from the control level in the other groups. Levels of FSH and LH were lower in the rats treated with estradiol benzoate (groups II and IV) than in the group-I rats.

Prolactin receptors in the mammary glands

The dissociation constant (K_D) values for prolactin binding to the receptor varied from 0.80 to 1.67 nM in the 4 groups (Table III). The maximum number of binding sites was significantly higher in the rats treated with progesterone (group III) than in the control rats; this number was also higher than that in the control group in the rats treated with estradiol benzoate plus progesterone, but the difference was not significant.

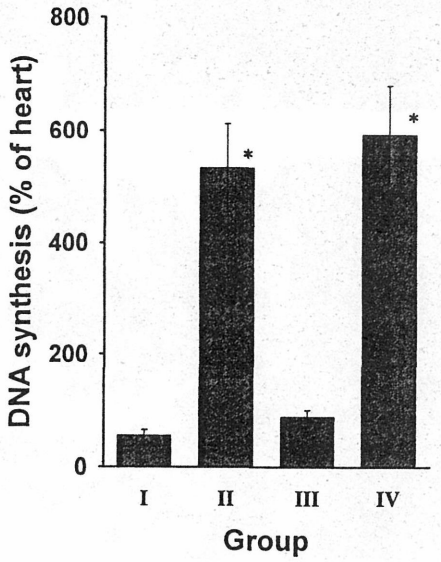

FIGURE 2 – Effects of hormone treatment on DNA synthesis in mammary glands. Results are expressed as a percentage of the DNA synthesis rate in the heart. Columns and vertical bars show the mean and SE of data from 5 rats each in groups I (control), II (estradiol benzoate), III (progesterone) and IV (estradiol benzoate + progesterone). *Difference from control (group I): $p \leq 0.01$.

DNA synthesis in the mammary glands and mammary development

^{3}H-thymidine incorporation into DNA in mammary glands was significantly higher than the control level in rats treated with estradiol benzoate (group II) and in those treated with estradiol benzoate plus progesterone (group IV). No increase in ^{3}H-thymidine incorporation was observed in the mammary glands of rats treated with progesterone (group III) (Fig. 2).

Whole mounts of mammary glands were prepared to examine the degree of differentiation before irradiation. Findings that reflected cell proliferation in the mammary glands of animals treated with estradiol benzoate (groups II and IV) were obtained from morphological observations in the whole-mount specimens (Fig. 3). In these rats, highly expanded lactiferous ducts and well-developed lobuloalveoli were observed (Fig. 3*b,d*), while the progesterone-treated rats showed expansion of the lactiferous ducts (Fig. 3*c*). The development was remarkable in rats treated with estradiol benzoate and progesterone in combination (Fig. 3*d*). Lactiferous ducts with lower expansion and undeveloped lobuloalveoli were detected in the mammary glands of control rats (Fig. 3*a*).

Steroid hormone receptors in mammary tumors

In the tumors obtained from estradiol-benzoate-treated rats (group II), estrogen receptors (ER) were expressed in 56% of the examined tissues and in 54% of the examined tumors obtained from progesterone-treated rats (group III), whereas all tumor tissues obtained from rats treated with estradiol benzoate plus progesterone (group IV) were ER^+ (Table IV).

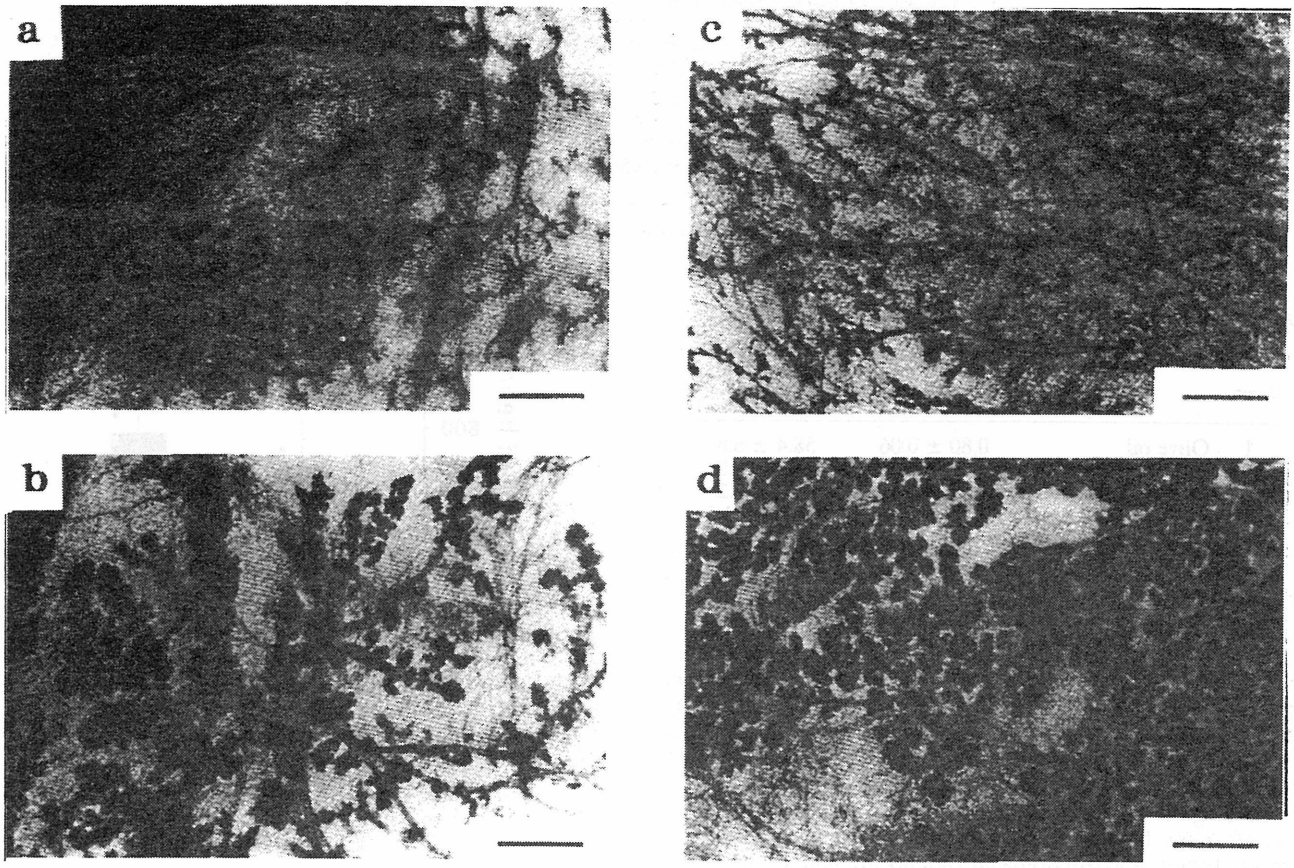

FIGURE 3 – Whole mounts of mammary glands from *(a)* group I (control), *(b)* group II (estradiol benzoate), *(c)* group III (progesterone), and *(d)* group IV (estradiol benzoate + progesterone). Scale bars, 1 mm.

Conversely, tumors which expressed neither ER nor PgR (ER^- PgR^-) were detected only in the rats treated with estradiol benzoate (group II) and in those treated with progesterone (group III). These 2 groups (groups II and III) were compared; 39% of tumors in the former group were ER^+ PgR^+, while in the latter group only 23% of all tumors were ER^+ PgR^+.

DISCUSSION

We have already reported that whole-body γ-ray irradiation of Wistar-MS rats and subsequent DES treatment resulted in the induction of mammary tumors (Inano *et al.,* 1991, 1993; Suzuki *et al.,* 1994). In the present study, a high incidence of mammary tumors was observed in both estradiol-benzoate-treated and progesterone-treated groups. However, the hormonal environments of these 2 groups were not the same. A high dose of estradiol stimulates prolactin gene expression (Maurer, 1982) and secretion (Raymond *et al.,* 1978) in the pituitary. We found here that the serum prolactin level was highest in the estradiol benzoate-treated group. Although the effect of prolactin on the up-regulation of prolactin receptors is well known (Djiane and Durand, 1977), we found that the maximum number of binding sites for prolactin in rats treated with estradiol benzoate was not different from that in the control group. Prolactin receptors in the mammary gland are reduced by high concentrations of estradiol in serum (Nagasawa *et al.,* 1986) and these receptors are up-regulated by high concentrations of LH (Guillaumot *et al.,* 1986). In our study, the concentration of LH in serum was reduced by estradiol and no increase was observed in prolactin receptors. Stimulation of DNA synthesis by estradiol benzoate has been attributed to high levels of prolactin. Zwierzchowski *et al.* (1987) reported that prolactin increased the rate of DNA synthesis in rabbit mammary glands; this may also occur in rat mammary glands. Prolactin itself is known to be the dominant factor in eliciting the activity of estrogen receptors in mouse mammary glands (Muldon, 1987). In this case, these mechanisms can be extrapolated to the interaction of hormones in rat mammary glands. Thus, this effect of estradiol in increasing prolactin levels in serum and the effect of prolactin in enhancing the activity of estrogen receptors, caused by the injection of estradiol benzoate, was synergistic. In the group that received estradiol benzoate it could be concluded that the high rate of DNA synthesis and mammary cell mitosis caused by prolactin contributed to the induction of mammary tumors by irradiation.

In the group that received daily injection of progesterone, high serum levels of this hormone were successfully maintained to the level during late pregnancy. In this group, DNA synthesis occurred at almost the same rate as in the control group. Progesterone has been reported to play a major role in stimulating DNA synthesis and the proliferation of ductal epithelial cells in mammary glands (Haslam, 1988). We observed no significant elevation of DNA synthesis in rats treated with progesterone, although the effect of progesterone on mammary growth was observed morphologically; it was not as remarkable as in the group treated with estradiol benzoate plus progesterone in combination. The maximum number of binding sites for prolactin receptors was highest in this group. These results suggest that progesterone increases the sensitivity of mammary glands to prolactin. In the progesterone-treated group, the situation was different from that in the estradiol-benzoate-treated group, the high level of progesterone with the low level of estradiol in serum at irradiation increasing the incidence of mammary tumors. These results indicate that prolactin and progesterone play an important

TABLE IV - ESTROGEN AND PROGESTERONE RECEPTORS IN MAMMARY TUMORS

Group	Treatment	Number of tumors tested	Number of tumors			
			ER^+PgR^+	ER^+PgR^-	ER^-PgR^+	ER^-PgR^-
I	Olive oil	2	2	0	0	0
II	Estradiol benzoate	18	7	3	3	5
III	Progesterone	13	3	4	1	5
IV	Estradiol benzoate + progesterone	7	6	1	0	0

ER, estrogen receptor; PgR, progesterone receptor.

role in tumorigenesis by sensitizing tissue to irradiation, but not by stimulating DNA synthesis.

Morphologically, estradiol and progesterone have a synergistic effect in the development of mammary glands. However, these 2 hormones did not synergistically affect the incidence of mammary tumors, the incidence of these tumors in rats treated with estradiol benzoate plus progesterone being almost the same as that in the control group. The serum prolactin level in this group was lower than that in the rats treated with estradiol benzoate alone, presumably because progesterone inhibits estrogen-induced prolactin gene expression in the rat pituitary (Cho *et al.*, 1993). When levels of both estradiol and progesterone in serum were high, the incidence of mammary tumors was reduced by the inhibition of prolactin synthesis due to the action of progesterone. On comparing this group with the estradiol-benzoate-treated group, DNA synthesis was not reduced, although estrogen-induced prolactin levels decreased concomitantly with progesterone levels. Additional studies are needed to determine the inhibitory mechanism of progesterone on estrogen-dependent mammary tumorigenesis induced by radiation.

In an earlier study (Inano *et al.*, 1991), we reported that gradually increased concentrations of progesterone and estradiol were observed in rats when prolactin levels were low during pregnancy and that irradiation in late pregnancy was the most effective way of initiating mammary tumors, suggesting that the contribution of estradiol and progesterone in the initiation of tumors is greater than that of prolactin. In conclusion, our present findings suggest that estrogen treatment increases the level of serum prolactin and its receptor in mammary glands, causing cell proliferation and thus increasing the population at risk of irradiation-induced tumors, and that the mechanism responsible for γ-radiation-induced estrogen-dependent tumorigenesis in rat mammary glands is different from that of tumorigenesis that is dependent on high progesterone levels. The differences we observed in the rate of ER^+ and PgR^+ tumors and the differences in the incidence of adenocarcinoma among mammary tumors occurring in estradiol-benzoate-treated and progesterone-treated rats support this idea.

ACKNOWLEDGEMENTS

This work was partly supported by a project research grant "Experimental Studies on the Radiation Health, Detriment and its Modifying Factors" and also by grants to H.Y. from the Research Development Corporation of Japan (JRDC) and The Foundation for Life Science Research.

REFERENCES

BURTON, K., Determination of DNA concentration with diphenylamine. *Meth. Enzymol.*, **12**, 163–166 (1968).

CHO, B.N., SUH, Y.H., YOON, Y.D., LEE, C.C. and KIM, K., Progesterone inhibits the estrogen-induced prolactin gene expression in the rat pituitary. *Mol. cell. Endocrinol.*, **93**, 47–52 (1993).

CHUNG, L.W.K. and COFFEY, D.S., Biochemical characterization of prostatic nuclei. II. Relationship between DNA synthesis and protein synthesis. *Biochim. biophys. Acta*, **247**, 584–596 (1971).

DJIANE, J. and DURAND, P., Prolactin-progesterone antagonism in self-regulation of prolactin receptors in the mammary gland. *Nature (Lond.)*, **266**, 641–643 (1977).

DULBECCO, R., HENAHAN, M. and ARMSTRONG, B., Cell types and morphogenesis in the mammary gland. *Proc. nat. Acad. Sci. (Wash.)*, **79**, 7346–7350 (1982).

GUILLAUMOT, P., SABBAGH, I., BERTRAND, J. and COHEN, H., Prolactin receptor regulation by LH in the rat mammary gland. *Biochem. Biophys. Res. Comm.*, **135**, 1076–1083 (1986).

HASLAM, S.Z., Progesterone effects on deoxyribonucleic acid synthesis in normal mouse mammary glands. *Endocrinology*, **122**, 464–470 (1988).

HUNTER, W.M. and GREENWOOD, F.C., Preparation of iodine-131 labeled human growth hormone of high specific activity. *Nature (Lond.)*, **194**, 495–496 (1962).

INANO, H., SUZUKI, K., ISHII-OHBA, H., IKEDA, K. and WAKABAYASHI, K., Pregnancy-dependent initiation in tumorigenesis of Wistar rat mammary glands by ^{60}Co irradiation. *Carcinogenesis*, **12**, 1085–1090 (1991).

INANO, H., SUZUKI, K., ISHII-OHBA, H., YAMANOUCHI, H., TAKAHASHI, M. and WAKABAYASHI, K., Promotive effects of diethylstilbestrol, its metabolite (Z,Z-dienestrol) and a stereoisomer of the metabolite (E,E-dienestrol) in tumorigenesis of rat mammary glands pregnancy-dependently initiated with radiation. *Carcinogenesis*, **14**, 2157–2163 (1993).

MAURER, R.A., Estradiol regulates the transcription of the prolactin gene. *J. biol. Chem.*, **257**, 2133–2136 (1982).

MULDON, T.G., Prolactin mediation of estrogen-induced changes in mammary tissue estrogen and progesterone receptors. *Endocrinology*, **121**, 141–149 (1987).

NAGASAWA, H., OHTA, K., NAKAJIMA, K., NOGUCHI, Y., MIURA, K., NIKI, K. and NAMIKI, H., Interrelationship between pituitary and ovarian hormones in normal and neoplastic growth of mammary glands of mice. *In:* A. Angeli, H.L. Bradlow and L. Dogliotti (eds.), *Endocrinology of the breast: basic and clinical aspects, Ann. N.Y. Acad. Sci.*, **464**, 301–315 (1986).

POSNER, B.I., KELLY, P.A., SHIU, R.P.C. and FRIESON, H.G., Studies of insulin, growth hormone and prolactin binding: tissue distribution, species variation and characterization. *Endocrinology*, **95**, 521–531 (1974).

RAYMOND, V., BEAULIEU, M., LABRIE, F. and BOISSIER, J., Potent antidopaminergic activity of estradiol at the pituitary level on prolactin release. *Science (Wash.)*, **200**, 1173–1175 (1978).

ROTHSCHILD, T.C., BOYLAN, E.S., CALHOON, R.E. and VODERHAAR, B.K., Transplacental effects of diethylstilbestrol on mammary development and tumorigenesis in female ACL rats. *Cancer Res.*, **47**, 4508–4516 (1987).

SUZUKI, K., ISHII-OHBA, H., YAMANOUCHI, H., WAKABAYASHI, K., TAKAHASHI, M. and INANO, H., Susceptibility of lactating rat mammary glands to gamma-ray-irradiation-induced tumorigenesis. *Int. J. Cancer*, **56**, 413–417 (1994).

TAYA, K., WATANABE, G. and SASAMOTO, S., Radioimmunoassay for progesterone, testosterone and estradiol-17β using ^{125}I-iodohistamine radioligands. *Jap. J. Animal Reprod.*, **31**, 186–197 (1985).

WELSCH, C.W. and NAGASAWA, H., Prolactin and murine mammary tumorigenesis. A review. *Cancer Res.*, **37**, 951–963 (1977).

WHO, *Histological Typing of Breast Tumors*, 2nd ed., pp. 15–25, WHO, Geneva (1981).

ZWIERZCHOWSKI, L., NIEDBALSKI, W. and KLECZKOWSKA, D., Effects of prolactin, progesterone, pregnancy and lactation on DNA synthesis and DNA polymerase activities in rabbit mammary gland. *J. Endocrinol.*, **114**, 139–145 (1987).

RADIATION RESEARCH 145, 708–713 (1996)
0033-7587/96 $5.00

Susceptibility of Fetal, Virgin, Pregnant and Lactating Rats for the Induction of Mammary Tumors by Gamma Rays

Hiroshi Inano, Keiko Suzuki, Makoto Onoda and Hiroshi Yamanouchi[1]

The First Research Group, National Institute of Radiological Sciences, 9-1, Anagawa-4-chome, Inage-ku, Chiba-shi 263, Japan

Inano, H., Suzuki, K., Onoda, M. and Yamanouchi, H. Susceptibility of Fetal, Virgin, Pregnant and Lactating Rats for the Induction of Mammary Tumors by Gamma Rays. *Radiat. Res.* 145, 708–713 (1996).

Pregnant Wistar-MS rats received a whole-body irradiation of 0–2.6 Gy γ rays at day 20 of pregnancy. The mother rats were implanted with a diethylstilbestrol (DES) pellet 30 days after weaning, and the female pups delivered by the irradiated mother were treated with DES after maturation. Lactating rats were irradiated with γ rays 21 days after parturition and then treated with DES. Virgin rats 70 days of age were also irradiated and then administered DES. The rats which received intrauterine irradiation did not develop mammary tumors at doses less than 2.1 Gy and showed a low incidence of tumors at 2.6 Gy. In virgin rats, the maximum tumor incidence was obtained with 1 Gy. The incidence of total mammary tumors in the mother rats and lactating rats increased in a dose-dependent manner with increasing doses of γ rays up to 2.1 Gy. With 0.1–1 Gy, the incidence of adenocarcinoma in the mother rats was significantly lower than that observed in the lactating rats. However, the incidence in the mother rats irradiated with 1.0–1.5 Gy was significantly higher than that of virgin rats treated with the corresponding γ-ray doses. These findings suggest that the susceptibility of the mammary glands to radiation depends upon the differentiation at the time of exposure.

INTRODUCTION

The carcinogenicity of radiation for the human breast has been studied in a survey of atomic bomb survivors in Hiroshima and Nagasaki (*1*) and of women treated with X rays for acute postpartum mastitis in New York (*2*). In general, the relative risk of breast cancer incidence increases linearly up to an average dose to the breast of about 4 Gy and diminishes at higher doses (*1, 2*). However, the dose–response effects of radiation-induced mammary tumorigenesis depend upon age at the time of irradiation (*3*). The incidence of mammary adenocarcinoma and fibroadenoma in rats also increases in a dose-dependent manner with increasing doses of radiation (*4, 5*), but there are no differences among the age groups irradiated between 24–225 days of age (*6*). Radiation-induced tumorigenesis of the mammary glands in mature rats is considered to be influenced by the developmental stage of the glands at the time of exposure (*7*). Whole-body irradiation (2.6 Gy) of pregnant (*8*) or lactating rats (*9*) results in a higher incidence of mammary tumors than that observed in irradiated virgin rats. However, the relationship of the γ-ray doses and of the developmental stages of the mammary gland to radiation-induced mammary tumorigenesis is not clearly understood. The present study was designed to investigate the dose–response effect of radiation on the induction of mammary tumors in rats in various mammary developmental stages including the fetal, virgin, pregnant and lactating phases.

MATERIALS AND METHODS

Materials. [2,4,6,7-^{3}H]Estradiol-17β (specific activity, 4.0 TBq/mmol) and [17α-methyl-^{3}H]17α,21-dimethyl-19-norpregna-4,9-diene-3,20-dione (R5020) (specific activity, 3.0 TBq/mmol) were purchased from Du Pont/NEN (Boston). Each diethylstilbestrol (DES) pellet contained 3 mg of DES mixed with 27 mg of cholesterol in a medical grade Silastic tube (2.0 mm inner diameter, 3.2 mm outer diameter; Dow Corning, Midland, MI) (*10*).

Animals and treatment. The rats used in the present study were treated and handled according to the "Recommendations for Handling of Laboratory Animals for Biomedical Research" compiled by the Committee of the Safety and Handling Regulations for Laboratory Animal Experiments in our Institute. Wistar-MS rats bred at our Institute were kept at 23 ± 1°C in a controlled light environment (14 h light/10 h dark). They received water and food *ad libitum*. Pregnant rats received whole-body irradiation with various doses (0–2.6 Gy) of γ rays (0.15 Gy/min) from a ^{60}Co source at day 20 of pregnancy (presence of vaginal plug denotes day 1). As shown in Fig. 1, the mother rats were then implanted with a DES pellet 30 days after termination of nursing, and the female pups delivered by the irradiated mother rats were treated with the DES pellets by implantation after maturation, at 141 days of age. Lactating rats were irradiated with 0–2.6 Gy 21 days after parturition, and 1 month later, the DES pellets were implanted. Virgin rats 70 days of age were also irradiated with 0–2.6 Gy γ rays and administered the DES pellets. The pellets were replaced every 8 weeks until the end of the experiment. The release of the synthetic estrogen was estimated to be 0.4 μg/day (*10*). The rats were observed for 1 year for detection of palpable mammary tumors starting from the time of pellet implantation. When palpable tumors reached more than 2 cm in diameter, the rats bearing them were killed by CO_2 asphyxiation and the

[1]Present address: First Department of Anatomy, Wakayama Medical College, 27, 9-Banchou, Wakayama-shi 640, Japan.

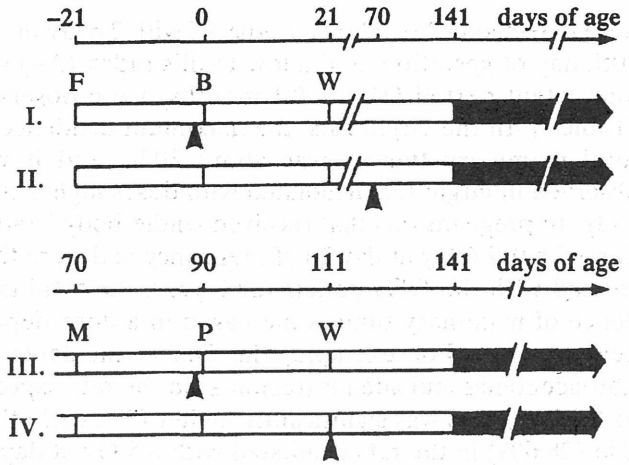

FIG. 1. Experimental schedule of γ irradiation and implantation of DES pellet for (I) fetal, (II) virgin, (III) pregnant and (IV) lactating rats. (▲), γ irradiation with ^{60}Co; F, fertilization; B, birth; W, weaning; M, mating; P, parturition; closed bar, period of DES treatment.

tumors were removed for histological examination and analyses of steroid receptors.

Histological examination. All mammary tumors were fixed in 10% formalin buffered with 0.1 *M* sodium phosphate solution (pH 7.2) immediately after isolation and embedded in paraffin as described previously (*8*). Each section (4 μm thick) was prepared and stained with hematoxylin and eosin. The tumors were classified as fibroadenoma or adenocarcinoma according to the criteria for the classification of rat mammary tumors (*11*). Before the irradiation the inguinal mammary glands of three rats each in the virgin, pregnant and lactating groups were prepared as whole mounts by the method of Rothschild *et al.* (*12*), with some modifications.

Assay for steroid receptors in mammary tumors. The cytosol fraction of the tumor tissues (1.0 g) was prepared by the methods described previously (*12*). Estrogen receptors (ER) and progesterone receptors (PgR) were analyzed by a Scatchard plot analysis with [2,4,6,7-^{3}H]estradiol-17β and [17α-*methyl*-^{3}H]R5020, respectively, as radioligands (*12*).

Statistical analysis and Iball's index. Statistical analyses were conducted using Fisher's exact probability test for incidence of mammary tumors and Dunnett's test for the level of significance of the difference by multiple comparisons. Iball's index was defined so that the ratio of incidence (%) to the average latent period in days was multiplied by 100 (*13*).

RESULTS

Developmental Stages of Mammary Glands at the Time of Irradiation

Whole mounts of inguinal mammary glands were prepared to examine the degree of differentiation at the time of irradiation. No preparation of mammary glands of the fetal rats was obtained, because the tissue was not sufficiently developed. Virgin rats 70 days of age had elongated and branched ducts and no alveolar bud in any area of the mammary glands (Fig. 2a). The mammary glands of the pregnant rats developed and differentiated progressively into a small lobule of alveoli (Fig. 2b). Differentiated lobulo-alveolar structures filled with milk were observed in the mammary glands of lactating rats (Fig. 2c).

Development of Mammary Tumors

Mammary tumors did not develop during the 1-year observation period in all of the mature rats that received less than 2.1 Gy intrauterine irradiation at fetal day 20 and were then implanted with the DES pellets after maturation (Fig. 3). Only 2 fibroadenomas (incidence, 7.4%)

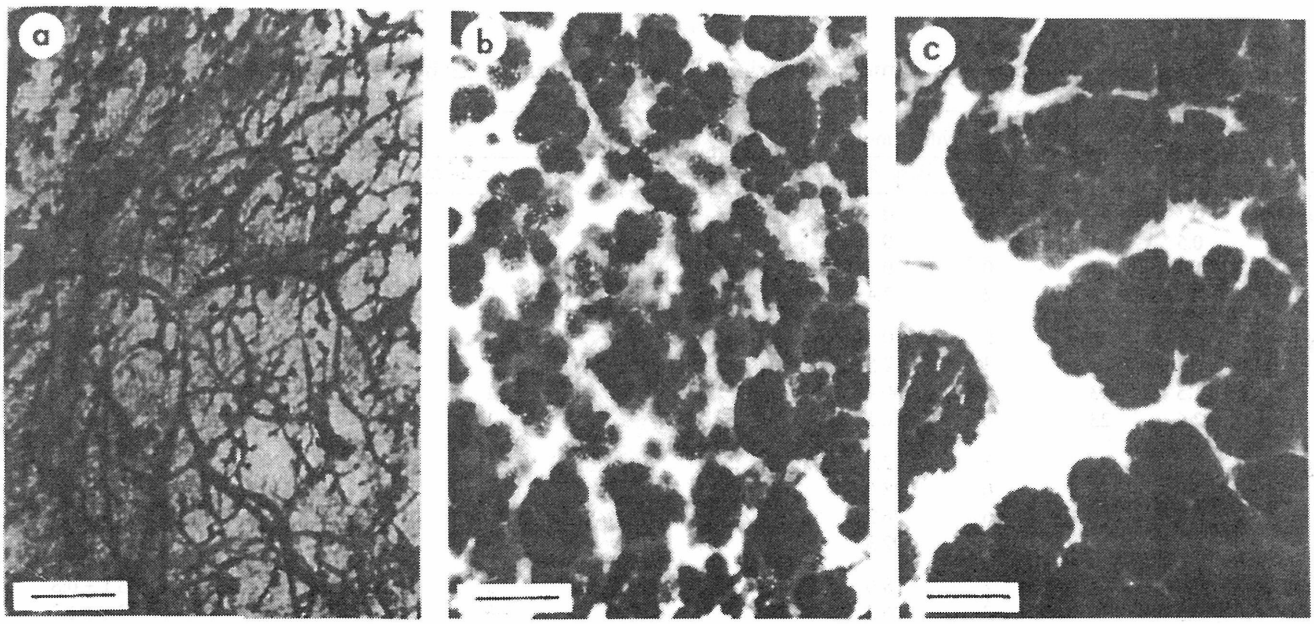

FIG. 2. Whole-mount preparation of mammary glands in three different preparations. Panel a: Virgin at 70 days of age; panel b: day 20 of pregnancy; panel c: day 21 of lactation. Scale bars, 1 mm.

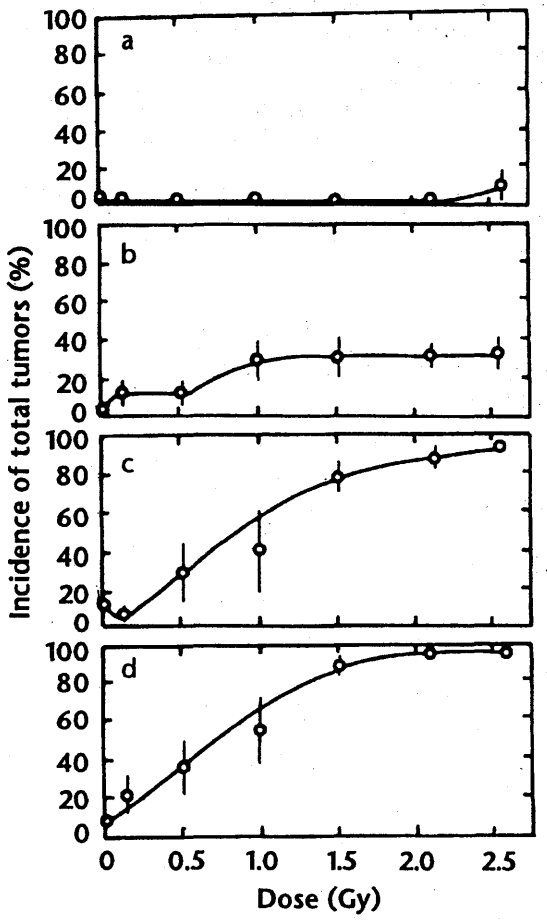

FIG. 3. Cumulative incidence of total mammary tumors obtained after 1-year observation period in rats irradiated during various phases of development of the mammary glands: fetal (a), virgin (b), pregnant (c) and lactating (d) periods. Values represent mean ± SE.

were detected in 2 of 27 rats irradiated with 2.6 Gy on the 20th day of gestation, and a low Iball's index (2.4) and long latent period (11.5 ± 0.1 months) were observed (Table I). In the virgin rats, the maximum incidence of total mammary tumors was about 30%, and it was observed in virgin rats irradiated with doses higher than 1 Gy. In pregnant rats that received whole-body irradiation with 0–2.6 Gy at day 20 of pregnancy and were then treated with the DES pellets for 1 year, the total incidence of mammary tumors increased in a dose-dependent manner. For example, the 76.2% incidence of fibroadenomas and adenocarcinomas in the rats exposed to 1.5 Gy γ rays was significantly higher ($P < 0.01$) than that (28.6%) in the rats irradiated with 0.5 Gy at day 20 of pregnancy, but was not significantly different ($P = 0.129$) from that (92.3%) observed in the pregnant rats irradiated with 2.6 Gy. An increasing number of tumors per tumor-bearing rat and a shortened latent period were observed with increasing radiation doses up to 2.6 Gy.

Lactating rats irradiated with γ rays 21 days after parturition showed a pattern of total mammary tumor incidence similar to that of the pregnant rats. A significantly higher incidence (36.8%) of total mammary tumors was observed in the rats irradiated with 0.5 Gy γ rays during the late lactating period compared to that (8.0%) in the nonirradiated rats. Moreover, the total incidence (85.0%) of mammary tumors in lactating rats irradiated with 1.5 Gy was higher compared with that with 0.5 Gy. The difference in incidence was not significant between the groups exposed to 1.5 Gy and 2.6 Gy. The highest Iball's index (41.7) for tumorigenesis was obtained in rats irradiated in the late lactating period with 2.6 Gy followed by the DES

TABLE I
Induction of Mammary Tumors at Various Developmental Stages by Various Doses of Radiation

Group	Dose (Gy)	Number of rats	Rats with tumors		Number of tumors			Number of tumors per tumor-bearing rat	Latent period (months)	Iball's index
			Number	Percentage	Total	Fibroadenoma	Adenocarcinoma			
Fetal	0	20	0	0	0			0		0
	0.5	24	0	0	0			0		0
	1.5	23	0	0	0			0		0
	2.6	27	2	7.4	2	2	0	1.0 ± 0.0	11.5 ± 0.1	2.4
Virgin	0	20	0	0	0			0		0
	0.5	24	3	12.5	3	2	1	1.0 ± 0.0	10.6 ± 0.7	3.9
	1.5	23	7	30.4	9	8	1	1.3 ± 0.2	9.9 ± 0.4	10.1
	2.6	23	6	26.1	6	5	1	1.0 ± 0.0	9.1 ± 0.9	9.5
Pregnant	0	25	3	12.0	3	3	0	1.0 ± 0.0	10.4 ± 0.8	3.8
	0.5	21	6	28.6	8	7	1	1.2 ± 0.2	9.8 ± 0.6	9.6
	1.5	21	16	76.2	25	15	10	1.4 ± 0.2	8.9 ± 0.6	26.3
	2.6	26	24	92.3	38	21	17	1.8 ± 0.4	8.2 ± 0.6	39.1
Lactating	0	25	2	8.0	2	1	1	1.0 ± 0.0	6.1 ± 0.8	2.2
	0.5	19	7	36.8	10	3	7	1.2 ± 0.2	7.6 ± 1.3	15.9
	1.5	20	17	85.0	22	10	12	1.3 ± 0.2	7.5 ± 0.6	37.3
	2.6	24	22	91.7	31	16	15	1.3 ± 0.1	7.7 ± 0.4	41.7

treatment, the values being 17.4- and 4.4-fold higher than those in rats exposed to the same dose during the fetal and virgin period, respectively.

Adenocarcinomas induced with radiation and DES were found to be mainly of a papillotubular type and occasionally a solid-tubular type. Figure 4 shows the dose dependency of the development of mammary adenocarcinomas in the rats irradiated with 0–1.5 Gy γ rays in the virgin, pregnant and lactating groups. Compared with that in the pregnant group, the irradiation with 0.1–1 Gy γ rays in the lactating group induced a significantly ($P < 0.05$) higher incidence of adenocarcinomas, but the incidence of adenocarcinomas (60.0%) in the lactating group treated with 1.5 Gy was not significantly different ($P = 0.316$) from that in the pregnant group treated with the same dose. When pregnant rats were irradiated with <0.5 Gy γ rays, the incidence of adenocarcinoma was not significantly higher than that observed in virgin rats exposed at the same dose, but the incidence (47.6%) in rats irradiated with 1.5 Gy in pregnancy was 11.0-fold higher ($P < 0.01$) than that (4.3%) in the virgin rats irradiated at the corresponding dose.

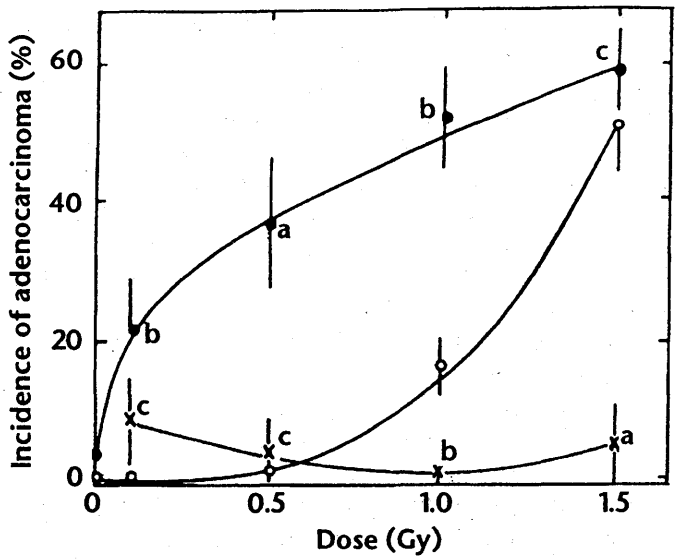

FIG. 4. Cumulative incidence of adenocarcinoma in rats irradiated at the virgin (×), pregnant (○) and lactating (●) stages. Values represent mean ± SE. [a]$P < 0.01$; [b]$P < 0.05$; [c]not significant compared with rats irradiated in pregnancy.

Estrogen and Progesterone Receptors in Mammary Tumors

The results of receptor analyses are shown in Table II. The majority of the mammary tumors induced in the virgin rats were ER^+PgR^+. The proportion of ER^+PgR^+ tumors compared to total tumors was 76.4 and 64.3% in rats irradiated at day 20 of pregnancy with 1.5 and 2.6 Gy, respectively. On the other hand, in the lactating group, the proportion of ER^+PgR^+ tumors induced by 1.5 and 2.6 Gy γ irradiation was only 11.2 and 22.2%, respectively, and that of PgR^- tumors was increased. This result for PgR^- was seen in 8 (89%) of the 9 tested tumor specimens induced by 1.5 Gy irradiation and in 7 (78%) of the 9 tumors induced by 2.6 Gy.

DISCUSSION

The induction of mammary tumors by radiation is known to be dependent on the developmental stage of the

TABLE II
Estrogen and Progesterone Receptors in Mammary Tumors

Group	Dose (Gy)	Tumors tested	Receptors[a]			
			ER^+PgR^+	ER^+PgR^-	ER^-PgR^+	ER^-PgR^-
Fetal	0	0	0	0	0	0
	0.5	0	0	0	0	0
	1.5	0	0	0	0	0
	2.6	2	0	1	1	0
Virgin	0	0	0	0	0	0
	0.5	3	2	1	0	0
	1.5	8	6	1	1	0
	2.6	6	3	1	1	1
Pregnant	0	1	0	0	0	1
	0.5	3	2	0	1	0
	1.5	17	13	1	3	0
	2.6	14	9	2	2	1
Lactating	0	2	2	0	0	0
	0.5	5	4	1	0	0
	1.5	9	1	6	0	2
	2.6	9	2	6	0	1

[a]ER, estrogen receptors; PgR, progesterone receptors.

mammary glands at the time of γ irradiation in Wistar-MS rats (*7, 14*), but it is independent of the physiological status of Sprague-Dawley rats at the time of X irradiation (*15*). The present study demonstrated that, at the doses tested (0.1–2.6 Gy), both pregnancy and lactation are associated with a significantly higher incidence of radiation-induced total mammary tumors than that obtained in virgin rats. Compared with mammary glands from virgin rats, the mammary glands from pregnant rats showed small lobules of alveoli, and those from lactating rats showed augmented well-differentiated lobulo-alveolar structure. The observation of mammary gland whole-mount preparations obtained at the time of irradiation revealed that the number of cells in the glands was increased during pregnancy and lactation. The rats irradiated with γ rays during pregnancy and lactation were implanted with the DES pellets, as a tumor promoter, 30 days after weaning. However, the numerous differentiated epithelial cells that were at risk for initiation by irradiation during the periods of pregnancy and lactation were absent from the glands at the time of the first DES implantation in the present experiments (data not shown). During post-lactational mammary gland involution, the bulk of the differentiated mammary epithelia which produce milk had regressed to a quiescent organ composed predominantly of adipose tissues surrounding a mammary epithelial tree, denuded by apoptosis (*16, 17*).

Clifton and colleagues (*18, 19*) have reported that the clonogens which they consider stem cells are the targets for initiation of mammary tumors by radiation. It is suggested that the high susceptibility of the mammary glands during pregnancy and lactation to tumor induction by radiation may be a cause of the higher radiosensitivity of the differentiated stem cells than that of undeveloped stem cells in fetal or virgin rats. The clonogens in pregnancy, or "pregnancy-type" stem cells, have a high susceptibility for the effects of γ rays that lead to an increase in fibroadenomas. After parturition, the clonogens found during pregnancy may be altered to "lactation-type" clonogens as a result of prolactin secreted from the pituitary glands during lactation. The high susceptibility to adenocarcinoma that has been demonstrated in rats irradiated with doses less than 1 Gy in lactation might be due to the presence of the lactation-type clonogens.

In chemical carcinogenesis, the mammary glands of young rats have higher susceptibility to tumorigenesis than those in aged ones (*20*). Chemically induced mammary tumors in virgin rats arose earlier than those induced by radiation. Treatment with human chorionic gonadotropin in young rats was observed to stimulate mammary gland differentiation, manifested as a progressive reduction in the number of terminal end buds and an increase in the number of alveolar buds and lobules, and to decrease the incidence of mammary adenocarcinoma after administration of 7,12-dimethylbenz(a)anthracene (*21, 22*). It is likely that the effect of human chorionic gonadotropin on the mammary glands is mediated by stimulation of estradiol secreted from the ovaries. The differentiated mammary glands show low susceptibility to the chemical carcinogens. Based on the findings described above, we conclude that radiation and chemical carcinogens may act on different types of stem cells in tumorigenesis.

ACKNOWLEDGMENTS

This work was partly supported by a project research grant, "Experimental Studies on the Radiation Health, Detriments and its Modifying Factors," and also by a grant for Special Programme of Bioregulation of the National Institute of Radiological Sciences. The authors wish to thank Dr. Ishii for her work in histological examination.

Received: August 30, 1995; accepted: January 16, 1996

REFERENCES

1. T. Wakabayashi, H. Kato, T. Ikeda and W. J. Schull, Studies of the mortality of atomic-bomb survivors, Report 7, Part III. Incidence of cancer in 1959–1978, based on the Tumor Registry, Nagasaki. *Radiat. Res.* **93**, 112–146 (1983).
2. R. E. Shore, L. H. Hempelmann, E. Kowaluk, P. S. Mansur, B. S. Pasternack, R. E. Albert and G. E. Haughie, Breast neoplasms in women treated with x-rays for acute postpartum mastitis. *J. Natl. Cancer Inst.* **59**, 813–822 (1977).
3. M. Tokunaga, J. E. Morman, M. Asano, S. Tokuda, H. Ezaki, I. Hishimori and Y. Tsuji, Malignant breast tumors among atomic bomb survivors, Hiroshima and Nagasaki, 1950–74. *J. Natl. Cancer Inst.* **62**, 1347–1359 (1979).
4. C. J. Shellabarger, D. Chmelevsky, A. M. Kellerer, J. P. Stone and S. Holtzman, Induction of mammary neoplasms in the ACI rat by 430-keV neutrons, X-rays, and diethylstilbestrol. *J. Natl. Cancer Inst.* **69**, 1135–1146 (1982).
5. C. J. Shellabarger, V. P. Bond, E. P. Cronkite and G. E. Aponte, Relationship of dose of total body ^{60}Co radiation to incidence of mammary neoplasia in female rats. In *Proceedings of a Symposium on Radiation-induced Cancer*, pp. 161–172. International Atomic Energy Agency, Vienna, 1969.
6. C. J. Shellabarger, A comparison of rat mammary carcinogenesis following total body irradiation at different ages. *Radiat. Res.* **59**, 103 (1974). [Abstract]
7. H. Yamanouchi, H. Ishii-Ohba, K. Suzuki, M. Onoda, K. Wakabayashi and H. Inano, Relationship between stages of mammary development and sensitivity to gamma-ray irradiation in mammary tumorigenesis in rats. *Int. J. Cancer* **60**, 230–234 (1995).
8. H. Inano, K. Suzuki, H. Ishii-Ohba, K. Ikeda and K. Wakabayashi, Pregnancy-dependent initiation in tumorigenesis of Wistar rat mammary glands by ^{60}Co-irradiation. *Carcinogenesis* **12**, 1085–1090 (1991).
9. K. Suzuki, H. Ishii-Ohba, H. Yamanouchi, K. Wakabayashi, M. Takahashi and H. Inano, Susceptibility of lactating rat mammary glands to gamma-ray-irradiation-induced tumorigenesis. *Int. J. Cancer* **56**, 413–417 (1994).
10. H. Inano, K. Suzuki, H. Ishii-Ohba, H. Yamanouchi, M. Takahashi and K. Wakabayashi, Promotive effects of diethylstilbestrol, its metabolite (Z,Z-dienestrol) and a stereoisomer of the metabolite (E,E-dienestrol) in tumorigenesis of rat mammary glands pregnancy-dependently initiated with radiation. *Carcinogenesis* **14**, 2157–2163 (1993).
11. *Histological Typing of Breast Tumors*, 2nd ed., pp. 15–25. World Health Organization, Geneva, 1981.
12. T. C. Rothschild, E. S. Boylan, R. E. Cahoon and B. K. Vonderhaar, Transplacental effects of diethylstilbestrol on mammary develop-

ment and tumorigenesis in female ACI rats. *Cancer Res.* **47**, 4508–4516 (1987).

13. J. Iball, The relative potency of carcinogenic compounds. *Am. J. Cancer* **35**, 188–190 (1939).
14. H. Inano, H. Yamanouchi, K. Suzuki, M. Onoda and K. Wakabayashi, Estradiol-17β as an initiation modifier for radiation-induced mammary tumorigenesis of rats ovariectomized before puberty. *Carcinogenesis* **16**, 1871–1877 (1995).
15. S. Holtzman, J. P. Stone and C. J. Shellabarger, Radiation-induced mammary carcinogenesis in virgin, pregnant, lactating and postlactating rats. *Cancer Res.* **42**, 50–53 (1982).
16. R. Strange, F. Li, S. Saurer, A. Burkhardt and R. R. Friis, Apoptotic cell death and tissue remodelling during mouse mammary gland involution. *Development* **115**, 49–58 (1992).
17. R. S. Guenette, H. B. Corbeil, J. Léger, K. Wong, V. Mézl, M. Mooibroek and M. Tenniswood, Induction of gene expression during involution of the lactating mammary gland of the rat. *J. Mol. Endocrinol.* **12**, 47–60 (1994).
18. K. H. Clifton, The clonogenic cells of the rat mammary and thyroid glands: their biology, frequency of initiation, and promotion/progression to cancer. In *Scientific Issues in Quantitative Cancer Risk Assessment* (S. H. Moolgavkar, Ed.), pp. 1–21. Birkhauser, Boston, 1990.
19. Y. Shimada, J. Yasukawa-Barnes, R. Y. Kim, M. N. Gould and K. H. Clifton, Age and radiation sensitivity of rat mammary clonogenic cells. *Radiat. Res.* **137**, 118–123 (1994).
20. C. Huggins, L. C. Grand and F. P. Brillantes, Mammary cancer induced by a single feeding of polynuclear hydrocarbons, and its suppression. *Nature* **189**, 204–207 (1961).
21. I. H. Russo, M. Koszalka and J. Russo, Effect of human chorionic gonadotropin on mammary gland differentiation and carcinogenesis. *Carcinogenesis* **11**, 1849–1855 (1990).
22. I. H. Russo, M. Koszalka, P. A. Gimotty and J. Russo, Protective effect of chorionic gonadotropin on DMBA-induced mammary carcinogenesis. *Br. J. Cancer* **62**, 243–247 (1990).

Volume 45(5): 663–674, 1997
The Journal of Histochemistry & Cytochemistry

ARTICLE

Distribution of Casein-like Proteins in Various Organs of Rat

Makoto Onoda and Hiroshi Inano

National Institute of Radiological Sciences, Chiba, Japan

SUMMARY Casein-like proteins were detected in various organs of rat by use of a specific antiserum raised against rat milk caseins. The antiserum specifically recognized α_1-, α_2-, β-, and γ-caseins in rat milk by Western blot analysis, whereas no immunoreactive band was observed in sera of rat and fetal bovine and in bovine caseins. Immunohistochemical studies of this antiserum on formalin-fixed mammary glands showed that immunoreactive caseins were localized to the apical portion of the cytoplasm in lactating mammary epithelial cells and in the luminal secretion, which indicates a directional secretion of caseins to the lumen by the mammary epithelial cells. With this antiserum, immunoreactive substances were detected in various organs, including the pancreatic ducts and islets of Langerhans, the secretory ducts of salivary glands, zona fasciculata cells and ganglion cells of adrenal gland, distal tubules and convoluted collecting tubules of kidney, epithelial cells of bronchioles and large pneumocytes of the lung, hair follicles, sebaceous glands, and the prickle cell layer of skin, uterine glands and epithelium of the endometrium, hepatic bile ducts, and brain. In Western blot analysis, major immunoreactive substances in the above organ extracts showed a similarity in molecular weight to α_2-casein of rat milk. Skin was the only tissue that expressed both α_2- and β-caseins. There were no other immunoreactive bands with similarity to β- and γ-caseins in the other organ extracts, but higher molecular weight immunoreactive bands (> 100 kD) were detected in some organ extracts, such as salivary gland, kidney, liver, lung, and uterus. These findings suggest that the α_2-casein-like substance is localized not only in the mammary gland but also in a variety of organs and may play an important role as a functional molecule in those organs.

(J Histochem Cytochem 45:663–674, 1997)

KEY WORDS
casein
antibody
immunohistochemistry
immunoblotting
mammary gland
organ
rat

CASEIN is one of the major components of milk, which is produced and secreted by the mammary gland epithelium under hormonal control during lactation (Hobbs et al. 1982; Topper and Freeman 1980). The caseins are acidic phosphoproteins and constitute almost 80% and >50% of rat (Jenness 1974) and mouse (Enami and Nandi 1977) milk protein, respectively. Therefore, casein (Hahm et al. 1990; Levine and Stockdale 1985; Bussolati et al. 1975) and α-lactalbumin (Hall et al. 1979; Woods et al. 1979) represent specific molecular markers of secretory activity and of the degree of differentiation of mammary gland epithelial cells.

Correspondence to: Dr. Makoto Onoda, The First Research Group, Natl. Inst. of Radiological Sciences, 4-9-1 Anagawa, Inageku, Chiba-shi, Chiba 263, Japan.

Received for publication August 12, 1996; accepted December 5, 1996 (6A4052).

Determination of casein by radioimmunoassay in the serum of patients with various malignancies, not only of the breast but also of other organs, raised concern about the specificity of casein production as a marker of mammary gland origin (Hendrick and Franchimont 1974). Pich et al. (1976) demonstrated casein-like proteins immunocytochemically in human tissues, including skin, lung, pancreas, endometrium, and kidney. However, it was reported by Barash et al. (1995) that no immunoreactive caseins were detected by immunoblot analysis in extracts of various tissues from mice, except in the mammary gland. In this context, we have attempted to clarify the presence of caseins and casein-like proteins in a variety of organs, because caseins could be a useful molecular marker to understand the secretory function and the differentiation mechanisms of epithelial cells, not only in mammary gland but in many other organs.

 0022-1554/97/$3.30

In this article we report the presence and localization of caseins and casein-like proteins in various organs of rat by use of immunohistochemistry and immunoblot analysis with a specific antiserum raised against rat α-, β-, and γ-caseins. The possible functional roles of casein-like proteins in organs other than the mammary gland are also discussed.

Materials and Methods

Materials and Animals

Reagents and chemicals were purchased from Sigma Chemical (St Louis, MO) unless stated otherwise in the text. All animals used in the present study were treated and handled according to the Recommendations for Handling of Laboratory Animals for Biomedical Research complied by the Committee of the Safety and Handling Regulations for Laboratory Animal Experiments in our Institute.

Preparation of Anti-casein Antiserum

Milk was collected from lactating Wistar–MS rats (Nippon SLC; Hamamatsu, Japan) and partially purified caseins (crude caseins) were obtained from diluted skimmed milk by isoelectric precipitation according to Hahm et al. (1990). The crude caseins were loaded onto a 12% gel of a minigel system for SDS-PAGE under reducing conditions. The proteins were electrotransferred from the gel to a nitrocellulose membrane (Onoda et al. 1991) and visualized with 0.2% Ponceau S. Subsequently, α-, β-, and γ-casein bands were excised from the membrane. By using this process the caseins were completely separated from an epithelial membrane antigen (EMA) which was present as an impurity in the crude casein preparations and showed a remarkable similarity of the tissue distribution (Ormerod et al. 1982). The casein-bound membranes were incubated together in 250 μl of DMSO for 1 hr to dissolve the membrane. An equal volume of 50 mM sodium carbonate buffer (pH 9.6) was vigorously mixed with the dissolved membrane to obtain a fine particulate suspension of protein/membrane/DMSO (Onoda and Djakiew 1993a,b; Abou–Zeid et al. 1987). The suspension was emulsified with 500 μl of Freund's complete adjuvant (DIFCO Laboratories; Detroit, MI) and injected SC into a male New Zealand White rabbit (Nippon SLC). Before inoculation, the rabbit was bled for the preparation of preimmune serum. Six weeks and 12 weeks after the first inoculation, another casein suspension emulsified with Freund's incomplete adjuvant (DIFCO) was injected SC. Three weeks after the last injection the rabbit was bled for the preparation of immune serum. Specificity of the immune serum was confirmed by Western blot analysis of caseins.

Immunoblot Analysis of Rat Caseins

Male and female Wistar–MS rats (8 to 16 weeks old) were sacrificed by decapitation and the following organs were isolated: lactating mammary gland, uterus, pancreas, salivary gland (submandibular gland and sublingual gland), kidney, liver, lung, thymus, brain, adrenal, skin from the abdominal area, testis, and prostate gland. The organs were minced and homogenized in ice-chilled 5 mM Tris-HCl buffer (pH 7.5) containing 0.25 M sucrose, 5 mM EGTA, and inhibitors (1 M PMSF, 2 mM sodium vanadate, 10 μg/ml aprotinin, 5 μg/ml leupeptin) (Onoda and Djakiew 1993a,b; van Haren et al. 1992). The homogenates were reconstituted in reducing sample buffer and loaded into the minigel system for SDS-PAGE. Subsequently, the separated proteins were electrotransferred to a nitrocellulose membrane (Onoda et al. 1991). The membrane was then soaked in 5% non-fat milk in 20 mM Tris-HCl buffer containing 500 mM sodium chloride (TBS, pH 7.5) for 2 hr to block nonspecific immunoreaction, rinsed twice for 10 min in TBS containing 0.05% Tween-20 (TTBS), and reacted overnight with anti-casein antiserum or pre-immune serum (1:5000–20,000 dilution) in TTBS containing 1% gelatin (Bio-Rad Labs; Richmond, CA). The membrane was washed in TTBS twice for 10 min, reacted with either horseradish peroxidase-conjugated goat anti-rabbit IgG (1:3000 dilution, Bio-Rad Labs) or alkaline phosphatase-conjugated goat anti-rabbit IgG (1:3000 dilution) in TTBS/gelatin for 1 hr and rinsed in TTBS twice and TBS once. The immunoreactivity was visualized by the following color development reactions (Onoda and Djakiew 1993a,b). For the horseradish peroxidase reaction, 4-chloro-1-naphthol (30 mg) was dissolved in ice-cold methanol (10 ml) and hydrogen peroxide (30 μl) was mixed with TBS (50 ml) at room temperature (RT). Both solutions were mixed, and the membrane was incubated in this mixture until color developed. Color development was stopped by replacement of the reaction mixture with distilled water. For the alkaline phosphatase reaction, 5% nitroblue tetrazolium (NBT) in 70% dimethylformamide and 5% 5-bromo-4-chloro-3-indolyl phosphate (BCIP) in dimethylformamide were freshly prepared. NBT and BCIP were then mixed with 100 mM Tris-HCl (pH 9.5) containing 100 mM sodium chloride and 5 mM magnesium chloride (alkaline phosphatase reaction buffer, APB) to a final concentration of 0.033% and 0.017%, respectively. Before color development, the protein-bound nitrocellulose membrane was washed in APB for 10 min and then the immunoreactive bands were visualized in APB containing NBT and BCIP. Color development was terminated by replacement of the reaction mixture with distilled water. The molecular weight of immunoreactive bands was estimated from plots of molecular weight vs relative mobility of rainbow marker standard proteins (Amersham; Arlington Heights, IL) that were run simultaneously with the sample proteins.

Immunohistochemistry of Casein-like Substance in Various Organs

The organs mentioned above were isolated, cut into small cubes, fixed in 10% neutral buffered formalin, usually for about 20 hr, and embedded in paraffin. Paraffin sections (2 μm in thickness) were placed on poly-lysine coated slide-glasses, allowed to dry for a few hours on a hotplate at 60C, and left at 37C overnight. The sections were deparaffinized in xylene, rehydrated in descending grades of ethyl alcohol, and brought to PBS. Streptavidin–biotin–peroxidase immunostaining was carried out using Histofine SAB-PO kits (Nichirei; Tokyo, Japan) as described previously (Inano et al. 1995). Endogenous peroxidase activity was inactivated by 3% hydrogen peroxide for 15 min at RT, sections were washed

twice in PBS for 5 min, then blocked by 10% normal goat serum for 30 min. Next, sections were incubated with anti-casein antiserum or pre-immune serum (1:1000–2000 dilution) at 4C overnight and washed twice in PBS. The sections were treated with biotinylated secondary antibody (goat anti-rabbit IgG) for 30 min at RT, washed twice in PBS, then incubated with streptavidin–peroxidase conjugate for 30 min and washed twice in PBS. Antibody localization on the specimens was visualized by the substrate–chromogen mixture [0.61 M Tris-HCl buffer (pH 7.4) containing 0.05% 3,3′-diaminobenzidine tetrahydrochloride and 0.01% hydrogen peroxide] and color development was stopped by replacement of the reaction mixture with distilled water. The sections were counterstained with hematoxylin, dehydrated, and mounted with a mounting reagent. Photomicrographs were taken under an Olympus BX50 microscope with an automatic camera.

Results

Specificity of Anti-casein Antiserum

The crude casein fraction obtained from the milk of Wistar–MS rats contained three major components (α-, β-, and γ-caseins), of which the apparent molecular weights were 41.4 ± 0.5 kD, 29.3 ± 0.3 kD, and 24.9 ± 0.3 kD, respectively (Figure 1). These values are similar to those of a previous report (Hahm et al. 1990) in which Sprague–Dawley CD rats were used for isolation of milk caseins. Furthermore, these molecular weights were clearly different from that of the EMA, since the EMA did not migrate very much in the running gel (7.5%) of SDS-PAGE and was concentrated at the top of the gel (Ormerod et al. 1982). The caseins were transferred to the nitrocellulose membrane and excised to raise a specific antiserum as described in Materials and Methods. The antiserum obtained recognized α_1-, β-, and γ-caseins in rat milk and crude caseins on the immunoblot analysis even at a dilution ratio of 5000-fold for visualization by the HRP-conjugated secondary antibody (Figure 2). In addition to these three major caseins, an immunoreactive band with an apparent molecular weight of 37.0 kD was detected by the anti-casein antiserum. This molecular species may be α_2-casein, which was immunologically recognized by a specific antibody directed against α_1-casein (Hahm et al. 1990; Hennighausen and Sippel 1982). Furthermore, the cloned α-casein cDNA hybridized equally well to both α-casein-specific mRNAs (Hennighausen and Sippel 1982). The α_2-casein was seldom observed in freshly prepared milk (Figure 1) but appeared in milk that had been stored for a longer period at 4C or repeatedly frozen and thawed. Meanwhile, the immunoreactive bands with this antiserum were not detected in rat serum, fetal bovine serum, bovine caseins (Figure 3) nor in mouse serum (data not shown). Furthermore, when the antiserum was absorbed with the crude caseins before immunoblot analysis, the immunoreactive bands were no longer detected by the pre-absorbed antiserum (data not shown). Because these results indicated the specificity of this anti-rat casein antiserum, we decided to employ this antiserum for further immunohistochemical studies of localization of caseins in various organs of rat.

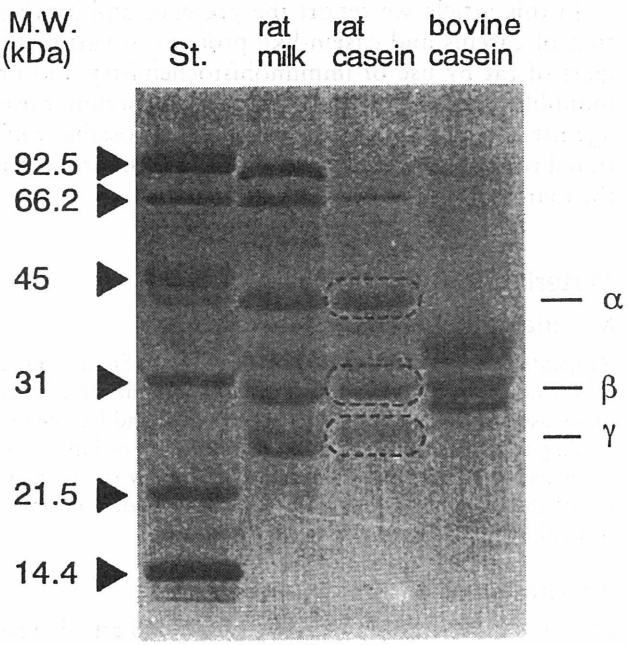

Figure 1 Partially purified (crude) rat caseins visualized by Coomassie Brilliant Blue staining after SDS-PAGE. Rat milk (10 μg), crude casein (5 μg), and bovine casein (10 μg) were loaded on the minigel system for SDS-PAGE and run as described in Materials and Methods.

Immunohistochemical Reaction of the Anti-casein Antiserum in Rat Mammary Glands

To validate the effectiveness and usefulness of the anti-casein antiserum for immunohistochemical study regarding the localization of caseins, paraffin-embedded sections were prepared from lactating rat mammary glands and analyzed with the antiserum as described in Materials and Methods. Immunoreactive staining with the antiserum was intense in the apical portion and the supranuclear cytoplasm of the epithelial cells surrounding the lumina of the alveoli and in the secretion of the lumina of the lactating mammary glands (Figures 4B and 4C). This result reconfirms the specificity of the anti-rat casein antiserum, because the anti-EMA antiserum stained only the luminal membranes and the surface of the fat globules, not the cell cytoplasm on lactating breast (Ormerod et al. 1982). Similar observations were noted in the primary duct structures of the lactating mammary glands (Figure 4D). In contrast, the immunoreactive signals with the antiserum were barely detected in the apical parts fac-

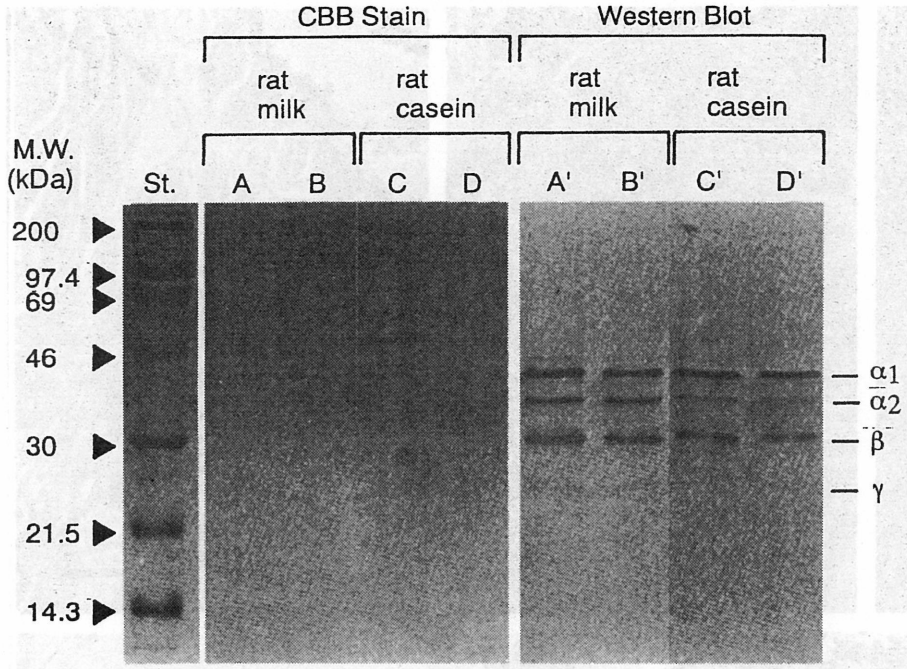

Figure 2 Immunoblot analysis of rat caseins. Immunoreactive caseins in rat milk (Lanes A', 0.25 μg and B', 0.125 μg) and crude rat casein (Lanes C', 0.25 μg and D', 0.125 μg) transferred to nitrocellulose were visualized by Western blot analysis with HRP-conjugated secondary antibody. Another set of milk and crude caseins (Lanes A–D) were not visualized by Coomassie Brilliant Blue (CBB) staining, although the loaded amount of protein was sufficient for visualization by Western blot analysis.

ing the unopened lumina of non-lactating and virgin rat mammary glands (Figure 4E). The absolute amount of reactive staining in virgin rat mammary glands appeared to be minute in comparison with the lactating rat. These findings indicate a directional secretion of caseins to the lumen by the epithelial cells of lactating mammary glands.

Because the anti-casein antiserum worked on the sections prepared from tissues fixed with 10% neutral buffered formalin and embedded in paraffin, we further investigated the presence and localization of caseins in a variety of organs.

Immunohistochemical Observation of Casein-like Substances in Various Organs

Immunoreactive staining with the anti-casein antiserum was detected in secretory organs such as the pancreas, adrenal gland, and salivary glands (Figure 5). In the pancreas, moderate amounts of casein-like immu-

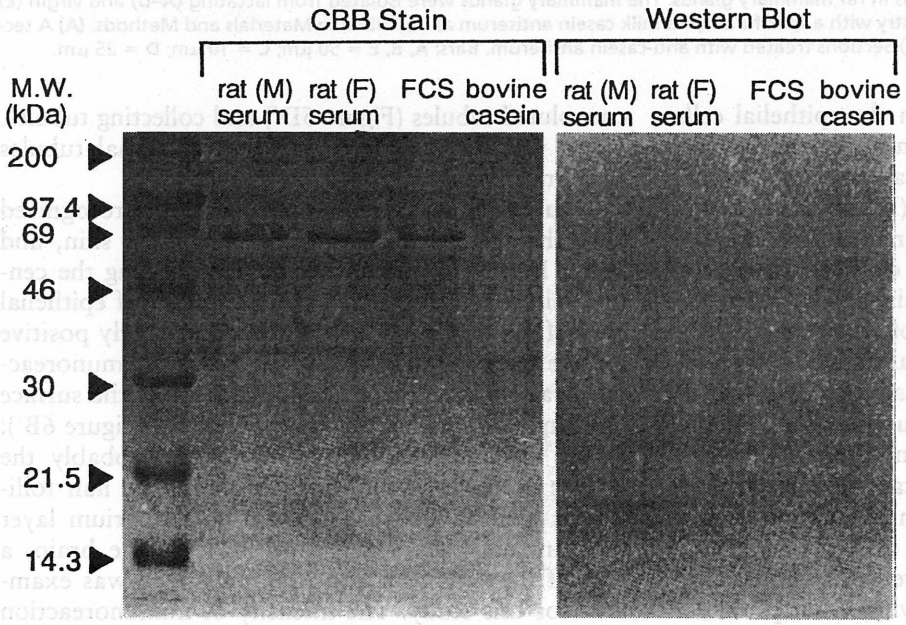

Figure 3 Immunoblot analysis of various kinds of sera and bovine casein. Two μg of male (M) and female (F) rat sera, fetal bovine serum (FCS), and bovine casein were loaded onto the SDS-PAGE system and the total protein was detected by visualization with CBB. However, the immmunoreactive caseins, in the same set of samples were not recognized by Western blot analysis using the antiserum against rat caseins.

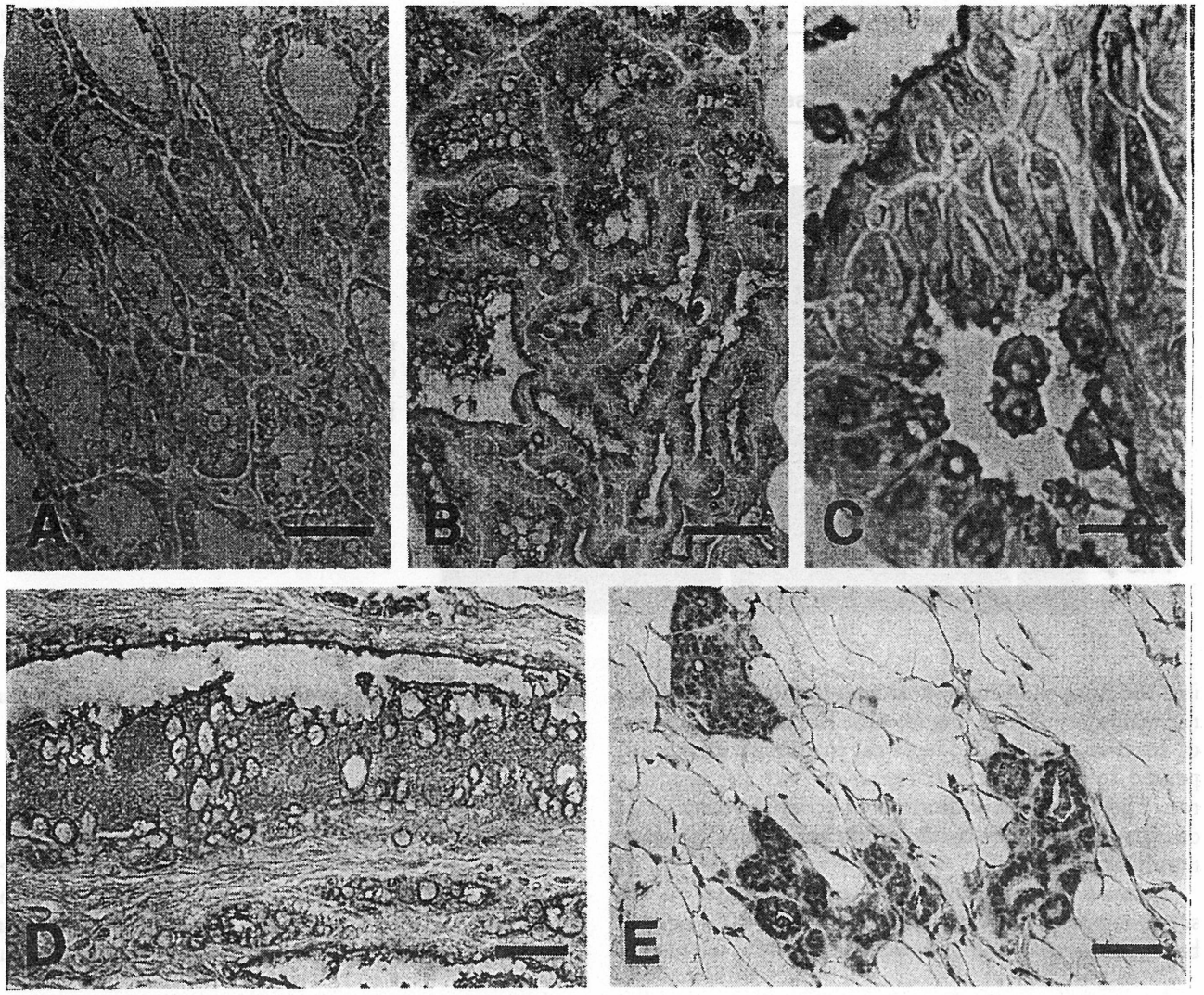

Figure 4 Immunohistochemistry of caseins in rat mammary glands. The mammary glands were isolated from lactating **(A–D)** and virgin **(E)** rats and proceeded to immunohistochemistry with a specific anti-rat milk casein antiserum as described in Materials and Methods. **(A)** A section treated with pre-immune serum. **(B–E)** Sections treated with anti-casein antiserum. Bars: **A, B, E** = 50 μm; **C** = 10 μm; **D** = 25 μm.

noreactive substances appeared in the epithelial cells of pancreatic exocrine ducts and in the endocrine cells of the islets of Langerhans, whereas the immunoreaction in acinar cells was negative (Figure 5A′). In the adrenal gland, cortical cells scattered in the zona fasciculata (Figure 5B′) and ganglion cells surrounded by medullary cells were strongly stained with the anti-casein antiserum. Epithelial cells of secretory ducts in both submandibular and sublingual glands showed intensive staining, and some glandular acini that stained brightly with hematoxylin in the submandibular gland were also positive for the antiserum (Figure 5C′). Figure 5 also shows immunoreactive staining with the anti-casein antiserum in the kidney. Intense immunoreaction was detected in the cytoplasm of epithelial cells of distal convoluted tubules, which were distinguished by the lack of brush borders (microvilli) from proximal convoluted tubules (Figure 5D′) and collecting tubules. There was no positive staining in proximal tubules and renal corpuscles.

Figure 6 shows the casein-like substance recognized with the specific antiserum in liver, lung, skin, and brain. In the liver, hepatic cells surrounding the central vein (Figure 6A′) and the cytoplasm of epithelial cells of the hepatic bile duct were apparently positive for the antiserum. In the lung, positive immunoreaction was observed in the epithelium lining the surface of bronchioles and in alveolar epithelium (Figure 6B′). In the skin, the epidermal cell layer (probably the prickle cell layer) was stained strongly, and hair follicles as well as sebaceous glands in the corium layer were intensely stained (Figure 6C′). In the brain, a part of the cerebrum and Ammon's horn was examined for this study. The intensity of immunoreaction

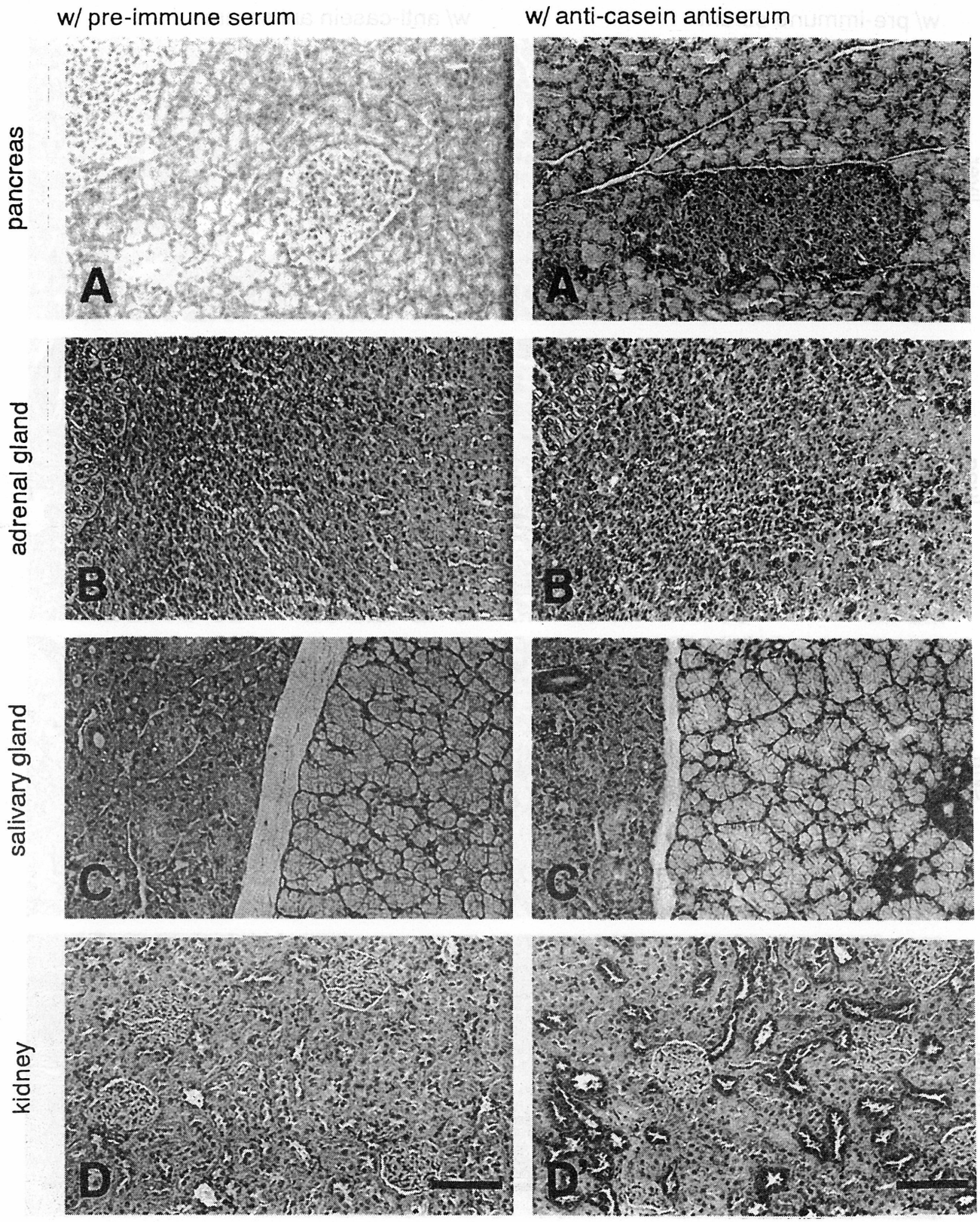

Figure 5 Immunohistochemical distribution of casein-like proteins in various organs of rat. Sections obtained from pancreas, adrenal gland, salivary gland and kidney were treated with either pre-immune serum (A–D) or anti-casein antiserum (A'–D'). Bars = 100 μm.

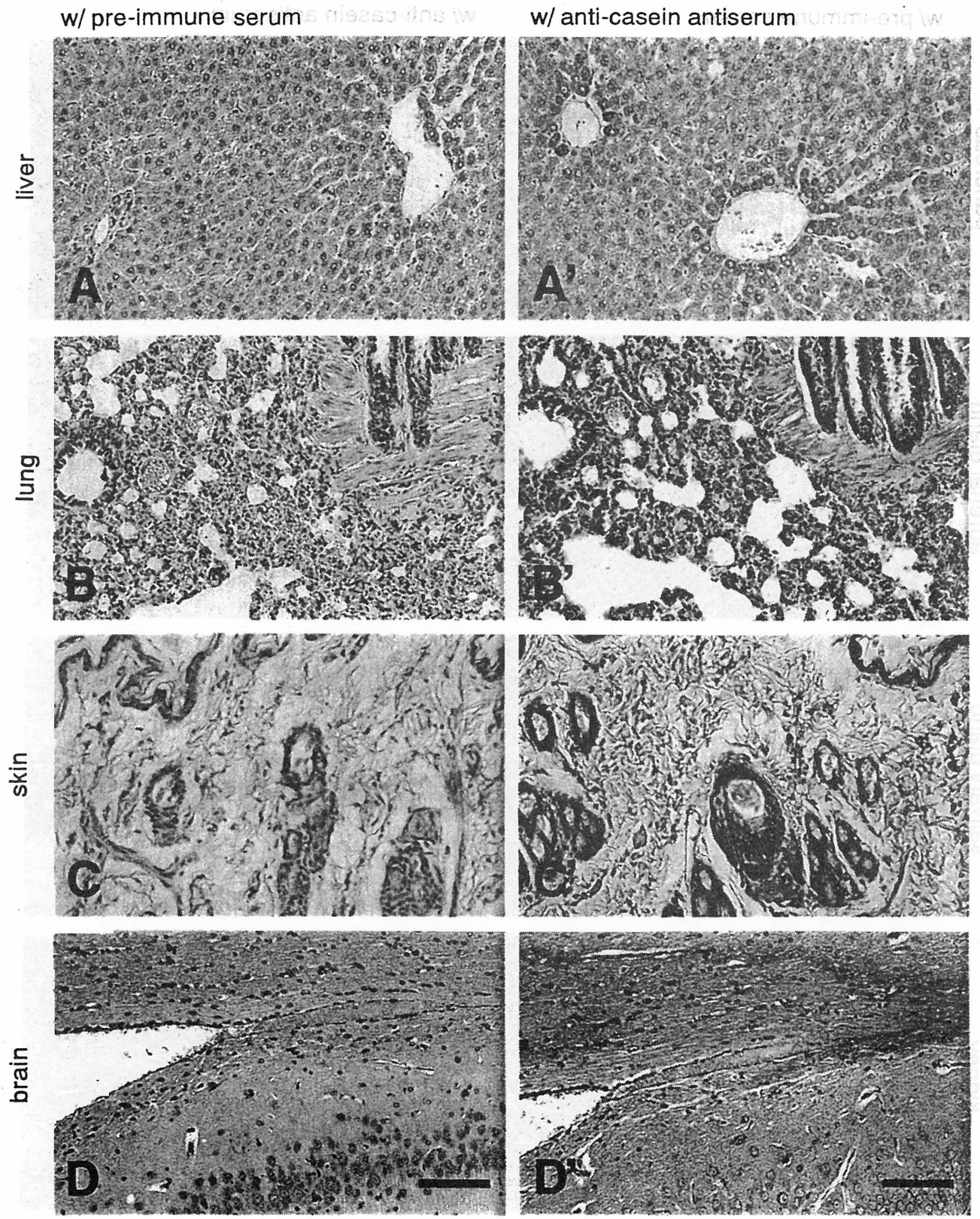

Figure 6 Immunohistochemical distribution of casein-like proteins in various organs of rat. Sections obtained from liver, lung, skin and brain (a portion of cerebrum and hippocampus) were treated with either pre-immune serum (**A–D**) or anti-casein antiserum (**A'–D'**). Bars = 100 μm.

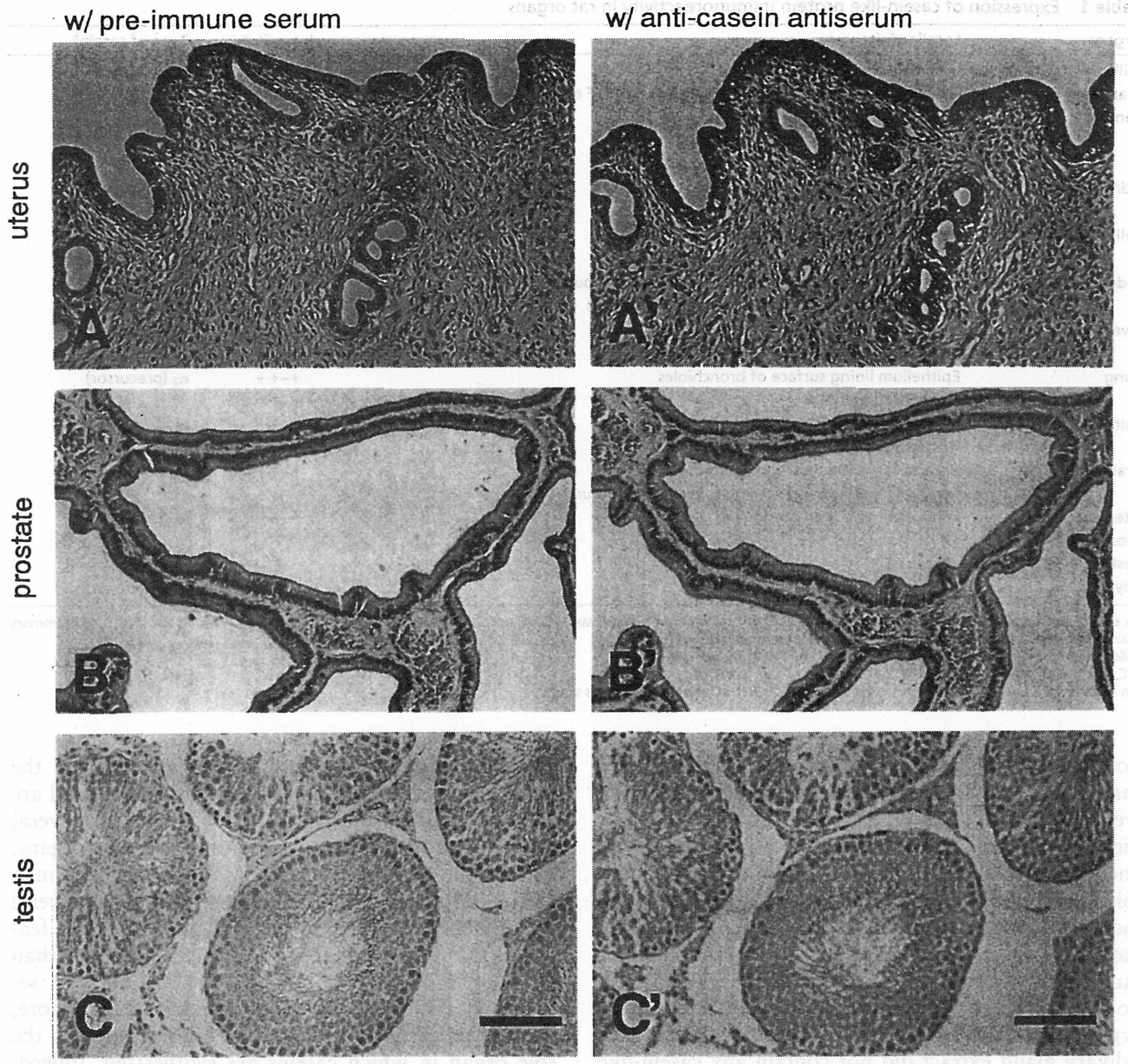

Figure 7 Immunohistochemical distribution of casein-like proteins in reproductive and accessory sex organs of rat. Sections obtained from uterus, prostate, and testis were treated with either pre-immune serum (A–C) or anti-casein antiserum (A'–C'). Bars = 100 μm.

with the antiserum was moderate and, in particular, the ventricular epithelium and chorioid plexus in the ventriculus cerebri showed intense immunoreaction (Figure 6D'). Interestingly, a part of the cerebral medulla (perhaps the cingulum bundle/corpus callosum) was relatively intense (Figure 6D').

Figure 7 presents the results of immunoreaction with the anti-casein antiserum in the reproductive and accessory sex organs. In the uterus, the epithelium of the endometrium and the uterine glands were strongly positive to the antiserum (Figure 7A'). However, the immunoreaction to the casein-like substance was inconclusive in the testis and prostate gland (Figures 7B' and 7C'). These results obtained from the immunohistochemical observation of casein-like substances in various organs are summarized with a semiquantitative assessment in Table 1.

Determination of Caseins in Various Organ Extracts by Immunoblot Analysis

As expected, the mammary gland extract contained caseins, and α_1-, α_2-, and β-caseins were abundant in the gland as well as in milk, whereas γ-casein was sel-

Table 1 Expression of casein-like protein immunoreactivity in rat organs

Organs	Localized site	Intensity[a]	Type of casein[b]
Milk			α_1, α_2, β, γ
Mammary gland	Apical portion and supranuclear cytoplasm of EC[c] of alveoli and primary ducts	+++	α_1, α_2, β, γ
Pancreas	EC of exocrine ducts	+–++	α_2
	Endocrine cells of islets of Langerhans	+–++	
	Acinar cells	–	
Adrenal gland	Cortical cells in zona fasciculata	++	α_2 (precursor)
	Ganglion cells	++	
Salivary gland	EC of secretory ducts	++	(precursor)
	Glandular acini	+	
Kidney	EC of distal convoluted tubules and collecting tubules	+–++	α_2 (precursor)
	Proximal convoluted tubules and renal corpuscles	–	
Liver	Hepatic cells surrounding central veins	+	α_2 (precursor)
	EC of hepatic bile ducts	+	
Lung	Epithelium lining surface of bronchioles	+–++	α_2 (precursor)
	Alveolar epithelium	+–++	
Skin	Epidermal cell layer (prickle cell layer)	++	α_2, β (precursor)
	Hair follicles and sebaceous glands	++	
Brain[d]	Ventricular epithelium and choroid plexus	+–++	α_2
	Cerebral medulla (cingulate bundle/corpus callosum)	+–++	
Uterus	Epithelium of endometrium and uterine glands	++	α_2 (precursor)
Prostate		?	
Testis		?	
Thymus	Not done		α_2 (precursor)

[a] A semiquantitative assessment of the immunohistochemical staining results was defined as follows: maximal intensity (+++) detected in the lactating mammary glands, moderate (++), weak (+), negative (–), and inconclusive (?).
[b] Molecular species of caseins were determined by Western blot analysis.
[c] EC, epithelial cells.
[d] In the brain, a part of the cerebrum and Ammon's horn was examined for this study.

dom detectable (Figure 8). The casein-like proteins that immunoreacted with the anti-casein antiserum were detected in many other organ extracts: pancreas, kidney, liver, lung, brain, uterus, skin, adrenal gland, and thymus (Figure 8). In these organ extracts, a major immunoreactive band had approximately a 37-kD molecular weight, which is similar to that of α_2-casein molecular species. In skin extract, a β-casein-like immunoreactive band was detected, whereas there were no such species of immunoreactive bands in the other organ extracts except for the mammary gland. The salivary gland extract did not contain any casein-like immunoreactive bands, although the secretory ducts of the salivary gland were strongly positive for the anti-casein antiserum in the immunohistochemical study (Figure 5C′). However, the salivary gland contained doublet immunoreactive bands in the higher molecular weight range. Interestingly, similar immunoreactive bands with higher molecular weights appeared in several organ extracts, including the adrenal gland, kidney, liver, lung, skin, uterus, and thymus, and are probably unprocessed precursors of the caseins (Barash et al. 1995).

Discussion

The ultimate function of the mammary gland obviously is to produce milk, which contains important substances for newborns, and it is known that the growth and differentiation of the mammary gland are basically controlled by multiple interactions of several peptide and steroid hormones from endocrine organs, such as the pituitary and ovary (Topper and Freeman 1980). Subsequently, development occurs in several phases, characterized by distinct morphological features. The major element of milk is casein (more than 50% of milk protein) which is synthesized and secreted by the mammary gland epithelium. Therefore, it has been believed that the mammary gland is the sole organ in which caseins are synthesized. Indeed, appreciable amounts of casein mRNAs are present in the rat mammary gland during pregnancy and lactation (Rosen et al. 1975), and cDNA clones corresponding to the mRNAs for the lactation-specific proteins, including caseins, have been isolated from a mammary-specific cDNA library (Hennighausen and Sippel 1982).

The observation that first localized the casein-like proteins in human organs other than the mammary gland was reported by Pich et al. (1976). Our present study confirmed the presence of casein-like immunoreactive substances in diverse organs of rat by use of a specific antiserum against rat caseins, although the amounts of casein-like substances in other organs were much less than that in the mammary gland and milk. One noteworthy finding was that the casein-like

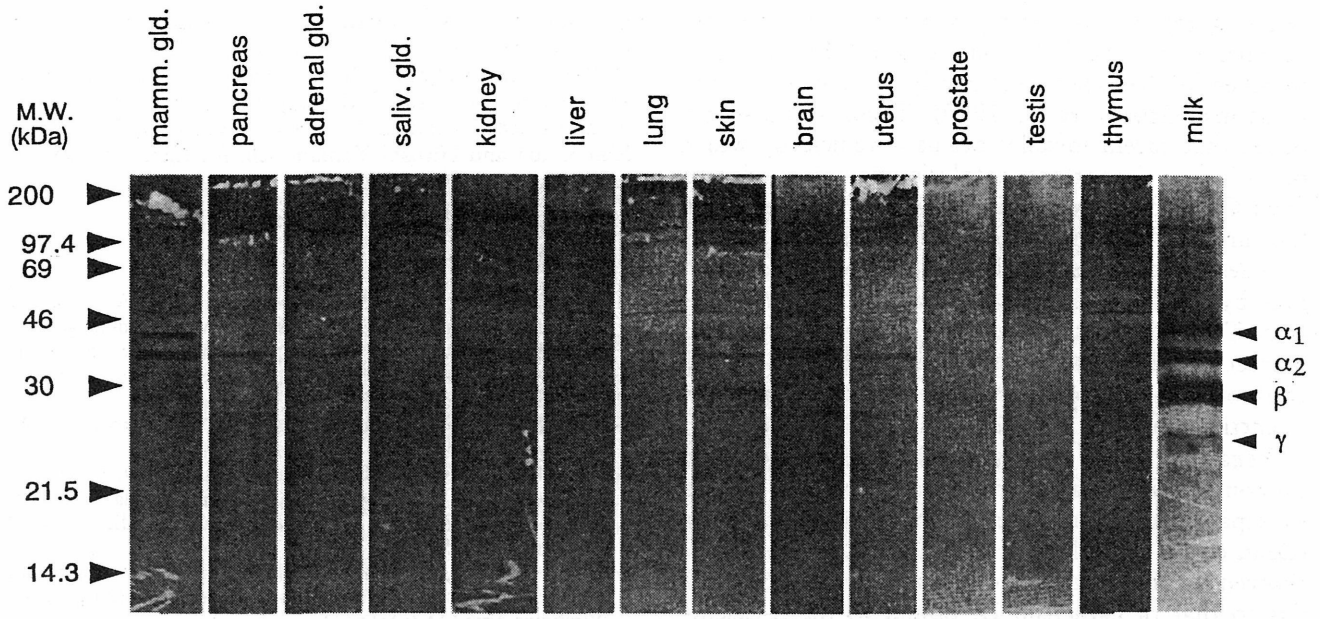

Figure 8 Immunoblot analysis of caseins and casein-like proteins in homogenates obtained from various organs. The homogenates were loaded onto the SDS-PAGE system and the immunoreactve substances were visualized as described above. The loaded amount of each homogenate was the following: mammary gland (30 μg), pancreas (120 μg), adrenal gland (80 μg), salivary gland (150 μg), kidney (150 μg), liver (150 μg), lung (150 μg), skin (25 μg), brain (150 μg), uterus (100 μg), prostate (80 μg), testis (30 μg), thymus (20 μg) and milk (0.03 μg).

substances were localized to the epithelium of exocrine ducts in a variety of organs, such as pancreas, salivary gland, kidney, and liver. In addition, the hormonally controlled organs, including the adrenal gland and uterus, also expressed the casein-like substances. Another observation in this study was that the α_2-casein-like protein was a major component of the casein-like protein expressed by organs. To our knowledge, this is the first time that the α_2-casein molecular species was identified in various organs by Western blot analysis with a specific antiserum. One possible explanation for this phenomenon is the hormonal regulation of casein expression in a variety of organs. It is well understood that the syntheses of the caseins (Terada et al. 1988; Enami and Nandi 1977; Banerjee 1976; Topper 1970) and their mRNAs (Hobbs et al. 1982; Ono and Oka 1980; Guyette et al. 1979; Matusik and Rosen 1978; Rosen et al. 1978; Banerjee 1976) are dependent on hormonal control. From these studies, it was deduced that prolactin, hydrocortisone, and insulin were essential for the synthesis of milk proteins and that progesterone suppressed casein synthesis, which is induced and maximized by three essential hormones. In addition, a significant level of mRNAs for caseins was found in virgin rat mammary glands, and the level increased coordinately during pregnancy and lactation (Hobbs et al. 1982). The proportions of each of the three casein (α-, β-, and γ-) mRNAs remained relatively constant throughout gestation and lactation. The concentration of mRNA for β-casein became higher than that of other casein mRNAs after gestation, whereas there was more α-casein mRNA than β-casein mRNA and the level of γ-casein mRNA was only 2% that of α-casein mRNA in the virgin rat mammary gland (Hobbs et al. 1982). In our study, the γ-casein-like protein was not detected by immunoblot analysis in the various organ extracts obtained from non-pregnant rats, and most of these organs were abundant in the α-casein-like protein (especially α_2-casein-like protein), except in the salivary gland. Therefore, these observations may reflect the hormonal regulation of casein-like proteins in various organs as well as in the mammary gland.

On the other hand, Ormerod et al. (1982) reported that human casein preparations were associated with small amounts of EMA, which was probably more immunogenic than casein, and that the immunization with such impure casein preparation might yield sera that react with EMA on tissue sections. However, in our present study, α-, β-, and γ-casein bands were excised from the nitrocellulose membrane after SDS-PAGE, electrotransfer, and visualization with Ponceau S. Furthermore, the distribution of staining in the lactating mammary glands was different from that obtained with the EMA antiserum, as described in Results. Therefore, it is unlikely that the casein emulsion used for the immunization in our study contained EMA.

Although the localization of caseins in a variety of organs is now certain, the physiological roles of casein and casein-like proteins remain obscure. There are in-

teresting reports that imply some possible roles for caseins. Cytotoxic T-lymphocytes (CTL) expressed members of the casein gene family, such as α-, β-, and κ-caseins (Grusby et al. 1990). These authors proposed that casein micelles act as a vehicle by which perforin, an important cytolytic mediator released from CTL on antigenic stimulation, is delivered onto the surface of target cells. In that report, the authors also described low levels of mRNA for α-casein in thymus by Northern blot analysis after PCR amplification. This is consistent with our finding that thymus extract contained an α_2-casein-like substance. Given these observations, caseins may be important as a sort of carrier protein in thymus and in CTL function.

Regarding other aspects, bovine α-casein was used for construction of a casein–Sepharose affinity column to separate acid proteases from renin in rat brain (Dzau et al. 1982; Hirose et al. 1978). These studies showed that the acid proteolytic activity, which is similar to that of cathepsin D, bound to the α-casein–Sepharose, whereas renin in the brain was eluted from the affinity column. Interestingly, the brain acid protease(s) also had angiotensin I-generating activity, which was not inhibited by the anti-renin antibody. These reports state that casein-like immunoreactive substance (α_2-casein) was detected throughout the section of rat brain. Therefore, casein in brain may act as a binding substance for some functional proteins, such as proteases, to regulate their activities and in turn maintain homeostasis. Furthermore, previous demonstrations by Young et al. (1986) and Simon et al. (1987) showed that casein was a substrate for serine esterases from cytolytic T-cells. Therefore, it is not unreasonable that α-casein may co-exist with such proteases in various organs, and is likely that caseins act as a substrate for certain proteases to control the proteolytic activities of enzymes in a variety of organs.

Although the specific anti-rat casein antiserum we generated provides a useful tool to analyze the mode of expression of the respective genes not only by immunohistochemistry but also by Western blotting, cloned cDNA probes in general would be superior to immunological methods for detection of specific markers in various organs. Therefore, the recognition of mRNAs for caseins or casein-like substances by specific cDNA probes would be a better approach to clarify the presence and localization of casein-like proteins in various organs. Furthermore, certain specific cDNAs will provide better understanding with regard to the regulation of respective genes by steroid and peptide hormones in various organs.

Acknowledgments

Supported by grants for the Special Project Research of Experimental Studies on the Radiation Health, Detriment and Its Modifying Factors, and for the Research Programme of Bioregulation Mechanism of the National Institute of Radiological Sciences.

We thank Dr Hiroshi Ohtsu, former Director of the Division of Physiology and Pathology, for his review of the immunohistochemical data. We are also grateful to Drs Hiroko Ishii–Ohba and Hiroshi Yamanouchi for their assistance in the preparation of the anti-casein antiserum.

Literature Cited

Abou–Zeid C, Filley E, Steele J, Rook GAW (1987) A simple new method for using antigens separated by polyacrylamide gel electrophoresis to stimulate lymphocytes in vitro after converting bands cut from Western blots into antigen-bearing particles. J Immunol Methods 98:5–10

Banerjee MR (1976) Responses of mammary cells to hormones. Int Rev Cytol 47:1–97

Barash I, Faerman A, Puzis R, Peterson D, Shani M (1995) Synthesis and secretion of casein by the mouse mammary gland: production and characterization of new polyclonal antibodies. Mol Cell Biochem 144:175–189

Bussolati G, Pich A, Alfani V (1975) Immunofluorescence detection of casein in human mammary dysplastic and neoplastic tissues. Virchows Arch [A] 365:15–21

Dzau V, Brenner A, Emmett NL (1982) Evidence for renin in rat brain: differentiation from other reninlike enzymes. Am J Physiol 242:E292–E297

Enami J, Nandi S (1977) Hormonal control of milk protein synthesis in cultured mouse mammary explants. Cell Differ 6:217–227

Grusby MJ, Mitchell SC, Nabavi N, Glimcher LH (1990) Casein expression in cytotoxic T lymphocytes. Proc Natl Acad Sci USA 87:6897–6901

Guyette WA, Matusik RJ, Rosen JM (1979) Prolactin-mediated transcriptional and post-transcriptional control of casein gene expression. Cell 17:1013–1023

Hahm HA, Ip MM, Darcy K, Black JD, Shea WK, Forczek S, Yoshimura M, Oka T (1990) Primary culture of normal rat mammary epithelial cells within a basement membrane matrix. II. Functional differentiation under serum-free conditions. In Vitro Cell Dev Biol 26:803–814

Hall L, Craig RK, Campbell PN (1979) mRNA species directing synthesis of milk proteins in normal and tumor tissue from human mammary gland. Nature 277:54–56

Hendrick JC, Franchimont P (1974) Radio-immunoassay of casein in the serum of normal subjects and of patiants with various malignancies. Eur J Cancer 10:725–730

Hennighausen LG, Sippel AE (1982) Characterization and cloning of the mRNAs specific for the lactating mouse mammary gland. Eur J Biochem 125:131–141

Hirose S, Yokosawa H, Inagami T (1978) Immunochemical identification of renin in rat brain and distinction from acid proteases. Nature 274:392–393

Hobbs AA, Richards DA, Kessler DJ, Rosen JM (1982) Complex hormonal regulation of rat gene expression. J Biol Chem 257: 3598–3605

Inano H, Ishii–Ohba H, Suzuki K, Yamanouchi H, Onoda M, Wakabayashi K (1995) Chemoprevention by dietary dehydroepiandrosterone against promotion/progression phase of radiation-induced mammary tumorigenesis in rats. J Steroid Biochem Mol Biol 54:47–53

Jenness R (1974) Biosynthesis and composition of milk. J Invest Dermatol 63:109–118

Levine JF, Stockdale FE (1985) Cell-cell interactions promote mammary epithelial cell differentiation. J Cell Biol 100:1415–1422

Matusik RJ, Rosen JM (1978) Prolactin induction of casein mRNA in organ culture: a model system for studying peptide hormone regulation of gene expression. J Biol Chem 253:2343–2347

Ono M, Oka T (1980) The differential actions of cortisol on the accumulation of α-lactalbumin and casein in midpregnant mouse mammary gland in culture. Cell 19:473–480

Onoda M, Djakiew D (1993a) A 29,000 Mr protein derived from round spermatid regulates Sertoli cell secretion. Mol Cell Endocrinol 93:53–61

Onoda M, Djakiew D (1993b) A 24,500 Da protein derived from rat germ cells is associated with Sertoli cell secretory function. Biochem Biophys Res Commun 197:688–695

Onoda M, Pflug B, Djakiew D (1991) Germ cell mitogenic activity is associated with nerve growth factor-like protein(s). J Cell Physiol 149:536–543

Ormerod MG, Bussolati G, Sloane JP, Steele K. Gugliotta P (1982) Similarities of antisera to casein and epithelial membrane antigen. Virchows Arch [Pathol Anat] 397:327–333

Pich A, Bussolati G, Carbonara A (1976) Immunocytochemical detection of casein and casein-like protein in human tissues. J Histochem Cytochem 24:940–947

Rosen JM, O'Neal DL, McHugh JE, Comstock JP (1978) Progesterone-mediated inhibition of casein mRNA and polysomal casein synthesis in the rat mammary gland during pregnancy. Biochemistry 17:290–297

Rosen JM, Woo SLC, Comstock JP (1975) Regulation of casein messenger RNA during the development of the rat mammary gland. Biochemistry 14:2895–2903

Simon MM, Simon HG, Fruth U, Epplen J, Muller–Hermelink HK, Kramer MD (1987) Cloned cytolytic T-effector cells and their malignant variants produce an extracellular matrix degrading trypsin-like serine proteinase. Immunology 60:219–230

Terada N, Wakimoto H, Oka T (1988) Regulation of milk protein synthesis by progesterone in cultured mouse mammary gland. J Steroid Biochem 29:99–104

Topper YJ (1970) Multiple hormone interactions in the development of mammary gland in vitro. Rec Prog Horm Res 26:287–308

Topper YJ, Freeman CS (1980) Multiple hormone interactions in the developmental biology of the mammary gland. Physiol Rev 60:1049–1106

van Haren L, Teerds KJ, Ossendorp BC, van Heusden GPH, Orly J, Stocco DM, Wirtz KWA, Rommerts FFG (1992) Sterol carrier protein 2 (nonspecific lipid transfer protein) is localized in membranous fractions of Leydig cells and Sertoli cells but not in germ cells. Biochim Biophys Acta 1124:288–296

Woods KL, Cove DH, Morrison JM, Heath DA (1979) The investigation of lactalbumin as a possible marker for human breast cancer. Eur J Cancer 15:47–51

Young JD-E, Leong LG, Liu C-C, Damiano A, Wall DA, Cohn ZA (1986) Isolation and characterization of a serine esterase from cytolytic T cell granules. Cell 47:183–194

Volume 46(11): 1269–1278, 1998
The Journal of Histochemistry & Cytochemistry
http://www.jhc.org

ARTICLE

Localization of Nitric Oxide Synthases and Nitric Oxide Production in the Rat Mammary Gland

Makoto Onoda and Hiroshi Inano

National Institute of Radiological Sciences, Chiba, Japan

SUMMARY We investigated nitric oxide (NO) production and the presence of nitric oxide synthase (NOS) in the mammary gland by use of an organ culture system of rat mammary glands. Mammary glands were excised from the inguinal parts of female Wistar–MS rats primed by implantation with pellets of 17β-estradiol and progesterone and were diced into approximately 3-mm cubes. Three of these cubes were cultured with 2 ml of 10% FCS/DMEM plus carboxy-PTIO (an NO scavenger, 100 μM) in the presence or absence of LPS (0.5 μg/ml) for 2 days. The amount of NO produced spontaneously by the cultured mammary glands was relatively minute at the end of the 2-day culture period, and the NO production was significantly enhanced by the presence of LPS. This enhancement of NO production was completely eliminated by addition of hydrocortisone (3 μM), an inhibitor of inducible NOS (iNOS), to the incubation medium. Immunoblot analyses with specific antisera against NOS isoforms such as iNOS, endothelial NOS (eNOS), and brain NOS (bNOS) showed immunoreactive bands of iNOS (122 ± 2 kD) and eNOS (152 ± 3 kD) in extracts prepared from the mammary glands in the culture without LPS. The immunoreactive band of iNOS was highly intense after the treatment of mammary glands with LPS, whereas the corresponding eNOS immunoreactive band was faded. The immunohistochemical study of anti-iNOS antiserum on frozen sections of the cultured mammary glands showed that an immunoreactive substance with the antiserum was localized to the basal layer (composed of myoepithelial cells of alveoli and lactiferous ducts) of the mammary epithelia and to the endothelium of blood vessels that penetrated into the interstitium of the mammary glands. Histochemical staining for NADPH-diaphorase activity, which is identical to NOS, showed localization similar to that of iNOS in the mammary glands. Similar observations were noted in the immunohistochemistry of eNOS. In contrast, the immunoreactive signal with the bNOS antiserum was barely detected in the epithelial parts of alveoli and lactiferous ducts of the mammary glands. These observations demonstrate that three isoforms of NOS are present not only in the endothelium of blood vessels but also in the parenchymal cells (the glandular epithelium) of the rat mammary gland, such as epithelial cells and myoepithelial cells, and suggest that NO may have functional roles in the physiology of the mammary glands. (J Histochem Cytochem 46:1269–1278, 1998)

KEY WORDS
nitric oxide
nitric oxide synthase
mammary gland
organ culture
immunohistochemistry
rat

NITRIC OXIDE (NO) is a unique biological messenger molecule that is synthesized from L-arginine by nitric oxide synthase (NOS) (Moncada et al. 1991; Schmidt et al. 1993; Bredt and Snyder 1994; Kröncke et al. 1995; Wolf 1997). This inorganic gaseous radical is released as a metabolic product of several types of cells, including endothelial, epithelial, neuronal, and phagocytic cells. Because of this variety of cell lineages, the functions of NO range from physiological to pathophysiological, including controlling blood pressure by blood vessel relaxation, regulating blood clotting through the inhibition of platelet aggregation, acting as a neurotransmitter in the central and peripheral nervous systems, and having a cytotoxic ability to kill tumor cells and intracellular parasites in the immune

Correspondence to: Dr. Makoto Onoda, First Research Group, Nat. Inst. of Radiological Sciences, 4-9-1 Anagawa, Inage-ku, Chiba-shi, Chiba, 263-8555, Japan.
Received for publication June 29, 1998; accepted June 30, 1998 (8A4713).

 0022-1554/98/$3.30

system (Moncada et al. 1991; Cifone et al. 1995; Dawson 1995; Vladutiu 1995; Kröncke et al 1997).

NOS has at least three distinct isoforms, including the neuronal (nNOS), brain (bNOS or NOS1), inducible (iNOS or NOS2), and endothelial (eNOS or NOS3) types (Mayer 1995; Wang and Marsden 1995). Although these were originally purified from the cerebellum (Bredt and Snyder 1990), cytokine-induced macrophages (Hevel et al. 1991; Stuehr et al. 1991; Yui et al. 1991), and the vascular endothelium (Förstermann et al. 1991; Pollock et al. 1991) and designated nNOS, iNOS and eNOS, respectively, the isoforms are now known to distribute across a wide spectrum of cell types and tissues. These include the adrenal gland (Afework et al. 1994, 1996; Tanaka and Chiba 1996), the digestive organs (Xue et al. 1994; Burrell et al. 1996; Chen et al. 1996), kidney (Bachmann et al. 1995; Fischer et al. 1995; Schwartz et al. 1997), bladder (Ehrén et al. 1995), liver (Bucher et al. 1997), pancreas (Umehara et al. 1997; Burrell et al. 1996), the female reproductive organs (Myatt et al. 1993; Ben-Shlomo et al. 1994; Huang et al. 1995; Chatterjee et al. 1996; Zackrisson et al. 1996), the male reproductive tract and its accessory organs (Burnett et al. 1995; Stéphan et al. 1995; Zini et al. 1996; Bloch et al. 1997), and many other tissues and organs. In addition to these organs and tissues, NOS isoforms were identified in human breast cancer and cancer cell lines (Thomsen et al. 1995; Zeillinger et al. 1996; Dueñas–Gonzalez et al. 1997). The presence and distribution of NOS isoforms in the normal mammary gland, in contrast, are not yet known. The aim of the present study was to investigate the presence and distribution of the NO-generating enzymes (NOS) in the rat mammary gland by using an organ culture system and immunobiological and immunohistochemical means. The possible functional roles of NO in the mammary gland are also discussed.

Materials and Methods

Materials and Animals

Reagents and chemicals were purchased from Sigma Chemical (St Louis, MO) unless stated otherwise. All animals used in the present study were treated and handled according to the "Recommendations for the Handling of Laboratory Animals for Biomedical Research" complied by the Committee of the Safety and Handling Regulations for Laboratory Animal Experiments in our Institute.

Organ Culture of Rat Mammary Glands

Female Wistar–MS rats (8-week-old) bred at Nippon SLC (Hamamatsu, Japan) were primed by implantation with pellets of 17β-estradiol (0.5 mg/3-week-release type; Innovative Research of America, Toledo, OH) and progesterone (35 mg/3-week-release type, Innovative Research). After 3 weeks of priming the rats were sacrificed by CO_2 asphyxiation and the inguinal mammary glands were excised aseptically for organ culture. The isolated mammary glands were diced into approximately 3-mm cubes, and three of these cubes were cultured in a well of 24-multiwell plate containing 2 ml of 10% fetal calf serum (FCS)/Dulbecco's modified Eagle's medium (DMEM) supplemented with antibiotics (100 U/ml penicillin, 100 μg/ml streptomycin) and an antimycotic (0.25 μg/ml amphotericin B) in a mixture of 5% CO_2/95% air at 37C for 2 days. The medium was then replaced with 10% FCS/DMEM plus 2-(4-carboxyphenyl)-4,4,5,5-tetramethylimidazole-1-oxyl 3-oxide (carboxy-PTIO, 100 μM; Dojindo Laboratories, Kumamoto, Japan) in the presence or absence of bacterial lipopolysaccharide (LPS, 0.5 μg/ml), and the culture was maintained for another 2 days. At the end of the culture, the conditioned media were collected for determination of the nitrite concentration as described below, and the cultured mammary glands were further processed for the preparation of mammary gland homogenates and frozen thin sections as described below.

Determination of Nitrite

NO produced and secreted by mammary glands into the culture medium was estimated by measuring the nitrite (NO_2^-) converted from NO with a Griess reagent mixture. The nitrite concentrations in conditioned media were determined immediately after the termination of the culture by a modification of a previously described colorimetric method (Green et al. 1982; Ben-Shlomo et al. 1994). Briefly, the Griess reagent mixture was freshly prepared by mixing equal volumes of stock Solution A (10% sulfanilamide, 40% phosphoric acid) and stock Solution B [1% *N*-(1-naphthyl) ethylenediamine dihydrochloride] before the measurement of nitrite. One part of the reagent mixture was transferred into 7 parts of the conditioned media appropriately diluted with PBS, and absorbance at either 545 nm or 570 nm was determined in a spectrophotometer. The nitrite concentration was then estimated from a standard curve that was simultaneously prepared for $NaNO_2$ in PBS. The slope of the standard curve was essentially the same whether DMEM or PBS was used as a diluent.

Preparation of Mammary Gland Homogenates and Immunoblot Analysis of Nitric Oxide Synthase Isoforms

The mammary glands cultured with or without LPS were minced and homogenized in ice-chilled 5 mM Tris-HCl buffer (pH 7.5) containing 0.25 M sucrose, 5 mM EGTA, and inhibitors (1 M phenylmethylsulfonyl fluoride, 2 mM sodium vanadate, 10 μg/ml aprotinin, 5 μg/ml leupeptin) (van Haren et al. 1992; Onoda and Djakiew 1993a,b). The homogenates were reconstituted in reducing sample buffer and loaded into the minigel system for SDS-PAGE. Subsequently, the separated proteins were electrotransferred to a nitrocellulose membrane (Onoda et al. 1991). The membrane was then soaked in 5% nonfat milk in 20 mM Tris-HCl-buffered saline containing 500 mM sodium chloride (TBS, pH 7.5) for 2 hr to block nonspecific immunoreaction, rinsed twice for 10 min in TBS containing 0.05% Tween 20 (TTBS), and reacted with either anti-iNOS antiserum (Affin-

ity Bioreagents; Golden, CO), anti-eNOS antiserum (Affinity Bioreagents), anti-bNOS antiserum (Affinity Bioreagents), or normal rabbit serum (NRS, 1:1000–2000 dilution) in TTBS containing 1% gelatin (Bio-Rad Labs; Richmond, CA) overnight. The membrane was washed in TTBS twice for 10 min, reacted with alkaline phosphatase-conjugated goat anti-rabbit IgG (1:3000 dilution) in TTBS/gelatin for 1 hr, and rinsed in TTBS twice and TBS once. The immunoreactivity was visualized by the following color development reactions (Onoda and Djakiew 1993a,b). For the alkaline phosphatase reaction, 5% nitroblue tetrazolium (NBT) in 70% dimethylformamide and 5% 5-bromo-4-chloro-3-indolyl phosphate (BCIP) in dimethylformamide were freshly prepared. Both NBT and BCIP reagents were then mixed with 100 mM Tris-HCl (pH 9.5) containing 100 mM sodium chloride and 5 mM magnesium chloride (alkaline phosphatase reaction buffer, APB) to a final concentration of 0.033% and 0.017%, respectively. Before color development, the protein-bound nitrocellulose membrane was washed in APB for 10 min and then the immunoreactive bands were visualized in APB containing NBT and BCIP. Color development was terminated by replacement of the reaction mixture with distilled water. The molecular weight of the immunoreactive bands was estimated from plots of molecular weight vs relative mobility of rainbow marker standard proteins (Amersham; Arlington Heights, IL), which were run simultaneously with the sample proteins. Anti-rat transferrin antiserum (Cappel Research Products; Durham, NC) and anti-rat caseins antiserum (Onoda and Inano 1997) were also used to confirm the presence of typical proteins produced by epithelial cells of the mammary glands.

Immunohistochemistry of Nitric Oxide Synthase Isoforms

The mammary glands incubated as mentioned above were cut into small cubes, fixed in 10% neutral buffered formalin at 4C, usually for about 20 hr, immersed in ascending grades of sucrose–PBS, and brought finally to 20% sucrose–5% glycerol–PBS. The fixed tissues then were embedded in Tissue-Tek OCT compound (Sakura Finetechnical; Tokyo, Japan) and frozen in hexane at −60C. Frozen sections (12 μm thick) were prepared in a Jung MC1900 cryostat (Leica; Nussloch, Germany), placed on gelatin–chromium (III)–potassium sulfate-coated slide glasses, and allowed to cool air-dry for a half hour. The sections were rehydrated in PBS before immunostaining. Streptavidin–biotin peroxidase immunostaining was carried out using Histofine SAB-PO kits (Nichirei; Tokyo, Japan) as described previously (Inano et al. 1995; Onoda and Inano 1997). Endogenous peroxidase activity was inactivated by 3% hydrogen peroxide for 15 min at room temperature (RT). The sections were washed twice in PBS for 5 min, then blocked by 10% normal goat serum for 30 min. Next, sections were incubated with either anti-NOS antisera or NRS (1:2000–3000 dilution) at 4C overnight and washed twice in PBS. The sections were treated with biotinylated second antibody (anti-rabbit IgG; goat) for 30 min at RT, washed twice in PBS, then incubated with streptavidin–peroxidase conjugate for 30 min and washed twice in PBS. Antibody localization on the specimens was visualized by the substrate–chromogen mixture [0.61 M Tris-HCl buffer (pH7.4) containing 0.05% 3,3′-diaminobenzidine tetrahydrochloride and 0.01% hydrogen peroxide], and color development was stopped by replacement of the reaction mixture with distilled water. The sections were counterstained with hematoxylin, dehydrated, and mounted with a mounting reagent. Immunostainings with anti-rat transferrin and anti-rat caseins were also carried out to validate the location of the mammary gland epithelium. Photomicrographs were taken under an Olympus BX50 microscope with an automatic camera.

NADPH-diaphorase Staining

The NADPH-diaphorase staining was performed according to the method described by Scherer–Singler (1983) with slight modification. Briefly, fixed frozen thin sections prepared as described above were rehydrated in PBS and incubated with a mixture of 1 mM NADPH (β) and 0.2 mM NBT in 50 mM Tris-HCl (pH 7.4) at 37C for 60 min. In the negative control sections, the NADPH (β) was omitted from the reaction mixture. After the staining, the sections were rinsed in PBS, counterstained in eosin, dehydrated, and mounted with a mounting reagent.

Statistical Analysis

Data are expressed as mean ± SE, and statistical comparisons among control and other groups were performed using ANOVA with StatView-J4.5 software (Abacus Concepts; Berkeley, CA) for Fisher's PLSD of multiple comparisons test. The level of significance was defined as $p<0.05$.

Results

NO Production by Cultured Mammary Glands

The amount of NO produced spontaneously by mammary glands in culture was relatively minute for the 2-day culture period, whereas the NO concentration in the conditioned media was significantly increased (by almost fivefold of the control) by the addition of LPS (0.5 μg/ml) to the culture system (Table 1). The secretion of NO from mammary glands cultured with LPS increased in a dose-dependent manner up to a concentration of 0.5 μg/ml, and was slightly inhibited at higher concentrations of LPS up to 2 μg/ml (Figure 1). This enhancement of NO secretion by the mammary

Table 1 Nitric oxide production by cultured rat mammary glands[a]

Treatment	Produced NO_2 (nmol/ml)[b]
Control	6.4 ± 0.4
w/LPS (0.5 μg/ml)	29.9 ± 1.9[c]
w/LPS, hydrocortisone (3 μM)	7.5 ± 0.6

[a]Three pieces of the mammary glands were cultured, and at the end of culture the conditioned media were collected for the determination of nitrite (NO_2^-) concentration. NO produced and secreted by mammary glands into culture medium was estimated by measuring nitrite converted from NO with Griess reagent as described in Materials and Methods.
[b]Values represent mean ± SE obtained from three independent experiments. Each experiment contained 6–8 cultures per replicate.
[c]Significant difference from control, $p<0.001$.

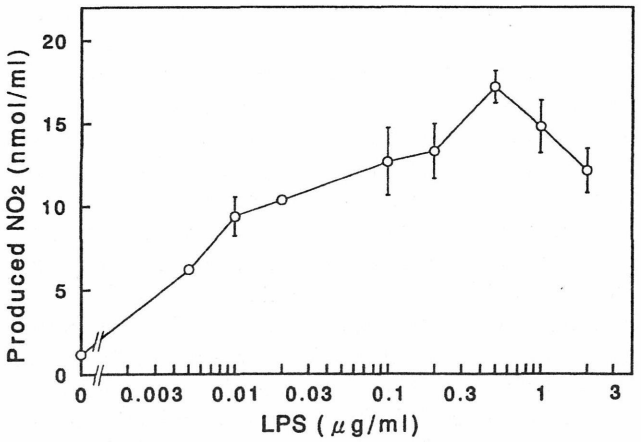

Figure 1 Enhancement of NO production in the cultured rat mammary glands by lipopolysaccharide (LPS). Three pieces of the mammary glands were cultured with the indicated doses of LPS for 2 days and the conditioned media were collected for the determination of the nitrite (NO_2^-) concentration as described in Materials and Methods. Each point and vertical bar represents the mean ± SE, respectively, obtained from three independent experiments. Each experiment contained three cultures per replicate.

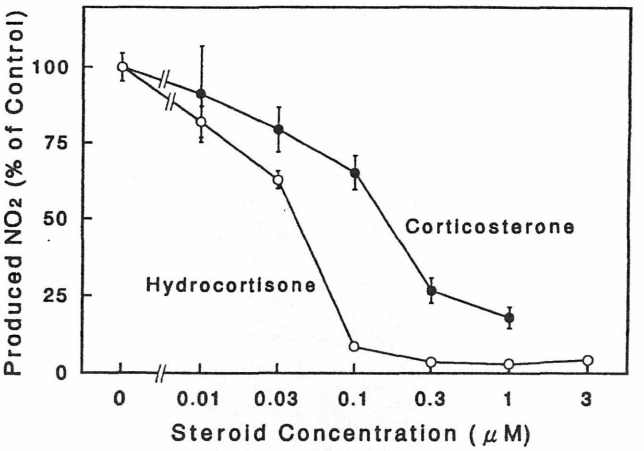

Figure 2 Effect of glucocorticoids on NO production by cultured rat mammary glands. Three pieces of the mammary glands were incubated for 2 days with LPS (0.5 μg/ml) in the presence of the indicated doses of steroids (hydrocortisone, open circles; corticosterone, solid circles), and the conditioned media were collected for the determination of nitrite (NO_2^-) concentration as described in Materials and Methods. Values presented are the percent of the control culture values (incubated without steroid). Each point and vertical bar represents the mean ± SE, respectively, obtained from three independent experiments. Each experiment contained three cultures per replicate.

glands in culture with LPS was completely eliminated by addition of 3 μM hydrocortisone to the culture (Table 1). Hydrocortisone and corticosterone inhibited NO production/secretion into the culture medium from mammary glands with LPS stimulation in a dose-dependent manner, and the median inhibition doses (ID_{50}) of hydrocortisone and corticosterone were approximately 40 nM and 150 nM, respectively (Figure 2). These findings suggest that the cultured rat mammary gland contains at least a certain cell population that responds to LPS stimulation and that this cell population produces NO.

Determination of NOS Isoforms in Mammary Gland Extracts by Immunoblot Analysis

The NOS isoforms that immunoreacted with anti-iNOS and anti-eNOS antisera were detected, respectively, in the mammary gland extracts obtained at the terminus of the organ culture of mammary glands (Figures 3 and 4). These immunoreactive bands of iNOS and eNOS had apparent molecular weights of 122 ± 2 kD and 152 ± 3 kD, respectively. In addition to this eNOS immunoreactive band (152 kD), in some cases a few other minor immunoreactive bands with molecular weights of approximately 97 kD, 78 kD, and 46 kD were detected by the anti-eNOS antibody (data not shown). These molecular species may be immunoreactive degradation products of eNOS, which were produced during the preparation of mammary gland extract owing to the presence of certain proteases (Zini et al. 1996). The quantity of immunoreactive band with anti-iNOS antiserum was apparently increased in the mammary gland extract treated with LPS during the culture period (Figure 3), and this increase in iNOS expression was well reflected in the enhancement of NO concentration in the conditioned

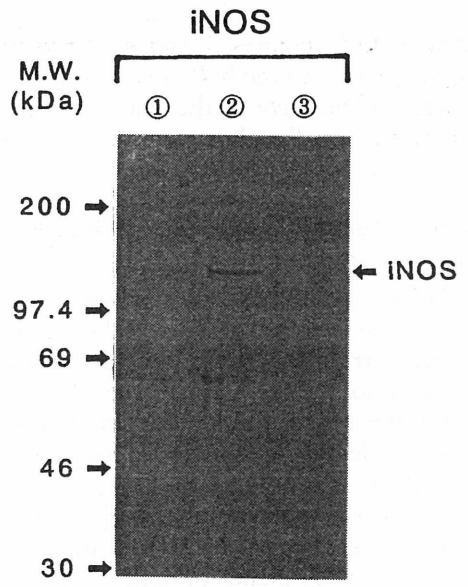

Figure 3 Immunoblot analysis of iNOS in extracts obtained from cultured rat mammary glands. The homogenates (10 μg/lane) were loaded onto the SDS-PAGE system and the immunoreactive substances were visualized by Western blot analysis with an alkaline phosphatase-conjugated secondary antibody as described in Materials and Methods. Lane 1, control; Lane 2, control + LPS (0.5 μg/ml); Lane 3, control + LPS + hydrocortisone (3 μM).

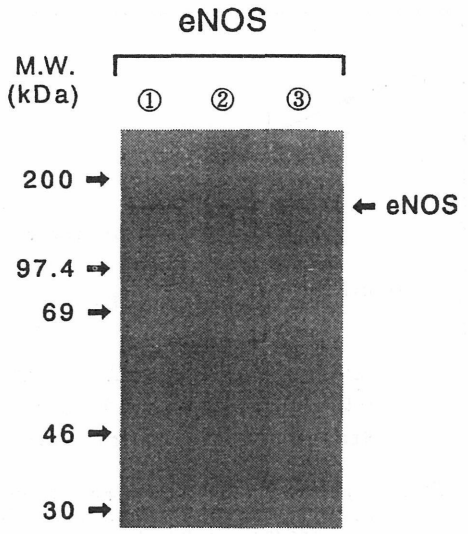

Figure 4 Immunoblot analysis of eNOS in extracts obtained from cultured rat mammary glands. The homogenates (18 μg/lane) were loaded onto the SDS-PAGE system and the immunoreactive substances were visualized as described in Materials and Methods. Lane 1, control; Lane 2, control + LPS (0.5 μg/ml); Lane 3, control + LPS + hydrocortisone (3 μM).

medium (Table 1). The eNOS expression was clearly diminished in the mammary gland extract after the treatment with LPS (Figure 4), although the gross production of NO was significantly enhanced in the culture with LPS treatment (Table 1). Hydrocortisone (3 μM) obviously suppressed not only the iNOS expression but also that of eNOS in the mammary glands cultured with LPS (Figures 3 and 4). Unfortunately, the immunoreaction to the bNOS with anti-bNOS antiserum was inconclusive in the mammary gland extracts obtained in all culture conditions (data not shown).

Immunohistochemical Observation of NOS Isoforms in Mammary Gland

Because the presence of NOS isoforms in the rat mammary gland was demonstrated by the immunoblot analyses, we carried out immunohistochemical staining of NOS isoforms in the rat mammary glands obtained after the organ culture with or without LPS stimulation to identify the particular location of NOS isoforms with specific antisera.

The immunoreactive signal of iNOS was clearly localized to the basal layers of alveoli and lactiferous ducts of the mammary glands obtained from the organ culture with LPS treatment (Figures 5b and 5b′). These component cells are probably myoepithelial cells, because the staining pattern of mammary epithelial cells with anti-transferrin and anti-casein antisera was evidently different from the iNOS staining pattern in the alveoli and lactiferous ducts (Figure 6). In addition to the mammary parenchymal cells, the endothelial cell layers of mammary blood vessels were also intensively stained with iNOS antiserum (Figure 5b). Similar immunoreactivity with anti-iNOS antiserum was present in the mammary glands obtained from organ cultures without LPS treatment, although less intense staining with anti-iNOS antiserum was noted (data not shown). The histochemical staining of NADPH-diaphorase activity, which is identical to NOS (Dawson et al. 1991; Hope et al. 1991), showed similarity to the iNOS immunoreactive staining pattern (Figure 7). The immunostaining pattern of eNOS in the non-LPS-treated mammary glands was identical to that observed in the immunostaining of iNOS (Figures 5c and 5c′). In contrast, the immunohistochemistry with anti-bNOS antiserum showed positive immunoreactivity in the epithelial cell layers of alveoli and lactiferous ducts of the mammary glands, although the staining intensity was relatively weak (Figures 5d and 5d′). A positive immunoreaction with anti-bNOS antiserum was not detected in the blood vessels of the mammary glands (Figure 5d).

Discussion

Nitric oxide is increasingly appreciated as a major regulator in the nervous, immune, and cardiovascular systems. Apart from being an autocrine and paracrine mediator of homeostasis, NO has been found to inflict damage on important biomolecules, and it was suggested to contribute to the cytocidal action of macrophages and to many pathological events. Recent reports also implicate the overproduction of NO in inflammation, arthritis, myositis, and other diseases, and a role of NO in the carcinogenic process and tumor progression has been described (Esumi et al. 1995; Doi et al. 1996; Tamir and Tannenbaum 1996). In fact, NOS isoforms are expressed in breast cancer cell lines (Zeillinger et al. 1996) and are correlated with breast cancer metastasis (Thomsen et al. 1995; Dueñas–Gonzalez et al. 1997).

The tentative presence of NOS activity in the mammary gland was first reported by Thomsen et al. (1995) in human breast cancer and normal tissue and by Lacasse et al. (1996) in goat and cow mammary glands. The former report described that NOS activity was detectable only in invasive tumors compared with benign or normal tissue, that iNOS immunoreactivity was predominantly within tumor-associated macrophages, and that bNOS was observed in vascular endothelial and myoepithelial cells in breast tumors. In the latter study, eNOS activity was detected only in the vascular endothelium and secretory epithelium of the two species. In our present study, however, it was demonstrated by immunoblot analysis and immunohistochemical criteria that three isoforms of NOS are present

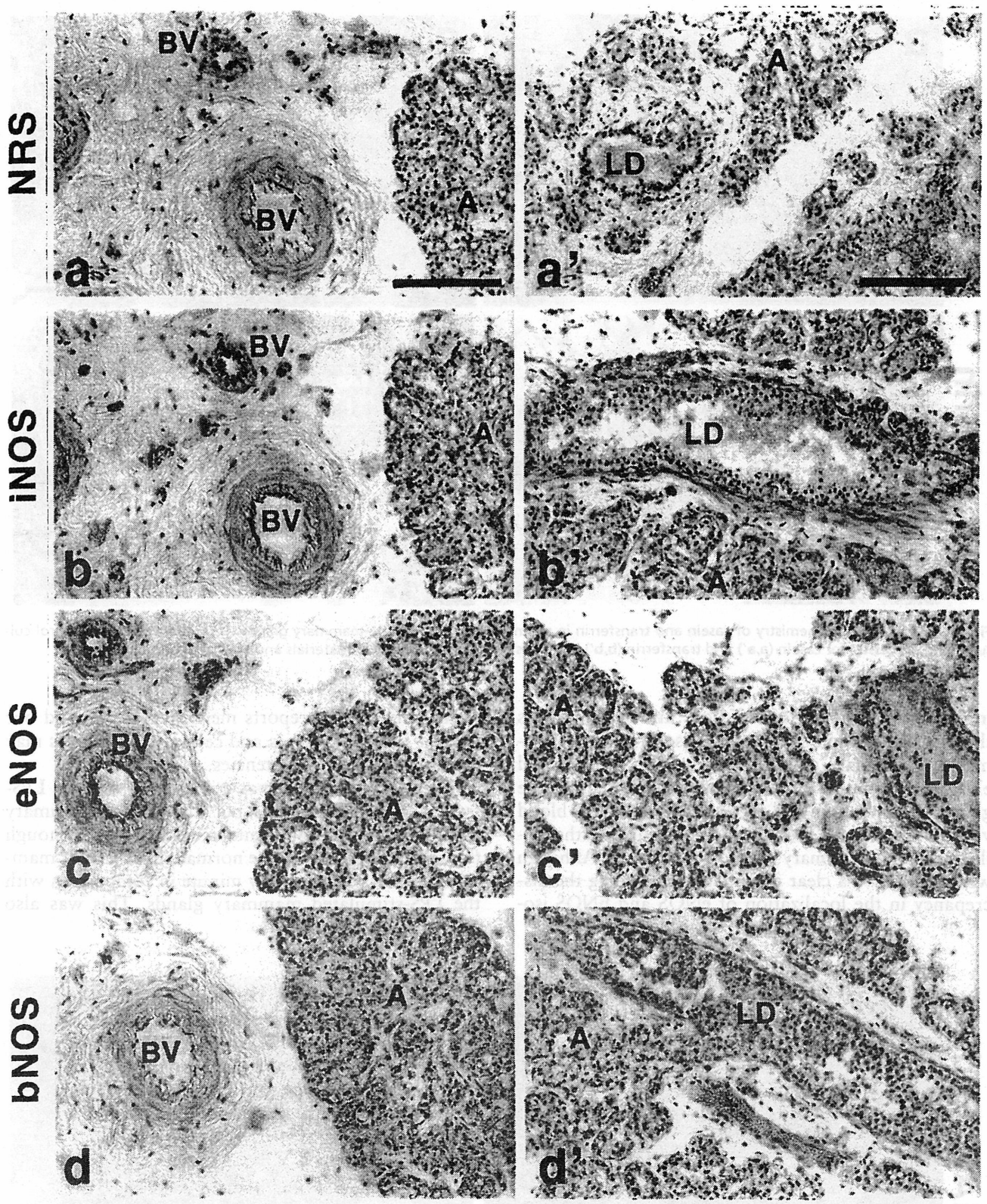

Figure 5 Immunohistochemistry of NOS isoforms in rat mammary glands. The mammary glands were isolated from hormone-primed Wistar–MS rats, cultured, and subjected to immunohistochemistry with specific antisera against NOS isoforms as described in Materials and Methods. For iNOS immunostaining (**b,b'**), the mammary glands were obtained from LPS-treated cultures, and the mammary glands obtained from control cultures were processed for eNOS (**c,c'**) and bNOS (**d,d'**) immunostaining. Normal rabbit serum (NRS) was used for detection of nonspecific immunoreactions (**a,a'**). Alveoli (A), lactiferous ducts (LD), and blood vessels (BV) are indicated. Bars = 100 μm.

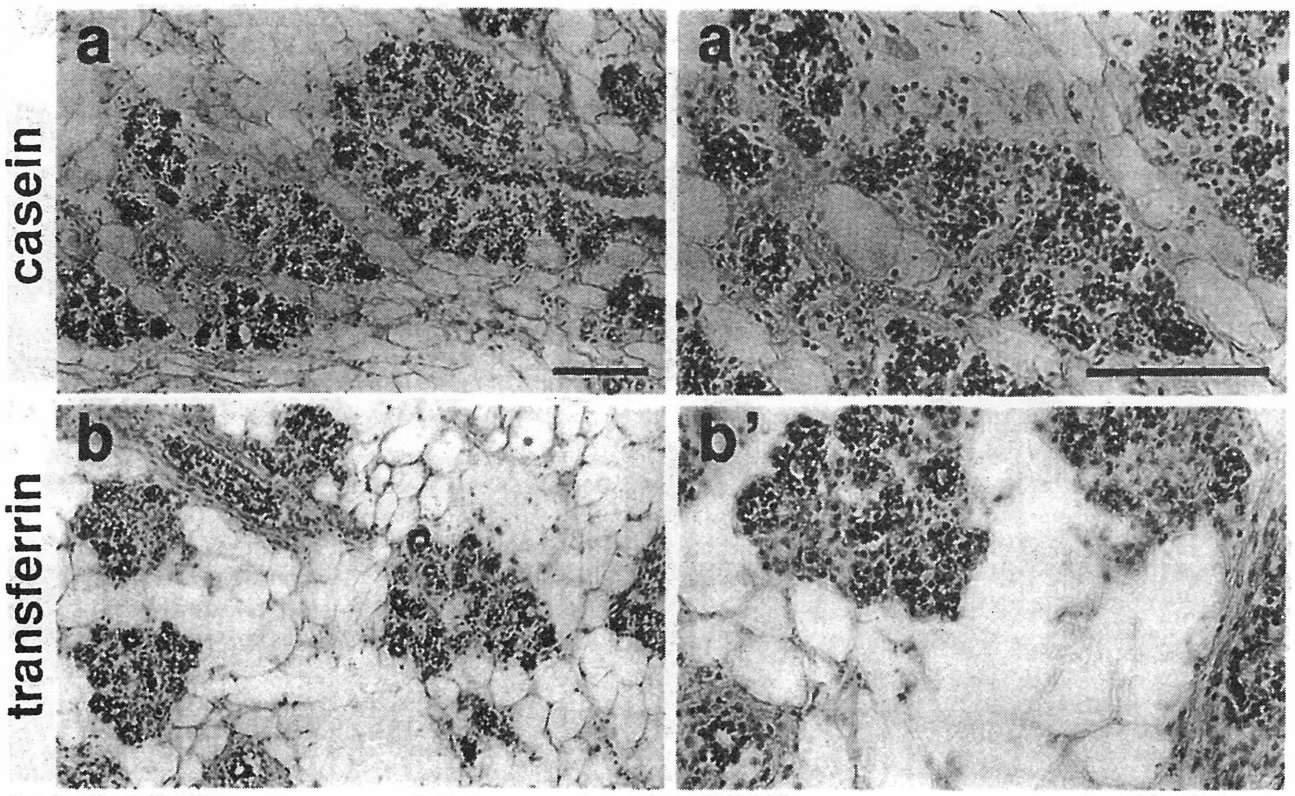

Figure 6 Immunohistochemistry of casein and transferrin in rat mammary glands. The mammary glands were obtained from control cultures and processed for casein (a,a') and transferrin (b,b') immunostaining as described in Materials and Methods. Bars = 100 μm.

in the rat mammary gland. To our knowledge, this is the first observation of three NOS isoforms in the normal rat mammary glands. We found that iNOS and eNOS isoforms localize to myoepithelial cells of the glandular epithelium and the endothelial cells of blood vessels, whereas the bNOS isoform is found in the epithelial cells of mammary parenchymal glands. Although we do not have a clear explanation regarding the discrepancy in the localization of eNOS and bNOS isoforms between the reports mentioned above and our present findings, species and cell type differences may account for the inconsistencies.

Interestingly, iNOS was present not only in LPS-treated mammary glands but also in the mammary glands that were not stimulated with LPS, although the amount of iNOS in the normal unstimulated mammary glands was relatively minute in comparison with the LPS-stimulated mammary glands. This was also

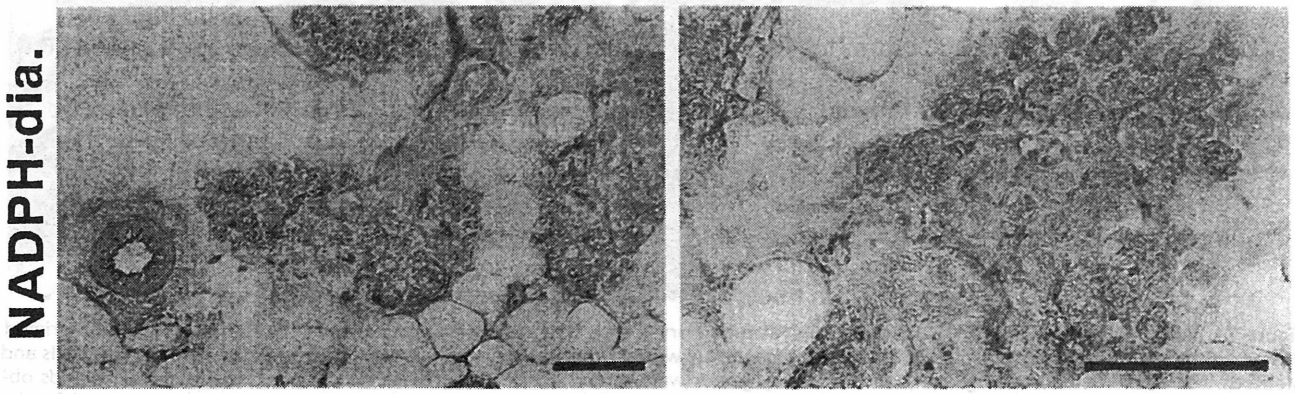

Figure 7 Histochemistry of NADPH-diaphorase activity in rat mammary glands. The mammary glands shown here were obtained from LPD-treated cultures and processed for NADPH-diaphorase activity staining as described in Materials and Methods. Bars = 100 μm.

reflected as spontaneous NO production in the NO concentration of culture medium in the mammary gland organ cultures without LPS stimulation. This is suggestive of a basal expression of iNOS and of other constitutive NOS isoforms in the unstimulated rat mammary glands. Because there are precedents for the expression of iNOS isoform in normal rat kidney (Morrissey et al. 1994) and guinea pig skeletal muscle (Gath et al. 1996,1997), it is not unlikely that the iNOS isoform is constitutively expressed to some extent in the normal rat mammary gland. However, it should be noted that the inevitable stress given to the isolated tissues during the dissection process and the subsequent culture conditions may have contributed to the induction of the iNOS isoform in the normal mammary glands.

Another surprising finding of our study is that the expression of the eNOS isoform in the mammary gland declined after the exposure of the mammary glands to LPS in the culture, although the iNOS-derived NO production masked a reduced NO production by eNOS in the cultures with LPS treatment. The downregulation of constitutive NOS expression by iNOS was recently reported not only for eNOS in cultured bovine coronary venular endothelial cells (Lu et al. 1996) and rat glomerular cells (Schwartz et al. 1997) but also for bNOS in the skeletal muscle of guinea pig (Gath et al. 1997), although these isoforms are usually considered to be constitutively expressed genes. It was suggested by Schwartz et al. (1997) that NO autoinhibition via complex interactions among NOS isoforms after LPS treatment may contribute to renal function. In addition, Lu et al. (1996) showed that LPS decreased the eNOS expression in cultured bovine coronary venular endothelial cells at protein and mRNA levels in a dose- and time-dependent manner, and concluded that the reduction of eNOS by LPS treatment resulted from an increased degradation rate of its transcripts. Therefore, it is likely that similar downregulation mechanisms occur in a reciprocal modulation of the eNOS and iNOS expressions of the mammary gland after the LPS exposure.

It is known that the growth and differentiation of the mammary gland are essentially controlled by multiple interactions of several peptide and steroid hormones from endocrine organs, such as the pituitary, ovary, and adrenal gland. Subsequently, development occurs in several phases, characterized by distinct morphological features (Topper and Freeman 1980). However, it was reported recently that release of these hormones from the endocrine organs is influenced by an NO-generating system. Higher levels of NO produced by iNOS in anterior pituitary cells may attenuate prolactin (PRL) and growth hormone (GH) release during emergency conditions of immune and inflammatory reactions, whereas low amounts of NO produced constitutively may take charge of subtle physiological adaptation (Vankelecom et al. 1997). Steroidogenesis in cultured ovarian cells is also suppressed by an inhibitory action of NO on P-450 aromatase activity (Masuda et al. 1997). Therefore, it is likely that development of the mammary gland is indirectly regulated through the NO-generating system by which hormone release is controlled in the endocrine organs. Conversely, steroids have been shown to regulate the NO synthesis in diverse types of cells and organs. Various glucocorticoids, mineralocorticoids, and sex steroids inhibited the spontaneous formation of nitrite in the medium of cultured rat hepatocytes (Pittner and Spitzer 1993). Yallampalli et al. (1994) showed that steroid hormones modulate the production of NO in the rat uterus, contributing to uterine contractility during pregnancy and the initiation of term or preterm labor. Taken together, these observations indicate that it is plausible that an NO-generating system may closely participate in the regulation of morphological and functional features of the mammary gland, because the growth and differentiation of the mammary gland are dependent on the hormonal conditions, which change with the developmental stages of this complicated gland.

Involution of the mammary gland is a tissue remodeling process, of which an integral component is the apoptosis of mammary epithelial cells (Furth et al. 1997). After lactation the mammary gland enters into an involutional process, which culminates in the return of the tissue to a quiescent stage within a short period. The beginning of this irreversible involution stage is characterized by decreased systemic hormone levels and proteinase action. Perplexingly, there a considerable number of studies have shown contrary effects of NO (i.e., apoptosis induction and cell protection by NO). The expression of cell-cycle control proteins, such as c-Myc and P53, increased after incubation with NO donors in vascular smooth muscle cells, whereas Bcl-2 protein, a survival protein, decreased (Nishio and Watanabe 1998). Wang and co-workers (1997) detected iNOS expression in the glomerular and tubulointerstitial cells of Class IV lupus nephritis in which p53 overexpression was correlated. These studies suggested that NO production plays a role in the occurrence of apoptosis through proto-oncoprotein expression. However, the mechanism of the inhibition of hepatocyte apoptosis by NO has been shown by Kim and colleagues (1997); who postulated that NO prevents apoptosis in hepatocytes by inhibiting caspase-3-like protease activity via a cGMP-dependent mechanism and by inhibition of caspase-3-like activity through protein S-nitrosylation. Although the roles of NO in apoptosis are still controversial, perhaps because NO can be either beneficial or detrimental depending on the cell type, it might help our understanding of the

precise roles of the NO-generating system in mammary gland physiology to clarify the stage-specificity of the expression of NOS isoforms, which may be influenced by pituitary, ovarian, and adrenal hormones.

In any event, our present data demonstrate that the presence of three NOS isoforms in the rat mammary gland is certain and that these NOS isoforms may correlate with mammary gland development and regulatory functions. Additional studies are needed to elucidate the precise roles of NO in the physiology and pathophysiology of the mammary gland.

Acknowledgments

Supported by grants for Special Project Research for Experimental Studies on Radiation Health, Detriment and Its Modifying Factors, and for Research Programme on Bioregulatory Mechanisms of the National Institute of Radiological Sciences.

We are grateful to Dr Yuji Ishikawa, Senior Researcher in the Division of Biology and Oncology, for helpful advice on the preparation of the frozen sections from cultured mammary glands.

Literature Cited

Afework M, Lincoln J, Belai A, Burnstock G (1996) Increase in nitric oxide synthase and NADPH-diaphorase in the adrenal gland of streptozotocin-diabetic Wistar rats and its prevention by ganglioside. Int J Dev Neurosci 14:111–123

Afework M, Tomlinson A, Burnstock G (1994) Distribution and colocalization of nitric oxide synthase and NADPH-diaphorase in adrenal gland of developing, adult and aging Sprague-Dawley rats. Cell tissue Res 276:133–141

Bachmann S, Bosse HM, Mundel P (1995) Topography of nitric oxide synthesis by localizing constitutive NO synthases in mammalian kidney. Am J Physiol 268:F885–898

Ben-Shlomo I, Kokia E, Jackson MJ, Adashi E, Payne DW (1994) Interleukin-1β stimulates nitrite production in the rat ovary: evidence for heterogous cell-cell interaction and for insulin-mediated regulation of the inducible isoform of nitric oxide synthase. Biol Reprod 51:310–318

Bloch W, Klotz T, Loch C, Schmidt G, Engelmann U, Addicks K (1997) Distribution of nitric oxide synthase implies a regulation of circulation, smooth muscle tone, and secretory function in the human prostate by nitric oxide. Prostate 33:1–8

Bredt DS, Snyder SH (1990) Isolation of nitric oxide synthase, a calmodulin-requiring enzyme. Proc Natl Acad Sci USA 87:682–685

Bredt DS, Snyder SH (1994) Nitric oxide: a physiologic messenger molecule. Annu Rev Biochem 63:175–195

Bucher M, Ittner KP, Zimmermann M, Wolf K, Hobbhahn J, Kurtz A (1997) Nitric oxide synthase isoform III gene expression in rat liver is up-regulated by lipopolysaccharide and lipoteichoic acid. FEBS Lett 412:511–514

Burnett AL, Ricker DD, Chamness SL, Maguire MP, Crone JK, Bredt DS, Snyder SH, Chang TSK (1995) Localization of nitric oxide synthase in the reproductive organs of the male rat. Biol Reprod 52:1–7

Burrell MA, Montuenga LM, Carcia M, Villaro AC (1996) Detection of nitric oxide synthase (NOS) in somatostatin-producing cells of human and murine stomach and pancreas. J Histochem Cytochem 44:339–346

Chatterjee S, Gangula PRR, Dong Y-L, Yallampalli C (1996) Immunocytochemical localization of nitric oxide synthase-III in reproductive organs of female rats during the oestrous cycle. Histochem J 28:715–723

Chen K, Inoue M, Okada A (1996) Expression of inducible nitric oxide synthase mRNA in rat digestive tissues after endotoxin and its role in intestinal mucosal injury. Biochem Biophys Res Commun 224:703–708

Cifone MG, Cironi L, Meccia MA, Roncaioli P, Festuccia C, De Nuntiis G, D'Alo S, Santoni A (1995) Role of nitric oxide in cell-mediated tumor cytotoxicity. Adv Neuroimmunol 5:443–461

Dawson VL (1995) Nitric oxide: role in neurotoxicity. Clin Exp Pharmacol Physiol 22:305–308

Dawson TM, Bredt DS, Fotuhi M, Hwang PM, Snyder SH (1991) Nitric oxide synthase and neuronal NADPH diaphorase are identical in brain and periopheral tissues. Proc Natl Acad Sci USA 88:7797–7801

Doi K, Akaike T, Horie H, Noguchi Y, Fujii S, Beppu T, Ogawa M, Maeda H (1996) Excessive production of nitric oxide in rat solid tumor and its implication in rapid tumor growth. Cancer 77: 1598–1604

Dueñas-Gonzalez A, Isales CM, del Mar Abad-Hernandez M, Gonzalez-Sarmiento R, Sangueza O, Rodriguez-Commes J (1997) Expression of inducible nitric oxide synthase in breast cancer correlates with metastatic disease. Mod Pathol 10:645–649

Ehrén I, Hammarström M, Adolfsson J, Wiklund NP (1995) Induction of calcium-dependent nitric oxide synthase by sex hormones in the guinea-pig urinary bladder. Acta Physiol Scand 153:393–394

Esumi H, Ogura T, Kurashima Y, Adachi H, Hokari A, Weisz A (1995) Implication of nitric oxide synthase in carcinogenesis: analysis of the human inducible nitric oxide synthase gene. Pharmacogenetics 5:S166–170

Fischer E, Schnermann S, Briggs JP, Kriz W, Ronco PM, Bachmann S (1995) Ontogeny of NO synthase and renin in juxtaglomerular apparatus of rat kidneys. Am J Physiol 268:F1164–1176

Förstermann U, Pollock JS, Schmidt HHHW, Heller M, Murad F (1991) Calmodulin-dependent endothelium-derived relaxing factor/nitric oxide synthase activity is present in the particulate and cytosolic fractions of bovin aortic endothelial cells. Proc Natl Acad Sci USA 88:1788–1792

Furth PA, Bar-Peled U, Li M (1997) Apoptosis and mammary gland involution: reviewing the process. Apoptosis 2:19–24

Gath I, Closs EI, Gödtel-Armbrust U, Schmitt S, Nakane M, Wessler I, Förstermann U (1996) Inducible NO synthase II and neuronal NO synthase I are constitutively expressed in different structures of guinea pig skeletal muscle: implications for contractile function. FASEB J 10:1614–1620

Gath I, Gödtel-Armbrust U, Förstermann U (1997) Expressional downregulation of neuronal-type NO synthase I in guinea pig skeletal muscle in response to bacterial lipopolysaccharide. FEBS Lett 410:319–323

Green LC, Wagner DA, Glogowski J, Skipper PL, Wishnok JS, Tannenbaum SR (1982) Analysis of nitrate, nitrite and [^{15}N]nitrate in biological fluids. Anal Biochem 126:131–138

Hevel JM, White KA, Marletta MA (1991) Purification of the inducible murine macrophage nitric oxide synthase. Identification as a flavoprotein. J Biol Chem 266:22789–22791

Hope BT, Michael GJ, Knigge KM, Vincent SR (1991) Neuronal NADPH diaphorase is a nitric oxide synthase. Proc Natl Acad Sci USA 88:2811–2814

Huang J, Roby KF, Pace JL, Russell SW, Hunt JS (1995) Cellular localization and hormonal regulation of inducible nitric oxide synthase in cycling mouse uterus. J Leukocyte Biol 57:27–35

Inano H, Ishii-Ohba H, Suzuki K, Yamanouchi H, Onoda M, Wakabayashi K (1995) Chemoprevention by dietary dehydroepiandrosterone against promotion/progression phase of radiation-induced mammary tumorigenesis in rats. J Steroid Biochem Mol Biol 54:47–53

Kim YM, Talanian RV, Billiar TR (1997) Nitric oxide inhibits apoptosis by preventing increases in caspase-3-like activity via two distinct mechanisms. J Biol Chem 272:31138–31148

Kröncke K-D, Fehsel K, Kolb-Bachofen V (1995) Inducible nitric oxide synthase and its product nitric oxide, a small molecule with complex biological activities. Biol Chem Hoppe Seyler 376:327–343

Kröncke K-D, Fehsel K, Kolb-Bachofen V (1997) Nitric oxide: cytotoxicity versus cytoprotection—how, why, when, and where? Nitric Oxide Biol Chem 1:107–120

Lacasse P, Farr VC, Davis SR, Prosser CG (1996) Local secretion of nitric oxide and the control of mammary blood flow. J Dairy Sci 79:1369–1374

Lu J-L, Schmiege LM III, Kuo L, Liao JC (1996) Downregulation of endothelial constitutive nitric oxide synthase expression by lipopolysaccharide. Biochem Biophys Res Commun 225:1–5

Masuda M, Kubota T, Kumada S, Aso T (1997) Nitric oxide inhibits steroidogenesis in cultured porcine granulosa cells. Mol Hum Reprod 3:285–292

Mayer B (1995) Biochemistry and molecular pharmacology of nitric oxide synthases. In Vincent SR, ed. Nitric Oxide in the Nervous System. London, Academic Press, 21–42

Moncada S, Palmer RMJ, Higgs EA (1991) Nitric oxide: physiology, pathophysiology, and pharmacology. Pharmacol Rev 43: 109–142

Morrissey JJ, McCracken R, Kaneto H, Vehaskari M, Montani D, Klahr S (1994) Location of an inducible nitric oxide synthase mRNA in the normal kidney. Kidney Int 45:998–1005

Myatt L, Brockman DE, Eis A, Pollock JS (1993) Immunohistochemical localization of nitric oxide synthase in the human placenta. Placenta 14:487–495

Nishio E, Watanabe Y (1998) NO induced apoptosis accompanying the change of oncoprotein expression and the activation of CPP32 protease. Life Sci 62:239–245

Onoda M, Djakiew D (1993a) A 29,000 Mr protein derived from round spermatid regulates Sertoli cell secretion. Mol Cell Endocrinol 93:53–61

Onoda M, Djakiew D (1993b) A 24,500 Da protein derived from rat germ cells is associated with Sertoli cell secretory function. Biochem Biophys Res Commun 197:688–695

Onoda M, Inano H (1997) Distribution of casein-like proteins in various organs of rat. J Histochem Cytochem 45:663-674

Onoda M, Pflug B, Djakiew D (1991) Germ cell mitogenic activity is associated with nerve growth factor-like protein(s). J Cell Physiol 149:536–543

Pittner RA, Spitzer JA (1993) Steroid hormones inhibit induction of spontaneous nitric oxide production in cultured hepatocytes without changes in arginase activity or urea production. Proc Soc Exp Biol Med 202:499–504

Pollock JS, Förstermann U, Mitchell JA, Warner TD, Schmidt HHHW, Nakane M, Murad F (1991) Purification and characterization of particulate endothelium-derived relaxing factor synthase from cultured and native bovine aortic endothelial cells. Proc Natl Acad Sci USA 88:10480–10484

Scherer-Singler U, Vincent SR, Kimura H, McGeer EG (1983) Demonstration of a unique population of neurons with NADPH-diaphorase histochemistry. J Neurosci Methods 9:229–234

Schmidt HHHW, Lohmann SM, Walter U (1993) The nitric oxide and cGMP signal transduction system: regulation and mechanism of action. Biochim Biophys Acta 1178:153–175

Schwartz D, Mendonca M, Schwartz I, Xia Y, Satriano J, Wilson CB, Blantz RC (1997) Inhibition of constitutive nitric oxide synthase (NOS) by nitric oxide generated by inducible NOS after lipopolysaccharide administration provokes renal dysfunction in rats. J Clin Invest 100:439–448

Stéphan J-P, Guillemois C, Jégou B, Bauché F (1995) Nitric oxide production by Sertoli cells in response to cytokines and lipopolysaccharide. Biochem Biophys Res Commun 213:218–224

Stuehr DJ, Cho HJ, Kwon NS, Weise MF, Nathan CF (1991) Purification and characterization of the cytokine-induced macrophage nitric oxide synthase: an FAD- and FMN-containing flavoprotein. Proc Natl Acad Sci USA 88:7773–7777

Tamir S, Tannenbaum SR (1996) The role of nitric oxide (NO·) in the carcinogenic process. Biochim Biophys Acta 1288:F31–36

Tanaka K, Chiba T (1996) Ultrastructural localization of nerve terminals containing nitric oxide synthase in rat adrenal gland. Neurosci Lett 204:153–156

Thomsen LL, Miles DW, Happerfield L, Bobrow LG, Knwles RG, Moncada S (1995) Nitric oxide synthase activity in human breast cancer. Br J Cancer 72:41–44

Topper YJ, Freeman CS (1980) Multiple hormone interactions in the developmental biology of the mammary gland. Physiol Rev 60:1049–1106

Umehara K, Kataoka K, Ogura T, Esumi H, Kashima K, Ibata Y, Okamura H (1997) Comparative distribution of nitric oxide synthase (NOS) in pancreas of the dog and rat: immunocytochemistry of neuronal type NOS and histochemistry of NADPH-diaphorase. Brain Res Bull 42:469–478

van Haren L, Teerds KJ, Ossendorp BC, van Heusden GPH, Orly J, Stocco DM, Wirtz KWA, Rommerts FFG (1992) Sterol carrier protein 2 (non-specific lipid transfer protein) is localized in membranous fractions of Leydig cells and Sertoli cells but not in germ cells. Biochim Biophys Acta 1124:288–296

Vankelecom H, Matthys P, Denef C (1997) Involvement of nitric oxide in the interferon-γ-induced inhibition of growth hormone and prolactin secretion in anterior pituitary cell cultures. Mol Cell Endocrinol 129:157–167

Vladutiu AO (1995) Role of nitric oxide in autoimmunity. Clin Immunol Immunopathol 76:1–11

Wang Y, Marsden PA (1995) Nitric oxide synthases: gene structure and regulation. Adv Pharmacol 34:71–90

Wang JS, Tseng HH, Shih DF, Jou HS, Ger LP (1997) Expression of inducible nitric oxide synthase and apoptosis in human lupus nephritis. Nephron 77:404–411

Wolf G (1997) Nitric oxide and nitric oxide synthase: biology, pathology, localization. Histol Histopathol 12:251–261

Xue C, Pollock J, Schmidt HH, Ward SM, Sanders KM (1994) Expression of nitric oxide synthase immunoreactivity by interstitial cells of the canine proximal colon. J Auton Nerv Syst 49:1–14

Yallampalli C, Byam-Smith M, Nelson SO, Garfield RE (1994) Steroid hormones modulate the production of nitric oxide and cGMP in the rat uterus. Endocrinology 134:1971–1974

Yui Y, Hattori R, Kosuga K, Eizawa H, Hiki K, Kawai C (1991) Purification of nitric oxide synthase from rat macrophages. J Biol Chem 266:12544–12547

Zackrisson U, Mikuni M, Wallin A, Delbro D, Hedin L, Brännström M (1996) Cell-specific localization of nitric oxide synthases (NOS) in the rat ovary during follicular development, ovulation and leuteal formation. Hum Reprod 11:2667–2673

Zeillinger R, Tantscher E, Schneeberger C, Tschugguel W, Eder S, Sliutz G, Huber JC (1996) Simultaneous expression of nitric oxide synthase and estrogen receptor in human breast cancer cell lines. Breast Cancer Res Treat 40:205–207

Zini A, O'Bryan MK, Magid MS, Schlegel PN (1996) Immunohistochemical localization of endothelial nitric oxide synthase in human testis, epididymis, and vas deferens suggests a possible role for nitric oxide in spermatogenesis, sperm maturation, and programmed cell death. Biol Reprol 55:935–941

Carcinogenesis vol.20 no.6 pp.1011–1018, 1999

Chemoprevention by curcumin during the promotion stage of tumorigenesis of mammary gland in rats irradiated with γ-rays

Hiroshi Inano[4], Makoto Onoda, Naoshi Inafuku[1], Megumi Kubota[1], Yasuhiro Kamada[1], Toshihiko Osawa[2], Hisae Kobayashi[3] and Katsumi Wakabayashi[3]

First Research Group, National Institute of Radiological Sciences, 9-1 Anagawa-4-chome, Inage-ku, Chiba-shi 263-8555, [1]Ryukyu Bio-Resource Development Co. Ltd, 606-2 Toyohara, Motobu-cho 905-0204, Okinawa, [2]Laboratory of Food and Biodynamics, Nagoya University Graduate School of Bioagricultural Sciences, Furo-cho, Chikusa-ku, Nagoya-shi 464-8601 and [3]Institute for Molecular and Cellular Regulation, Gunma University, Showa-machi, Maebashi-shi 371-8512, Japan

[4]To whom correspondence should be addressed
Email: inano@nirs.go.jp

We have evaluated the chemopreventive effects of curcumin on diethylstilbestrol (DES)-induced tumor promotion of rat mammary glands initiated with radiation. Sixty-four pregnant rats received whole body irradiation with 2.6 Gy γ-rays from a ^{60}Co source at day 20 of pregnancy and were divided into two groups after weaning. In the control group of 39 rats fed a basal diet and then implanted with a DES pellet for 1 year, 33 (84.6%) developed mammary tumors. Twenty-five rats were fed diet containing 1% curcumin immediately after weaning and received a DES pellet, as for the control. The administration of dietary curcumin significantly reduced the incidence (28.0%) of mammary tumors. Multiplicity and Iball's index of mammary tumors were also decreased by curcumin. Rats fed the curcumin diet showed a reduced incidence of the development of both mammary adenocarcinoma and ER(+)PgR(+) tumors in comparison with the control group. On long-term treatment with curcumin, body weight and ovarian weight were reduced, but liver weight was increased. Compared with the control rats, the curcumin-fed rats showed a significant reduction in serum prolactin, whereas estradiol-17β and progesterone concentrations were not significantly different between the two groups. Curcumin did not have any effect on the concentration of free cholesterol, cholesterol ester and triglyceride. Feeding of the curcumin diet caused a significant increase in the concentrations of tetrahydrocurcumin, arachidonic acid and eicosapentaenoic acid and a significant decrease in thiobarbituric acid-reactive substance concentration in serum. Whole mounts of the mammary glands showed that curcumin yielded morphologically indistinguishable proliferation and differentiation from the glands of the control rats. These findings suggest that curcumin has a potent preventive activity during the DES-dependent promotion stage of radiation-induced mammary tumorigenesis.

Introduction

Epidemiological surveys suggest that diet has an impact on cancer incidence. Frequent consumption of vegetables and fruits decreases the risk for human cancer (1–3). Recently, attention has been focused on identifying dietary phytochemicals which have the ability to inhibit the processes of carcinogenesis. Extracts of plants or their fractionated ingredients were found to possess inhibitory effects against chemically induced carcinogenesis (4). Curcumin (Figure 1) is a major component of turmeric, the dried rhizome of *Curcuma longa* L. which is commonly used as a yellow coloring and flavoring agent in food in Asian countries. Commercial grade curcumin has shown anticarcinogenic activity in animals as indicated by ability to block colon tumor initiation induced by azoxymethane (5) and skin tumor promotion induced by phorbol ester (6). Furthermore, curcumin has been reported to possess anti-inflammatory activity and is a potent inhibitor of reactive oxygen-generating enzymes such as lipoxygenase/cyclooxygenase (7,8), xanthine dehydrogenase/oxidase (9) and nitric oxide synthase (NOS) (10,11). Lack of a mutagenic effect of curcumin was also reported in the presence or absence of a rat liver microsomal activation system in the Ames test with *Salmonella typhimurium* (12). Bhavanishankar *et al.* (13) found that an alcohol extract (including curcumin) of turmeric was non-toxic, although curcumin has been reported to inhibit the growth of a wide variety of tumor cells, whereas normal cells were found to be relatively resistant (14). In the present study, we have evaluated the chemopreventive effects of curcumin on diethylstilbestrol (DES)-induced tumor promotion of rat mammary glands initiated with radiation and the endocrinological and pharmacological activities of the agent are discussed.

Abbreviations: DES, diethylstilbestrol; ER, estrogen receptor; FSH, follicle stimulating hormone; LH, luteinizing hormone; LPS, lipopolysaccharide; MDA, malondialdehyde; NOS, nitric oxide synthase; PgR, progesterone receptor; TBARS, thiobarbituric acid-reactive substances.

Materials and methods

Materials

Curcumin, commonly used in foods as a coloring agent, was obtained from Aldrich Chemical Co. (Milwaukee, WI). Diet containing 1% (w/w) curcumin was prepared in biscuit form by Funabashi Farm (Chiba, Japan). A basal diet (MB-1) of the same form was used for the control experiments. The major components of MB-1 are as follows: total carbohydrate, 54.1%; protein, 24.6%; fat, 4%; fiber, 3.8%; moisture, 7.7%; ash, 5.8%. DES, cholesterol and sulfatase were purchased from Sigma (St Louis, MO). β-Glucuronidase was purchased from Wako Pure Chemical Industies Ltd (Osaka, Japan). Pellets were prepared in a medical grade Silastic tube (Dow Corning Co., Midland, MI) and were filled with 3 mg DES mixed with 27 mg cholesterol. [2,4,6,7-^{3}H]Estradiol-17β (sp. act. 4 TBq/mmol), [17α-methyl-^{3}H]R5020 (sp. act. 3 TBq/mmol) and non-labeled R5020 (17α,21-dimethyl-19-nor-4,9-pregnadiene-3,20-dione) were purchased from Du Pont/NEN Research Products (Boston, MA).

Animals and treatment

The rats used in the present study were treated and handled according to the *Recommendations for Handling of Laboratory Animals for Biomedical Research* compiled by the Committee on the Safety and Handling Regulations for Laboratory Animal Experiments in our Institute. Wistar-MS rats from a stock colony of Nippon SLC Co. (Hamamatsu, Japan) were kept at 23 ± 1°C in a controlled environment (14 h light/10 h dark). They received water and food *ad libitum*. Sixty-four pregnant rats received whole body irradiation with 2.6 Gy γ-rays (0.15 Gy/min) from a ^{60}Co source at day 20 of pregnancy (the presence of a vaginal plug denoting day 1) and were divided into two groups after weaning. Serving as the control group, 39 rats were fed a basal diet (MB-1) and were then implanted with a DES pellet at 1 month after weaning.

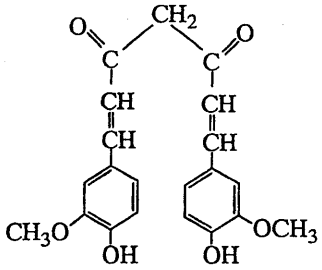

Fig. 1. Chemical structure of curcumin [chemical name 1,7-bis(4'-hydroxy-3'-methoxyphenyl)-1,6-heptadiene-3,5-dione].

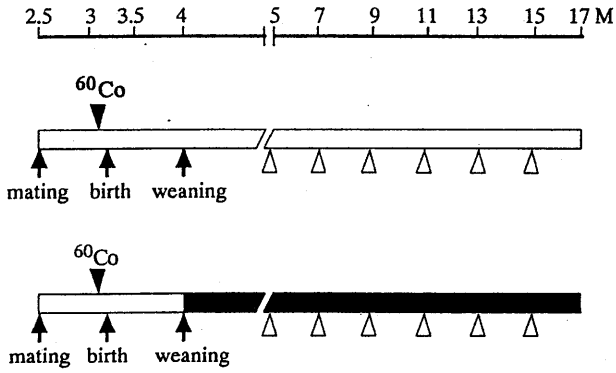

Fig. 2. Experimental schedule in this study. Open bar, control diet (MB-1); closed bar, diet containing 1% curcumin; open arrowhead, implantation with DES pellet; closed arrowhead, whole body irradiation with 2.6 Gy γ-rays at day 20 of pregnancy; M, months old.

Twenty-five rats were fed diet containing 1% curcumin immediately after weaning and received a DES pellet at 1 month after termination of nursing (Figure 2). The pellets were replaced every 8 weeks. The rate of release of DES from the pellet was 0.38 ± 0.01 μg/day (15). The rats were examined for palpable mammary tumors for 1 year starting from the date of pellet implantation. When mammary tumors >2 cm in diameter were detected, the rats were killed by CO_2 asphyxiation and the tumors were removed. Each mammary tumor was divided into two portions: one portion was fixed in 10% neutral buffered formalin for histopathological examination and the other was trimmed off surrounding normal tissue and immediately frozen at −80°C until use for receptor assays. The remaining rats were killed 1 year after administration of the DES pellet and were autopsied to ascertain whether they had any non-palpable mammary tumors. Tumor incidence was calculated from the number of rats with tumors within 1 year. Iball's index of mammary tumors was calculated as follows: the ratio of incidence (%) to the average latency period in days×100 (16).

Assays

A blood sample was collected by cardiocentesis under anesthesia and serum prepared as usual. The sera were frozen immediately and stored at −80°C until the assay was started. For assays of total curcuminoids (free form plus conjugates), serum was incubated with 10 mM McIlvaine buffer (pH 5.0) containing 20% ascorbic acid, 0.17% EDTA, 500 U β-glucuronidase and 40 U sulfatase at 37°C for 60 min (17). Curcumin and its metabolites were extracted with ethylacetate and then analyzed by HPLC with a multiwavelength detector on a Develosil ODS-HG-5 column (4.6×250 mm; Nomura Chemical Co., Seto, Japan) eluted with a mixture of acetonitrile:water (1:1 v/v) containing 0.1% trifluoroacetic acid as solvent system at a flow rate of 1 ml/min. The chromatogram was monitored at a wavelength of 430 nm for detection of curcumin and at 280 nm for tetrahydrocurcumin (18). Concentrations of prolactin, luteinizing hormone (LH) and follicle stimulating hormone (FSH) were determined with NIDDK radioimmunoassay kits (the National Hormone and Pituitary Program, Rockville, MD). Estradiol-17β, progesterone, cholesterol and triglyceride were assayed by commercially available kits. Fatty acids were extracted from serum with hexane and were treated with 14% trifluorobenzene dissolved in methanol:methanol:benzene (35:35:30) for 10 min in boiling water for esterification. The methyl esters of fatty acids were analyzed by gas chromatography with a hydrogen flame ionization detector (19). For assay of lipid peroxidation products, the serum was mixed with 20% trichloroacetic acid and 0.67% thiobarbituric acid and then heated for 15 min in boiling water. The concentration of thiobarbituric acid-reactive substances (TBARS) extracted with *n*-butanol was estimated by absorption at 530 nm. TBARS were expressed as malondialdehyde (MDA) amounts, using freshly produced MDA as standard prepared from 1,1,3,3-tetramethoxypropane with HCl (20).

Whole mounts of mammary glands

After feeding of a diet containing curcumin for 1 year, the inguinal mammary glands were dissected from the inner surface of the skin, retaining as much of the connective tissue as possible, and spread and dried slightly on filter paper. After fixing in 10% formalin buffered with 0.1 M phosphate buffer (pH 7.2) and defatting with ethyl ether, the preparations were stained with alum carmine, destained in ethanol and stored in cedar oil (21).

Histological examination of mammary tumors

All mammary tumors were fixed immediately in 10% formalin buffered with 0.1 M phosphate buffer (pH 7.2). Each paraffin section (4 μm in thickness) was prepared and stained with hematoxylin and eosin. The tumors were classified as adenocarcinoma or fibroadenoma according to the criteria for the classification of rat mammary tumors (22).

Assay of steroid receptors

The tissues obtained from all mammary tumors >2.0 cm in diameter were homogenized in 10 mM Tris–HCl buffer (pH 7.4) containing 1.5 mM EDTA and 1 mM dithiothreitol. Homogenates were centrifuged at 105 000 *g* for 60 min at 4°C and the obtained cytosol fraction was used for assay of the estrogen receptor (ER) and progesterone receptor (PgR). The receptors were analyzed by a dextran-coated charcoal method using [2,4,6,7-^{3}H]estradiol-17β and [17α-methyl-^{3}H]R5020, respectively, as radioligands (23,24). Maximum binding sites and dissociation constant (K_d) values for the receptors were determined by a Scatchard plot analysis (25).

Statistical analysis

Body weight, organ weight, tumor incidence, tumor multiplicity, latency period and biochemical parameters in serum were compared between the rats fed the control and curcumin diets. All statistical analyses were performed using StatView-J4.5 software (Abacus Concepts, Berkeley, CA). Tumor incidence, which is expressed as the percentage of rats with tumors, was analyzed statistically by χ^2 test. The cumulative proportions of rats with tumors (incidence curves) were calculated by the product-limit method where rats which died or were killed without mammary tumors were included and the difference between groups was tested for statistical significance by the Mantel–Cox test. Numbers of adenocarcinomas and fibroadenomas in the groups were analyzed by Fisher's exact probability test. Tumor multiplicity, expressed as mean number of tumors/rat, was analyzed by unpaired *t*-test. Differences in body weight, organ weight, latency period and biochemical parameters between the groups were analyzed statistically by Student's *t*-test. Differences were considered statistically significant at $P < 0.05$.

Results

Prevention by curcumin of the development of mammary tumors

For control experiments, of the 39 pregnant rats which were administered whole body irradiation with 2.6 Gy γ-rays at day 20 of pregnancy and then treated with DES after nursing, 33 (84.6%) rats developed mammary tumors during the experimental period of 1 year (Figure 3). The administration of dietary 1% curcumin together with DES implantation in the 25 experimental rats significantly decreased the incidence (28.0%) of total mammary tumors ($P < 0.0001$). The number of mammary tumors/tumor-bearing rat in the curcumin-fed group was half (NS, $P = 0.092$) that in the rats fed the control diet (1.9 ± 0.2). The Iball's index for overall development of mammary tumors in the curcumin-fed rats was also one-third of that in the control group (Table I). No significant difference in the latency period was observed between the control and curcumin-fed groups. The administration of dietary curcumin together with DES implantation in the irradiated rats significantly decreased the cumulative incidence curve ($P < 0.0001$) of mammary tumors for the 1 year period, compared with the control diet group (Figure 4). The appearance of the first palpable tumors was delayed by ~2.5 months in the curcumin-fed group compared with that in the control group.

Table I. Development of mammary tumors in rats fed control diet and curcumin diet

Diet	No. of rats used	No. of mammary tumors			Multiplicity[a,b]	Latency period[b,c]	Iball's index
		Fibroadenoma (%)	Adenocarcinoma (%)	Total			
Control	39	44 (69.8%)	19 (30.2%)	63	1.9 ± 0.2	9.3 ± 0.4	29.8
Curcumin	25	6 (85.7%)	1 (14.3%)	7	1.0 ± 0.0	9.7 ± 0.7	9.5

[a]Number of mammary tumors/tumor-bearing rat.
[b]Means ± SE.
[c]Months.

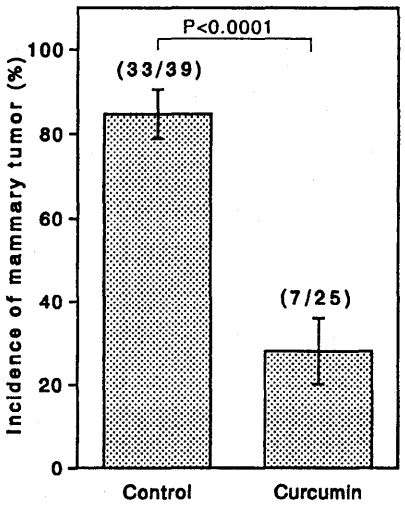

Fig. 3. Incidence of mammary tumors in γ-ray-irradiated rats. Bar, SD. The numbers in parentheses on the top of the bar represent the actual number of rats bearing tumors and rats used.

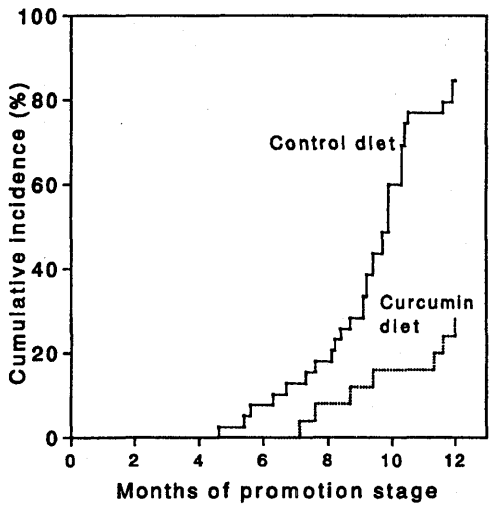

Fig. 4. Cumulative incidence of development of mammary tumors in irradiated rats treated with DES and curcumin. Statistical evaluation of the cumulative proportion data (incidence curves) by Mantel–Cox test yielded $P < 0.0001$, indicating a significant difference between the control diet and curcumin-containing diet groups. Solid and dotted lines represent control diet and curcumin diet groups, respectively.

Histological characterization of mammary tumors

All of the mammary tumors induced in the control group and curcumin-fed group were examined histologically. The proportion of adenocarcinomas and fibroadenomas in total tumors was 30.2 and 69.8%, respectively, in rats fed the control diet (Table I). By the administration of curcumin, the proportion (14.3%) of adenocarcinomas was decreased to half of that in the control group, conversely, one might say that the proportion (85.7%) of fibroadenomas was 1.2-fold higher than that in the control rats. However, no significant difference ($P = 0.664$) in the proportion of adenocarcinomas and fibroadenomas was observed between the two groups.

Table II. Biological effects of long-term administration of curcumin

	Control diet[a] ($n = 39$)	Curcumin diet[a] ($n = 25$)
Body weight (g)	245 ± 6	227 ± 5[b]
Liver (g)	10.6 ± 0.4	12.7 ± 0.4[c]
Adrenals (mg)	91.8 ± 2.6	84.4 ± 3.2
Uterus (mg)	579 ± 34	501 ± 27
Ovaries (mg)	70.5 ± 6.0	51.8 ± 3.2[b]
Pituitary gland		
Normal gland (mg)	13.0 ± 0.9 ($n = 17$)	13.1 ± 2.8 ($n = 22$)
Gland with tumor (mg)	32.4 ± 4.7 ($n = 22$)	47.7 ± 14.4 ($n = 3$)

[a]Mean ± SE.
[b]Significant difference between control and curcumin diet groups, $P < 0.05$.
[c]Significant difference between control and curcumin diet groups, $P < 0.01$.

Biological effects of long-term treatment with curcumin

Body weight and organ weight values at the end of the experiment are summarized in Table II. A significant reduction ($P < 0.05$) in body weight was observed in rats fed the diet containing 1% curcumin for 1 year in spite of similar calorie intake ($P = 0.570$) in both curcumin-fed (63.7 ± 1.1 kcal/rat/day) and control (62.6 ± 1.6 kcal/rat/day) groups. The weights of adrenals and uterus were decreased slightly by the administration of curcumin, but no significant difference was observed ($P = 0.075$ for adrenal and $P = 0.086$ for uterus). The treatment with curcumin increased liver weight significantly ($P < 0.01$), but ovarian weight was reduced markedly ($P < 0.05$). No change in weight of normal pituitary gland was observed between the control and curcumin-fed groups ($P = 0.525$). Interestingly, when the 39 control rats were autopsied, 22 (56.4%) were found to have developed pituitary tumors, while the pituitary tumor incidence (12.0%) in the curcumin-fed rats was one-fifth of that in the control rats ($P < 0.0005$).

Serum concentration of curcuminoids, hormones, lipids and TBARS

The serum concentrations of curcumin and its metabolites were measured 1 year after the administration of dietary curcumin together with DES implantation in the irradiated rats. Curcumin and tetrahydrocurcumin were estimated as 6.0 ± 2.0 and 112 ± 27 ng/ml serum, respectively (Table III). The serum estradiol-17β concentration in the rats fed the

Table III. Effect of curcumin on serum concentrations of hormones, lipids, TBARS and curcumin

Substances assayed (units)	Control diet[a] (n = 5)	Curcumin diet[a] (n = 5)
Estradiol-17β (pg/ml)	6.9 ± 0.2	3.6 ± 0.8
Progesterone (ng/ml)	118.7 ± 28.9	156.9 ± 35.2
Prolactin (ng/ml)	324 ± 116	65.8 ± 7.1[b]
LH (ng/ml)	0.30 ± 0.05	0.39 ± 0.18
FSH (ng/ml)	5.2 ± 1.1	6.3 ± 0.6
Cholesterol ester (mg/dl)	82.3 ± 20.6	110.0 ± 8.3
Free cholesterol (mg/dl)	23.0 ± 4.4	16.0 ± 2.4
Triglyceride (mg/dl)	105.6 ± 17.6	90.0 ± 3.0
TBARS (nmol MDA/ml)	10.8 ± 0.4	9.3 ± 0.5[b]
Curcumin (ng/ml)	ND[c]	6.0 ± 2.0
Tetrahydrocurcumin (ng/ml)	ND[c]	112.0 ± 27.0

[a]Mean ± SE.
[b]Significant difference between control and curcumin diet groups, $P < 0.05$.
[c]Not detected.

Table IV. Effect of curcumin on the fatty acid profile in serum

Fatty acid	Concentration[a] (μg/ml serum)	
	Control diet (n = 4)	Curcumin diet (n = 5)
Palmitic acid ($C_{16:0}$)	597 ± 47	609 ± 54
Stearic acid ($C_{18:0}$)	323 ± 27	411 ± 30
Oleic acid ($C_{18:1}$)	420 ± 53	396 ± 66
Linoleic acid ($C_{18:2}$)	585 ± 23	509 ± 32
Linolenic acid ($C_{18:3}$)	35 ± 2	36 ± 4
Arachidonic acid ($C_{20:4}$)	390 ± 47	541 ± 32[c]
Eicosapentaenoic acid ($C_{20:5}$)	97 ± 15	188 ± 11[b]
Docosahexanoic acid ($C_{22:6}$)	265 ± 19	254 ± 15
Total saturated fatty acids (S)	920 ± 60	1020 ± 64
Total unsaturated fatty acids (U)[d]	1792 ± 125	1924 ± 98
Total polyunsaturated fatty acids (PU)[e]	787 ± 66	1019 ± 33[c]
S/U	0.51	0.53
S/PU	1.17	1.00

[a]Mean ± SE.
[b]Significant difference between control and curcumin diet groups, $P < 0.01$.
[c]Significant difference between control and curcumin diet groups, $P < 0.05$.
[d]$C_{18:1}$, $C_{18:2}$, $C_{18:3}$, $C_{20:4}$, $C_{20:5}$, $C_{22:6}$.
[e]$C_{18:3}$, $C_{20:4}$, $C_{20:5}$, $C_{22:6}$.

curcumin diet was reduced to 52% of that obtained in rats fed the control diet, but no significant difference was observed between the two groups (P = 0.203). The progesterone concentration in the rats fed the curcumin diet was 1.3-fold higher than that in the control rats (P = 0.427). The serum prolactin concentration of the curcumin-fed rats was 80% less than that of control rats ($P < 0.05$). No changes in LH (P = 0.631) and FSH (P = 0.410) concentrations were observed in the curcumin-fed rats. Also, curcumin did not have any effect on the concentrations of free cholesterol (P = 0.249), cholesterol ester (P = 0.188) and triglyceride (P = 0.409). The serum concentration of TBARS was significantly decreased by long-term treatment with curcumin ($P < 0.05$).

Fatty acid profile in serum

The serum concentrations of fatty acids were measured 1 year after the start of the administration of dietary curcumin together with DES implantation in the irradiated rats (Table IV). With regard to unsaturated fatty acids, the serum concentrations of arachidonic acid ($P < 0.05$) and eicosapentaenoic acid ($P < 0.01$) in rats fed the curcumin diet were significantly higher than in rats in the control group. However, no significant change was observed in concentrations of the other fatty acids such as oleic acid (P = 0.797), linoleic acid (P = 0.114), linolenic acid (P = 0.894) and docosahexanoic acid (P = 0.658). The sum of the polyunsaturated fatty acids (≥ three unsaturated bonds) was increased significantly ($P < 0.05$) by treatment with curcumin and total unsaturated fatty acids (≥ one unsaturated bond) was not affected by curcumin (P = 0.427). With regard to saturated fatty acids, the serum stearic acid concentration in rats fed the curcumin diet was 1.3-fold higher than that in control rats, but no significant difference was observed between the two groups (P = 0.071). Fatty acid ratios of total saturated fatty acids to total unsaturated fatty acids (S/U) and of total saturated fatty acids to total polyunsaturated fatty acids (S/PU) were not significantly altered by long-term administration of curcumin.

Effect of curcumin on development of mammary glands

At the end of the experiment, whole mounts of inguinal mammary glands were prepared to examine the effects of curcumin on the development and differentiation of the glands by long-term treatment. In the irradiated rats fed the control diet, mammary glands showed many alveolar buds with branched lactiferous ducts due to the DES implantation (Figure 5a and b). The whole mounts (Figure 5c and d) showed that the mammary glands in rats fed curcumin diet exhibited less proliferation and differentiation than those of the glands of control rats, because both number and size of alveolar buds were small.

ER and PgR in mammary tumors

Table V shows the results of analysis of ER and PgR in the cytosol fraction obtained from homogenates of mammary tumors >2.0 cm in diameter. Many (74.2%) of the mammary tumors that developed in rats fed the control diet were ER(+)PgR(+) and only one tumor (3.2%) was ER(–)PgR(–). Conversely, rats fed the curcumin diet showed increased numbers (57.1%) of ER(–)PgR(–) tumors and decreased numbers (14.3%) of ER(+)PgR(+).

Discussion

In our previous study, it was found that whole body irradiation of pregnant rats results in a higher incidence of mammary tumors than that observed in irradiated virgin rats (26) and we suggested that the mammary cells in the differentiated glands of pregnant rats are particularly susceptible to radiation. Although numerous proliferated epithelial cells in the glands are removed rapidly by the involution process after weaning, the origin of the mammary tumors initiated by radiation during pregnancy appears to be the cells that are not removed during involution, which proliferate in the presence of DES as the tumor promoter. Reddy and Aggarwal (14) have reported that curcumin could inhibit the growth of tumor cells, whereas normal cells are found to be relatively resistant. We would suggest that one possible mechanism in the chemoprevention of mammary tumors by long-term treatment with curcumin is inhibition of the proliferation of preneoplastic cells or tumor origin cells initiated by radiation.

Data presented herein indicate that curcumin markedly reduces tumorigenesis in mammary glands in irradiated rats during DES-dependent promotion. Curcumin has been shown

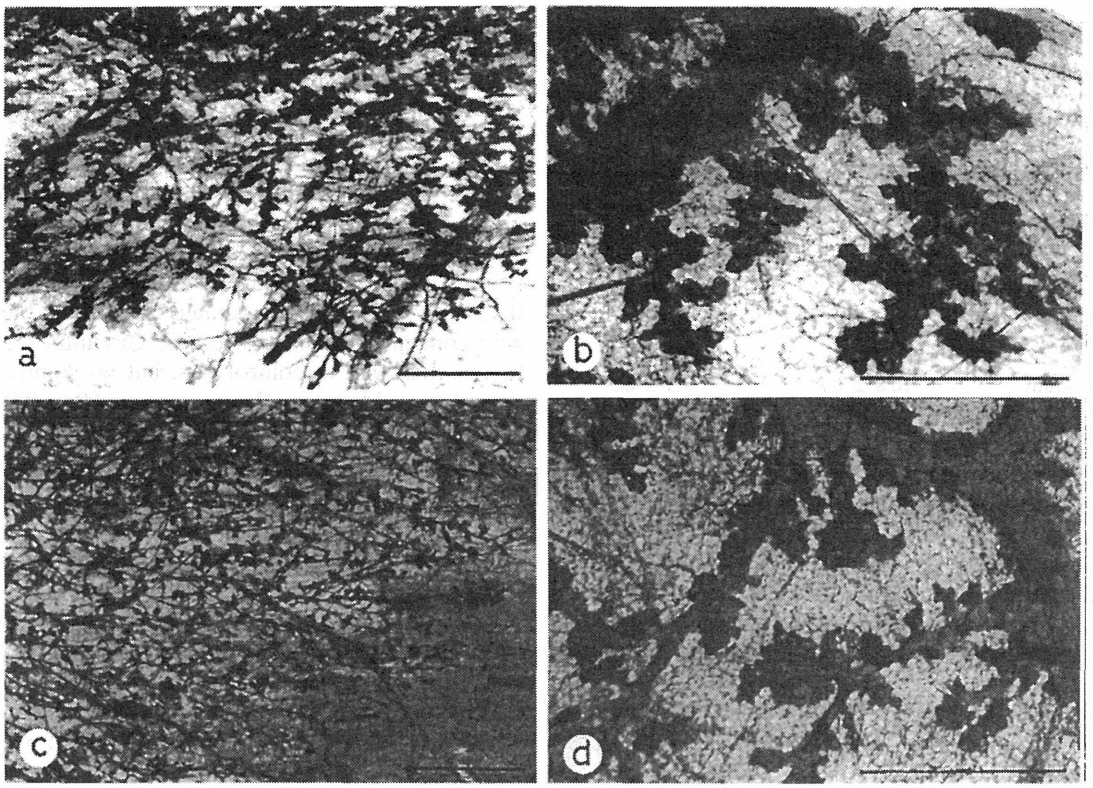

Fig. 5. Whole mount observation of inguinal mammary glands of rats. (**a** and **b**) Control rats fed basal diet (MB-1); (**c** and **d**) rats fed diet containing 1% curcumin. Scale bars: a and c, 3 mm; b and d, 1 mm.

Table V. ER and PgR in mammary tumors

Diet (no. of tumors tested)	Receptor			
	ER(+)PgR(+)	ER(+)PgR(–)	ER(–)PgR(+)	ER(–)PgR(–)
Control (n = 31)	23	2	5	1
Curcumin (n = 7)	1	1	1	4

to display antitumor properties in animals, as indicated by its ability to prevent tumorigenesis in skin (27), colon (28) and oral cavity (29) induced by chemical carcinogens. In the 7,12-dimethylbenz[*a*]anthracene-induced mammary tumor model in rats, when curcumin was administered by i.p. injection at 100 mg/kg body wt (30) or in a diet containing 1% curcumin (5) prior to dosing with the chemical carcinogen, the incidence of animals with tumors was not significantly altered. However, administration of a concentration twice as high as the above doses of curcumin slightly decreased tumor incidence to 85% of the control group. Therefore, our results are the first to show that curcumin markedly inhibits tumorigenesis in mammary glands. Also, incidence (12.0%) of pituitary tumors in curcumin-fed rats indicated less than half of that (28.0%) in the control group. However, it is inconclusive whether the reduced incidence was caused by an antipromotion effect of curcumin, because of a lack of data on experimental groups given DES without radiation and with or without curcumin in the present study. Further research is needed to establish the mechanism of prevention of pituitary tumors by curcumin.

Yokoro *et al.* (31) have reported that rat mammary tumorigenesis was mediated through estrogenic stimulation of prolactin release from the pituitary gland. In our current study, chemoprevention by curcumin of mammary tumor promotion by DES was associated with a significant decrease (20% of the control value) in serum concentration of prolactin in rats fed the curcumin diet. This result is consistent with other reports in which inhibition of mammary gland DNA synthesis by 2-bromo-α-ergocryptine-induced prolactin suppression resulted in a decrease in mammary tumorigenesis in rats (32). Also, in previous works, a decrease in prolactin concentration and chemoprevention of radiation-induced mammary tumors resulted from administration of either dietary dehydroepiandrosterone (33) or bezafibrate (34) in the presence of DES implantation.

Holder *et al.* (35) and Ravindranath and Chandrasekhara (36) have reported the absorption, metabolism and excretion of curcumin administered orally. Curcumin was metabolized to tetrahydrocurcumin during absorption through the intestine. Almost all the curcuminoids were conjugated to the glucuronide and/or sulfate forms in liver and excreted mainly in the feces after enterohepatic circulation of the metabolites. Using rats fed a diet containing 1% curcumin for 1 year in the present experiment, serum concentrations (free form plus conjugates) of curcumin and its metabolites were measured. Concentration of tetrahydrocurcumin was ~20-fold higher than that of

curcumin. Tetrahydrocurcumin exhibited a significant inhibitory effect on 12-*O*-tetradecanoylphorbol-13-acetate-induced superoxide anion radical generation (37) and a greater inhibitory effect on lipid peroxidation of erythrocyte membrane ghosts induced by *t*-butylhydroperoxide than curcumin (18,38). It was shown that feeding a diet containing 0.5% tetrahydrocurcumin resulted in a significant repression of 1,2-dimethylhydrazine-induced formation of aberrant crypt foci, which are regarded as a precursor lesion for colon cancer (39). Tetrahydrocurcumin may have the same important physiological and pharmacological properties as curcumin *in vivo* due to the β-diketone moiety as well as phenolic hydroxy groups.

An increase in peroxidase activity in the mammary glands is observed to accompany sexual maturity (40). Recently, it was reported by Roy *et al.* (41) that oxidation of DES by the peroxidase activity of cytochrome P-4501A1 produces some reactive intermediates, presumably the semiquinone and quinone of DES, and curcumin is a potent inhibitor of cytochrome P-4501A1 (42). Superoxide anion radicals are generated by redox cycling between DES and its quinone (43) and reduce iron, which in turn reduces hydrogen peroxide, the secondary product of one-electron auto-oxidation of superoxide anion radicals, to hydroxyl radicals (44,45). The unsaturated fatty acids present in the cell membrane are susceptible to hydroxyl radicals, which are much more reactive than superoxide anion radicals. Peroxidation of polyunsaturated fatty acids containing three or more double bonds by oxygen free radicals induces them to produce lipid hydroperoxides or TBARS, such as MDA. In this paper, the concentrations of arachidonic acid and eicosapentaenoic acid during ingestion of the curcumin diet were higher than those in rats fed the control diet and the amounts of TBARS derived from hydroperoxidized fatty acids induced by DES were also significantly reduced by curcumin. These findings suggest that curcumin inhibits peroxidation of polyunsaturated fatty acids in the presence of DES. Huang *et al.* (7,8) also showed that the antitumor promotion activity of curcumin is associated with suppression of arachidonic acid metabolism. Arachidonic acid metabolism is known to produce free radicals in living cells. Curcumin appears to be a potent scavenger of oxygen free radicals, such as superoxide anion radicals (37,46) and hydroxyl radicals (47,48). Its antioxidant activity is further shown by its capacity to inhibit lipid peroxidation. For instance, curcumin suppresses the lipid peroxide levels in serum and liver of rats irradiated with γ-rays (49) and of renal epithelial (LLC-PK_1) cells incubated with hydrogen peroxide (50). Lipid peroxides are toxic to cells because they decrease membrane fluidity and permeability and induce DNA damage and, ultimately, result in cell injury (51). Shalini and Srinivas (52) have shown that curcumin inhibits lipid peroxide-induced DNA damage. The role of free radicals in the tumor promotion stage has been reviewed (53,54). From the above findings, curcumin may scavenge the free radicals derived from DES metabolism and exhibit antipromotion activity. Our observations support the hypothesis that one aspect of the antitumor activity of curcumin during the promotion stage may be linked to reduction of free radicals.

Furthermore, our results demonstrate that the serum concentration of eicosapentaenoic acid in the rats fed the curcumin diet was ~2-fold higher than that in control rats. Eicosapentaenoic acid is an ω-3 polyunsaturated fatty acid. Growth of a human breast cancer cell line (MDA-MB-231) (55) and of a rat mammary adenocarcinoma (R3230AC) (56) is suppressed by ω-3 polyunsaturated fatty acids. Recently, it was reported that dietary ω-3 polyunsaturated fatty acids reduce the activities and levels of both HMG-CoA reductase (57) and cyclooxygenase-2 (58) in rat mammary glands. Inhibition of HMG-CoA reductase is known to suppress a post-translational processing of $p21^{ras}$ (59) and prevent tumorigenesis in mammary glands (60) and colon (61). Inhibition of $p21^{ras}$ processing may inhibit malignant transformation (62). Cyclooxygenase-2 is usually not expressed in various organs, but its expression in certain cell types can be rapidly induced by mitogens and hormones (63). Intake of the cyclooxygenase-2 inhibitor nabumetone during the time corresponding to the post-initiation phase has a chemopreventive effect on *N*-methyl-*N*-nitrosourea-induced mammary carcinogenesis in rats (64). In addition, reduced expression of cyclooxygenase-2 in the mammary glands of rats fed ω-3 polyunsaturated fatty acids was accompanied by a decreased level of $p21^{ras}$ protein (58). Therefore, it is likely that prevention of mammary carcinogenesis may occur in curcumin-fed rats having increased concentrations of serum ω-3 polyunsaturated fatty acids, such as eicosapentaenoic acid.

Also, dietary ω-3 polyunsaturated fatty acids reduced the activity of NOS in lipopolysaccharide (LPS)-stimulated macrophage cells (65). In rat mammary glands, certain isoforms of NOS localize to myoepithelial cells of the glandular epithelium and marked expression of i-NOS is observed after exposure to LPS, an inflammatory agent (66). Excessive NO produced in inflamed tissues could contribute to the process of carcinogenesis (67,68). Chan *et al.* have found that curcumin reduced NO production in LPS- and interferon-γ-stimulated peritoneal cells (69). This may result from one or more mechanisms: reduction of i-NOS gene expression (11) and/or scavenging of NO molecules (70). Thus, inhibition of NO synthesis by NOS inhibitors gives reduced growth of rat mammary adenocarcinoma (71).

Finally, Gross and Dreyfuss (72,73) have reported that the incidence of radiation-induced tumors in rats was significantly reduced by calorie restriction. In our present experiments, rats fed the curcumin diet had a significant reduction in body weight. However, food intake was not reduced by chronic curcumin treatment. Body weight in rats fed the curcumin diet was reduced to 93% of that observed in rats fed the control diet. The reduction is statistically significant, but would be relatively low for prevention of the development of radiation-induced mammary tumors. From the above-mentioned, it is likely that a reduction in body weight in rats fed the curcumin diet did not contribute to the prevention of development of mammary tumors.

In conclusion, the DES-dependent promotion of radiation-induced mammary tumorigenesis was markedly inhibited by administration of dietary curcumin. The mechanism of chemoprevention involves both endocrinological and pharmacological effects of curcumin during tumor development in the radiation-initiated cells. These results provide useful information for further development of compounds as chemopreventive agents for human clinical trials.

Acknowledgements

This work was partly supported by a project research grant for Experimental Studies on Radiation Health, Detriment and its Modifying Factors and also by a grant from the Special Program for Bioregulation of the National Institute of Radiological Sciences. We thank Dr J.Ueda for valuable discussions concerning antioxidant activity of curcumin and Mrs M.Takahashi for excellent assistance in the care of the animals.

References

1. Armstrong,B. and Doll,R (1975) Environmental factors and cancer incidence and mortality in different countries, with special reference to dietary practices. *Int. J. Cancer*, **15**, 617–631.
2. Phillips,R.L. (1975) Role of life-style and dietary habits in risk of cancer among seventh-day adventists. *Cancer Res.*, **35**, 3513–3522.
3. Freudenheim,J.L., Marshall,J.R., Vena,J.E., Laughlin,R., Brasure,J.R., Swanson,M.K., Nemoto,T. and Graham,S. (1996) Premenopausal breast cancer risk and intake of vegetable, fruits and related nutrients. *J. Natl Cancer Inst.*, **88**, 340–348.
4. Stoner,G.D. and Mukhtar,H. (1995) Polyphenols as cancer chemopreventive agents. *J. Cell. Biochem.*, **22**, 169–180.
5. Pereira,M.A., Grubbs,C.J., Barnes,L.H. *et al.* (1996) Effects of the phytochemicals, curcumin and quercetin, upon azoxymethane-induced colon cancer and 7,12-dimethylbenz[*a*]anthracene-induced mammary cancer in rats. *Carcinogenesis*, **17**, 1305–1311.
6. Huang,M.T., Smart,R.C., Wong,C.-Q. and Conney,A.H. (1988) Inhibitory effect of curcumin, chlorogenic acid, caffeic acid, and ferulic acid on tumor promotion in mouse skin by 12-*O*-tetradecanoyl phorbol-13-acetate. *Cancer Res.*, **48**, 5941–5946.
7. Huang,M.T., Lysz,T., Ferraro,T., Abidi,T.F., Laskin,J.D. and Conney,A.H. (1991) Inhibitory effect of curcumin on *in vitro* lipoxygenase and cyclooxygenase activities in mouse epidermis. *Cancer Res.*, **51**, 813–819.
8. Conney,A.H., Lysz,T., Ferraro,T., Abidi,T.F., Manchand,P.S., Laskin,J.D. and Huang,M.-T. (1991) Inhibitory effect of curcumin and some related dietary compounds on tumor promotion and arachidonic acid metabolism in mouse skin. *Adv. Enzyme Regul.*, **31**, 385–396.
9. Lin,J.-K. and Shih,C.-A. (1994) Inhibitory effect of curcumin on xanthine dehydrogenase/oxidase induced by phorbol-12-myristate-13-acetate in NIH3T3 cells. *Carcinogenesis*, **15**, 1717–1721.
10. Brouet,I. and Ohshima,H. (1995) Curcumin, an anti-tumor promoter and anti-inflammatory agent, inhibit induction of nitric oxide synthase in activated macrophages. *Biochem. Biophys. Res. Commun.*, **206**, 533–540.
11. Chan,M.M.-Y., Huang,H.-I., Fenton,M.R. and Fong,D. (1998) *In vivo* inhibition of nitric oxide synthase gene expression by curcumin, a cancer preventive natural product with anti-inflammatory properties. *Biochem. Pharmacol.*, **55**, 1955–1962.
12. Jensen,N.J. (1982) Lack of mutagenic effect of turmeric oleoresin and curcumin in the *Salmonella*/mammalian microsome test. *Mutat. Res.*, **105**, 393–396.
13. Bhavanishankar,T.N., Murthy,K.N. and Murthy,V.S. (1986) Toxicity studies on turmeric (*Curcuma longa* L.); long-term toxicity studies in albino rats and monkeys. *J. Food Sci. Technol.*, **23**, 287–290.
14. Reddy,S. and Aggarwal,B.B. (1994) Curcumin is a non-competitive and selective inhibitor of phosphorylase kinase. *FEBS Lett.*, **341**, 19–22.
15. Inano,H., Suzuki,K., Ishii-Ohba,H., Yamanouchi,H., Takahashi,M. and Wakabayashi,K. (1993) Promotive effects of diethylstilbestrol, its metabolite (*Z,Z*-dienestrol) and a stereoisomer of the metabolite (*E,E*-dienestrol) in tumorigenesis of rat mammary glands pregnancy-dependently initiated with radiation. *Carcinogenesis*, **14**, 2157–2163.
16. Iball,J. (1939) The relative potency of carcinogenic compounds. *Am. J. Cancer*, **35**, 188–190.
17. Lee,M.-J., Wang,Z.-Y., Li,H., Chen,L., Sun,Y., Gobbo,S., Balentine,D.A. and Yang,C.S. (1995) Analysis of plasma and urinary tea polyphenols in human subjects. *Cancer Epidemiol. Biomarker Prev.*, **4**, 393–399.
18. Sugiyama,Y., Kawakishi,S. and Osawa,T. (1996) Involvement of the β-diketone moiety in the antioxidative mechanism of tetrahydrocurcumin. *Biochem. Pharmacol.*, **52**, 519–525.
19. Santillo,M., Mondola,P., Milone,A., Gioielli,A, and Bifulco,M. (1996) Ascorbate administration to normal and cholesterol-fed rats inhibits *in vitro* TBARS formation in serum and liver homogenates. *Life Sci.*, **58**, 1101–1108.
20. Buege,J.A. and Aust,S.D. (1978) Microsomal lipid peroxidation. *Methods Enzymol.*, **52**, 302–310.
21. Inano,H., Yamanouchi,H., Suzuki,K., Onoda,M. and Wakabayashi,K. (1995) Estradiol-17β as an initiation modifier for radiation-induced mammary tumorigenesis of rats ovariectomized before puberty. *Carcinogenesis*, **16**, 1871–1877.
22. Russo,J., Gusterson,B.A., Rogers,A.E., Russo,I.H., Wellings,S.R. and van Zwieten,M.J. (1990) Comparative study of human and rat mammary tumorigenesis. *Lab. Invest.*, **62**, 244–278.
23. Johnson,R.B., Nakamura,R.M. and Libby,R.M. (1975) Simplified Scatchard plot assay for oestrogen receptor in human breast cancer. *Clin. Chem.*, **21**, 1725–1730.
24. Johnson,R.B. and Nakamura,R.M. (1978) Simplified Scatchard plot assay for progesterone receptor in breast cancer: comparison with single-point and multipoint assay. *Clin. Chem.*, **24**, 1170–1176.
25. Scatchard,G. (1949) The attractions of proteins for small molecules and ions. *Ann. NY Acad. Sci.*, **51**, 660–672.
26. Inano,H., Suzuki,K., Onoda,M. and Yamanouchi,H. (1996) Susceptibility of fetal, virgin, pregnant and lactating rats for the induction of mammary tumors by gamma rays. *Radiat. Res.*, **145**, 708–713.
27. Limtrakul,P., Lipigorngoson,S., Namwong,O., Apisariyakul,A. and Dunn,F.W. (1997) Inhibitory effect of dietary curcumin on skin carcinogenesis in mice. *Cancer Lett.*, **116**, 197–203.
28. Rao,C.V., Rivenson,A., Simi,B. and Reddy,B.S. (1995) Chemoprevention of colon carcinogenesis by dietary curcumin, a naturally occurring plant phenolic compound. *Cancer Res.*, **55**, 259–266.
29. Tanaka,T., Makita,H., Ohnishi,M., Hirose,H., Wang,A., Mori,H., Satoh,K., Hara,A. and Ogawa,H. (1994) Chemoprevention of 4-nitroquinoline 1-oxide-induced oral carcinogenesis by dietary curcumin and hesperidin: comparison with the protective effect of β-carotene. *Cancer Res.*, **54**, 4653–4659.
30. Singletary,K., MacDonald,C., Wallig,M. and Fisher,C. (1996) Inhibition of 7,12-dimethylbenz[*a*]anthracene (DMBA)-induced mammary tumorigenesis and DMBA–DNA adduct formation by curcumin. *Cancer Lett.*, **103**, 137–141.
31. Yokoro,K., Nakano,M., Ito,A., Nakago,K., Kodama,Y. and Hamada,K. (1977) Role of prolactin in rat mammary carcinogenesis: detection of carcinogenicity of low-dose carcinogens and of persisting dormant cancer cells. *J. Natl Cancer Inst.*, **58**, 1777–1783.
32. Welsch,C.W. and Nagasawa,H. (1977) Prolactin and murine mammary tumorigenesis: a review. *Cancer Res.*, **37**, 951–963.
33. Inano,H., Ishii-Ohba,H., Suzuki,K., Yamanouchi,H., Onoda,M. and Wakabayashi,K. (1995) Chemoprevention by dietary dehydroepiandrosterone against promotion/progression phase of radiation-induced mammary tumorigenesis in rats. *J. Steroid Biochem. Mol. Biol.*, **54**, 47–53.
34. Inano,H., Suzuki,K. and Wakabayashi,K. (1996) Chemoprevention of radiation-induced mammary tumors in rats by bezafibrate administered together with diethylstilbestrol as a promoter. *Carcinogenesis*, **17**, 2641–2646.
35. Holder,G.M., Plummer,J.L. and Ryan,A.J. (1978) The metabolism and excretion of curcumin (1,7-bis-(4-hydroxy-3-methoxyphenyl)-1,6-heptadiene-3,5-dione) in the rat. *Xenobiotica*, **8**, 761–768.
36. Ravindranath,V. and Chandrasekhara,M. (1980) Absorption and tissue distribution of curcumin in rats. *Toxicology*, **16**, 259–265.
37. Nakamura,Y., Ohta,Y., Murakami,A., Osawa,T. and Ohigashi,H. (1998) Inhibitory effects of curcumin and tetrahydrocurcuminoids on the tumor promoter-induced reactive oxygen species generation in leukocytes *in vitro* and *in vivo*. *Jpn. J. Cancer Res.*, **89**, 361–370.
38. Osawa,T., Sugiyama,Y., Inayoshi,M. and Kawakishi,S. (1995) Antioxidative activity of tetrahydrocurcuminoids. *Biosci. Biotechnol. Biochem.*, **59**, 1609–1612.
39. Kim,J.M., Araki,S., Kim,D.J. *et al.* (1998) Chemopreventive effects of carotenoids and curcumins on mouse colon carcinogenesis after 1,2-dimethylhydrazine initiation. *Carcinogenesis*, **19**, 81–85.
40. Chan,J.K.T. and Shyamala,G. (1983) An evaluation of peroxidase as a marker for estrogen action in normal mammary glands of mice. *Endocrinology*, **113**, 2202–2209.
41. Roy,D., Bernhardt,A., Strobel,H.W. and Liehr,J.G. (1992) Catalysis of the oxidation of steroid and stilbene estrogens to estrogen quinone metabolites by the β-naphthoflavone-inducible cytochrome P-4501A family. *Arch. Biochem. Biophys.*, **296**, 450–456.
42. Oetari,S., Sudibyo,M., Commandeur,J.N.M., Samhoedi,R. and Vermeulen, N.P.E. (1996) Effects of curcumin on cytochrome P-450 and glutathione S-transferase activities in rat liver. *Biochem. Pharmacol.*, **51**, 39–45.
43. Epe,B., Schiffmann,D. and Metzler,M. (1986) Possible role of oxygen radicals in cell transformation by diethylstilbestrol and related compounds. *Carcinogenesis*, **7**, 1329–1334.
44. Wyllie,S. and Liehr,J.G. (1997) Release of iron form ferritin storage by redox cycling of stilbene and steroid estrogen metabolites: a mechanism of induction of free radical damage by estrogen. *Arch. Biochem. Biophys.*, **346**, 180–186.
45. McCord,J.M. and Day,E.D.,Jr (1978) Superoxide-dependent production of hydroxyl radical catalyzed by iron–EDTA complex. *FEBS Lett.* **86**. 139–142.
46. Sreejayan,N. and Rao,M.N.A. (1996) Free radical scavenging activity of curcumin. *Arzneimittelforschung*, **46**, 169–171.
47. Reddy,A.C.P. and Lokesh,B.R. (1994) Studies on the inhibitory effects of curcumin and eugenol on the formation of reactive oxygen species and the oxidation of ferrous iron. *Mol. Cell. Biochem.*, **137**, 1–8.
48. Shih,C.-A. and Lin,J.-K. (1993) Inhibition of 8-hydroxydeoxyguanosine

formation by curcumin in mouse fibroblast cells. *Carcinogenesis*, **14**, 709–712.
49. Nishigaki,I., Kuttan,R., Oku,H., Ashoori,F., Abe,H. and Yagi,K. (1992) Suppressive effect of curcumin on lipid peroxidation induced in rats by carbon tetrachloride or ^{60}Co-irradiation. *J. Clin. Biochem. Nutr.*, **13**, 23–29.
50. Cohly,H.H.P., Taylor,A., Angel,M.F. and Salahudeen,A.K. (1998) Effect of turmeric, turmerin, and curcumin on H_2O_2-induced renal epithelial (LLC-PK_1) cell injury. *Free Radic. Biol. Med.*, **24**, 49–54.
51. Freeman,B.A. and Crapo,J.D. (1982) Biology of disease, free radicals and tissue injury. *Lab. Invest.*, **47**, 412–416.
52. Shalini,V.K. and Srinivas,L. (1987) Lipid peroxide induced DNA damage: protection by turmeric (*Curcuma longa*). *Mol. Cell. Biochem.*, **77**, 3–10.
53. Copeland,E.S. (1983) A National Institute of Health Workshop Report, free radical in promotion, a chemical pathology study section workshop. *Cancer Res.*, **43**, 5631–5637.
54. Cerutti,P.A. (1985) Prooxidant states and tumor promotion. *Science*, **227**, 375–381.
55. Rose,D.P. and Connolly,J.M. (1990) Effects of fatty acids and inhibitors of eicosanoid synthesis on the growth of a human breast cancer cell line in culture. *Cancer Res.*, **50**, 7139–7144.
56. Karmali,R.A., Marsh,J. and Fuchs,C. (1984) Effect of omega-3 fatty acids on growth of a rat mammary tumor. *J. Natl Cancer Inst.*, **73**, 457–461.
57. El-Sohemy,A. and Archer,M.C. (1997) Regulation of mevalonate synthesis in rat mammary glands by dietary n-3 and n-6 polyunsaturated fatty acids. *Cancer Res.*, **57**, 3685–3687.
58. Badawi,A.F., El-Sohemy,A., Stephen,L., Ghoshal,A.K. and Archer,M.C. (1998) The effect of dietary n-3 and n-6 polyunsaturated fatty acids on the expression of cyclooxygenase 1 and 2 and levels of $p21^{ras}$ in rat mammary glands. *Carcinogenesis*, **19**, 905–910.
59. Schulz,S. and Nyce,J.W. (1991) Inhibition of protein isoprenylation and $p21^{ras}$ membrane association by dehydroepiandrosterone in human colonic adenocarcinoma cells *in vitro*. *Cancer Res.*, **51**, 6563–6567.
60. Inano,H., Suzuki,K., Onoda,M. and Wakabayashi,K. (1997) Anti-carcinogenic activity of simvastatin during the promotion phase of radiation-induced mammary tumorigenesis of rats. *Carcinogenesis*, **18**, 1723–1727.
61. Narisawa,T., Fukaura,Y., Terada,K., Umezawa,A., Tanida,N., Yazawa,K. and Ishikawa,C. (1994) Prevention of 1,2-dimethylhydrazine-induced colon tumorigenesis by HMG-CoA reductase inhibitors, pravastatin and simvastatin, in ICR mice. *Carcinogenesis*, **15**, 2045–2048.
62. Kohl,N.E., Mosser,S.D., deSolms,S.J., Giuliani,E.A., Pompliano,D.L., Graham,S.L., Smith,R.L., Scolnick,E.M., Oliff,A. and Gibbs,J.B. (1993) Selective inhibition of *ras*-dependent transformation by a farnesyltransferase inhibitor. *Science*, **260**, 1934–1937.
63. DeWitt,D. and Smith,W.L. (1995) Yes, but do they still get headaches? *Cell*, **83**, 345–348.
64. Matsunaga,K., Yoshimi,N., Yamada,Y., Shimizu,M., Kawabata,K., Ozawa,Y., Hara,A. and Mori,H. (1998) Inhibitory effects of nabumetone, a cyclooxygenase-2 inhibitor, and esculetin, a lipoxygenasae inhibitor, on *N*-methyl-*N*-nitrosourea-induced mammary carcinogenesis in rats. *Jpn. J. Cancer Res.*, **89**, 496–501.
65. Ohata,T., Fukuda,K., Takahashi,M., Sugimura,T. and Wakabayashi,K. (1997) Suppression of nitric oxide production in lipopolysaccharide-stimulated macrophage cells by ω-3 polyunsaturated fatty acids. *Jpn. J. Cancer Res.*, **88**, 234–237.
66. Onoda,M. and Inano,H. (1998) Localization of nitric oxide synthases and nitric oxide production in the rat mammary gland. *J. Histochem. Cytochem.*, **46**, 1269–1278.
67. Ohshima,H. and Bartsch,H. (1994) Chronic infections and inflammatory processes as cancer risk factors: possible role of nitric oxide in carcinogenesis. *Mutat. Res.*, **305**, 253–264.
68. Wink,D.A., Vodovotz,Y., Laval,J., Laval,F., Dewhirst,M.W. and Mitchell,J.B. (1998) The multifaceted roles of nitric oxide in cancer. *Carcinogenesis*, **19**, 711–721.
69. Chan,M.M.-Y., Ho,C.-T., and Huang,H.-I. (1995) Effects of three dietary phytochemicals from tea, rosemary and turmeric on inflammation-induced nitrite production. *Cancer Lett.*, **96**, 23–29.
70. Sreejayan and Rao,M.N.A. (1996) Nitric oxide scavenging by curcuminoids. *J. Pharm. Pharmacol.*, **49**, 105–107.
71. Meyer,R.E., Shan,S., DeAngelo,J., Dodge,R.K., Bonaventura,J., Ong,E.T. and Dewhirst,M.W. (1995) Nitric oxide synthase inhibition irreversibly decreases perfusion in the R3230AC rat mammary adenocarcinoma. *Br. J. Cancer*, **71**, 1169–1174.
72. Gross,L. and Dreyfuss,Y. (1984) Reduction in the incidence of radiation-induced tumors in rats after restriction of food intake. *Proc. Natl Acad. Sci. USA*, **81**, 7596–7598.
73. Gross,L. and Dreyfuss,Y. (1990) Prevention of spontaneous and radiation-induced tumors in rats by reduction of food intake. *Proc. Natl Acad. Sci. USA*, **87**, 6795–6797.

Received October 20, 1998; revised December 29, 1998; accepted February 11, 1999

NITRIC OXIDE: Biology and Chemistry
Vol. 4, No. 5, pp. 505–515 (2000)
doi:10.1006/niox.2000.0305, available online at http://www.idealibrary.com on IDEAL®

Effect of Curcumin on the Production of Nitric Oxide by Cultured Rat Mammary Gland

Makoto Onoda[1] and Hiroshi Inano

First Research Group, National Institute of Radiological Sciences, 4-9-1 Anagawa, Inage-ku, Chiba-shi, Chiba 263-8555 Japan

Received April 19, 2000

We have hypothesized that one aspect of the antitumor activity of curcumin (diferuloylmethane) during the promotion stage of mammary gland tumorigenesis may be linked to reduction of free radicals (Inano *et al.*, Carcinogenesis, 20: 1011–1018, 1999). Nitric oxide (NO) has been found to inflict damage on important biomolecules, and the overproduction of NO in diseases may be implicated in carcinogenesis and tumor progression. We have reported that the presence of three isoforms of nitric oxide synthases (NOS) and NO generation in the mammary gland correlate with the mammary gland development and mammary carcinogenesis. We, therefore, investigated the inhibitory activity of curcumin for the production of NO in rat mammary glands by using an organ culture system to validate the effectiveness and usefulness of curcumin in the pathophysiology of the mammary gland. A diced mammary gland (approximately 3 mm cubes) from the inguinal part of a female Wistar-MS rat treated with estradiol and progesterone was cultured with 2 ml of 5% FCS/DMEM in the presence or absence of LPS (0.5 μg/ml) for 2–3 days. Curcumin (~100 μM) was added at the same time to the LPS-treated cultures. In some experiments, curcumin was added to the culture after the LPS had been washed out. The NO production was significantly increased (by almost 20-fold compared to the control) by the addition of LPS to the culture system. This enhancement of NO production by LPS was reduced to 76 and to 56% by addition of 30 and 100 μM curcumin, respectively, to the culture. When LPS was eliminated from the culture after prestimulation for 1 day, the production of NO by the mammary gland dropped off, although some NO was still detectable. Curcumin did not further inhibit the production of NO by the prestimulated mammary gland after the elimination of LPS from the culture. The inducible nitric oxide synthase (iNOS, 122 kDa) and endothelial nitric oxide synthase (eNOS, 152 kDa) isoforms were detected in the mammary gland extracts at the end of the organ culture. The quantity of iNOS was apparently increased in the gland treated with LPS, while the eNOS expression was clearly diminished. Curcumin (100 μM) obviously suppressed the iNOS expression in the mammary glands cultured with LPS, and a recovery in the eNOS expression was observed. On the other hand, curcumin exhibited scavenging activity for the NO released from *N*-ethyl-2-(1-ethyl-2-hydroxy-2-nitrosohydrazino)-ethanamine (NOC 12), a NO donor compound, in the coincubation mixture. These results indicate that curcumin has the ability to inhibit iNOS induction by LPS in the mammary gland and to scavenge NO radicals, which might explain, at least partly, its therapeutic properties in inflammation of the mammary gland. © 2000 Academic Press

Key Words: curcumin; nitric oxide; nitric oxide synthase; mammary gland.

[1] To whom correspondence should be addressed. Fax: +81-43-255-6819. E-mail: onoda@nirs.go.jp.

1089-8603/00 $35.00

Nitric oxide (NO)[2] is a reactive free radical that is synthesized from L-arginine by nitric oxide synthase (NOS), and a unique biological messenger molecule (1–4). Recent reports implicate the overproduction of NO in inflammation, and a role for NO in the carcinogenic process and tumor progression has been described (5–7). NOS has at least three distinct isoforms, including the neuronal (nNOS) same as brain (bNOS), inducible (iNOS), and endothelial (eNOS) types (8, 9), and these isoforms are expressed in breast cancer cell lines (10, 11) and are correlated with breast cancer metastasis (11, 12). In a previous report we showed that three isoforms of NOS are present in the rat mammary gland (13). By immunohistochemical study with specific antibodies against NOS isoforms, eNOS and iNOS were localized to the basal layer (composed of myoepithelial cells of alveoli and lactiferous ducts) of mammary epithelia and to the endothelium of blood vessels in the mammary glands. In contrast, the immunoreactive signal of bNOS was barely detected in the epithelial parts of alveoli and lactiferous ducts. In addition, the production of NO in the mammary gland was significantly increased by treatment with lipopolysaccharide (LPS) as a proinflammatory agent (13). It has then been suggested that the presence of these NOS isoforms and NO generation in the mammary gland correlate with mammary gland development and mammary carcinogenesis.

Curcumin, the yellow pigment and a major component of turmeric, has long been used as a spice and coloring agent in food, as well as a naturally occurring medicine. Recently, curcumin has shown to possess diversified chamical, biological, and pharmacological properties, such as antioxidant (14, 15) and anti-inflammatory (16, 17) activities. Furthermore, the anti-carcinogenic activity of curcumin has been reported in a variety of chemically induced tumors including digestive organ (18, 19) and skin (20) tumors, and in cell lines (21–23). We have reported a preventive activity of curcumin against the diethylstilbestrol-dependent promotion of radiation-induced mammary tumorigenesis in rats (24), and it has been proposed that reduction of free radicals by curcumin may participate partly in the antitumor activity of curcumin during the promotion stage of mammary gland tumorigenesis. In this context, we examined the effect of curcumin on the generation by the rat mammary gland and scavenging of NO in culture to elucidate the effectiveness and usefulness of curcumin in the pathophysiology of the mammary gland.

[2] Abbreviations used: NO, nitric oxide; NOS, nitric oxide synthase; nNOS, neuronal NOS; bNOS, brain NOS; iNOS, inducible NOS; eNOS, endothelial NOS; LPS, lipopolysaccharide; FCS, fetal calf serum; DMEM, Dulbecco's modified Eagle's medium; PBS, phosphate-buffered saline; NBT, nitroblue tetrazolium; BCIP, 5-bromo-4-chloro-3-indolyl phosphate; NOC 12, *N*-ethyl-2-(1-ethyl-2-hydroxy-2 nitrosohydrazino)ethanamine; DES, diethylstilbestrol; cAK, cyclic AMP-dependent protein kinase; BSA, bovine serum albumin; IKK, IκB kinase.

MATERIALS AND METHODS

Materials and animals. Curcumin (1, 7-bis[4-hydroxy-3-methoxyphenyl]-1, 6-heptadiene-3, 5-dione, purity ≥95%) was obtained from Cayman Chemical (Ann Arbor, MI). The other reagents and chemicals were purchased from Sigma Chemical Company (St. Louis, MO) unless described otherwise. All animals used in the present study were treated and handled according to the *Recommendations for the Handling of Laboratory Animals for Biomedical Research* complied by the Committee of the Safety and Handling Regulations for Laboratory Animal Experiments in our Institute.

Organ culture of rat mammary glands. The isolation and culture of rat mammary glands were essentially carried out as previously described (13). Female Wistar-MS (8-week-old) rats bred at Nippon SLC Co. (Hamamatsu, Japan) were primed by implantation with pellets of 17β-estradiol (0.5 mg/3-week-release type, Innovation Research of America, Toledo, OH) and progesterone (35 mg/3-week-release type, Innovation Research of America). After 3 weeks of priming, the rats were sacrificed by carbon dioxide asphyxiation and the inguinal mammary glands were excised asceptically for organ culture. The isolated mammary glands were diced into approximately 3-mm cubes, and each cube was cultured in the well of 24-multiwell plates containing 2 ml of 5% fetal calf serum (FCS)/Dulbecco's modified Eagle's medium (DMEM) supplemented with antibiotics

(100 U/ml penicillin, 100 μg/ml streptomycin) and antimycotic (0.25 μg/ml amphotericin B) in a mixture of 5% CO_2/95% air at 37°C for 2 days. The medium was then replaced with 5% FCS/DMEM in the presence or absence of bacterial lipopolysaccharide (0.5 μg/ml), and the culture was maintained for another 2 days. Curcumin (100-fold concentration) dissolved or suspended in absolute ethanol was added at the same time to the LPS-treated cultures. Curcumin was dissolvable in 5% FCS/DMEM even though a concentration (100 μM as a final concentration) as reported by others (25, 26) when a stock suspension (10 mM) of curcumin was added and agitated vigorously. In some experiments, curcumin was added to the culture after the LPS had been washed out following prestimulation for 1 day of the mammary glands. Ethanol (20 μl/2 ml of medium/well) as a vehicle of equal volume without curcumin was also added to the control culture. At the end of the culture, the conditioned media were collected for the determination of the nitrite concentration as described below, and the cultured mammary glands were further processed for the preparation of mammary gland homogenates as described below.

Determination of the nitrite concentration. The amount of NO produced and secreted by mammary glands into the culture medium was estimated by measuring the nitrite (NO_2^-) converted from NO, with a Griess reagent mixture. The nitrite concentrations in conditioned media were determined immediately after the termination of the culture by a modification of a previously described colorimetric method (27, 28). Briefly, the Griess reagent mixture was freshly prepared by mixing equal volumes of stock solution A (10% sulfanilamide, 40% phosphoric acid) and stock solution B (1% *N*-(1-naphthyl)ethylenediamine dihydrochloride) prior to the measurement of nitrite. One part of the reagent mixture was transferred into 7 parts of the conditioned media appropriately diluted with phosphate-buffered saline (PBS), and absorbance at either 545 or 570 nm was determined in a spectrophotometer. The nitrite concentration was then estimated from a standard curve which was simultaneously prepared for $NaNO_2$ (~10 nmol/ml) in PBS. The slope of the standard curve was essentially the same whether DMEM or PBS was used as a diluent.

Preparation of mammary gland homogenates and immunoblot analysis of nitric oxide synthase isoforms. The mammary glands cultured under various conditions were minced and homogenized in ice-chilled 5 mM Tris-HCl buffer (pH 7.5) containing 0.25 M sucrose, 5 mM EGTA, and inhibitors (1 M phenylmethylsulfonyl fluoride, 2 mM sodium vanadate, 10 μg/ml aprotinin, 5 μg/ml leupeptin) (13, 29). The homogenates were reconstituted in reducing sample buffer and loaded into the minigel system for SDS-PAGE. Subsequently, the separated proteins were electrotransferred to a nitrocellulose membrane. The membrane was then soaked in 5% nonfat milk in 20 mM Tris-HCl-buffered saline containing 500 mM sodium chloride (TBS, pH 7.5) for 2 h to block nonspecific immunoreactions, rinsed twice for 10 min in TBS containing 0.05% Tween 20 (TTBS), and reacted with either anti-iNOS antiserum (Affinity Bioreagents, Inc., Golden, CO), anti-eNOS antiserum (Affinity Bioreagents, Inc.) or normal rabbit serum (NRS, 1:1000–2000 dilution) in TTBS containing 1% gelatin (Bio-Rad Labs., Richmond, CA) overnight. The membrane was washed in TTBS twice for 10 min, reacted with alkaline phosphatase-conjugated goat anti-rabbit IgG (1:3000 dilution) in TTBS/gelatin for 1 h, and rinsed in TTBS twice and TBS once. The immunoreactivity was visualized by the following color development reactions. For the alkaline phosphatase reaction, 5% nitroblue tetrazolium (NBT) in 70% dimethylformamide and 5% 5-bromo-4-chloro-3-indolyl phosphate (BCIP) in dimethylformamide were freshly prepared. Both NBT and BCIP reagents were then mixed with 100 mM Tris-HCl (pH 9.5) containing 100 mM sodium chloride and 5 mM magnesium chloride (alkaline phosphatase reaction buffer, APB) to a final concentration of 0.033 and 0.017%, respectively. Prior to color development, the protein-bound nitrocellulose membrane was washed in APB for 10 min, and then the immunoreactive bands were visualized in APB containing NBT and BCIP. Color development was terminated by replacement of the reaction mixture with distilled water. The molecular weight of the

immunoreactive bands was estimated from plots of molecular weight vs relative mobility of rainbow marker standard proteins (Amersham, Arlington Heights, IL) which were run simultaneously with the sample proteins.

Nitric oxide scavenging by curcumin. To validate the nitric oxide-scavenging potency of curcumin, a nitric oxide-releasing substance, *N*-ethyl-2-(1-ethyl-2-hydroxy-2-nitrosohydrazino)ethanamine (NOC 12) (Dojindo Laboratories, Kumamoto, Japan), dissolved in 0.1 N NaOH at a 1000-fold concentration was added to PBS in the presence or absence of curcumin (30 or 100 μM). The half-life for NOC 12 in PBS at 37°C is 100 min, and this NO donor releases the full 2 equiv of NO in solution during its decomposition (Manufactory's brochure). The reaction mixture was transferred immediately into a water bath and incubated at 37°C for 2 h. At the end of the incubation, the reaction mixture was placed on ice and collected for measurement of the nitrite converted from NO as described above.

Statistic analysis. Data are expressed as the mean ± SE, and statistical comparisons between the control and other groups were performed using ANOVA with StatView-J4.5 software (Abacus Concepts Inc., Berkeley, CA) for Fisher's PLSD of multiple comparisons test. The level of significance was defined as $P < 0.05$.

RESULTS

Inhibition of NO production in LPS-stimulated rat mammary glands by curcumin. Rat mammary glands cultured with 5% FCS/DMEM spontaneously produced and secreted NO into the culture madia for the 2-day culture period, although the amount of NO was relatively minute and the nitrite converted from NO was barely detected by the Griess reagent assay system (Table I). The NO concentration in the conditioned media of rat mammary glands was significantly increased (by almost 15- to 20-fold compared to the control) by the addition of LPS (0.5 μg/ml) to the culture system (Table I). The secretion of NO from mammary glands cultured with LPS increased in a time-dependent manner up to a 48-h culture period. This enhancement was reduced in a dose-dependent manner to 82, 80, 76, and 56% by addition of 3, 10, 30, and 100 μM curcumin, respectively, to the culture (Fig. 1). In the other control cultures, prepared simultaneously without the addition of ethanol to confirm the nonspecific cellular toxicity of the vehicle, a similar profile of NO production was observed (data not shown). This, therefore, suggests that ethanol possesses no cellular toxicity at the concentration (1%) used in the culture. Curcumin also at the range of concentrations used in the experiments did not affect the determination of the nitrite concentration with the Griess reagent mixture (data not shown).

TABLE I

Nitric Oxide Production by the LPS-Stimulated Rat Mammary Glands in Culture[a]

Treatment	Nirtite produced (nmol/ml)[b]	
	24 h	48 h
Control	0.38 ± 0.10	0.73 ± 0.06
With LPS (0.5 μg/ml)	5.66 ± 0.30[c]	13.57 ± 0.73[c]

[a] One piece of the mammary gland (approximately 3-mm cubes) was cultured, and the conditioned media were collected for the determination of nitrite (NO_2^-) concentration at the culture period indicated. NO produced and secreted by mammary glands into culture medium was estimated by measuring nitrite converted from NO with Giess reagent as described under Materials and Methods.

[b] Values represent the mean ± SE obtained from three independent experiments. Each experiment contained four cultures per replicate.

[c] Significant difference from control, $P < 0.001$.

In the culture in which LPS was added for 1 day and washed out, the level of NO production over the following 2 days was significantly lower than that in the culture treated with LPS continuously, although still enough NO was produced to be detected by Griess assay in the prestimulated mammary glands (Groups 1 and 2 in Table II). This indicates that continuous stimulation by LPS is necessary for the excess generation of NO in the mammary gland. A similar tendency was observed in the cultures treated by the combination of LPS prestimulation and curcumin (30 and 100 μM) administration, although the absolute amount of NO produced was less in these cultures (Groups 3 to 6 in Table II). Curcumin exhibited again the inhibitory activity of

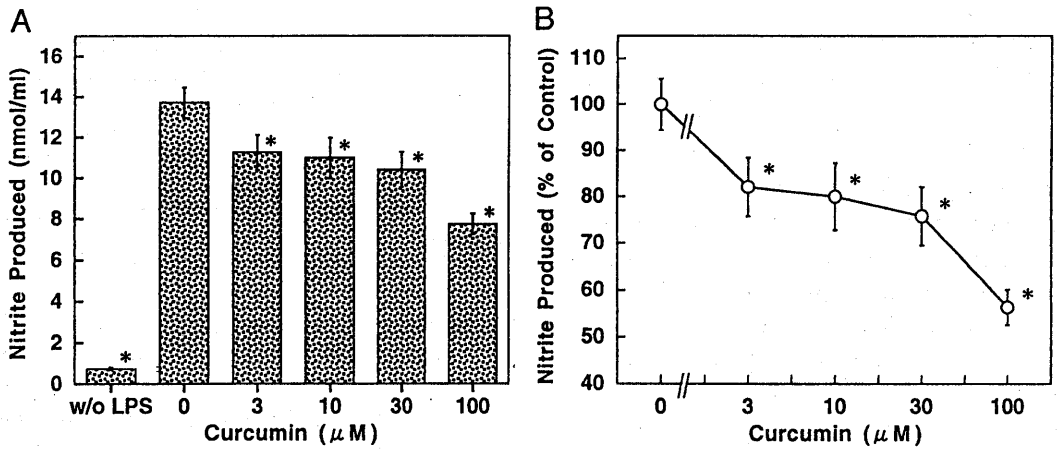

FIG. 1. Inhibition of NO production in LPS-stimulated rat mammary glands by curcumin. A piece of the mammary gland was cultured in the presence or absence of LPS (0.5 μg/ml) for 2 days, after which the conditioned medium was collected for the determination of the nitrite (NO_2^-) concentration. The curcumin concentration was maintained throughout the culture period. The actual concentration of the nitrite and relative concentration to the LPS-stimulated control culture are indicated in A and B, respectively. Each value and vertical bar represents the mean ± SE, respectively, obtained from four independent experiments. Each experiment contained four cultures per replicate. *Significant difference from LPS alone control, $P < 0.001$.

NO production by the mammary gland in a dose-dependent manner in both LPS-contained and LPS-depleted cultures (Table II).

Suppression of NOS expression in the mammary gland by curcumin. The iNOS (122 kDa) and eNOS (152 kDa) isoforms that immunoreacted with anti-iNOS and anti-eNOS antisera, respectively, were detected in the mammary gland extracts obtained from the organ culture (Fig. 2 and Fig. 3). In both cases, a few other immunoreactive bands were detected. These molecular species may be immunoreactive degradation products of iNOS and eNOS, pro-

TABLE II

NO Production by the LPS-Prestimulated Rat Mammary Gland and Effect of Curcumin on NO Production[a]

Group	Pretreatment	Treatment	Nitrite produced (nmol/ml)[b] 24 h	48 h
1	With LPS (0.5 μg/ml)	With LPS (0.5 μg/ml)	7.63 ± 1.00	13.41 ± 1.60
2	With LPS (0.5 μg/ml)	Without LPS	4.33 ± 0.56[c]	5.61 ± 0.64[d]
3	With LPS (0.5 μg/ml), curcumin (30 μM)	With LPS (0.5 μg/ml), curcumin (30 μM)	5.94 ± 0.84	10.75 ± 1.32
4	With LPS (0.5 μg/ml), curcumin (30 μM)	Without LPS, with curcumin (30 μM)	2.58 ± 0.42[c]	3.48 ± 0.54[d]
5	With LPS (0.5 μg/ml), curcumin (100 μM)	With LPS (0.5 μg/ml), with curcumin (100 μM)	3.20 ± 0.23	6.21 ± 0.27
6	With LPS (0.5 μg/ml), curcumin (100 μM)	Without LPS, with curcumin (100 μM)	2.08 ± 0.20[c]	2.70 ± 0.56[d]

[a] One piece of the mammary gland (approximately 3-mm cubes) was precultured with LPS (0.5 μg/ml) and curcumin (30 or 100 μM) for 1 day, and then the culture was continued with the fresh medium indicated for another 2 days. Nitrite (NO_2^-) concentration at the culture period indicated was determined as described under Materials and Methods.

[b] Values represent the mean ± SE obtained from three independent experiments. Each experiment contained three cultures per replicate.

[c] Significant difference from LPS-treated culture for a pair of treatments, $P < 0.01$.

[d] Significant difference from LPS-treated culture for a pair of treatments, $P < 0.001$.

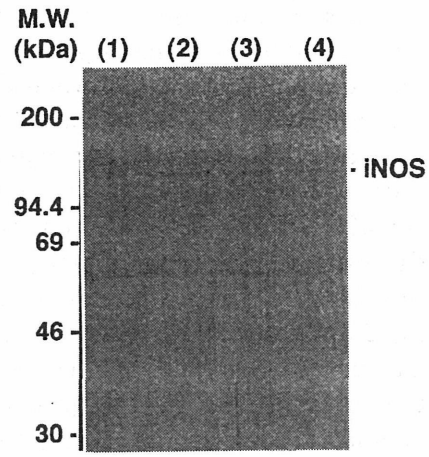

FIG. 2. Immunoblot analysis of iNOS in extracts obtained from cultured rat mammary glands. The homogenates (25 μg/lane) were loaded onto the SDS-PAGE system and the immunoreactive substances were visualized by Western blot analysis with an alkaline phosphatase-conjugated secondary antibody as described under Materials and Methods. Lane 1, nonstimulated control; Lane 2, control + LPS (0.5 μg/ml); Lane 3, control + LPS + curcumin (30 μM); Lane 4, control + LPS + curcumin (100 μM).

duced during the preparation of mammary gland extracts owing to the presence of certain proteases (13, 30). The quantity of immunoreactive iNOS was markedly increased in the gland treated with LPS (Lane 2 in Fig. 2), while the eNOS expression was apparently diminished in the corresponding tissue extract (Lane 2 in Fig. 3). This downregulation of constitutive eNOS expression by iNOS was consistent with a previous report (13). Curcumin (100 μM) clearly suppressed the expression of iNOS in the mammary glands cultured with LPS (Lane 4 in Fig. 2), whereas the reduced expression of eNOS was recovered in the mammary glands treated with LPS and curcumin (Lane 4 in Fig. 3). This decrease in iNOS expression following curcumin treatment was well reflected in the decline in NO concentration in the conditioned medium (Fig. 1). By the way, this recovery of the reduced expression of constitutive eNOS indicates that the function of protein synthesis still remains intact in the mammary glands treated with LPS and curcumin, and that curcumin at the concentrations used is not detrimental to the mammary glands in this culture system. Hence, the reduction of iNOS expression did not result from the cellular toxicity of curcumin used.

Scavenging of NO released from NOC 12 by curcumin. Incubation of NOC 12 resulted in a linear dose-dependent NO release (Fig. 4). The released NO from NOC 12 into the buffer were 53 ± 4, 38 ± 1, 24 ± 1, and 10 ± 1 nmol/ml at 40, 30, 20, and 10 μM of NOC 12, respectively, in a 2-h incubation period at 37°C. These values were suitable for the theoretical values based on the half-life (100 min) of NOC 12. The presence of curcumin (30 and 100 μM) significantly reduced the NO concentration in the mixture. NO scavenging by curcumin was greater in the mixture incubated with lower concentrations of NOC 12. For instance, the NO concentration was significantly reduced by curcumin at 100 μM to 40 and 65% of that of the control mixture containing 10 and 40 μM NOC 12, respectively, indicating a direct NO-scavenging property of curcumin. A similar tendency was seen with 30 μM curcumin, although the reduction ratio was less than that with 100 μM curcumin.

Scavenging of NO secreted from the mammary gland into the culture medium by curcumin. The scavenging of NO by curcumin was examined in the rat mammary gland culture system in order to establish to what extent the scavenging ability of curcumin contributes to the regulation of the extracel-

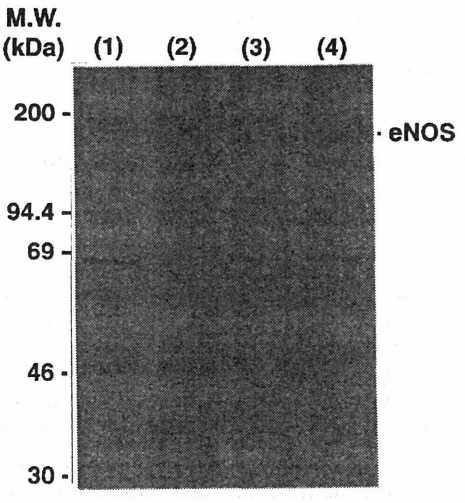

FIG. 3. Immunoblot analysis of eNOS in extracts obtained from cultured rat mammary glands. The homogenates (25 μg/lane) were processed as described in the legend of Fig. 2 and under Materials and Methods. Lane 1, nonstimulated control; Lane 2, control + LPS (0.5 μg/ml); Lane 3, control + LPS + curcumin (30 μM); Lane 4, control + LPS + curcumin (100 μM).

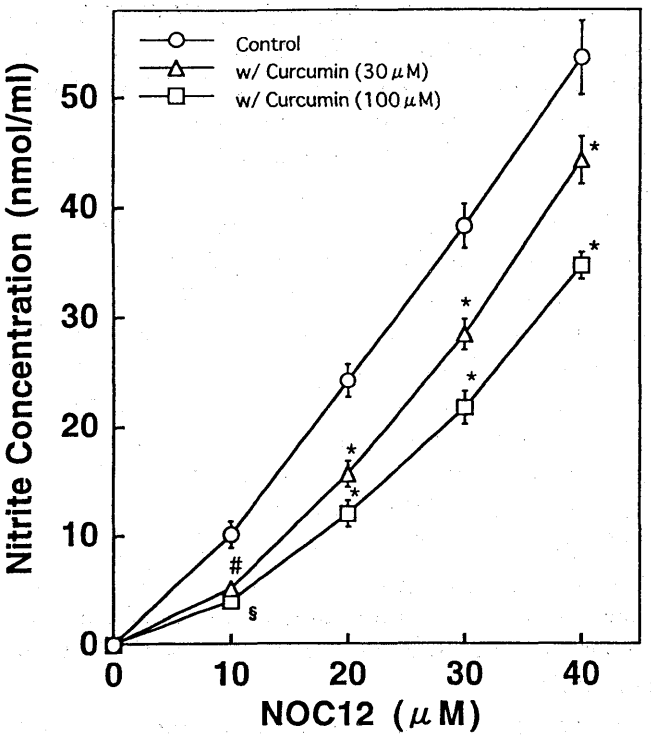

FIG. 4. Release from NOC 12 and scavenging by curcumin of NO. NOC 12 in PBS was mixed with curcumin (30 or 100 μM) dissolved in alcohol and incubated at 37°C for 2 h. The nitrite concentration was determined immediately after the incubation with Griess reagent mixture as described under Materials and Methods. Values represent the mean ± SE obtained from three independent experiments. Each experiment contained two tubes per replicate. *Significant difference from control (NOC 12 alone), $P < 0.001$. §Significant difference from control (NOC 12 alone), $P < 0.01$. #Significant difference from control (NOC 12 alone), $P < 0.05$.

lular NO secreted into the culture medium. Curcumin was added to the mammary gland culture after a prestimulation for 1 day and then the elimination by washing out of LPS. In this culture, *de novo* induction of iNOS in the mammary glands did not occur without LPS stimulation. The production and secretion of NO during the next 2 days declined significantly, although NO was still generated from the iNOS remaining in the prestimulated mammary gland (Group 2 in Table III). However, curcumin (30 and 100 μM), unexpectedly, did not reduce the NO concentration any further in the prestimulated mammary gland cultures (Groups 3 and 4 in Table III). NO concentrations were slightly increased with curcumin treatment in the prestimulated mammary gland cultures, although its minute enhancement was not significant from the culture without curcumin (Groups 3 and 4 in Table III). This indicates that curcumin did not affect the generation of NO by iNOS induced by the prestimulation with LPS, nor did it scavenge NO under these culture conditions.

DISCUSSION

We showed in a previous work that the diethylstilbestrol (DES)-dependent promotion of radiation-induced mammary tumorigenesis was markedly inhibited by administration of dietary curcumin, and hypothesized that the antitumor activity of cur-

TABLE III

Effect of Curcumin on NO Production and Scavenging in the LPS-Prestimulated Rat Mammary Gland Culture[a]

Group	Pretreatment	Treatment	Nitrite produced (nmol/ml)[b] 24 h	48 h
1	With LPS (0.5 μg/ml)	With LPS (0.5 μg/ml)	7.63 ± 1.00	13.41 ± 1.60
2	With LPS (0.5 μg/ml)	Without LPS	4.33 ± 0.56[c]	5.61 ± 0.64[d]
3	With LPS (0.5 μg/ml)	Without LPS, with curcumin (30 μM)	4.62 ± 1.82[c,e]	6.81 ± 2.28[d,e]
4	With LPS (0.5 μg/ml)	Without LPS, with curcumin (100 μM)	5.14 ± 1.35[c,e]	8.03 ± 2.01[d,e]

[a] One piece of the mammary gland (approximately 3-mm cubes) was precultured with LPS (0.5 μg/ml) for 1 day, and then the culture was continued with the fresh medium indicated for another 2 days. Nitrite (NO_2^-) concentration at the culture period indicated was determined as described under Materials and Methods.

[b] Values represent the mean ± SE obtained from three independent experiments. Each experiment contained three cultures per replicate.

[c] Significant difference from LPS-treated culture (Group 1), $P < 0.01$.

[d] Significant difference from LPS-treated culture (Group 1), $P < 0.001$.

[e] Not significantly different from the culture without LPS and curcumin (Group 2).

cumin during the promotion stage may be implicated in the reduction of free radicals (24). Furthermore, in our previous report three isoforms of NOS, NO-radical-generating enzymes, were localized to the parenchymal cells (the glandular epithelium) of the rat mammary gland, such as epithelial cells and myoepithelial cells, and it was proposed that these NOS isoforms may correlate with mammary gland development and regulatory functions (13). In this context, in the current study we have examined the effect of curcumin on NO generation by treatment with LPS, a proinflammatory agent, in the rat mammary gland in culture to validate the effectiveness and usefulness of curcumin in the pathophysiology of mammary gland originated in the overproduction of free radicals.

The inhibitory activity of curcumin on inflammation-induced nitrite production in macrophages has been shown by Brouet and Ohshima (31) and Chan *et al.* (32), and relatively low concentrations of curcumin ($IC_{50} < 10$ μM) inhibit NO production by cultured macrophages. Activated macrophages in the presence of curcumin (10 μM) contained significantly reduced amounts of a 130-kDa iNOS protein and iNOS mRNA compared with those cultured in the absence of curcumin (31). In our present study, NO production by the LPS-stimulated rat mammary gland was significantly decreased in the presence of curcumin in the culture system, and a decrease in the amount of a 122-kDa iNOS was also observed in the LPS-stimulated mammary gland cultured with curcumin. A considerably higher concentration of curcumin (100 μM), however, was required to obtain a certain degree of inhibition of the NO production (56% of control) and iNOS expression (Fig. 1 and Fig. 2). A difference in responsiveness to curcumin between a single pure population of macrophages and the mixed population of the mammary gland cells may explain why a higher concentration of curcumin is needed to obtain a certain degree of inhibitory activity for the NO generation by the cultured rat mammary gland. Since, the cultured mammary tissue contains a variety of cells, such as epithelial, myoepithelial, stromal, and adipose cells, the transportation of curcumin to the target cells (probably myoepithelial cells of alveoli and lactiferous ducts of mammary epithelia and the endothelial cells of blood vessels in the gland) might be hindered in these jammed cell populations, and the curcumin consumption by these populations may be greater than that by a single cell population.

On the other hand, curcumin at 30 μM reduced by approximately 50% the amount of NO generated from NOC 12 (10 μM) for 2 h at 37°C in the PBS mixture (Fig. 4). Sreejayan and Rao (33) reported a similar result whereby curcumin reduced the amount of nitrite formed (less than 10 μM in their experimental conditions) by the reaction between oxygen and NO generated from sodium nitroprusside (5 mM) and that curcumin at 20 μM scavenged approximately 50% of the NO generated. This indicates that curcumin is a potent NO scavenger. However, curcumin did not effect the NO generation by iNOS induced by the LPS prestimulation, and curcumin, unexpectedly, did not further reduce the NO concentration by scavenging in the medium obtained from the culture of LPS-prestimulated mammary gland (Table III). On the contrary, curiously, slight increases of NO concentrations were observed in the prestimulated mammary gland cultures, although those minute enhancements were not significant from the culture without curcumin (Table III). This loss of inhibitory activity of curcumin on the NO scavenging and the NO production by the cultured rat mammary gland in the current study may be attributed to the decomposition of curcumin at neutral pH (34) and the presence of serum albumin in the culture medium (34, 35). When curcumin is incubated in 0.1 M phosphate buffer and serum-free medium, at pH 7.2 and 37°C, about 90% of it decomposes within 30 min. This decomposition of curcumin is pH dependent and occurs faster at neutral-basic conditions. Curcumin is more stable in cell culture medium containing 10% FCS; less than 20% of it decomposed within 1 h, and after incubation for 8 h, about 50% of curcumin remained (34). Curcumin inhibits the catalytic subunit of cyclic AMP-dependent protein kinase (cAK) in a fashion that is competitive with respect to both ATP and synthetic peptide substrate. In the presence of bovine serum albumin (BSA, 0.8 mg/ml), the inhibition of cAK by curcumin is largely overcome; therefore, it is likely that BSA either binds curcumin or occludes a curcumin-binding region on cAK (35). Hence, the

culture conditions, such as pH regulation and the presence of a certain binding protein, may affect the intrinsic properties of curcumin. Furthermore, curcumin scavenges other free radicals including hydroxy radicals and superoxide radicals (15). Therefore, curcumin degradation kinetics might progress faster through the reaction with radicals in the culture medium. Taken together, the NO-scavenging activity of curcumin might be secluded by ingredient(s) in the culture medium and/or decline by the decomposition under neutral pH conditions of culture.

Interestingly, the NO generation by iNOS was not disturbed by the presence of curcumin after the prestimulation with LPS (Table III). It is, therefore, likely that curcumin does not affect the posttranslational processes of iNOS. Recently, it has been reported that the pleiotropic effects of curcumin are at least partly due to inhibition of the transcription factors NF-κB and AP-1 (25, 26, 36, 37). NF-κB and AP-1 activations are important steps for cell proliferation and both activities are required for proinflammatory gene expression including expression of immediate-early or early genes. Curcumin inhibits IκBα degradation and the nuclear import of NF-κB in bovine endothelial cells, and the inhibition of AP-1 by curcumin is due to a direct interaction of curcumin with AP-1 binding to its DNA-binding motif. Thus, curcumin inhibits NF-κB and AP-1 and reduces the expression of certain endothelial genes controlled by both transcription factors (37). The inhibition of apoptosis by curcumin in rat thymocytes induced by dexamethasone treatment is accompanied by a partial suppression of AP-1 activity, and a complete suppression of AP-1 activity is observed in proliferating thymocytes treated with concanavalin A (36). Moreover, Jobin *et al.* (26) reported that curcumin blocks gene expression by inhibiting the signal leading to IκB kinase (IKK) activation, subsequent IκBα phosphorylation/degradation, NF-κB activation, and DNA binding of NF-κB in the intestinal epithelial cells, and concluded that curcumin potently inhibits cytokine-mediated NF-κB activation by blocking a signal leading to IKK activity. Therefore, it is plausible that similar inhibitory mechanisms of curcumin for these transcription factors occur in the mammary gland. Since curcumin acts at a level upstream of or parallel to NF-κB inducing kinase and IKK, once the iNOS gene expression through a transactivation of NF-κB is triggered by LPS during the prestimulation period, the NO generation by iNOS induced is not inhibited any further by curcumin in the mammary gland culture in which the stimulus had washed out. This is a possible explanation for why curcumin did not further inhibit the production of NO by the prestimulated mammary gland after the elimination of LPS from the culture (Table III).

Furthermore, since direct interaction between curcumin and LPS is very likely in the culture medium, LPS-active sites and/or binding sites might be occluded. This could not be ruled out as a possible mechanism for the inhibitory activity of curcumin on the NO generation by LPS-induced iNOS in the mammary gland, although many other mechanisms, such as arachidonic acid metabolism modification (38) and kinase modification (35, 39), may apply to the inhibitory activity of curcumin on the NO generation in the mammary gland. In any event, although its precise mode of action remains elusive, the results of the current study indicate that curcumin has inhibitory activity for iNOS induction by LPS in the mammary gland and scavenging activity for NO radicals, and suggest that the therapeutic properties of curcumin in inflammation, cancer, and other pathological conditions of mammary glands might be explained, at least partly, by its ability to inhibit iNOS expression and to scavenge NO. Finally, the use of natural anti-inflammatory products provides an attractive and safe alternative for modulating inflammatory disorders.

ACKNOWLEDGMENT

This study was supported by a grant for Research Programme on Bioregulatory Mechanisms of the National Institute of Radiological Sciences.

REFERENCES

1. Moncada, S., Palmer, R. M. J., and Higgs, E. A. (1991). Nitric oxide: Physiology, pathophysiology, and pharmacology. *Pharmacol. Rev.* **43,** 109–142.
2. Bredt, D. S., and Snyder, S. H. (1994). Nitric oxide: A physiologic messenger molecule. *Annu. Rev. Biochem.* **63,** 175–195.

3. Kröncke, K.-D., Fehsel, K., and Kolb-Bachofen, V. (1995). Inducible nitric oxide synthase and its product nitric oxide, a small molecule with complex biological activities. *Biol. Chem. Hoppe-Seyler* **376,** 327–343.
4. Wolf, G. (1997). Nitric oxide and nitric oxide synthase: Biology, pathology, localization. *Histol. Histopathol.* **12,** 251–261.
5. Esumi, H., Ogura, T., Kurashima, Y., Adachi, H., Hokari, A., and Weisz, A. (1995). Implication of nitric oxide synthase in carcinogenesis: Analysis of the human inducible nitric oxide synthase gene. *Pharmacogenetics* **5,** S166–S170.
6. Doi, K., Akaike, T., Horie, H., Noguchi, Y., Fujii, S., Beppu, T., Ogawa, M., and Maeda, H. (1996). Excessive production of nitric oxide in rat solid tumor and its implication in rapid tumor growth. *Cancer* **77,** 1598–1604.
7. Tamir, S., and Tannenbaum, S. R. (1996). The role of nitric oxide (NO ·) in the carcinogenic process. *Biochim. Biophys. Acta* **1288,** F31–F36.
8. Mayer, B. (1995). Biochemistry and molecular pharmacology of nitric oxide synthases. *In* Nitric Oxide in the Nervous System (Vincent, S. R., Ed.), pp. 21–42, Academic Press, London.
9. Wang, Y., and Marsden, P. A. (1995). Nitric oxide synthases: Gene structure and regulation. *Adv. Pharmacol.* **34,** 71–90.
10. Zeillinger, R., Tantscher, E., Schneeberger, C., Tschugguel, W., Eder, S., Sliutz, G., and Huber, J. C. (1996). Simultaneous expression of nitric oxide synthase and estrogen receptor in human breast cancer cell lines. *Breast Cancer Res. Treat.* **40,** 205–207.
11. Orucevie, A., Bechberger, J., Green, A. M., Shapiro, R. A., Billiar, T. R., and Lala, P. K. (1999). Nitric-oxide production by murine mammary adenocarcinoma cells promotes tumor-cell invasiveness. *Int. J. Cancer* **81,** 889–896.
12. Dueñas-Gonzalez, A., Isales, C. M., del Mar Abad-Hernandez, M., Gonzalez-Sarmiento, R., Sangueza, O., and Rodriguez-Commes, J. (1997). Expression of inducible nitric oxide synthase in breast cancer correlates with metastatic disease. *Modern Pathol.* **10,** 645–649.
13. Onoda, M., and Inano, H. (1998). Localization of nitric oxide synthases and nitric oxide production in the rat mammary gland. *J. Histochem. Cytochem.* **46,** 1269–1278.
14. Ruby, A. J., Kuttan, G., Babu, K. D., Rajasekharan, K. N., and Kuttan, R. (1995). Anti-tumor and anti-oxidant activity of natural curcuminoids. *Cancer Lett.* **94,** 79–83.
15. Sreejayan, N., and Rao, M. N. A. (1996). Free radical scavenging activity of curcuminoids. *Arzneim.-Forsch./Drug Res.* **46,** 169–171.
16. Satoskar, R. R., Shah, S. J., and Shenoy, S. G. (1986). Evaluation of antiinflammatory property of curcumin (diferuloylmethane) in patients with postoperative inflammation. *Int. J. Clin. Pharmacol. Ther. Toxicol.* **24,** 651–654.
17. Huang, M-T., Lysz, T., Ferraro, T., Abidi, T. F., Laskin, J. D., and Conney, A. H. (1991). Inhibitory effects of curcumin on in vitro lipoxygenase and cyclooxygenase activities in mouse epidermis. *Cancer Res.* **51,** 813–819.
18. Huang, M-T., Lou, Y-R., Ma, W., Newmark, H. L., Reuhl, K. R., and Conney, A. H. (1994). Inhibitory effects of dietary curcumin on forestomach, duodenal and colon carcinogenesis in mice. *Cancer Res.* **54,** 5841–5847.
19. Pereira, M. A., Grubbs, C. J., Barnes, L. H., Li, H., Olson, G. R., Eto, I., Juliana, M., Whitaker, L. M., Kelloff, G. J., Steele, V. E., and Lubet, R. A. (1996). Effects of the phytochemicals, curcumin and quercetin, upon azoxymethane-induced colon cancer and 7,12-dimethylbenz[a]anthracene-induced mammary cancer in rats. *Carcinogenesis* **17,** 1305–1311.
20. Huang, M-T., Ma, W., Yen, P., Xie, J. G., Han, J., Frenkel, K., Grunberger, D., and Conney, A. H. (1997). Inhibitory effects of topical application of low doses of curcumin on 12-O-tetradecanoylphorbol-13-acetate-induced tumor promotion and oxidized DNA bases in mouse epidermis. *Carcinogenesis* **18,** 83–88.
21. Verma, S. P., Salamone, E., and Goldin, B. (1997). Curcumin and genistein, plant natural products, show synergistic inhibitory effects on the growth of human breast cancer MCF-7 cells induced by estrogenic pesticides. *Biochem. Biophys. Res. Commun.* **233,** 692–696.
22. Kuo, M.-L., Huang, T.-S., and Lin, J.-K. (1996). Curcumin, an antioxidant and anti-tumor promoter, induces apoptosis in human leukemia cells. *Biochim. Biophys. Acta* **1317,** 95–100.
23. Khar, A., Ali, A. M., Pardhasaradhi, B. V. V., Begum, Z., and Anjum, R. (1999). Antitumor activity of curcumin is mediated through the induction of apoptosis in AK-5 tumor cells. *FEBS Lett.* **445,** 165–168.
24. Inano, H., Onoda, M., Inafuku, N., Kubota, M., Kamada, Y., Osawa, T., Kobayashi, H., and Wakabayashi, K. (1999). Chemoprevention by curcumin during the promotion stage of tumorigenesis of mammary gland in rats irradiated with γ-rays. *Carcinogenesis* **20,** 1011–1018.
25. Chen, Y.-R., and Tan, T.-H. (1998). Inhibition of the c-Jun N-terminal kinase (JNK) signaling pathway by curcumin. *Oncogene* **17,** 173–178.
26. Jobin, C., Bradham, C. A., Russo, M. P., Juma, B., Narula, A. S., Brenner, D. A., and Sartor, R. B. (1999). Curcumin blocks cytokine-mediated NF-κB activation and proinflammatory gene expression by inhibiting inhibitory factor I-κB kinase activity. *J. Immunol.* **163,** 3474–3483.
27. Green, L. C., Wagner, D. A., Glogowski, J., Skipper, P. L., Wishnok, J. S., and Tannenbaum, S. R. (1982). Analysis of nitrate, nitrite, and [^{15}N]nitrate in biological fluids. *Anal. Biochem.* **126,** 131–138.
28. Ben-Shlomo, I., Kokia, E., Jackson, M. J., Adashi, E., and Payne, D. W. (1994). Interleukin-1β stimulates nitrite production in the rat ovary: Evidence for heterogous cell-cell interaction and for insulin-mediated regulation of the induc-

ible isoform of nitric oxide synthase. *Biol. Reprod.* **51,** 310–318.

29. van Haren, L., Teerds, K. J., Ossendorp, B. C., van Heusden, G. P. H., Orly, J., Stocco, D. M., Wirtz, K. W. A., and Rommerts, F. F. G. (1992). Sterol carrier protein 2 (non-specific lipid transfer protein) is localized in membranous fractions of Leydig cells and Sertoli cells but not in germ cells. *Biochim. Biophys. Acta* **1124,** 288–296.
30. Zini, A., O'Bryan, M. K., Magid, M. S., and Schlegel, P. N. (1996). Immunohistochemical localization of endothelial nitric oxide synthase in human testis, epididymis, and vas deferens suggests a possible role for nitric oxide in spermatogenesis, sperm maturation, and programmed cell death. *Biol. Reprod.* **55,** 935–941.
31. Brouet, I., and Ohshima, H. (1995). Curcumin, an anti-tumor promoter and anti-inflammatory agent, inhibits induction of nitric oxide synthase in activated macrophages. *Biochem. Biophys. Res. Commun.* **206,** 533–540.
32. Chan, M. M.-Y., Ho, C.-T., and Huang, H.-I. (1995). Effects of three dietary phytochemicals from tea, rosemary and turmeric on inflammation-induced nitrite production. *Cancer Lett.* **96,** 23–29.
33. Sreejayan, and Rao, M. N. A. (1997). Nitric oxide scavenging by curcuminoids. *J. Pharm. Pharmacol.* **49,** 105–107.
34. Wang, Y. J., Pan, M. H., Cheng, A. L., Lin, L. I., Ho, Y. S., Hsieh, C. Y., and Lin, J. K. (1997). Stability of curcumin in buffer solutions and characterization of its degradation products. *J. Pharmaceut. Biomed. Anal.* **15,** 1867–1876.
35. Hasmeda, M., and Polya, G. M. (1996). Inhibition of cyclic AMP-dependent protein kinase by curcumin. *Phytochemistry* **42,** 599–605.
36. Sikora, E., Bielak-Zmijewska, A., Piwocka, K., Skierski, J., and Radziszewska, E. (1997). Inhibition of proliferation and apoptosis of human and rat T lymphocytes by curcumin, a curry pigment. *Biochem. Pharmacol.* **54,** 899–907.
37. Bierhaus, A., Zhang, Y., Quehenberger, P., Luther, T., Haase, M., Muller, M., Mackman, N., Ziegler, R., and Nawroth, P. P. (1997). The dietary pigment curcumin reduces endothelial tissue factor gene expression by inhibiting binding of AP-1 to the DNA and activation of NF-kappa B. *Thromb. Haemostasis* **77,** 772–782.
38. Zhang, F., Altorki, N. K., Mestre, J. R., Subbaramaiah, K., and Dannenberg, A. J. (1999). Curcumin inhibits cyclooxygenase-2 transcription in bile acid- and phorbol ester-treated human gastrointestinal epithelial cells. *Carcinogenesis* **20,** 445–451.
39. Chen, H. W., and Huang, H. C. (1998). Effect of curcumin on cell cycle progression and apoptosis in vascular smooth muscle cells. *Br. J. Pharmacol.* **124,** 1029–1040.

RADIATION RESEARCH 153, 68–74 (2000)
0033-7587/00 $5.00

Inhibitory Effects of WR-2721 and Cysteamine on Tumor Initiation in Mammary Glands of Pregnant Rats by Radiation

Hiroshi Inano,[a,1] Makoto Onoda,[a] Keiko Suzuki,[a] Hisae Kobayashi[b] and Katsumi Wakabayashi[b]

[a]*First Research Group, National Institute of Radiological Sciences, 9-1, Anagawa-4-chome, Inage-ku, Chiba-shi 263-8555, Japan; and*
[b]*Institute for Molecular and Cellular Regulation, Gunma University, Showa-machi, Maebashi-shi 371-8512, Japan*

Inano, H., Onoda, M., Suzuki, K., Kobayashi, H. and Wakabayashi, K. Inhibitory Effects of WR-2721 and Cysteamine on Tumor Initiation in Mammary Glands of Pregnant Rats by Radiation. *Radiat. Res.* 153, 68–74 (2000).

We evaluated the effect of WR-2721 [*S*-2-(3-aminopropylamino)-ethylphosphorothioic acid] and cysteamine (2-mercaptoethylamine) on the development of radiation-induced mammary tumors in rats. Pregnant rats were treated with WR-2721 or cysteamine 30 min prior to whole-body irradiation with γ rays from a ^{60}Co source at a dose of 1.5 or 2.6 Gy. Additional pregnant rats were given saline and then exposed to γ rays at a dose of 0, 1.5 or 2.6 Gy as a control. All rats were implanted with pellets of diethylstilbestrol, a tumor promoter, 1 month after termination of nursing and were observed for 1 year to detect palpable mammary tumors. No mammary tumors developed in the saline-injected nonirradiated rats. However, when rats were irradiated with 1.5 or 2.6 Gy after saline treatment, the incidence of mammary tumors was high (71.4 and 92.3%, respectively). Administration of WR-2721 or cysteamine prior to irradiation with 1.5 Gy significantly decreased the tumor incidence (23.8 and 20.8%, respectively). Tumor prevention by either agent was less effective at the higher dose. The appearance of the first mammary tumor occurred later in rats treated with WR-2721 or cysteamine than in the control rats. An increasing rate of adenocarcinoma in the control group was observed with increasing dose from 1.5 Gy up to 2.6 Gy. However, the development of adenocarcinoma did not increase after pretreatment with WR-2721 or cysteamine in rats irradiated with 2.6 Gy. Many of the mammary tumors that developed in the control rats were of the ER$^+$PgR$^+$ type. Administration of WR-2721 produced no tumors of the ER$^+$PgR$^+$ type. Cysteamine treatment increased the development of ER-negative tumors. The serum concentration of progesterone was significantly higher in rats treated with WR-2721 or cysteamine than in the control rats. On the other hand, the estradiol-17β concentration was reduced by treatment with WR-2721, but not significantly compared to the control. WR-2721 and cysteamine had no effect on the prolactin concentration of the irradiated rats. The results suggest that administration of WR-2721 or cysteamine prior to the irradiation has a potent preventive effect on the initiation phase during mammary tumorigenesis. © 2000 by Radiation Research Society

INTRODUCTION

The generation of oxygen radical species by radiation exposure is considered one of the most important mechanisms of radiation-induced carcinogenesis. The aminothiols *S*-2-(3-aminopropylamino)ethylphosphorothioic acid (WR-2721) and cysteamine are potent radioprotectors. WR-2721 is a prodrug that requires dephosphorylation catalyzed by alkaline phosphatase in the plasma membrane (*1*) to generate the free thiol form, 2-(aminopropylamino)ethanethiol (WR-1065), as the active form of a radioprotector. Protection against the effects of radiation by WR-1065 (*2*) and cysteamine (*3*) is considered to be due to the scavenging of free radicals produced by the interaction of radiation and biological molecules. WR-2721 has antitransforming (*4*), antimutagenic (*5*) and anticlastogenic (*6*) properties. However, little information is available on the *in vivo* effects of these agents on the development of radiation-induced tumors. There are only two reports that radiation-induced sarcoma (*7*) and lymphoreticular tumors (*8*) were suppressed by administration of WR-2721 prior to γ irradiation. Previous studies in our laboratory have demonstrated that γ irradiation of rats in late pregnancy or in late lactation induced mammary tumors at a higher incidence than in virgin rats irradiated in the presence of a tumor promoter (*9–11*). The susceptibility of the mammary glands to radiation depends on estrogen-stimulated development in pregnancy (*9*) and on prolactin-stimulated differentiation in lactation (*10*). Also, our results suggested that estrogen is a direct or indirect sensitizer for tumor initiation by radiation (*12*). The present study was designed to evaluate the chemopreventive activity of the aminothiols against radiation-induced initiation of mammary tumors in rats during pregnancy.

MATERIALS AND METHODS

Materials

WR-2721 was kindly supplied by Dr. Mikio Shikita, former Director of the Division of Chemical Pharmacology in this Institute. Diethylstil-

[1] To whom correspondence should be addressed.

bestrol (DES) and cysteamine were obtained from Sigma (St. Louis, MO). [2,4,6,7-^{3}H]Estradiol-17β (specific activity 4 TBq/mmol) and [17α-methyl-^{3}H]17α,21-dimethyl-19-nor-pregn-4,9-diene-3,20-dione (R5020) (specific activity 3 TBq/mmol) were purchased from NEN Life Science Products (Boston, MA). Pellets were prepared in a medical-grade Silastic tube (Dow Corning Co., Midland, MI, 1.98 mm i.d., 3.18 mm o.d.) and were filled with 3 mg of DES mixed with 27 mg of cholesterol.

Animals and Treatment

The rats used in the present study were treated and handled according to the "Recommendations for Handling of Laboratory Animals for Biomedical Research" compiled by the Committee for Safety and Handling Regulations for Laboratory Animal Experiments in our Institute. Wistar-MS rats from a stock colony of Nippon SLC Co. (Hamamatsu, Japan) were housed in a temperature-controlled room at 23 ± 1°C and maintained under a light schedule of 14 h light/10 h dark. They received water and food *ad libitum*. One hundred sixty pregnant rats were divided into groups as follows at day 20 of pregnancy (the presence of a vaginal plug denoting day 1): 24 rats (group S_0) served as a control with i.p. injection of saline (1.5 ml) and no radiation exposure; 21 (group $S_{1.5}$) and 26 rats (group $S_{2.6}$) were given i.p. injection of 1.5 ml saline and 30 min later received whole-body irradiation with 1.5 and 2.6 Gy of γ rays (0.15 Gy/min), respectively, from a ^{60}Co source; 21 (group $W_{1.5}$) and 23 (group $W_{2.6}$) were treated by i.p. injection of WR-2721 (50 mg/1.5 ml saline per rat) 30 min prior to irradiation and received whole-body irradiation with 1.5 and 2.6 Gy of γ rays, respectively; 24 (group $C_{1.5}$) and 21 rats (group $C_{2.6}$) were injected i.p. with cysteamine (25 mg/1.5 ml saline/rat) and then exposed to whole-body irradiation with 1.5 and 2.6 Gy of γ rays, respectively. The drugs were dissolved in saline immediately before use. The interval between the injection and irradiation was chosen based on previous observations on the maximal protection by WR-2721 against lung micrometastases (*13*). All rats were implanted with DES pellets in the interscapular area under light anesthesia by sodium pentobarbiturate at 1 month after termination of nursing. The pellet was renewed every 8 weeks. The rate of release of DES from the pellet was approximately 0.38 ± 0.01 μg DES/day (*14*). The rats were examined for palpable mammary tumors for 1 year starting from the date of pellet implantation. When mammary tumors >2 cm in diameter were detected, the rats were killed by CO_2 asphyxiation and the tumors were removed. Each mammary tumor was divided in two portions: One portion was fixed in 10% neutral-buffered formalin for histopathological examination, and the other was trimmed of surrounding normal tissue and immediately frozen at −80°C until used for the receptor assay. The remaining rats were killed 1 year after the start of administration of DES and were autopsied to ascertain whether they had any nonpalpable mammary tumors. Tumor incidence was calculated from the number of rats with tumors within 1 year. Iball's index (*15*) and the protection index (*16*) were calculated according to the following equations:

$$\text{Iball's index} = [\text{incidence (\%)/latent period (days)}] \times 100;$$

$$\text{Protection index} = [(\text{incidence of } S_{irr}) - (\text{incidence of } S_0)] \div [(\text{incidence of } Exp_{irr}) - (\text{incidence of } S_0)];$$

where S_0 is the rats treated with saline and no radiation, S_{irr} is the rats treated with saline and then whole-body irradiation with 1.5 or 2.6 Gy, and Exp_{irr} is the rats treated with a radioprotective reagent and then whole-body irradiation with 1.5 or 2.6 Gy.

Radioimmunoassay of Hormones

A blood sample collected from each rat by cardiocentesis under anesthesia was allowed to clot and was centrifuged to obtain serum. The sera were immediately frozen and stored at −80°C until the assay was started. Concentrations of prolactin, luteinizing hormone (LH) and follicle-stimulating hormone (FSH) were determined with NIDDK radioimmunoassay kits (the National Hormone and Pituitary Program, Rockville, MD). Estradiol-17β was measured by a modification of the method of Watanabe *et al.* (*17*). The serum concentration of progesterone was assayed with a commercially available kit (BioMerieux, Marcy-l'Etoile, France).

Histological Examination

The removed mammary tumors were immediately fixed in 10% formalin neutralized with 0.1 *M* phosphate buffer (pH 7.2). Paraffin sections (4 μm thick) were prepared and stained with hematoxylin and eosin. The tumors were classified as adenocarcinoma or fibroadenoma according to the criteria for the classification of mammary tumors (*18*).

Assay of Steroid Receptors

The tissues obtained from all mammary tumors >2 cm in diameter were homogenized in 10 m*M* Tris-HCl buffer (pH 7.4) containing 1.5 m*M* EDTA-Na and 1 m*M* dithiothreitol, and the cytosol fraction was obtained from the homogenates by centrifugation at 105,000*g* for 1 h at 4°C. Estrogen receptor (ER) and progesterone receptor (PgR) in the cytosol fraction were analyzed by dextran-coated charcoal methods using [2,4,6,7-^{3}H]estradiol-17β (*19*) and [17α-methyl-^{3}H]R5020 (*20*), respectively, as radioligands. Maximum binding sites for the receptors were determined by a Scatchard plot analysis (*21*).

Statistical Analysis

Statistical analyses were conducted using the χ^2 test for the incidence of mammary tumors, and an analysis of variance (ANOVA) with post hoc Scheffe's test for body weight, organ weight, hormone concentration and latent period. The cumulative proportions of rats with tumors (incidence curves) were calculated by the product-limit method where rats which died or were sacrificed without mammary tumors were included, and the difference between groups was tested for statistical significance by the Mantel-Cox test. The analyses were performed using StatView-J4.5 software (Abacus Concepts, Berkeley, CA). *P* values of less than 5% were considered significant.

RESULTS

Prevention of Radiation-Induced Mammary Tumors by WR-2721 and Cysteamine

Mammary tumors did not develop during the 1-year observation period in any of the rats in group S_0 that were treated with saline but were not irradiated at day 20 of pregnancy and then were implanted with the DES pellet. Of the 21 rats in the control group ($S_{1.5}$) treated with saline with whole-body irradiation with 1.5 Gy γ rays at day 20 of pregnancy and then with DES after weaning, 15 (71.4%) developed mammary tumors during the experimental period (Table 1). The administration of WR-2721 30 min prior to irradiation with 1.5 Gy in the pregnant rats (group $W_{1.5}$) significantly decreased the incidence of total mammary tumors (23.8%, $P < 0.005$). Treatment of pregnant rats (group $C_{1.5}$) with cysteamine before whole-body irradiation with 1.5 Gy also decreased the incidence of mammary tumors in the 1-year period (20.8%, $P < 0.001$). An increased incidence was observed in the rats exposed to the higher dose (2.6 Gy) of radiation. Of the 26 pregnant rats (group $S_{2.6}$) that received whole-body irradiation with 2.6 Gy after

TABLE 1
Prevention of the Development of Radiation-Induced Mammary Tumors by Treatment with WR-2721 or Cysteamine

Group	Treatment prior to irradiation	Dose (Gy)	Rats used	Rats with mammary tumors (%)	No. of tumors			Latent period (months)	No. of tumors/rat	Iball's index	Protection index
					Total	Fibro-adenoma	Adeno-carcinoma				
S_0	Saline	0	24	0 (0)	0	0	0		0		
$S_{1.5}$	Saline	1.5	21	15 (71.4)	25	18	7	8.9 ± 0.6	1.6 ± 0.2	28.5	
$W_{1.5}$	WR-2721	1.5	21	5 (23.8)[a]	9	7	2	11.0 ± 0.2[b]	1.8 ± 0.8	7.2	3.0
$C_{1.5}$	Cysteamine	1.5	24	5 (20.8)[c]	6	4	2	11.0 ± 0.3[b]	1.2 ± 0.2	6.3	3.4
$S_{2.6}$	Saline	2.6	26	24 (92.3)	38	21	17	8.2 ± 0.6	1.6 ± 0.4	39.1	
$W_{2.6}$	WR-2721	2.6	23	10 (43.5)[d]	18	15[d]	3[d]	8.5 ± 0.5	1.8 ± 0.2	20.5	2.1
$C_{2.6}$	Cysteamine	2.6	21	14 (66.7)[e]	21	15	6	9.3 ± 0.3	1.6 ± 0.9	23.9	1.4

[a] Significant difference ($P < 0.005$) from group $S_{1.5}$ by the χ^2 test.
[b] Significant difference ($P < 0.05$) from group $S_{1.5}$ by Scheffe's test.
[c] Significant difference ($P < 0.001$) from group $S_{1.5}$ by the χ^2 test.
[d] Significant difference ($P < 0.005$) from group $S_{2.6}$ by the χ^2 test.
[e] Significant difference ($P < 0.05$) from group $S_{2.6}$ by the χ^2 test.

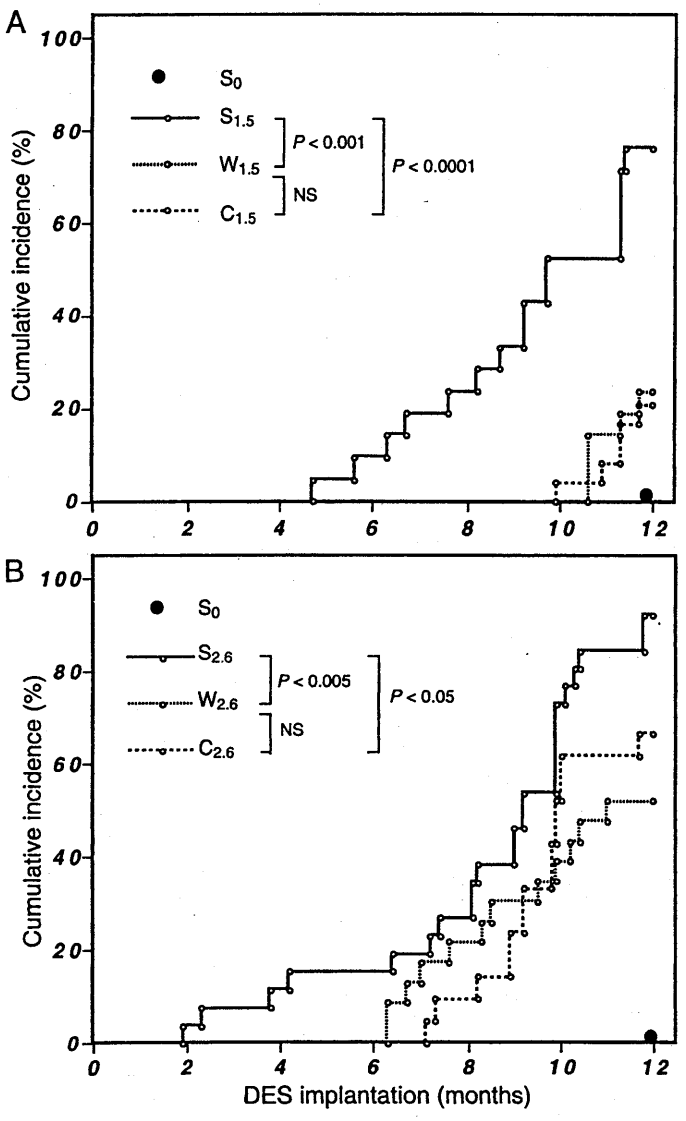

FIG. 1. Cumulative incidence of the development of mammary tumors in rats irradiated with 1.5 (panel A) and 2.6 Gy (panel B) as a function of time after implantation of DES pellets.

saline injection, 24 rats (92.3%) developed mammary tumors during the 1-year period. In the experimental groups, rats were injected with WR-2721 (group $W_{2.6}$) or cysteamine (group $C_{2.6}$) 30 min prior to irradiation with 2.6 Gy. A decreased incidence of total mammary tumors was observed in group $W_{2.6}$ (43.4%, $P < 0.005$) and group $C_{2.6}$ (66.6%, $P < 0.05$).

As shown in Fig. 1A, the administration of WR-2721 (group $W_{1.5}$) or cysteamine (group $C_{1.5}$) before irradiation with 1.5 Gy significantly decreased the cumulative incidence curves of mammary tumors ($P < 0.001$ and $P < 0.0001$, respectively) for the 1-year period compared to group $S_{1.5}$. The appearance of the first mammary tumor occurred 5–6 months later in group $W_{1.5}$ and group $C_{1.5}$ than in group $S_{1.5}$. Also, as shown in Fig. 1B, the cumulative incidence in rats treated with WR-2721 (group $W_{2.6}$) or cysteamine (group $C_{2.6}$) prior to the irradiation with 2.6 Gy was significantly decreased ($P < 0.005$ and $P < 0.05$, respectively) compared to that in the rats injected with saline (group $S_{2.6}$). The appearance of the first palpable tumors was delayed by approximately 4.5 and 5 months in group $W_{2.6}$ and group $C_{2.6}$, respectively, compared to that in group $S_{2.6}$. There were significant differences ($P < 0.05$) in the average latent period until the appearance of mammary tumors, when rats were injected with WR-2721 or cysteamine prior to irradiation with 1.5 Gy during pregnancy, but not with 2.6 Gy. No significant difference was observed among the groups irradiated with 1.5 or 2.6 Gy in the number of tumors per tumor-bearing rat. Iball's index for overall tumor development in rats in group $W_{1.5}$ and group $C_{1.5}$ was 20–25% of that in group $S_{1.5}$, while in group $W_{2.6}$ and group $C_{2.6}$ it was 50–60% of that in group $S_{2.6}$. Protection indexes for WR-2721 and cysteamine were 3.0 and 3.4, respectively, when rats were injected with those agents prior to irradiation with 1.5 Gy during pregnancy. Increasing the dose to 2.6 Gy was associated with a reduction in the protection indexes for WR-2721 and cysteamine. Based on the results

TABLE 2
Estrogen Receptor (ER) and Progesterone Receptor (PgR) in Radiation-Induced Mammary Tumors

Group	Tumors tested	ER/PgR +/+	+/−	−/+	−/−
$S_{1.5}$	17	13	1	3	0
$W_{1.5}$	4	0	2	1	1
$C_{1.5}$	6	2	0	2	2

showing prevention of development of mammary tumors in rats irradiated with 1.5 Gy by treatment with WR-2721 or cysteamine, we decided to measure the organ weights, hormone concentrations in serum, and hormone receptors in the tumors of rats irradiated with this dose.

Histological Examination of Mammary Tumors

Adenocarcinoma was seen in 7 (28%) of the 25 tumors that developed in rats (group $S_{1.5}$) that were irradiated with 1.5 Gy after injection with saline (Table 1). The proportion (22 and 33%, respectively) of adenocarcinoma in group $W_{1.5}$ and $C_{1.5}$ was not significantly different from that in group $S_{1.5}$. An increasing proportion (17 of the 38 tumors, 45%) of adenocarcinoma was observed when the dose was increased to 2.6 Gy (group $S_{2.6}$). When rats irradiated with 2.6 Gy were pretreated with WR-2721 or cysteamine, the proportion of adenocarcinoma was 16% (group $W_{2.6}$) and 29% (group $C_{2.6}$) of the total tumors. The reduced proportion of adenocarcinoma in group $W_{2.6}$ was significantly different from that in group $S_{2.6}$, but not group $C_{2.6}$.

Expression of Estrogen Receptor (ER) and Progesterone Receptor (PgR) in Mammary Tumors

Table 2 shows the results of the steroid receptor expression assay in the mammary tumors (>2 cm in diameter) that developed in rats irradiated with 1.5 Gy. Many (76%) of the mammary tumors that developed in the rats injected with saline prior to irradiation were of the ER^+PgR^+ type, and no tumor was ER^-PgR^-. Induction of ER^+PgR^+ type tumors was eliminated by treatment with WR-2721 prior to irradiation. Figure 2 shows the maximum binding sites for ER and PgR in fibroadenoma and adenocarcinoma obtained from the rats that were irradiated with 1.5 Gy after treatment with WR-2721 or cysteamine at day 20 of pregnancy. Administration of cysteamine increased the development of ER-negative tumors. However, the concentration of PgR in adenocarcinoma obtained from the rats treated with cysteamine was higher than that in fibroadenoma.

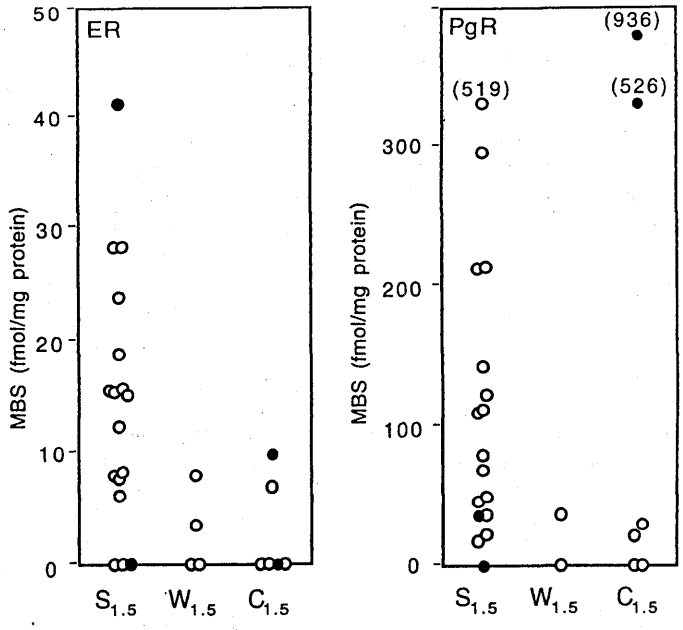

FIG. 2. Maximum binding sites (MBS) of the estrogen receptor (ER) and progesterone receptor (PgR) in mammary tumors. Open circles and closed circles represent fibroadenoma and adenocarcinoma, respectively.

Serum Concentration of Hormones

The serum concentrations of ovarian and pituitary hormones were measured 1 year after the implantation of DES in the irradiated rats. The progesterone concentrations in the group $W_{1.5}$ and group $C_{1.5}$ rats were 3.4- ($P < 0.01$) and 2.1- ($P < 0.05$) fold higher, respectively, than that of the rats in group $S_{1.5}$ (Table 3). On the other hand, the estradiol-17β level was reduced to 48% of that observed in rats in group $S_{1.5}$ by the administration of WR-2721 prior to irradiation with 1.5 Gy, but it was not significantly different by statistical analysis. The estradiol-17β concentration in rats in group $C_{1.5}$ was also decreased to below the

TABLE 3
Hormone Concentration in Serum of Rats Irradiated with γ Rays after Treatment with WR-2721 or Cysteamine

Group (*n*)	Progesterone (ng/ml)	Estradiol-17β (pg/ml)	Prolactin (ng/ml)	LH (ng/ml)	FSH (ng/ml)
S_0 (5)	34.2 ± 7.9	4.8 ± 2.3	176 ± 32	0.35 ± 0.03	5.7 ± 2.6
$S_{1.5}$ (5)	25.4 ± 3.8	4.0 ± 2.2	219 ± 53	0.22 ± 0.02[a]	5.3 ± 0.7
$W_{1.5}$ (5)	86.2 ± 9.3[a,b]	1.9 ± 1.0	238 ± 36	0.18 ± 0.02[a]	6.6 ± 0.5
$C_{1.5}$ (5)	55.3 ± 11.7[c]	<0.2	195 ± 41	0.11 ± 0.03[c]	5.3 ± 0.2

[a] Significant difference ($P < 0.01$) from group S_0 by Scheffe's test.
[b] Significant difference ($P < 0.01$) from group $S_{1.5}$ by Scheffe's test.
[c] Significant difference ($P < 0.05$) from group $S_{1.5}$ by Scheffe's test.

TABLE 4
Mean Body and Organ Weights of Rats Irradiated with γ Rays after Treatment with WR-2721 or Cysteamine

Group (*n*)	Body weight (g)	Liver (g)	Adrenals (mg)	Uterus (mg)	Ovaries (mg)	Pituitary (mg)
S_0 (16)	255 ± 8	9.9 ± 0.2	92 ± 2	603 ± 29	54 ± 4	15 ± 1
$S_{1.5}$ (11)	257 ± 9	15.6 ± 1.0[a]	98 ± 7	497 ± 29[a]	58 ± 5	24 ± 9[a]
$W_{1.5}$ (7)	251 ± 18	11.4 ± 0.4[b]	103 ± 5	586 ± 24	62 ± 5	19 ± 2
$C_{1.5}$ (11)	231 ± 6	9.4 ± 0.3[b]	92 ± 2	535 ± 23	59 ± 3	16 ± 1[c]

[a] Significant difference ($P < 0.01$) from group S_0 by Scheffe's test.
[b] Significant difference ($P < 0.01$) from group $S_{1.5}$ by Scheffe's test.
[c] Significant difference ($P < 0.05$) from group $S_{1.5}$ by Scheffe's test.

level detectable by the radioimmunoassay (0.2 pg/ml). In addition, WR-2721 and cysteamine had no effect on the serum concentrations of prolactin and FSH in the irradiated rats.

Biological Effects of Treatment with WR-2721 and Cysteamine Prior to Irradiation with 1.5 Gy

No significant difference in body weight was observed among the rats that were irradiated after treatment with WR-2721 or cysteamine (Table 4). The livers of rats in group $S_{1.5}$ were significantly hypertrophied by the irradiation ($P < 0.01$), but the radiation-induced enlargement did not occur after pretreatment with WR-2721 or cysteamine. The uterus was atrophied in the saline-injected rats after irradiation with 1.5 Gy (group $S_{1.5}$) ($P < 0.01$) but was not reduced after the treatment with WR-2721 or cysteamine. Irradiated rats implanted with DES (group $S_{1.5}$) had hypertrophic pituitary glands and few pituitary tumors.

DISCUSSION

The results presented in this paper show that WR-2721 and cysteamine can effectively protect mammary glands against the initiation of tumorigenesis by radiation, and that the effectiveness of the radioprotection depends on the dose of radiation. It is considered that the dose of the radioprotector and the interval between the administration of these compounds and the radiation exposure are important factors that influence radioprotection. In preliminary experiments, when pregnant rats at day 20 were treated with an i.p. injection of a higher dose (100 mg/rat) of WR-2721 than that used in the present experiments, rats were not able to deliver full-term pups. Based on those results, we chose 50 mg/rat as the dose of WR-2721 for subsequent work. On the other hand, maximal protection against radiation damage depended on the interval between drug and radiation treatments. Milas *et al.* (*7*) have reported that a sarcoma incidence of 93% in control mice was reduced to 30% by the administration of WR-2721 30 min prior to irradiation. Protection against the detrimental effects of radiation by WR-2721 was observed only when the radioprotector was present in tissues during irradiation (*22, 23*). Utley *et al.* (*24*) demonstrated that WR-1065, an active form of the radioprotector, is a major metabolite of the drug in tissues within 15–30 min after treatment with WR-2721. Based on their reports, we examined the radioprotective effects of the administration of WR-2721 30 min prior to irradiation. The administration of WR-2721 or cysteamine prior to irradiation at 1.5 Gy suppressed the incidence of mammary tumors, which was 71.4% in saline-injected rats, to 23.8 or 20.8%, respectively. The modes of action of WR-2721 that have been proposed include induction of intracellular hypoxia by oxidation of the thiol moiety of the WR-1065 molecule (*25*). Also, Liu *et al.* (*26*) demonstrated that WR-1065 is effective in repressing *Myc* expression. Reduced expression of *Myc* can lead to lower rates of exponential cell growth and a lengthening of the time required for transition from G_0 to S phase (*27*). Moreover, protection of mammalian cells from the cytotoxic effects of γ rays by WR-1065 is accompanied by a substantial reduction in the yield of single- and double-strand breaks in the DNA (*28–30*).

Scott *et al.* have reported that administration of cysteamine rapidly depletes plasma prolactin by inhibition of dopamine-β-hydroxylase (*31*). Since the action of prolactin in the mammary glands is related to a higher incidence of mammary tumors induced by radiation (*10*), the reduction of the prolactin level at the time of irradiation is one of the possible mechanisms of the preventive action of cysteamine. In addition to this action, it was reported that cysteamine scavenges free radicals produced by radiation (*3*). At the end of the experiments, a reduction in the serum estradiol-17β level was observed in the irradiated rats that had been treated with WR-2721 or cysteamine. The mechanism of the reduction is unclear, but a low level of estradiol-17β is considered to be one of the mechanisms of prevention of radiation-induced mammary tumors by WR-2721 or cysteamine.

Another possible explanation for the reduction in the risk of radiation-induced mammary tumors by WR-2721 or cysteamine is that the effect of these thiol compounds was manifested only on delay of tumor appearance. The slopes of the appearance of tumors with time are similar in the saline-injected group and the thiol-treated group in the observation period of 1 year.

The results of the present study demonstrate that admin-

istration of WR-2721 or cysteamine prior to irradiation at 1.5 Gy reduced the number of ER/PgR$^{+/+}$ tumors, and ER/PgR$^{-/-}$ tumors appeared. Although a low level of serum estradiol-17β was observed in the irradiated rats that had been treated with WR-2721 or cysteamine, the serum concentration of prolactin was not reduced. The prolactin concentrations in rats of group $S_{1.5}$, group $W_{1.5}$ and group $C_{1.5}$ remained at a high level during the experimental period, because of the continuous administration of DES. In our previous studies of chemoprevention of radiation-induced mammary tumors, a similar phenomenon was seen when dietary simvastatin was administered together with implantation of DES during the promotion phase (*32*).

The results of this study show clearly that treatment with cysteamine at a lower dose than that of WR-2721 in pregnant rats prior to irradiation decreased the incidence of mammary tumors induced by radiation. On the other hand, when rats received 2-β-aminoethylisothiouronium-Br·HBr (AET), another radioprotector, prior to exposure to X rays, the incidence and the total number of mammary tumors were not reduced (*33*). In a study of chemical carcinogenesis in mammary glands, Marquardt *et al.* reported that treatment of Sprague-Dawley rats with cysteamine 20 min prior to and 5 and 24 h after the administration of 7,12-dimethylbenz[a]anthracene (DMBA) reduced the number of mammary tumors that formed (*34*). Accumulating evidence also suggests an important role for reactive oxygen radicals in the multistage carcinogenesis in mammary glands by DMBA (*35*). Werts and Gould (*36*) demonstrated that decreases in susceptibility to DMBA-induced mammary tumors were correlated with increased activity of superoxide dismutase in mammary glands.

The goal of our program is the complete prevention of radiation-induced mammary tumors, and we are using rats in which there is no spontaneous development of mammary tumors to test the effectiveness of different agents. The administration of radioprotective aminothiols such as WR-2721 and cysteamine prior to irradiation has a potent preventive effect on the initiation phase after exposure γ rays during mammary tumorigenesis.

ACKNOWLEDGMENTS

This work was partly supported by a project research grant for Experimental Studies on Radiation Health, Detriment and its Modifying Factors and also by a grant from the Special Program for Bioregulation, of the National Institute of Radiological Sciences.

Received: April 26, 1999; accepted: September 3, 1999

REFERENCES

1. J. Nakamura, L. M. Shaw and D. Q. Brown, Hydrolysis of WR-2721 by mouse liver cell fractions. *Radiat. Res.* **109**, 143–152 (1987).
2. L. G. Littlefield, E. E. Joiner, S. P. Colyer, F. Sallam and E. L. Frome, Concentration-dependent protection against X-ray-induced chromosome aberrations in human lymphocytes by the aminothiol WR-1065. *Radiat. Res.* **133**, 88–93 (1993).
3. B. W. Henderson and A. C. Miller, Effects of scavengers of reactive oxygen and radical species on cell survival following photodynamic treatment *in vitro*; Comparison to ionizing radiation. *Radiat. Res.* **108**, 196–205 (1986).
4. E. K. Balcer-Kubiczek, G. H. Harrison, C. K. Hill and W. F. Blakely, Effects of WR-1065 and WR-151326 on survival and neoplastic transformation in C3H/10T1/2 cells exposed to TRIGA or JANUS fission neutrons. *Int. J. Radiat. Biol.* **63**, 37–46 (1993).
5. D. J. Grdina, Y. Kataoka, I. Basic and J. Perrin, The radioprotector WR-2721 reduces neutron-induced mutations at the hypoxanthine-guanine phosphoribosyl transferase locus in mouse splenocytes when administered prior to or following irradiation. *Carcinogenesis* **13**, 811–814 (1992).
6. J. L. Schwartz, S. M. Giovanzzi, T. Karrison, C. Jones and D. J. Grdina, 2-[(Aminopropyl)amino]ethanethiol-mediated reduction in ^{60}Co γ-ray and fission-spectrum neutron-induced chromosome damage in V79 cells. *Radiat. Res.* **113**, 145–154 (1988).
7. L. Milas, N. Hunter, L. C. Stephens and L. J. Peters, Inhibition of radiation carcinogenesis in mice by *S*-2-(3-aminopropylamino)-ethylphosphorothioic acid. *Cancer Res.* **44**, 5567–5569 (1984).
8. D. J. Grdina, B. A. Carnes, D. Grahn and C. P. Sigdestad, Protection against late effects of radiation by *S*-2-(3-aminopropylamino)ethylphosphorothioic acid. *Cancer Res.* **51**, 4125–4130 (1991).
9. H. Inano, K. Suzuki, H. Ishii-Ohba, K. Ikeda and K. Wakabayashi, Pregnancy-dependent inhibition in tumorigenesis of Wistar rat mammary glands by ^{60}Co-irradiation. *Carcinogenesis* **12**, 1085–1090 (1991).
10. K. Suzuki, H. Ishii-Ohba, H. Yamanouchi, K. Wakabayashi, M. Takahashi and H. Inano, Susceptibility of lactating rat mammary glands to gamma-ray-irradiation-induced tumorigenesis. *Int. J. Cancer* **56**, 413–417 (1994).
11. H. Inano, K. Suzuki, M. Onoda and H. Yamanouchi, Susceptibility of fetal, virgin, pregnant and lactating rats for the induction of mammary tumors by gamma rays. *Radiat. Res.* **145**, 708–713 (1996).
12. H. Inano, H. Yamanouchi, K. Suzuki, M. Onoda and K. Wakabayashi, Estradiol-17β as an initiation modifier for radiation-induced mammary tumorigenesis of rats ovariectomized before puberty. *Carcinogenesis* **16**, 1871–1877 (1995).
13. L. Milas, N. Hunter, B. O. Reid and H. D. Thames, Jr., Protective effects of *S*-2-(3-aminopropylamino)ethylphosphorothioic acid against radiation damage of normal tissue and a fibrosarcoma in mice. *Cancer Res.* **42**, 1888–1897 (1982).
14. H. Inano, K. Suzuki, H. Ishii-Ohba, H. Yamanouchi, M. Takahashi and K. Wakabayashi, Promotive effects of diethylstilbestrol, its metabolite (Z,Z-dienestrol) and a stereoisomer of the metabolite (E,E-dienestrol) in tumorigenesis of rat mammary glands pregnancy-dependently initiated with radiation. *Carcinogenesis* **14**, 2157–2163 (1993).
15. J. Iball, The relative potency of carcinogenic compounds. *Am. J. Cancer* **35**, 188–190 (1939).
16. D. J. Grdina, B. Nagy and C. P. Sigdestad, Radioprotectors in treatment therapy to reduce risk in secondary tumors induction. *Pharmacol. Ther.* **39**, 21–25 (1988).
17. G. Watanabe, K. Taya and S. Sasamoto, Dynamics of ovarian inhibin secretion during the oestrous cycles of rats. *J. Endocrinol.* **126**, 151–157 (1990).
18. J. Russo, B. A. Gusteron, A. E. Rogers, I. H. Russo and S. R. Wellings, Comparative study of human and rat mammary tumorigenesis. *Lab. Invest.* **61**, 244–278 (1990).
19. R. B. Johnson, R. M. Nakamura and R. M. Libby, Simplified Scatchard plot assay for estrogen receptor in human breast tumor. *Clin. Chem.* **21**, 1715–1730 (1975).
20. R. B. Johnson and R. M. Nakamura, Simplified Scatchard plot assay for progesterone receptor in breast cancer: Comparison with single-point and multipoint assay. *Clin. Chem.* **24**, 1170–1176 (1978).
21. G. Scatchard, The attractions of proteins for small molecules and ions. *Ann. NY Acad. Sci.* **51**, 660–672 (1949).
22. D. J. Grdina, C. P. Sigdestad and B. A. Carnes, Protection by WR-

1065 and WR-151326 against fission-neutron-induced mutations at the HGPRT locus in V79 cells. *Radiat. Res.* **117**, 500–510 (1989).

23. D. J. Grdina, B. Nagy, C. K. Hill, R. L. Wells and C. Peraino, The radioprotector WR-1065 reduces radiation-induced mutations at the hypoxanthine-guanine phosphoribosyl transferase locus in V79 cells. *Carcinogenesis* **6**, 929–931 (1985).
24. J. F. Utley, N. Seaver, G. L. Lewton and R. C. Fahey, Pharmacokinetics of WR-1065 in mouse tissue following treatment with WR-2721. *Int. J. Radiat. Oncol. Biol. Phys.* **10**, 1525–1528 (1984).
25. J. W. Purdie, E. R. Inhaber, H. Schneider and J. Labelle, Interaction of cultured mammalian cells with WR-2721 and its thiol WR-1065: Implications for mechanisms of radioprotection. *Int. J. Radiat. Biol.* **43**, 517–527 (1983).
26. S-C. Liu, J. S. Murley, G. Woloschak and D. J. Grdina, Repression of c-myc gene expression by the thiol and disulfide forms of the cytoprotector amifostine. *Carcinogenesis* **18**, 2457–2459 (1997).
27. K. D. Hanson, M. Shichiri, M. R. Follansbee and J. M. Sedivy, Effects of c-myc expression on cell cycle progression. *Mol. Cell. Biol.* **14**, 5748–5755 (1994).
28. D. Murray, S. C. vanAnkeren, L. Milas and R. E. Meyn, Radioprotective action of WR-1065 on radiation-induced DNA strand breaks in cultured Chinese hamster ovary cells. *Radiat. Res.* **113**, 155–170 (1980).
29. C. P. Sigdestad, S. H. Treacy, L. A. Knapp and D. J. Grdina, The effect of 2-[(aminopropyl)amino]ethanethiol (WR-1065) on radiation induced DNA double strand damage and repair in V79 cells. *Br. J. Cancer* **55**, 477–482 (1987).
30. P. H. M. Lohman, O. Vos, C. V. van Sluis and J. A. Cohen, Chemical protection against breaks induced in DNA of human and bacterial cells by X-irradiation. *Biochim. Biophys. Acta* **224**, 339–352 (1970).
31. J. S. Scott, C. A. Lakin and J. R. Oliver, The effect of cysteamine, cystamine, and the structurally related compounds taurine, *N*-acetylcysteine, and D-penicillamine on plasma prolactin level in normal and estrogen-primed hyperprolactinemic rats. *Endocrinology* **121**, 812–818 (1987).
32. H. Inano, K. Suzuki, M. Onoda and K. Wakabayashi, Anti-carcinogenic activity of simvastatin during the promotion phase of radiation-induced mammary tumorigenesis of rats. *Carcinogenesis* **18**, 1723–1727 (1997).
33. C. J. Shellabarger and R. W. Schmidt, Mammary neoplasia in partial-body-irradiated rats treated with AET. *Radiat. Res.* **30**, 507–514 (1967).
34. H. Marquardt, M. D. Sapozink and M. S. Zedeck, Inhibition by cysteamine-HCl of oncogenesis induced by 7,12-dimethylbenz(a)anthracene without affecting toxicity. *Cancer Res.* **34**, 3387–3390 (1974).
35. M. Hirose, A. Masuda, S. Fukushima and N. Ito, Effects of subsequent antioxidant treatment on 7,12-dimethylbenz[a]anthracene-induced carcinogenesis of the mammary glands, ear duct and forestomach in Sprague-Dawley rats. *Carcinogenesis* **9**, 101–104 (1988).
36. E. D. Werts and M. N. Gould, Relationship between cellular superoxide dismutase and susceptibility to chemical induced cancer in the rat mammary gland. *Carcinogenesis* **7**, 1197–1201 (1986).

INT. J. RADIAT. BIOL 2000, VOL. 76, NO. 8, 1113–1120

Prevention of radiation-induced mammary tumours in rats by combined use of WR-2721 and tamoxifen

H. INANO*†, M. ONODA†, K. SUZUKI†, H. KOBAYASHI‡ and K. WAKABAYASHI‡

(Received 27 October 1999; accepted 5 January 2000)

Abstract.
Purpose: This investigation evaluated the inhibitory effect of S-2-(3-aminopropylamino)-ethylphosphorothioic acid (WR-2721) against the initiation of mammary tumourigenesis by irradiation, and the antipromotion activity of tamoxifen in the development of radiation-initiated mammary tumours.
Materials and methods: Lactating rats were injected with WR-2721 and then irradiated with γ-rays (1.5 Gy) at day 21 of lactation. The rats were divided into three groups 1 month after irradiation and were implanted with a pellet either of cholesterol as an inert control, diethylstilbestrol (DES) as a tumour-promoting agent, or DES combined with tamoxifen. For the control experiments, non-irradiated and irradiated rats receiving saline instead of WR-2721 were treated with a pellet by the same procedures.
Results: The highest incidence (85%) for tumourigenesis of mammary glands was observed in the irradiated rats that had been previously injected with saline following treatment with DES Administration of WR-2721 prior to the irradiation significantly decreased the incidence of mammary tumours to 52.2%. The treatment with DES pellets combined with tamoxifen in the irradiated rats previously injected with saline also markedly suppressed the incidence of mammary tumours even further to 4.4%. Also, the development of mammary tumours was completely prevented in the rats treated with WR-2721 prior to irradiation and then implanted with DES pellets combined with tamoxifen.
Conclusions: These results suggest that the administration of WR-2721 prior to irradiation has an inhibitory effect on the initiation phase, resulting in a partial reduction of mammary tumour development, and that the combination of WR-2721 at the initiation phase with tamoxifen at the promotion phase is quite effective in preventing mammary tumourigenesis induced by radiation.

1. Introduction

Early work with radioprotectors focused on acute biological effects, such as haematopoietic and gastrointestinal deaths, in sublethally irradiated mice (Yuhas and Storer 1969). One benefit of chemical radioprotection would be the inhibition of radiation-induced carcinogenesis (Liu *et al.* 1997). Whole-body irradiation of late pregnant or late lactating rats results in a higher incidence of mammary tumours than in irradiated virgin rats in the presence of diethylstilbestrol (DES) as a tumour-promoting agent (Inano *et al.* 1991, 1996a, Suzuki *et al.* 1994). Experiments done in our laboratory using pregnant rats have demonstrated that radiation-induced mammary tumours were partially suppressed by administration of WR-2721 prior to irradiation (Inano *et al.* 2000). In that study, we used a relatively low dose (50 mg/pregnant rat at day 20) of WR-2721 to minimize the toxicity during pregnancy. WR-2721 is a phosphorothioate pro-drug which is ultimately cleaved to the radioprotective thiol, 2-(aminopropylamino)ethanethiol (WR-1065), by alkaline phosphatase in the plasma membrane (Nakamura *et al.* 1987). Tamoxifen is the most widely used drug for the treatment of estrogen receptor positive breast cancer (Early Breast Cancer Trialist's Collaborative Group 1998), and also is under investigation as a chemopreventive in healthy women who are at high risk of breast cancer because of their family history (Fisher *et al.* 1998). The incidence of mammary tumours in rats induced by 7,12-dimethylbenz[a]anthracene (DMBA) (Jordan 1976) and irradiation (Welsch *et al.* 1981) can be partially suppressed by the administration of tamoxifen for periods prior to the development of these tumours. These observations were confirmed by Lemon *et al.* (1989), who reported that long-term treatment with tamoxifen after irradiation also considerably reduced the incidence of mammary carcinoma from 83% in controls to 14%. But, in neither of these studies, did tamoxifen prevent completely radiation-induced mammary tumours from developing. The objective of the present study is the characterize the potency of a combination of WR-2721 with tamoxifen to protect against rat mammary tumourigenesis initiated by γ-rays during lactation and then promoted by DES.

2. Materials and methods

2.1. *Materials*

DES and cholesterol were purchased from Sigma (St Louis, MO, USA). Tamoxifen was kindly supplied

*Author for correspondence.
†First Research Group, National Institute of Radiological Sciences, 9-1, Anagawa-4-chome, Inage-ku, Chiba-shi 263-8555, Japan. E-mail: inano@nirs.go.jp
‡Institute for Molecular and Cellular Regulation, Gunma University, Showa-machi, Maebashi-shi 371-8512, Japan.

International Journal of Radiation Biology ISSN 0955-3002 print/ISSN 1362-3095 online © 2000 Taylor & Francis Ltd
http://www.tandf.co.uk/journals

by AstraZeneca (Macclesfield, England). WR-2721 was kindly supplied by Dr Mikio Shikita, the former Director of the Division of Chemical Pharmacology in this Institute. Four kinds of sustained-release pellets were prepared in a medical grade Silastic tube (1.98 mm inner diameter, 3.18 mm outer diameter; Dow Corning, Midland, MI, USA) for tumour promotion. Cholesterol pellets were filled with 30 mg of cholesterol alone in the tube. DES pellets and tamoxifen pellets were filled with 3 mg of DES mixed with 27 mg of cholesterol, and with 9 mg of tamoxifen mixed with 21 mg of cholesterol in the tube, respectively. DES pellets combined with tamoxifen were filled with 3 mg of DES, 9 mg of tamoxifen and 18 mg of cholesterol in the medical tube.

2.2. *Animals and treatment*

The rats used in the present study were treated and handled according to the Recommendations for the Handling of Laboratory Animals for Biomedical Research compiled by the Committe of Safety and Handling Regulations for Laboratory Animal Experiments in our Institute. Wistar-MS rats bred in this Institute were kept at 23±1°C in a light-controlled environment (14 h light–10 h dark). They received water and food *ad libitum*. One hundred and eighty eight multiparous rats, at 7 months old, were divided into eight groups at day 21 of lactation (table 1). In groups S_{0c} and S_{0d}, 25 and 30 lactating rats, respectively, were injected with saline (1.5 ml/rat, i.p.) 21 days after parturition, and 1 month later, the cholesterol and DES pellets were implanted in the interscapular area under light anaesthesia by sodium pentobarbiturate, respectively. In groups $S_{1.5c}$ and $S_{1.5d}$, 23 and 20 lactating rats, respectively, were injected with saline 30 min before whole-body irradiation with 1.5 Gy γ-rays (15 cGy/min) from a ^{60}Co source at day 21 of lactation, and then were treated with cholesterol and DES, respectively, by the same procedures used for groups S_{0c} and S_{0d}. In groups $W_{1.5c}$ and $W_{1.5d}$, 21 and 23 lactating rats, respectively, were injected with WR-2721 (50 mg/1.5 ml saline/rat, i.p.) 30 min before the irradiation at day 21 of lactation, and were treated with cholesterol and DES, respectively, by the same procedures used for groups S_{0c} and S_{0d}. In groups $S_{1.5dt}$ and $W_{1.5dt}$, 23 lactating rats in each were injected with saline and WR-2721, respectively, 30 min before the irradiation at 1.5 Gy γ-rays at day 21 of lactation, and implanted with a tamoxifen pellet in the interscapular area immediately after the irradiation. One month later, the tamoxifen pellet was removed, and a DES pellet combined with tamoxifen was implanted in the same area. The pellets of cholesterol, DES and DES combined with tamoxifen were renewed every 8 weeks during the experimental period. The rates of release of DES and tamoxifen were calculated from weight loss of the pellets, and were estimated to be approximately 0.38±0.01 μg/day and 1.14±0.03 μg/day, respectively. The rats were observed for 1 year for detection of palpable mammary tumours starting from the time of the first pellet implantation. Tumour incidence was calculated from the number of rats with mammary tumours within 1 year. When palpable tumours reached more than 2 cm in diameter, the rats bearing them were killed by CO_2 asphyxiation and tumours were removed for histological examination.

2.3. *Radioimmunoassay of hormones*

Sera were obtained from a blood sample collected from each rat by cardiocentesis under anaesthesia at the end of experiments. The sera were frozen at −80°C until the assay was started. Estradiol-17β was measured by a modification of the method of Watanabe *et al.* (1990). The serum concentration of progesterone was assayed using a commercially available kit (BioMerieux, Marcy-l'Etoile, France). Concentrations of prolactin, luteinizing hormone (LH), thyroid stimulating hormone (TSH) and follicle stimulating hormone (FSH) were determined with

Table 1. Sequence of events that comprised the experiment design.

Group	Treatment before irradiation	Irradiation with γ-rays (Gy)	Treatment after irradiation	Number of rats/group
S_{0c}	Saline	0	Cholesterol	25
S_{0d}	Saline	0	DES	30
$S_{1.5d}$	Saline	1.5	DES	20
$S_{1.5c}$	Saline	1.5	Cholesterol	23
$S_{1.5dt}$	Saline	1.5	Tamoxifen + DES	23
$W_{1.5d}$	WR-2721	1.5	DES	23
$W_{1.5c}$	WR-2721	1.5	Cholesterol	21
$W_{1.5dt}$	WR-2721	1.5	Tamoxifen + DES	23

NIDDK radioimmunoassay kits (National Hormone and Pituitary Program, Rockville, MD, USA).

2.4. *Histological examination of tumours*

The removed mammary tumours were fixed in 10% formalin neutralized by 0.1 M phosphate buffer (pH 7.2) and embedded in paraffin. Each paraffin section (4 μm in thickness) was prepared and stained with hematoxylin and eosin. The tumours were classified as adenocarcinoma or fibroadenoma according to the criteria for the classification of rat mammary tumours (Russo *et al.* 1990).

2.5. *Iball's index and statistical analysis*

Iball's index was calculated as follows: the ratio of the incidence (%) to the average latency period in days was multiplied by 100 (Iball 1939). All statistical analyses were performed using StatView-J4.5 software (Abacus Concepts Inc., Berkeley, CA, USA). Statistical analyses were conducted by χ^2 test for the incidence of mammary tumours, and by one-way analysis of variance (ANOVA) with *post hoc* Scheffés test for body weight, organ weight, latency period and hormone concentrations. The cumulative percentage of rats with tumours (incidence curves) was calculated by the product-limit method where rats which died or were sacrificed without mammary tumours were included, and the difference between groups was tested for statistical significance by the Mantel-Cox test. Probability values less than 5% were considered significant.

3. Results

3.1. *Prevention of radiation-induced mammary tumours by WR-2721 and tamoxifen*

When 25 (S_{0c}) and 30 (S_{0d}) rats were treated with saline, were not irradiated in lactation but then implanted with the pellets of cholesterol and DES, respectively, only one rat (4%) in group S_{0c} and six rats (20%) in group S_{0d} developed mammary tumours during the experimental period (figure 1). When 20 lactating rats ($S_{1.5d}$) were treated with saline prior to the irradiation with 1.5 Gy and then implanted with DES pellets, 17 (85%) rats developed mammary tumours over the 1-year period. A lower incidence (52.2% and 4.4%) for the tumourigenesis was observed in the irradiated rats administered WR-2721 30 min prior to the irradiation ($W_{1.5d}$) or implanted with DES pellets combined with tamoxifen ($S_{1.5dt}$) instead of DES pellets, respectively. No mammary tumour developed during the 1-year observation period in any of the rats in group $W_{1.5dt}$ that were treated with WR-2721 prior to the irradiation

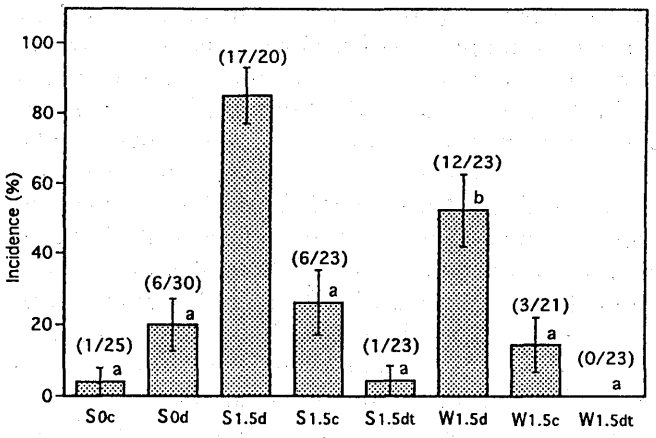

Figure 1. Effects of WR-2721 and tamoxifen on the incidence of radiation-induced mammary tumours. The numbers in parentheses on the top of the bar are the actual number of rats bearing tumours/rats used. Significant difference from group $S_{1.5d}$, (*a*) $p<0.0001$ and (*b*) $p<0.05$. Each column and vertical bar present the incidence (%)$\pm$SD, respectively. Abbreviations and treatment in each group were summarized in table 1.

and then implanted with DES pellets combined with tamoxifen. The results for the statistical analysis of incidence of total mammary tumours are summarized in figure 2.

As shown in figure 3, the administration of WR-2721 prior to the irradiation ($W_{1.5d}$) significantly decreased the cumulative incidence curve of mammary tumours ($p<0.01$) during the 1-year period, compared with group $S_{1.5d}$ without WR-2721. The administration of tamoxifen in the irradiated rats pretreated with saline ($S_{1.5dt}$, $p<0.0001$) or WR-2721 ($W_{1.5dt}$, $p<0.0001$) markedly reduced the cumulative incidence curves compared to group $S_{1.5d}$. As shown in table 2, treatment with WR-2721 prior to the

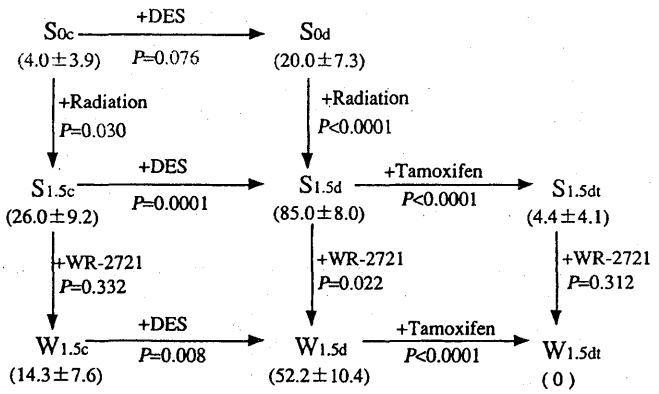

Figure 2. Statistical analysis of incidence of total mammary tumours. The number in parentheses presents the incidence (%)$\pm$SD of total mammary tumours. Statistical analyses were conducted by χ^2 test. Abbreviations and treatment in each group were summarized in table 1.

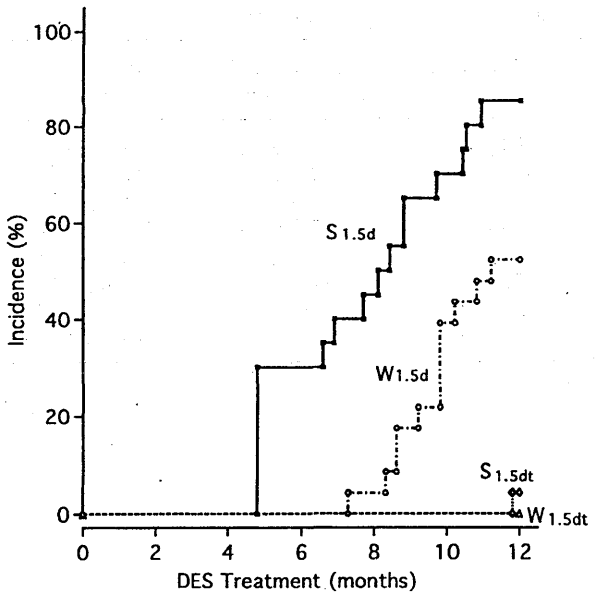

Figure 3. Cumulative incidence curves for radiation-induced mammary tumours. The administration of WR-2721 prior to irradiation ($W_{1.5d}$) significantly decreased ($p<0.01$) the cumulative incidence curve of the tumours, compared with group $S_{1.5d}$. The administration of tamoxifen in the irradiated rats pretreated with saline ($S_{1.5dt}$, $p<0.0001$) or WR-2721 ($W_{1.5dt}$, $p<0.0001$) markedly reduced the cumulative incidence curve relative to group $S_{1.5d}$. Abbreviations and treatment in each group were summarized in table 1.

irradiation in late lactation ($W_{1.5d}$) prolonged significantly ($p<0.05$) the latency period (9.5 ± 0.3 months) and decreased slightly ($p=0.427$) the number of tumours per rat (1.2 ± 0.1) compared with that (7.4 ± 0.6 months and 1.5 ± 0.3, respectively) of group $S_{1.5d}$. Furthermore, an extended period of latency (11.9 months) lasting until the appearance of palpable tumour was observed on treatment with DES pellets combined with tamoxifen ($S_{1.5dt}$). The highest Iball's index (38.3) for the development of overall tumours was obtained in group $S_{1.5d}$, the value being 2.1-fold higher than that with treatment by WR-2721 ($W_{1.5d}$) and 22-fold that with the tamoxifen treatment ($S_{1.5dt}$).

By histological examination, the percentage of adenocarcinomas among the tumours was shown to be 42% and 47% in group $S_{1.5d}$ and $W_{1.5d}$, respectively. No adenocarcinoma was detected in rats treated with DES pellets combined with tamoxifen during the promotion phase ($S_{1.5dt}$ and $W_{1.5dt}$).

3.2. *Hormone concentration in serum*

The serum concentrations of pituitary and ovarian hormones were measured 1 year after the implantation of the promoter (table 3). The prolactin concentration in the irradiated rats treated with DES ($S_{1.5d}$) was significantly higher ($p<0.05$) than that in rats treated with cholesterol ($S_{1.5c}$). Treatment with DES pellets combined with tamoxifen ($S_{1.5dt}$) caused a 82% reduction ($p<0.05$) of the prolactin level compared with rats implanted with DES pellets ($S_{1.5d}$). In the irradiated rats previously injected with WR-2721, the prolactin concentration in rats implanted with DES pellets ($W_{1.5d}$) was 8.8-fold higher ($p<0.01$) than that in rats without DES ($W_{1.5c}$). The hyperprolactinemia by DES in group $W_{1.5d}$ was decreased ($p<0.01$) to the level of that in group $W_{1.5c}$ by the treatment with DES pellets combined with tamoxifen ($W_{1.5dt}$).

In the irradiated rats previously injected with saline ($S_{1.5d}$) or WR-2721 ($W_{1.5d}$), the serum estradiol-17β concentration was low on long-term treatment with DES, compared with the corresponding control groups without DES ($S_{1.5c}$ and $W_{1.5c}$), and this low level of estrogen recovered during the implantation of DES pellets combined with tamoxifen. However, there were no significant differences between group $S_{1.5d}$ and group $S_{1.5c}$ ($p=0.596$), group $S_{1.5d}$ and

Table 2. Mammary tumourigenesis in rats treated with WR-2721 prior to irradiation and with tamoxifen during the promotion stage.

Group	No. of tumours*			Latency period (months)	No. of tumours/rat	Iball's index
	FA	AC	Total			
S_{0c}	1	0	1	12.0	1.0	1.1
S_{0d}	4	3	7	7.7 ± 0.6	1.2 ± 0.2	12.9
$S_{1.5d}$	15	11	26	7.4 ± 0.6	1.5 ± 0.3	38.3
$S_{1.5c}$	7	3	10	9.3 ± 1.4	1.7 ± 0.5	9.2
$S_{1.5dt}$	1	0	1	11.9	1.0	1.7
$W_{1.5d}$	8	7	15	9.5 ± 0.3†	1.2 ± 0.1	18.3
$W_{1.5c}$	1	3	4	8.4 ± 2.5	1.3 ± 0.3	5.6
$W_{1.5dt}$			0	—	—	—

Abbreviations and treatment in each group were summarized in table 1.
*FA, fibroadenoma; AC, adenocarcinoma.
†Significant difference ($p<0.05$) from group $S_{1.5d}$ by Scheffés test.

Table 3. Hormone concentration in serum of rats at the end of the experiments.

Group	LH (ng/ml)	FSH (ng/ml)	TSH (ng/ml)	Prolactin (ng/ml)	Estradiol-17β (pg/ml)	Progesterone (ng/ml)
S_{0c}	0.58±0.15	2.6±0.5	1.7±0.5	96±12‡	14.9±4.5	129.8±12.1
S_{0d}	0.33±0.03†	6.8±0.6†	1.7±0.4	305±125	2.7±0.8	85.1±5.3
$S_{1.5c}$	0.50±0.07	2.4±0.7	1.8±0.2	95±19	13.5±10.3	122.2±27.4
$S_{1.5d}$	0.30±0.06†	5.2±1.1	2.1±0.4	324±117†	7.0±2.7	117.8±24.5
$S_{1.5dt}$	0.26±0.06*	7.1±2.2†	2.6±0.4	59±14‡	30.5±18.0	38.3±17.9†
$W_{1.5c}$	0.34±0.05†	6.0±0.4	1.1±0.2	71±11	11.3±4.2	250.6±33.9*
$W_{1.5d}$	0.24±0.02*	3.2±0.3	2.5±0.1§	623±95*,§	4.6±1.6	36.8±7.7*,§
$W_{1.5dt}$	0.28±0.06*	7.1±1.8†	2.4±0.5¶	85±18‖	12.9±11.1	68.6±15.1§

Abbreviations and treatment in each group were summarized in table 1.
*Significant difference ($p<0.01$) from group $S_{1.5c}$ by Scheffés test.
†Significant difference ($p<0.05$) from group $S_{1.5c}$ by Scheffés test.
‡Significant difference ($p<0.05$) from group $S_{1.5d}$ by Scheffés test.
§Significant difference ($p<0.01$) from group $W_{1.5c}$ by Scheffés test.
¶Significant difference ($p<0.05$) from group $W_{1.5c}$ by Scheffés test.
‖Significant difference ($p<0.01$) from group $W_{1.5d}$ by Scheffés test.

group $S_{1.5dt}$ ($p=0.065$), group $W_{1.5d}$ and group $W_{1.5c}$ ($p=0.564$) or group $W_{1.5d}$ and group $W_{1.5dt}$ ($p=0.476$). Following treatment with DES, the progesterone concentration in the irradiated rats previously injected with WR-2721 ($W_{1.5d}$) was reduced to 15% ($p<0.01$) of that observed in rats with cholesterol ($W_{1.5c}$). But, the progesterone concentration of rats in group $S_{1.5d}$ was comparable ($p=0.887$) to that in the corresponding control group ($S_{1.5c}$).

3.3. *Biological changes during the experiments*

The body weight in saline ($S_{1.5d}$, $p<0.01$) or WR-2721 ($W_{1.5d}$, $p<0.01$)-injected rats receiving DES was reduced to 60–70% of that in the control rats ($S_{1.5c}$ or $W_{1.5c}$) implanted with cholesterol pellets, in spite of the similar food intake (table 4). No increase in body weight was observed after administration of tamoxifen together with DES ($S_{1.5dt}$ and $W_{1.5dt}$), compared with in rats in group $S_{1.5d}$ and $W_{1.5d}$, respectively. The saline ($S_{1.5d}$) or WR-2721 ($W_{1.5d}$)-treated rats receiving DES had hypertrophied pituitary glands compared with the corresponding control groups ($S_{1.5c}$ and $W_{1.5c}$), but a significant difference ($p<0.05$) was observed only between groups $W_{1.5d}$ and $W_{1.5c}$. The DES-induced hypertrophy of pituitary glands was inhibited ($p<0.05$) by the administration of DES pellets combined with tamoxifen ($W_{1.5dt}$). The weight of ovaries in saline-injected rats receiving DES ($S_{1.5d}$) decreased to about 60% ($p<0.01$) of that in the control rats receiving cholesterol ($S_{1.5c}$), and did not recover on administration of the DES pellets combined with tamoxifen ($S_{1.5dt}$). The same findings were observed in WR-2721-injected rats treated with DES alone, or with a combination of DES and tamoxifen. No hepatic or uterine tumours were obtained in the rats ($S_{1.5dt}$ and $W_{1.5dt}$) implanted with DES pellets combined with tamoxifen.

Table 4. Body weight and organ weight of rats at the end of the experiments.

Group	Body weight (g)	Liver (g)	Uterus (mg)	Ovaries (mg)	Pituitary gland (mg)
S_{0c}	377±11	15.5±0.7	579±117	96.8±11.9	16.2±1.2
S_{0d}	274±19*	11.8±0.7*	489±39	84.0±3.4	19.0±4.0
$S_{1.5c}$	369±12	15.2±1.0	559±71	96.4±8.5	16.0±2.0
$S_{1.5d}$	271±13*	13.4±0.5	445±31	54.5±6.9*	21.2±1.7
$S_{1.5dt}$	279±7*	11.2±0.3*	387±113†	66.5±4.7*	13.6±0.6
$W_{1.5c}$	392±8	12.8±0.4*	665±73	105.7±7.9	20.9±6.1
$W_{1.5d}$	243±8*,‡	12.8±0.4†	521±47	60.5±1.8*,‡	67.3±35.6§
$W_{1.5dt}$	259±6*,‡	11.2±0.5*	639±137	71.0±6.1*,‡	17.9±7.5¶

Abbreviations and treatment in each group were summarized in table 1.
*Significant difference ($p<0.01$) from group $S_{1.5c}$ by Scheffés test.
†Significant difference ($p<0.05$) from group $S_{1.5c}$ by Scheffés test.
‡Significant difference ($p<0.01$) from group $W_{1.5c}$ by Scheffés test.
§Significant difference ($p<0.05$) from group $W_{1.5c}$ by Scheffés test.
¶Significant difference ($p<0.05$) from group $W_{1.5d}$ by Scheffés test.

4. Discussion

Our focus has been on the prevention of radiation-induced mammary tumours by synthetic chemicals and natural products. This area has received less attention than the prevention of mammary tumours induced by chemical carcinogens such as DMBA and N-methyl-N-nitrosourea (MNU) (El-Bayoumg 1994). After irradiation with 2.6 Gy γ-rays at day 20 of pregnancy, treatment with lipid lowering agents such as bezafibrate (Inano *et al.* 1996b) or simvastatin (Inano *et al.* 1997), during the promotion by DES reduced the incidence of mammary tumour from about 90% in control to 27% or 36%, respectively. In other experiments on chemoprevention of radiation-induced mammary tumours done in our laboratory, similar effects of tumour prevention were seen on the administration of dietary dehydroepiandrosterone which has multifunctional activities (Inano *et al.* 1995a). Also, we have previously evaluated the chemopreventive effects of curcumin, a natural antioxidant product in rhizomes of *Curcuma longa* Linn, on the DES-induced promotion of tumour in mammary glands initiated with radiation (Inano *et al.* 1999). The administration of dietary curcumin suppressed the incidence from 85% in control to 28%. The goal of our programme is the complete prevention of radiation-induced mammary tumours, but a tumour-free state can not be obtained in the irradiated rats by the treatment with bezafibrate, simvastatin, dehydroepiandrosterone and curcumin, respectively, during the promotion phase with DES. The present experiments used lactating rats which had a similar susceptibility to radiation as developed mammary glands of pregnant rats (Inano *et al.* 1996a). The high incidence (85%) of mammary tumours in rats ($S_{1.5d}$) irradiated at day 21 of lactation and then administered with DES as promoter was decreased to 52.2% by treatment with WR-2721 prior to irradiation ($W_{1.5d}$), and also to 4.4% by addition of tamoxifen to DES pellets ($S_{1.5dt}$).

As stated in the Introduction, an inhibitory effect of tamoxifen on radiation-induced mammary tumours was reported by two groups, Welsch *et al.* (1981) and Lemon *et al.* (1989). Treatment of female rats with tamoxifen for 60 days, i.e. 30 days before and 30 days after irradiation, or for 60 days beginning at 30 days after irradiation with 4 Gy γ-rays reduced the incidence of adenocarcinoma from 55% in control to 24% or 36%, respectively (Welsch *et al.* 1981). The investigation by the former group reported the results of effects of short-term tamoxifen treatment on the promotion of radiation-induced tumours. The latter group have reported that a long-term treatment of tamoxifen started two weeks after irradiation suppressed the mammary cancer incidence from 83% in control to 14% (Lemon *et al.* 1989). From their results, tamoxifen is recognized to have anti-initiation and anti-promotion activities in radiation-induced mammary tumourigenesis. In the present study, treatment with DES pellets combined with tamoxifen caused a significant reduction of prolactin concentration compared with rats implanted with DES pellets, as a tumour promoter. Lieberman *et al.* (1983a, b) have demonstrated that the inhibition of estrogen-stimulated prolactin synthesis by anti-estrogen, tamoxifen, caused by a competitive interaction with estrogen to ER in pituitary cells. Tamoxifen treatment was consistently more effective in suppressing mammary tumourigenesis in mice than early ovariectomy (Jordan *et al.* 1991). In a previous study, rats were ovariectomized bilaterally before and after sexual maturation and then were irradiated to evaluate the role of ovarian hormones in the sensitivity for the initiation of mammary tumours by radiation (Inano *et al.* 1995b, Yamanouchi *et al.* 1995). The tumour incidence of the ovariectomized rats was 26% and 30%, respectively. The mammary glands of the ovariectomized rats were exposed to estrogens synthesized in extraovarian tissues, such as adipocytes (Cleland *et al.* 1983, Rink *et al.* 1996). Therefore, mammary tumourigenesis was not suppressed completely by ovariectomy before irradiation. The main preventive effect of tamoxifen appears to be the competitive inhibition of DES binding to ER in the pituitary gland and/or mammary gland.

In the initiation phase of radiation-induced carcinogenesis, cellular DNA is damaged either directly or by radiation-produced reactive free radical oxygen. The generation of reactive free radical oxygen by radiation exposure has been considered one of the most important mechanisms of radiation-induced carcinogenesis. WR-2721 is a pro-drug which requires dephosphorylation by alkaline phosphatase to generate a free aminothiol form, WR-1065 (Nakamura *et al.* 1987), before it becomes an active radical scavenger (Littlefield *et al.* 1993). Also, the modes of action of WR-2721 include induction of intracellular hypoxia by oxidation of the thiol moiety of WR-1065 molecule (Purdie *et al.* 1983). Moreover, protection of mammalian cells from the cytotoxic effects of γ-rays by WR-1065 is accompanied by a substantial reduction in the yield of single- and double-strand breaks in the DNA (Lohman *et al.* 1970, Murray *et al.* 1980, Sigdestad *et al.* 1987). WR-1065 may afford protection against radiation-induced mutation through polyamine-like processes, e.g. stabilization of chromatin structure and influence on DNA repair systems (Clark *et al.* 1997). Little is known about the inhibitory effect of WR-2721 on

radiation-induced tumours, such as sarcoma (Milas *et al.* 1984) and lymphoreticular tumours (Grdina *et al.* 1991). Recently, we evaluated the preventive effect of WR-2721 on the development of radiation-induced mammary tumours in rats. Administration of WR-2721 prior to irradiation with 1.5 and 2.6 Gy at day 20 of pregnancy decreased the incidence from 71.4% in control to 23.8%, and from 92.3% in control to 43.5%, respectively, in the presence of DES, as a tumour-promoting agent (Inano *et al.* 2000). Protection against radiation-induced tumours by WR-2721 was observed only when the radioprotector was present in tissues during irradiation (Grdina *et al.* 1985, 1989). However, it has been very difficult to completely prevent the development of radiation-induced mammary tumours using the synthetic radical scavenger alone, because of its toxicity. In this work, we have completely prevented the formation of mammary tumours in rats by a combination treatment which was administered with WR-2721 prior to irradiation and then with tamoxifen during the period of DES-dependent promotion.

Acknowledgements

This work was partly supported by a project grant for Experimental Studies on Radiation Health, Detriment and its Modifying Factors and also by a grant from the Special Program for Bioregulation, of the National Institute of Radiological Sciences.

References

Clark, L. S., Albertini, R. J. and Nicklas, J. A., 1997, The aminothiol WR-1065 protects T lymphocytes from ionizing radiation-induced deletions of the HPRT gene. *Cancer Epidemiology, Biomarkers and Prevention*, **6,** 1033–1037.

Cleland, W. H., Mendelson, C. R. and Simpson, E. R., 1983, Aromatase activity of membrane fractions of human adipose tissue stromal cells and adipocytes. *Endocrinology*, **113,** 2155–2160.

Early Breast Cancer Trialist's Collaborative Group, 1998, Tamoxifen for early breast cancer. An overview of the randomized trials. *Lancet*, **351,** 1451–1467.

El-Bayoumg, K., 1994, Evaluation of chemopreventive agents against breast cancer and proposed strategies for future clinical intervention trials. *Carcinogenesis*, **15,** 2395–2420.

Fisher, B., Costantino, J. P., Wickerham, D. L., Redmond, C. K., Kavanah, M., Cronin, W. M., Vogel, V., Robidoux, A., Dimitrov, N., Atkins, J., Daly, M., Wieand, S., Tan-Chiu, E., Ford, L., Wolmark, N. and Other National Surgical Adjuvant Breast and Bowel Project Investigators, 1998, Tamoxifen for prevention of breast cancer: Report of the national surgical adjuvant breast and bowel project P-1 study. *Journal of the National Cancer Institute*, **90,** 1371–1388.

Grdina, D. J., Nagy, B., Hill, C. K., Wells, R. L. and Peraino, C., 1985, The radioprotector WR-1065 reduces radiation-induced mutations at the hypoxanthine-guanine phosphoribosyl transferase locus in V79 cells. *Carcinogenesis*, **6,** 929–931.

Grdina, D. J., Sigdestad, C. P. and Carnes, B. A., 1989, Protection by WR-1065 and WR-151326 against fission-neutron-induced mutations at the HGPRT locus in V79 cells. *Radiation Research*, **117,** 500–510.

Grdina, D. J., Carnes, B. A., Grahn, D. and Sigdestad, C. P., 1991, Protection against late effects of radiation by S-2-(3-aminopropylamino)ethylphosphorothioic acid. *Cancer Research*, **51,** 4125–4130.

Iball, J., 1939, The relative potency of carcinogenic compounds. *American Journal of Cancer*, **35,** 188–190.

Inano, H., Ishii-Ohba, H., Suzuki, K., Yamanouchi, H., Onoda, M. and Wakabayashi, K., 1995a, Chemoprevention by dietary dehydroepiandrosterone against promotion/progression phase of radiation-induced mammary tumourigenesis in rats. *Journal of Steroid Biochemistry and Molecular Biology*, **54,** 47–53.

Inano, H., Onoda, M., Inafuku, N., Kubota, M., Kamada, Y., Osawa, T., Kobayashi, H. and Wakabayashi, K., 1999, Chemoprevention by curcumin during promotion stage of tumorigenesis of mammary glands in rats irradiated with gamma-rays. *Carcinogenesis*, **20,** 1011–1018.

Inano, H., Onoda, M., Suzuki, K., Kobayashi, H. and Wakabayashi, K., 2000, Inhibitory effects of WR-2721 and cysteamine on tumor initiation of developed mammary glands in pregnant rats by radiation. *Radiation Research*, **153,** 68–74.

Inano, H., Suzuki, K., Ishii-Ohba, H., Ikeda, K. and Wakabayashi, K., 1991, Pregnancy-dependent initiation in tumourigenesis of Wistar rat mammary glands by ^{60}Co-irradiation. *Carcinogenesis*, **12,** 1085–1090.

Inano, H., Suzuki, K., Onoda, M. and Wakabayashi, K., 1997, Anti-carcinogenic activity of simvastatin during the promotion phase of radiation-induced mammary tumorigenesis of rats. *Carcinogenesis*, **18,** 1723–1727.

Inano, H., Suzuki, K., Onoda, M. and Yamanouchi, H., 1996a, Susceptibility of fetal, virgin, pregnant and lactating rats for the induction of mammary tumors by gamma-rays. *Radiation Research*, **145,** 708–713.

Inano, H., Suzuki, K. and Wakabayashi, K., 1996b, Chemoprevention of radiation-induced mammary tumors in rats by bezafibrate administered together with diethylstilbestrol as a promoter. *Carcinogenesis*, **17,** 2641–2646.

Inano, H., Yamanouchi, H., Suzuki, K., Onoda, M. and Wakabayashi, K., 1995b, Estradiol-17β as an initiation modifier for radiation-induced mammary tumourigenesis of rats ovariectomized before puberty. *Carcinogenesis*, **16,** 1871–1877.

Jordan, V. C., 1976, Effect of tamoxifen (ICI46,474) on initiation and growth of DMBA-induced rat mammary carcinoma. *European Journal of Cancer*, **12,** 419–424.

Jordan, V. C., Lababidi, M. K. and Langan-Fahey, S., 1991, Suppression of mouse mammary tumorigenesis by long-term tamoxifen therapy. *Journal of National Cancer Institute*, **83,** 492–496.

Lemon, H. M., Kumar, P. F., Peterson, C., Rodriguez-Sierra, J. F. and Abbo, K. M., 1989, Inhibition of radiogenic mammary carcinoma in rats by estriol or tamoxifen. *Cancer*, **63,** 1685–1692.

Lieberman, M. E., Gorski, J. and Jordan, V. C., 1983a, An estrogen receptor model to describe the regulation of prolactin synthesis by antiestrogens *in vitro*. *Journal of Biological Chemistry*, **258,** 4741–4745.

Lieberman, M. E., Jordan, V. C., Fritsch, M., Santos, M. A. and Gorski, J., 1983b, Direct and reversible inhibition

of estradiol-stimulated prolactin synthesis by antiestrogens *in vitro*. *Journal of Biological Chemistry*, **258,** 4734–4740.

LITTLEFIELD, L. G., JOINER, E. E., COLYER, S. P., SALLAM, F. and FROME, E. L., 1993, Concentration-dependent protection against X-ray-induced chromosome aberrations in human lymphocytes by the aminothiol WR-1065. *Radiation Research*, **133,** 88–93.

LIU, S.-C., MURLEY, J. S., WOLOSCHAK, G. and GRDINA, D. J., 1997, Repression of c-myc gene expression by the thiol and disulfide forms of the cytoprotector amifostine. *Carcinogenesis*, **18,** 2457–2459.

LOHMAN, P. H. M., VOS, O., VAN SLUIS, C. V. and COHEN, J. A., 1970, Chemical protection against breaks induction in DNA of human and bacterial cells by X-irradiation. *Biochimica et Biophysica Acta*, **224,** 339–352.

MILAS, L., HUNTER, N., STEPHENS, L. C. and PETERS, L. J., 1984, Inhibition of radiation carcinogenesis in mice by S-2-(3-aminopropylamino)ethylphosphorothioic acid. *Cancer Research*, **44,** 5567–5569.

MURRAY, D., VAN ANKEREN, S. C., MILAS, L. and MEYN, R. E., 1980, Radioprotective action of WR-1065 on radiation-induced DNA strand breaks in cultured Chinese hamster ovary cells. *Radiation Research*, **113,** 155–170.

NAKAMURA, J., SHAW, L. M. and BROWN, D. Q., 1987, Hydrolysis of WR-2721 by mouse liver cell fractions. *Radiation Research*, **109,** 143–152.

PURDIE, J. W., INHABER, E. R., SCHNEIDER, H. and LABELLE, J., 1983, Interaction of cultured mammalian cells with WR-2721 and its thiol WR-1065: Implications for mechanisms of radioprotection. *International Journal of Radiation Biology*, **43,** 517–527.

RINK, J. D., SIMPSON, E. R., BARNARD, J. J. and BULUN, S. E., 1996, Cellular characterization of adipose tissue from various body sites of women. *Journal of Clinical Endocrinology and Metabolism*, **81,** 2443–2447.

RUSSO, J., GUSTERON, B. A., ROGERS, A. E., RUSSO, I. H. and WELLINGS, S. R., 1990, Comparative study of human and rat mammary tumorigenesis. *Laboratory Investigation*, **61,** 244–278.

SIGDESTAD, C. P., TREACEY, S. H., KNAPP, L. A. and GRDINA, D. J., 1987, The effect of 2-[(aminopropyl)amino]ethanethiol (WR-1065) on radiation induced DNA double strand damage and repair in V79 cells. *British Journal of Cancer*, **55,** 477–482.

SUZUKI, K., ISHII-OHBA, H., YAMANOUCHI, H., WAKABAYASHI, K., TAKAHASHI, M. and INANO, H., 1994, Susceptibility of lactating rat mammary glands to gamma-ray-irradiation-induced tumorigenesis. *International Journal of Cancer*, **56,** 413–417.

WATANABE, G., TAYA, K. and SASAMOTO, S., 1990, Dynamics of ovarian inhibin secretion during the oestrous cycles of rats. *Journal of Endocrinology*, **126,** 151–157.

WELSCH, C. W., GOODRICH-SMITH, M., BROWN, C. K., MIGLORIE, N. and CLIFTON, K. H., 1981, Effect of an estrogen antagonist (tamoxifen) on the initiation and progression of γ-irradiation-induced mammary tumors in female Sprague–Dawley rats. *European Journal of Cancer and Clinical Oncology*, **17,** 1255–1258.

YAMANOUCHI, H., ISHII-OHBA, H., SUZUKI, K., ONODA, M., WAKABAYASHI, K. and INANO, H., 1995, Relationship between stages of mammary development and sensitivity to gamma-ray irradiation in mammary tumorigenesis in rats. *International Journal of Cancer*, **60,** 230–234.

YUHAS, J. M. and STORER, J. B., 1969, Chemoprotection against three models of radiation death in the mouse. *International Journal of Radiation Biology*, **15,** 233–237.

Carcinogenesis vol.21 no.10 pp.1835–1841, 2000

Potent preventive action of curcumin on radiation-induced initiation of mammary tumorigenesis in rats

Hiroshi Inano[1,6], Makoto Onoda[1], Naoshi Inafuku[2], Megumi Kubota[2], Yasuhiro Kamada[2,5], Toshihiko Osawa[3], Hisae Kobayashi[4] and Katsumi Wakabayashi[4]

[1]First Research Group, National Institute of Radiological Sciences, 9-1 Anagawa-4-chome, Inage-ku, Chiba-shi 263-8555, [2]Ryukyu Bio-Resource Development Co. Ltd, 606-2 Toyohara, Motobu-cho 905-0204, Okinawa, [3]Laboratory of Food and Biodynamics, Nagoya University Graduate School of Bioagricultural Sciences, Furo-cho, Chikusa-ku, Nagoya-shi 464-8601 and [4]Institute for Molecular and Cellular Regulation, Gunma University, Showa-machi, Maebashi-shi 371-8512, Japan

[5]Present address: Okinawa Industrial Technology Center, 12-2 Suzaki, Gushikawa-shi 904-2234, Okinawa, Japan

[6]To whom correspondence should be addressed
Email: inano@nirs.go.jp

This investigation evaluated the preventive effect of curcumin on radiation-induced tumor initiation in rat mammary glands. Fifty-four female rats were mated and then divided into two groups at day 11 of pregnancy. As the control group, 27 rats were fed a basal diet during the experimental period. As the experimental group, 27 rats were fed a diet containing 1% curcumin between day 11 of pregnancy and parturition (day 23 of pregnancy). All rats of both groups received whole body irradiation with 1.5 Gy γ-rays from a ^{60}Co source at day 20 of pregnancy and were then implanted with a diethylstilbestrol pellet 1 month after weaning. A high incidence (70.3%) of mammary tumorigenesis was observed in the control group. The tumor incidence (18.5%) was significantly reduced in the rats fed curcumin during the initiation stage. The appearance of the first palpable tumor was delayed by 6 months in the curcumin-fed group and the average latent period until the appearance of mammary tumors was 2.5 months longer in the curcumin-fed group than in the control group. By histological examination, the proportion of adenocarcinoma (16.7%) in total tumors in the curcumin-fed rats was found to be decreased to half that (32.1%) in the control group. Compared with the control rats, the body weight of rats in the experimental group was decreased slightly by administration of the curcumin diet from day 11 of pregnancy, in spite of a similar intake of diet, but had recovered to the level of the control by the end of the experiment. At the time of irradiation, curcumin did not have any effect on organ weight or on the development and differentiation of mammary glands of pregnant rats. In addition, the serum concentrations of fatty acids, thiobarbituric acid-reactive substances and ovarian and pituitary hormones, except LH, remained at the control level. Also, no change in litter size and body weight of pups born from curcumin-fed rats indicated no toxicity of curcumin. These results suggest that curcumin does not have any side-effects and is an effective agent for chemoprevention acting at the radiation-induced initiation stage of mammary tumorigenesis.

Abbreviations: curcumin, 1,7-bis(4′-hydroxy-3′-methoxyphenyl)-1,6-heptadiene-3,5-dione; DES, diethylstilbesterol; DMBA, 7,12-dimethylbenz[*a*]anthracene; ER, estrogen receptor; FSH, follicle-stimulating hormone; IL, interleukin; iNOS, inducible nitric oxide synthase; IκB, inhibitory protein κB; LH, luteinizing hormone; LPS, lipopolysaccharide; MDA, malondialdehyde; NF-κB, nuclear factor κB; resveratrol, 3,5,4′-trihydroxy-*trans*-stilbene; TBARS, thiobarbituric acid-reactive substances; WR-2721, *S*-2-(3-aminopropylamino)ethylphosphorothioic acid.

Introduction

Tumor initiation by radiation in mammary glands is dependent upon cell stage, because estrogen is a direct or indirect sensitizer for tumor initiation by radiation (1,2). Previous studies in our laboratory have demonstrated that administration of aminothiols, such as *S*-2-(3-aminopropylamino)ethylphosphorothioic acid (WR-2721) and cysteamine, prior to irradiation has a potent preventive effect at the initiation stage of mammary tumorigenesis (3). The protection against radiation offered by WR-2721 (4) and cysteamine (5) is considered to be due to the scavenging of free radicals produced by the interaction of biological molecules and radiation. WR-2721 and cysteamine are toxic at effective doses (6,7), therefore, we have undertaken an evaluation of less toxic phytochemicals whose anti-oxidant properties may make the potential chemopreventive agents for radiation-induced mammary tumorigenesis. A recent study has indicated that phytochemicals with anti-oxidant and anti-inflammatory properties can inhibit tumor initiation and promotion in mouse skin (8). 1,7-Bis(4′-hydroxy-3′-methoxyphenyl)-1,6-heptadiene-3,5-dione (curcumin), a major pigment in turmeric obtained from the powdered rhizomes of *Curcuma longa* L., possesses both anti-inflammatory and anti-oxidant properties (9) and has no toxicity (10). In the 7,12-dimethylbenz[*a*]anthracene (DMBA)-induced mammary tumor model, when rats were fed a diet containing 1% curcumin prior to dosing with the chemical carcinogen, the incidence of animals with tumors was not significantly altered (11). Because radiation is the only proven relevant human breast carcinogen, we have attempted to evaluate the preventive effects of curcumin on radiation-induced initiation of mammary tumorigenesis and on estrogen-induced tumor promotion in rat mammary glands initiated with radiation in our research series. Our previous study suggested that when administered orally for a long period, curcumin has potent preventive activity during tumor promotion in radiation-initiated mammary tumorigenesis (12). In the present study we have carried out further investigations of the chemopreventive effects of dietary curcumin on radiation-induced initiation.

Materials and methods

Materials

Diethylstilbestrol (DES), cholesterol and sulfatase were purchased from Sigma (St Louis, MO). β-Glucuronidase was purchased from Wako Pure Chemical Industries (Osaka, Japan). Pellets were prepared in a medical Silastic tube (Dow Corning, Midland, MI) and were filled with 3 mg DES mixed with

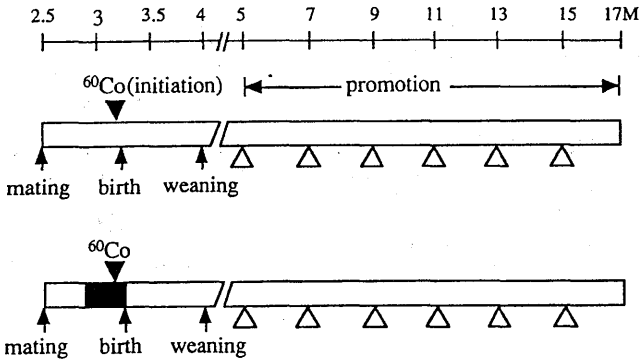

Fig. 1. Experimental schedule in this study. Open bar, control diet (MB-1); closed bar, diet containing 1% curcumin; closed arrowhead, whole body irradiation with 1.5 Gy γ-rays at day 20 of pregnancy for tumor initiation; open arrowhead, implantation with DES pellet for tumor promotion; M, months old.

27 mg cholesterol. Curcumin, commonly used in food as a coloring agent, was obtained from Aldrich Chemical Co. (Milwaukee, WI). Diet containing 1% (w/w) curcumin was prepared in biscuit form by Funabashi Farm (Chiba, Japan). A basal diet (MB-1) of the same form was used for the control experiments. The major components of MB-1 are as follows: total carbohydrate, 54.1%; protein, 24.6%; fat, 4%; fiber, 3.8%; moisture, 7.7%; ash, 5.8%. [2,4,6,7-^{3}H]Estradiol-17β (sp. act. 4 TBq/mmol) was purchased from Du Pont/NEN Research Products (Boston, MA).

Animals and treatment

The rats used in the present study were treated and handled according to the *Recommendations for Handling of Laboratory Animals for Biomedical Research* compiled by the Committee on the Safety and Handling Regulations for Laboratory Animal Experiments in our Institute. Wistar-MS rats from a stock colony of Nippon SLC Co. (Hamamatsu, Japan) were kept at 23 ± 1°C in a controlled environment (14 h light/10 h dark). They received water and food *ad libitum*. For experiments on the prevention of mammary tumors, 54 female rats, 2.5 months old, were mated and then randomized into two groups of 27 rats each at day 11 of pregnancy (the presence of a vaginal plug denoting day 1). The control rats were fed a basal diet (MB-1) throughout the experimental period, received whole body irradiation with 1.5 Gy γ-rays (0.15 Gy/min) from a ^{60}Co source at day 20 of pregnancy and were then implanted with a DES pellet at 1 month after weaning (Figure 1). The experimental group rats were fed the diet containing 1% curcumin between day 11 of pregnancy and parturition (day 23 of pregnancy) and implanted with a DES pellet at 1 month after termination of nursing. The pellets were replaced every 8 weeks. The rate of release of DES from the pellet was 0.38 ± 0.01 μg/day (13). The rats were examined for palpable mammary tumors for 1 year starting from the date of pellet implantation. When mammary tumors >2 cm in diameter were detected, the rats were killed by CO_2 asphyxiation and the tumors were removed for further observation. Each mammary tumor was fixed in 10% neutral buffered formalin for histopathological examination. The remaining rats were killed 1 year after administration of the DES pellet and were autopsied to ascertain whether they had any non-palpable mammary tumors and pituitary tumors. Tumor incidence was calculated from the number of rats that developed tumors within 1 year. Iball's index of mammary tumors was calculated as follows: the ratio of incidence (%) to the average latency period in days×100 (14). For studies on the morphological and biochemical effects of the treatment with curcumin, separate experiments were carried out for which 20 pregnant rats were divided into two groups of 10 rats each at day 11 of pregnancy. Control rats were fed the basal diet and the curcumin group the diet containing 1% curcumin. At day 20 of pregnancy, corresponding to the time of irradiation for tumor initiation described above, six rats in each group were killed for biochemical and morphological studies. The remaining four dams in each group bore pups at full-term gestation. Body weights of dams and newborn pups were measured after parturition.

Assays

A blood sample, collected from each rat by cardiocentesis under anesthesia, was allowed to clot and was centrifuged to obtain serum. The sera were immediately frozen and stored at –80°C until the assay was started. Concentrations of prolactin, luteinizing hormone (LH) and follicle-stimulating hormone (FSH) were determined with NIDDK radioimmunoassay kits (the National Hormone and Pituitary Program, Rockville, MD). The serum concentrations of estradiol-17β and progesterone were assayed with commercially available radioimmunoassay kits. For assays of total curcuminoids (free form plus conjugates), serum was incubated with 10 mM McIlvaine buffer (pH 5.0) containing 20% ascorbic acid, 0.17% EDTA, 500 U β-glucuronidase and 40 U sulfatase at 37°C for 60 min (15). Curcumin and its metabolites were extracted with ethylacetate and then analyzed by HPLC with a multiwavelength detector on a Develsoil ODS-HG-5 column (4.6×250 mm; Nomura Chemical Co., Seto, Japan) eluted with a mixture of acetonitrile:water (1:1 v/v) containing 0.1% trifluoroacetic acid at a flow rate of 1 ml/min. The chromatogram was monitored at a wavelength of 430 nm for detection of curcumin and at 280 nm for tetrahydrocurcumin (16). Fatty acids were extracted from serum with hexane and were treated with 14% trifluorobenzene dissolved in methanol: methanol:benzene (35:35:30 v/v/v) for 10 min in boiling water for esterification. The methyl esters of fatty acids were analyzed by gas chromatography with a hydrogen flame ionization detector (17). For assay of lipid peroxidation products, the serum was mixed with 20% trichloroacetic acid and 0.67% thiobarbituric acid and heated for 15 min in boiling water. The concentration of thiobarbituric acid-reactive substances (TBARS) extracted with n-butanol was estimated by absorption at 530 nm. TBARS were expressed as malondialdehyde (MDA) equivalents, using freshly produced MDA as the standard prepared from 1,1,3,3-tetramethoxypropane with HCl (18). The estrogen receptor (ER) in mammary glands was analyzed by the dextran-coated charcol method, using [2,4,6,7-^{3}H]estradiol-17β (19) as the radioligand. Maximum binding sites for the receptor were determined by a Scatchard plot analysis (20).

Histological examination

The removed mammary glands and mammary tumors were immediately fixed in 10% formalin neutralized with 0.1 M phosphate buffer (pH 7.2). Paraffin sections (4 μm thick) were prepared and stained with hematoxylin and eosin. The tumors were classified as fibroadenoma or adenocarcinoma according to the criteria for the classification of mammary tumors (21).

Statistical analysis

Statistical analyses were conducted using the χ^2 test for incidence of mammary tumors and for the proportion of adenocarcinoma and fibroadenoma and Student's *t*-test for the level of significance of the difference between two mean values of body weight, organ weight, hormone and fatty acid concentrations, latent period and multiplicity. The cumulative proportions of rats with tumors (incidence curves) were calculated by the product-limit method where rats which died or were killed without mammary tumors were included and the difference between groups was tested for statistical significance by the Mantel–Cox test. The analyses were performed using StatView-J4.5 software (Abacus Concepts, Berkeley, CA). *P* values <5% were considered significant.

Results

Development of irradiation-induced mammary tumors in rats fed curcumin

When the control rats received whole body irradiation with 1.5 Gy γ-rays, a tumor initiator, at day 20 of pregnancy and then were implanted with DES, a tumor promoter, after weaning, a high incidence (70.3%) of tumorigenesis of the mammary glands was observed. The tumor incidence (18.5%) in the rats fed curcumin during the initiation stage was about 25% ($P < 0.0001$) of that in the control rats (Table I). The administration of dietary curcumin during initiation by irradiation significantly decreased the cumulative incidence curve of the mammary tumors for the 1 year period ($P < 0.0001$), compared with the control diet group (Figure 2). The appearance of the first palpable tumors was delayed by 6 months in the curcumin-fed group, compared with the control group. Also, the average latent period until the appearance of total mammary tumors was delayed by ~2.5 months in the curcumin-fed group (11.2 ± 0.2 months) compared with the control group (8.7 ± 0.4 months) ($P < 0.005$). There were no significant differences ($P = 0.495$) between the two groups in the number of mammary tumors per tumor-bearing rat. Iball's index for overall development of mammary tumors in the curcumin-fed rats was 20% of that in the control group. Histological examination was performed for all of the mammary tumors that developed in the control and curcumin-fed rats.

Table I. Development of mammary and pituitary tumors in irradiated rats fed curcumin during the initiation stage

Diet	No. of rats used	Mammary tumors							Pituitary tumours
		Rats with tumors (% incidence)	FA (%)	AC (%)	Total	Multiplicity[a,b]	Latency period[b] (months)	Iball's index	Rats with tumours (% incidence)
Control	27	19 (70.3%)	19 (67.9%)	9 (32.1%)	28	1.5 ± 0.2	8.7 ± 0.4	26.5	8 (29.6%)
Curcumin	27	5 (18.5 %)[c]	5 (83.3%)	1 (16.7%)	6	1.2 ± 0.2	11.2 ± 0.2[d]	5.0	5 (18.5%)[e]

[a]Number of mammary tumors/tumor-bearing rat.
[b]Mean ± SE.
[c]Significant difference ($P < 0.0001$) from the control group by the χ^2 test.
[d]Significant difference ($P < 0.005$) from the control group by Student's t-test.
[e]No significant difference ($P = 0.340$) from the control group by the χ^2 test.

Table II. Biological effect at the time of irradiation (day 20 of pregnancy) of curumin treatment

Diet	Body weight (g)	Liver (g)	Adrenal (mg)	Pituitary (mg)	Litter size (n)	Body weight of fetus (g)
Control ($n = 6$)	298 ± 6.3	13.7 ± 0.4	99.5 ± 3.7	10.5 ± 0.6	10.5 ± 0.8	2.05 ± 0.06
Curcumin ($n = 6$)	271 ± 6.7[a]	13.1 ± 0.4	105.0 ± 5.3	9.0 ± 0.5	10.5 ± 0.9	2.21 ± 0.07

[a]Significant difference ($P < 0.05$) from the control group by Student's t-test.

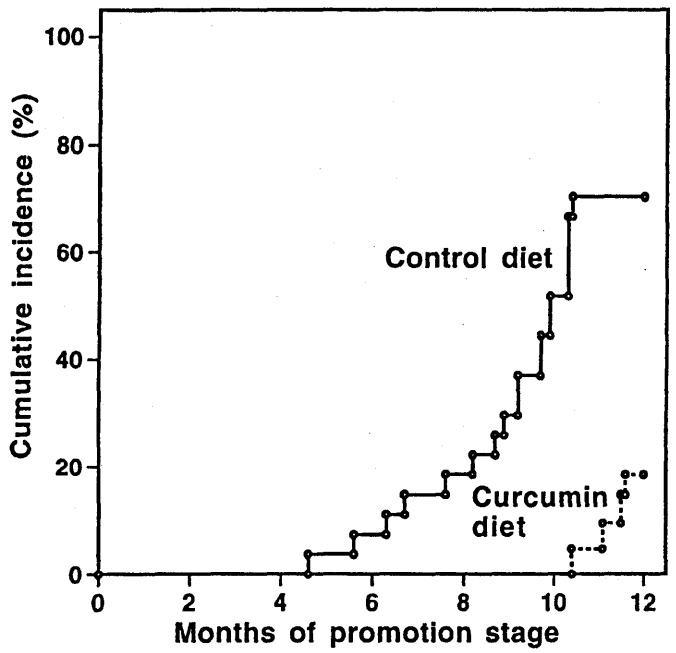

Fig. 2. Cumulative incidence of development of mammary tumors in irradiated rats treated with DES. Solid and dotted lines represent the control diet and the curcumin diet groups, respectively. Statistical evaluation of the cumulative proportion data (overall incidence curves) by the Mantel–Cox test yielded $P < 0.0001$, indicating a significant difference between the control diet and curcumin-containing diet groups during the observation period.

The proportion of adenocarcinoma and fibroadenoma in total tumors was 32.1 and 67.9%, respectively, in rats fed the control diet (Table I). In the curcumin-fed group, the proportion (16.7%) of adenocarcinoma was decreased to 50% of that in the control group. Conversely, the proportion (83.3%) of fibroadenoma was 1.2-fold higher than that in the control group. However, no significant difference ($P = 0.450$) in the proportion of adenocarcinoma and fibroadenoma was observed between the two groups with the χ^2 test.

Biological effects at the time of initiation of curcumin administration during pregnancy

Body weight of dams was decreased to 91% of that observed in rats fed the control diet by administration of the curcumin diet from day 11 of pregnancy, in spite of a similar intake of diet throughout the experiment. No change in weight of liver ($P = 0.262$), adrenal gland ($P = 0.378$) or pituitary gland ($P = 0.079$) of dams at day 20 of pregnancy was observed between the control and curcumin-fed groups (Table II). The litter size of curcumin-fed rats was comparable with that of the rats fed the control diet. In addition, the body weight of fetuses at day 20 of pregnancy was increased slightly by the administration of curcumin, but no significant difference was observed ($P = 0.109$). Also, the body weight (5.6 ± 0.1 g) of pups (1 day-old) born to curcumin-fed dams was the same as that of pups of the dams fed the control diet (5.6 ± 0.1 g).

Biochemical effects at the time of initiation of curcumin administration during pregnancy

Serum concentrations of ovarian and pituitary hormones were measured 10 days after the start of the administration of dietary curcumin, the time corresponding to initiation with radiation. No significant differences in estradiol-17β ($P = 0.677$) and progesterone ($P = 0.223$) concentrations were observed between the two groups (Table III). In addition, curcumin did not have any effect on the concentrations of prolactin ($P = 0.502$) and FSH ($P = 0.883$). However, the concentration of LH in the rats fed the curcumin diet was increased to 1.8-fold of that observed in rats fed the control diet ($P < 0.05$). No significant difference ($P = 0.592$) in TBARS was observed on administration of curcumin for 10 days. The serum concentration of curcumin in rats fed the curcumin diet was below the level detectable by HPLC (4 ng/ml). The tetrahydrocurcumin concentration was 39 ± 10 ng/ml in the curcumin-fed rats.

Table III. Serum concentrations of hormones, TBARS and curcumin at the time of irradiation (day 20 of pregnancy) in the rats fed curcumin

Substances assayed (units)	Control diet[a]	Curcumin diet[a]
Estradiol-17β (pg/ml)	33.1 ± 1.7	35.0 ± 4.6
Progesterone (ng/ml)	196.4 ± 11.6	214.3 ± 11.6
Prolactin (ng/ml)	2.9 ± 0.5	4.1 ± 1.6
LH (ng/ml)	0.23 ± 0.05	0.41 ± 0.06[b]
FSH (ng/ml)	4.13 ± 0.24	4.18 ± 0.23
TBARS (nmol MDA/ml)	12.1 ± 0.9	12.7 ± 0.8
Curcumin (ng/ml)	ND[c]	<4.0
Tetrahydrocurcumin (ng/ml)	ND[c]	39 ± 10

[a]Mean ± SE (n = 6).
[b]Significant difference ($P < 0.05$) from the control group by Student's t-test.
[c]Not detected.

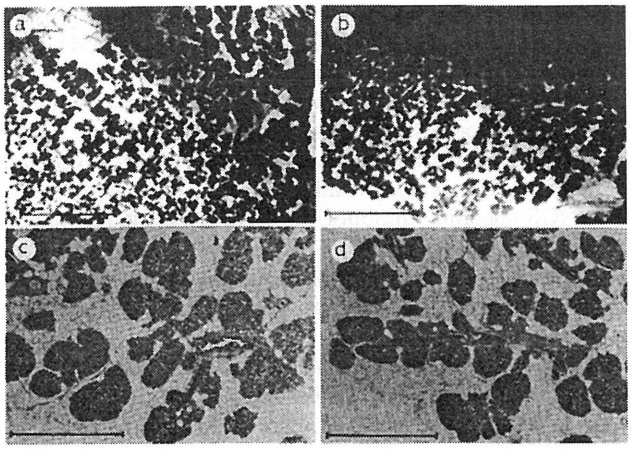

Fig. 3. Whole mount and histological observations in inguinal mammary glands of rats. (**a** and **c**) Control rats fed the basal diet (MB-1); (**b** and **d**) rats fed the diet containing 1% curcumin. Scale bars: a and b, 5 mm; c and d, 1 mm.

Histological observations of and number of ER in mammary glands at the time of initiation

Whole mounts of inguinal mammary glands corresponding to the time of irradiation were prepared to examine the effects of curcumin on development and differentiation of the glands in pregnant rats. On day 20 of pregnancy, mammary glands of rats fed the control diet showed many alveolar buds with branched lactiferous ducts (Figure 3a). The whole mounts showed that the mammary glands in pregnant rats fed the curcumin diet exhibited the same development as the glands of control rats (Figure 3b). On histological examination, no significant differences were observed in the population of parenchymal cells (the glandular epithelium) in the glands of pregnant rats fed the curcumin diet compared with those in control rats (Figure 3c and d). These observations at the time of irradiation were consistent with the finding of no significant differences in the number of ER in the mammary glands of control (10.9 ± 1.0 fmol/mg protein) and curcumin-fed rats (10.0 ± 0.5 fmol/mg protein) (P = 0.466).

Effect of curcumin on the fatty acid profile in serum at the time of initiation

The serum concentrations of fatty acids were measured 10 days after the start of administration of dietary curcumin, corresponding to the day of irradiation. No significant change was observed in the concentrations of the fatty acids assayed

Table IV. Effect of curcumin on the fatty acid profile in serum at the time of irradiation (day 20 of pregnancy)

Fatty acid	Concentration (μg/ml serum)[a]	
	Control diet	Curcumin diet
Palmitic acid (C16:0)	721 ± 82	725 ± 89
Stearic acid (C18:0)	424 ± 20	408 ± 22
Oleic acid (C18:1)	488 ± 61	530 ± 81
Linoleic acid (C18:2)	749 ± 86	662 ± 82
Linolenic acid (C18:3)	45.8 ± 7.4	36.9 ± 6.0
Arachidonic acid (C20:4)	509 ± 14	450 ± 28
Eicosapentaenoic acid (C20:5)	49.4 ± 4.7	63.2 ± 8.5
Docosahexanoic acid (C22:6)	398 ± 28	430 ± 37
Total saturated fatty acids (S)	1145 ± 101	1133 ± 108
Total unsaturated fatty acids (U)[b]	2100 ± 256	2108 ± 213
Total polyunsaturated fatty acids (PU)[c]	1002 ± 43	899 ± 109
S/U	0.54	0.54
S/PU	1.14	1.26

[a]Mean ± SE (n = 6).
[b]C18:1, C18:2, C18:3, C20:4, C20:5, C20:6.
[c]C18:3, C20:4, C20:5, C20:6.

Table V. Biological effects at the end of the experiment (17 months old) of curcumin treatment during the initiation stage

	Control diet[a]	Curcumin diet[a]
Body weight (g)	255 ± 7	244 ± 5
Liver (g)	15.2 ± 0.8	10.6 ± 0.6[b]
Ovaries (mg)	57.2 ± 5.5	51.5 ± 3.2
Uterus (mg)	501 ± 23	618 ± 37[c]
Pituitary gland		
Normal gland (mg)	15.8 ± 0.8	14.7 ± 0.9
Gland with tumor (mg)	70.4 ± 21.8	49.4 ± 12.3

[a]Mean ± SE.
[b]Significant difference ($P < 0.01$) from the control group by Student's t-test.
[c]Significant difference ($P < 0.05$) from the control group by Student's t-test.

(Table IV). With regard to unsaturated fatty acids, the serum concentrations of linoleic acid (P = 0.487), linolenic acid (P = 0.628) and arachidonic acid (P = 0.093) were slightly decreased by the administration of dietary curcumin. However, the concentrations of eicosapentaenoic acid (P = 0.912) and docosahexanoic acid (P = 0.505) were weakly increased in rats fed the curcumin diet. Ratios of total saturated fatty acids to total unsaturated fatty acids (S/U) and of total saturated fatty acids to total polyunsaturated fatty acids (S/PU) were not significantly altered by 10 days administration of curcumin.

Biological effects at the end of the curcumin treatment experiment

The final body weights and organ weights are summarized in Table V. No significant changes in body weight were observed between the control and curcumin-fed groups (P = 0.253). Treatment with curcumin during initiation by radiation decreased the liver weight ($P < 0.01$) and increased the uterus weight ($P < 0.05$) significantly. When the 27 control rats were autopsied, eight (29.6%) were found to have developed pituitary tumors; the pituitary tumor incidence (18.5%) in the curcumin-fed rats was two-thirds of that in the control rats (P = 0.340) (Table I). No change in weight of normal pituitary

glands (P=0.389) and pituitary glands with tumors (P = 0.493) was observed between the control and curcumin-fed groups.

Discussion

Explanations of the cytotoxic effects of radiation have previously emphasized the involvement of reactive oxygen species such as the superoxide anion (O_2^-) and the hydroxyl radical ($^{\cdot}OH$) (22,23). McLennan *et al.* have reported that O_2^- may be non-toxic, but it is a precursor in the formation of $^{\cdot}OH$, which is the most toxic radical resulting from radiation (24). The involvement of oxygen-derived free radicals in the carcinogenic process correlates well with the protective effects of free radical scavengers, as seen by inhibition of the development of radiation-induced mammary tumors by administration of WR-2721 prior to irradiation (3,25). A recent study indicated that reactive oxygen radical species generated by radiation increased the frequency of a tandem CC→TT double substitution in the DNA strand (26).

Chemoprevention is a rapidly growing field in cancer research which focuses on inhibiting and delaying the onset of carcinogenesis. A large number of natural products have been evaluated as potential chemopreventive agents (27,28). Recent studies on components of plants indicated that phenolic compounds with anti-oxidant and/or anti-inflammatory properties can inhibit tumor initiation and promotion in mouse skin (8). Most of the natural anti-oxidants have either a phenolic group or a β-diketone group (29,30). Curcumin is a unique compound, having both phenolic and β-diketone functional groups, and would be expected to have remarkable anti-oxidant and free radical scavenging activities (31,32). Curcumin not only exhibits the above properties, but also enhances the activities of anti-oxidant enzymes such as superoxide dismutase, catalase and glutathione peroxidase (33). Furthermore, curcumin is a potent inhibitor of oxygen radical-generating enzymes such as cyclooxygenase-2 (34,35).

The formation of chromosomal aberrations (36) and micronucleated polychromatic erythrocytes (37) caused by whole body exposure to γ-rays were significantly inhibited by oral administration of curcumin. Also, curcumin suppressed lipid peroxidation in rats irradiated with γ-rays (38,39). Earlier studies from our laboratory demonstrated a marked preventive effect of curcumin on DES-dependent promotion in radiation-initiated mammary tumorigenesis (12). The data presented herein indicate that administration of curcumin for 12 days, i.e. 9 days before and 3 days after irradiation, also markedly reduced radiation-induced initiation in mammary tumorigenesis in rats. Curcumin has been shown to display anti-initiation activities, as indicated by its ability to prevent tumorigeneses induced in the colon by azoxymethane (40), mouth by 4-nitroquinoline-1-oxide (41), skin by benzo[*a*]pyrene (42) and duodenum by *N*-ethyl-*N'*-nitro-*N*-nitrosoguanidine (43). It was suggested that many chemical carcinogens act by forming free radicals (44–46). We would suggest that one possible mechanism of the anti-initiation activity of curcumin is the scavenging of free radicals produced by a variety of chemical carcinogens or radiation as tumor initiator at target sites. However, dietary curcumin did not lower the cumulative incidence or affect tumor multiplicity in the initiation stage of DMBA-induced mammary tumorigenesis (11,47). The reason why no protective effect of curcumin was observed in the chemical carcinogenesis of mammary glands is still not known.

Nitric oxide plays a key role in physiological as well as pathological processes, including inflammation and cancer. The enhancement of NO production by irradiation was attributed to high levels of expression of inducible nitric oxide synthase (iNOS) (48). Excessive production of NO by activated iNOS may result in the formation of toxic intermediates, such as peroxynitrite ($ONOO^-$) and N_2O_3, causing tissue damage and genotoxicity (49,50), and thus has potential carcinogenic effects (51). In immunohistochemical experiments, iNOS expression was apparently increased in the basal layers of alveoli and lactiferous ducts of the mammary glands treated with lipopolysaccharide (LPS) as an inflammatory agent and this increase was reflected in an enhancement of NO production (52). Furthermore, NO production by LPS-stimulated mammary glands was significantly decreased in the presence of curcumin, as was the amount of a 122 kDa iNOS (53). On the other hand, 3,5,4'-trihydroxy-*trans*-stilbene (resveratrol), a phytopolyphenol isolated from the seeds and skins of grapes, inhibited the expression of LPS-induced iNOS (54) and decreased LPS-stimulated NO production (55). Mgbonyebi *et al.* (56) have reported that resveratrol is a potential chemopreventive agent for both ER-positive and ER-negative breast cancers. Also, formation of azoxymethane-induced colonic aberrant crypt foci was significantly suppressed in the presence of an iNOS-specific inhibitor, *S,S'*-1,4-phenylene-*bis*(1,2-ethanediyl)*bis*-isothiourea (57). These findings suggest that suppression of iNOS activity by curcumin in the mammary gland of irradiated rats helps to prevent radiation-induced tumor initiation.

The transcription factor nuclear factor κB (NF-κB) has been implicated in the inducible expression of a variety of genes involved in inflammatory and immune responses (58). Singh and Aggarwal have reported that curcumin inhibits the NF-κB activation pathway at a step before inhibitory protein κB (IκB) α phosphorylation (59). Recently, Jobin *et al.* (60) have reported that interleukin (IL)-1β-mediated expression of the adhesion molecule, intercellular adhesion molecule-1, and the chemokine IL-8 were reduced by blockade of transcriptional activation cascades, such as cytokine-induced NF-κB DNA binding activity, RelA nuclear translocation, IκBα degradation, IκB Ser32 phosphorylation and IκB kinase activity, by curcumin. Their results suggest that curcumin blocks a signal upstream of the NF-κB-inducing kinase, but below the junction of the IL-1β signal pathways. NF-κB is activated by radiation (61,62). Activation of NF-κB may be particularly important for cell survival in response to oxidative stress induced by radiation, but it has been shown recently that inhibition of NF-κB activation enhances radiation-induced apoptosis (63,64). We would suggest that another possible mechanism of the chemopreventive activity of curcumin for mammary tumorigenesis is elimination of radiation-initiated tumor origin cells from the mammary gland by apoptosis.

At the time corresponding to initiation with radiation, no detectable serum curcumin was observed in rats fed the curcumin diet. It was shown that curcumin administered orally was metabolized to tetrahydrocurcumin during absorption through the intestine (65,66). In fact, tetrahydrocurcumin was detected in serum of rats fed the diet containing curcumin for 9 days in the present study. Tetrahydrocurcumin exhibited a significant inhibitory effect on O_2^- generation induced by 12-*O*-tetradecanoylphorbol-13-acetate (67) and on lipid peroxidation of erythrocyte membrane ghosts induced by t-butylhydroperoxide compared with curcumin (16,68). Also,

feeding of a diet containing tetrahydrocurcumin resulted in a significant repression of 1,2-dimethylhydrazine-induced formation of aberrant crypt foci, which are regarded as a precursor lesion for colon cancer (69). The results obtained from the present study thus suggest that tetrahydrocurcumin has potential as a chemopreventive agent for radiation-initiated mammary tumorigenesis.

Finally, Wahlström and Blennow (70) found no apparent toxic effects of curcumin at doses of up to 5 g/kg body wt in rats when given orally. In the present study, pregnant rats consumed 18.2 ± 0.3 g of diet containing 1% curcumin/day, which corresponds to 0.67 g curcumin/kg/day, for 12 days. Body weight in pregnant rats fed the curcumin diet was reduced to 91% of that observed in rats fed the control diet. The reduction was significant, but would be too low to indicate a toxic action of curcumin. Therefore, it is likely that a reduction in body weight occurs in curcumin-fed rats having a decreased concentration of serum triglycerides (12). Curcumin did not have any adverse effects on growth or teratogenesis of fetuses nor on organ weight or serum concentrations of hormones of dams, suggesting no toxic effect when administered orally. Lack of a mutagenic effect of curcumin was also reported in the presence or absence of a rat hepatic microsomal activation system in the Ames test with *Salmonella typhimurium* (71).

In conclusion, radiation-induced initiation of mammary tumorigenesis was markedly inhibited by administration of dietary curcumin. Oral administration of curcumin did not produce any side-effects on endocrinological and physiological status. These results raise the possibility of clinical application of curcumin in the management of radio-diagnosis to diminish tissue damage by radiation.

Acknowledgements

We thank Mrs M.Takahashi for excellent assistance in the care of the animals. This work was partly supported by a grant from the Special Program for Bioregulation of the National Institute of Radiological Sciences.

References

1. Inano,H., Yamanouchi,H., Suzuki,K., Onoda,M. and Wakabayashi,K. (1995) Estradiol-17β as an initiation modifier for radiation-induced mammary tumorigenesis of rats ovariectomized before puberty. *Carcinogenesis*, **16**, 1871–1877.
2. Yamanouchi,H., Ishii-Ohba,H., Suzuki,K., Onoda,M., Wakabayashi,K. and Inano,H. (1995) Relationship between stages of mammary development and sensitivity to γ-ray irradiation in mammary tumorigenesis in rats. *Int. J. Cancer*, **60**, 230–234.
3. Inano,H., Onoda,M., Suzuki,K., Kobayashi,H. and Wakabayashi,K. (2000) Inhibitory effects of WR-2721 and cysteamine on tumor initiation in mammary glands of pregnant rats by radiation. *Radiat. Res.*, **153**, 68–74.
4. Littlefield,L.G., Joiner,E.E., Colyer,S.P., Sallam,F. and Frome,E.L. (1993) Concentration-dependent protection against X-ray-induced chromosome aberrations in human lymphocytes by the aminothiol WR-1065. *Radiat. Res.*, **133**, 88–93.
5. Henderson,B.W. and Miller,A.C. (1986) Effects of scavengers of reactive oxygen and radical species on cell survival following photodynamic treatment *in vitro*; comparison to ionizing radiation. *Radiat. Res.*, **108**, 196–205.
6. Kligerman,M.M., Glover,D.J., Turrisi,A.T., Norfleet,A.L., Yuhas,J.M., Coia,L.R., Simone,C., Glick,J.H. and Goodman,R.L. (1984) Toxicity of WR-2721 administration in single and multiple doses. *Int. J. Radiat. Oncol. Biol. Phys.*, **10**, 1771–1776.
7. Devi,P.U., Navalkha,P.L., Kumar,S., Kumar,A., Jagetia,G.C., Surana,M., Gupta,S. and Pareek,B.P. (1984) Studies on toxic effect of WR-2721 in mouse. *Indian J. Med. Sci.*, **38**, 65–69.
8. Huang,M.-T., Smart,R.C., Wong,C.-Q. and Conney,A.H. (1988) Inhibitory effect of curcumin, chlorogenic acid, caffeic acid and ferulic acid on tumor promotion in mouse skin by 12-O-tetradecanoylphorbol-13-acetate. *Cancer Res.*, **48**, 5941–5946.
9. Ammon,H.P.T. and Wahl,M.A. (1991) Pharmacology of *Curcuma longa*. *Planta Med.*, **57**, 1–7.
10. Shankar,T.N., Shantha,N.V., Ramesh,H.P., Murthy,I.A. and Murthy,V.S. (1980) Toxicity studies on turmeric (*Curcuma longa*): acute toxicity studies in rats, guinea pig and monkeys. *Indian J. Exp. Biol.*, **18**, 73–75.
11. Pereira,M.A., Grubbs,C.J., Barnes,L.H., Li,H., Olson,G.R., Eto,I., Jukiana,M., Whitaker,L.M., Kelloff,G.J., Steele,V.E. and Lubet,R.A. (1996) Effects of the phytochemicals, curcumin and quercetin, upon azoxymethane-induced colon cancer and 7,12-dimethylbenz[*a*]anthracene-induced mammary cancer in rats. *Carcinogenesis*, **17**, 1305–1311.
12. Inano,H., Onoda,M., Inafuku,N., Kubota,M., Kamada,Y., Osawa,T., Kobayashi,H. and Wakabayashi,K. (1999) Chemoprevention by curcumin during the promotion stage of tumorigenesis of mammary glands in rats irradiated with γ-rays. *Carcinogenesis*, **20**, 1011–1018.
13. Inano,H., Suzuki,K., Ishii-Ohba,H., Yamanouchi,H., Takahashi,M. and Wakabayashi,K. (1993) Promotive effects of diethylstilbestrol, its metabolite (Z,Z-dienestrol) and a stereoisomer of the metabolite (E,E-dienestrol) in tumorigenesis of rat mammary glands pregnancy-dependently initiated with radiation. *Carcinogenesis*, **14**, 2157–2163.
14. Iball,J. (1939) The relative potency of carcinogenic compounds. *Am. J. Cancer*, **35**, 188–190,
15. Lee,M.-J., Wang,Z.-Y., Li,H., Chen,L., Sun,Y., Gobbo,S., Balentine,D.A. and Yang,C.S. (1995) Analysis of plasma and urinary tea polyphenols in human subjects. *Cancer Epidemiol. Biomarkers Prev.*, **4**, 393–399.
16. Sugiyama,Y., Kawakishi,S. and Osawa,T. (1996) Involvement of β-diketone moiety in the antioxidative mechanism of tetrahydrocurcumin. *Biochem. Pharmacol.*, **52**, 519–525.
17. Ozawa,A., Takayanagi,K., Fujita,T., Hirai,A., Hamazaki,A., Terano,T., Tamura,Y. and Kumagai,A. (1982) Determination of long chain fatty acids in human total plasma lipids using gas chromatography. *Bunseki Kagaku*, **31**, 87–91.
18. Buege,J.A. and Aust,S.D. (1978) Microsomal lipid peroxidation. *Methods Enzymol.*, **52**, 302–310.
19. Johnson,R.B., Nakamura,R.M. and Libby,R.M. (1975) Simplified Scatchard plot assay for estrogen receptor in human breast cancer. *Clin. Chem.*, **21**, 1725–1730.
20. Scatchard,G. (1949) The attractions of proteins for small molecules and ions. *Ann. N. Y. Acad. Sci.*, **51**, 660–672.
21. Russo,J., Gusterson,B.A., Rogers,A.E., Russo,I.H., Wellings,S.R. and van Zwieten,M.-J. (1990) Comparative study of human and rat mammary tumorigenesis. *Lab. Invest.*, **62**, 244–278.
22. Buc-Calderon,P., Defresne,M.P., Barvais,C. and Roberfroid,M. (1989) *N*-acyl dehydroalanines protect from radiation toxicity and inhibit radiation carcinogenesis in mice. *Carcinogenesis*, **10**, 1641–1644.
23. Riley,P.A. (1994) Free radicals in biology: oxidative stress and the effects of ionizing radiation. *Int. J. Radiat. Biol.*,**65**, 27–33.
24. McLennan,G., Oberley,L.W. and Autor,A.P. (1980) The role of oxygen-derived free radicals in radiation-induced damage and death of nondividing eucaryotic cells. *Radiat. Res.*, **84**, 122–132.
25. Inano,H., Onoda,M., Suzuki,K., Kobayashi,H. and Wakabayashi,K. (2000) Prevention of radiation-induced mammary tumors in rats by combined use of WR-2721 and tamoxifen. *Int. J. Radiat. Biol.*, in press.
26. Reid,T.M. and Loeb,L.A. (1993) Tandem double CC TT mutations are produced by reactive oxygen species. *Proc. Natl Acad. Sci. USA*, **90**, 3905–3907.
27. Sharma,S., Stutzman,J.D., Kelloff,G.J. and Steele,V.E. (1994) Screening of potential chemopreventive agents using biochemical markers of carcinogenesis. *Cancer Res.*, **54**, 5848–5855.
28. Ohigashi,H., Murakami,A. and Koshimizu,K. (1996) An approach to functional food: cancer preventive potential of vegetables and fruits and their active constituents. *Nutr. Rev.*, **54**, S24–S28.
29. Masuda,T. and Jitoe,A. (1994) Antioxidative and antiinflammatory compounds from tropical gingers: isolation, structure determination and activities of cassumunins A, B and C, new complex curcuminoids from *Zingiber cassumunar*. *J. Agric. Food Chem.*, **42**, 1850–1856.
30. Subramanian,M., Sreejayan, Rao,M.N.A., Devasagayan,T.P.A. and Singh,B.B. (1994) Diminution of singlet oxygen-induced DNA damage by curcumin and related antioxidants. *Mutat. Res.*, **311**, 249–255.
31. Reddy,A.C.P. and Lokesh,B.R. (1994) Studies on the inhibitory effects of curcumin and euganol on the formation of reactive oxygen species and the oxidation of ferrous iron. *Mol. Cell. Biochem.*, **137**, 1–8.

32. Toda,S., Miyase,T., Arichi,H., Tanizawa,H. and Takino,Y. (1985) Natural antioxidants III. Antioxidative components isolated from rhizome of *Curcuma longa* L. *Chem. Pharm. Bull.*, **33**, 1725–1728.
33. Reddy,A.C.P. and Lokesh,B.P. (1994) Effect of dietary turmeric (*Curcuma longa*) on iron-induced lipid peroxidation in rat liver. *Food Chem. Toxicol.*, **32**, 279–283.
34. Huang,M.T., Lysz,T., Ferraro,T., Abidi,T.F., Laskin,J.D. and Conney,A.H. (1991) Inhibitory effect of curcumin on *in vitro* lipoxygenase and cyclooxygenase activities in mouse epidermis. *Cancer Res.*, **51**, 813–819.
35. Zhang,F., Altorki,N.K., Mester,J.R., Subbaramaiah,K. and Dannenberg,A.J. (1999) Crucumin inhibits cyclooxygenase-2 transcription in bile acid- and phorbol ester-treated human gastrointestinal epithelial cells. *Carcinogenesis*, **20**, 445–451.
36. Thresiamma,K.C., George,J. and Kuttan,R. (1998) Protective effect of curcumin, ellagic acid and bixin on radiation induced genotoxicity. *J. Exp. Clin. Cancer Res.*, **17**, 431–434.
37. Abraham,S.K., Sarma,L. and Kesavan,P.C. (1993) Protective effects of chlorogenic acid, curcumin and β-carotene against γ-radiation-induced *in vivo* chromosomal damage. *Mutat. Res.*, **303**, 109–112.
38. Nishigaki,I., Kuttan,R., Oku,H., Ashoori,F., Abe,H. and Yagi,K. (1992) Suppressive effect of curcumin on lipid peroxidation induced in rats by carbon tetrachloride or ^{60}Co-irradiation. *J. Clin. Biochem. Nutr.*, **13**, 23–29.
39. Sreejayan,N., Rao,M.N.A., Priyadarsini,K.I. and Devasagayan,T.P.A. (1997) Inhibition of radiation-induced lipid peroxidation by curcumin. *Int. J. Pharmaceut.*, **151**, 127–130.
40. Rao,C.V., Simi,B. and Reddy,B.S. (1993) Inhibition by dietary curcumin of azoxymethane-induced ornithine decarboxylase, tyrosine protein kinase, arachidonic acid metabolism and aberrant crypt foci formation in the rat colon. *Carcinogenesis*, **14**, 2219–2225.
41. Tanaka,T., Makita,H., Ohnishi,M., Hirose,H., Wang,A., Mori,H., Satoh,K., Hara,A. and Ogawa,H. (1994) Chemoprevention of 4-nitroquinoline-1-oxide-induced oral carcinogenesis by dietary curcumin and hesperidin: comparison with the protective effect of β-carotene. *Cancer Res.*, **54**, 4653–4659.
42. Huang,M.-T., Wang,Z.Y., Georgiadis,C.A., Laskin,J.D. and Conney,A.H. (1992) Inhibitory effects of curcumin on tumor initiation by benzo[*a*]pyrene and 7,12-dimethylbenz[*a*]anthracene. *Carcinogenesis*, **13**, 2183–2186.
43. Huang,M.-T., Lou,Y.-R., Ma,W., Newmark,H.L., Reuhl,K.R. and Conney,A.H. (1994) Inhibitory effects of dietary curcumin on forestomach, duodenal and colon carcinogenesis in mice. *Cancer Res.*, **54**, 5841–5847.
44. Nagata,C., Inomata,M., Kodama,M. and Tagashira,Y. (1968) Electron spin resonance study on the interaction between the chemical carcinogens and tissue components III. Determination of the structure of the free radical produced either by stirring 3,4-benzopyrene with albumin or incubating with liver homogenates. *Gann*, **59**, 289–298.
45. Nagata,V., Nakadate,M., Ioki,Y. and Imamura,A. (1972) Electron spin resonance study on the free radical production from N-methyl-N′-nitro-N-nitrosoguanidine. *Gann*, **63**, 471–481.
46. Varnes,M.E. and Biaglow,J.E. (1979) Interactions of the carcinogen 4-nitroquinoline-1-oxide with the non-protein thiols of mammalian cells. *Cancer Res.*, **39**, 2960–2965.
47. Singletary,K., MacDonald,C., Iovinellr,M., Fisher,C. and Wallig,M. (1998) Effect of the β-diketones diferuloylmethane (curcumin) and dibenzoylmethane on rats mammary DNA adducts and tumors induced by 7,12-dimethylbenz[*a*]anthracene. *Carcinogenesis*, **19**, 1039–1043.
48. Ibuki,Y. and Goto,R. (1997) Enhancement of NO production from resident peritoneal macrophages by *in vitro* gamma-irradiation and its relationship to reactive oxygen intermediates. *Free Radic. Biol. Med.*, **22**, 1029–1035.
49. Tamir,S. and Tannenbaum,S.R. (1996) The role of nitric oxide (NO) in the carcinogenic process. *Biochim. Biophys. Acta*, **1288**, F31–F36.
50. Wink,D.A., Vodovotz,Y., Laval,J., Laval,F., Dewhirst,M. and Mitchell,J.B. (1998) The multifaceted roles of nitric oxide in cancer. *Carcinogenesis*, **19**, 711–721.
51. Ohshima,H. and Bartsch,H. (1994) Chronic infections and inflammatory processes as cancer risk factors: possible role of nitric oxide in carcinogenesis. *Mutat. Res.*, **305**, 253–264.
52. Onoda,M. and Inano,H. (1998) Localization of nitric oxide synthases and nitric oxide production in the rat mammary gland. *J. Histochem. Cytochem.*, **46**, 1269–1278.
53. Onoda,M. and Inano,H. (2000) Effect of curcumin on the production of nitric oxide by cultured mammary gland. *Arch. Biochem. Biophys. B Nitric Oxide Biol. Chem.*, in press.
54. Jang,M. and Pezzuto,J.M. (1999) Cancer chemopreventive activity of resveratrol. *Drug. Exp. Clin. Res.*, **25**, 65–77.
55. Wadsworth,T.L. and Koop,D.R. (1999) Effects of the wine polyphenols quercetin and resveratrol on pro-inflammatory cytokine expression in RAW 264.7 macrophages. *Biochem. Pharmacol.*, **57**, 941–949.
56. Mgbonyebi,O.P., Russo,J. and Russo,I.H. (1998) Antiproliferative effect of synthetic resveratrol on human breast epithelial cells. *Int. J. Oncol.*, **12**, 865–869.
57. Rao,C.V., Kawamori,T., Hamid,R. and Reddy,B.S. (1999) Chemoprevention of colonic aberrant crypt foci by an inducible nitric oxide synthase-selective inhibitor. *Carcinogenesis*, **20**, 641–644.
58. Barnes,P.J. and Karin,M. (1997) Nuclear factor-κB, a pivotal transcription factor in chronic inflammatory diseases. *New Engl. J. Med.*, **336**, 1066–1071.
59. Singh,S. and Aggarwal,B.B. (1995) Activation of transcription factor NF-κB is suppressed by curcumin (diferuloylmethane). *J. Biol. Chem.*, **270**, 24995–25000.
60. Jobin,C., Bradham,C.A., Russo,M.P., Juma,B., Narula,A.S., Brenner,D.A. and Sartor,R.B. (1999) Curcumin blocks cytokine-mediated NF-κB activation and proinflammatory gene expression by inhibiting inhibitory factor IκB kinase activity. *J. Immunol.*, **163**, 3474–3483.
61. Weichsellaum,R.R., Hallahan,D., Fuks,Z. and Kufe,D. (1994) Radiation induction of immediate early genes: effectors of the radiation-stress response. *Int. J. Radiat. Oncol. Biol. Phys.*, **30**, 229–234.
62. Zhou,D., Brown,S.A., Yu,T., Chen,G., Barve,S., Kang,B.C. and Tompson,J.S. (1999) A high dose of ionizing radiation induces tissue-specific activation of nuclear factor-κB *in vivo*. *Radiat. Res.*, **151**, 703–709.
63. Wang,C.-Y., Mayo,M.W. and Baldwin,A.S. (1996) TNF- and cancer therapy-induced apoptosis: potentiation by inhibition of NF-κB. *Science*, **274**, 784–787.
64. Yamagishi,N., Miyakoshi,J. and Takebe,H. (1997) Enhanced radiosensitivity by inhibition of nuclear factor κB activation in human malignant glioma cells. *Int. J. Radiat. Biol.*, **72**, 157–162.
65. Holder,G.M., Plummer,J.L. and Ryan,A.J. (1978) The metabolism and excretion of curcumin (1,7-bis-(4-hydroxy-3-methoxyphenyl)-1,6-heptadiene-3,5-dione) in the rat. *Xenobiotica*, **8**, 761–768.
66. Ravindranath,V. and Chandrasekhara,N. (1981) *In vitro* studies on the intestinal absorption of curcumin in rats. *Toxicology*, **20**, 251–257.
67. Nakamura,Y., Ohto,Y., Murakami,A., Osawa,T. and Ohigashi,H. (1998) Inhibitory effects of curcumin and tetrahydrocurcuminoids on the tumor promoter-induced reactive oxygen species generation in leukocytes *in vitro* and *in vivo*. *Jpn. J. Cancer Res.*, **89**, 361–370.
68. Osawa,T., Sugiyama,Y., Inayoshi,M. and Kawakishi,S. (1995) Antioxidative activity of tetrahydrocurcuminoids. *Biosci. Biotechnol. Biochem.*, **59**, 1609–1612.
69. Kim,J.M., Araki,S., Kim,D.J., Park,C.B., Takatuka,N., Baba-Toriyama,H., Ota,T., Nir,Z., Khachik,F., Shimidzu,N., Tanaka,Y., Osawa,T., Uraji,T., Murakoshi,M., Nishino,H. and Tsuda,H. (1998) Chemopreventive effects of carotenoids and curcumins on mouse colon carcinogenesis after 1,2-dimethylhydrazine initiation. *Carcinogenesis*, **19**, 81–85.
70. Wahlström,B. and Blennow,G. (1978) A study on the fate of curcumin in the rats. *Acta Pharmacol. Toxicol.*, **43**, 86–92.
71. Jensen,N.J. (1982) Lack of mutagenic effect of turmeric oleoresin and curcumin in the Salmonella/mammalian microsome test. *Mutat. Res.*, **105**, 393–396.

Received March 24, 2000; revised June 26, 2000; accepted June 30, 2000

IMPROVED SYNTHESIS OF 1-DEOXYNOJIRIMYCIN AND FACILE SYNTHESIS OF ITS STEREOISOMERS FROM (*S*)-PYROGLUTAMIC ACID DERIVATIVE

Nobuo Ikota,*,[a] Jun-ichi Hirano,[b] Ranjith Gamage,[a] Hidehiko Nakagawa,[a] and Hiroko Hama-Inaba[a]

National Institute of Radiological Sciences,[a] 9-1, Anagawa-4-chome, Inage-ku, Chiba 263, Japan and Faculty of Science, Toho University,[b] 2-2-1, Miyama Funabashi, Chiba 274, Japan

Abstract-----Improved synthesis of 1-deoxynojirimycin (**9**) from (*E*)-α,β-unsaturated ester (**1**) and facile synthesis of 1-deoxy-azasugars (**14** and **15**) from **10** where both substrates (**1** and **10**) prepared from (*S*)-pyroglutamic acid were described.

1-Deoxynojirimycin and its stereoisomers show interesting biological activities such as glycosidase inhibitory activity[1a-c] and their synthesis has been a subject of recent research.[1c-f] We have already reported the synthesis of 1-deoxynojirimycin from (*S*)-pyroglutamic acid [2] and the improvement of stereoselectivity for the newly formed asymmetric centers.[3] In continuation of our studies on the synthesis of chiral polyhydroxylated amines, we describe here a further improvement for the synthesis of 1-deoxynojirimycin (**9**) and the facile synthesis of 1-deoxyazasugars (**14** and **15**) from (*S*)-pyroglutamic acid.

We have found the dihydroxylation of **1** with potassium osmate (0.08 equiv.) using hydroquinidine 1,4-phthalazinediyl diether (0.20 equiv.) as a chiral ligand[4] in the presence of $K_3Fe(CN)_6$ (3 equiv.), K_2CO_3 (3 equiv.), and $MeSO_2NH_2$ (1 equiv.) in *tert*-BuOH-H_2O (1:1) at 0°C for 12 h gives the diol (**2a**) as a sole diastereomer in 84% yield. A complete diastereoselectivity for this dihydroxylation was confirmed by conversion of the crude diol into the corresponding diacetate, and the diacetate (**3b**) was not detected in the ^1H NMR spectrum of the crude poduct. On the other hand, the double asymmetric induction for the dihydroxylation of (*Z*)-α,β-unsaturated ester (**4**)[5] was not effective (up to 20% d.e. was observed using hydroquinidine 1,4-phthalazinediyl diether and hydroquinine 1,4-phthalazinediyl diether as chiral ligands, while 31% d.e. was obtained without chiral ligand[5]).

The alcohol (**5**) was obtained from **2a** *via* the corresponding MOM ether (**2c**) by the same procedure as reported previously.[3] A high diastereoselectivity was also observed for the introduction of vinyl group to the aldehyde derived from **5** by the method of Swern.[6] Thus, the reaction of the aldehyde with the reagent prepared from vinylmagnesium bromide and copper bromide-dimethyl sulfide complex[7] at -78°C

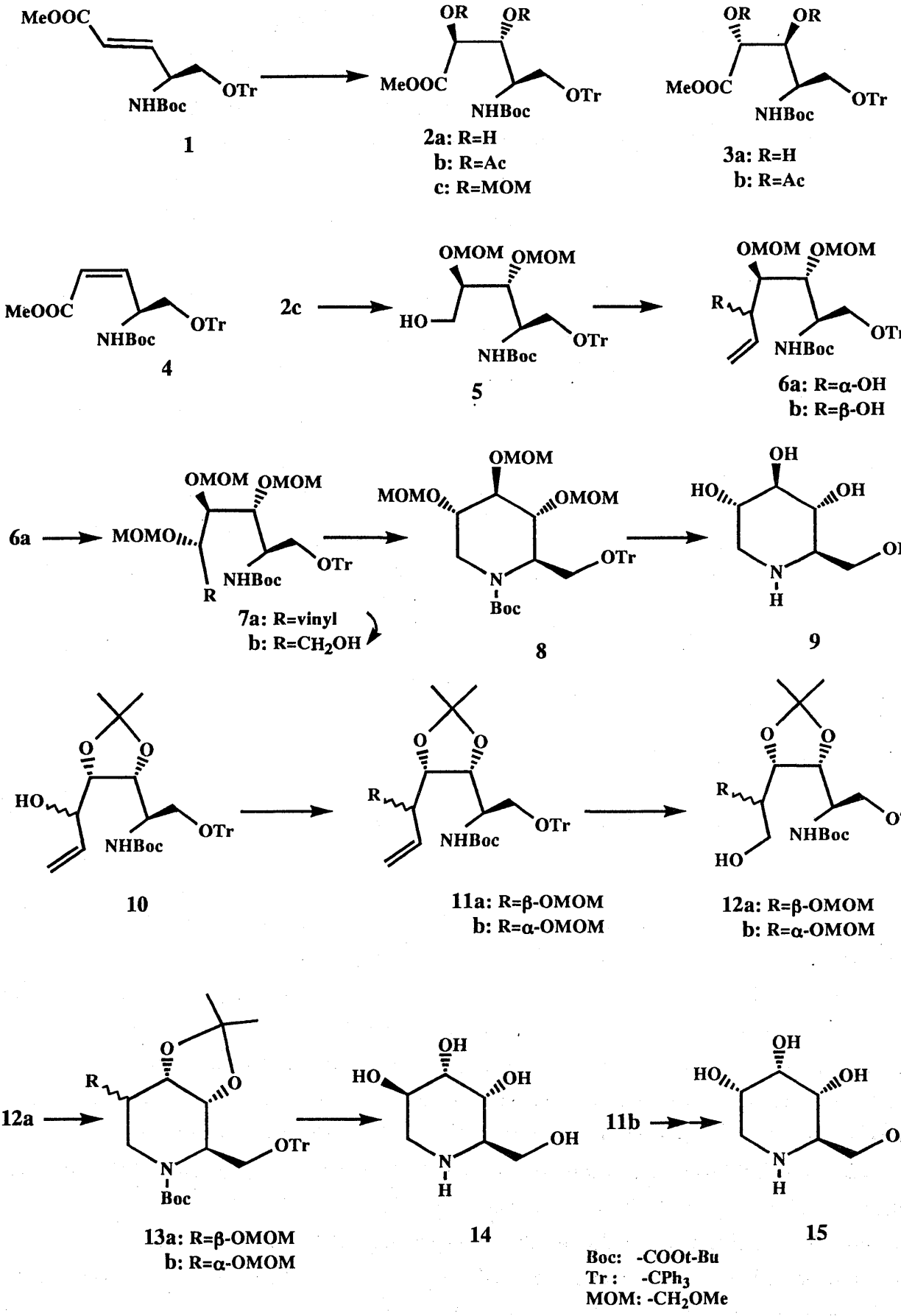
MeOOC
NHBoc
OTr
1
OR
OR
2a: R=H
b: R=Ac
c: R=MOM
3a: R=H
b: R=Ac
4
2c
OMOM
HO
5
R
6a: R=α-OH
b: R=β-OH
6a
MOMO
7a: R=vinyl
b: R=CH2OH
Boc
8
9
10
11a: R=β-OMOM
b: R=α-OMOM
12a: R=β-OMOM
b: R=α-OMOM
12a
13a: R=β-OMOM
b: R=α-OMOM
14
11b
15
Boc: -COOt-Bu
Tr : -CPh3
MOM: -CH2OMe

gave **6a** and **6b** in a ratio of 15:1 in 51% yield. The major diastereomer (**6a**) was converted into a corresponding MOM ether (**7a**) and was treated with ozone in methylene chloride followed by reductive work-up with $NaBH_4$ to give the alcohol (**7b**) in 53% yield. Mesylation (methanesulfonyl chloride (MsCl), triethylamine (TEA), CH_2Cl_2) followed by cyclization with potassium *tert*-butoxide in THF gave the fully protected piperidine derivative (**8**) in 71% yield. Hydrolysis of **8** with MeOH-10% HCl (1:1) at 70°C followed by treatment with Dowex 50W-X8 (H^+ form) gave 1-deoxynojirimycin (**9**) (mp 195-197°C, $[\alpha]_D$ +46.5° (c=0.5, H_2O), lit.,[1b] mp 196°C, $[\alpha]_D$ +47° (H_2O)) in 80% yield.
1-Deoxyazasugars (**14** and **15**) were synthesized starting from the inseparable diastereomeric mixture (**10**), which was prepared from (*S*)-pyroglutamic acid for the synthesis of 1,7a-diepialexine.[8] The compound (**10**) was converted into the corresponding MOM ethers (89% yield, **11a** : **11b**= 2.3:1), which were separated by column chromatography. Major diastereomer (**11a**) was transformed to the alcohol (**12a**, O_3, then $NaBH_4$), which was then cyclized into the piperidine derivative (**13a**) *via* mesylate (MsCl, TEA, CH_2Cl_2; then *tert*-BuOK, THF) in 62% yield. Cleavage of all protecting groups in **13a** with acidic conditions (MeOH:10% HCl=1:1, 70°C) gave **14** (hydrochloride of **14**: mp 103-105°C, $[\alpha]_D$ +54.3°(H_2O)) in 85% yield. In the same reaction sequence, **11b** was converted into **15** (mp 149-150°C, $[\alpha]_D$ +28.1° (c=0.8, H_2O), lit.,[9] $[\alpha]_D$ +25.7° (c=0.65, H_2O)) in 58% yield.

EXPERIMENTAL

General methods.---------Melting points were determined on a hot stage apparatus and are uncorrected. IR spectra were measured with a JEOL JIR-110 FT-IR spectrophotometer. ^1H and ^{13}C NMR spectra were recorded on a JEOL JNM-FX100 (100 Mz) spectrometer. Data are recorded in parts per million (ppm) downfield from internal tetramethylsilane. MS spectra were taken on a JEOL JMS-D302 spectrometer. Optical rotations were measured in $CHCl_3$ solution at 20°C on a JASCO DIP-360 polarimeter unless otherwise mentioned. The organic solvents were dried over $MgSO_4$ before vacuum evaporation and a column chromatography was carried out with silica gel (Wakogel C-200).

1,1-Dimethylethyl *N*-[(1*R*,2*R*,3*S*)-2,3-dihydroxy-3-methoxycarbonyl-1-(trityloxymethyl)propanyl]carbamate (2a) Potassium osmate dihydrate (54.5 mg, 0.15 mmol) was added to a mixture of hydroquinidine 1,4-phthalazinedil diether (288 mg, 0.37 mmol), $K_3Fe(CN)_6$ (1.82 g, 5.5 mmol), K_2CO_3 (770 mg, 5.5 mmol), and $MeSO_2NH_2$ (174 mg, 1.85 mmol) in a *tert*-BuOH-H_2O (1:1, 18 mL) at rt. Then, **1** (900 mg, 1.85 mmol) was added at 0°C. After being stirred at 0°C for 12 h, Na_2SO_3 (4 g) was added and the mixture was stirred for 30 min, and extracted with AcOEt. The organic extracts were washed with H_2O, 1 N aqueous KOH, H_2O, and saturated aqueous NaCl. Drying followed by evaporation gave a residue, which was purified by column chromatography (AcOEt:hexane=2: 1) to give **2a** (805 mg, 84%) as an oil, $[\alpha]_D$ -7.9° (c=1.5); IR ν_{max} 3444, 1748, 1708, 1166, 1086 cm^{-1}; ^1H NMR ($CDCl_3$): 1.41 (9H, s, *t*-Bu), 2.80-3.02(1H, br s, OH), 3.15-3.29 (1H, m, CH), 3.49-3.96(2H, m, 2xCH), 3.75(3H, s, OCH_3), 3.96-4.46(3H, m, 2xCH, OH), 5.15(1H, d, *J*=8 Hz, NH), 7.07-7.78 (15H, m, aromatic protons); ^{13}C NMR ($CDCl_3$): 27.92(q), 52.09(d), 62.13(t), 70.76(d), 71.54(d), 79.72(s), 86.49(s), 126.70, 127.48, and 128.20(each d), 143.27(s),

156.23(s), 172.60(s); MS *m/z* 520(M^+-1). A part of the crude diol was converted to the corresponding diacetate (excess pyridine and acetic anhydride, room temperature, 13 h). Diacetate (**3b**) was not detected in the ^1H NMR spectrum of the crude diacetate.

1,1-Dimethylethyl *N*-[(1*R*,2*R*,3*R*,4*S*)- and (1*R*,2*R*,3*R*,4*R*)-2,3-Bis(methoxymethoxy)-4-hydroxy-1-trityloxymethyl-5-hexenyl]carbamate (6a and 6b) The preparation of alcohol (**5**) and Swern oxidation were peformed by the same procedure as previously described.[3] [Vinyl-Cu]·$MgBr_2$ prepared by addition of vinylmagnesium bromide (4.2 mL of 1.0 M solution in THF) to the copper bromide-dimethyl sulfide complex (816 mg, 4 mmol) in ether-dimethyl sulfide (5:1, 5 mL) was added at -78°C to the crude aldehyde prepared from **5c** (480 mg, 0.83 mmol). After being stirred at -78°C for 1 h, the mixture was treated with saturated aqueous NH_4Cl (10 mL) and extracted with AcOEt. The organic layers were washed with half-saturated aqueous NaCl. Drying followed by evaporation gave a residue, which was purified by column chromatography (AcOEt:hexane=1:2.5) to give **6a** (241 mg, 48%, $[\alpha]_D$ -15.0° (c=1.1), lit.,[3] $[\alpha]_D$ -15.3° (c=1)) and **6b** (16 mg, 3.2%, $[\alpha]_D$ -22.5° (c=1.6), lit.,[3] $[\alpha]_D$ -22.0° (c=1)) as oils, which were identical to the authentic samples.[3]

1,1-Dimethylethyl *N*-[(1*R*,2*R*,3*R*,4*S*)-2,3,4-Tris(methoxymethoxy)-1-trityloxymethyl-5-hexenyl]carbamate (7a) A mixture of **6a** (230 mg, 0.38 mmol), *N*,*N*-diethylaniline (570 mg, 3.82 mmol), and chloromethyl methy ether (310 mg, 3.82 mmol) in CH_2Cl_2 (5 mL) was stirred at rt for 48 h. After addition of AcOEt (100 mL), the mixture was washed with 5% aqueous HCl, H_2O, saturated aqueous $NaHCO_3$, and H_2O. Drying followed by evaporation gave a residue, which was purified by column chromatography(AcOEt:hexane= 1: 4) to give **7a** (176 mg, 71%) as an oil, $[\alpha]_D$ +4.3° (c=1.6, MeOH) ; IR $\nu_{max.}$ (neat) 1708, 1500, 1218, 1028 cm^{-1}; ^1H NMR($CDCl_3$): 1.40(9H, s, *t*-Bu), 3.10-4.03(5H, m, CH_2, 3xCH), 3.25, 3.28, 3.29, and 3.41 (9H, each s, 3xOCH_3), 4.10-4.35(1H, m, CH), 4.42-4.80(6H, m, 3xCH_2), 5.14-5.90(4H, m, -C<u>H2</u>=C<u>H</u>, NH), 7.10-7.53(15H, m, aromatic protons); ^{13}C NMR($CDCl_3$): 27.97(q), 50.68(d), 55.26(q), 55.69(q), 55.99(q), 62.38(t), 77.14(d), 77.87(d), 78.41(s), 79.43(d), 86.25(s), 93.51(t), 97.51(t), 98.63(t), 119.24(t), 126.55, 127.33, and 128.26(each d), 134.05(d), 143.27(s), 155.16(s); Anal. Calcd for $C_{37}H_{49}NO_9$: C, 68.18; H, 7.58; N, 2.15. Found: C, 67.77; H, 7.85; N, 1.88.

1,1-Dimethylethyl *N*-[(1*R*,2*R*,3*R*,4*S*)-2,3,4-Tris(methoxymethoxy)-1-trityloxymethyl-5-hydroxypentyl]carbamate (7b) A solution of **7a** (170 mg, 0.26 mmol) in CH_2Cl_2 (1 mL) was added at -78°C to 2 mL of CH_2Cl_2 saturated with ozone, then ozone was bubbled for further 5 min at -78°C. Then, this solution was added to a suspension of $NaBH_4$ (61 mg, 1.6 mmol) in EtOH (2 mL) at 0°C. After being stirred at 0°C for 15 min, the mixture was diluted with AcOEt-benzene (1:2, 100 mL) and washed with half-saturated aqueous NaCl. Drying followed by evaporation gave a residue, which was purified by column chromatography (AcOEt:hexane=3:2) to give **7b** (128 mg, 75 %) as an oil, $[\alpha]_D$ -12.8° (c=1.2) ; IR $\nu_{max.}$ (neat) 3448, 1708, 1450, 1158, 1026 cm^{-1}; ^1H NMR($CDCl_3$): 1.40(9H, s, *t*-Bu), 3.10-3.31(2H, m, CH_2), 3.21, 3.30, and 3.39 (each 3H, each s, 3xOCH_3), 3.57-4.20(6H, m, CH_2, 4xCH), 4.55(4H, br s, 2xOCH_2O), 4.50-4.70(1H, m, OH), 4.66(2H, br s, OCH_2O), 5.50(1H, d, J=9 Hz, NH), 7.10-7.48(15H, m, aromatic protons); ^{13}C NMR($CDCl_3$): 28.21(q), 50.44(d), 55.70(q), 55.89(q), 56.14(q), 62.33(t), 77.14(d), 78.75(s),

80.45(d), 80.99(d), 86.49(s), 97.56(t), 98.09(t), 98.68(t), 126.75, 127.53, and 128.45(each d), 143.41(s), 155.16(s); MS *m/z* 655(M^+).

(2*R*,3*R*,4*R*,5*S*)-*N*-*tert*-Butoxycarbonyloxy-3,4,5-tri(methoxymethoxy)-2-(trityloxymethyl)piperidine (8) A mixture of **7b** (120 mg, 0.18 mmol), methanesulfonyl chloride (41 mg, 0.36 mmol), and TEA (37 mg, 0.36 mmol) in CH_2Cl_2 (3 mL) was stirred at 0° C for 30 min. After dilution with AcOEt, the mixture was washed with H_2O, saturated aqueous $NaHCO_3$, and H_2O. Drying followed by evaporation gave a residue, which was treated with potassium *tert*-butoxide(40 mg, 0.35 mmol) in THF (2 mL) at rt for 30 min. After dilution with AcOEt, the mixture was washed with half-saturated aqueous NaCl. Drying followed by evaporation gave a residue, which was purified by column chromatography (AcOEt:hexane =1:2) to give **8** (82 mg, yield 71%) as an oil, $[\alpha]_D$ +7.5° (c=1.4) ; IR ν max. (neat) 1688, 1418, 1038 cm^{-1}; ^1H NMR($CDCl_3$): 1.49(9H, s, *t*-Bu), 3.10-3.60(1H, m, CH_2), 3.32(6H, s, 2xCH_3), 3.45 (3H, s, OCH_3), 3.61-4.26(5H, m, 2xCH_2, 3xCH), 4.26-4.98(2H, m, 2xCH), 4.62(2H, br s, OCH_2O), 4.80(4H, br s, 2xOCH_2O), 7.11-7.64(15H, m, aromatic protons); ^{13}C NMR($CDCl_3$): 28.26(q), 39.62 and 40.74(t), 54.77(d), 55.46(q), 61.25(t), 71.73(d), 73.09(d), 75.63(d), 79.63(s), 86.35(s), 94.70 and 95.66(t), 126.75, 127.53, and 128.50(each d), 127.53, and 128.45(each d), 143.66(s), 154.96(s); MS *m/z* 636(M^+-1).

1-Deoxynojirimycin (9)

A mixture of **8** (65 mg, 0.10 mmol), 10% aqueous HCl (2 mL), and MeOH (2 mL) was stirred at 70°C for l h. After removal of the methanol *in vacuo*, the mixture was washed with AcOEt(x2) and the aqueous layer was placed on a Dowex 50W-X8 (H^+ form) column (10 ml), washed with 20 ml of H_2O, and eluted with 1 N NH_4OH. Freeze-drying of the appopriate fractions gave a residue, which was crystallized from MeOH-ether to give **9** (13 mg, 80%), which was identical to the authentic sample,[2] mp 195-197°C, $[\alpha]_D$ +46.5° (c=0.8, H_2O) ; ^{13}C NMR(D_2O, internal standard:dioxane δ=67.4): 49.56 (t), 61.35(d), 62.23(t), 71.73(d), 72.36 (d), 79.24(d).

1,1-Dimethylethyl *N*-[(1*R*,2*R*,3*S*,4*R*)- and (1*R*,2*R*,3*S*,4*S*)-2,3-Isopropylidenedioxy-4-methoxymethoxy-1-trityloxymethyl-5-hexenyl]carbamate (11a and 11b) These samples (**11a**, 368 mg, 62%; **11b**, 160 mg, 27%) were obtained from **10** (550 mg, 0.98 mmol) as an oil after column chromatography (AcOEt:hexane= 1: 4) in the same manner as described above for the preparation of **2c**. **11a**: $[\alpha]_D$ -42.2° (c=0.4) ; IR ν max. (neat) 1714, 1496, 1376, 1164 cm^{-1} ; ^1H NMR ($CDCl_3$):1.39(6H, s, 2xCH_3), 1.44(9H, s, *t*-Bu), 3.08-3.51(2H, m, CH_2), 3.32(3H, s, OCH_3), 4.10-4.41(4H, m, 4xCH), 4.41-4.80(2H, m, OCH_2O), 4 .90(1H, d, J=9 Hz, NH), 5.17-5.46(2H, m, $C\underline{H}_2$=CH), 5.71-6.16(1H, m, CH_2=C<u>H</u>), 7.07-7.59(15H, m, aromatic protons);^{13}C NMR($CDCl_3$): 25.34(q), 26.31(q), 28.12(q), 49.85(d), 55.46(q), 63.35(t), 76.07(d), 79.09(s), 79.77(d), 86.16(s), 94.44(t), 108.47(s), 118.42(t), 126.70, 127.48, and 128.35(each d), 135.37(d), 143.70(s), 154.77(s). **11b**: mp 128-130°C(AcOEt-hexane) ; $[\alpha]_D$ -29.8° (c=0.5) ; IR ν max. (nujol) 1710, 1498, 1374, 1166 cm^{-1}; ^1H NMR($CDCl_3$):1.36(6H, s, 2xCH_3), 1.43(9H, s, *t*-Bu), 3.01-3.35(2H, m, CH_2), 3.38(3H, s, OCH_3), 4.03-4.80(6H, m, CH_2, 4xCH), 4.90(1H, d, J=9 Hz, NH), 5.18-5.51(2H, m, $C\underline{H}_2$=CH), 5.60-6.01(1H, m, CH_2=C<u>H</u>), 7.07-7.59(15H, m, aromatic protons);^{13}C NMR($CDCl_3$): 24.71(q), 26.17(q), 28.17(q), 49.51(d), 55.60(q), 63.50(t), 75.44(d), 75.87(d), 78.75(d), 79.19(s), 86.16(s), 93.27(t),

108.13(s), 120.56(t), 126.75, 127.53, and 128.40(each d), 134.01(d), 143.75(s), 154.91(s); Anal. Calcd for $C_{36}H_{45}NO_7$: C, 71.62; H, 7.51; N, 2.32. Found: C, 71.33; H, 7.79; N, 2.11.

1,1-Dimethylethyl *N*-[(1*R*,2*R*,3*S*,4*R*)-2,3-Isopropylidenedioxy-4-methoxymethoxy-1-trityloxymethyl-5-hydroxypentyl]carbamate (12a) This sample (230 mg, 76%) was obtained from **11a** (300 mg, 0.50 mmol) as an oil after column chromatography (AcOEt:hexane= 2:3) in the same manner as described above for the preparation of **7b**, $[\alpha]_D$ -30.7° (c=0.6); IR ν max. (neat) 3444, 1708, 1062 cm^{-1}; ^1H NMR($CDCl_3$):1.39(15H, s, 2xCH_3, *t*-Bu), 2.98-3.50(2H, m, CH_2), 3.38(3H, s, OCH_3), 3.65-3.85(3H, m, OH, CH_2), 3,98-4.55(4H, m, 4xCH), 4.60-4.97(3H, m, 2xCH, NH), 7.14-7.55(15H, m, aromatic protons); ^{13}C NMR($CDCl_3$): 25.49(q), 26.36(q), 28.12(q), 49.51(d), 55.50(q), 63.20(t), 64.47(t), 75.34(d), 77.72(s), 79.57(d), 80.45(d), 86.25(s), 97.22(t), 108.72(s), 126.75, 127.58, and 128.35(each d), 143.66(s), 155.10(s); MS *m/z* 607(M^+).

(2*R*,3*R*,4*S*,5*R*)-*N*-*tert*-Butoxycarbonyloxy-3,4-isopropylidenedioxy-5-methoxymethoxy-2-(trityloxymethyl)piperidine (13a) This sample (126 mg, 82%) was obtained from **12a** (160 mg, 0.26 mmol) as an oil after column chromatography (AcOEt:hexane= 1: 3) in the same manner as described above for the preparation of **8**, $[\alpha]_D$ -44.5° (c=0.4) ; IR ν max. (neat) 1694, 1408, 1228, 1090 cm^{-1}; ^1H NMR($CDCl_3$):1.30(6H, s, 2xCH3), 1.46(9H, s, t-Bu), 2.84-3.18(3H, m, CH_2, CH), 3.32(3H, s, OCH_3), 3.50-3.83(1H, m, CH), 3.83-4.23(3H, m, 3xCH), 4.49-4.87(3H, m, CH, OCH_2O), 7.13-7.53(15H, m, aromatic protons); ^{13}C NMR($CDCl_3$): 25.44(q), 27.24(q), 27.87(q), 40.64 and 42.05(t), 51.75 and 52.63(d), 54.72(q), 62.81 and 63.50(t), 72.36 and 72.09(d), 74.07 and 74.67(d), 75.77 and 76.51(d), 79.53(s), 86.64(s), 94.73 and 94.97(t), 107.55(s), 126.65, 127.38, and 128.11(each d), 143.12(s), 154.67(s); MS *m/z* 588(M^+-1).

(2*R*,3*R*,4*S*,5*R*)-2-Hydroxymethyl-3,4,5-piperidinetriol (14) This sample (19 mg, 85%) was obtained from **13a** (80 mg, 0.14 mmol) as an oil in the same manner as described above for the preparation of **9**, $[\alpha]_D$ +17.9° (c=1.3, H_2O) ; ^1H NMR(D_2O, DHO: δ=4.70): 2.53-3.01(3H, m), 3.58-3.97(5H, m); ^{13}C NMR(D_2O, internal standard:dioxane δ=67.4): 45.42(t), 56.43(d), 61.69(t), 67.05(d), 70.22(d), 71.48(d). Hydrochloride of **14**: mp 103-105°C (MeOH-ether): $[\alpha]_D$ +54.3° (c=0.7, H_2O) ; ^1H NMR(D_2O, DHO:δ=4.70): 3.05-3.47(3H,m), 3.65-4.20(5H,m); ^{13}C NMR(D_2O, internal standard: dioxane δ=67.4): 44.78(t), 56.72(d), 59.06(t), 64.47(d), 67.05(d), 69.34(d); Anal. Calcd for $C_6H_{14}NO_4Cl$: C, 36.10; H, 7.07; N, 7.02. Found: C, 35.87; H, 7.32; N, 6.81.

Physical and nmr data of 12b, 13b, and 15 **12b**:$[\alpha]_D$ -43.9° (c=0.4) ; ^1H NMR($CDCl_3$):1.25 and 1.32(6H, each s, 2xCH3), 1.45(9H, s, *t*-Bu), 3.11-3.58(2H, m, CH_2), 3.41(3H, s, OCH_3), 3.58-3.83(3H, m, OH, CH_2), 3.85-4.50(4H, m, 4xCH), 4.69 and 4,76(2H, AB q, J=7 Hz, OCH_2O), 5.04(1H, d, J=8 Hz, NH), 7.11-7.58(15H, m, aromatic protons); ^{13}C NMR($CDCl_3$): 24.80(q), 26.60(q), 28.07(q), 50.05(d), 55.46(q), 63.35(t), 76.12(d), 79.09(s), 79.53(d), 86.06(s), 96.92(t), 107.79(s), 126.55, 127.38, and 128.31(each d), 143.60(s), 154.82(s). **13b**: $[\alpha]_D$ -42.1° (c=0.4) ; ^1H NMR($CDCl_3$) : 1.31 and 1.47(6H, each s, 2xCH_3), 1.42(9H, s, *t*-Bu), 2.92-3.60(4H, m, CH_2, 2xCH), 3.31(3H, s, OCH_3), 3.60-3.97(1H, m, CH), 4.10-4.51(3H, m, 3xCH), 4.60(2H, s, OCH_2O), 7.01-7.50(15H, m, aromatic protons); ^{13}C NMR($CDCl_3$): 23.88(q), 25.97(q), 28.17(q), 39.08 and 40,74(each t), 53.16(d),

108.13(s), 120.56(t), 126.75, 127.53, and 128.40(each d), 134.01(d), 143.75(s), 154.91(s); Anal. Calcd for $C_{36}H_{45}NO_7$: C, 71.62; H, 7.51; N, 2.32. Found: C, 71.33; H, 7.79; N, 2.11.

1,1-Dimethylethyl *N*-[(1*R*,2*R*,3*S*,4*R*)-2,3-Isopropylidenedioxy-4-methoxymethoxy-1-trityloxymethyl-5-hydroxypentyl]carbamate (12a) This sample (230 mg, 76%) was obtained from **11a** (300 mg, 0.50 mmol) as an oil after column chromatography (AcOEt:hexane= 2:3) in the same manner as described above for the preparation of **7b**, $[\alpha]_D$ -30.7° (c=0.6); IR ν max. (neat) 3444, 1708, 1062 cm^{-1}; ^1H NMR($CDCl_3$):1.39(15H, s, 2xCH_3, *t*-Bu), 2.98-3.50(2H, m, CH_2), 3.38(3H, s, OCH_3), 3.65-3.85(3H, m, OH, CH_2), 3,98-4.55(4H, m, 4xCH), 4.60-4.97(3H, m, 2xCH, NH), 7.14-7.55(15H, m, aromatic protons); ^{13}C NMR($CDCl_3$): 25.49(q), 26.36(q), 28.12(q), 49.51(d), 55.50(q), 63.20(t), 64.47(t), 75.34(d), 77.72(s), 79.57(d), 80.45(d), 86.25(s), 97.22(t), 108.72(s), 126.75, 127.58, and 128.35(each d), 143.66(s), 155.10(s); MS *m/z* 607(M^+).

(2*R*,3*R*,4*S*,5*R*)-*N*-*tert*-Butoxycarbonyloxy-3,4-isopropylidenedioxy-5-methoxymethoxy-2-(trityloxymethyl)piperidine (13a) This sample (126 mg, 82%) was obtained from **12a** (160 mg, 0.26 mmol) as an oil after column chromatography (AcOEt:hexane= 1: 3) in the same manner as described above for the preparation of **8**, $[\alpha]_D$ -44.5° (c=0.4) ; IR ν max. (neat) 1694, 1408, 1228, 1090 cm^{-1}; ^1H NMR($CDCl_3$):1.30(6H, s, 2xCH3), 1.46(9H, s, t-Bu), 2.84-3.18(3H, m, CH_2, CH), 3.32(3H, s, OCH_3), 3.50-3.83(1H, m, CH), 3.83-4.23(3H, m, 3xCH), 4.49-4.87(3H, m, CH, OCH_2O), 7.13-7.53(15H, m, aromatic protons); ^{13}C NMR($CDCl_3$): 25.44(q), 27.24(q), 27.87(q), 40.64 and 42.05(t), 51.75 and 52.63(d), 54.72(q), 62.81 and 63.50(t), 72.36 and 72.09(d), 74.07 and 74.67(d), 75.77 and 76.51(d), 79.53(s), 86.64(s), 94.73 and 94.97(t), 107.55(s), 126.65, 127.38, and 128.11(each d), 143.12(s), 154.67(s); MS *m/z* 588(M^+-1).

(2*R*,3*R*,4*S*,5*R*)-2-Hydroxymethyl-3,4,5-piperidinetriol (14) This sample (19 mg, 85%) was obtained from **13a** (80 mg, 0.14 mmol) as an oil in the same manner as described above for the preparation of **9**, $[\alpha]_D$ +17.9° (c=1.3, H_2O) ; ^1H NMR(D_2O, DHO: δ=4.70): 2.53-3.01(3H, m), 3.58-3.97(5H, m); ^{13}C NMR(D_2O, internal standard:dioxane δ=67.4): 45.42(t), 56.43(d), 61.69(t), 67.05(d), 70.22(d), 71.48(d). Hydrochloride of **14**: mp 103-105°C (MeOH-ether): $[\alpha]_D$ +54.3° (c=0.7, H_2O) ; ^1H NMR(D_2O, DHO:δ=4.70): 3.05-3.47(3H,m), 3.65-4.20(5H,m); ^{13}C NMR(D_2O, internal standard: dioxane δ=67.4): 44.78(t), 56.72(d), 59.06(t), 64.47(d), 67.05(d), 69.34(d); Anal. Calcd for $C_6H_{14}NO_4Cl$: C, 36.10; H, 7.07; N, 7.02. Found: C, 35.87; H, 7.32; N, 6.81.

Physical and nmr data of 12b, 13b, and 15 **12b**:$[\alpha]_D$ -43.9° (c=0.4) ; ^1H NMR($CDCl_3$):1.25 and 1.32(6H, each s, 2xCH3), 1.45(9H, s, *t*-Bu), 3.11-3.58(2H, m, CH_2), 3.41(3H, s, OCH_3), 3.58-3.83(3H, m, OH, CH_2), 3.85-4.50(4H, m, 4xCH), 4.69 and 4,76(2H, AB q, J=7 Hz, OCH_2O), 5.04(1H, d, J=8 Hz, NH), 7.11-7.58(15H, m, aromatic protons); ^{13}C NMR($CDCl_3$): 24.80(q), 26.60(q), 28.07(q), 50.05(d), 55.46(q), 63.35(t), 76.12(d), 79.09(s), 79.53(d), 86.06(s), 96.92(t), 107.79(s), 126.55, 127.38, and 128.31(each d), 143.60(s), 154.82(s). **13b**: $[\alpha]_D$ -42.1° (c=0.4) ; ^1H NMR($CDCl_3$) : 1.31 and 1.47(6H, each s, 2xCH3), 1.42(9H, s, *t*-Bu), 2.92-3.60(4H, m, CH_2, 2xCH), 3.31(3H, s, OCH_3), 3.60-3.97(1H, m, CH), 4.10-4.51(3H, m, 3xCH), 4.60(2H, s, OCH_2O), 7.01-7.50(15H, m, aromatic protons); ^{13}C NMR($CDCl_3$): 23.88(q), 25.97(q), 28.17(q), 39.08 and 40,74(each t), 53.16(d),

55.26(q), 63.59(t), 70.17(d), 71.63(s), 74.21(d), 79.67(s), 86.98(s), 95.36(t), 108.33(s), 126.94, 127.62, and 128.35(each d), 143.21(s), 154.86(s). **15**: mp 149-150°C (MeOH-ether): $[\alpha]_D$ +28.1° (c=0.8, H_2O); ^1H NMR(D_2O, DHO: δ=4.70):2.39-2.87(3H, m), 3.30-3.80(4H, m), 3.90-4.05(1H, m); ^{13}C NMR(D_2O, internal standard:dioxane δ=67.4): 44.44(t), 55.36(d), 62.03(t), 68.91(d), 69.39(d), 72.27(d); Anal. Calcd for $C_6H_{13}NO_4$: C, 44.16; H, 8.03; N, 8.58. Found: C, 43.90; H, 8.37; N, 8.34.

ACKNOWLEGDEMENT

The authors are grateful to Professor K. Koga (University of Tokyo) for spectral measurements. Partial financial supports by a Grant-in-Aid for Scientific Research (No. 07672307) from Ministry of Education, Science, Sports and Culture, Japan, and a grant from the Japan Research Foundation for Optically Active Compounds are gratefully acknowledged. This study was performed through Special Coordination Funds of the Science and Technology Agency of the Japanese Government.

REFERENCES AND NOTES

1. a) S. Inoue, T. Tsuruoka, T. Ito, and T. Niida, *Tetrahedron*, 1968, **23**, 2125; b) D. D. Schnidt, W. Frommer, L. Muler, and E. Truseeheiy, *Naturwissenschaften*, 1979, **66**, 584 ; c) R. C. Bernotas and B. Ganem, *Tetrahedron Lett.*, 1985, **26**, 1123 ; d) G. W. J. Fleet, L. E. Fellows, and P. W. Smith, *Tetrahedron*, 1987, **43**, 979; e) H. Iida, N. Yamazaki, and C. Kibayashi, *J. Org. Chem.*, 1987, **52**, 3337; f) T. Kiguchi, K. Tajiri, I. Ninomiya, T. Naito, and H. Hiramatsu, *Tetrahedron Lett.*, 1995, **36**, 253.
2. N. Ikota, *Heterocycles*, 1989, **29**, 1469.
3. N. Ikota, *Heterocycles*, 1995, **41**, 983.
4. K. B. Sharpless, W. Amberg, Y. L. Bennani, G. A. Crispino, J. Hartung, K-S. Jeong, H.-L. Kwong, K. Morikawa, Z-M. Wang, D. Xu, and X-L. Zhang, *J. Org. Chem.*, 1992, **57**, 2768.
5. N. Ikota, *Heterocycles*, 1993, **36**, 2035.
6. A. J. Mancuso, S.-L. Huang, and D. Swern, *J. Org. Chem.*, 1978, **43**, 2480.
7. K. Mead and T.L. Macdonald, *J. Org. Chem.*, 1985, **50**, 422.
8. N. Ikota, *Tetrahedron Lett.*, 1992, **33**, 2553.
9. N. Asano, K. Oseki, H. Kizu, and K. Matsui, *J. Med. Chem.*, 1994, **37**, 3701.

Received, 3rd February, 1997

Vol. 45, No. 6, September 1998 BIOCHEMISTRY *and* MOLECULAR BIOLOGY INTERNATIONAL
Pages 1129–1138

SPIN TRAPPING FOR NITRIC OXIDE PRODUCED IN LPS-TREATED MOUSE USING VARIOUS NEW DITHIOCARBAMATE IRON COMPLEXES HAVING SUBSTITUTED PROLINE AND SERINE MOIETY

Hidehiko Nakagawa‡, Nobuo Ikota‡, Toshihiko Ozawa‡*,
Toshiki Masumizu§, and Masahiro Kohno§
‡National Institute of Radiological Sciences, Chiba,
and §Analytical Instruments Division, JEOL Ltd., Tokyo, Japan

Received May 6, 1998

Summary

Four dithiocarbamate derivatives of 4-substituted L-proline and *N*-methyl-L-serine were synthesized, and their iron complexes were prepared in Tris-HCl buffer solution. These complexes were used as spin trapping reagents for nitric oxide in ESR spectrometry, and compared with each other in regard to their spin trapping properties *in vivo*. When the synthesized complexes were injected to lipopolysaccharide-treated mice intravenously, the nitric oxide adducts were detected both in the liver and in the blood except *N*-dithiocarboxy-4-(methoxymethyl)oxy-L-proline iron complex, whose nitric oxide adduct was detected mostly in the blood. When the exogenous nitric oxide adduct of this complex was injected, it was not detected in the liver, too. It is considered that this complex can trap nitric oxide in the blood by excluding the accumulation of the nitric oxide adduct in the liver.

Keyword; nitric oxide, dithiocarbamate iron complex, spin trapping, L-proline derivative, distribution

Introduction

Oxygen radicals are thought not only to be toxic compounds in oxidative stress but also to be important modulators or messengers in biological responses. Nitric oxide, a free radical molecule like oxygen radicals, is an endogenous compound which plays important roles in biological systems such as vasodilation, neural transmission, and excitotoxicity (1-8). Nitric oxide is considered to be relatively unstable under biological conditions, and to have a short life time *in vivo*. Because of this chemical property, it is difficult to detect and estimate nitric oxide directly in biological systems.

Abbreviations: LPS; lipoporisaccharide, MGD; *N*-methyl-D-glucamine dithiocarbamate, DTCS; *N*-dithiocarboxysarcosine, DTCP; *N*-dithiocarboxy-L-proline, DTCMP; *N*-dithiocarboxy-4-*trans*-methoxymethyl-L-proline, DTCTP; *N*-dithiocarboxy-4-*trans*-(2-tetrahydropyranyl)oxymethyl-L-proline, MSD; *N*-methyl-L-serine dithiocarbamate, L-NMMA; N^G-monomethyl-L-arginine, $Fe(DTC)_2$; dithiocarbamate iron complex, NOFe(DTC)2 derivative; nitric oxide adduct of $Fe(DTC)_2$ derivative, NOFe(DTCMP)2; nitric oxide adduct of $Fe(DTCMP)_2$, NOFe(MGD)2; nitric oxide adduct of $Fe(MGD)_2$, NOFe(MSD)2; nitric oxide adduct of $Fe(MSD)_2$.

*To whom correspondence should be addressed at: National Institute of Radiological Sciences, 9-1, Anagawa-4, Inage-ku, Chiba 263, Japan. Fax No: +81-43-255-6819, e-mail: ozawa@nirs.go.jp.

Spin trapping method is a useful method for the detection of unstable radicals. Radicals are trapped by non-radical spin trapping reagents, so-called spin traps, and converted to relatively stable radical adducts, spin adducts, which can be observed with an ESR spectrometer. For this purpose, the spin traps should have high reactivities and selectivities for the short-lived radicals to be detected. This method has been used to detect some reactive oxygen species and free radicals such as hydroxyl radical, superoxide, and thiyl radicals (9-14).

Although spin trapping of nitric oxide in biological systems, *e.g.* in a mouse body, has been reported (15-23), the distribution of spin adducts were not considered to reflect the site of the nitric oxide production because the nitric oxide adducts of the spin traps used previously have tendency to accumulate in the liver of mice (17, 21). Using these spin traps, the amount of the nitric oxide adduct may only represent the total nitric oxide producibility, but do not reflect the production in blood. In this study, we synthesized dithiocarbamate of proline derivatives and serine, and investigated their iron complexes as the improved spin traps for nitric oxide. Then we found that the nitric oxide adducts of all the synthesized iron complexes could be detected in the liver and the blood except one of the complexes, $Fe(DTCMP)_2$, which had the property that its nitric oxide adduct was not detected in the liver but detected in the blood, unlike typical known spin traps for nitric oxide.

Methods

All chemicals used in this study were purchased from Wako Chemical Ind. (Osaka, Japan) and Aldrich (Milwaukee, WI, USA). Ar gas and pure N_2 gas were from Nippon Sanso (Tokyo, Japan), NO gas from Sumitomo Seika (Osaka, Japan). Animals were purchased from SLC (Hamamatsu, Japan) and kept in air-conditioned and light-controlled rooms.

1) Synthesis of N-dithiocarboxy-L-proline derivatives (1-3), N-dithiocarboxy-N-methyl-L-serine (4) and their iron complexes (5-8) (24) (Fig. 1)

To L-proline and *N*-methyl-L-serine solution in pre-cooled aqueous ammonia, carbon disulfide in a small amount of ethanol was slowly added at 0°C. After becoming homogenous, the mixture was lyophilized to yield pale yellow powder of *N*-dithiocarboxy-L-proline (1), and *N*-dithiocarboxy-*N*-methyl-L-serine (4). After modification of the hydroxyl group in 4-*trans*-hydroxy-L-proline to methoxymethyl or tetrahydropyranyl ether, these 4-substituted L-prolines were similarly converted to the corresponding dithiocarbamates (2, 3). The structures of all dithiocarbamate derivatives were confirmed by a ^1H- and ^{13}C-NMR spectra. Each dithiocarbamate was mixed with ferrous sulfate (2.2:1) in 40mM Tris HCl buffer (pH 7.4) under anaerobic conditions to yield dark red or dark green colored complex solution. Prepared complexes were stored under anaerobic conditions at 4°C.

2) Measurement of the affinity for nitric oxide and the hydrophobicity of $Fe(DTC)_2$ derivatives.

a) Measurement of the affinity of $Fe(DTC)_2$ derivatives for nitric oxide.

The aqueous solution of nitric oxide was prepared by bubbling of gaseous nitric oxide to Ar gas-bubbled 40mM Tris-HCl buffer under anaerobic conditions. The concentration of prepared solution was determined using Griess reaction as follows: the prepared nitric oxide solution was diluted with non Ar gas-purged Tris-HCl buffer and mixed with Griess reagent (25). The concentration was determined from the calibration curve of authentic $NaNO_2$ solution. The concentrations of all prepared nitric oxide solutions in Tris buffer were in the range of 6-7mM.

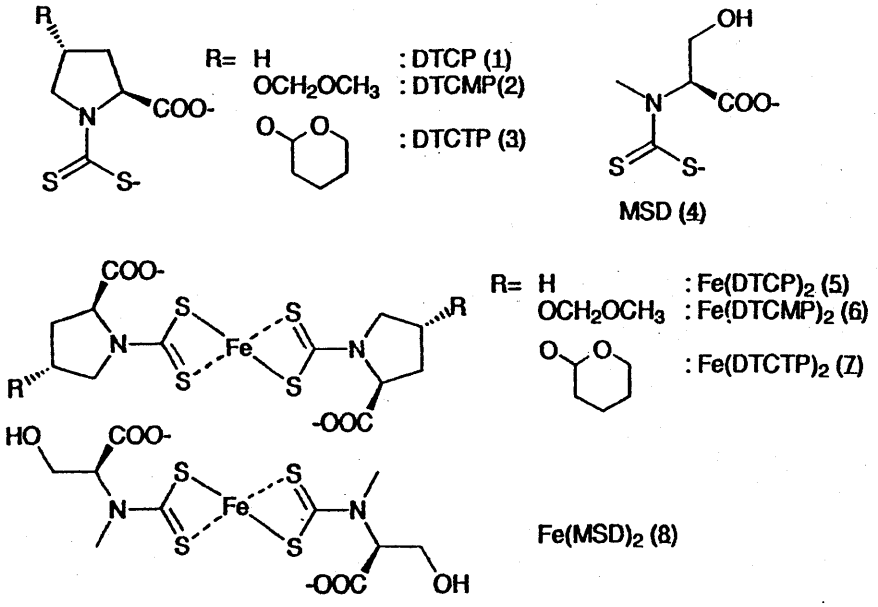

Fig. 1 Structures of synthesized dithiocarbamates and their iron complexes.

Various amounts of the nitric oxide solution were added to the 0.5mM solution of Fe(DTC)2 derivatives, and the aliquots of the mixture were measured with a 9.5GHz ESR spectrometer (JES RE-1X, JEOL, Tokyo). The amount of nitric oxide adduct was determined from the ESR signal intensity. ESR measurement was carried out at the following settings; microwave frequency was 9.43GHz, power 10mW, modulation frequency and range 100kHz/0.125mT.

b) Measurement of Rf values of synthesized Fe(DTC)2 derivatives on reversed-phase thin layer chromatography.

Synthesized Fe(DTC)2 derivatives were developed on PLC RP-18F254S (Merck, Darmstat, Germany). The mobile phase was a mixture of Tris-HCl (40mM, pH7.4) and acetonitrile (v/v 2:1). A single black-colored spot was detected and its Rf value was determined.

3) Measurement of endogenous nitric oxide trapped by Fe(DTC)2 derivatives in living mice treated with lipopolysaccharide (LPS)

To the ICR mice (5w, female) which were treated with LPS (E. coli 026B6, 5 or 10mg/kg i.v.) 5 hr before, the synthesized Fe(MSD)2 and Fe(MGD)2 (110mg/kg as iron) were injected subcutaneously. The spectra of the mouse body (upper abdomen) were measured 2 hr after the treatment of the iron complex using a low frequency ESR spectrometer with a loop-gap resonator (JEOL). The spectra were accumulated on the computed analyzing system 30 times. ESR measurement settings were follows; microwave frequency and power 1.1GHz/4.0mW, modulation frequency and width 100kHz/1.25mT.

4) Measurement of endogenous NO trapped by Fe(DTC)2 derivatives in LPS-treated mouse liver and blood.

Synthesized Fe(DTC)2 derivatives (23mg/kg as Fe) as spin traps were intravenously injected to mice (ddY, male, 5w) which had been pretreated with LPS (E.coli 026:B6, 250mg/kg) intravenously. For the inhibitory experiment, N^G-monomethyl-L-arginine (L-NMMA) (100mg/kg) was additionally injected 3 times at 1 hr intervals intraperitoneally. At 15 or 30 min after injection of the spin traps, whole blood was collected and measured by 9.5GHz ESR spectroscopy within 6 min at the following settings; microwave frequency and power 9.43GHz/10mW, modulation frequency and range 100kHz/0.125mT. Immediately after the collection of the blood, the liver was removed and homogenized with an equal volume of 40mM Ar gas-bubbled Tris-HCl buffer. The

liver homogenate was measured under the same conditions as for the blood. The relative signal intensity for the standard signal of Mn^{2+} doped in MgO was calculated for each sample. The relative signal intensity in liver homogenate was converted to the relative intensity in the liver.

5) Measurement of the NO-trapping abilities of Fe(DTC)2 derivatives in the LPS-pretreated mouse liver homogenate.

Five hours after LPS-treatment (250mg/kg, i.v.), the liver of the anesthetized mouse (ddY, female, 5w) was perfused with phosphate buffered saline (12ml) and then removed. The liver (ca 1.2g) was homogenized with phosphate buffered saline (3.5ml) on ice bath. The liver homogenate was freshly prepared for each experiment.

To 200μl of the liver homogenate was added 4μl of 50mM Fe(DTC)2 derivative and the mixture was incubated at 37°C for 20 min. After incubation, 40μl of 6mM nitric oxide solution in Tris-HCl buffer (40mM, pH7.4) was added to the homogenate, and the aliquot of the mixture was measured with a 9.5GHz ESR spectrometer with in 4 min. ESR conditions were the same as described above. The formation of nitric oxide adduct was represented in a percentage for the non-incubated control. The accurate concentration of the nitric oxide solution was determined by the same way as described above, and the excess amount of nitric oxide was used for the complex.

6) Measurement of exogenously treated NOFe(DTC)2 derivatives in lipopolysaccharide-treated mouse liver and blood.

To prepare for NOFe(DTC)2 derivatives, gaseous nitric oxide was bubbled into the 50mM solution of the synthesized complex for 10 min. The aliquot (0.2ml) of the resulted solution was intravenously injected to a mouse (ddY, female, 5w) 5hr after LPS (E.coli, 026B6) treatment. At the sampling time, the blood was collected, and the liver was immediately removed and homogenized with Ar-bubbled Tris-HCl buffer (40mM, pH7.4) on ice bath within 4 min. ESR spectra of the blood and the liver samples were measured with 9.5GHz ESR spectrometer soon after collection and homogenization, respectively. The condition for the measurement was same as the experiment 2) described above.

Results

The synthesized dithiocarbamate iron complexes shown in Fig. 1 were all water-soluble. They produced the spin adducts with nitric oxide *in vitro*, which could be detected with a 9.5GHz ESR spectrometer. The amount of the nitric oxide adduct formed *in vitro* was dependent on the dose of nitric oxide, and was similar among the iron complexes examined in Tris-HCl buffer solution. It is therefore confirmed that the synthesized iron complexes have the similar nitric oxide-trapping ability (data not shown).

When Fe(MSD)2 was injected subcutaneously to the LPS (E. coli 026B6)-pretreated mice, the ESR signal of nitric oxide trapped by the iron complex was detected in the living mouse body using a low frequency ESR spectrometer with a loop-gap resonator (Fig. 2). Using Fe(MGD)2 complex, the nitric oxide-adduct could be also detected in the LPS-treated mice body, but the signal intensity was weaker than in the case of Fe(MSD)2.

When these iron complexes as spin traps were intravenously injected to the mice pretreated with LPS (E.coli 026B6, 250mg/kg i.v.), the nitric oxide adducts of the iron complexes were detected in the liver and the blood (Fig. 3a, Table 1, 2) using a 9.5GHz ESR spectrometer. These nitric oxide adducts were shown to be produced from the endogenous nitric oxide because the pretreatment of L-NMMA, nitric oxide synthase inhibitor, decreased the formation of the nitric

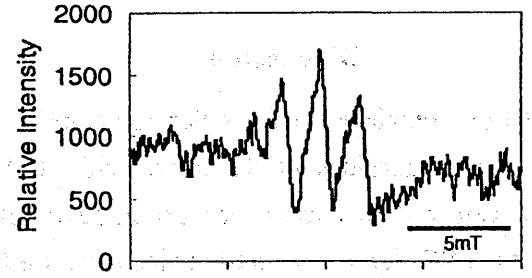

Fig. 2 In vivo ESR spectrum of nitric oxide trapped by Fe(MSD)2 in the body of LPS-treated mouse.
To the ICR mice (5w, female) which were treated with LPS (E. coli 026B6, 5 or 10mg/kg i.v.) 5 hr before, the synthesized Fe(MSD)2 and Fe(MGD)2 (110mg/kg as iron) were injected subcutaneously. The spectra of the mouse body (upper abdomen) were measured 2 hr after the treatment of the iron complex using a low frequency ESR spectrometer with a loop-gap resonator. The measurement conditions were as discribed in the Methods.

oxide adduct (Fig. 3b). The formation of the nitric oxide adducts of the tested iron complexes were different each other at 5.5 hr after LPS treatment. Using Fe(DTCMP)2 (8), its nitric oxide adduct was hardly detected in the liver, but detected in the blood. In the case of the other spin traps, the amount of the detected nitric oxide adducts were larger in the liver than in the blood. The ratio of the ESR signal intensity in the liver and in the blood also differed from each other (Fig. 4).

By reversed-phase TLC analysis, the complexes were found to have diverse Rf values, i.e. different hydrophobicities (Table 3), which was assumed to be due to its functional group at 4-position in the pyrrolidine ring. However, no relation between the liver/blood ratio of the signal intensity and the Rf value were observed.

For the estimation of the stability or the metabolism of the synthesized iron complexes in the liver of the LPS-pretreated mouse, the change of the spin trapping abilities of these complexes during the incubation in the liver homogenate were examined. The liver homogenate was freshly prepared from the LPS-treated mouse liver. The iron complexes were incubated in the homogenate at 37°C for 20 min, and then their nitric oxide-trapping abilities were estimated. After incubation, the trapping abilities of all the tested iron complexes, including Fe(DTCMP)2, were little changed, and rather increased†. The stability of the nitric oxide adducts themselves in the liver homogenate were also examined, and found they were stable in the homogenate for 20 min incubation.

When exogenous NOFe(DTCMP)2 was injected into the tail vein of the LPS-pretreated mouse, the ESR signal of the nitric oxide adduct in the blood was detected after injection. However, the signals were hardly detected in the liver at any sampling time. (Fig. 5).

† The increase of the trapping abilities was considered to be due to the reduction of the iron complexes in the liver homogenate. The addition of the reductant such as L-ascorbate or cysteamine in phosphate buffered saline also caused the increase of the trapping ability of long-time stored spin traps. These iron complexes were assumed to have been partly oxidized by small amounts of remaining oxygen. So, in the experiment *in vivo*, the iron complexes freshly prepared as possible were used.

Discussion

Although the synthesized iron complexes had similar nitric oxide-trapping ability in the experiment *in vitro*, the ESR signal intensities of the nitric oxide adducts detected in LPS-pretreated mice liver and blood were different from each other. Especially, unlikely other iron complexes, $Fe(DTCMP)_2$ gives the ESR signal of its nitric oxide adduct actually only in the blood. This result means that $Fe(DTCMP)_2$ should have different property from other iron complexes *in vivo*. Using $Fe(MSD)_2$, endogenous nitric oxide induced by LPS was trapped and detected in the

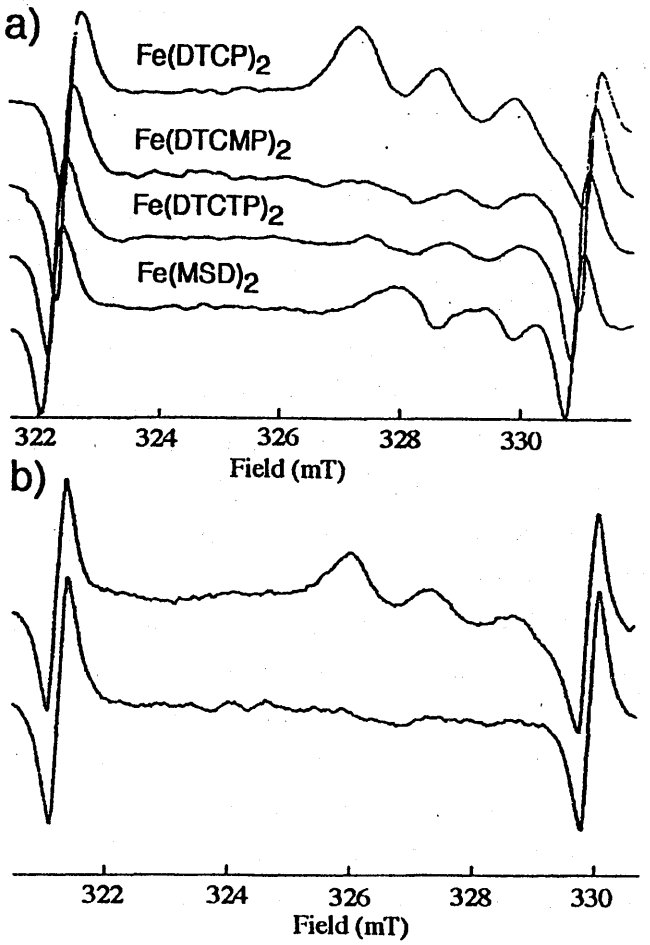

Fig. 3 ESR spectra of nitric oxide adducts of $Fe(DTC)_2$ derivatives in LPS-pretreated mouse blood.
The spectra were modified by the computer using the smoothing method for excluding noises. $Fe(DTC)_2$ derivatives as spin traps were injected intravenously to the mice (ddY, male, 5w) which had been pretreated with lipopolysaccharide (LPS, E.coli 026:B6, 250mg/kg) intravenously. The collected blood was measured with 9.5GHz ESR spectrometer within 6 min at the following settings; microwave frequency and power 9.43GHz/10mW, scan range 10mT, modulation frequency and range 100kHz/0.125mT. a); ESR spectra were measured at 5.5 hr after LPS treatment and at 0.5 hr after the injection of $Fe(DTC)_2$ derivatives. b); Spectra from $Fe(DTCP)_2$-injected mice (upper) and from L-NMMA- and $Fe(DTCP)_2$-injected mice (lower) after LPS-treatment.

Table 1 Relative signal intensity of nitric oxide adducts in LPS-treated mouse blood

$Fe(DTC)_2$	time after LPS teatment (hr)		
	3	5	7
$Fe(DTCP)_2$	0.126	0.213	0.190
$Fe(DTCMP)_2$	0.067	0.117	0.149

Each $Fe(DTC)_2$ derivative as a spin trap was injected intravenously. At 30 min after injection, the whole blood was collected and measured with a 9.5GHz ESR spectrometer. Treatment and measurement conditions are described in the Methods section.

Table 2 Relative signal intensity of nitric oxide adducts in mouse liver and blood after LPS-treatment

$Fe(DTC)_2$	liver	blood	liver/blood ratio
$Fe(DTCP)_2$	0.70	0.37	1.89
$Fe(DTCMP)_2$	0.04	0.11	0.364
$Fe(DTCTP)_2$	0.77	0.11	6.81
$Fe(MSD)_2$	4.09	0.2	20.9

The liver/blood ratio was the average of two or three samples. Signal intensities were measured in mouse liver homogenate and blood at 0.5 hr after intravenous injection of $Fe(DTC)_2$ and at 5.5 hr after LPS treatment.

living mice body by a low frequency ESR spectrometer. However, we do not succeeded to detect the nitric oxide adduct of $Fe(DTCMP)_2$ yet. These results are consistent with the *ex vivo* evidence that $NOFe(MSD)_2$ was accumulated to the liver but $NOFe(DTCMP)_2$ was not.

When these iron complexes were incubated in the liver homogenate from the LPS-pretreated mouse, the trapping abilities of all the tested complexes, including $Fe(DTCMP)_2$, were not so changed after the incubation for 20 min. Therefore, it was found that they were not decomposed so rapidly in the liver. The difference of the liver/blood ratio between $Fe(DTCMP)_2$ and the other complexes is not attributed to the metabolism of these iron complexes in the liver.

However, in the case of the injection of $NOFe(DTCMP)_2$, the nitric oxide adduct was hardly detected in the liver. These results suggest that $NOFe(MGD)_2$ and $NOFe(MSD)_2$ were accumulated in the liver, but $NOFe(DTCMP)_2$ was not accumulated in the liver. Although the bolus exogenous spin adduct gradually decreased in the blood, nitric oxide adduct of $Fe(DTCMP)_2$ produced *in vivo* could be detected for over an hours in the blood of the LPS-pretreated mouse, because the spin adduct was continuously produced in the LPS-treated mouse body.

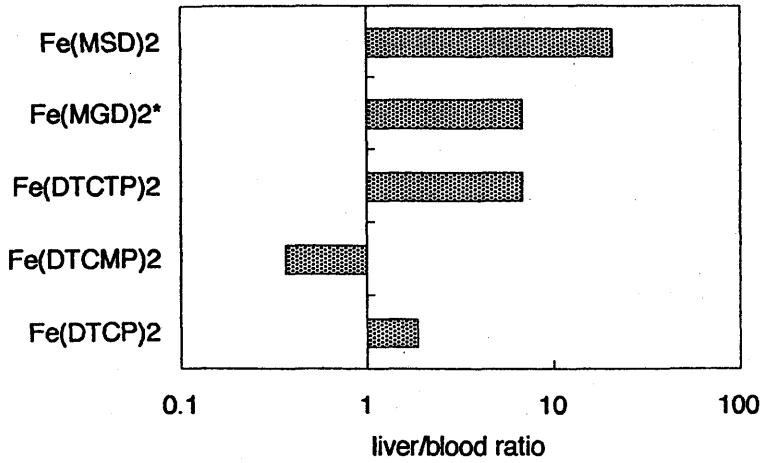

Fig. 4 Ratio of the amount of nitric oxide adducts between the liver and the blood of LPS-treated mouse.
The ratio between the liver and the blood was calculated by dividing the relative signal intensities in the liver by that in the blood. The ratio of $Fe(MGD)_2$ (asterisked) was calculated from the result of a subcutaneous administration given in the literature (17). When $Fe(MGD)_2$ was injected intravenously, the ratio was larger than that in the case of subcutaneous injection.

Table 3 Rf values of dithiocarbamate iron complexes in reversed-phase thin layer chromatography

complex	Rf value
$Fe(DTCP)_2$	0.18
$Fe(DTCMP)_2$	0.21
$Fe(DTCTP)_2$	0.049
$Fe(MGD)_2$	0.47
$Fe(DTCS)_2$	0.33
$Fe(MSD)_2$	0.73

Complexes were developed on RP-18 F254S (C18) (Merck, Darmstat, Germany) with Tris-HCl (pH7.4, 40mM):acetonitrile (2:1, v/v) as the mobile phase. The complexes above the dotted line have a proline moiety and below have a linear strucure.

The nitric oxide adduct of $Fe(DTCMP)_2$ was not detected in the liver either in the case of detecting the spin adduct of the endogenous nitric oxide nor in the case of injecting the exogenous $NOFe(DTCMP)_2$. While, in the mouse liver homogenate, $Fe(DTCMP)_2$ hold the ability to form the nitric oxide adduct with the additive nitric oxide even after the incubation. This means $Fe(DTCMP)_2$ was not decomposed in the mouse liver homogenate for the incubation. If the injected $Fe(DTCMP)_2$ could be accumulated in the liver tissue, the ESR signal of the nitric oxide adduct should be detected in the liver, but actually it was not detected. In any urine sample from

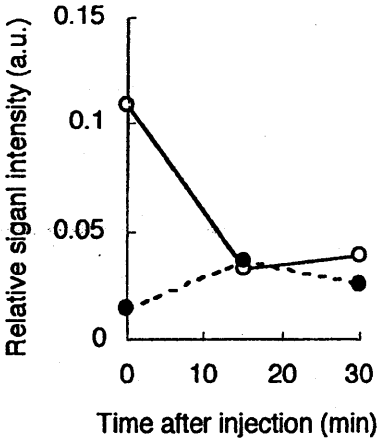

Fig. 5 Relative signal intensity in liver homogenate and blood from the mouse treated with exogenous NOFe(DTCMP)2.
The blood and liver were collected at 0, 15 or 30 min after injection of Fe(DTCMP)2 to the LPS-pretreated mice. The relative siganl intensity in the blood (open circle, solid line) and the liver homogenate (closed circle, dotted line) were measured with a 9.5 GHz ESR spectrometer.

the LPS-pretreated mouse after the injection of Fe(DTCMP)2, no spin adduct signals were detected. Therefore, the nitric oxide adducts formed in the mouse were not excreted within the measurement time. According to these results, it is suggested that Fe(DTCMP)2 did not distribute in the liver or NOFe(DTCMP)2 was not accumulated in the liver, and that the detected signal may reflect the nitric oxide produced in the blood.

In conclusion, four dithiocarbamate iron complexes were synthesized as spin traps for nitric oxide by the modification of the functional group of the ligand, and applied to the detection of nitric oxide in the LPS-treated mouse liver and blood. All the synthesized iron complexes was shown to have the trapping ability for nitric oxide *in vivo*. Especially, using Fe(MSD)2, its nitric oxide adduct was detected in the LPS-treated living mice body with low frequency ESR spectrometer (JEOL, Tokyo, Japan). The nitric oxide adducts of Fe(DTCP)2, Fe(DTCTP)2 and Fe(MSD)2 could be detected in the liver and the blood in ex vivo experiments. Another iron complex, Fe(DTCMP)2, had a unique property to give the nitric oxide adduct only in the blood, which may reflect the amount of nitric oxide in the blood.

References

1. Moncada, S., Palmer, R. M. J., and Higgs, E. A. (1991) *Pharmacol. Rev.*, 43, 109-142.
2. Lipton, S. A., Choi, Y.-B., Pan, Z.-H., Lei, S. Z., Chen, H.-S. V., Sucher, N. J., Loscalzo, J., Singel, D. J., and Stamler, J. S. (1993) *Nature*, 364, 626-632.
3. Iadecola, C., Pelligrino, D. A., Moskowitz, M. A., and Lassen, N. A. (1994) *J. Cereb. Blood Flow Metab.*, 14, 175-192.
4. Haley, J. E., Dickenson, A. H., and Schachter, M. (1992) *Neuropharmacol.*, 31, 251-258.
5. Palmer, R. M., Ashton, D. S., and Moncada, S. (1988) *Nature*, 333, 664-666.
6. Kumura, E., Yoshimine, T., Tanaka, S., Hayakawa, T., Shiga, T., and Kosaka, H. (1994) *Neurosci. Lett.*, 177, 165-167.

7. Lancaster, F. E. (1995) *Metab. Brain Dis.*, 10, 125-132.
8. Cooper, C. E., and Brown, G. C. (1995) *Biochem. Biophys. Res. Commun.*, 212, 404-412.
9. Zweier, J. L., Kuppusamy, P., and Lutty, G. A. (1988) *Proc. Natl. Acad. Sci. USA*, 85, 4046-4050.
10. Kwak, H.-S., Yim, H.-S., Chock, P. B., and Yim, M. B. (1995) *Proc. Natl. Acad. Sci. USA*, 92, 4582-4586.
11. Bradshaw, T. P., McMillian, D. C., Crouch, R. K., and Jollow, D. J. (1995) *Free Rad. Biol. Med.*, 18, 279-285.
12. Ozawa, T., and Hanaki, A. (1986) *Biochem. Biophys. Res. Commun.*, 136, 657-664
13. Ozawa, T., and Hanaki, A. (1987) *Biochem. Biophys. Res. Commun.*, 142, 410-416
14. Ozawa, T., and Hanaki, A. (1991) *J. Chem. Soc., Chem. Commun.*, 330-332
15. Lai, C.-S., and Komarov, A. M. (1995) *in* Bioradicals Detected by ESR Spectroscopy (Ohya-Nichiguchi, H., and Packer, L., Eds.), pp.163-171, Birkhauser Verlag, Basel, Switzerland.
16. Mordvintcev, P., Mulsch, A., Busse, R., and Vanin, A. (1991) *Anal. Biochem.*, 199, 142-146.
17. Lai, C.-S., and Komarov, A. M. (1994) *FEBS Lett.*, 345, 120-124.
18. Komarov,A., Mattson, D., Jones, M. M., Singh, P. K., and Lai, C.-S. (1993) *Biochem. Biophys. Res. Commun.*, 195, 1191-1198.
19. Mulsch, A., Mordvintcev, P., Bassenge,E., Jung, F., Clement, B., and Busse, R. (1995) *Circulation*, 92, 1876-1882.
20. Komarov, A. M., and Lai, C.-S. (1995) *Biochim. Biophys. Acta*, 1272, 29-36.
21. Quaresima, V., Takehara, H., Tsushima, K., Ferrari, M., and Utsumi, H. (1996) *Biochem. Biophys. Res. Commun.*, 221, 729-734.
22. Yoshimura, T., Yokoyama, H., Fujii, S., Takayama, F., Oikawa, K., and Kamada, H. (1996) *Nature Biotechnol.*, 14, 992-994.
23. Kuppusamy, P., Ohnishi, S. T., Numagami, Y., Ohnishi, T., and Zweier, J. L. (1995) *J. Cereb. Blood Flow Metab.*, 15, 899-903.
24. Shinobu, L. A., Jones, S. G., and Jones, M. M. (1984) *Acta Pharmacol. Toxicol.*, 54, 189-194.
25. Green, L. C., Wagner, D. A., Glogowski, J., Skipper, P. L., Wishnok, J. S., and Tannenbaum, S. R. (1982) *Anal. Biochem.*, 126, 131-138.

7. Lancaster, F. E. (1995) *Metab. Brain Dis.*, 10, 125-132.
8. Cooper, C. E., and Brown, G. C. (1995) *Biochem. Biophys. Res. Commun.*, 212, 404-412.
9. Zweier, J. L., Kuppusamy, P., and Lutty, G. A. (1988) *Proc. Natl. Acad. Sci. USA*, 85, 4046-4050.
10. Kwak, H.-S., Yim, H.-S., Chock, P. B., and Yim, M. B. (1995) *Proc. Natl. Acad. Sci. USA*, 92, 4582-4586.
11. Bradshaw, T. P., McMillian, D. C., Crouch, R. K., and Jollow, D. J. (1995) *Free Rad. Biol. Med.*, 18, 279-285.
12. Ozawa, T., and Hanaki, A. (1986) *Biochem. Biophys. Res. Commun.*, 136, 657-664
13. Ozawa, T., and Hanaki, A. (1987) *Biochem. Biophys. Res. Commun.*, 142, 410-416
14. Ozawa, T., and Hanaki, A. (1991) *J. Chem. Soc., Chem. Commun.*, 330-332
15. Lai, C.-S., and Komarov, A. M. (1995) *in* Bioradicals Detected by ESR Spectroscopy (Ohya-Nichiguchi, H., and Packer, L., Eds.), pp.163-171, Birkhauser Verlag, Basel, Switzerland.
16. Mordvintcev, P., Mulsch, A., Busse, R., and Vanin, A. (1991) *Anal. Biochem.*, 199, 142-146.
17. Lai, C.-S., and Komarov, A. M. (1994) *FEBS Lett.*, 345, 120-124.
18. Komarov,A., Mattson, D., Jones, M. M., Singh, P. K., and Lai, C.-S. (1993) *Biochem. Biophys. Res. Commun.*, 195, 1191-1198.
19. Mulsch, A., Mordvintcev, P., Bassenge,E., Jung, F., Clement, B., and Busse, R. (1995) *Circulation*, 92, 1876-1882.
20. Komarov, A. M., and Lai, C.-S. (1995) *Biochim. Biophys. Acta*, 1272, 29-36.
21. Quaresima, V., Takehara, H., Tsushima, K., Ferrari, M., and Utsumi, H. (1996) *Biochem. Biophys. Res. Commun.*, 221, 729-734.
22. Yoshimura, T., Yokoyama, H., Fujii, S., Takayama, F., Oikawa, K., and Kamada, H. (1996) *Nature Biotechnol.*, 14, 992-994.
23. Kuppusamy, P., Ohnishi, S. T., Numagami, Y., Ohnishi, T., and Zweier, J. L. (1995) *J. Cereb. Blood Flow Metab.*, 15, 899-903.
24. Shinobu, L. A., Jones, S. G., and Jones, M. M. (1984) *Acta Pharmacol. Toxicol.*, 54, 189-194.
25. Green, L. C., Wagner, D. A., Glogowski, J., Skipper, P. L., Wishnok, J. S., and Tannenbaum, S. R. (1982) *Anal. Biochem.*, 126, 131-138.

ELSEVIER

Mutation Research 403 (1998) 85–94

MR
Fundamental and Molecular Mechanisms of Mutagenesis

Radio-sensitive murine thymoma cell line 3SB: characterization of its apoptosis-resistant variants induced by repeated X-irradiation

Hiroko Hama-Inaba [a,*], Bing Wang [b], Masahiko Mori [b], Tadashi Matsushima [c], Toshiyuki Saitoh [d], Mitsuko Takusagawa [a], Takeshi Yamada [c,e], Masahiro Muto [f], Harumi Ohyama [b]

[a] *Bioregulation Research Group, National Institute of Radiological Sciences, Chiba 263-8555, Japan*
[b] *Division of Radiobiology and Biodosimetry, National Institute of Radiological Sciences, Chiba 263-8555, Japan*
[c] *Division of Biomolecular Science, Graduate School of Science, Toho University, Miyama, Funabashi 274-8510, Japan*
[d] *Genome Research Group, National Institute of Radiological Sciences, Chiba 263-8555, Japan*
[e] *Department of Biology, Toho University School of Medicine, Tokyo 143-8540, Japan*
[f] *Division of Biology and Oncology, National Institute of Radiological Sciences, Chiba 263-8555, Japan*

Received 25 November 1997; revised 3 March 1998; accepted 3 March 1998

Abstract

3SB, a mouse thymoma cell line, is one of the most radio-sensitive cells ($D_0 = 0.3$ Gy), and its rapid apoptosis (4 h after 5 Gy irradiation, 90% apoptosis) seems to play a decisive role in enhancing the radiosensitivity. To understand the molecular mechanisms underlying extremely high radiosensitivity and rapid apoptosis, we attempted to isolate X-ray-resistant (XR) variants from 3SBH5, a stable subclone of 3SB, by repeating exposure of the cells to 2–5 Gy X-rays. Four independent stable XR variants, R111, R223, R316 and R429, were isolated by the repeated irradiation protocols. All XR cells possessed about 3 times higher D_{10} values than that of their parental 3SBH5. They were also resistant to apoptosis; only 10% cells underwent apoptosis 4 h after 5 Gy irradiation. The p53 protein was induced in all the cell lines after 5 Gy X-irradiation. These variants showed a cross resistance to a chemical reagent daunorubicin (DNR) that is known to be involved in the ceramide-mediated apoptosis. DNR, as well as C2-ceramide (5 μM) induced apoptosis in parental 3SBH5 cell, but not in two XR variants, R233 and R316 cells. Present result suggests that the induction of X-ray resistance by repeated X-irradiation might be achieved, at least partly, by the enhanced resistance to the ceramide-mediated apoptosis.

Keywords: Thymoma; Radiation-induced apoptosis; Ceramide; p53; Daunorubicin

1. Introduction

Cellular radiation sensitivity varies considerably from one cell line to the other, and has long been a

* Corresponding author. Bioregulation Research Group, National Institute of Radiological Sciences, Anagawa 4-9-1, Inage-ku, Chiba 263-8555, Japan. Fax: +81-43-255-6819; E-mail: inabahir@nirs.go.jp

research focus in the field of radiation biology. The factors most generally believed to influence cellular sensitivity to ionizing radiation are the amount of initial DNA damage by a given dosage and DNA repair capacity. Recently, it became evident that the vulnerability to apoptosis could also contribute to the cellular radiation sensitivity. But it is still unclear whether there is a direct or quantitative relationship between DNA damage, apoptosis and the cellular radiation sensitivity.

Apoptosis is a distinct mode of cell death that is responsible for deletion of cells in normal tissues; it also occurs in specific pathologic contexts, and is relevant to a wide spectrum of biological phenomena. Several lymphocytic tumor cell lines have been reported to undergo interphase death-type apoptosis. A mouse thymoma cell line 3SB established in our institute from the lymphoma in B10 Thy1.1 mouse underwent apoptosis shortly after low dose X-irradiation [1,2]. It showed the typical apoptotic changes such as chromatin condensation and DNA fragmentation, and more than 90% of the cells underwent apoptosis within 4 h after 5 Gy X-irradiation. The D_0 value, estimated by the colony forming assay was 0.3 Gy, indicating that 3SB is one of the most radio-sensitive cell lines.

It has been identified that apoptosis is the common form of radiation-induced cell death in interphase of thymocytes [3]. Hence, the high radiosensitivity of 3SB seems to reflect the nature of its parental thymocytes. Experiments using p53 knockout mice demonstrated that p53 is required for apoptosis of thymocytes by DNA-damaging agents including ionizing radiation, but not for apoptosis by glucocorticoids or calcium [4,5].

Ceramide, a lipid component of eukaryotic cell membranes, has been shown to mediate the effects of radiation in inducing apoptosis in several cell lines [6–8]. Acid sphingomyelinase, an enzyme participating in hydrolysis of sphingomyelin to generate ceramide, plays a role in this response to ionizing radiation in lymphoblasts [9]. Thus, there must be multiple pathways in the apoptosis induction by radiation depending on the type of cells, and/or the physical conditions of cells.

Mammalian cell mutants with different sensitivity can be good models for studying the basis of radiosensitivity. In this study, in order to analyze the mechanisms responsible for the high radiosensitivity of 3SB, radio-resistant variants were systematically isolated from a stable subclone (3SBH5) of 3SB by repeated X-irradiation. Using four variants isolated independently, the relationship between the radiosensitivity and apoptosis induction was examined. Implication of the ceramide-mediated apoptosis in the enhanced radiosensitivity of 3SB was explored.

2. Materials and methods

2.1. Cells and culture conditions

Murine thymic lymphoma cell line, 3SB, was established from thymoma induced in B10 Thy1.1 mouse by split-dose X-irradiation (four exposures of 1.61 Gy at 8-day intervals) [1]. Cells were grown in suspension culture in Dulbecco's modified Eagle medium (MEM; Nissui Seiyaku, Tokyo, Japan) supplemented with 7% fetal bovine serum (Biowhittaker, MD, USA) inactivated at 53°C, 30 min, 10 mM HEPES, 150 μM asparagine, 100 nM MEM non-essential amino acids solution (Gibco, BRL), 50 units/ml penicillin, and 50 ng/ml streptomycin (Gibco) at 37°C at high humidity in incubators containing 5% CO_2 in air.

The fetal calf serum for the culture was selected to make colonies in soft agar with plating efficiency more than 60% (when 3×10^2 cells were plated).

2.2. X-irradiation

Cells in exponentially growing phase were irradiated using an X-ray machine (Pantak 320S, Shimadzu, Kyoto, Japan) at the dose rates of 0.8–1.2 Gy/min (200 kVp, 19 mA with filters of 0.5 mm Cu and 0.5 mm Al).

2.3. Variant isolation and survival assays

The protocols for isolation of X-ray-resistant (XR) variants by repeated X-irradiation are shown in Section 3. For X-ray survival assays, cells ($3–6 \times 10^5$/ml) in growth medium were irradiated with various doses of X-rays and appropriate number of cells were plated in 6 ml soft-agar (0.29% Agar, Noble, Difco, Detroit, 10% fetal calf serum) medium. The plates were incubated at 37°C in a CO_2 incubator for 2 weeks. Survival curves were constructed

using mean values obtained from more than three independent experiments.

Survival curves for chemicals were constructed as previously described [10]. Briefly, appropriate number of log-phase cells (2×10^2–10^5) in growth medium were plated on a dish, and 6 ml of soft agar medium containing various concentrations of mitomycin-C (MMC; Sigma), diepoxybutane (DEB; Sigma), daunorubicin (DNR) (Sigma), methylmethanesulfonate (MMS; Wako Junyaku, Tokyo) was poured onto each dish. After incubation of the plates for 10–14 days in a CO_2 incubator at 37°C, visible colonies were counted. Experiments were repeated at least 3 times, and typical survival curves were used.

2.4. Detection and counting of apoptotic cells

Cells with condensed chromatin were judged as apoptotic cells. The number of apoptotic cells was scored after fixation with 1% glutaraldehyde (TAAB) in 0.1 M phosphate buffer at pH 7.4 and subsequent staining with Hoechst 33342. Apoptosis induced by X-irradiation, DNR and C2-ceramide (Funakoshi, Tokyo, Japan) was examined. In DNR experiments, apoptotic cells were counted by trypan blue-staining, since cell death under the conditions used resulted solely from apoptosis, and therefore apoptotic cells could be counted by the dye-exclusion test. Experiments were repeated at least twice, and the results shown are mean values.

2.5. Detection of DNA fragmentation on gel electrophoresis

Detection of DNA fragmentation on gel electrophoresis was performed according to the method of Ramachandra and Studzinski [11] with a slight modification. Briefly, DNA fragments were extracted with phosphate–citrate buffer, and subsequently treated with RNase and proteinase K. Samples thus obtained were subjected to agarose gel electrophoresis.

2.6. SDS-PAGE and Western blotting for p53 detection

The cells were harvested at various time points after irradiation (2–8 h) by 0.5, 2 and 5 Gy and treated with SDS-polyacrylamide gels electrophoresis (PAGE) sample lysis buffer. The lysates were subjected to 10% SDS-PAGE, and were then electrotransfered to PVDF membrane (BioRad). The residual binding sites were blocked by incubating the filters with 5% dry milk (Yukijirushi) in phosphate-buffered saline and 0.05% Tween 20 overnight at 4°C. The filters were incubated with anti-p53 antibody (Ab 4; Calbiochem) for 1.5 h. After washing twice with phosphate-buffered saline and Tween 20, blots were incubated with anti-mouse IgG alkaline phosphatase-conjugated (BioRad). The antibody complexes signals were detected with NBT/BCIP color reaction.

3. Results

3.1. Isolation of 3SB subclones

A total of 10 subcell clones of 3SB were picked up from the soft agar plates, and were grown in suspension. One of these cell lines showing similar clonogenic and apoptotic sensitivity to X-irradiation as the parental cell [2] was selected as the standard subclone of 3SB, designated 3SBH5, and used throughout in this study. It had high plating efficiency (> 70%) and diploid chromosome number. 3SBH5 showed stable sensitivity to X-rays after continuous culture for 2 months (data not shown) when the medium was changed every other days. Doubling time of the cell was about 12 h.

3.2. Induction and isolation of X-ray-resistant cell lines from 3SB5H by repeated X-irradiation

Four independent dishes containing 3SBH5 cells at exponentially growing phase (6×10^5/ml, 5 ml) were irradiated 4 times with 2 Gy X-rays, and then one time with 2 Gy or 3 Gy for dishes 1 and 2, and dishes 3 and 4, respectively, at the first stage with intervals of 3 to 5 days. The cells were further irradiated repeatedly 2 times with 3 Gy, and subsequently 4 and 5 Gy twice with same intervals (stage 2). At the end of the repeated irradiation (stage 1 and 2), 10–20 colonies were picked up from soft agar-plates for survival assays. The most resistant clones,

R111, R223, R316 and R429, from these four dishes were selected and used for further experiments.

The majority of these cells had diploid chromosomes (data not shown) and stable sensitivity to X-rays even after continuous culture and freezing. Measurements of survival of the cells revealed a gradual increase in radio-resistance. Surviving fractions of the cells in the course of the selection were 10^{-4}, $3–5 \times 10^{-3}$, 10^{-2} and $4–8 \times 10^{-2}$ following irradiation with 3 Gy for the original 3SBH5, the cells at the end of stage 1, stage 2 and XR cells, respectively.

3.3. Radio-resistance of XR variants

Fig. 1 shows X-ray-survival curves for 3SBH5 and its XR variants. The survival curve for 3SBH5 was clearly steeper than those for the resistant variants, and D_{10} values were 0.7 and 2.2–2.6 Gy for 3SBH5 and XR cells, respectively. Thus, the resistant variants obtained by the repeated exposure had 3.1–3.7 times higher D_{10} value compared with that of 3SBH5. These results indicate clearly an enhanced radio-resistance of the XR variants.

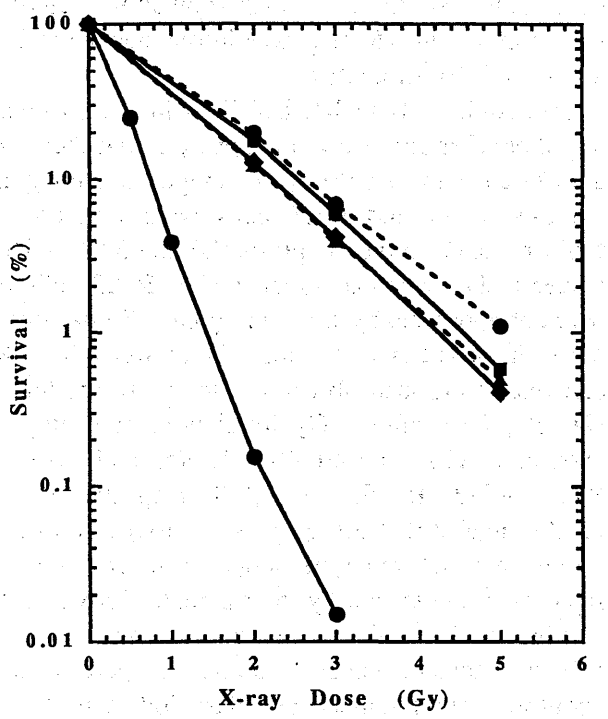

Fig. 1. X-ray dose survival curves of 3SBH5 and XR cells. —●— 3SBH5, ---●--- R111, —♦— R223, ---▲--- R316, —■— R429. Data are means ± S.E. of three independent experiments.

It is of interest to note that the survival curves for all cell lines had no shoulder. Four XR-variants had almost similar sensitivity. No cell clone having higher resistance could be found (see Section 4)

3SBH5 cells were not so sensitive to UV compared with UV-sensitive mouse lymphoma cell line, Q31 [12]. All of XR variants were slightly resistant to UV (data not shown).

3.4. Reduced sensitivity of the XR cells to radiation-induced apoptosis

3SBH5 cells were extremely sensitive to radiation-induced apoptosis, and died by apoptosis shortly after X-irradiation as having shown in our previous paper [2] with 3SB. Unlike 3SBH5 cells, all XR variants were fairly resistant to radiation-induced apoptosis as shown in Fig. 2a. Making a marked contrast to 3SBH5 cells which showed 90% apoptosis, apoptosis in XR cells was lower than 10 to 20% 4 h after 2 Gy irradiation.

Apoptotic cells in XR cell lines increased gradually thereafter and it became apparent that there was a difference in sensitivity to apoptosis among the variants. R111 and R316 cells were found to be fairly resistant to the apoptosis (20 and 32% at 20 h, respectively), whereas about half of R223 cells underwent apoptosis by this time point. Similar differences in sensitivity to apoptosis between four XR cell lines were also observed after 5 Gy irradiation. Namely, 20 h after 5 Gy irradiation, percentage of apoptotic cells reached 40, 75, 45, and 50% for R111, R223, R315, and R429, respectively. The results suggest that the apoptosis in four XR variants might be a delayed type apoptosis in contrast to a rapid type one shown by their parental 3SBH5 cells.

Fig. 2b shows that induction of apoptosis in XR cells was dose-dependent, although the percentage of apoptotic cells remained less than 50% 4 h after 20 Gy irradiation.

Fig. 3 illustrates the DNA ladder obtained with the experiments with 3SBH5 and XR cells 4 h after

R111, R223, R316 and R429, from these four dishes were selected and used for further experiments.

The majority of these cells had diploid chromosomes (data not shown) and stable sensitivity to X-rays even after continuous culture and freezing. Measurements of survival of the cells revealed a gradual increase in radio-resistance. Surviving fractions of the cells in the course of the selection were 10^{-4}, $3–5 \times 10^{-3}$, 10^{-2} and $4–8 \times 10^{-2}$ following irradiation with 3 Gy for the original 3SBH5, the cells at the end of stage 1, stage 2 and XR cells, respectively.

3.3. Radio-resistance of XR variants

Fig. 1 shows X-ray-survival curves for 3SBH5 and its XR variants. The survival curve for 3SBH5 was clearly steeper than those for the resistant variants, and D_{10} values were 0.7 and 2.2–2.6 Gy for 3SBH5 and XR cells, respectively. Thus, the resistant variants obtained by the repeated exposure had 3.1–3.7 times higher D_{10} value compared with that of 3SBH5. These results indicate clearly an enhanced radio-resistance of the XR variants.

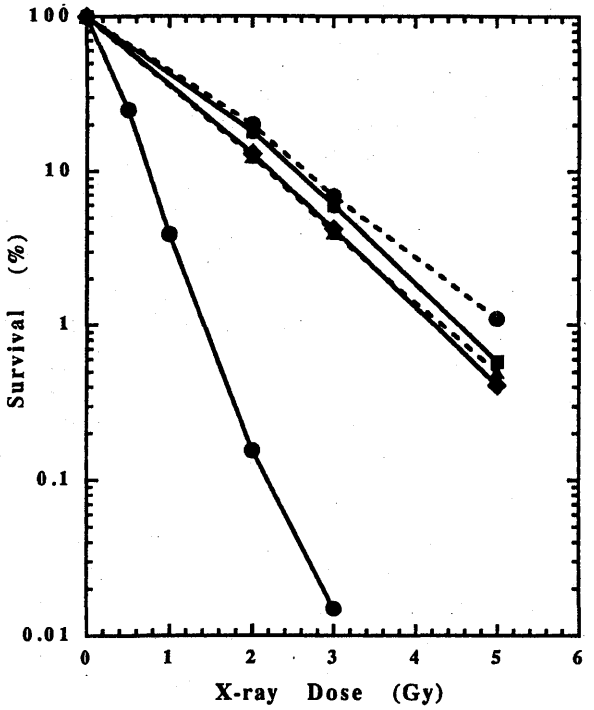

Fig. 1. X-ray dose survival curves of 3SBH5 and XR cells. —●— 3SBH5, ---●--- R111, —♦— R223, ---▲--- R316, —■— R429. Data are means ± S.E. of three independent experiments.

It is of interest to note that the survival curves for all cell lines had no shoulder. Four XR-variants had almost similar sensitivity. No cell clone having higher resistance could be found (see Section 4)

3SBH5 cells were not so sensitive to UV compared with UV-sensitive mouse lymphoma cell line, Q31 [12]. All of XR variants were slightly resistant to UV (data not shown).

3.4. Reduced sensitivity of the XR cells to radiation-induced apoptosis

3SBH5 cells were extremely sensitive to radiation-induced apoptosis, and died by apoptosis shortly after X-irradiation as having shown in our previous paper [2] with 3SB. Unlike 3SBH5 cells, all XR variants were fairly resistant to radiation-induced apoptosis as shown in Fig. 2a. Making a marked contrast to 3SBH5 cells which showed 90% apoptosis, apoptosis in XR cells was lower than 10 to 20% 4 h after 2 Gy irradiation.

Apoptotic cells in XR cell lines increased gradually thereafter and it became apparent that there was a difference in sensitivity to apoptosis among the variants. R111 and R316 cells were found to be fairly resistant to the apoptosis (20 and 32% at 20 h, respectively), whereas about half of R223 cells underwent apoptosis by this time point. Similar differences in sensitivity to apoptosis between four XR cell lines were also observed after 5 Gy irradiation. Namely, 20 h after 5 Gy irradiation, percentage of apoptotic cells reached 40, 75, 45, and 50% for R111, R223, R315, and R429, respectively. The results suggest that the apoptosis in four XR variants might be a delayed type apoptosis in contrast to a rapid type one shown by their parental 3SBH5 cells.

Fig. 2b shows that induction of apoptosis in XR cells was dose-dependent, although the percentage of apoptotic cells remained less than 50% 4 h after 20 Gy irradiation.

Fig. 3 illustrates the DNA ladder obtained with the experiments with 3SBH5 and XR cells 4 h after

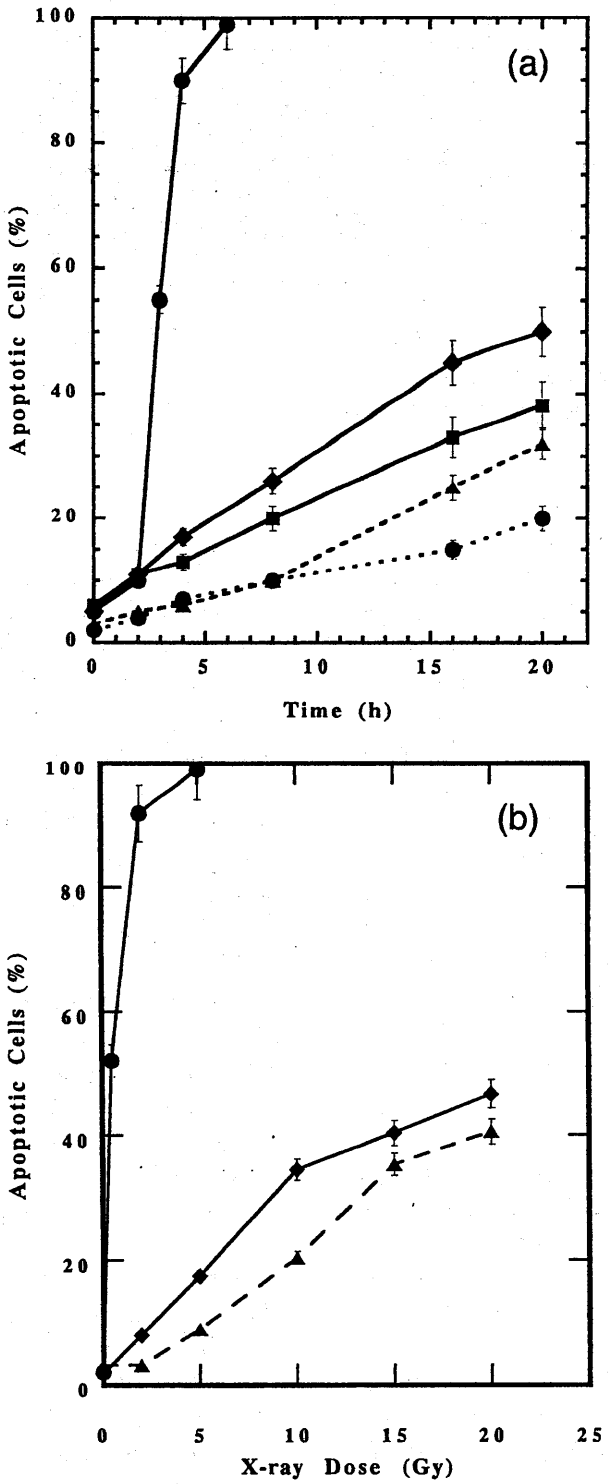

Fig. 2. Induction of apoptosis in 3SBH5 and XR cells. Symbols for the cells are the same as in Fig. 1. (a) Induction of apoptosis following 2 Gy X-irradiation. Control for each cell line is not shown. Apoptotic cells were not increased without X-irradiation. (b) Dose-dependent induction of apoptosis 4 h after X-irradiation. Data are means ± S.E.

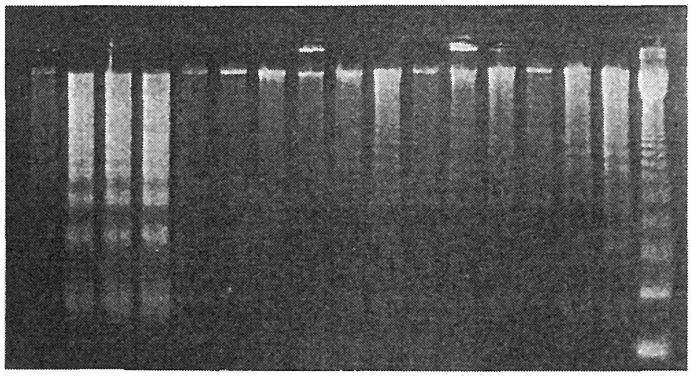

Fig. 3. DNA fragmentation analysis following X-irradiation. Cells were harvested 4 h after irradiation and DNA fragments extracted from same number of cells were subjected to agarose gel electrophoresis.

1–10 Gy irradiation, using the same samples as shown in Fig. 2b. DNA samples extracted from the identical number of cells were subjected to the electrophoresis. The so-called 'ladder pattern' of the fragmented DNA on the gel electrophoresis confirmed clearly resistance of XR variants to the radiation-induced apoptosis as well as the dose-dependent increase in apoptosis.

Thus, all the XR variants underwent dose- and time-dependent apoptosis with the sensitivity markedly lower than that of 3SBH5. It can be concluded from these results that the radio-resistance of XR variants could be, at least partly, interpreted in terms of the enhanced resistance to apoptosis.

3.5. Cross resistance to genotoxic / anti-cancer agents

Next, we examined the cross resistance of the XR variants to other genotoxic or anti-cancer agents, the mode of action of which are well known, expecting that the findings to be obtained might shed light on the mechanisms underlying the enhanced radio-resistance.

First, the sensitivity of XR cells to MMS, an alkylating agent, was examined. As shown in Fig. 4a, the sensitivities were lower than that of 3SBH5 cells, indicating that the variants became resistant also to this alkylating agent. However, the degree of resistances of XR cells to MMS were not parallel to that to X-rays shown in Fig. 1, suggesting that the mechanisms underlying induction of radio-resistance both to radiation and to MMS are partly common but not completely identical.

DNR, having anthraquinone structure, is known as an agent generating active oxygen in cells, and acts against membrane, as well as intercalate to DNA. DNR can trigger apoptosis, which was recently reported to be mediated by a signal pathway via sphingomyelin- or ceramide synthase-derived ceramide [13,14].

Fig. 4b shows that SBH5 is extremely sensitive to DNR, suggesting an important role of the ceramide-mediated apoptosis in their extreme radiosensitivity. On the other hand, all the XR cells were resistant to DNR in almost same extent observed with the enhanced resistance to X-rays.

These results suggest that the enhanced radiosensitivity of XR variants could be attributed to the suppression of the sensitivity to ceramide-mediated apoptosis.

MMC which is known as a bifunctional DNA-damaging agent and causes DNA–DNA, or DNA–protein crosslinks. It has semiquinone structure and generates active oxygen which causes damages to DNA or proteins [15]. All the variants were resistant to MMC and also to DEB in the same extent (data not shown).

These results indicate clearly that X-ray-sensitive 3SBH5 cells were also sensitive to MMC, DEB, and

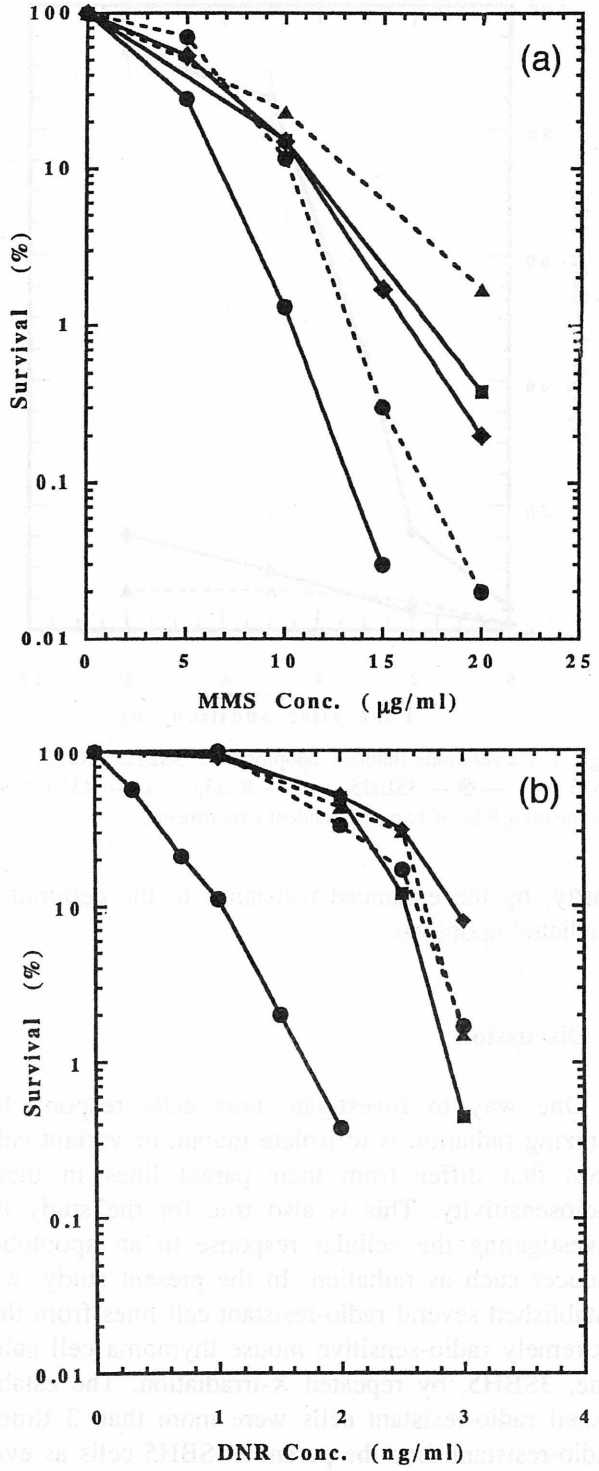

Fig. 4. Survival curves of the cells for (a) MMS and (b) DNR. Symbols for the cells are the same as in Fig. 1.

DNR, and the sensitivity of the variants to ionizing radiation varied in parallel with the sensitivity to these agents, and suggest that these agents and X-rays could induce apoptosis using a common pathway, and the changes in sensitivity might be attributable to the altered sensitivity to apoptosis.

3.6. Increase in p53 following X-irradiation

As p53 is considered to be key molecule in radiation-induced apoptosis in various cells including thymocytes, induction of p53 following X-irradiation was tested. As shown in Fig. 5, p53 protein is not detectable in any strains without irradiation, and X-rays induced significant p53 protein accumulation in a time-dependent manner in both sensitive and resistant XR cell lines. Western blot analysis showed a marked increase in p53 protein by 4 h post-irradiation, and then the levels of p53 in all cells decreased with time. The p53 of these variants seems to be normal in structure and in functions. The result suggests that the radiation-induced accumulation of p53 in XR cells is not directly related to the changes in radiosensitivity in these cells.

3.7. Apoptosis induced by daunorubicin and C2-ceramide

The involvement of apoptosis in the radiosensitivity changes is suggested, we examined induction of apoptosis by DNR.

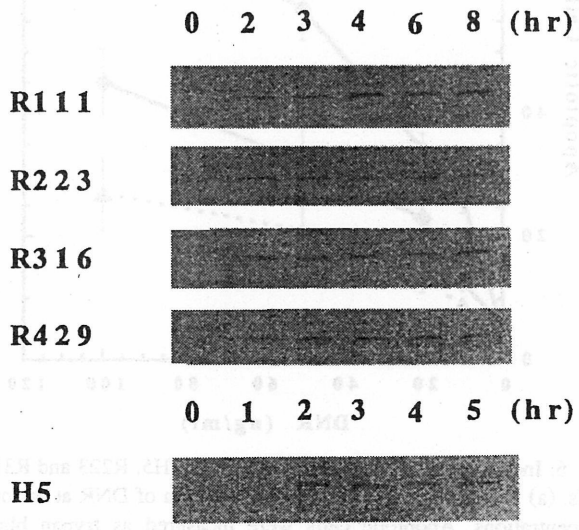

Fig. 5. Relative levels of cellular p53 protein measured by immunoblot analysis using whole cell extract (20 μg/lane) prepared from cells at 0, 1, 2, 3, 4, 5 h for 3SBH5 and at 0, 2, 3, 4, 6, 8 h for XR variants after irradiation with 5 Gy X-ray.

Following exposure to 50 ng/ml (−0.1 μM) DNR, about 60% of 3SBH5 underwent apoptosis at 6 h as shown in Fig. 6. While, R316 showed resistance to apoptosis induced by DNR even at the high concentration. These facts suggest that R316 cell was resistant to DNR.

Ceramide has been shown to mediate apoptosis by ionizing radiation and DNR in several cell lines. Then, we examined the effect of C2-ceramide on apoptosis induction in 3SBH5 and XR cells. As shown in Fig. 7, 3SBH5 underwent apoptosis shortly after the addition of 5 μM ceramide. About 90% of 3SBH5 cells underwent apoptosis at 5 h, indicating that the apoptosis proceeded so rapidly as induced by X-irradiation. On the contrary, R223 and R316 cells showed a low level apoptosis even after 8 h (about 20% for R223 and 8% for R316 cells).

The above result suggests strongly that X-ray resistance of XR cells might be achieved, at least partly, by the enhanced resistance to the ceramide-mediated apoptosis.

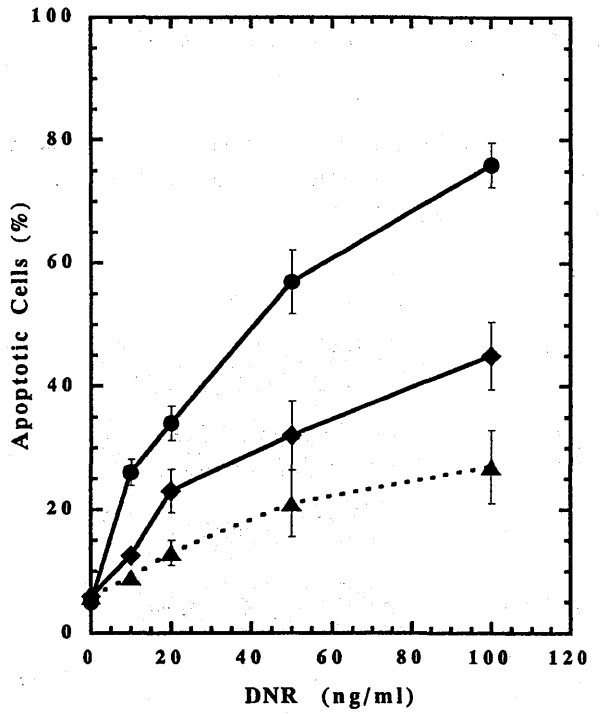

Fig. 6. Induction of apoptosis by DNR in 3SBH5, R223 and R316 cells. (a) Apoptotic cells (%) 6 h after addition of DNR at various concentrations. Apoptotic cells were measured as trypan blue-stained cells. (DNR at high concentration gave damages to cells causing loss by breakdown through centrifugation and fixation). —●— 3SBH5, —♦— R223, ---▲--- R316. Data are means ± S.E. of two independent experiments.

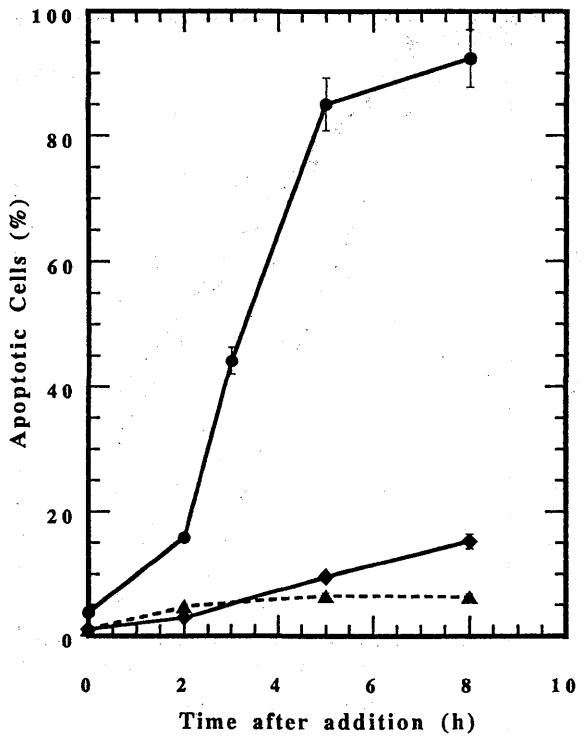

Fig. 7. C2-ceramide-induced apoptosis in 3SBH5, R223, and R316 cells. —●— 3SBH5, —♦— R223, ---▲--- R316. Data are means ± S.E. of two independent experiments.

4. Discussion

One way to investigate how cells respond to ionizing radiation is to isolate mutant or variant cell lines that differ from their parent lines in their radiosensitivity. This is also true for the study in investigating the cellular response to an apoptotic inducer such as radiation. In the present study, we established several radio-resistant cell lines from the extremely radio-sensitive mouse thymoma cell subline, 3SBH5, by repeated X-irradiation. The established radio-resistant cells were more than 3 times radio-resistant than the parental 3SBH5 cells as evidenced by the ratio of D_{10} doses.

There are so far only a few studies on establishment of the radio-resistant variants by repeating exposure of cells to X-rays. Russell et al. [16] obtained a radio-resistant variant from a human neuroblastoma cell line by subjecting the cells to a regime of

fractionated X-irradiation. The D_{10} values estimated from their results have shown that the increased radio-resistance of the variant is about 1.5 times higher than that of the parental cells. In our preliminary study using ethyl methane sulfonate (EMS), several clones having only intermediate sensitivity were obtained. Mutation frequency of X-ray-resistant cells was about 10^{-6}. While by using EMS treatment followed by repeated X-irradiation, and further EMS treatment of the resistant clones, more resistant clones to X-ray-induced apoptosis were obtained [17]. The clone which was the most resistant to X-ray-induced apoptosis had mutation in p53, while original 3SB had functional wild type $p53^{+/+}$.

It is generally known that the variants thus obtained are often unstable. The radio-resistant variant from a human neuroblastoma lost their radio-resistant phenotype after three passages in the absence of radiation-selective pressure [16]. Unlike these cell lines, our variants' XRs established here, as well as their parental 3SBH5, maintained their original radiosensitivity over, at least, several months under normal culture conditions without any treatment.

One of the most interesting findings of this study is that the increased radio-resistance of the variants can be explained by the reduced vulnerability of the cells to the radiation-induced apoptosis (Fig. 2a,b, Fig. 3). After 2 Gy, 3SBH5 underwent apoptosis and died 100% by 6 h, whereas XR cells exhibited few apoptotic death within 4 h, and then a gradual increase in dead cells at most up to 50% at 20 h, showing a remarkable difference in sensitivity to apoptosis between the parental and variant cells. Our present findings are consistent with the reported results [16] in which a radio-resistant variant from a human neuroblastoma is less prone to radiation-induced apoptosis.

Radiation-induced apoptosis can be classified into three types in relation to cell cycle progression, namely, rapid interphase death type apoptosis which occurs shortly after irradiation, delayed interphase death type apoptosis occurring after prolonged arrest in G2 phase, and mitotic (reproductive) death type apoptosis appearing after one or more mitosis [18]. Fig. 2a shows clearly that the apoptosis in the parental 3SBH5 cells represents a typical rapid interphase death type, while XR cells lost the ability to undergo this type apoptosis in response to low dose X-rays (2 Gy). With time after the irradiation, the XR cells began to show apoptosis and dead cells increased gradually possibly by delayed interphase death type and/or mitotic death type apoptosis. With increasing radiation dose up to 20 Gy, apoptotic cells increased also in XR cells within 4 h after irradiation, suggesting that rapid interphase death type apoptosis appeared in response only to the higher radiation dose due to the decreased susceptibility to radiation-induced apoptosis.

Since p53-knockout mouse experiments [4,5] revealed that p53 gene is essential to the radiation-induced apoptosis in thymocytes, a lot of experimental studies have implicated the normal or 'wild type' p53 protein in the cellular response including apoptosis to ionizing radiation and other DNA damaging agents [19]. The p53 mutations are frequently associated with decreased radiosensitivity in a number of tumor cells as a consequence of a diminished ability to undergo apoptosis. Our present results (Fig. 5), however, demonstrate that wild type p53 is expressed in all variant cell lines after irradiation. Therefore, the decreased sensitivity in the variant cells could not be attributed to the p53 mutation.

The existence of cross resistance between X-rays and genotoxic/anticancer drugs, DNR, MMC and DEB, gave us a promising clue to elucidate the mechanisms underlying the enhanced radio-resistance (Fig. 4a). Clonogenic survival assay clearly demonstrates that all XR cells were also resistant to the anticancer agents in the same extent as the radiation. DNR is known to induce apoptosis by triggering ceramide generation [13,14]. Recent studies investigating mechanisms of radiation-mediated apoptosis demonstrate that the production of the lipid second messenger ceramide immediately following X-rays [6–9]. DNR treatment for 6 h could indeed elicit apoptosis markedly in the parental 3SBH5 cells in dose-dependent manner, but in a XR cell, it is in a much less extent (Fig. 6). These findings indicate that ceramide-mediated pathway is involved in rapid apoptosis induced by radiation in 3SBH5 cells. Further support for this view was obtained by the experiment in which C2-ceramide (5 μM) induced apoptosis extensively in 3SBH5, but at restricted levels in XR cells (Fig. 7).

Recently, Michael et al. [20] reported that resistance to radiation-induced apoptosis in Burkitt's

lymphoma cells was associated with defects in ceramide signaling. Burkitt's lymphoma cell line, BL30A, sensitive to ionizing radiation induced apoptosis, generated ceramide about 4-fold of non-irradiated-cells by 10 min post-irradiation (10 Gy). Chmura et al. [7] reported that a murine lymphoid WEHI-231 subline, made deficient in ceramide production was found to be resistant to apoptosis compared with the parental subline following X-irradiation.

Together, our results show that XR cells have lost the sensitivity to the ceramide-mediated apoptosis leading eventually to getting strong resistance against radiation. Further studies are, however, needed to explore in detail the mechanism underlying the process causing the loss of the cellular sensitivity to the ceramide-mediated apoptosis.

Acknowledgements

We thank Dr. I. Hayata (Division of Radiobiology and Biodosimetry), Dr. N. Ikota, Dr. T. Ozawa (Bioregulation Research Group) and Dr. T. Hori (Genome Research Group) of National Institute of Radiobiological Sciences for their kind support throughout this work. This work was supported in part by a Special Grant for Promoted Research from NIRS.

References

[1] M. Muto, E. Kubo, H. Kamisaku, T. Sado, Phenotypic characterization of thymic prelymphoma cells of B10 mice treated with split-dose irradiation, J. Immunol. 144 (1990) 849–853, I.R.

[2] H. Ohyama, M. Muto, T. Yamada, Apoptosis in newly established radio-sensitive mouse lymphoma cell line, in: T. Suhagara, L.A. Sagan, T. Aoyama (Eds.), Low Dose Irradiation and Biological Defense Mechanisms, Elsevier, Amsterdam, 1992, pp. 361–364.

[3] T. Yamada, H. Ohyama, Radiation-induced interphase death of rat thymocytes is internally programmed (apoptosis), Int. J. Radiat. Biol. 53 (1988) 65–75.

[4] S.W. Lowe, E.M. Schmitt, S.W. Smith, B.A. Osborne, T. Jacks, p53 is required for radiation-induced apoptosis in mouse thymocytes, Nature 362 (1993) 847–849.

[5] A.R. Clarke, A.A. Purdie, D.J. Harrison, R.G. Morris, C.C. Bird, M.I. Hooper, A.H. Wyllie, Thymocyte apoptosis induced by p53-dependent and independent pathways, Nature 362 (1993) 849–852.

[6] A. Haimovitz-Friedman, C. Kan, D. Ehleiter, R. Persand, M. McLoughlin, Z. Fuks, R.N. Kulensnich, Ionizing radiation acts on cellular membranes to generate ceramide and initiate apoptosis, J. Exp. Med. 180 (1994) 525–535.

[7] S.J. Chmura, E. Nodzenski, M.A. Beckett, D.W. Kufe, J. Quintans, R.R. Weichselbaum, Loss of ceramide production confers resistance to radiation-induced apoptosis, Cancer Res. 57 (1997) 1270–1275.

[8] Y.A. Hannan, Functions of ceramide in coordinating cellular responses to stress, Science 274 (1996) 1855–1859.

[9] P. Santana, L.A. Pena, A. Haimovitz-Friedman, S. Martin, D. Green, M. McLoughlin, C. Cordon-Cardo, E.H. Schuchman, Z. Fuks, R. Kolesnick, Acid sphingomyelinase-deficient human lymphoblasts and mice are defective in radiation-induced apoptosis, Cell 86 (1996) 189–199.

[10] H. Hama-Inaba, N. Hieda-Shiomi, T. Shiomi, K. Sato, Isolation and characterization of mitomycin-C-sensitive mouse lymphoma cell mutants, Mutation Res. 108 (1983) 405–416.

[11] S. Ramachandra, G.P. Studzinski, Morphological and biochemical criteria of apoptosis, in: G.P. Studzingski (Ed.), Cell Growth and Apoptosis: A Practical Approach, IRL Press, Oxford, 1995, pp. 119–142.

[12] K. Sato, N. Hieda, Isolation of mammalian cell mutant sensitive to 4-nitroquinoline-1-oxide, Int. J. Radiat. Biol. 35 (1979) 83–87.

[13] J.-P. Jaffrezou, T. Levade, A. Bettaieb, N. Andrieu, C. Bezombes, N. Maestre, S. Vermeersch, A. Rousse, G. Laurent, Daunorubicin-induced apoptosis: triggering of ceramide generation through sphingomyelin hydrolysis, EMBO J. 15 (1996) 2417–2424.

[14] R. Bose, M. Verheij, A. Haimovitz-Friedman, K. Scotto, Z. Fuks, R. Kolesnick, Ceramide synthase mediates daunorubicin-induced apoptosis: an alternative mechanism for generating death signals, Cell 82 (1995) 405–414.

[15] H. Hama-Inaba, Y. Shimazu, M. Takusagawa, K. Sato, M. Morimyo, CHO-K1 cell mutants sensitive to active oxygen-generating agents: I. Isolation and genetic studies, Mutation Res. 311 (1994) 95–102.

[16] J. Russell, T.E. Wheldon, P. Stanton, A radio-resistant variant derived from a human neuroblastoma cell line is less prone to radiation-induced apoptosis, Cancer Res. 55 (1995) 4915–4921.

[17] H. Kawai, Y. Kitamura, O. Nikaido, M. Tatsuka, H. Ohyama, H. Hama-Inaba, M. Muto, F. Suzuki, Isolation and characterization of apoptosis-resistant mutant from a radio-sensitive mouse lymphoma cell, Radiat. Res. 149 (1997) 41–51.

[18] I.R. Radford, T.K. Murphy, Radiation response of mouse lymphoid and myeloid cell lines: III. Different signals can lead to apoptosis and may influence sensitivity to killing by DNA double-strand breakage, Int. J. Radiat. Biol. 65 (1994) 229–239.

[19] C.E. Canman, M.B. Kastan, Role of p53 in apoptosis, Adv. Pharmacol. 41 (1997) 429–460.

[20] J.M. Michael, M.F. Lavin, D.J. Watters, Resistance to radiation-induced apoptosis in Burkitt's lymphoma cells is associated with defective ceramide signaling, Cancer Res. 57 (1997) 3600–3605.

Pergamon

Tetrahedron 54 (1998) 8985–8998

TETRAHEDRON

Stereoselective Synthesis of Alexine Stereoisomers from (*S*)-Pyroglutamic Acid

Nobuo Ikota,[a,*] Hidehiko Nakagawa,[a] Shigeru Ohno,[a] Keiichi Noguchi,[b] and Kenji Okuyama[b]

[a]National Institute of Radiological Sciences, 4-9-1, Anagawa, Inage-ku, Chiba-shi 263-8555 , Japan

[b]Department of Biotechnology, Tokyo University of Agriculture and Technology, Nakacho 2-24-16, Koganei, Tokyo 184-8588, Japan

Received 20 April 1998; accepted 1 June 1998

Abstract: Four stereoisomers of alexine (1,7a-diepialexine (**1a**), 1,7,7a-triepialexine (**1b**), 1-epi-alexine (**30a**), and 1,7-diepialexine (**30b**)), the polyhydroxylated pyrrolizidine alkaloid, were synthesized from (*S*)-pyroglutamic acid derivative (**6**).

Alexines[1] are polyhydroxylated pyrrolizidine alkaloid with a carbon substituent at C-3 and five adjacent asymmetric carbons, and have been shown to possess interesting biological activities such as inhibitory activity toward glucosidase and antiviral activity. Alexine and its stereoisomers have been synthesized to evaluate the structural basis of biological activity from sugars as the starting materials.[2] In a continuation of our synthetic studies to utilize optically active pyroglutamic acid derivatives for natural product synthesis and asymmetric reaction,[3] we have already reported a stereocontrolled synthesis[4] of 1,7a-diepialexine **1a** and 1,7,7a-triepi-alexine **1b** *via* a none-carbohydrate based approach utilizing (*S*)-pyroglutamic acid derivative. The details of this work and further synthetic studies on alexine stereoisomers (**30a** and **30b**) are presented here.

According to our retrosynthetic analysis as shown in Scheme 1, **1a** could be obtained from **2**, which might be synthesized by alkylation of the aldehyde **3** derived from a protected 3,4-dihydroxy-2,5-dihydroxy-methylpyrrolidine derivative **4**. The polyhydroxylated pyrrolidine **4** could be in turn prepared from (*S*)-pyroglutamic acid. Since optically active 3,4-dihydroxy-2,5-dihydroxymethylpyrrolidines have interesting biological activities, the synthesis of (2*R*,3*R*,4*S*,5*R*)- and (2*R*,3*R*,4*S*,5*S*)-3,4-dihydroxy-2,5-dihydroxy-methylpyrrolidine derivatives (**13b** and **14b**) from (*S*)-pyroglutamic acid has been first examined as shown in Scheme 2. An enone **7** was obtained by the reaction of (3*R*,4*R*,5*R*)-1-(*tert*-butoxycarbonyl)-3,4-isopropylidenedioxy-5-trityloxymethyl-2-pyrrolidinone **6**,[3c] prepared from the unsaturated lactam **5** by dihydroxylation with a catalytic amount of OsO_4 in the presence of *N*-methylmorpholine *N*-oxide followed by isopropylidenation, with vinylmagnesium bromide[5] in tetrahydrofuran (THF) at -40 - -50°C in 93% yield. Reduction of **7** with $NaBH_4$ in the presence of $CeCl_3$ in MeOH[6] gave an allylic alcohol **10** as a mixture of inseparable diastereomers in 91% yield. Ozonolysis of the allylic alcohol **10** followed by workup with $NaBH_4$ gave diols **11a** and **12a**, which were separated by column chromatography (**11a**: **12a** = 2.4:1). The both diols were converted to the corresponding *tert*-butyldimethylsilyl ethers **11b** and **12b** by *tert*-butyldimethylsilyl chloride (1.2 equiv.) and imidazole in dimethylformamide (DMF) in 48% and 19% yields from **10**, respectively. Silyl ethers **11b** and **12b** were converted to the mesylate by methanesulfonyl chloride

Scheme 1

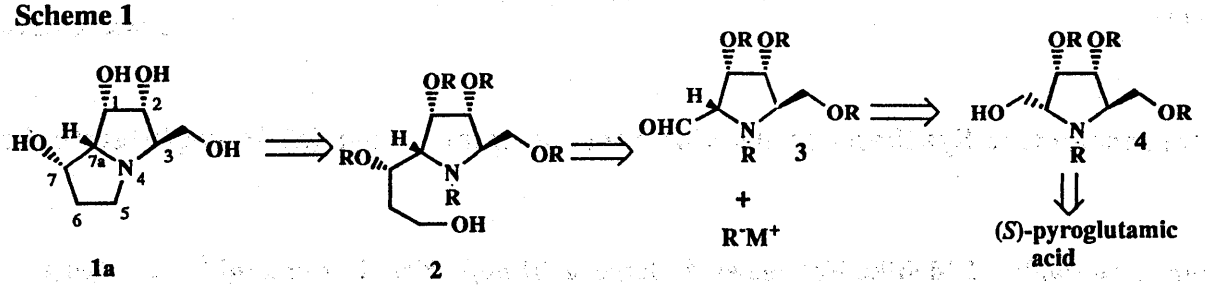

Scheme 2

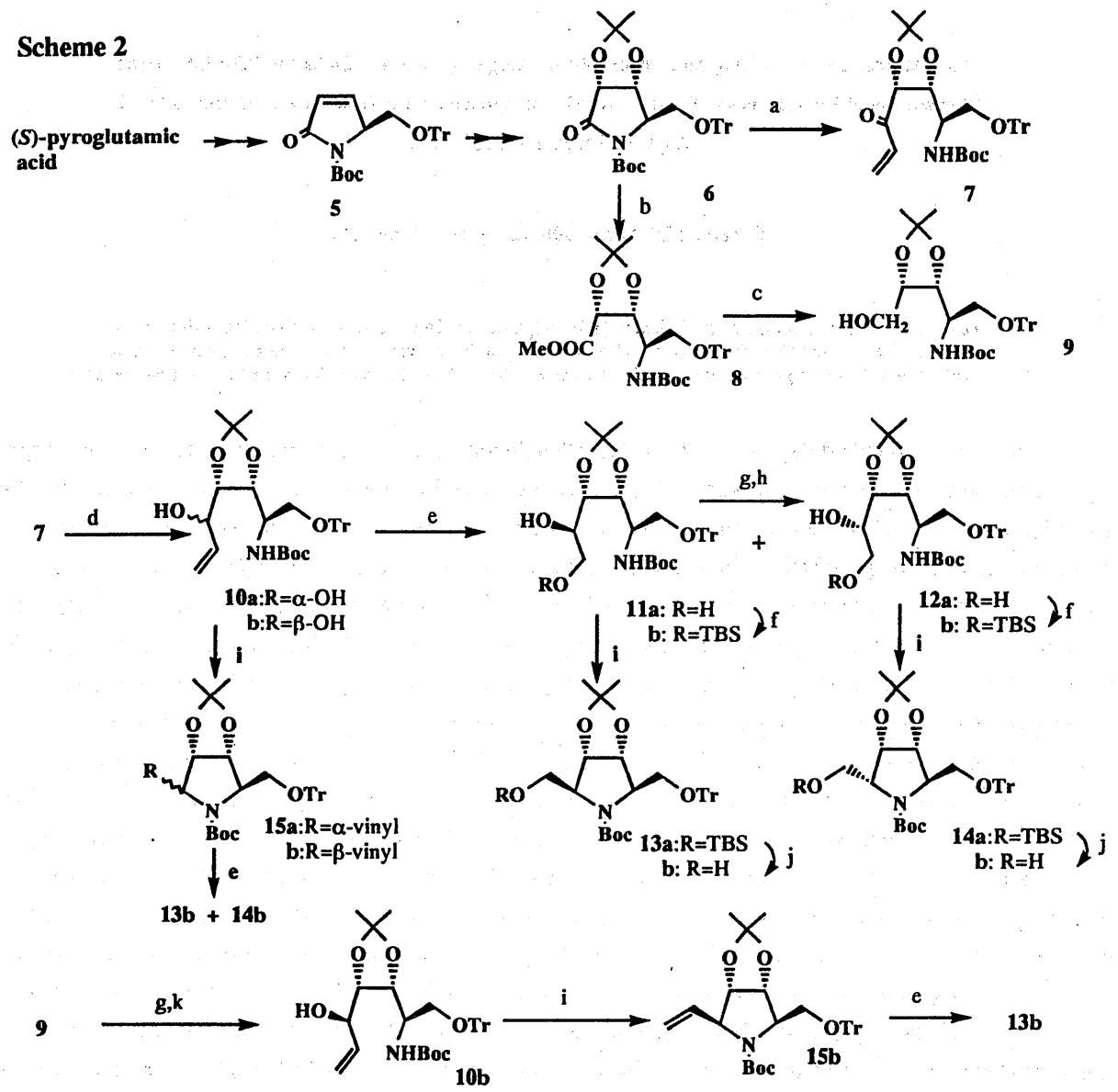

Reagents and conditions: (a) vinylmagnesium bromide, THF, -40 - -50°C; (b) aq LiOH, THF-MeOH, then CH_2N_2. ether; (c) $NaBH_4$, EtOH; (d) $NaBH_4$, $CeCl_3 \cdot 7H_2O$, MeOH; (e) O_3, CH_2Cl_2, -78°C, then $NaBH_4$, EtOH; (f) *tert*-butyldimethylsilyl chloride, imidazole, DMF, 0°C; (g) Swern oxidation, -20°C; (h) $NaBH_4$, EtOH, -78°C; (i) MsCl, TEA, CH_2Cl_2, then *tert*-BuOK, THF; (j) tetrabutylammonium fluoride, THF; (k) vinylmagnesium bromide, THF, -78°C

and triethylamine (TEA) in methylene chloride followed by cyclization with potassium *tert*-butoxide to yield the fully protected pyrrolidines **13a** and **14a** by intramolecular S_N2 displacement in 75% and 78% yields, respectively. Removal of the *tert*-butyldimethylsilyl group in **13a** and **14a** with tetrabutylammonium fluoride in THF gave the alcohols **13b** and **14b** in 78% and 82% yields, respectively. The structure of **13b** and **14b** and optical purity of **14b** were confirmed by the conversion of **13b** and **14b** into the hydrochlorides of the corresponding *meso*- and (2*R*,3*R*,4*S*,5*R*)-2,5-dihydroxymethyl-3,4-dihydroxypyrrolidines by acidic treatment.[3c,4] The diols **13b** and **14b** were also prepared from the allylic alcohol **10**. Mesylation of **10** followed by cyclization with potassium *tert*-butoxide in THF gave the pyrrolidine **15** as an inseparable diastereomeric mixture in 68% yield,[7] from which the diols **13b** and **14b** were isolated by treatment with ozone followed by $NaBH_4$ reduction in EtOH in 60% and 25% yields, respectively. Since (2*R*,3*R*,4*S*,5*R*)-5-hydroxymethylpyrrolidine **14b** was the desired compound for the synthesis of 1,7a-diepialexine, selective conversion of **11b** into **12b** was examined by employing oxidation-reduction procedure. Thus, oxidation of **11b** by the method of Swern [8] followed by reduction with $NaBH_4$ in EtOH at -78°C gave **12b** with very high diastereoselectivity (**12b**:**11b**=18:1) in 73% yield, which was already converted into the pyrrolidine **14b**.

On the other hand, (2*R*,3*R*,4*S*,5*S*)-5-hydroxymethylpyrrolidine **13b** was the intermediate for the preparation of 1-epialexines (**30**). Although **10b** was obtained predominantly by the reduction of enone **7**, the selective formation of **10b** was examined by vinylation of the aldehyde derived from an alcohol **9**. The lactam ring opening of **6** (aqueous lithium hydroxide in THF-MeOH) followed by esterification with diazomethane and subsequent reduction of the resulting methyl ester **8** with sodium borohydride gave the alcohol **9** in 79% yield from **6**. Swern oxidation of **9** followed by treatment with vinylmagnesium bromide in THF at -78°C gave the allylic alcohol **10b** in 71% yield, which was converted into the pyrrolidine **13b** *via* the 5-vinylpyrrolidine **15b** in 72 % yield.

The construction of pyrrolizidine skeleton was shown in Scheme 3. The carbon unit required for the pyrrolizidine ring was introduced using a diastereoselective allylation of the aldehyde[9] derived from the alcohols **13b** and **14b**. Swern oxidation of the alcohol **14b** followed by treatment with either allylmagnesium chloride in THF or allyllithium in ether-THF at -78°C afforded **16** predominantly (allylmagnesium chloride: **16**/**19**=2.5/1, yield 84%; allyllithium: **16**/**19**=5.4/1, yield 81%; the ratio was determined by HPLC analysis (Waters, radial pak cartridge silica (10 μ), AcOEt:hexane=1:4 as eluants)).[10] The reaction of the aldehyde derived from **14b** with allyltrimethylsilane in the presence of $TiCl_4$ in methylene chloride at -78°C for 5 min afforded **16** selectively. However, the yield was very low due to the instability of the aldehyde toward strong acidic conditions. On the other hand, the aldehyde derived from **13b** was very unstable and only the trace of aldehyde was obtained after aqueous workup for Swern oxidation. Therefore, allylmagnesium chloride in THF was directly added to crude Swern oxidation mixture of **13b** in THF at -78°C[11] to afford allylic alcohols **23** and **26** in 52% and 25% yields after column chromatography, respectively. The stereochemistry of newly formed asymmetric carbon for the major isomer **23** was established to be *S* by x-ray crystallography of **23** after the conversion into its methoxymethyl ether **24** as shown in Figure 1.[12] The hydroxy group in **16** was protected as the methoxymethyl ether (chloromethyl methyl ether, *N*,*N*-diethyl-aniline, methylene chloride), and selective transformation of *N*-*tert*-butoxycarbonyl group in **17** into *N*-benzyl group by treatment with *tert*-butyldimethylsilyl trifluoromethanesulfonate[13] in the presence of 2,6-lutidine followed by successive treatments with tetrabutylammonium fluoride in THF and benzyl

Scheme 3

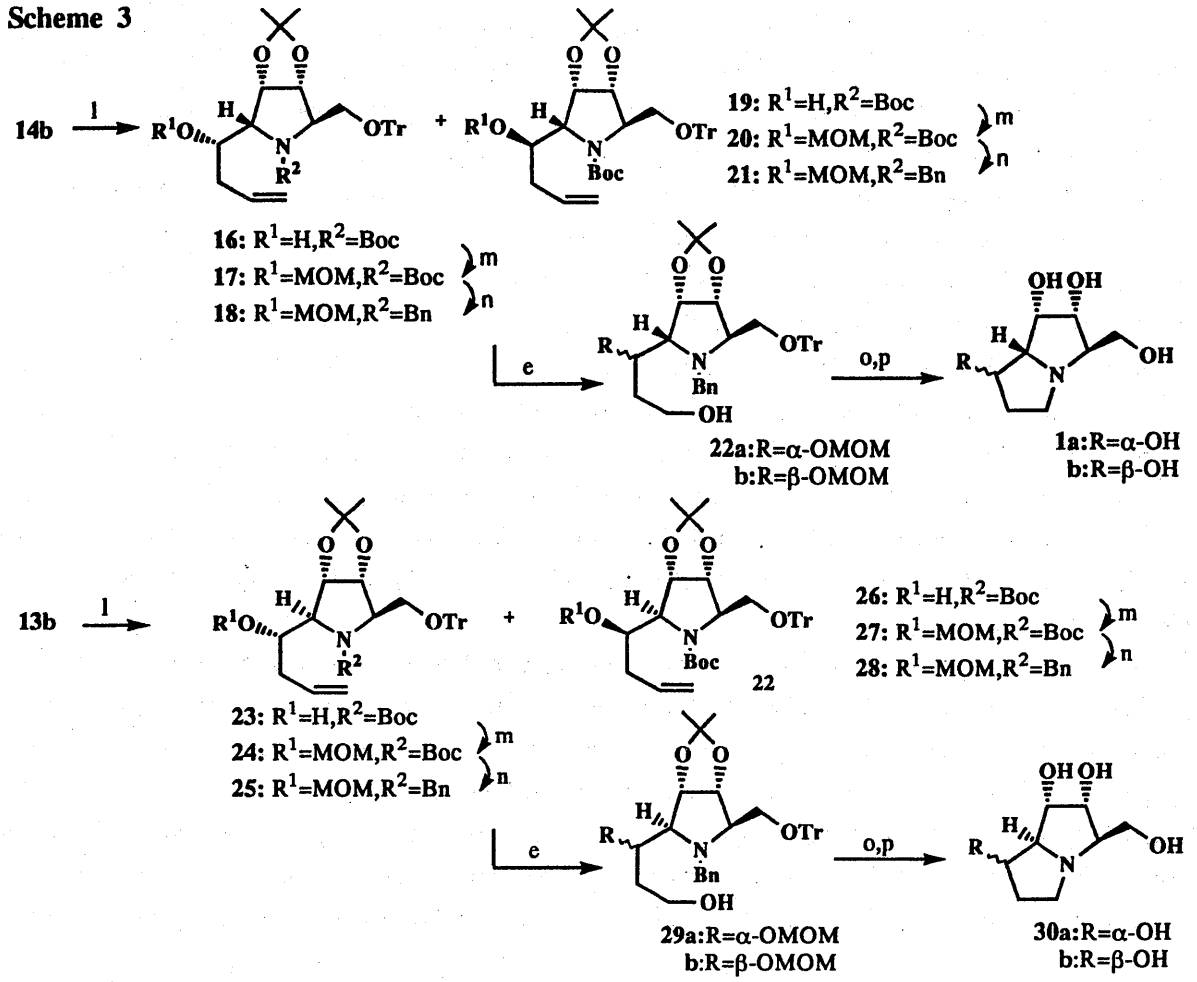

Reagents and conditions: (l) Swern oxidation, then allylation, -78°C; (m) chloromethyl methyl ether, *N,N*-diethylaniline, CH_2Cl_2; (n) *tert*-butyldimethylsilyl trifluoromethanesulfonate, 2,6-lutidine, CH_2Cl_2, then (j), then BnBr, K_2CO_3, acetone; (o) MsCl, TEA, CH_2Cl_2, then 10% Pd-C, H_2, HCl- EtOH. (p) 10% HCl-MeOH, 70°C, then Dowex 50W-X8

Figure 1 ORTEP structure of **24**

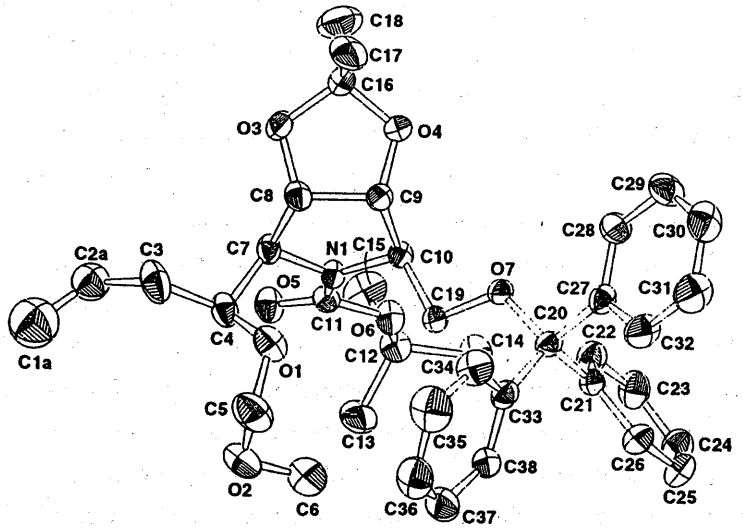

bromide in the presence of potassium carbonate in acetone to furnish **18** in 58% yield. Ozonolysis of **18** followed by reductive workup with $NaBH_4$ gave the alcohol **22a** in 58% yield. Mesylation of **22a** gave a mesylate, which was spontaneously cyclized to give the pyrrolizidine derivative. After hydrogenation of the protected pyrrolizidine with 10% palladium on carbon in EtOH under atmospheric hydrogen in the presence of hydrogen chloride to remove *N*-benzyl group, acidic treatment with 10% HCl-MeOH (1:1) at 70°C to cleave the acetonide and trityl groups afforded the 1,7a-diepialexine **1a** ($[\alpha]_D^{20}$ +12.5° (c=0.6, H_2O), lit. $[\alpha]_D^{20}$ +12° (c=1.17, H_2O),[1c] $[\alpha]_D^{20}$ +8.5° (c=0.41, H_2O),[1d] $[\alpha]_D^{20}$ +13.3° (c=0.1, H_2O)[2c]) in 52% yield after purification by ion exchange chromatography (Dowex 50W-X8, H^+ form). Its spectral data (^1H and ^{13}C NMR) were identical with those reported for **1a**. By a parallel series of reactions, the allylic alcohols, **19**, **23**, and **26** were converted to 1,7,7a-triepialexine **1b** (oil, $[\alpha]_D^{20}$ +4.7° (c=0.5, H_2O), lit. $[\alpha]_D^{20}$ +11.7° (c=1, H_2O),[2c]), 1-epialexine **30a** ($[\alpha]_D^{20}$ +34.8° (c=0.5, H_2O), and 1,7-diepialexine **30b** ($[\alpha]_D^{20}$ +37.0° (c=0.7, H_2O), in 13-21% yields.

Since we have synthesized various optically active 2,5-dihydroxymethyl-3,4-dihydroxypyrrolidine derivatives,[3e,f] this approach utilizing (S)-pyroglutamic acid derivative could be efficient synthetic method for the preparation of the alexine stereoisomers.

Experimental

Melting points were determined on a hot stage apparatus and are uncorrected. Ir spectra were measured with a JEOL JIR-110 FT-IR spectrophotometer. ^1H and ^{13}C nmr spectra were recorded on a JEOL JNM-FX100 (100 Mz) spectrometer. Data are recorded in parts per million (ppm) downfield from internal tetramethylsilane. Mass spectra were taken on a JEOL JMS-D302 spectrometer. Optical rotations were measured on a JASCO DIP-360 polarimeter. The organic solvents were dried over $MgSO_4$ before vacuum evaporation and a column chromatography was carried out with silica gel (Wakogel C-200).

1,1-Dimethylethyl *N*-[(1*R*,2*R*,3*R*)-2,3-isopropylidenedioxy-1-trityloxymethyl-5-hexen-4-onyl]carbamate (7). Vinylmagnesium bromide (4.8 ml of 0.98 M solution in THF) was added to a solution of (3*R*,4*R*,5*R*)-*N*-*tert*-butoxycarbonyl-3,4-isopropylidenedioxy-5-trityloxymethyl-2-pyrrolidinone (**6**, 1.74 g, 3.29 mmol) in THF (15 ml) at -40 - -50°C and the mixture was stirred at -40 - -50°C for 3 h. After addition of saturated aqueous NH_4Cl (10 ml), the mixture was diluted with AcOEt and washed with half-saturated aqueous NaCl. Drying followed by evaporation and purification of the residue by column chromatography (AcOEt:hexane=1:3) gave the enone **7** (1.69 g, 93%) as crystals, mp 104-105°C (AcOEt-hexane), $[\alpha]_D^{20}$ -85.1° (c=0.4, $CHCl_3$); IR ν_{max} (nujol) 1700, 1240, 1170, 698, 623 cm^{-1}; ^1H NMR($CDCl_3$) δ: 1.36(12H, s, CH_3, *t*-Bu), 1.60(3H, s, CH_3), 3.16(1H, dd, *J*=9 and 3.4 Hz, CH), 3.30-3.58(1H, m, CH), 4.10-4.36(2H, m, NH, CH), 4.46-4.62(2H, m, 2xCH), 5.13(1H,dd, *J*=2 and 10.5 Hz, CH=C<u>H</u>2), 5.39(1H, dd, *J*=2 and 17 Hz, CH=C<u>H</u>2), 6.16(1H, dd, *J*=10.5 and 17 Hz, C<u>H</u>=CH2), 6.70-7.93(15H, m, aromatic protons) ^{13}C NMR δ:25.29(q), 25.73(q), 28.22(q), 61.16(d), 62.92(t), 80.16(s), 80.80(s), 84.06(s), 87.08(s), 88.40(s), 112.56(s), 114.32(t), 127.04, 127.72, and 128.46(aromatic carbons), 141.07(d), 143.36(s), 153.65 (s). *Anal.* Calcd for C_{34} $H_{39}NO_6$: C,73.22; H, 7.05; N, 2.35. Found: C, 72.98; H, 6.86; N. 2.31.

1,1-Dimethylethyl *N*-[(1*R*,2*R*,3*S*,4*S*)- and (1*R*,2*R*,3*S*,4*R*)-4-Hydroxy-2,3-isopropylidenedioxy-1-trityloxymethyl-5-hexenyl]carbamate(10). A mixture of **7** (1.48 g, 2.7 mmol), $CeCl_3 \cdot 7H_2O$ (1.0 g, 2.7 mmol), and $NaBH_4$ (200 mg, 5.3 mmol) in MeOH (20 ml) was stirred at 0°C for 10 min, then at room temperature for 1 hr. After dilution with AcOEt, the mixture was washed with half-saturated aqueous NaCl. Drying followed by evaporation and purification of the residue by column chromatography (AcOEt:hexane=1:3) gave an inseparable diastereomeric mixture of **10** (1.35 g, 91%) as an oil, $[\alpha]_D^{20}$ -38.5° (c=1.2, $CHCl_3$); IR ν_{max} (film) 3450, 1704, 1496, 1375, 1220, 756, 704 cm^{-1}; ^1H NMR($CDCl_3$) δ: 1.39

(15H, s, *t*-Bu, 2xCH3), 2.35-2.50 and 2.90-3.00(1H, br s, OH), 3.00-3.25(1H, m, CH), 3.30-3.50(1H, m, CH), 3.90-4.60(4H, m, 4xCH), 4.70-5.10(1H, m, NH), 5.10-5.50(2H, m,CH=C<u>H2</u>), 5.77-6.16(1H, m, C<u>H</u>=CH2), 7.10-7.58(15H, m , aromatic protons). ^{13}C NMR δ: 24.70(q) and 25.33(q), 26.65(q) and 27.19 (q), 28.11(q), 49.89(d), 63.20(t) and 63.34(t) , 69.82(d) and 69.92(d), 75.57(d) and 76.30(d), 79.52(d) and 80.20(d), 79. 91(s), 86.30(s), 107.98(s), 115.92(t) and 116.22(t), 126.79, 127.57, and 128.40(aromatic carbons), 137.51(d) and 137.65(d), 143.70(s), 155.10(s) and 155.63(s). MS *m/z* 559 (M^+).

1,1-Dimethylethyl *N*-[(1*R*,2*R*,3*S*,4*R*)- and (1*R*,2*R*,3*S*,4*S*)-4,5-Dihydroxy-2,3-isopropylidenedioxy-1-(trityloxymethyl)pentyl]carbamate (11a and 12a). A solution of **10** (1.2 g, 2.15mmol) in CH_2Cl_2 (9 ml) was added at -78°C to 9 ml of CH_2Cl_2 saturated with ozone, and ozone was bubbled further 5 min at -78°C. Then, this solution was added to a suspension of $NaBH_4$ (570 mg, 15 mmol) in EtOH (9 ml) at 0°C. After being stirred at 0°C for 15 min, the mixture was diluted with AcOEt-benzene (1:1, 100 ml), and washed with half-saturated aqueous NaCl. Drying followed by evaporation gave a residue, which was purified by column chromatography (AcOEt:hexane=3:2) to give **11a** (641 mg, 53%) and **12a** (266 mg, 22%). **11a** (polar isomer): mp 135-137°C, $[\alpha]_D^{20}$ -50.5° (c=1.1, $CHCl_3$); IR ν max (nujol) 1670, 1249, 1087, 758, 704 cm^{-1}; ^{1}H NMR($CDCl_3$) δ: 1.39(15H, br s, 2xCH3, *t*-Bu), 2.30(1H, br s, OH), 2.94(1H, br s, OH), 3.07-3.12(1H, m, CH), 3.40-3.44(1H, m, CH), 3.50-3.80 (3H, m, 3xCH), 4.13-4.40(3H, m, CH), 4.90(1H, d, *J*=10 Hz, NH), 7.15-7.40(15H, m, aromatic protons); ^{13}C NMR($CDCl_3$) δ: 24.85(q), 26.66(q), 28.17(q), 49.95(d), 63.20(t), 64.71(t), 68.81(d), 75.43(d), 77.24 (d), 79.87(s), 86.35(s), 108.18(s), 126.85, 127.62, and 128.45(aromatic carbons), 143.70(s).155.60(s). *Anal.* Calcd for $C_{33}H_{41}NO_7$: C,70.31; H, 7.33; N 2.49 . Found: C, 70.12 ; H, 7.56 ; N.2.38. **12a** (less polar isomer): $[\alpha]_D^{20}$ -28.9° (c=1.5, $CHCl_3$); IR ν max (film) 3429, 1699, 1450, 1375, 1220, 1057, 758, 704 cm^{-1}; ^{1}H NMR($CDCl_3$) δ: 1.38(15H, br s, 2xCH3, *t*-Bu), 2.34-2.90(2H, br s, 2xOH), 2.90-3.20(1H, m, CH), 3.26-3.51(1H, m, CH), 3.51-3.90(3H, m, 3xCH), 3.90-4.57(3H, m, CH), 5.00(1H, d, *J*=8 Hz, NH), 7.05-7.56(15H, m, aromatic protons); ^{13}C NMR($CDCl_3$) δ: 25.44(q), 27.53(q), 28.17(q), 50.00(d), 63.50(t), 64.32(t), 68.51(d), 76.36(d), 78.11(d), 80.31(s), 86.49(s), 108.03(s), 126.89, 127.67, and 128.50(aromatic carbons), 143.70(s), 156.23(s). MS *m/z* 563(M^+).

1,1-Dimethylethyl *N*-[(1*R*,2*R*,3*S*,4*R*)- and (1*R*,2*R*,3*S*,4*S*)-4-hydroxy-2,3-isopropylidenedioxy-5-*tert*-butyldimetylsilyloxy-1-(trityloxymethyl)pentyl]carbamate (11b and 12b). A mixture of **11a** (1.25 g, 2.2mmol), *tert*-butyldimethylsilyl chloride (435 mg, 2.9 mmol), and imidazole (635 mg, 7.2 mmol) in DMF (15 ml) was stirred at 0°C for 1 h. After dilution with AcOEt (2:1, 100 ml), the mixture was washed with half-saturated aqueous NaCl . Drying followed by evaporation gave a residue, which was purified by column chromatography (AcOEt:hexane=1:5) to give **11b** (1.37 g, 91%) as crystals. The compound **12b** was obtained from **12a** in 86% yield as an oil in the same manner as described above for the preparation of **11b**. **11b**: mp 54-56°C, $[\alpha]_D^{20}$ -39.8° (c=0.3, $CHCl_3$); IR ν max (nujol) 3432, 1710, 1500, 1373, 1252, 1166, 1075, 773, 702 cm^{-1} ; ^{1}H NMR($CDCl_3$) δ: 0.05(6H,s, 2xCH3), 0.88(9H, s, *t*-Bu), 1.38(15H, s, 2xCH3, *t*-Bu), 2.60(1H, br s, OH), 3.02-3.20(1H, m, CH), 3.34-3.89(4H, m, 4xCH)), 4.05-4.58(3H,m ,3xCH), 4.96(1H, d, *J*=7 Hz, NH), 7.07-7.59(15H, m, aromatic protons); ^{13}C NMR($CDCl_3$) δ:-5.46(q), -3.65(q), 18.18(s), 24.95(q), 25.78(q), 26.51(q), 28.21(q), 50.24(d), 63.25(t), 64.47(t), 68.95(d), 75.29(d), 75.83(d), 79.48(s), 86.30(s), 108.03(s), 126.80, 127.58, and 128.50(aromatic carbons), 143.80 (s).155.35(s). *Anal.* Calcd for C39 $H_{55}NSiO_7$: C,69.09; H, 8.18; N, 2.07. Found: C, 68.87; H, 8.39; N. 1.82. **12b**: $[\alpha]_D^{20}$ -28.1° (c=0.8, $CHCl_3$); IR ν max (film) 3434, 1710, 1500, 1373, 1252, 1075, 773, 702 cm^{-1}; ^{1}H NMR($CDCl_3$) δ: 0.07(6H,s, 2xCH3), 0.90(9H, s, *t*-Bu), 1.18(3H, s, CH3), 1.27(3H, s, CH3), 1.43(9H, s, *t*-Bu), 2.82(1H, br s, OH), 3.22-3.33(2H, m, 2xCH), 3.52-3.90(3H, m, 3xCH), 4.00-4.45(3H, m, 3xCH), 5.06(1H, d, *J*=7 Hz, NH), 7.10-7.62(15H, m, aromatic protons); ^{13}C NMR($CDCl_3$) δ: -5.55(q), -3.65(q), 18.17(s), 25.49(q), 25.73(q), 27.34(q), 28.31(q), 50.29(d), 63.45(t), 64.47(t), 68.37(d), 76.78(d), 79.04(d), 86.20(s), 107.94(s), 126.65, 127.48, and 128.58(aromatic carbons), 143.85(s).155.25(s). HRMS *m/z* (M^+) calcd for $C_{39}H_{55}NSiO_7$ 677.3748, found 677.3737.

Conversion of 11b into 12b by Swern oxidation followed by reduction with $NaBH_4$. Dimethyl sulfoxide (660 mg, 8.52 mmol) was added at -78°C to a solution of oxalyl chloride (492 mg, 3.9

mmol)) in CH_2Cl_2 (12 ml). The mixture was stirred at - 78°C for 2 min, and then a solution of **11b** (1.2 g, 1.77 mmol) in CH_2Cl_2 (6 ml) was added at - 20°C over a period of 5 min. The whole was strirred at - 20 °C for 15 min, then TEA (1.24 ml, 8.86 mmol) was added and the reaction mixture was stirred at - 20°C for 5 min, then allowed to warm to room temperature. After addition of H_2O (10 ml), the aqueous layer was extracted with ether. The organic layers were washed with half-saturated aqueous NaCl. Drying followed by evaporation gave the crude ketone, which was dissolved in EtOH (4 ml) and treated with $NaBH_4$ (640 m g, 16.8 mmol) at -78°C for 20 min. After addition of AcOEt (100 ml), the mixture was washed with half-saturated aqueous NaCl. Drying followed by evaporation gave a residue, which was purified by column chromatography (AcOEt:hexane=1:4) to give **12b** (876 mg, 73%) and **11b**(48 mg, 4%) as an oil. Physical and NMR data were identical with those of authentic samples.

***(2R,3R,4S,5S)*- and *(2R,3R,4S,5R)*-*N*-*tert*-Butoxycarbonyl-3,4-isopropylidenedioxy-2-trityloxymethyl-5-(*tert*-butyldimethylsilyloxymethyl)pyrrolidine (13a and 14a).** A mixture of **11b** (1.34 g, 1.98 mmol), methanesulfonyl chloride (300 mg, 2.64 mmol), and TEA (264 mg, 2.64 mmol) in CH_2Cl_2 (16 ml) was stirred at 0° C for 1 h. After dilution with AcOEt, the mixture was washed with H_2O, saturated aqueous $NaHCO_3$, and H_2O. Drying followed by evaporation gave a residue, which was treated with potassium *tert*-butoxide (560 mg, 5 mmol) in THF (16 ml) at 0°C for 20 min. After dilution with AcOEt, the mixture was washed with half-saturated aqueous NaCl. Drying followed by evaporation gave a residue, which was purified by column chromatography (AcOEt:hexane =1:4) to give **13a** (978 mg, 75%) as an oil. The compound **14a** was obtained from **12b** in 78% yield as an oil in the same manner as described above for the preparation of **13a**. **13a**: $[\alpha]_D^{20}$ -18.9°(c=0.7, $CHCl_3$); IR ν_{max} (film) 1695, 1390, 1250, 1066, 758, 704 cm^{-1}; ^1H NMR($CDCl_3$) δ: -0.13(6H,s, 2xCH_3), 0.76(9H, s, *t*-Bu), 1.28(12H, s, CH_3, *t*-Bu), 1.44(6H, s, 2xCH_3), 2.69-3.15(1H, m CH), 3.15-3.77(3H, m, 2xCH), 3.77-4.25(2H, m, 2xCH)), 4.61(2H,br s, 2xCH), 7.11-7.55(15H, m, aromatic protons); ^{13}C NMR($CDCl_3$) δ: -5.51(q), 18.18(s), 25.44(q), 25.83(q), 27.29(q), 28.17(q), 62.18(t), 63.35(t), 64.37(d), 65.74(d), 79.57(s), 81.14(d), 82.40 (d), 86.49(s), 111.30(s), 126.84, 127.62, and 128.50(aromatic carbons), 143.468(s).153.89(s). HRMS *m/z* (M^+) calcd for $C_{39}H_{53}NSiO_6$ 659.3642, found 659.3613. **14a**: $[\alpha]_D^{20}$ -37.9° (c=0.5, $CHCl_3$); IR ν_{max} (film) 1697, 1375, 1084, 758, 704 cm^{-1}; ^1H NMR($CDCl_3$) δ: 0.05(6H,s, 2xCH_3), 0.88(9H, s, *t*-Bu), 1.27 (12H, s, CH_3, *t*-Bu), 1.42(3H, s, CH_3), 2.82-3.17(1H, m CH), 3.17-3.45(1H, m, CH), 3.60-4.22(4H, m, 4xCH)), 4.33-4.98(2H,m, 2xCH), 6.89-7.75(15H, m, aromatic protons); ^{13}C NMR($CDCl_3$) δ: -5.55(q), -5.31(q), 18.13(s), 24.81(q), 25.78(q), 26.31(q), 28.21(q), 59.89(t), 63.45(t), 63.55(d), 64.81(d), 79.33(s), 80.26(d), 86.94(s), 110.52(s), 126.84, 127.67, and 128.35(aromatic carbons), 143.41(s).154.08(s). HRMS *m/z* (M^+) calcd for $C_{39}H_{53}NSiO_6$ 659.3642, found 659.3624.

***(2R,3R,4S,5S)*- and *(2R,3R,4S,5R)*-*N*-*tert*-Butoxycarbonyl-3,4-isopropylidenedioxy-2-trityloxymethyl-5-hydroxymethylpyrrolidine(13b and 14b).** A mixture of **14a** (920 mg, 1.4 mmol) in THF (10 ml) and tetrabutylammonium fluoride (4 ml of a 1M solution in THF) was stirred at room temperature for 30 min. After dilution with AcOEt, the mixture was washed with half-saturated aqueous NaCl. Drying followed by evaporation gave a residue, which was purified by column chromatography (AcOEt:hexane=1:1) to give **14b** (630 mg, 82%) as crystals. The compound **13b** was obtained from **13a** in 78% yield as crystals after column chromatography (AcOEt : hexane= 1 : 1) in the same manner as described above for the preparation of **14b**. **14b**: mp 145°C (AcOEt-hexane), $[\alpha]_D^{20}$ -49.1° (c=1.6, $CHCl_3$); IR ν max (nujol) 3376, 1674, 1060, 762, 706 cm^{-1}; ^1H NMR($CDCl_3$) δ:1.27(3H, s, CH3), 1.33(9H,s, *t*-Bu), 1.41(3H, s, CH_3), 3.01-3.15(1H, m CH), 3.29-3.57(1H, m, CH), 3.75-4.23(4H, m, 4xCH)), 4.50(1H, d, *J*=6 Hz, CH), 4.88(1H, m, CH), 5.40(1H, br s, OH), 7.15-7.44(15H, m, aromatic protons) ; ^{13}C NMR ($CDCl_3$) δ:24.51(q), 25.88(q), 28.17(q), 62.72(t), 63.25(t), 63.54(d), 65.74(d), 80.31(d), 80.60(s), 80.70 (d), 87.13(s), 110.86(s), 126.99, 127.77, and 128.26(aromatic carbons), 143.17(s).155.49(s). *Anal.* Calcd for C_{33} $H_{39}NO_6$: C,72.63; H,7.20 , N; 2.57. Found: C,72.42 ; H, 7.41 ; N.2.31. **13b**: mp 90-92°C(AcOEt-hexane) , $[\alpha]_D^{20}$ -23.1° (c=1.1, $CHCl_3$); IR ν_{max} (nujol) 3423, 1674, 1065, 760, 704 cm^{-1}; ^1H NMR($CDCl_3$) δ: 1.29(12H, s, *t*-Bu), 1.43(3H, s, CH_3), 3.10-3.25(2H, m CH_2), 3.50-3.70(3H, m, CH_2, OH), 3.90-4.10(2H, m, 2xCH)), 4.30-4.65(2H, m, 2xCH), 7.10-7.45(15H, m, aromatic protons);

^{13}C NMR($CDCl_3$) δ: 25.54(q), 27.48(q), 28.28(q), 63.33(t), 64.50(d), 65.32(t), 67.19(d), 80.84(d), 81.63(d), 81.83(d), 87.31(s), 111.81(s), 127.22, 127.88, and 128.70(aromatic carbons), 143.32(s), 156.16(s). Anal. calcd for $C_{33}H_{39}NO_6$: C, 72.63; H, 7.20, N; 2.57. Found: C,72.53; H, 7.48; N.2.61.

(2*R*,3*R*,4*S*,5*R*)- and (2*R*,3*R*,4*S*,5*S*)-*N*-*tert*-Butoxycarbonyl-3,4-isopropylidenedioxy-2-trityloxymethyl-5-vinylpyrrolidine (15). A mixture of **10** (800 mg, 1.43 mmol), methanesulfonyl chloride (229 mg, 1.99 mmol), and TEA (202 mg, 1.99 mmol) in CH_2Cl_2 (15 ml) was stirred at 0°C for 30 min. After dilution with AcOEt, the mixture was washed with H_2O, saturated aqueous $NaHCO_3$, and H_2O. Drying followed by evaporation gave a residue, which was treated with potassium *tert*-butoxide (400 mg, 3.58 mmol) in THF (15ml) at 0°C for 15 min, then at room temperature for 30 min. After dilution with AcOEt, the mixture was washed with half-saturated aqueous NaCl. Drying followed by evaporation gave a residue, which was purified by column chromatography (AcOEt:hexane =1:4) to give an inseparable diastereomeric mixture **15** (526 mg, 68%) as an oil; ^1H NMR($CDCl_3$) δ: 1.30(3H, s, CH_3), 1.40(9H, S, *t*-Bu), 1.48(3H, s, CH_3), 2.90-3.25(2H, m, CH_2), 4.20-4.65(4H, m, 4xCH), 4.65-5.30(2H, m, CH=C<u>H</u>2), 5.50-6.00(1H, m, C<u>H</u>=CH_2), 7.10-7.50(15H, m, aromatic protons). ^{13}C NMR δ: 24.66(q) and 25.34(q), 25.83(q) and 27.19(q), 28.26(q), 63.06(t) and 64.03(t), 65.54(d), 67.10(d), 79.82(s), 81.57(d) and 81.87(d), 84.46(d), 86.84(s), 111.25 and 111.59(s)., 114.86 and 115.88(t), 126.89, 127.67, and 128.54(aromatic carbons), 136.69(d), 142.53(s) and 143.51(s), 154.13(s). MS *m/z* 541 (M^+).

(2*R*,3*R*,4*S*,5*S*)- and (2*R*,3*R*,4*S*,5*R*)-*N*-*tert*-Butoxycarbonyl-3,4-isopropylidenedioxy-5-hydroxymethyl-2-trityloxymethylpyrrolidine (13b and 14b) from 15. The compounds **13b** (351 mg, 60%) and **14b** (146 mg, 25%) were obtained from **15** (580 mg, 1.1 mmol) as crystals after column chromatography (AcOEt : hexane= 1 : 2) in the same manner as described above for the preparation of **11a** and **12a** from **10**. Physical and NMR data were identical with those of authentic samples.

1,1-Dimethylethyl *N*-[(1*R*,2*R*,3*R*)-2,3-Isopropylidenedioxy-3-methoxycarbonyl-1-(trityloxymethyl)propyl]carbamate (8). A mixture of **6** (1.0 g, 1.89 mmol) and 2 ml of 2M solution of lithium hydroxide in 7 ml of THF-MeOH (1:1) was stirred at room temperature for 2 h. After removal of the solvents *in vacuo*, the aqueous layer was acidified with 10% aqueous citric acid and extracted with AcOEt. The AcOEt extracts were washed with saturated aqueous NaCl. Drying followed by evaporation gave a residue, which was treated with ethereal diazomethane at room temperature. After evaporation of the solvent *in vacuo*, the residue was purified by column chromatography (AcOEt:hexane=1: 2.5) to give **8** (954 mg, 90 %) as crystals, mp 124°C (AcOEt-hexane), $[\alpha]_D^{20}$ -46.8° (c=0.9, $CHCl_3$); IR ν_{max} (nujol) 1760, 1716, 1161, 1082, 758, 704 cm^{-1}; ^1H NMR($CDCl_3$) δ: 1.37(12H, s, CH_3, *t*-Bu), 1.46(3H, s, CH_3), 3.06-3.44(2H, m, CH_2), 3.66(3H, s, $COOCH_3$), 3.66-4.10(1H, m, CH), 4.45-4.83(3H, m, 2xCH, NH), 7.06-7.52(15H, m, aromatic protons); ^{13}C NMR($CDCl_3$) δ:25.49(q), 26.66(q),28.17(q), 50.48(d), 52.14(q), 62.72(t), 76.12(d), 76.41(d), 79.24(s), 86.25(s), 110.62(s), 126.80, 127.58, 128.40(aromatic carbons), 143.66(s)., 154.62(s), 169.48(s). *Anal.* Calcd for $C_{33}H_{39}NO_7$: C, 70.57; H, 7.00; N, 2.49. Found: C, 70.42; H, 7.25; N, 2.30.

1,1-Dimethylethyl *N*-[(1*R*,2*R*,3*S*)-4-hydroxy-2,3-isopropylidenedioxy-1-(trityloxymethyl)butyl]carbamate (9). A mixture of $NaBH_4$ (230 mg, 6.1 mmol) and **8** (850 mg, 1.52 mol) in EtOH (10 ml) was stirred at room temperature for 8 h. After addition of AcOEt (100 ml), the mixture was washed with half-saturated aqueous NaCl. Drying followed by evaporation gave a residue, which was purified by column chromatography (AcOEt:hexane=2:1) to give **9** (710 mg, 88%) as crystals, mp 100-102°C (ether-hexane), $[\alpha]_D^{20}$ -38.5° (c=0.7, $CHCl_3$); IR ν_{max} (nujol) 3432, 1707, 1498, 1167, 1045, 758, 704 cm^{-1}; ^1H NMR($CDCl_3$) δ: 1.35(15H, s, 2xCH3, *t*-Bu), 2.42(1H, br s, OH), 3.05-3.09(1H, m, CH), 3.30-3.45(1H, m, CH), 3.50-3.65(1H, m, CH), 3.70-3.95(2H, m, CH2), 4.20-4.40(2H, m, 2xCH), 4.78(1H, d, *J*=9 Hz, NH),7.16-7.50(15H, m, aromatic protons); ^{13}C NMR($CDCl_3$) δ: 25.56(q), 27.99(q),28.29(q), 49.56(d), 61.25(t), 63.37(t), 75.43(d), 78.22(d), 80.16(s), 86.56(s), 108.41(s), 127.03, 127.79, 128.61 (aromatic carbons), 143.84(s)., 155.69(s). *Anal.* Calcd for $C_{32}H_{39}NO_6$: C, 72.02; H, 7.37; N, 2.62. Found: C, 71.82; H, 7.58; N, 2.43.

1,1-Dimethylethyl *N*-[(1*R*,2*R*,3*S*,4*R*)-4-Hydroxy-2,3-isopropylidenedioxy-1-trityloxymethyl-5-hexenyl]carbamate(10b) from 9. Swern oxidation of **9** (540 mg, 1.01 mmol) in

CH_2Cl_2 was performed in the same manner as described above for the preparation of **12b** from **11b**. The crude aldehyde was dissolved in THF (6ml). Then, vinylmagnesium bromide (2.1 ml of 1 M solution in THF) was added at -78°C. After being stirred at -78°C for 30 min, the mixture was treated with saturated aqueous NH_4Cl and extracted with AcOEt. The organic layers were washed with half-saturated aqueous NaCl. Drying followed by evaporation gave a residue, which was purified by column chromatography (AcOEt:hexane=1:2) to give **10b** (401 mg, 71%) as an oil. **10b**: $[\alpha]_D^{20}$ -39.8° (c=1.2, $CHCl_3$); IR ν max (film) 3456, 1716, 1493, 1377, 1161 cm^{-1}; ^1H NMR($CDCl_3$) δ: 1.37(15H, s, *t*-Bu, 2xCH_3), 2.36(1H, brs, OH), 3.11(1H, dd, *J*=3 and 8.5 Hz, CH), 3.42(1H, dd, *J*=2 and 8.5 Hz, CH), 3.90-4.45(4H, m, 4xCH), 4.65-4.95(1H, m , NH), 5.05-5.40(2H, m , CH=C<u>H2</u>), 5.65-7.05(1H, m, C<u>H</u>=CH_2), 7.10-7.50(15H, m , aromatic protons); ^{13}C NMR($CDCl_3$) δ: 24.75(q), 26.70(q), 28.21(q), 49.95(d), 63.25(t), 69.98(d), 75.53(d), 79.58(d and s)), 86.35(s), 108.13(s), 116.03(t), 126.84, 127.62, and 128.50(aromatic carbons), 137.56(d), 143.75(s), 155.25(s). MS *m/z* 559 (M^+).

(2*R*,3*R*,4*S*,5*S*)-*N*-*tert*-Butoxycarbonyl-3,4-isopropylidenedioxy-2-trityloxymethyl-5-vinylpyrrolidine (15b). This compound **15b** (306 mg, 88%) was obtained from **10b** (360 mg, 0.64 mmol) as an oil in the same manner as described above for the preparation of **13a**, $[\alpha]_D^{20}$ -51.0° (c=0.7, $CHCl_3$); IR ν max (film) 1377, 1167, 1051, 758, 704 cm^{-1}; ^1H NMR($CDCl_3$) δ: 1.30(3H, s, CH_3), 1.40(9H, S, *t*-Bu), 1.47(3H, s, CH_3), 2.90-3.25(2H, m, CH_2), 4.20-4.65(4H, m, 4xCH), 4.65-5.30(2H, m, CH=C<u>H2</u>), 5.50-6.00(1H, m, C<u>H</u>=CH_2), 7.11-7.55(15H, m, aromatic protons) ; ^{13}C NMR($CDCl_3$) δ: 25.39(q), 27.24(q), 28.31(q), 63.11(t), 64.03(d), 67.05(d), 79.82(s), 81.91(d), 84.55(d), 86.88(s), 111.64 (s), 115.93(t), 127.20, 128.26, and 128.98(aromatic carbons), 136.73(d), 143.14(s), 153.79(s). MS *m/z* 541(M^+).

(2*R*,3*R*,4*S*,5*S*)-*N*-*tert*-Butoxycarbonyl-5-hydroxymethyl-3,4-isopropylidenedioxy-2-(trityloxymethyl)pyrrolidine (13b). This compound **13b** (207 mg, 82%) was obtained from **15b** (250 mg, 0.46 mmol) as crystals after column chromatography (AcOEt : hexane= 1 : 1) in the same manner as described above for the preparation of **11a** and **12a** from **10**. Physical and NMR data were identical with those of an authentic sample.

(2*R*,3*R*,4*S*,5*R*)-*N*-*tert*-Butoxycarbonyl-3,4-isopropylidenedioxy-2-trityloxymethyl-5-[(1*S*)- and (1*R*)-1-hydroxy-3-butenyl]pyrrolidine(16 and 19). A) Allylation with Grignard Reagent: Swern oxidation of **14b** (800 mg, 1.47 mmol) was performed in the same manner as described above for the preparation of **12b** from **11b**. The crude aldehyde was dissolved in THF (14 ml) and treated with allylmagnesium chloride (1.7 ml of a 2 M solution in THF) at - 78°C. After being stirred at - 78°C for 1 h, the mixture was quenched with 5 ml of 10% aqueous NH_4Cl and extracted with AcOEt. The organic layers were washed with half-saturated aqueous NaCl. Drying followed by evaporation and purification of the residue by column chromatography (AcOEt : hexane= 1 : 4) gave **16** (516 mg, 60%) and **19** (206 mg, 24%). **16** (less polar isomer): mp 93-94°C (AcOEt-hexane), $[\alpha]_D^{20}$ -29.9° (c=1, $CHCl_3$); IR ν max (nujol) 3342, 1672, 1417, 1207, 1171, 1130, 698, 623 cm^{-1}; ^1H NMR($CDCl_3$) δ: 1.29(3H, s, CH_3), 1.34(9H,s , *t*-Bu), 1.41 (3H, s, CH_3), 2.11-2.89(2H,m, CH_2), 2.98-3.44(2H,m, 2xCH), 3.66-3.92(1H, m, CH), 3.92-4.36 (2H, m, 2xCH), 4.45-4.87(2H, m, 2xCH), 5.00-5.25(2H, m, CH=C<u>H2</u>), 5.76-6.34(1H,m, C<u>H</u>=CH_2), 6.34-6.55 (1H, br s, OH), 6.90-7.61(15H, m, aromatic protons) ; ^{13}C NMR($CDCl_3$) δ: 22.05(q), 26.61(q), 28.17(q), 37.91(t), 63.11(t), 65.49(d), 67.95(d), 69.34(d), 79.57(d), 80.45(s), 80.70(d), 86.98(s), 110.06 (s), 116.32 (t), 126.99, 127.77, and 128.35(aromatic carbons), 135.37(d), 143.27(s).155.21(s). *Anal.* Calcd for $C_{36}H_{43}NO_6$: C, 73.82; H, 7.40; N, 2.39. Found: C, 73.591; H,7.62; N, 2.23. **19** (polar isomer) : $[\alpha]_D^{20}$ -57.1° (c=1, $CHCl_3$); IR ν max (film) 3435, 1680, 1403, 1243, 1081, 758, 704 cm^{-1}; ^1H NMR ($CDCl_3$) δ: 1.25(3H, s, CH_3), 1.33(9H, s , *t*-Bu), 1.47(3H, s, CH_3), 1.95-2.67(2H,m, CH_2), 2.87-3.17 (1H,m, CH), 3.43-3.65(1H, m, CH), 3.91-4.56(4H, m, 3xCH, OH), 4.73-5.34(4H, m, 4xCH), 5.69-6.18(1H, m, C<u>H</u>=CH_2), 6.70-7.93(15H, m, aromatic protons); ^1H NMR($CDCl_3$) δ: 23.63(q), 25.24(q), 28.21(q), 37.86(t), 63.38(d), 63.59(t), 67.98(d), 69.98(d), 79.92(d), 80.70(s), 80.94(d), 87.18(s), 110.96 (s), 115.64(t), 127.09, 127.87, and 128.35(aromatic carbons), 136.64(d), 143.27(s).156.03(s). HRMS *m/z* (M^+) calcd for $C_{36}H_{43}NO_6$ 585.3090, found 585.3140.

B) Allylation with Allyllithium: 1.85 ml of allyllithium[14] (about 1 M in ether, prepared from tetraallyltin (1 equiv.) and phenyllithium (4 equv.) in ether) was added at -78°C to a solution of the crude aldehyde prepared from **14b** (500 mg, 0.92 mmol). The mixture was stirred at - 78°C for 1 h. After addition of 10% aqueous NH_4Cl (6ml), the reaction mixture was diluted with AcOEt, and washed with half-saturated aqueous NaCl. Drying followed by evaporation and purification of the residue by column chromatography (AcOEt : hexane= 1 : 4) gave **16** (363 mg, 68%) and **19** (72 mg, 13%).

C) Allylation with Allyltrimethylsilane and $TiCl_4$: A solution of $TiCl_4$ (160 mg, 0.843 mmol) in CH_2Cl_2 (1 ml) was added to a solution of allytrimethylsilane (115 mg, 1.0 mmol) and the aldehyde prepared from **14b** (230 mg, 0.42 mmol) in CH_2Cl_2 (2.5 ml) at - 78°C over a period of 5 min. After being stirred at - 78°C for 10 min , the mixture was basified with 10% aqueous NaOH and extracted with AcOEt. The AcOEt extracts were washed with half-saturated aqueous NaCl. Drying followed by evaporation and purification of the residue by column chromatography (AcOEt:hexane=1:4) gave **16** (52 mg, 21%).

***(2R,3R,4S,5S)*-*N*-*tert*-Butoxycarbonyl-3,4-isopropylidenedioxy-2-trityloxymethyl-5-[(1*S*)- and (1*R*)-1-hydroxy-3-butenyl]pyrrolidine (23 and 26).** Dimethyl sulfoxide (590mg, 7.5 mmol) was added at - 78°C to a solution of oxalyl chloide (440 mg, 3.4 mmol) in THF (8 ml). The mixture was stirred at -40 - -50°C for 3 min. Then a solution of **13b** (850 mg, 1.56 mmol) in THF (3 ml) was added at -10 °C. After being stirred at -10°C for 40 min, TEA (787 mg, 7.8 mmol) was added. Then the mixture was recooled at -78°C, and vinylmagnesium bromide (7.3 ml of 1 M solution in THF) was added at -78°C. The mixture was stirred at -78°C for 30 min, and then treated with EtOH (1 ml) and saturated aqueous NH_4Cl (5 ml). After dilution with AcOEt, the mixture was washed with half-saturated aqueous NaCl. Drying followed by evaporation gave a residue, which was purified by column chromatography (AcOEt :hexane=1:4) to give **23** (476 mg, 52%) and **26** (227 mg, 25%) as an oil. **23**(polar isomer): $[\alpha]_D^{20}$ -23.2° (c=1, $CHCl_3$); IR ν max (film) 3480, 1695, 1379, 1219, 1167, 1066, 758, 706 cm^{-1} ; ^1H NMR($CDCl_3$) δ: 1.29(3H, s, CH_3), 1.37(9H,s , *t*-Bu), 1.42(3H, s, CH_3), 1.96-2.40(2H,m, CH_2), 3.13-3.50(3H,m, CH_2, CH), 3.50-3.91(1H, br s, OH), 3.91-4.33(2H, m, 2xCH), 4.33-4.82(2H, m, 2xCH), 4.82-5.25(2H, m, CH=C<u>H</u>$_2$), 5.42-5.98 (1H, m, C<u>H</u>=CH_2),6.92-7.58(15H, m, aromatic protons); ^{13}C NMR($CDCl_3$) δ: 25.19(q), 27.14(q), 28.02 (q), 38.16(t), 62.96(t), 64.57(d), 68.37(d), 70.32(d), 79.53(d), 79.72(s), 81.87(d), 86.88(s), 111.06(s), 117.49(t), 126.75, 127.48, and 128.35(aromatic carbons), 134.05(d), 143.12(s).154.38(s). HRMS *m/z* (M^+) calcd for $C_{36}H_{43}NO_6$ 585.3090, found 585.3130. **26** (less polar isomer); $[\alpha]_D^{20}$ -20.1° (c=0.7, $CHCl_3$); IR ν max (film) 3496, 1693, 1379, 1221, 1167, 1068, 758, 704 cm^{-1}; ^1H NMR($CDCl_3$) δ: 1.28 (3H, s, CH_3), 1.37(9H, s, *t*-Bu), 1.43(3H, s, CH_3), 1.84-2.50(2H, m, CH_2), 3.08-3.80(4H, m, CH_2, CH, OH), 3.92-4.30(2H, m, 2xCH), 4.34-4.68(2H, m, 2xCH), 4.83-5.19(2H, m, CH=C<u>H</u>$_2$), 5.48-6.03(1H, m, C<u>H</u>=CH_2),7.00-7.57(15H, m, aromatic protons).^{13}C NMR($CDCl_3$) δ: 25.49(q), 27.39(q), 28.22(q), 38.84(t), 63.21(t), 64.96(d), 68.81(d), 73.19(d), 80.74(s), 81.96(d), 82.40(d), 87.23(s), 111.54(s), 117.54(t), 127.04, 127.77, and 128.65(aromatic carbons), 134.40(d), 143.36(s), 156.76(s). HRMS *m/z* (M^+) calcd for $C_{36}H_{43}NO_6$ 585.3090, found 585.3075.

***(2R,3R,4S,5R)*-*N*-*tert*-Butoxycarbonyl-3,4-isopropylidenedioxy-2-trityloxymethyl-5-[(1*S*)-1-methoxymethyloxy-3-butenyl]pyrrolidine(17).** A mixture of **16** (330 mg, 0.56 mmol), *N*,*N*-diethylaniline (673 mg, 4.5 mmol), and chloromethyl methy ether (363 m g, 4.5 mmol) in CH_2Cl_2 (5 ml) was stirred at room temperature for 40 h. After addition of AcOEt (100 ml), the mixture was washed with 5% aqueous HCl, H_2O, saturated aqueous $NaHCO_3$, and H_2O. Drying followed by evaporation gave a residue, which was purified by column chromatography (AcOEt:hexane=1: 3) to give **17** (300 mg, 85%) as crystals, **17**: mp 126-127°C(AcOEt-hexane), $[\alpha]_D^{20}$ -68.5° (c=0.9, $CHCl_3$); IR ν max (nujol) 1699, 1040, 762, 706 cm^{-1}; ^1H NMR($CDCl_3$) δ: 1.28(3H, s, CH_3), 1.32(9H,s , *t*-Bu), 1.50(3H, s, CH_3), 2.15-2.84(2H, m, 2xCH), 2.99-3.24(1H, m, CH), 3.30-3.71(1H, m, CH), 3.31(3H, s, OCH_3), 3.90-4.20(3H, m, CH), 4.23-5.23(6H, m, 4xCH, CH=C<u>H</u>$_2$), 5.64-6.17(1H, m, C<u>H</u>=CH_2), 6.94-7.56(15H, m, aromatic protons) ; ^{13}C NMR($CDCl_3$) δ: 23.93(q), 25.83(q), 28.26(q), 36.21(t), 55.55(q), 63.50(d and t), 64.32(d), 80.41(s and d), 81.19(d), 87.08(s), 97.80(t), 111.11(s), 115.98(t), 126.99, 127.77, and 128.45, (aromatic carbons),

137.23 (d), 143.41(s), 154.18(s). *Anal.* Calcd for $C_{38}H_{47}NO_7$: C, 72.47; H, 7.52, N 2.22. Found: C, 72.51 ; H,7.68 ; N.2.31.

(2*R*,3*R*,4*S*,5*R*)-*N*-Benzyl-3,4-isopropylidenedioxy-2-trityloxymethyl-5-[(1*S*)-1-methoxymethyloxy-3-butenyl]pyrrolidine(18). *tert*-Butyldimethylsilyl trifluoromethanesulfonate (370 mg, 1.4 mmol) was added at room temperature to a solution of **17** (180 mg, 0.29 mmol) and 2,6-lutidine (150 mg, 1.4 mmol) in CH_2Cl_2 (3 ml) .The mixture was stirred at room temperature for 3 h and quenched with saturated aqueous NH_4Cl solution. The product was extracted with ether and the combined ether layers were washed with half-saturated aqueous NaCl . Drying followed by evaporation gave a residue, which was dissolved in THF (2 ml) and tetrabutylammonium fluoride (1 ml of a 1M solution in THF) was added. After being stirred at room temperature for 30 min, the mixture was diluted with AcOEt and washed with half-saturated aqueous NaCl. Drying followed by evaporation gave a residue, which was benzylated with benzyl bromide (180 mg, 1.1 mmol) in the presence of K_2CO_3 (200 mg) in acetone (3 ml) at room temperature for 2 h. Filtration followed by evaporation and purification with column chromatography (AcOEt:hexane=1: 6) gave **18** (103 mg, 58%) as an oil, $[\alpha]_D^{20}$ -60.9° (c=1.3, $CHCl_3$); IR ν_{max} (film) 1448, 1211, 1151, 1037, 740, 704 cm^{-1}; ^1H NMR($CDCl_3$) δ: 1.35(3H, s, CH_3), 1.55(3H,s CH_3), 2.54-2.82(2H, m, 2xCH), 2.92-3.74(5H, m, 3xCH, CH_2OTr), 3.30(3H, s, OCH_3), 3.40-4.23(2H, m, 2xCH), 4.58-5.26(6H, m, 2xCH2, 2xCH), 5.68-6.14(1H, m, C<u>H</u>=CH_2), 6.86-7.763(20H, m, aromatic protons); ^{13}C NMR($CDCl_3$) δ: 24.41(q), 24.98(q), 36.11(t), 51.31(t), 55.75(q), 60.82(t), 64.27(d), 66.71(d), 78.65(d), 81.38(d), 81.72(d), 87.23(s), 96.58(t), 110.91(s), 116.42(t), 126.31, 126.94, and 127.72, 128.00, 128.65 (aromatic carbons), 135.30(d), 139.42(s), 143.46(s). HRMS *m/z* (M^+) calcd for $C_{40}H_{45}NO_5$ 619.3298, found 619.3282.

(2*R*,3*R*,4*R*,5*R*)-*N*-Benzyl-3,4-isopropylidenedioxy-2-trityloxymethyl-5-[(1*S*)-1-methoxymethyloxy-3-hydroxypropanyl]pyrrolidine(22a). This sample **22a** (114 mg, 58%) was obtained from **18** (195 mg, 0.31 mmol) as an oil after column chromatography (AcOEt : hexane= 1 : 4) in the same manner as described above for the preparation of **11a** and **12a** from **10**, $[\alpha]_D^{20}$ -26.9° (c=0.5, $CHCl_3$). IR ν_{max} (film) 3460, 1374,1247, 1047, 758, 704 cm^{-1}; ^1H NMR($CDCl_3$) δ: 1.32(3H, s, CH_3), 1.57(3H,s CH_3), 1.80-2.43 (3H, CH_2, OH), 2.89-3.27(4H,m, CH_2, 2xCH), 3.34(3H, s, OCH_3), 3.42-4.20(4H, m, 4xCH), 4.50--5.10 (5H, m, 5xCH), 6.86-7.52(20H, m, aromatic protons); ^{13}C NMR($CDCl_3$) δ: 24.46(q), 26.02(q), 33.97(t), 51.09(t), 55.65(q), 59.68(t), 60.52(t), 63.69(d), 66.76(d), 76.94(d), 81.33(d), 81.43(d), 87.08(s), 96.92(t), 110.76(s), 126.21, 126.80, and 127.43, 127.53, 127.87, and 128.46(aromatic carbons), 135.64(d), 143.17 (s). HRMS *m/z* (M^+) calcd for $C_{39}H_{45}NO_6$ 623.3247, found 623.3288.

1,7a-Diepialexine(1a). A mixture of **22a** (80 mg, 0.13 mmol), methanesulfonyl chloride (22 mg, 0.19 mmol), and TEA (19 mg, 0.19 mmol) in CH_2Cl_2(1.5 ml) was stirred at room temperature for 16 h. After addition of 20 ml of CH_2Cl_2, the mixture was washed with H_2O. Drying followed by evaporation gave a residue, which was hydrogenated using 10% palladium on carbon (25 mg) in EtOH (2 ml) in the presence of hydrogen chloride at room temperature for 1h under hydrogen at atmospheric pressure. The mixture was filtered and concentrated *in vacuo*, and the residue was treated with 10% aqueous HCl (1 ml) and MeOH (1 ml) at 70°C for l h. After removal of the methanol *in vacuo*, the insoluble materials were filtered off, and the filtrate was placed on a Dowex 50W-X8 (H^+ form) column (15 ml), washed with 30 ml of H_2O, and eluted with 0.6 N NH_4OH. Freeze-drying of the appropriate fractions gave 1,7a-diepialexine (**1a**, 13 mg, 52%) as an oil, $[\alpha]_D^{20}$ +12.5° (c=0.6, H_2O); ^1H NMR(D_2O) δ: 2.01(2H, m), 3.00(1H, m), 3.09(1H, m), 3.20(1H, m), 3.53(1H, dd), 3.62(1H, dd), 3.80(1H, dd), 3.91(1H, dd), 4.38(1H, m), 4.55(1H, m); ^{13}C NMR(D_2O, dioxane δ=67.40) 36.01(t), 52.92(t), 63.20(t), 67.00(d), 70.85(d), 72.80(d), 73.73(d), 75.09(d). HRMS (FAB): *m/z* $(M+H)^+$ calcd for $C_8H_{16}NO_4$ 190.1080, found 190.1088.

Physical and NMR data for 20, 21, 22b, 1b, 24, 25, and 27-30. **20**: oil, $[\alpha]_D^{20}$ -71.5° (c=0.7, $CHCl_3$); IR ν_{max} (film) 1695, 1373, 1043, 758, 704 cm^{-1}; ^1H NMR($CDCl_3$) δ: 1.28(3H, s, CH_3), 1.40 (9H, s, *t*-Bu), 1.51(3H, s, CH_3), 2.43-2.74(2H, m, 2xCH), 2.86-3.20(1H, m, CH), 3.30-3.70(1H, m, CH), 3.34(3H, s, OCH_3), 3.94-4.43(3H, m, 3xCH), 4.43-5.31(6H, m, 4xCH, CH=C<u>H</u>$_2$), 5.66-6.17(1H, m,

CH=CH_2), 6.90-7.63(15H, m, aromatic protons); ^{13}C NMR($CDCl_3$) δ: 24.41(q), 25.19(q), 28.21(q), 36.74 (t), 55.11(q), 62.62(d), 64.86(d), 76.31(d), 79.48(d), 81.33(d), 86.88(s), 97.22(t), 110.06(s), 116.17(t), 126.89, 127.67, and 128.31, (aromatic carbons), 135.81(d), 143.36(s), 154.18(s). HRMS *m/z* (M^+) calcd for $C_{38}H_{47}NO_7$ 629.3353, found 629.3362. **21**:oil, $[\alpha]_D^{20}$ -55.9° (c=1.3, $CHCl_3$); IR ν max (film) 1488, 1215, 1153, 1038, 756, 704 cm^{-1}; ^1H NMR($CDCl_3$) δ: 1.31(3H, s, CH_3), 1.55(3H, s, CH_3), 1.90-2.56(2H, m, 2xCH), 2.72-3.30(5H,m, 3xCH, CH_2OTr), 3.30(3H, s, OCH_3), 3.60-4.20(2H, m, 2xCH), 4.50-5.20 (6H, m, 2xCH_2, 2xCH), 5.68-6.17(1H, m, CH=C, 6.84-7.72(20H, m, aromatic protons); ^{13}C NMR($CDCl_3$) δ: 24.12(q), 25.88(q), 36.45(t), 51.75(t), 55.51(q), 61.11(t), 63.40(d), 68.17(d), 77.92(d), 81.33(d), 82.30 (d), 87.23(s), 96.53(t), 110.26(s), 115.88(t), 126.26, 126.94, and 127.72, 128.01, 128.60(aromatic carbons), 137.17(d), 139.12(s), 143.41(s). HRMS *m/z* (M^+) calcd for $C_{40}H_{45}NO_5$ 619.3298, found 619.3290. **22b**: oil, $[\alpha]_D^{20}$ -70.5° (c=0.5, $CHCl_3$); IR ν max (film) 3440, 1450, 1377, 1215, 1032, 756, 704 cm^{-1}; ^1H NMR($CDCl_3$) δ: 1.29(3H, s, CH_3), 1.53(3H,s CH_3), 2.10-2.63(3H, CH_2, OH), 3.00-3.24(3H,m, CH_2, CH), 3.32(3H, s, OCH_3), 3.57-3.86(3H, m, 3xCH), 3.97-4.31(3H, m, 3xCH), 4.50-4.98(4H, m, 4xCH), 6.88-7.56(20H, m, aromatic protons); ^{13}C NMR($CDCl_3$) δ: 24.07(q), 25.92(q), 34.06(t), 51.80(t), 55.75 (q), 60.57(t), 61.16(t), 63.59(d), 67.93(d), 76.36(d), 81.48(d), 82.26(d), 87.28(s), 96.53(t), 110.96(s), 126.41, 126.99, and 127.22, 128.06, and 128.59(aromatic carbons), 138.88(d), 143.41(s). HRMS *m/z* (M^+) calcd for $C_{39}H_{45}NO_6$ 623.3247, found 623.3268. **1b**: oil, $[\alpha]_D^{20}$ +4.7° (c=0.5, H_2O); ^1H NMR(D_2O) δ: 1.83(1H,m), 2.18(1H,m), 2.81(2H, m), 3.21(1H, m), 3.34(1H,m), 3.61(1H,dd), 3.78 (1H, m), 3.88(1H, m), 4.16(1H, m), 4.53(1H, m); ^{13}C NMR(D_2O, dioxane δ=67.40) δ: 35.29(t), 53.81 (t), 62.97(t), 69.30(d), 70.81(d), 70.91(d), 73.34(d), 74.90(d). HRMS (FAB): *m/z* $(M+H)^+$ calcd for $C_8H_{16}NO_4$ 190.1080, found 190.1086. **24**: mp 118-119°C ; $[\alpha]_D^{20}$ -43.5° (c=0.7, $CHCl_3$); IR ν max (nujol) 1697, 1165, 1029, 760, 708 cm^{-1}; ^1H NMR($CDCl_3$) δ:1.31(3H, s, CH_3), 1.35(9H, s,*t*-Bu), 1.44(3H, s, CH_3), 2.05-2.48(2H, m, 2xCH), 2.65-2.90(1H, m, CH), 3.02(3H, s, OCH_3), 3.15-3.50(1H, m, CH), 3.50-3.90(2H, m, 2xCH), 3.90-4.19(2H,m, 2xCH), 4.20-4.65(3H, m, 3xCH), 4.90-5.20(2H, m, CH=CH_2), 5.45-5.95(1H, m, CH=CH_2), 7.14-7.53(15H, m, aromatic protons); ^{13}C NMR($CDCl_3$) δ: 25.58(q), 27.39(q), 28.31(q), 36.69(t), 55.21(q), 63.06(t), 63.93(d), 67.35(d), 76.41(d), 78.94(d), 79.91(s), 82.40(d), 86.45(s), 96.19(t), 111.45(s), 117.68(t), 126.84, 127.72, and 128.50, (aromatic carbons), 133.72 (d), 143.95(s), 154.18(s). *Anal.* Calcd for $C_{38}H_{47}NO_7$: C, 72.47 ; H, 7.52; N, 2.22 , Found: C,72.53 ; H,7.68 ; N, 2.01. **27**: oil, $[\alpha]_D^{20}$ -30.1° (c=1.1, $CHCl_3$); IR ν max (film) 1691, 1165, 1036, 758, 706 cm^{-1}; ^1H NMR($CDCl_3$) δ:1.29(3H, s, CH_3), 1.41(9H,s CH_3), 1.46(3H, s, CH_3), 1.78-2.28(2H, m, 2xCH), 2.88-3.13(1H, m, CH), 3.10(3H, s, OCH_3), 3.18-3.85(2H, m, 2xCH), 4.00-4.65(6H,m, CH2, 4xCH), 4.85-5.10(2H, m, CH=CH_2), 5.49-6.05(1H, m, CH=CH_2), 7.14-7.53(15H, m, aromatic protons); ^{13}C NMR($CDCl_3$) δ: 25.49(q), 27.39(q), 28.21(q), 35.18(t), 55.65(q), 63.01(t), 66.03(d), 66.42(d), 77.681(d), 79.82(d), 82.30(s), 83.52(d), 86.20(s), 95.22(t), 111.11(s), 116.86(t), 126.70., 127.58, and 128.55, (aromatic carbons), 134.59(d), 143.90(s), 155.30(s). HRMS : *m/z* (M^+) calcd for $C_{38}H_{47}NO_7$, 629.3353, found 629.3268. **25**: oil, $[\alpha]_D^{20}$ -24.2° (c=0.5, $CHCl_3$); IR ν max (film) 1446, 1377, 1215, 1036, 756, 704 cm^{-1}; ^1H NMR($CDCl_3$) δ:1.39(3H, s, CH_3), 1.56(3H, s, CH_3), 2.28-2.56(2H, m, 2xCH), 2.90-3.67(5H, m, CH_2, 3xCH), 3.34(3H, s, OCH_3), 3.80-4.20(2H,m, 2xCH), , 4.40-4.60(2H, m, 2xCH), 4.60-4.80 (2H,m, 2xCH), 5.00-5.30(2H, m, 2xCH), 5.52-5.69(1H, m, CH=CH_2), 7.13-7.61(20H, m, aromatic protons); ^{13}C NMR($CDCl_3$) δ: 25.58(q), 27.78(q), 37.13(t), 55.41(q), 58.48(t), 65.30(t), 68.17(d), 71.63 (d), 76.65(d), 80.66(d), 82.60(d), 86.50(s), 96.88(t), 111,50(s), 117.15(t), 126.75, 127.57, 128.55, 128.01, 128.54, and 129.33(aromatic carbons), 134.74(d), 138.20(s), 143.90(s). HRMS : *m/z* (M^+) calcd for $C_{40}H_{45}NO_5$, 619.3298, found 619.3308. **28**: oil, $[\alpha]_D^{20}$ +12.8° (c=0.9, $CHCl_3$); IR ν max (film) 1446, 1375, 1215, 1035, 758, 704 cm^{-1}; ^1H NMR($CDCl_3$) δ:1.12(3H, s, CH3), 1.29(3H,s CH_3), 1.70-2.52(2H, m, 2xCH), 2.65-3.25(5H, m, CH_2, 3xCH), 3.11(3H, s, OCH_3), 3.60 and 3.82(2H, AB *J*=13.5 Hz, CH_2Ph), 4.05-4.50(4H, m, CH_2, 2xCH), 4.50-5.00(2H,m, CH=CH_2), 5.20-5.70(1H, m, CH=CH_2), 6.83-7.43(20H, m, aromatic protons); ^{13}C NMR($CDCl_3$) δ: 25.54(q), 27.78(q), 34.45(t), 55.36(q), 59.16 (t), 64.66(t), 60.24(d), 70.71(d), 77.92(d), 81.87(d), 82.21(d), 86.49(s), 96.14(t), 111,50(s), 116.37(t), 126.70, 126.89, 127.53, 127.96, 128.54, and 129.13(aromatic carbons), 135.71(d), 138.68(s), 143.90(s). HRMS : *m/z* (M^+)

CH=CH_2), 6.90-7.63(15H, m, aromatic protons); ^{13}C NMR($CDCl_3$) δ: 24.41(q), 25.19(q), 28.21(q), 36.74 (t), 55.11(q), 62.62(d), 64.86(d), 76.31(d), 79.48(d), 81.33(d), 86.88(s), 97.22(t), 110.06(s), 116.17(t), 126.89, 127.67, and 128.31, (aromatic carbons), 135.81(d), 143.36(s), 154.18(s). HRMS *m/z* (M^+) calcd for $C_{38}H_{47}NO_7$ 629.3353, found 629.3362. **21**:oil, $[\alpha]_D^{20}$ -55.9° (c=1.3, $CHCl_3$); IR ν max (film) 1488, 1215, 1153, 1038, 756, 704 cm^{-1}; ^{1}H NMR($CDCl_3$) δ: 1.31(3H, s, CH_3), 1.55(3H, s, CH_3), 1.90-2.56(2H, m, 2xCH), 2.72-3.30(5H,m, 3xCH, CH_2OTr), 3.30(3H, s, OCH_3), 3.60-4.20(2H, m, 2xCH), 4.50-5.20 (6H, m, 2xCH_2, 2xCH), 5.68-6.17(1H, m, CH=C, 6.84-7.72(20H, m, aromatic protons); ^{13}C NMR($CDCl_3$) δ: 24.12(q), 25.88(q), 36.45(t), 51.75(t), 55.51(q), 61.11(t), 63.40(d), 68.17(d), 77.92(d), 81.33(d), 82.30 (d), 87.23(s), 96.53(t), 110.26(s), 115.88(t), 126.26, 126.94, and 127.72, 128.01, 128.60(aromatic carbons), 137.17(d), 139.12(s), 143.41(s). HRMS *m/z* (M^+) calcd for $C_{40}H_{45}NO_5$ 619.3298, found 619.3290. **22b**: oil, $[\alpha]_D^{20}$ -70.5° (c=0.5, $CHCl_3$); IR ν max (film) 3440, 1450, 1377, 1215, 1032, 756, 704 cm^{-1}; ^{1}H NMR($CDCl_3$) δ: 1.29(3H, s, CH_3), 1.53(3H,s CH_3), 2.10-2.63(3H, CH_2, OH), 3.00-3.24(3H,m, CH_2, CH), 3.32(3H, s, OCH_3), 3.57-3.86(3H, m, 3xCH), 3.97-4.31(3H, m, 3xCH), 4.50-4.98(4H, m, 4xCH), 6.88-7.56(20H, m, aromatic protons); ^{13}C NMR($CDCl_3$) δ: 24.07(q), 25.92(q), 34.06(t), 51.80(t), 55.75 (q), 60.57(t), 61.16(t), 63.59(d), 67.93(d), 76.36(d), 81.48(d), 82.26(d), 87.28(s), 96.53(t), 110.96(s), 126.41, 126.99, and 127.22, 128.06, and 128.59(aromatic carbons), 138.88(d), 143.41(s). HRMS *m/z* (M^+) calcd for $C_{39}H_{45}NO_6$ 623.3247, found 623.3268. **1b**: oil, $[\alpha]_D^{20}$ +4.7° (c=0.5, H_2O); ^{1}H NMR(D_2O) δ: 1.83(1H,m), 2.18(1H,m), 2.81(2H, m), 3.21(1H, m), 3.34(1H,m), 3.61(1H,dd), 3.78 (1H, m), 3.88(1H, m), 4.16(1H, m), 4.53(1H, m); ^{13}C NMR(D_2O, dioxane δ=67.40) δ: 35.29(t), 53.81 (t), 62.97(t), 69.30(d), 70.81(d), 70.91(d), 73.34(d), 74.90(d). HRMS (FAB): *m/z* $(M+H)^+$ calcd for $C_8H_{16}NO_4$ 190.1080, found 190.1086. **24**: mp 118-119°C ; $[\alpha]_D^{20}$ -43.5° (c=0.7, $CHCl_3$); IR ν max (nujol) 1697, 1165, 1029, 760, 708 cm^{-1}; ^{1}H NM CDCl3) δ:1.31(3H, s, CH_3), 1.35(9H, s,*t*-Bu), 1.44(3H, s, CH_3), 2.05-2.48(2H, m, 2xCH), 2.65-2.90(1H, m, CH), 3.02(3H, s, OCH_3), 3.15-3.50(1H, m, CH), 3.50-3.90(2H, m, 2xCH), 3.90-4.19(2H,m, 2xCH), 4.20-4.65(3H, m, 3xCH), 4.90-5.20(2H, m, CH=CH_2), 5.45-5.95(1H, m, CH=CH_2), 7.14-7.53(15H, m, aromatic protons); ^{13}C NMR($CDCl_3$) δ: 25.58(q), 27.39(q), 28.31(q), 36.69(t), 55.21(q), 63.06(t), 63.93(d), 67.35(d), 76.41(d), 78.94(d), 79.91(s), 82.40(d), 86.45(s), 96.19(t), 111.45(s), 117.68(t), 126.84, 127.72, and 128.50, (aromatic carbons), 133.72 (d), 143.95(s), 154.18(s). *Anal.* Calcd for $C_{38}H_{47}NO_7$: C, 72.47 ; H, 7.52; N, 2.22 , Found: C,72.53 ; H,7.68 ; N, 2.01. **27**: oil, $[\alpha]_D^{20}$ -30.1° (c=1.1, $CHCl_3$); IR ν max (film) 1691, 1165, 1036, 758, 706 cm^{-1}; ^{1}H NMR($CDCl_3$) δ:1.29(3H, s, CH_3), 1.41(9H,s CH_3), 1.46(3H, s, CH_3), 1.78-2.28(2H, m, 2xCH), 2.88-3.13(1H, m, CH), 3.10(3H, s, OCH_3), 3.18-3.85(2H, m, 2xCH), 4.00-4.65(6H,m, CH2, 4xCH), 4.85-5.10(2H, m, CH=CH_2), 5.49-6.05(1H, m, CH=CH_2), 7.14-7.53(15H, m, aromatic protons); ^{13}C NMR($CDCl_3$) δ: 25.49(q), 27.39(q), 28.21(q), 35.18(t), 55.65(q), 63.01(t), 66.03(d), 66.42(d), 77.681(d), 79.82(d), 82.30(s), 83.52(d), 86.20(s), 95.22(t), 111.11(s), 116.86(t), 126.70., 127.58, and 128.55, (aromatic carbons), 134.59(d), 143.90(s), 155.30(s). HRMS : *m/z* (M^+) calcd for $C_{38}H_{47}NO_7$, 629.3353, found 629.3268. **25**: oil, $[\alpha]_D^{20}$ -24.2° (c=0.5, $CHCl_3$); IR ν max (film) 1446, 1377, 1215, 1036, 756, 704 cm^{-1}; ^{1}H NMR($CDCl_3$) δ:1.39(3H, s, CH_3), 1.56(3H, s, CH_3), 2.28-2.56(2H, m, 2xCH), 2.90-3.67(5H, m, CH_2, 3xCH), 3.34(3H, s, OCH_3), 3.80-4.20(2H,m, 2xCH), , 4.40-4.60(2H, m, 2xCH), 4.60-4.80 (2H,m, 2xCH), 5.00-5.30(2H, m, 2xCH), 5.52-5.69(1H, m, CH=CH_2), 7.13-7.61(20H, m, aromatic protons); ^{13}C NMR($CDCl_3$) δ: 25.58(q), 27.78(q), 37.13(t), 55.41(q), 58.48(t), 65.30(t), 68.17(d), 71.63 (d), 76.65(d), 80.66(d), 82.60(d), 86.50(s), 96.88(t), 111,50(s), 117.15(t), 126.75, 127.57, 128.55, 128.01, 128.54, and 129.33(aromatic carbons), 134.74(d), 138.20(s), 143.90(s). HRMS : *m/z* (M^+) calcd for $C_{40}H_{45}NO_5$, 619.3298, found 619.3308. **28**: oil, $[\alpha]_D^{20}$ +12.8° (c=0.9, $CHCl_3$); IR ν max (film) 1446, 1375, 1215, 1035, 758, 704 cm^{-1}; ^{1}H NMR($CDCl_3$) δ:1.12(3H, s, CH3), 1.29(3H,s CH_3), 1.70-2.52(2H, m, 2xCH), 2.65-3.25(5H, m, CH_2, 3xCH), 3.11(3H, s, OCH_3), 3.60 and 3.82(2H, AB *J*=13.5 Hz, CH_2Ph), 4.05-4.50(4H, m, CH_2, 2xCH), 4.50-5.00(2H,m, CH=CH_2), 5.20-5.70(1H, m, CH=CH_2), 6.83-7.43(20H, m, aromatic protons); ^{13}C NMR($CDCl_3$) δ: 25.54(q), 27.78(q), 34.45(t), 55.36(q), 59.16 (t), 64.66(t), 60.24(d), 70.71(d), 77.92(d), 81.87(d), 82.21(d), 86.49(s), 96.14(t), 111,50(s), 116.37(t), 126.70, 126.89, 127.53, 127.96, 128.54, and 129.13(aromatic carbons), 135.71(d), 138.68(s), 143.90(s). HRMS : *m/z* (M^+)

calcd for $C_{40}H_{45}NO_5$, 619.3298, found 619.3334. **29a**: oil, $[\alpha]_D^{20}$ -37.9° (c=1.1, $CHCl_3$); IR ν max (film) 3380, 1446,1379, 1217, 1072, 1033, 756, 704 cm^{-1}; ^1H NMR($CDCl_3$) δ:1.36(3H, s, CH_3), 1.42 (3H,s, CH_3), 1.50-1.75(2H, m, CH_2), 2.63(1H, br s, OH), 2.81-3.04(2H,m, 2xCH), 3.04-3.45(2H, m, 2xCH), 3.25(3H, s, OCH_3), 3.45-3.78(2H, m, 2xCH), 3.80-3.96(2H, m, CH_2), 4.22-4.70(5H, m, 5xCH), 7.04-7.52(20H, m, aromatic protons); ^{13}C NMR($CDCl_3$) δ:25.53(q), 27.73(q), 34.89(t), 55.65(t), 58.18(t), 59.01(t), 65.01(t), 68.07(d), 72.90(d), 79.77(d), 82.21(d), 86.55(s), 97.99(t), 116.69(s), 126.80, 127.09, 127.58, 128.55,and 129.33 (aromatic carbons), 137.81(d), 143.85(s). HRMS : *m/z* (M^+) calcd for $C_{39}H_{45}NO_6$ 623.3247, found 623.3262. **29b**: oil, $[\alpha]_D^{20}$ +11.9° (c=0.4, $CHCl_3$); IR ν max (film) 3373, 1450, 1377,1217, 1070, 1034, 757, 704 cm^{-1}; ^1H NMR($CDCl_3$) δ:1.24(3H, s, CH_3), 1.38(3H, s, CH_3), 1.60(1H, br s, OH), 1.75-1.90(1H, m, CH), 3.00-3.13(3H,m, 3xCH), 3.18-3.30(3H, m, 3xCH), 3.23(3H, s, OCH_3), 3.40-3.50(2H, m, 2xCH), 3.60-4.00(2H, m, CH_2), 4.26-4.42(4H, m, 4xCH), 7.11-7.41(20H, m, aromatic protons); ^{13}C NMR($CDCl_3$) δ:25.66(q), 27.86(q), 32.91(t), 55.68(q), 60.36(t), 64.71(t), 69.25(d), 70.65(d), 76.97(d), 80.26(d), 81.65(d), 86.30(s), 96.41(t), 111.95(s), 126.95, 127.34, 127.74, 128.22, 128.30, 128.72, and 129.59 (aromatic carbons), 138.15(s), 143.98(s). HRMS : *m/z* (M^+) calcd for $C_{39}H_{45}NO_6$ 623.3247, found 623.3257. **1-Epialexine (30a)**: oil, $[\alpha]_D^{20}$ +34.8° (c=0.5, H_2O); IR ν max (film) 3332, 1674, 1631, 1597, 1342, 1099, 1042 cm^{-1}; ^1H NMR(D_2O) δ:1.67(1H, m), 2.06(1H,m), 2.75-3.03(2H,m), 3.09-3.40(2H,m), 3.55-3.90(3H,m), 3.90-4.20(2H, m); ^{13}C NMR(D_2O, dioxane δ= 67.40) δ 34.11(t), 46.02(t), 59.35(t), 65.54(d), 71.49(d), 73.97(d), 74.56(d), 76.95(d), HRMS (FAB): *m/z* $(M+H)^+$ calcd for $C_8H_{16}NO_4$ 190.1080, found 190.1085. **1,7-diepialexine (30b)**: oil, $[\alpha]_D^{20}$ +37.0° (c=0.7, H_2O); IR ν max (film) 3346, 1670, 1632, 1597, 1319, 1092, 1036 cm^{-1}; ^1H NMR($CDCl_3$) δ:1.89(2H, m), 3.15(2H,m), 3.38(1H,m), 3.69(1H,m), 3.72-3.94(3H,m), 4.17(1H, m), 4.41(1H,m); ^{13}C NMR(D_2O, dioxane δ=67.40) δ 35.05(t), 46.36(t), 58.99(t), 64.16(d), 69.68(d), 70.14(d), 72.28(d), 76.36(d), HRMS (FAB): *m/z* $(M+H)^+$ calcd for $C_8H_{16}NO_4$ 190.1080, found 190.1089.

Acknowledgment : We are grateful to Professor K. Koga (University of Tokyo) and Professor A. Nakagawa (Chiba University) for spectral measurements. Partial financial supports by a Grant-in-Aid for Scientific Research (No. 07672307) from Ministry of Education, Science, Sports and Culture, Japan, and a grant from the Japan Research Foundation for Optically Active Compounds are gratefully acknowledged. This study was performed through Special Coordination Funds of the Science and Technology Agency of the Japanese Government.

References and Notes

1. a) Nash, R. J.; Fellows, L. E.; Dring, J. V.; Fleet, G. W. J.; Derome, A. E.; Hamor, T. A.; Scofield, A. M; Watkin, D. J. *Tetrahedron Lett.* **1988**, 29, 2487-2490; b) Nash, R.J.; Fellows, L.E.; Plant, A. C.; Fleet, G. W. J.; Derome, A. E.; Baird, P.D.; Hegarty, M. P.; Scofield, A.M.,*Tetrahedron* **1988**, 44, 5959-5964; c) Harris, C. M.; Harris, T. M.; Molyneux, R. J.; Tropea, J. E.; Elbein, A. D. *Tetrahedron Lett.* **1989**, 30, 5685-5688; d) Nash, R. J.; Fellows, L. F.; Dring, J. V. ; Fleet, G. W. J.; Grigdhar, A.; Ramsden, N. G.; Peach, J. M.; Hegarty, M. P.; Scofield, A. M. *Phytochemistry* **1990**, 29, 111-114; e) Winchester, B; Daher, S. A.; Carpenter, N. C.; Bello, I. C. ; Choi, S. S.; Fairbanks, A. J.; Fleet, G. W. J., *Biochem. J.* **1993**, 290,.743-749; e) Scofield, A. M.; Witham, P.; Nash, R. J.; Kite, G. C.; Fellows, L. E. *Comp. Biochem. Physiol, A: Physiol* . **1995**, 112A, 187-196.
2. Some representative syntheses ; a) Fleet, G. W. J.; Haraldsson, M. ; Nash, R. J.; Fellows, L. E. *Tetrahedron Lett.* **1988**, 29, 5441-5444 ; b) Peason, W.H.; Hines, J. V. *Tetrahedron Lett.*, **1991**, 32, 5513-5516; c) Choi. S.; Bruce, I.; Fairbanks, A. J.; Fleet, G. W. J.; Jones, A. H.; Nash, R. J.; Fellows, L. E. *Tetrahedron Lett.* **1991**, 32, 5517-5520 ; d) Funeaux, R. H.; Gainsford, G. J.; Mason, J. M.; Tyler, P.C. *Tetrahedron* **1994**, 50, 2131-2160.
3. a) Ikota, N. ; Hanaki, A. *Chem. Pharm. Bull.* **1987**, 35, 2140-2143 ; b) Ikota, N. ; Hanaki, A. *Heterocycles* **987**, 26, 2369-2370; c) Ikota, N.; Hanaki, A. *Chem. Pharm. Bull.* **1989**, 37, 1087-1089 ; d) Ikota, N. *Chem. Pharm. Bull.* **1990**, 38, 2712-2718 ; e) Ikota, N. *Heterocycles* **1993**,

36, 2035-2050 ; f) Ikota, N., *Heterocycles* **1995**, 41, 983, g) Ikota, N. ; Hama-Inaba, H. *Chem. Pharm. Bull.* **1996**, 44, 587-589; h) Ikota, N.; Hirano, J.; Gamaga, R.; Nakagawa, H.; Hama-Inaba, H. *Heterocycles* **1997**, 46, 637-643.

4. Preliminary communication, Ikota, N., *Tetrahedron Lett.* **1992**, 33, 2553-2556.
5. Ohta, T.; Hosoi, A.; Kimura, T.; Nozoe, S. *Chem. Lett.* **1987**, 2091-2094.
6. Luche, J. C.; Hahn, L. R.; Crabbe, P. *J. Chem. Soc., Chem. Commun.* **1978**, 601602.
7. We have described the pyrrolidine **15b** was obtained as a sole product in this conversion.[4] However, the repeated experiments revealed that the diastereomeric mixture (ratio about 2-2.5:1=**15b**: **15a**) was always formed.
8. Mancus, A. J.; Huang, S. L.; Swern, D. *J. Org. Chem.* **1978**, 43, 2480-2482.
9. Hamana, H.; Ikota, N.; Ganem, B. *J. Org. Chem.* **1987**, 52, 5492-5493.
10. Oxidation of **16** by the method of Swern gave a ketone which on reduction with sodium borohydride in EtOH at -78°C resulted in the formation of **16** and **19** in 1:1.2 ratio.
11. Ireland, R.E.; Norbeck, D.W. *J. Org.Chem.* **1985**, 50, 2198-2200.
12. X-ray analysis of **24** : $C_{38}H_{47}N0_7$, Mr = 629.8 g mol^{-1}, colourless crystals, crystal size 0.20 x 0.10 x 0.60 mm, a =9.232(3), b =22.944(2), c =9.292(2) Å, β=114.16(2)°, V=1795.8 $Å^3$, T=300 K, dcal=1.165 g cm^{-3}, μ = 0.8 cm^{-1}, Z = 2, monoclinic, space group $P2_1$ (No. 4), Rigaku AFC-5R diffractometer, λ=0.71069 Å, scan mode ω–2θ, 5673 measured reflections (+h, +k, ±1) $[(\sin\theta)/\lambda]_{max}$ = 0.70 $Å^{-1}$, 5382 independent reflections, 3417 observed reflections [$I \geq 3\sigma(I)$], structure solved by direct methods (SHELXS-86, Sheldrick, G. M. Acta Cryst. **1990**, A46, 467-473), final refinement by least-squares (SHELXL-93, Sheldrick, G. M. Program for Crystal Structure Refinement, Univ. of Goettingen, Gernany, 1993), all the H atoms were located geometrically calculated position and refined using a dreiding model, C1 and C2 carbon atoms are disordered over two site, R = 0.055 (based on F), Rw = 0.166 (based on F^2) for 413 refined parameters and 8 restraints [$w = 1/\{\sigma^2(Fo^2) + (0.0727 * P)^2 + 0.28 * P\}$, $P = \{\max(Fo^2, 0) + 2 * Fc^2\}/3$], residual electron density 0.22 e $Å^{-3}$. Atomic coordinates and e.s.d's have been deposite at the Cambridge Crystallographic Data Centre.
13. Sakaitani, M.; Ohfune, Y. *Tetrahedron Lett.* **1985**, 26, 5543-5546.
14. Seyferth, D.; Weiner, M. A. *J. Org. Chem.* **1961**, 26, 4797-4800.

ANTIOXIDANTS & REDOX SIGNALING
Volume 1, Number 2, 1999
Mary Ann Liebert, Inc.

Short Communication

Endogenous and New Synthetic Antioxidants for Peroxynitrite: Selective Inhibitory Effect of 5-Methoxytryptamine and Lipoic Acid on Tyrosine Nitration by Peroxynitrite

HIDEHIKO NAKAGAWA,[1] ERIKA SUMIKI,[2] NOBUO IKOTA,[1]
YOSHIKAZU MATSUSHIMA,[2] and TOSHIHIKO OZAWA[1]

ABSTRACT

The inhibitory effects of endogenous and synthetic compounds on the nitration and oxidation of L-tyrosine by peroxynitrite were examined. Nitration and oxidation activities of L-tyrosine by peroxynitrite were estimated by monitoring the formation of 3-nitrotyrosine and dityrosine with a high-performance liquid chromatography-ultraviolet (HPLC-UV)-fluorescence detector system. Glutathione and synthetic compounds ((2*S*,3*R*,4*S*)-*N*-ethylmercapto-3,4-dihydroxy-2-hydroxymethylpyrrolidine, L-*N*-dithiocarboxyproline) inhibited both the nitration and the oxidation reactions of L-tyrosine effectively. On the other hand, 5-methoxytryptamine and lipoic acid inhibited only the nitration reaction of L-tyrosine, and instead increased the oxidation reaction. It was assumed that 5-methoxytryptamine and lipoic acid reacted only with the nitrating species of peroxynitrite. This is the first report of a selective inhibitor for the nitrating reaction of peroxynitrite. Antiox. Redox Signal. 1, 239–244, 1999.

INTRODUCTION

Peroxynitrite (ONOO-) is formed from nitric oxide (NO) and superoxide *in vivo*. It has been reported to have a high activity for the oxidation of various biological components and for the nitration of free tyrosine and protein tyrosine residues. Because the nitration of tyrosine residues is one of the characteristic reactions of peroxynitrite, the presence of nitrotyrosine in tissues or cell cultures is often used as the marker of the production of peroxynitrite. Peroxynitrite causes various types of oxidative damage, for example, low-density lipoprotein (LDL) oxidation, lipid peroxidation, DNA strand breakage, and so on (White *et al.*, 1994; Darley-Usmar *et al.*, 1992, 1995). Additionally, the nitration of tyrosine is assumed to prevent the phosphorylation of tyrosine residues in the substrate proteins of tyrosine kinase (Gow *et al.*, 1996; Kong *et al.*, 1996). The oxidation and nitration activities of peroxynitrite play the pathological roles in oxidative stress. Various typical antioxidants were reported to have the inhibitory effects on the nitration of the tyrosine (Whiteman *et al.*,

[1]Bioregulation Research Group, National Institute of Radiological Sciences, Chiba 263, Japan.
[2]Kyoritsu College of Pharmacy, Tokyo 115, Japan.

1996a,b). In a few reports, the fluorescent product, which was assumed to be dityrosine as an oxidation product, was formed simultaneously with the nitrotyrosine formation in the reaction of L-tyrosine and peroxynitrite (Van der Vliet *et al.*, 1994). In this study, the formation of nitrotyrosine and dityrosine in the reaction of L-tyrosine and peroxynitrite was confirmed, and then the inhibitory effects of the endogenous compounds and synthesized antioxidants on each of the oxidation and nitration reaction by peroxynitrite were examined.

MATERIALS AND METHODS

Chemicals

L-Tyrosine, 2,4-dihydroxy-DL-phenylalanine, *p*-fluoro-L-phenylalanine, glutathione (reduced form), and *dl*-lipoic acid were purchased from Wako Pure Chemical Ind. (Osaka, Japan). 3-Nitro-L-tyrosine, and 5-methoxytryptamine were from Aldrich (Milwaukee, WI). All reagents used were analytical grade. NEMP ((2*S*,3*R*,4*S*)-*N*-ethylmercapto-3,4-dihydroxy-2-hydroxymethylpyrrolidine) was obtained by hydrolysis of the precursor compound synthesized as described previously (Ikota and Hama-Inaba, 1996). DTCP (L-*N*-dithiocarboxyproline) was synthesized according to Shinobu *et al.* (1984). The structures and purity of synthesized NEMP and DTCP were confirmed by ^{1}H- and ^{13}C-nuclear magnetic resonance (NMR) spectroscopy.

Peroxynitrite preparation

Peroxynitrite was synthesized as alkaline solution according to Whiteman *et al.* (1996b). Briefly, 1 ml of 1 *M* hydrogen peroxide (H_2O_2) was mixed with 1 ml of 1 *M* $NaNO_2$ in the glass tube under the acidic condition on an ice bath, and then rapidly quenched with 2 ml of 1.5 *M* NaOH. The quenched solution was treated with MnO_2 immediately, and then it was slowly frozen with dry-ice/acetone and the top layer of the frozen solution was collected. The concentrated peroxynitrite solution (25–126 m*M*) was obtained. The concentration of the peroxynitrite solution was determined spectrophotometrically from the absorbance at 302 nm (molar absorption coefficient = 1,670 M^{-1} cm^{-1}), and the prepared peroxynitrite solution was stored at −20°C until use. The stock solution was diluted to the desired concentration with 0.01 *N* NaOH after determining the concentration of the stock solution spectrophotometrically. The peroxynitrite solution without MnO_2 treatment was also prepared and used, but the formation of 3-nitro-L-tyrosine, 2,2′-dityrosine, and L-dopa were not significantly affected. H_2O_2 and sodium nitrite did not give any oxidized and nitrated products from L-tyrosine in this system.

Assignment of the dityrosine in the analytical experiment

The authentic sample of 2,2′-dityrosine was prepared from L-tyrosine and hydrogen peroxide in the presence of horseradish peroxidase at pH 9.5 at 37°C according to Gross and Sizer. (1959) and Nomura *et al.* (1990) with a slight modification. The reaction product was analyzed using HPLC with fluorescence detector, and the main product was confirmed as 2,2′-dityrosine by comparing its excitation and emission spectra (λmax; ex 295 nm and em 410 nm) with the reported ones in the literature (Lehrer and Fasman, 1967).

Reaction of peroxynitrite with L-tyrosine and analytical conditions

To the L-tyrosine (final concentration, 0–2 mM) solution in 0.1 *M* sodium phosphate buffer, pH 7.4, peroxynitrite (final concentration, 0–8 m*M*) was added at 37°C. After 10 min of incubation, *p*-fluorotyrosine (final concentration, 0.91 m*M*) was added to the reaction mixture as an internal standard, and the aliquot of the mixture was analyzed by the high-performance liquid chromatography ultraviolet (HPLC-UV)-fluorescence detector system. The HPLC conditions were as follows: column, TSK-GEL ODS 80-Ts 4.6 × 150 mm (TOSOH Corp., Tokyo, Japan); eluent, 0.1 *M* potassium phosphate, pH 3.5; flow rate, 1.0 ml/min; detection, absorbance at 274 nm and fluorescence at 410 nm (ex 295 nm). The 3-nitro-L-tyrosine produced was quantified with the standard curve. The reaction of peroxynitrite and L-tyrosine was also carried out at pH 9.5 and pH 11.5 as same manner.

Effects of various compounds on nitrotyrosine and dityrosine formation

In the presence of various concentrations of testing compounds, L-tyrosine (1 m*M*) was incubated with peroxynitrite (0.2 m*M*) at 37°C for 10 min in neutral buffer solution, pH 7.4. After addition of fluorotyrosine as an internal standard, the formation of 3-nitro-L-tyrosine and 2,2'-dityrosine were estimated, and the IC_{50} value of each testing compound was determined both for 3-nitro-L-tyrosine and for 2,2'-dityrosine formation. The amount of 3-nitro-L-tyrosine formed was determined with the standard curve. The fluorescent product formation was represented as the percent for the fluorescence intensity in the control experiment.

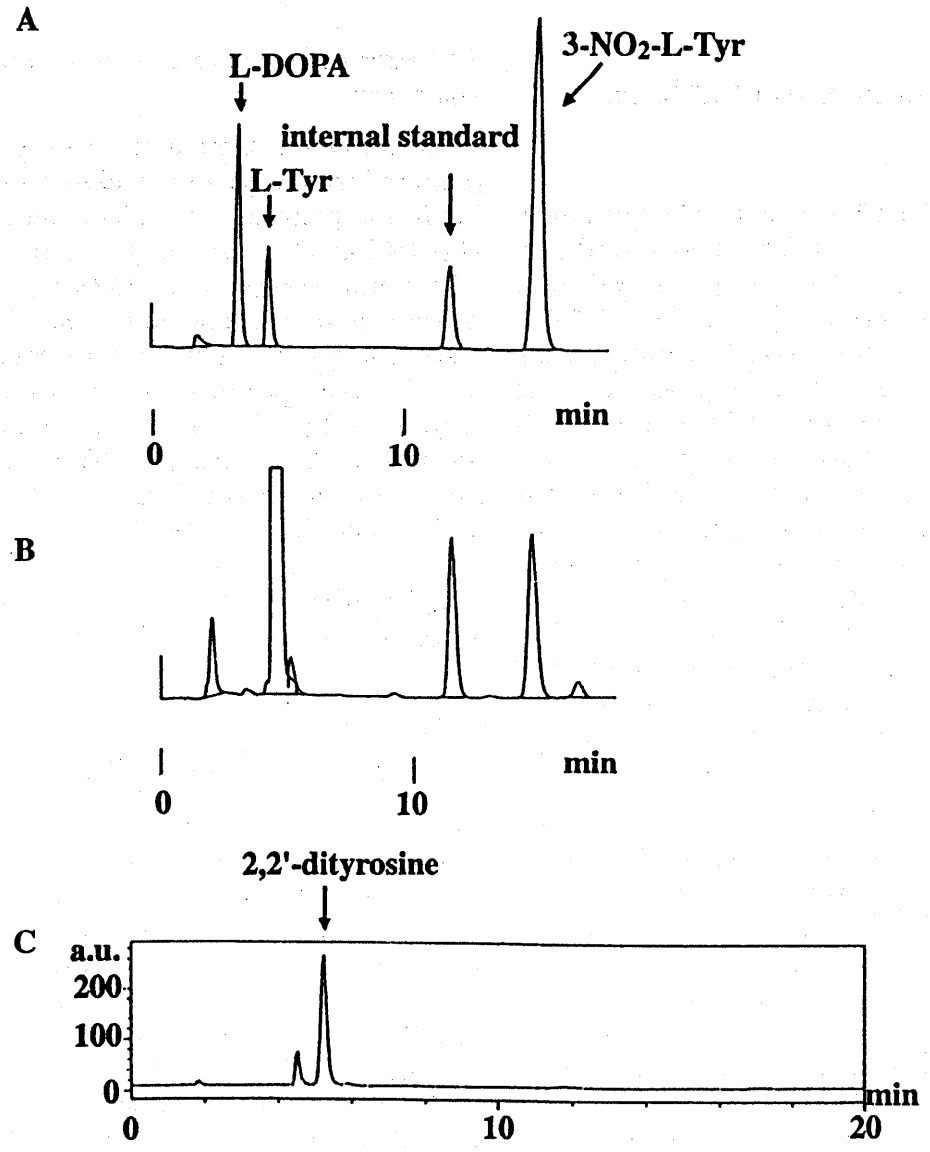

FIG. 1. HPLC charts of the authentic and reaction products. A. The authentic mixture of L-dopa, L-tyrosine (L-Tyr), *p*-fluoro-L-tyrosine (internal standard), and 3-nitro-L-tyrosine (3-NO_2-L-Tyr); output from UV (274 nm) detector. **B.** The reaction mixture of 1 m*M* L-tyrosine and 0.2 m*M* peroxynitrite; output from UV (274 nm). **C.** The reaction mixture monitored by fluorescence detector (ex 295 nm, em 410 nm). The HPLC condition was as described in Materials and Methods.

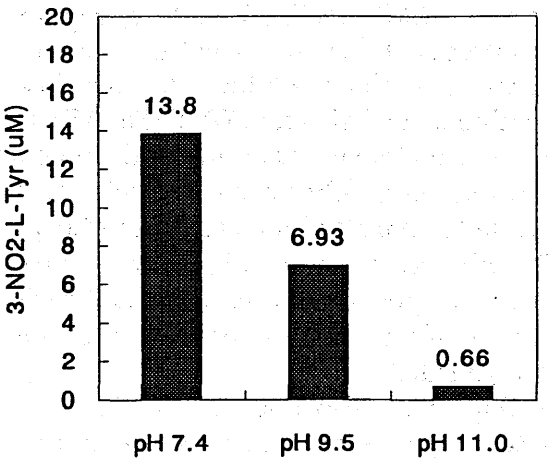

FIG. 2. 3-Nitro-L-tyrosine formation by peroxynitrite with L-tyrosine at different pH. In the phosphate buffer (pH 7.4–11.0), L-tyrosine (1 mM) was treated with peroxynitrite (0.2 mM) as described in Materials and Methods. The amount of 3-nitro-L-tyrosine formed for the 10 min reaction was determined by HPLC with the standard curve.

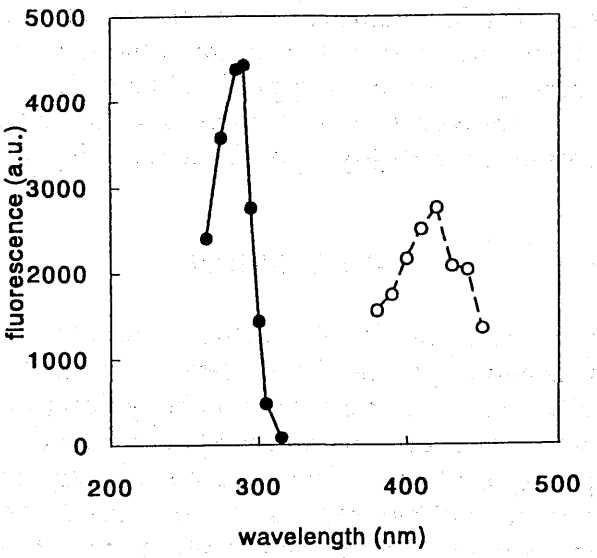

FIG. 3. Excitation and fluorescence spectra of the fluorescent product from the reaction of L-tyrosine and peroxynitrite. (●) excitation spectra monitored at 410 nm fluorescence; (○) fluorescence spectra excited by 295 nm light.

RESULTS

Reaction of peroxynitrite with L-tyrosine

The reaction products of peroxynitrite with L-tyrosine were analyzed by HPLC and a tandemly jointed UV-fluorescence detector system. In the reaction of peroxynitrite and L-tyrosine, it was confirmed that 3-nitrotyrosine was detected as a major product, as reported (Van der Vliet *et al.*, 1994) (Fig. 1). The formation of 3-nitro-L-tyrosine was dependent on the concentration of both of L-tyrosine and peroxynitrite, and was suppressed under higher pH conditions (Fig. 2). These results suggest that 3-nitrotyrosine was a reaction product of L-tyrosine and a protonated form of peroxynitrite (peroxynitrous acid) rather than an anion form. It was also confirmed that a fluorescent product was formed (Van der Vliet *et al.*, 1994), which was assigned as 2,2′-dityrosine by comparing its retention time and fluorescence spectra (Fig. 3) with the authentic sample prepared as described in Materials and Methods.

Effects of synthetic and endogenous compounds on the nitration and oxidation reaction by peroxynitrite

Inhibitory effects of synthetic compounds and endogenous compounds on the reaction of peroxynitrite with L-tyrosine were examined. In the presence of 5-methoxytryptamine (1 in Fig. 4) and *dl*-lipoic acid (2), it was shown that the formation of 2,2′-dityrosine was not inhibited, but rather increased, and 3-nitrotyrosine was significantly inhibited. Glutathione, a typical antioxidant, inhibited the formation of both 3-nitrotyrosine and 2,2′-dityrosine. The synthetic compounds NEMP (3 in Fig. 4) and DTCP (4 in Fig. 4) also effectively inhibited the formation of 3-nitrotyrosine and 2,2′-dityro-

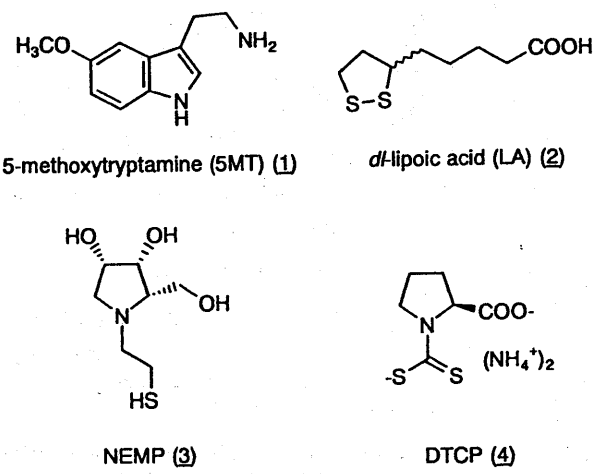

FIG. 4. Structures of endogenous and synthetic compounds used in the inhibitory experiment.

sine. The IC_{50} values of these compounds were almost the same as that of glutathione in this reaction. L-cystine, a typical oxidized form of thiol, showed weak inhibition of the 3-nitrotyrosine and 2,2'-dityrosine formation (Fig. 5).

DISCUSSION

From the results of the reaction of peroxynitrite and L-tyrosine, 3-nitro-L-tyrosine and 2,2'-dityrosine were considered to be typical products of the nitration and oxidation reaction of peroxynitrite with L-tyrosine, respectively. The formation of 3-nitrotyrosine was dependent on the concentration of peroxynitrite and L-tyrosine. In neither case of the treatment of decomposed peroxynitrite nor hydrogen peroxide with L-tyrosine was 3-nitrotyrosine formed.

The formation of 3-nitrotyrosine by peroxynitrite was effectively inhibited by glutathione, NEMP, DTCP, 5-methoxytryptamine, and lipoic acid (Fig. 5A). The formation of 2,2'-dityrosine was also inhibited by low doses of glutathione, NEMP, and DTCP (Fig. 5B). In the case of 5-methoxytryptamine and lipoic acid, however, the 2,2'-dityrosine formation was not inhibited and instead increased at the low dose (Fig. 5B). From this result, 5-methoxytryptamine and lipoic acid were suggested to be selective inhibitors for the tyrosine nitration by peroxynitrite.

L-Dopa was also detected in this reaction mixture, but its amount was decreased at a higher concentration of peroxynitrite due to the further oxidation of dopa by peroxynitrite. Actually, the further oxidation product peak of L-dopa by the reaction with peroxynitrite was detected at a retention time of 16–17 min under this condition using the HPLC-electrochemical detector system. The formation of L-dopa was also not affected in the presence of 5-

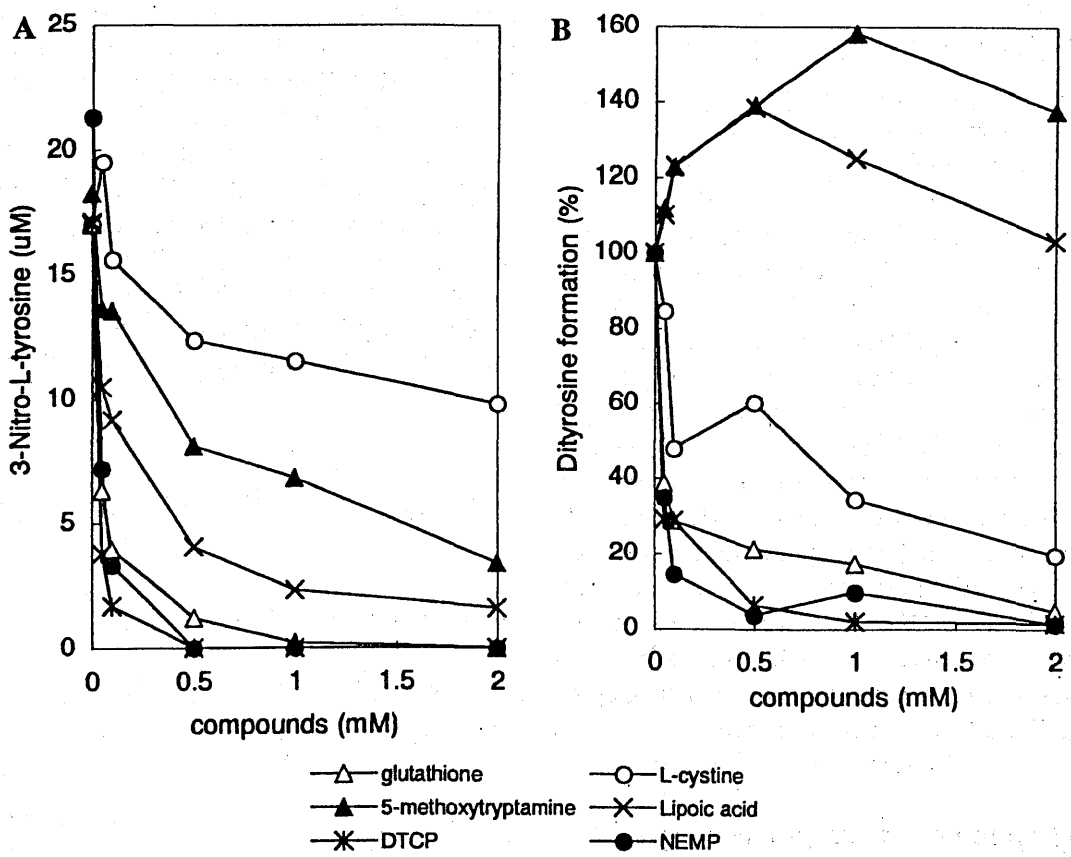

FIG. 5. Formation of 3-nitro-L-tyrosine and 2,2'-dityrosine by L-tyrosine and peroxynitrite reaction in the presence of endogenous and synthetic compounds. L-Tyrosine (1 m*M*) was treated with 0.2 m*M* peroxynitrite, and then the formation of 3-nitro-L-tyrosine and 2,2'-dityrosine was measured as described in Materials and Methods. **A.** 3-Nitro-L-tyrosine formation (μM). **B.** 2,2'-Dityrosine formation as percent for the formation without test compounds.

methoxytryptamine or *dl*-lipoic acid. On the other hand, in the presence of glutathione, NEMP, and DTCP, the formation of L-dopa was first increased and then decreased in a dose-dependent manner, accompanied by the decrease of the further oxidation product of L-dopa. This also suggested that glutathione, NEMP, and DTCP inhibited the oxidation reaction of peroxynitrite and L-tyrosine, but 5-methoxytryptamine or *dl*-lipoic acid did not affect it.

By monitoring the formation of 3-nitro-L-tyrosine and 2,2'-dityrosine simultaneously, it was revealed that 5-methoxytryptamine and *dl*-lipoic acid have a selective inhibitory activity for the nitration reaction of peroxynitrite. This result suggests that the nitration and the oxidation by peroxynitrite may proceed at least partly in the separate way. These reagents are assumed to play potentially important roles against reactive oxygen/nitrogen species (ROS/RNS), and are suggested to be useful tools for investigating ROS/RNS reactions. Further investigation regarding the reaction mechanisms of tyrosine with peroxynitrite and the functional damages and modifications of proteins by peroxynitrite, as well as the protective activity of these compounds found in this study, are now in progress.

ABBREVIATIONS

DTCP, L-*N*-dithiocarboxyproline; H_2O_2, hydrogen peroxide; HPLC-UV, high-performance liquid chromatography-ultraviolet; LDL, low-density lipoprotein; NEMP, (2*S*, 3*R*, 4*S*)-*N*-ethylmercapto-3,4-dihydroxy-2-hydroxymethylpyrrolidine; NMR, nuclear magnetic resonance; NO, nitric oxide; RNS, reactive nitrogen species; ROS, reactive oxygen species.

REFERENCES

DARLEY-USMAR, V.M., HOGG, N., O'LEARY, V.J., WILSON, M.T., and MONCADA, S. (1992). The simultaneous generation of superoxide and nitric oxide can initiate lipid peroxidation in human low density lipoprotein. Free Rad. Res. Commun. **17**, 9–20.

DARLEY-USMAR, V., WISEMAN, H., and HALLIWELL, B. (1995). Nitric oxide and oxygen radicals: A question of balance. FEBS Lett. **369**, 131–135.

GOW, A.J., DURAN, D., MALCOLM, S., and ISCHIROPOULOS, H. (1996). Effects of peroxynitrite-induced protein modifications on tyrosine phosphorylation and degradation, FEBS Lett. **385**, 63–66.

GROSS, A.J., and SIZER, I.W. (1959). The oxidation of tyramine, tyrosine and related compounds by peroxidase. J. Biol. Chem. **234**, 1611–1614.

IKOTA, N., and HAMA-INABA, H. (1996). Chiral pyrrolidine derivatives as catalyst for the enantioselective addition of diethylzinc to aldehydes. Chem. Pharm. Bull. **44**, 587–589.

KONG, S.-K., YIM, M.B., STADTMAN, E.R., and CHOCK, P.B. (1996). Peroxynitrite disables the tyrosine phosphorylation regulatory mechanism: Lymphocyte-specific tyrosine kinase fails to phosphorylate nitrated cdc2(6-20)NH2 peptide. Proc. Natl. Acad. Sci. USA **93**, 3377–3382.

LEHRER, S.S., and FASMAN, G.D. (1967). Ultraviolet irradiation effects in poly-L-tyrosine and model compounds. Identification of bityrosine as photoproduct. Biochemistry **6**, 757–767.

NOMURA, K., SUZUKI, N., and MATSUMOTO, S. (1990). Pulcherosine, a novel tyrosine-derived trivalent cross-linking amino acid from the fertilization envelope of sea urchin embryo. Biochemistry, 29, 4525–4534.

SHINOBU, L.A., JONES, S.G., and JONES, M.M. (1984). Sodium N-methyl-D-glucamine dithiocarbamate and cadmium intoxication. Acta Pharmacol. Toxicol. **54**, 189–194.

VAN DER VLIET, A., O'NEILL, C.A., HALLIWELL, B., CROSS, C.E., and KAUR, H. (1994). Aromatic hydroxyl and nitration of phenylalanine and tyrosine by peroxynitrite. FEBS Lett. **339**, 89–92.

WHITE, C.R., BROCK, T.A., CHANG, L.Y., CRAPO, J., BRISCOE, P., KU, D., BRADLEY, W.A., GIANTURCO, S.H., GORE, J., FREEMAN, B.A., and TARPEY, M.M. (1994). Superoxide and peroxynitrite in atherosclerosis. Proc. Natl. Acad. Sci. USA **91**, 1044–1048.

WHITEMAN, M., and HALLIWELL, B. (1996a). Protection against peroxynitrite-dependent tyrosine nitration and alpha 1-antiproteinase inactivation by ascorbic acid. A comparison with other biological antioxidants. Free Rad. Res. **25**, 275–283.

WHITEMAN, M., TRITSCHLER, H., and HALLIWELL, B. (1996b). Protection against peroxynitrite-dependent tyrosine nitration and alpha 1-antiproteinase inactivation by oxidized and reduced lipoic acid. FEBS Lett. **379**, 74–76.

Address reprint requests to:
Dr. Toshihiko Ozawa
Bioregulation Research Group
National Institute of Radiological Sciences
9-1, Anagawa-4, Inage-ku
Chiba 263, Japan

E-mail: ozawa@nirs.go.jp

Scavengers for Peroxynitrite: Inhibition of Tyrosine Nitration and Oxidation with Tryptamine Derivatives, α-Lipoic Acid and Synthetic Compounds

Hidehiko NAKAGAWA,[a] Erika SUMIKI,[b] Mitsuko TAKUSAGAWA,[a] Nobuo IKOTA,[a] Yoshikazu MATSUSHIMA,[b] and Toshihiko Ozawa*,[a]

Bioregulation Research Group, National Institute of Radiological Sciences,[a] 4–9–1, Anagawa, Inage-ku, Chiba 263–8555 and Kyoritsu College of Pharmacy,[b] 1–5–30, Shibakoen, Minato-ku, Tokyo 105–8512, Japan.
Received August 25, 1999; accepted November 2, 1999

The inhibitory effects of various endogenous and synthetic compounds on the nitration and oxidation of L-tyrosine by peroxynitrite were examined. Nitrating and oxidizing activities were monitored by the formation of 3-nitrotyrosine and dityrosine with a HPLC–UV–fluorescence detector system, respectively. Glutathione, serotonin and synthetic sulfur- and selenium-containing compounds inhibited both the nitration and oxidation reaction of L-tyrosine effectively. However, 5-methoxytryptamine, melatonin and α-lipoic acid only inhibited the nitration reaction, and enhanced the formation of an oxidation product. This is important evidence that there are different intermediates in the nitrating and oxidizing reactions of L-tyrosine by peroxynitrite. It was suggested that 5-methoxytryptamine, melatonin and α-lipoic acid reacted only with the nitrating intermediate of peroxynitrite and inhibited nitration of L-tyrosine. Actually, the DNA strand breakage, which is believed to be a typical reaction of hydroxyl radical-like species, caused by peroxynitrite was not effectively inhibited by 5-methoxytryptamine. 5-Methoxytryptamine, melatonin and α-lipoic acid were viewed as useful reagents for investigating the mechanisms of damage by peroxynitrite *in vitro*.

Key words peroxynitrite; scavenger; melatonin-related compound; 5-methoxytryptamine; nitrotyrosine; synthetic selenium compound

Reactive oxygen species are well-known and important components of oxidative stress in several diseases. Recently, nitric oxide and its oxidized species, called reactive nitrogen species, have been suggested to be involved in the damage caused by oxidative stress. Peroxynitrite (PN) is one of the reactive nitrogen species, and is formed from nitric oxide and superoxide *in vivo*.[1,2] This compound is a highly reactive oxidant and causes nitration on the aromatic ring of free tyrosine and protein tyrosine residues.[3] Since the nitration of tyrosine residues is a characteristic reaction of PN, the presence of nitrotyrosine in tissues or cell cultures is often used as a marker of the production of PN. It was reported that PN induced various oxidative damages, for example, LDL (low density lipoprotein) oxidation, lipid peroxidation, DNA strand breakage and so on.[4—13] Additionally, the nitration of tyrosine is assumed to prevent the phosphorylation of tyrosine residues in the substrate proteins of tyrosine kinase,[14,15] and to affect tyrosine phosphorylation in the cell signal transduction.[16] This would suggest that the oxidizing and nitrating reactions of PN play pathological roles in the oxidative stress. Although Pfeiffer and Mayer[17] reported 3-nitrotyrosine formation by PN produced from nitric oxide and superoxide *in vivo* was below the detection limit of the HPLC method, the scavenging of PN in assays involving tyrosin nitration and oxidation *in vitro* is a useful research tool to provide information on the antioxidant profiles.

The nitration of tyrosine and other aromatic amino acids is one typical reaction of PN, as reported by Van der Vliet *et al.*[13] and the formation of a fluorescent product assumed to be dityrosine, as an oxidation product, was detected in the reaction of L-tyrosine with PN. Various typical antioxidants were reported to have inhibitory effects on the nitration of tyrosine.[18,3] However, the inhibitory effects of typical antioxidants on the oxidation reaction of peroxynitrite have not been evaluated. We have briefly communicated[19] that 5-methoxytryptamine (5MT) and α-lipoic acid (LA) are selective inhibitors for tyrosine nitration by PN, but not for oxidative dityrosine formation. The details of this work and further investigations of PN and its scavengers are described in this paper. The formation of nitrotyrosine and dityrosine in the reaction of L-tyrosine and PN was analyzed simultaneously, and then the inhibitory effect of various endogenous compounds and synthesized antioxidants was examined. A selective inhibitor for the nitration was applied to inhibit the PN-caused DNA strand breakage.

Experimental

Chemicals L-Tyrosine, 3,4-dihydroxy-DL-phenylalanine (DOPA), *p*-fluoro-L-phenylalanine, glutathione (reduced form), serotonin, L-cystine and *dl*-LA were purchased from Wako Pure Chemical Ind. (Osaka, Japan). 3-Nitro-L-tyrosine, 5-MT, melatonin and 2-methyl-2-nitrosopropane (MNP) were from Aldrich (Milwaukee, WI, U.S.A.). 5,5′-Dimethyl-1-pyrroline-*N*-oxide (DMPO) was from LABOTEC Co., Ltd. (Tokyo, Japan). *N-tert*-butyl-α-phenylnitrone (PBN) was from Sigma (St. Louis, MO, U.S.A.). Plasmid pBR322 was purchased from Takara Shuzo Co., Ltd. (Shiga, Japan) and Tris–Borate–EDTA (TBE) buffer was from Gibco BRL (Rockville, MD, U.S.A.). All reagents used were of analytical grade.

Synthesis of Antioxidants (2*S*,3*R*,4*S*)-*N*-ethylmercapto-3,4-dihydroxy-2-hydroxymethylpyrrolidine (NEMP) (4) was obtained by hydrolysis of the precursor compound synthesized as described previously.[20] L-*N*-dithiocarboxyproline (DTCP) (3) was synthesized according to Shinobu *et al.*[21] Briefly, L-proline (1.15 g) was dissolved in 7 ml of concentrated aqueous ammonia solution in an ice bath. Carbon disulfide (1.2 eq) in a small amount of ethanol was added to the L-proline solution at 0—4 °C dropwise. After the reaction mixture had become a homogenous solution, it was lyophilized and yielded pale orange powder (97.6%). The structures and purity of synthesized NEMP and DTCP were confirmed by ^{1}H- and ^{13}C-NMR spectroscopy. DTCP$(NH_4)_2$: ^{1}H-NMR (D_2O) δ: 1.84—1.96 (2H, m), 1.84—2.27 (2H, dm), 3.68—3.85 (2H, m), 4.69—4.73 (1H, m); ^{13}C-NMR (D_2O) δ: 24.20 (t), 31.05 (t), 55.20 (t), 69.00 (d), 179.72 (s), 205.32 (s). NEMP·HCl: ^{1}H-NMR (D_2O) δ: 2.68—2.90 (2H, m, CH_2), 3.13—3.48 (3H, m), 3.48—3.83 (2H, m), 3.85—4.05 (2H, m), 4.35—4.55 (2H, m); ^{13}C-NMR (D_2O) δ: 19.64 (t), 57.01 (t), 58.14 (t), 59.30 (t), 69.78 (d), 70.76 (d); $[\alpha]_D^{20}$ +36.5° (c=0.5,

H_2O)

(2*R*,3*R*,4*S*)-2-amino-3,4-dihydroxy-5-phenylselenopentan-1-ol (ADPP) (**5**) and (2*S*,4*RS*)-2-amino-4-phenylseleno-5-carboxybutan-1-ol (APCB) (**6**) were also synthesized from the corresponding precursors,[22,23] and their structures and purity were confirmed by ^{1}H- and ^{13}C-NMR spectroscopy. ADPP·HCl: mp 137—140 °C: ^{1}H-NMR (D_2O) δ: 2.92—3.16 (2H, m), 3.31—3.46 (1H, m), 3.54—3.67 (1H, m), 3.67—3.82 (2H, m), 3.85—4.00 (1H, m), 7.18—7.35 (3H, m), 7.44—7.59 (2H, m); ^{13}C-NMR (D_2O) δ: 31.18 (t), 56.28 (d), 58.85 (t), 69.72 (d), 70.78 (d), 128.50 (d), 129.50 (s), 130.38 (d), 133.64 (d); $[\alpha]_D^{20}$ +19.4° (*c*=0.3, H_2O). APCB·HCl (1 : 1 mixture): mp 167—170 °C (dec.); ^{1}H-NMR (D_2O) δ: 1.85—2.14 (2H, m), 3.34—3.59 (2H, m), 3.61—3.86 (2H, m), 7.22—7.42 (3H, m), 7.43—7.62 (2H, m); ^{13}C-NMR (D_2O) δ: 31.15 and 31.29 (t), 39.08 and 39.22 (d), 52.15 and 52.42 (d), 61.11 and 61.48 (t), 125.72 (s), 130.35 and 130.40 (d), 130.63 and 130.70 (d), 137.40 and 137.62 (d), 176.26 (s); $[\alpha]_D^{20}$ −14.7° (*c*=0.4, H_2O).

PN Preparation PN was synthesized as an alkaline solution according to Whiteman and Halliwell.[18] Briefly, 1 ml of 1 M H_2O_2 was mixed with 1 ml of 1 M $NaNO_2$ in a glass tube under acidic conditions in an ice bath, and then rapidly quenched with 2 ml of 1.5 M NaOH. The resulting solution was slowly frozen with dry-ice/acetone and the top layer of the frozen solution was collected. A concentrated peroxynitrite solution (25 to 126 mM) was obtained. The concentration of the PN solution was determined photometrically from the absorbance at 302 nm (ε=1670 M^{-1} cm^{-1}), and the prepared PN solution was stored at −20 °C until used. The stock solution was diluted to the desired concentration with 0.01 N NaOH after determining concentration of the solution photometrically, and used for experiments mentioned below. Although unreacted hydrogen peroxide and sodium nitrite were assumed to be present in the prepared PN solution, neither of these residual reagents gave any oxidized or nitrated products in this system.

ESR Spin Trapping of Tyrosyl Radical The production of free radical intermediates during the reaction of PN with L-tyrosine was measured by the ESR-spin trapping method using MNP as a spin trapping reagent. Briefly, to 0.1 M phosphate buffer solution (pH 9.5) containing 1 mM L-tyrosine, 80 mM MNP and 0.2 mM diethylenetriaminepentaacetic acid (DTPA), 100 μl of 20 mM PN solution (2 mM as final concentration) was added. Immediately, ESR spectra of the aliquot were measured at room temperature using a 9.5 GHz ESR spectrometer (FE-2X, JEOL Co., Ltd., Tokyo, Japan). Measurement conditions were as follows: microwave power: 10 mW, microwave frequency: 9.45 GHz, modulation frequency and width: 100 kHz and 0.8 G, response and sweep time: 1.0 s and 16 min/100 G, amp. gain: 2×1000.

Reaction of PN with L-Tyrosine To the L-tyrosine (final 0 to 2 mM) solution in 0.1 M sodium phosphate buffer (pH 7.4), PN (final 0 to 8 mM) was added at 37 °C. After 10 min incubation at 37 °C, *p*-fluorotyrosine (final 0.91 mM) was added to the reaction mixture as an internal standard, then an aliquot of the mixture was analyzed with a HPLC–UV–fluorescence detector system (TOSOH Corp., Tokyo). The HPLC conditions were as follows:column: TSK-GEL ODS 80-Ts 4.6×150 mm (TOSOH Corp.), mobile phase: 0.1 M potassium phosphate (pH 3.5), flow rate: 1.0 ml/min. The produced 3-nitro-L-tyrosine and 2,2′-dityrosine were detected by monitoring the absorbance at 274 nm and the fluorescence at 410 nm (ex. 295 nm), respectively. The detected 3-nitro-L-tyrosine was quantified using a standard curve. The formation of dityrosine was confirmed by comparing the retention time and the excitation/fluorescence spectra of a detected peak with the enzymatically synthesized authentic sample, as described previously.[19] Percent changes of the produced dityrosine were calculated from the fluorescence peak area.

For the detection of dopa, the reaction mixture was analyzed by HPLC with an electrochemical detector (TOSOH Corp.). The formation of dopa was detected by monitoring the detector current at 550 mV of electrode potential. The other HPLC conditions were the same as for the detection of 3-nitrotyrosine and 2,2′-dityrosine.

Effects of Various Compounds on Nitrotyrosine and Dityrosine Formation In the presence of various concentrations of testing compounds, L-tyrosine (1 mM) was incubated with PN (0.2 mM) at 37 °C for 10 min in neutral buffer solution (pH 7.4). After the addition of fluorotyrosine as an internal standard, the formation of 3-nitro-L-tyrosine and 2,2′-dityrosine were estimated. When a testing compound showed inhibitory activity, its IC_{50} value was determined for 3-nitro-L-tyrosine and for 2,2′-dityrosine formation.

Effects of 5-MT on PN-Induced Plasmid DNA Strand Scission DNA strand scission of pBR322 plasmid by PN was detected in the presence and absence of 5-MT with agarose gel electrophoresis and ethidium bromide staining. Plasmid pBR322 (2.5 μl of 0.2 μg/ml solution, final 0.05 μg/μl) and PN (2.5 μl of 0.2 mM to 10 mM alkaline solution, final 0.05—2.5 mM) were added to PBS (phosphate buffered saline solution) (5 μl) in this order, and the solution was vortexed for 60 s. For the inhibitory experiment on 5-MT, 0.05 μg/μl of pBR322 and 1 mM PN were used. An aliquot of this reaction mixture was loaded on 2% agarose gel with loading buffer (containing bromophenol blue and sucrose). Electrophoresis was performed in TBE buffer at 50 V for 50 min using a Mupid electrophoresis system (Advance Co., Ltd., Tokyo, Japan). After the electrophoresis, the gel was stained with ethidium bromide (1 μg/ml) for 30 min and washed for 30 min, and then three forms of pBR322 plasmid DNA, supercoiled (SC), open-circular (OC) and linear (LN), were detected using a UV luminometer.

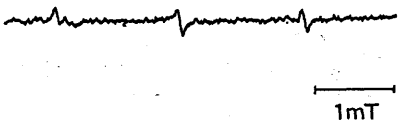

Fig. 1. ESR Spectrum of Spin Adduct of MNP with Tyrosyl Radical

PN was added to the mixture of L-tyrosine and MNP in 0.1 M sodium phosphate buffer (pH7.4).

Results

Synthesized PN was mixed with L-tyrosine in sodium phosphate buffer at neutral pH, and the products of the reaction of L-tyrosine with PN were analyzed by HPLC with a UV and fluorescence detector system. It was confirmed that 3-nitrotyrosine was formed as a major product in the reaction mixture of PN and L-tyrosine, as reported.[13] The formation of 3-nitro-L-tyrosine was dependent on the concentration of PN and L-tyrosine. The formation of a fluorescent product,[13] which was identified as 2,2′-dityrosine by comparing its retention time and fluorescence spectra with the authentic sample prepared as described in Experimental, was also confirmed.[19]

To investigate the possibility of the formation of radical species during the reaction of PN, the ESR-spin trapping method was used. MNP was used for spin trapping of radical species during the reaction of PN with tyrosine. In the case of 1 mM L-tyrosine, 2 mM PN and *ca.* 80 mM MNP at pH 9.5, a triplet ESR signal (a^N=15.8 G) was observed (Fig. 1), while only a trace of the same ESR signal was detected at pH 7.4. From its hyperfine splitting constant, it was identified as a MNP-tyrosyl radical adduct.[24] This result showed that tyrosyl radical could be involved in the reaction of L-tyrosine with PN. In the reaction of PN with tyrosine at pH 9.5, the products were the same as those at pH 7.4 by HPLC analysis. The same intermediates could be involved in the reaction both at pH 7.4 and 9.5.

The inhibitory effects of the test compounds (Fig. 2), including glutathione, synthetic selenium- and sulfur-containing compounds, and endogenous compounds, on the reaction of PN with L-tyrosine were examined (Figs. 3, 4, Table 1). The formation of 3-nitrotyrosine and 2,2′-dityrosine was detected with UV absorption at 270 nm and fluorescence at 410 nm excited with 295 nm light, respectively. All tested compounds were water-soluble at the concentration tested except melatonin, which was used after being well dispersed in water by sonication. Glutathione, serotonin and synthetic compounds, DTCP (**3**) and NEMP (**4**) effectively inhibited both the formation of 3-nitrotyrosine and 2,2′-dityrosine, and L-cystine had a very weak inhibitory effect on the 3-nitrotyrosine formation.[19] Synthetic compounds, ADPP (**5**) and APCB (**6**), also inhibited the formation of 3-nitro-L-tyrosine and 2,2′-dityrosine. In the case of 5-MT, melatonin and *dl*-LA, the formation of 2,2′-dityrosine was not inhibited, but

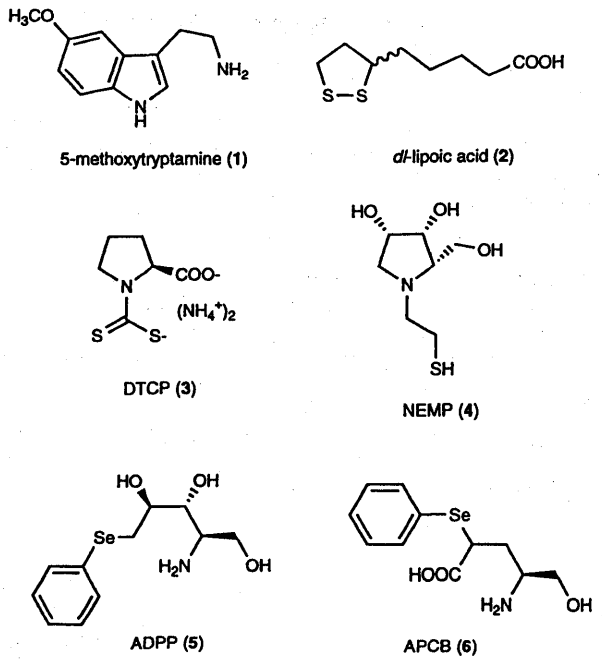

Fig. 2. Structures of Tested Compounds

The structures of endogenous and synthetic compounds used here are shown, except melatonin, serotonin, glutathione and L-cystine.

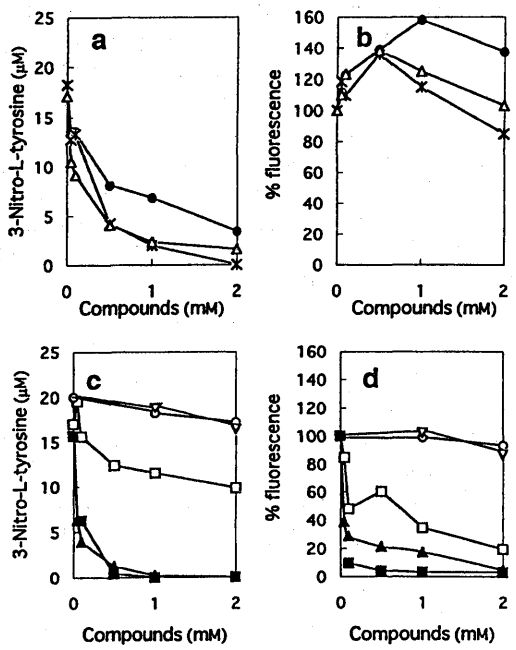

Fig. 3. Inhibitory Effects of Endogenous Compounds and DMPO on the Formation of 3-Nitro-L-tyrosine and 2,2′-Dityrosine by PN

PN and L-tyrosine were mixed in sodium phosphate buffer at pH 7.4 in the presence of various concentrations of test compounds. The formation of 3-nitro-L-tyrosine and 2,2′-dityrosine in the reaction mixture was detected. panel a and c: formation of 3-nitro-L-tyrosine, panel b and d: percent change of 2,2′-dityrosine fluorescence at 410 nm (ex. 295 nm). closed circles: 5-MT, asterisks: melatonin, open triangles: *dl*-LA, open squares: L-cystine, closed triangles: glutathione, closed squares: serotonin, open circles: DMPO, inverted triangles: PBN.

rather enhanced, although 3-nitrotyrosine was significantly inhibited.[19] Melatonin also inhibited the formation of 3-nitrotyrosine without inhibiting the formation of 2,2′-dityrosine (Fig. 3). Thus, these three reagents are thought to be a new type of inhibitor for the PN reaction because of their selective inhibitory activity for the nitration. Although some

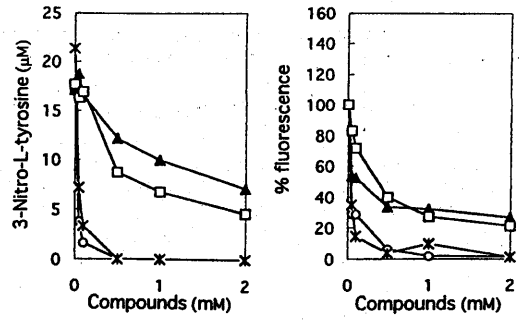

Fig. 4. Inhibitory Effects of Synthetic Compounds on the Formation of 3-Nitro-L-tyrosine and 2,2′-Dityrosine by PN

PN and L-tyrosine were mixed in sodium phosphate buffer at pH 7.4 in the presence of various concentrations of test compounds. The formation of 3-nitro-L-tyrosine and 2,2′-dityrosine in the reaction mixture was detected. panel a: formation of 3-nitro-L-tyrosine, panel b: percent change of 2,2′-dityrosine fluorescence at 410 nm (ex. 295 nm). open circles: DTCP, asterisks: NEMP, open squares: APCB, closed triangles: ADPP.

Table 1. Inhibitory Effects of Endogenous and Synthetic Compounds on 3-Nitro-L-Tyrosine and 2,2′-Dityrosine Formation

Compound	IC_{50} value (mM)	
	3-Nitro-L-tyrosine	2,2′-Dityrosine
Glutathione	0.04	0.042
Serotonin	0.08	0.055
L-Cystine	—[a]	—[b]
5-MT (1)	0.44	—[c]
Melatonin	0.29	—[c]
dl-LA (2)	0.15	—[c]
DTCP (3)	0.032	0.035
NEMP (4)	0.038	0.038
ADPP (5)	1.53	0.15
APCB (6)	0.50	0.37

a) The compound did not inhibit the formation more than 50%. *b*) The IC_{50} value was not calculated. *c*) The formation of 2,2′-dityrosine was enhanced.

radical species may be involved in this reaction based on the results obtained from the ESR experiment, the formation of both 3-nitrotyrosine and 2,2′-dityrosine was little affected by DMPO and PBN even at high concentration (>5 mM).

Without antioxidant compounds, a small amount of DOPA, another oxidized product of L-tyrosine by PN, was also detected in the reaction mixture using HPLC with an electrochemical detector. When glutathione or DTCP was used as the test compound, the amount of dopa detected first increased and then decreased with increase in the concentration of the test compound (Fig. 5). The initial increase of DOPA formation at a low concentration of test compound was assumed to be due to inhibition of further DOPA oxidation. When DOPA was treated with PN, a new product was detected by HPLC, which was considered to be the oxidized and polymerized product of DOPA. This dopa-derived product was also detected in the reaction mixture of PN and L-tyrosine. In the presence of 5-MT and LA, however, the formation of dopa was not affected. This result also supports that 5-MT and LA are selective inhibitors for the formation of 3-nitrotyrosine.

When the SC plasmid DNA was treated with 1 mM PN, DNA strand scission was observed as reported,[25] but in this concentration range, the SC form of DNA did not completely disappear. The OC (single strand scission) and LN (double

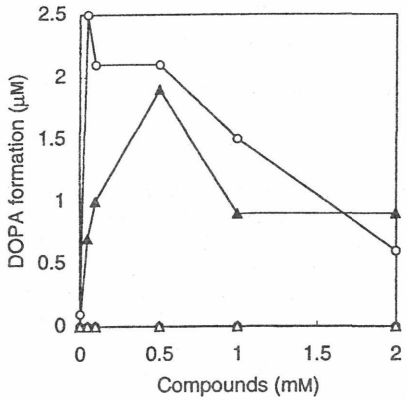

Fig. 5. The Formation of DOPA from L-Tyrosine with PN in the Presence of Test Compounds

PN and L-tyrosine were mixed in sodium phosphate buffer at pH 7.4 in the presence of various concentrations of test compounds. The formation of dopa in the reaction mixture was detected using a HPLC-electrochemical detector. open circles: DTCP, closed triangles: glutathione, closed circles: 5-MT, open triangles, *dl*-LA.

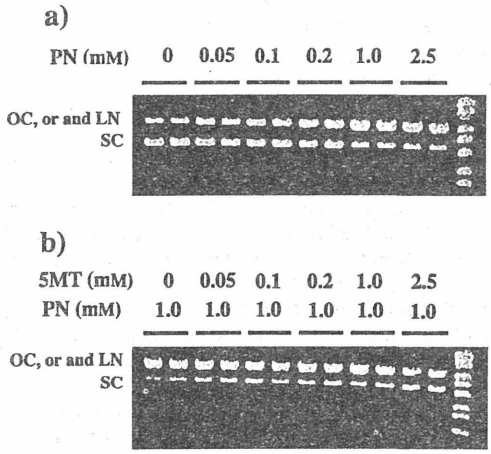

Fig. 6. Effect of 5-MT on the Plasmid DNA Scission by PN

Plasmid DNA pBR322 treated with PN was analyzed in the presence (a) and absence (b) of 5-MT by agarose gel electrophoresis and ethidium bromide staining. Three forms of pBR322 plasmid DNA, SC, OC and LN, were detected using a UV luminometer.

strand scission) form of DNA was increased in a dose dependent manner. This result showed that the DNA strands were broken by PN although its effect was less strong. In the presence of 5-MT, DNA strand breakage by 1 mM PN was not inhibited at less than 2 mM, and was only partly inhibited even at 5 mM of 5-MT (Fig. 6), although the tyrosine nitration by PN was effectively inhibited by 5-MT (IC_{50} value of 5-MT for 0.2 mM peroxynitrite=0.48 mM).

Discussion

From the HPLC analysis, 3-nitro-L-tyrosine and 2,2′-dityrosine were confirmed to be produced from the reaction of PN with L-tyrosine, indicating they are nitration and oxidation products, respectively. The amount of 3-nitrotyrosine formed was dependent on the concentration of PN and L-tyrosine. In the reaction of decomposed PN (dilution of PN in phosphate buffer at pH 7.4 resulted in rapid decomposition and this solution was used for the reaction with tyrosine instead of PN) or nitrite anion with L-tyrosine, 3-nitrotyrosine and 2,2′-dityrosine were not detected. In the case of hydrogen peroxide treatment, 3-nitrotyrosine was not detected, but a trace amount of dityrosine was formed. These results showed that the formation of 3-nitrotyrosine and 2,2′-dityrosine was the result of the reaction with PN, not with residual hydrogen peroxide, nitrate anion, or a decomposed product of PN.

Although there was a report on the inhibitory effects of glutathione and LA on tyrosine nitration,[3] the effects of antioxidants on the formation of dityrosine have not been investigated. Therefore, we studied the inhibitory effects of endogenous and newly synthetic potential antioxidants on the nitration and oxidation reaction by PN simultaneously. The formation of 3-nitrotyrosine by PN was effectively inhibited by glutathione, serotonin, the tested synthetic dithiocarbamate, thiol and selenium-containing compounds. The formation of 2,2′-dityrosine was also inhibited at a low concentration of glutathione and tested synthetic compounds. Thus, our synthetic compounds containing sulfur or selenium, DTCP, NEMP, ADPP and APCB, were as effective for the inhibition of PN reaction as was glutathione.

In the case of 5-MT, melatonin and LA, the formation of 3-nitrotyrosine was inhibited depending on the concentration. However the 2,2′-dityrosine formation was not inhibited, but rather increased at a lower dose. This result suggests that 5-MT, melatonin and LA selectively inhibited the nitration reaction of PN, and that the nitration and oxidation by PN proceeded, at least partly, *via* different intermediates. These endogenous compounds were selective scavengers for the nitrating intermediate of PN.

From the spin trapping study, tyrosyl radicals were shown to be formed in this reaction. This result supports the reaction pathway whereby PN is converted to a radical intermediate, and then a tyrosyl radical intermediate produced. However, the radical pathway in this reaction was not assumed to contribute much to the formation of nitrotyrosine and dityrosine, because DMPO and PBN, typical spin trapping reagents, did not affect their formation even at higher concentrations. Since dityrosine was thought to be formed by the dimerization of tyrosyl radicals, it was assumed that PN might react with tyrosine as a caged radical form such as [ONO·...·OH] without releasing free hydroxyl radicals.[26] As described above, 5-MT, melatonin and LA inhibited only the nitration reaction. If the nitration of L-tyrosine and the dityrosine formation were carried out with the caged radical species, the tyrosyl radical formation by ·OH-equivalent species and the addition of the NO_2·-equivalent species should occur simultaneously for the nitrotyrosine formation. In this case, it is unlikely that 5-MT, melatonin or LA is able to inhibit the nitration of tyrosine selectively, because it is impossible for these reagents to react only with the nitrating NO_2·-equivalent species in the caged radical pairs without interacting with the ·OH-equivalent species. Moreover, NO_2· also has the potential to subtract hydrogen atom from tyrosine to yield tyrosyl radicals. So, if 5-MT, melatonin or LA scavenges NO_2·-equivalent species selectively, they have to inhibit the formation of both nitrotyrosine and dityrosine. From the results of the experiments with 5-MT, melatonin and LA, it was suggested that there are at least partly independent pathways to form 3-nitrotyrosine and 2,2′-dityrosine. It was assumed that 2,2′-dityrosine was formed from the dimerization of tyrosyl radicals derived by a caged radical like [ONO·...·OH], and that 3-nitrotyrosine was formed

via a non-radical pathway, that is, electrophilic addition of nitronium cation, which may exist in a caged dipolar form such as $[ONO^+...^-OH]$.[26] For the selective inhibition of the nitration, 5-MT, melatonin and LA may scavenge only the caged dipolar intermediate.

In the reaction of plasmid DNA and PN, a SC form of DNA was changed to an OC and LN form by PN treatment, showing that PN caused DNA strand breakage, and suggesting that PN could produce a ·OH-equivalent intermediate. However, the extent of the cleavage appeared to be weaker than the effect of $Cu(en)_2$–H_2O_2 system, which was established to produce hydroxyl radicals,[27] so PN may not produce a large amount of free hydroxyl radicals. In the presence of 5-MT, the extent of the OC and LN DNA formation by PN was only slightly inhibited. This means that 5-MT had little effect on the DNA cleavage by the ·OH-equivalent intermediate of PN. This result suggested that 5-MT had no scavenging effect on the ·OH-equivalent intermediate of PN, as in the case of the reaction of PN with L-tyrosine.

In this study, the inhibitory effects of synthetic and endogenous compounds on the formation of 3-nitrotyrosine and 2,2′-dityrosine were investigated simultaneously. The synthetic compounds tested efficiently inhibited both 3-nitro-L-tyrosine and 2,2′-dityrosine formation, and 5-MT, melatonin and LA were found to have a selective inhibitory activity for the nitration reaction of PN. These results suggest that the nitration and the oxidation by PN proceed at least in part separately, and nitration-selective inhibitors, 5-MT, melatonin and LA, should be very useful compounds to investigate reactive nitrogen species (RNS). Further investigation of the functional damage and modifications of protein tyrosine residues by PN and the protective effects of the compounds found in this study are in progress.

Acknowledgments Partial financial support by Grant-in-Aids for Scientific Research (No. 10357021, 11771475) from the Ministry of Education, Science, Sports and Culture, Japan, and a grant from the Cosmetology Research Foundation are gratefully acknowledged. This study was performed through Special Coordination Funds of the Science and Technology Agency of the Japanese Government.

References

1) Beckman J. S., Beckman T. W., Chen J., Marshall P. A., Freeman B. A., *Proc. Natl. Acad. Sci. U.S.A.*, **87**, 1620—1624 (1990).
2) Huie R. E., Padmaja S., *Free Radic. Res. Commun.*, **18**, 195—199 (1993).
3) Whiteman M., Tritschler H., Halliwell B., *FEBS Lett.*, **379**, 74—76 (1996).
4) Darley-Usmar V. M., Wiseman H., Halliwell B., *FEBS Lett.*, **369**, 131—135 (1995).
5) Darley-Usmar V. M., Hogg N. O., Leary V. J., Wilson M. T., Moncada S., *Free Radic. Res. Commun.*, **17**, 9—20 (1992).
6) White C. R., Brock T. A., Chang L. Y., Crapo J., Briscoe P., Ku D., Bradley W. A., Gianturco S. H., Gore J., Freeman B. A., Tarpey M. M., *Proc. Natl. Acad. Sci. U.S.A.*, **91**, 1044—1048 (1994).
7) Salgo M. G., Bermudez E., Squadrito G. L., Pryor W. A., *Arch. Biochem. Biophys.*, **322**, 500—505 (1995).
8) Squadrito G. L., Jin X., Pryor W. A., *Arch. Biochem. Biophys.*, **322**, 53—59 (1995).
9) Radi R., Beckman J. S., Bush K. M., Freeman B. A., *Arch. Biochem. Biophys.*, **288**, 481—487 (1991).
10) Radi R., Beckman J. S., Bush K. M., Freeman B. A., *J. Biol. Chem.*, **266**, 4244—4250 (1991).
11) King P. A., Anderson V. E., Edwards J. O., Gustafson G., Plumb R. C., Suggs J. W., *J. Am. Chem. Soc.*, **114**, 5430—5432 (1992).
12) Pryor W. A., Jin X., Squadrito G. L., *Proc. Natl. Acad. Sci. U.S.A.*, **91**, 11173—11177 (1994).
13) Van der Vliet A. O., Neill C. A., Halliwell B., Cross C. E., Kaur H., *FEBS Lett.*, **339**, 89—92 (1994).
14) Kong S. K., Yim M. B., Stadtman E. R., Chock P. B., *Proc. Natl. Acad. Sci. U.S.A.*, **93**, 3377—3382 (1996).
15) Gow A. J., Duran D., Malcolm S., Ischiropoulos H., *FEBS Lett.*, **385**, 63—66 (1996).
16) Li X., DeSarno P., Song L., Beckman J. S., Jope R. S., *Biochem. J.*, **331**, 599—606 (1998).
17) Pfeiffer S., Mayer B., *J. Biol. Chem.*, **273**, 27280—27285 (1998).
18) Whiteman M., Halliwell B., *Free Radic. Res.*, **25**, 275—283 (1996).
19) Nakagawa H., Sumiki E., Ikota N., Matsushima, Y., Ozawa T., *Antioxi. Redox Signaling*, **1**, 239—244 (1999).
20) Ikota N., Hama-Inaba H., *Chem. Pharm. Bull.*, **44**, 587—589 (1996).
21) Shinobu L. A., Jones S. G., Jones M. M., *Acta Pharmacol. Toxicol.*, **54**, 189—194 (1984).
22) Ikota N., *Heterocycles*, **29**, 1469—1472 (1989).
23) Ikota N., Hanaki A., *Chem. Pharm. Bull.*, **38**, 2712—2718 (1990).
24) Barr D. D., Gunther M. R., Deterding L. J., Tomer K. B., Mason R. P., *J. Biol. Chem.*, **271**, 15498—15503 (1996).
25) Salgo M. G., Stone K., Squadrito G. L., Battista J. R., Pryor W. A., *Biochem. Biophys. Res. Commun.*, **210**, 1025—10330 (1995).
26) Richeson C. E., Mulder P., Bowry V. W., Ingold K. U., *J. Am. Chem. Soc.*, **120**, 7211—7219 (1998).
27) Ozawa T., Hanaki A., *J. Chem. Soc., Chem. Commun.*, **1991**, 330—332.

Induction of superoxide in glioma cell line U87 stimulated with lipopolysaccharide and interferon-γ: ESR using a new flow-type quartz cell

Hidehiko Nakagawa[a], Takashi Moritake[b], Koji Tsuboi[b], Nobuo Ikota[a], Toshihiko Ozawa[a,*]

[a] *National Institute of Radiological Sciences, 4-9-1, Anagawa, Inage-ku, Chiba 263-8555, Japan*
[b] *Department of Neurological Surgery, Institute of Clinical Medicine, University of Tsukuba, 1-1-1 Tennodai, Tsukuba-shi, Ibaraki 305-8575, Japan*

Received 1 February 2000; received in revised form 10 March 2000

Edited by Thomas L. James

Abstract The production of superoxide and nitric oxide induced in U87 glioma treated with lipopolysaccharide (LPS) and interferon-γ (IFN-γ) was examined by electron spin resonance (ESR) spectroscopy using a newly designed flow-type quartz cuvette without detaching cells from the culture plate. ESR spectra of 2,2,6,6-tetramethyl-4-hydroxy-1-piperidinyloxy (TEMPOL) with U87 cells on a quartz culture plate were measured at 15 min intervals. The signal intensity of TEMPOL decreased in the presence of U87 cells at the pseudo-first order rate. The signal decay was accelerated in the U87 cells treated with LPS/IFN-γ for 24 h, and was suppressed in the presence of superoxide dismutase and catalase. By the spin-trapping method, nitric oxide from U87 cells pretreated with LPS/IFN-γ for 24 h was measured by the ESR, but only a weak signal of nitric oxide adducts was detected. Further, the nitrite and nitrate levels in the medium did not increase for 24 h. By the ESR measurement of cells on culture plates without detachment stress, it was found that the production of superoxide was induced by LPS/IFN-γ, but that of nitric oxide was not, in U87 glioma cells.

Key words: Nitroxide spin label; Spin-trapping; Superoxide; Nitroxide; Glioma cell; Dithiocarboxysarcosine; Endotoxin

1. Introduction

Superoxide and nitric oxide are endogenous radical species, which are considered to play important roles not only in inflammation as protective factors, but also in signal transduction [1–4]. Recently, they have been reported to be involved in neurodegenerative diseases [5–7]. Just like immune cells such as macrophages in peripheral tissues, glial cells in the brain are considered to play a role in protecting against infection and oxidative stress. The production of nitric oxide and superoxide is suggested to be induced by treatment with cytokines or endotoxic reagents in several glioma cell lines. However, there have been only a few attempts to measure the induction of superoxide and nitric oxide [8–10]; by either a colorimetric method or an electrode-sensing method. The former method does not have good sensitivity, and for the latter, a special technique to make the electrodes is needed. Electron spin resonance (ESR) measurement is a useful way to detect radicals in biological systems. However, there have been no reports on the detection of superoxide and nitric oxide in glioma cells using ESR spectrometry. In this study, we investigated the production of superoxide and nitric oxide in a glioma cell line, U87, by measuring the superoxide-dependent spin decay of a nitroxide spin probe, and by spin-trapping of nitric oxide, respectively. The cells were measured by ESR without their detachment from culture glass plates, which does not enforce the stress caused by trypsinization or mechanical detachment, using a new cuvette and culture glass plates designed for adhesive cells.

*Corresponding author. Fax: (81)-43-255 6819.
E-mail: ozawa@nirs.go.jp

Abbreviations: ESR, electron spin resonance; LPS, lipopolysaccharide; IFN-γ, interferon-γ; TEMPOL, 4-hydroxy-2,2,6,6-tetramethylpiperidin-1-oxyl; Fe-DTCS, iron complex of *N*-dithiocarboxysarcosine; L-NMMA, *N*-monomethyl-L-arginine; SOD, superoxide dismutase; Cat, catalase

2. Materials and methods

2.1. Chemicals

Superoxide dismutase (SOD), catalase (Cat), interferon-γ (IFN-γ) and minimum essential medium were purchased from Sigma (St. Louis, MO, USA). Fetal bovine serum, a mixture of antibiotics (penicillin–streptomycin–neomycin) and trypsin were from Gibco BRL (Rockville, MD, USA). Lipopolysaccharide (LPS) was from Difco Laboratories (Detroit, MI, USA). *N*-Dithiocarboxysarcosine (DTCS) was from Dojindo Laboratories (Kumamoto, Japan) and 4-hydroxy-2,2,6,6-tetramethylpiperidin-1-oxyl (TEMPOL) was from Aldrich (Milwaukee, WI, USA). *N*-Methyl-D-glucamine dithiocarbamate (MGD) was synthesized by following the method of Shinobu et al. [11]. *N*-Methyl-D-glucamine, carbon disulfide, *N*-monomethyl-L-arginine (L-NMMA) and $FeSO_4 \cdot 7H_2O$ were from Wako Pure Chemical Industries (Osaka, Japan). All the chemicals and reagents were of analytical or biochemical grade.

2.2. Cell culture

U87 glioma cells were maintained in minimum essential medium with 10% fetal bovine serum and a mixture of antibiotics at 37°C inside a humidified incubator with 5% CO_2/95% air. Experimental cultures were grown on quartz slide glasses (82 mm × 8.7 mm × 0.2 mm). After confirming U87 cells were grown subconfluently, the culture medium was changed to minimum essential medium with 500 ng/ml LPS and 150 U/ml IFN-γ without fetal bovine serum. After treatment with LPS and IFN-γ for 24 h, U87 cells on slide glasses were washed with Hank's balanced buffer solution in a flow-type cuvette (sample space thickness = 0.5 mm), and subjected to ESR measurements. To detect nitrite and nitrate, U87 cells were seeded into 48 well cell culture plates at 7.3×10^4 cells per well, and incubated at 37°C with 5% CO_2 for 24 h.

2.3. ESR measurement of U87 cells on slide glass

A slide glass with U87 cells was directly inserted into the new flow-type quartz cuvette (Fig. 1) designed for measurement of adhesive cells (Radical Research, Tokyo, Japan). The cuvette was connected

to the flow system as shown in Fig. 1, in which the upstream of the cuvette was connected to a reservoir tank warmed at 37°C, and the downstream to a peristaltic pump connecting to a drain. The cuvette was set in the cavity of a ESR spectrometer (FR-30, JEOL, Tokyo, Japan). The cells in the cuvette were washed with Hank's balanced buffer solution at the rate of 0.5 ml/min for 2 min. The cells were treated with 7 μM TEMPOL (Fig. 2, 1), 10 mM DTCS-iron complex (Fe-DTCS) (DTCS, Fig. 2, 3) or 10 mM MGD-iron complex (Fe-MGD) (MGD, Fig. 2, 4) by introducing 2 ml solutions of these reagents into the cuvette at the rate of 0.5 ml/min, and then ESR spectra were measured. Because the total volume of the cuvette and tubes is 1.2 ml, the buffer solution inside the cuvette is discarded by adding 2 ml of the reagent solution.

2.4. TEMPOL signal decay with U87 cells

U87 cells on culture slide glasses were inserted into the flow-type cuvettes, and washed with Hank's balanced buffer solution. After a 2 ml solution of 7 μM TEMPOL in Hank's balanced buffer solution had been introduced into the cuvettes, ESR spectra were measured at 15 min intervals. ESR measurement conditions were as follows: field, 330–340 mT; modulation frequency, 100 kHz; modulation width, 0.2 mT; time constant, 1 s; sweep time, 8 min/10 mT; microwave frequency, 9.4 GHz; microwave power, 16 mW. The relative signal intensities of the lowest field signals of TEMPOL for MnO as an external standard were plotted as time lapsed. ESR spectra of 7 μM TEMPOL with LPS and IFN-γ-pretreated U87 cells were also measured in the presence of 100 U/ml SOD and 10 U/ml Cat. After the measurement, the cells on the slide glasses were trypsinized and enumerated.

2.5. Spin-trapping of nitric oxide with Fe-DTCS

Culture slide glasses with U87 cells were inserted into cuvettes and washed with Hank's balanced buffer solution. A 2 ml solution of 10 mM Fe-DTCS with or without SOD (1000 U/ml) or 10 mM Fe-MGD in 100 mM Tris–HCl buffer containing 0.25 M glucose was then introduced into each cuvette, and ESR spectra were measured at 8 min intervals. The measurement conditions were as for the TEMPOL measurements except that the field was 324–334 mT and time constant was 3 s.

2.6. Detection of nitrite/nitrate

U87 cells were treated with LPS/IFN-γ or L-NMMA for 24 h in minimum essential medium without fetal bovine serum. The concentration of nitrite and nitrate in the medium was measured with a NO_2/NO_3 detection kit-F (Dojindo, Kumamoto, Japan). Briefly, an aliquot of the medium was collected, and centrifuged at $1000 \times g$ for 15 min at room temperature. According to the instructions, 80 μl of the supernatant was treated with nitrate reductase and co-enzyme for 1 h at 37°C, and then reacted with 2,3-diaminonaphtalene under acidic conditions at room temperature for 15 min. After neutralization with sodium hydroxide, the fluorescence from naphtalenetriazole at 460 nm (excited at 355 nm) was measured with a fluorescence plate reader (Fluoroskan Acent, Labsystems, Helsinki, Finland).

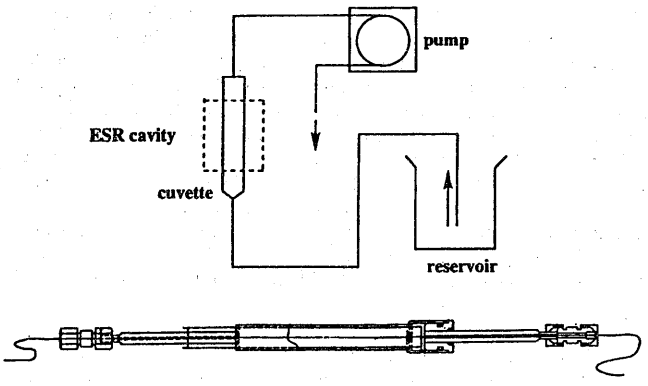

Fig. 1. The structure of the new flow-type quartz cell and a diagram of the ESR measurement system.

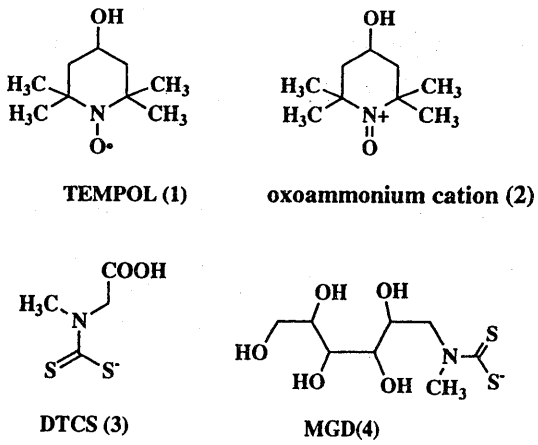

Fig. 2. Structure of TEMPOL (1), its oxoammonium cation (2), DTCS (3) and MGD (4).

3. Results

The effect of LPS with IFN-γ on the production of superoxide by U87 glioma cells was examined with a 9.5 GHz ESR spectrometer without detachment of the cells using an order-made flow-type cuvette designed for adhesive cells. The production of superoxide was evaluated by measuring the superoxide-dependent signal decay of TEMPOL. After a 2 ml solution of 7 μM TEMPOL in Hank's balanced buffer solution had been introduced into the cuvette, the ESR spectra of 7 μM TEMPOL were measured at 15 min intervals in the presence of U87 cells pretreated with or without 500 ng/ml LPS and 150 U/ml IFN-γ for 24 h. The relative intensities of the lowest field ESR signals of TEMPOL were measured and plotted as time lapsed. The decrease in the signal intensity of TEMPOL with U87 cells occurred at the pseudo-first order rate (Fig. 3).

Without U87 cells, the signal did not decay. The observed rate constant of the signal decay was increased in the case of U87 cells pretreated with LPS and IFN-γ (Figs. 3 and 4). The observed pseudo-first rate constants were calculated to be 3.05×10^{-3}/min/10^6 cells and 6.14×10^{-3}/min/10^6 cells in the case of non-treated cells and LPS/IFN-γ-pretreated cells, respectively. This increase of the rate constant by LPS/IFN-γ-pretreated U87 cells was inhibited in the presence of SOD and Cat (Fig. 4). The observed pseudo-first rate constant was calculated to be 3.39×10^{-3}/min/10^6 cells in the case of LPS/IFN-γ-pretreated cells with SOD and Cat. From the difference of the observed rate constants in the presence and absence of both SOD and Cat, the signal decay of TEMPOL with superoxide was calculated to be 2.75×10^{-3}/min/10^6 cells. Since the reaction rate constant of TEMPOL with superoxide has been calculated to be 3.90×10^7 M^{-1} min^{-1} [12], the concentration of superoxide in LPS/IFN-γ-treated U87 cells was estimated to be 70.5 pM/10^6 cells.

The effect of LPS with IFN-γ on the production of nitric oxide by U87 glioma cells was also examined by ESR using the flow-type cuvette without detachment of the cells. U87 cells on a culture slide glass were treated with 10 mM Fe-DTCS or 10 mM Fe-MGD for spin-trapping of nitric oxide from the cells [13,14]. ESR spectra were measured at 8 min intervals. In the case of U87 cells pretreated with LPS/IFN-γ, a trace amount of the ESR signal of the nitric oxide adduct of

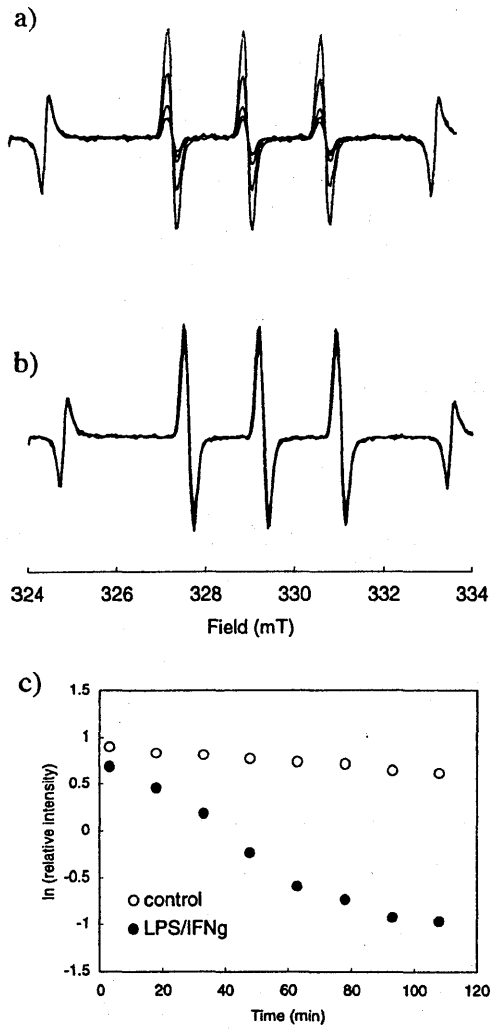

Fig. 3. ESR signal decay of TEMPOL with U87 glioma cells ESR spectra of the TEMPOL solution (the initial concentration is 7 μM) with U87 glioma cells cultivated on a quartz glass plate were obtained at 30 min intervals, (a) with LPS/IFN-γ-treated U87 cells, and (b) with control U87 cells. The time course of the relative signal intensity measured at 15 min intervals is presented in (c).

Fe-DTCS (NO-Fe-DTCS) was detected (Fig. 5) during the first scan (0–8 min after Fe-DTCS treatment), but no nitric oxide adducts were detected thereafter. The same result was obtained in the presence of SOD. Using MGD-ion complex, an ESR signal for nitric oxide adduct was not detected.

To evaluate the production of nitric oxide by U87 cells, the concentration of nitrite/nitrate accumulated for 24 h in the medium was measured with NO_2/NO_3 detection kit-F. It was not affected by treatment of LPS/IFN-γ, and decreased in the presence of L-NMMA (Fig. 6).

4. Discussion

The production of superoxide and nitric oxide by U87 glioma cells was measured by ESR without detachment of the cells using a flow-type cuvette designed for adhesive cells. The cuvette and the flow system made it possible to subject adhesive cells to ESR without the stress of detachment involving trypsinization and mechanical stress.

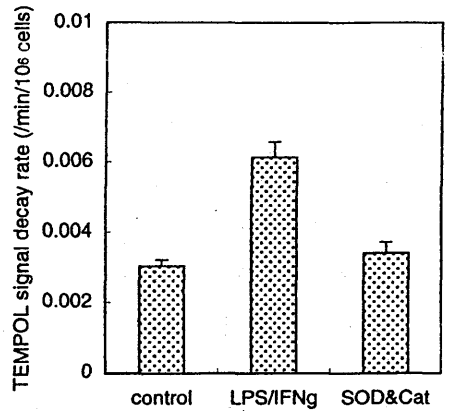

Fig. 4. Signal decay rate of TEMPOL by U87 glioma cells ESR spectra of the TEMPOL solution (the initial concentration is 7 μM) with U87 glioma cells on a quartz glass plate were obtained at 15 min intervals. The signal decay rate of TEMPOL with U87 glioma cells was calculated by measuring the decrease of ESR signal intensities of TEMPOL with U87 glioma cells treated with LPS/IFN-γ in the presence or absence of SOD and Cat. Values are presented as the mean ± S.E.M. of 3–5 experiments. One-way ANOVA indicated significant differences between groups ($P < 0.05$).

For evaluating the production of superoxide, the decay rate of TEMPOL signal was measured by ESR in the presence or absence of both SOD and Cat. The decay rate was increased by treatment with LPS/IFN-γ, but this increase was inhibited in the presence of both SOD and Cat to the control level (Fig. 4). This result suggested that superoxide production by U87 cells was induced by treatment with LPS/IFN-γ for 24 h. Nitroxide spin probes have been reported to act as a superoxide scavenger or a SOD-mimic [12,15–18]. TEMPOL was

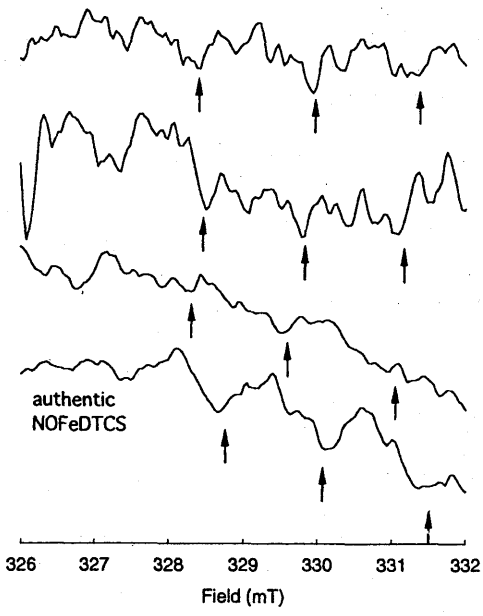

Fig. 5. ESR spectra of LPS and IFN-γ-treated U87 cells with Fe-DTCS U87 cells pretreated with LPS/IFN-γ for 24 h were treated with 10 mM of Fe-DTCS complex as a spin-trapping reagent for nitric oxide. ESR spectra were obtained from the U87 cells from 0 to 8 min after loading of Fe-DTCS. Each spectrum shows ESR signals obtained from independent samples except the bottom one, which is the signal from the authentic nitric oxide adduct of Fe-DTCS. In each spectrum, the weak signals from the nitric oxide adduct are indicated by arrows.

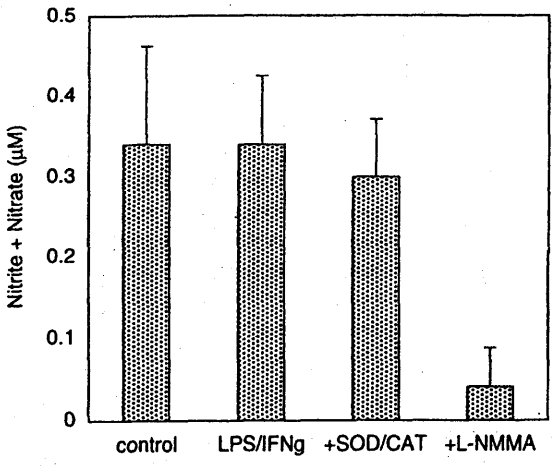

Fig. 6. Concentration of nitrite and nitrate in the culture media of U87 cells treated with LPS and IFN-γ. U87 cells at 7.3×10^4 cells per well were treated with LPS/IFN-γ for 24 h in culture media without serum and phenol red. After a reduction of nitrate to nitrite with nitrate reductase and a reaction with 2,3-diaminonaphtharene under acidic conditions, the concentration of nitrite in 80 μl of the media was evaluated by measuring the fluorescence intensity at 460 nm (excitation at 355 nm). Values are presented as the mean ± S.E.M. of 10 samples.

considered to act a SOD-mimic by the redox mechanism [11]. TEMPOL is readily oxidized by protonated superoxide to oxoammonium cation (Fig. 2, 2) which in turn oxidizes another superoxide to molecular oxygen [19]. According to these reports, TEMPOL catalytically reacts with superoxide, so that the signal intensity of TEMPOL might not decrease depending on the production of superoxide. However, the decay rate of signal intensity of TEMPOL was considered to reflect the production of superoxide in this study, because the concentration of TEMPOL was much higher than that of superoxide produced in the cells which was practically spent only in the reaction with TEMPOL. The reaction of the oxoammonium cation with superoxide is considered to be negligible as long as the concentration of TEMPOL is high enough in the system.

Although the decay rate of TEMPOL with LPS/IFN-γ-treated U87 cells decreased at the same level as that of the control in the presence of SOD and Cat, the signal still decayed. This slow decay is assumed to be due to biological reductants which have been reported to reduce nitroxide spin probes including TEMPOL [20,21].

The production of nitric oxide by LPS/IFN-γ-treated U87 glioma cells was also examined by ESR without detachment of the cells. However, only a weak ESR signal due to the nitric oxide adduct of Fe-DTCS (NO-Fe-DTCS) was detected (Fig. 5) from U87 cells pretreated with LPS/IFN-γ. From this result, it is not clear whether nitric oxide is induced by LPS/IFN-γ in U87 cells. From the concentration of the nitrite/nitrate that had accumulated over 24 h in the medium, it was apparent that no nitric oxide was produced on treatment with LPS/IFN-γ. Because the concentration of nitrite/nitrate was decreased in the presence of L-NMMA (Fig. 6), a small amount of nitric oxide may be produced by the control cells. The mechanism of induction of nitric oxide for endotoxin and/or for cytokines is considered to be different. Recently, it has been reported that nitric oxide was not produced in some malignant glioma cells, but was involved in the malignant progression of cancers [10]. The loss of the nitric oxide production induced in U87 cells by LPS/IFN-γ is consistent with the tumorigenic nature of U87 glioma cells.

In conclusion, it was found that treatment with LPS/IFN-γ for 24 h induced production of superoxide, but not nitric oxide in a glioma cell line, U87, by ESR for cells using a superoxide-sensitive spin probe, TEMPOL, and spin-trapping reagents for nitric oxide, Fe-DTCS and Fe-MGD. The use of new cuvettes designed for adhesive cells and quartz culture plates is an effective way to measure glioma cells by ESR without their detachment from the plates.

Acknowledgements: We thank Mr. M. Shinmei (Radical Research) for making the cuvette designed for adhesive cells. This work was supported by Special Coordination Funds of the Science and Technology Agency of the Japanese Government and by a Grant-in-Aid for Scientific Research, (A) No. 10357021, from The Ministry of Education, Science, Sports and Culture, Japan, to T.O.

References

[1] Fridovich, I. (1997) J. Biol. Chem. 272, 18515–18517.
[2] Hancock, J.T. (1997) Br. J. Biomed. Sci. 54, 38–46.
[3] Irani, K. and Goldschmidt-Clermont, P.J. (1998) Biochem. Pharmacol. 55, 1339–1346.
[4] Moncada, S., Palmer, R.M. and Higgs, E.A. (1991) Pharmacol. Rev. 43, 109–142.
[5] Dawson, V.L. and Dawson, T.M. (1998) Prog. Brain Res. 118, 215–229.
[6] Youdim, M.B., Lavie, L. and Riederer, P. (1994) Ann. N.Y. Acad. Sci. 738, 64–68.
[7] Beckman, J.S., Chen, J., Crow, J.P. and Ye, Y.Z. (1994) Prog. Brain Res. 103, 371–380.
[8] Haregewoin, A., Alexander, E.R., Black, P.M. and Loeffler, J.S. (1994) Exp. Cell Res. 210, 137–139.
[9] Manning, P., McNeil, C.J., Cooper, J.M. and Hillhouse, E.W. (1998) Free Radic. Biol. Med. 24, 1304–1309.
[10] Rieger, J., Stander, M., Loschmann, P.A., Heneka, M., Dichgans, J., Klockgether, T. and Weller, M. (1998) Oncogene 17, 2323–2332.
[11] Shinobu, L.A., Jones, S.G. and Jones, M.M. (1984) Acta Pharmacol. Toxicol. 54, 189–194.
[12] Krishna, M.C., Russo, A., Mitchell, J.B., Goldstein, S., Dafni, H. and Samuni, A. (1996) J. Biol. Chem. 271, 26026–26031.
[13] Yoshimura, T., Yokoyama, H., Fujii, S., Takayama, F., Oikawa, K. and Kamada, H. (1996) Nat. Biotechnol. 14, 992–994.
[14] Fujii, S., Suzuki, Y., Yoshimura, T. and Kamada, H. (1998) Am. J. Physiol. 274, G857–G862.
[15] Haseloff, R.F., Zollner, S., Kirilyuk, I.A., Grigor'ev, I.A., Reszka, R., Bernhardt, R., Mertsch, K., Roloff, B. and Blasig, I.E. (1997) Free Radic. Res. 26, 7–17.
[16] Offer, T., Mohsen, M. and Samuni, A. (1998) Free Radic. Biol. Med. 25, 832–838.
[17] Samuni, A., Mitchell, J.B., DeGraff, W., Krishna, C.M., Samuni, U. and Russo, A. (1991) Free Radic. Res. Commun. 12–13, 187–194.
[18] Samuni, A., Krishna, C.M., Riesz, P., Finkelstein, E. and Russo, A. (1988) J. Biol. Chem. 263, 17921–17924.
[19] Krishna, M.C., Grahame, D.A., Samuni, A., Mitchell, J.B. and Russo, A. (1992) Proc. Natl. Acad. Sci. USA 89, 5537–5541.
[20] Swartz, H.M., Sentjurc, M. and Morse, P.D.D. (1986) Biochim. Biophys. Acta 888, 82–90.
[21] Iannone, A., Bini, A., Swartz, H.M., Tomasi, A. and Vannini, V. (1989) Biochem. Pharmacol. 38, 2581–2586.

平成１３年 10 月刊行

放射線医学総合研究所
研究交流・情報室
千葉市稲毛区穴川４丁目９番１号（〒２６３－８５５５）
電話　千葉（０４３）２０６－３０２７（ダイヤルイン）
http://www.nirs.go.jp　　E-mail : kouryu@nirs.go.jp